TTI: 0-6982

Texas A&M Transportation Institute

Utilization of UHPC Bridge Superstructures in Texas—Volume 2: Structural Analysis, Design, and Full-Scale Testing of Precast, Pretensioned Girders

Technical Report 0-6982-R1-Vol2

Cooperative Research Program

TEXAS A&M TRANSPORTATION INSTITUTE
COLLEGE STATION, TEXAS

sponsored by the
Federal Highway Administration and the
Texas Department of Transportation
https://tti.tamu.edu/documents/0-6982-R1-Vol2.pdf

Technical Report Documentation Page

1. Report No.	2. Government Accession No.	3. Recipient's Catalog No.
FHWA/TX-23/0-6982-R1-Vol2		

4. Title and Subtitle	5. Report Date
UTILIZATION OF UHPC BRIDGE SUPERSTRUCTURES IN TEXAS—VOLUME 2: STRUCTURAL ANALYSIS, DESIGN, AND FULL-SCALE TESTING OF PRECAST, PRETENSIONED GIRDERS	Published: October 2023
	6. Performing Organization Code

7. Author(s)	8. Performing Organization Report No.
Mary Beth D. Hueste, John Mander, Stefan Hurlebaus, Anol Mukhopadhyay, Amreen Fatima, Hyeonki Hong, and Tevfik Terzioglu	Report 0-6982-R1-Vol2

9. Performing Organization Name and Address	10. Work Unit No. (TRAIS)
Texas A&M Transportation Institute The Texas A&M University System College Station, Texas 77843-3135	11. Contract or Grant No. Project 0-6982

12. Sponsoring Agency Name and Address	13. Type of Report and Period Covered
Texas Department of Transportation Research and Technology Implementation Office 125 E. 11th Street Austin, Texas 78701-2483	Technical Report: September 2018–October 2022
	14. Sponsoring Agency Code

15. Supplementary Notes

Project sponsored by the Texas Department of Transportation and the Federal Highway Administration.
Project Title: Utilization of UHPC Bridge Superstructures in Texas
URL: https://tti.tamu.edu/documents/0-6982-R1-Vol2.pdf

16. Abstract

The use of ultra-high performance concrete (UHPC) in Texas bridges has potential to produce substantial improvements to bridge construction. Advanced material properties and superior durability of UHPC can result in significant design and construction benefits. An analytical feasibility study showed that UHPC bridge girders provide increased design efficiency over conventional concrete (CC) girders, including reduced cross-sections, longer spans, and larger girder spacings. This study identified the desired material properties of nonproprietary UHPC for the fabrication of precast, pretensioned bridge girders with a CC deck slab. The characteristic material properties attained using the developed nonproprietary UHPC mixtures were used to design prototype bridge girders and full-scale Tx34 and Tx54 girder specimens with CC decks for laboratory testing. Three UHPC girder specimens were tested under the prototype design load demands to evaluate the girder response with respect to flexure, web shear, and interface shear. The fiber distribution and tensile strength impacted both the flexure and shear behavior. The flexure and shear performance were enhanced relative to CC girders. During flexure testing, no cracking was observed up to factored moment demands. The moment applied to each girder was 30–50 percent higher than the corresponding design-factored moment. The use of harped strands and minimum transverse reinforcement also enhanced the shear performance. The Tx34 girder with straight strands had a lower tensile strength, and the applied shear was slightly below the design-factored shear at the unreinforced end. For all other girder ends, the experimental shear capacity was at least twice the design-factored shear demand. Mild steel reinforcement in the shape of U-bars at the interface of the CC-UHPC composite section effectively transferred shear up to the design-factored loads with negligible slip, although some limited slip was observed at loads exceeding factored load demands. The selected prediction models and the recommended design approach provided results consistent with the measured behavior.

17. Key Words	18. Distribution Statement
Ultra-High Performance Concrete, UHPC, Full-Scale Girder Testing, Instrumentation, Flexure, Shear, Interface Shear, Composite Action, Transfer Length, Camber, Precast Girder	No restrictions. This document is available to the public through NTIS: National Technical Information Service Alexandria, Virginia https://www.ntis.gov

19. Security Classif. (of this report)	20. Security Classif. (of this page)	21. No. of Pages	22. Price
Unclassified	Unclassified	460	

Form DOT F 1700.7 (8-72) Reproduction of completed page authorized

UTILIZATION OF UHPC BRIDGE SUPERSTRUCTURES IN TEXAS—VOLUME 2: STRUCTURAL ANALYSIS, DESIGN, AND FULL-SCALE TESTING OF PRECAST, PRETENSIONED GIRDERS

by

Mary Beth D. Hueste, Ph.D., P.E.
Research Engineer
Texas A&M Transportation Institute

John Mander, Ph.D.
Research Engineer
Texas A&M Transportation Institute

Stefan Hurlebaus, Ph.D., P.E.
Research Scientist
Texas A&M Transportation Institute

Anol Mukhopadhyay, Ph.D.
Research Scientist
Texas A&M Transportation Institute

Amreen Fatima
Graduate Assistant Researcher
Texas A&M Transportation Institute

Hyeonki Hong
Graduate Assistant Researcher
Texas A&M Transportation Institute

and

Tevfik Terzioglu, Ph.D.
Post-Doctoral Research Associate
Texas A&M Transportation Institute

Report 0-6982-R1-Vol2
Project 0-6982
Project Title: Utilization of UHPC Bridge Superstructures in Texas

Sponsored by the
Texas Department of Transportation
and the
Federal Highway Administration

Published: October 2023

TEXAS A&M TRANSPORTATION INSTITUTE
College Station, Texas 77843-3135

DISCLAIMER

This research was sponsored by the Texas Department of Transportation (TxDOT) and the Federal Highway Administration (FHWA). The contents of this report reflect the views of the authors, who are responsible for the facts and the accuracy of the data presented herein. The contents do not necessarily reflect the official view or policies of FHWA or TxDOT. This report does not constitute a standard, specification, or regulation.

This report is not intended for construction, bidding, or permit purposes. The researcher in charge of the project was Mary Beth D. Hueste. The United States Government and the State of Texas do not endorse products or manufacturers. Trade or manufacturers' names appear herein solely because they are considered essential to the object of this report.

ACKNOWLEDGMENTS

This project was conducted at Texas A&M University and was supported by TxDOT and FHWA through the Texas A&M Transportation Institute (TTI) as part of Project 0-6982, Utilization of UHPC Bridge Superstructures in Texas.

The authors are grateful to the individuals who were involved with this project and provided invaluable assistance, including Tom Schwerdt (TxDOT, project manager), Robert Owens (TxDOT, project director), and the TxDOT Project Monitoring Committee: Ahmed Al-Basha, Biniam Aregawi, Rachel Cano, Geetha Chandar, Chad Dabbs, Jamie Farris, Igor Kafando, Andy Naranjo, Joe Roche, Prapti Sharma, and Jason Tucker.

Co-authors Amreen Fatima and Hyeonki Hong were the principal PhD students for the project, and this work was conducted as a major part of their doctoral research.

The authors also wish to acknowledge the students involved in the early stages of the project, particularly master's students Brittni Cooper and Jay Shah.

In addition, many students contributed to this project by helping with the laboratory work and precast plant production process: Stephin Joseph Anna, Victor Balangero, William (Jake) Irr, Nuzhat Kabir, Mikhail Lanier, Matthew Leffler, Isabel Mlo, Anirutthan Narayanan, Samir Palepu, Jay Parmar, Pushkar Shivechchhu, Arash Rockey, Nikhil Ganesh Tandel, Xincheng Ethan Wang, Seunghyun Yoon, and Zhen Zhang.

The support and assistance from the Center for Infrastructure Renewal staff is gratefully acknowledged, including Kai-wei (Victor) Liu, Rick Canatella, Tony Barbosa, Charles Droddy, Kirk Martin, and Dr. Peter Keating (director of the High-Bay Structural & Materials Testing Laboratory).

The TTI staff who supported the project are gratefully acknowledged, especially Madalyn Salcido, who provided overall administrative and business support for the project.

The research team is grateful for staff at Heldenfels Enterprises Inc., San Marcos, Texas, who supported this project by working with the research team to conduct a trial batch of the developed UHPC mixture and who fabricated the UHPC girder specimens at their precast plant.

TABLE OF CONTENTS

LIST OF FIGURES

LIST OF TABLES

LIST OF ACRONYMS

AASHTO	American Association of State Highway and Transportation Officials
AFGC	Association Française de Génie Civil/French Civil Engineering Association
ACI	American Concrete Institute
CC	Conventional concrete
CIP	Cast-in-Place
CMOD	Crack-Mouth Opening Displacement
CSA	Canadian Standard Association
DAfStb	German Committee for Structural Concrete (Deutscher Ausschuss für Stahlbeton)
DEMEC	Demountable mechanical
ESG	Embedded concrete gage
FHWA	Federal Highway Administration
FRC	Fiber-reinforced concrete
HBSMTL	High Bay Structures and Material Testing Laboratory
HPC	High-performance concrete
JSCE	Japan Society of Civil Engineers
KSG	Surface-mounted concrete strain gage
LRFD	Load and Resistance Factor Design
LVDT	Linear variable displacement transducer
LV	Linear variable displacement transducer
MOE	Modulus of elasticity
NCHRP	National Cooperative Highway Research Program
NSC	Normal strength concrete
PCI	Precast/Prestressed Concrete Institute
PCP	Precast Concrete Panel
PCSB	Prestressed Concrete Slab Beam
SG	Surface Concrete Strain Gage
SLS	Service Limit State
SP	String Potentiometer
SSG	Surface Steel Strain Gage
TC	Thermocouple
TxDOT	Texas Department of Transportation
UC-bars	U-Composite Bars
UHPC	Ultra-high performance concrete
UHP-FRC	Ultra-high performance fiber-reinforced concrete
ULS	Ultimate Limit State

1 INTRODUCTION

1.1 BACKGROUND AND SIGNIFICANCE

Ultra-high-performance concrete (UHPC) is being adopted as a favorable choice for several construction applications, including highway bridge girders. Higher prestressing force can be applied due to the higher compressive strength and enhanced tensile behavior of UHPC. Utilizing higher prestressing forces allows for longer spans, fewer girder lines, and more slender sections. The dense matrix associated with UHPC enhances the durability of the material and therefore increases the life span of the structure. These structural advantages of comparatively fewer material requirements and long-term benefits help to balance the higher material cost of UHPC mixtures. Although the implementation of UHPC has increased gradually in the United States, limited research has been conducted on the full-scale testing of UHPC girders with conventional concrete (CC) decks.

The cost of commercially available UHPC is significantly higher than CC, although nonproprietary UHPC mixtures developed from locally available materials provides a more economical option. The initial phase of this research project, documented in the Volume 1 report, led to the development of several nonproprietary UHPC mixtures, along with steel fibers, from material constituents local to the state of Texas. The finalized UHPC mixture for implementation, resulting from several parametric optimizations and a trial batch conducted in collaboration with a Texas precaster, was used to cast the full-scale girder test specimens.

1.2 OBJECTIVE AND SCOPE

There were three main objectives of this research: (1) conduct an analytical feasibility study to identify the material properties for which a nonproprietary UHPC mixture design should be developed to deliver the optimal design benefits; (2) develop a nonproprietary concrete mixture design to meet the needs identified in Objective 1; and (3) conduct experiments (full-scale and material-level) to study long-term mechanical properties in an effort to eliminate or minimize the use of ordinary reinforcing bars in UHPC applications.

An analytical feasibility study was conducted to assess the potential bridge girder design solutions that were suited to optimize the standard Texas Department of Transportation (TxDOT) shapes.

Several parameters were assessed to identify the advantages of the high compressive and tensile strength limits by increasing the prestressing force. The study also explored increasing the spacing between the girders by eliminating one girder line to make the overall bridge design more economical. Several other possibilities for future bridge construction were explored, including increasing the strand diameter and minimizing the bridge deck thickness. Based on feedback from TxDOT, two standard Texas I-shapes were selected for full-scale testing.

In collaboration with a Texas precast company, two Tx34 specimens and one Tx54 specimen were fabricated using the finalized UHPC mixture. The Tx34 specimens were both 50 ft long; one designed with an eccentric strand solution and the other designed with a harped strand solution. The Tx54 specimen was 70 ft long with harped strands. All three specimens were designed such that half the span had minimum web shear reinforcement while the other half had no transverse shear reinforcement. The objective was to study the enhanced tensile and shear strength of the UHPC girders. Transfer length measurements and camber were monitored. The girders were topped with a standard cast-in-place (CIP), 8.5 in. thick CC deck slab. The composite girders were tested in flexure and shear. The appendix shows the structural drawings of the three girder specimens provided to the precaster.

The results of the flexure and shear testing of the girder specimens are presented in this report volume and comparisons with theoretical predictions are drawn.

This Volume 2 report focuses on design and analysis of standard precast, pretensioned UHPC bridge girders in Texas made from the developed nonproprietary UHPC mixture. The design guidelines developed based on this experimental full-scale testing of the designed specimens serve as the starting point for the implementation of UHPC in Texas highway bridge girders.

This Volume 2 report documents the following aspects of the research project:

- Review of the literature and state of the practice related to design requirements, guidelines, and recommendations for UHPC structural components are summarized.
- An analytical feasibility study is conducted for typical Texas girder types and shapes to explore the design space and provide an evaluation for potential implementation of UHPC bridge girders.

- Two Tx34 and one Tx54 girder prototype designs were developed, and full-scale UHPC girder specimens were fabricated at a precast plant.
- Material models updated with companion small-scale material tests were applied to analyze the full-scale specimens and predict the UHPC girder performance during load testing.
- The UHPC girder designs were evaluated using the data from the full-scale flexure and shear tests.
- The performance of the UHPC girder specimens with and without the presence of minimum transverse reinforcement in shear was compared by providing minimum transverse steel in only half of the girder span for each specimen.
- Recommended design guidelines for UHPC girders are reviewed and evaluated based on the comparison of the full-scale girder response during testing versus theoretical and design predictions.

The Volume 1 report documents the details of the tasks focusing on the development of the nonproprietary UHPC mixtures and girder fabrication and assessment. The Volume 3 report includes guidelines for production of UHPC, design guidelines for precast, pretensioned UHPC bridge girders, and UHPC girder design examples.

1.3 RESEARCH PLAN

The findings of this research study support implementation of precast, pretensioned UHPC bridge girder in Texas. The following tasks were systematically undertaken to achieve the goals of this research project:

- Task 1. Project Management and Research Coordination
- Task 2. Review State of the Art and State of the Practice
- Task 3. Conduct Analytical Feasibility Study
- Task 4. Develop Nonproprietary UHPC Mixture Design
- Task 5. Material-Level Experiments for Selected Mixes
- Task 6. Full-Scale Experiments
- Task 7. Develop Design Guidelines and Examples

1.4 REPORT OUTLINE

This Volume 2 report consists of eight chapters that describe the literature review, methodology, preparation, and findings from Tasks 2, 3, and 6.

Chapter 1 describes the background, significance, objectives, and scope of this research study and plan and outlines the Volume 2 report.

Chapter 2 presents a literature review of the existing code provisions and publications for the structural design and analysis of UHPC. The structural behavior of UHPC, studied by several domestic and international researchers and code authorities, is documented. The experimental test data conducted on flexural, shear, and other structural members is summarized and reviewed for background. The information and recommendations provided by the latest design guidelines at national and international levels are presented. The information of recent drafts and other ongoing guidelines is summarized. This chapter also enumerates the research questions that arise from the literature review.

Chapter 3 presents a preliminary analytical feasibility study that was conducted to optimize the possible design alternatives that could be achieved using UHPC in standard TxDOT highway bridge girder members. Several standard TxDOT bridge girder shapes, such as prestressed concrete slab beams (PCSBs) and I-girders (Tx54 and Tx62), were evaluated using UHPC design strength values based on the literature. The diameter of the strands, the number of girder lines, the use of a thinner UHPC deck slab, and different tensile strengths were considered in evaluating the potential benefits of UHPC girders. The most feasible design solutions were selected to determine the target compressive and tensile strength of the UHPC to be attained by the nonproprietary mixture developed. Based on the feedback from TxDOT, Tx34 and Tx54 girder sections were selected for full-scale testing.

Chapter 4 describes the details of the full-scale test program. This chapter documents the testing plan, the instrumentation plan, and the details of the specimens of the selected Texas girder shapes. This chapter also summarizes the experimental test data of the companion specimens fabricated along with the full-scale girders.

Chapter 5 documents the flexural testing layout and the flexure analysis conducted prior to the testing. This chapter also details the full-scale flexure test results and the comparison with the theoretical predictions. The details of the flexure analysis used for the prediction are elaborated. The comparison of the experimental capacity with the service and factored demand loads and the analytical predictions are also presented in this chapter.

Chapter 6 discusses the shear testing layout and shear capacity predictions conducted for the full-scale testing. This chapter presents the comparison between the experimental and analytical capacity of the girder specimens. The performance of the specimens under shear with and without transverse web reinforcement is also evaluated. This chapter additionally presents the results for monitoring interface shear slip of the composite section at the CC deck and UHPC girder interface. The details of the analysis and the processing of the experimental data is elaborated upon. A comparison of the experimental shear capacity of the girder specimens with the service and factored demand loads and the analytical predictions is also documented.

Chapter 7 discusses the transfer length, camber predictions, and experimental results. The difference in transfer length estimates between CC and UHPC and the comparison between the experimental results of transfer length and the estimates are discussed. This chapter also presents the camber readings of the three girder specimens over time. The prediction of camber using the incremental time-step method is described and compared to the measured results.

Chapter 8 presents the overall summary of the report and the major takeaways that were obtained from the experimental testing of the composite UHPC girders.

The appendix of this volume contains detailed drawings describing the designs for the full-scale testing.

Based on the experimental and theoretical comparison of the girder specimens, recommendations and examples are developed for design of UHPC precast, pretensioned bridge girders in the Volume 3 report.

2 LITERATURE REVIEW

2.1 INTRODUCTION

This chapter presents a comprehensive literature review of the structural design philosophy and behavior of UHPC structural components. The existing code-based provisions and recommendations for UHPC are documented and summarized. In addition, the latest developments for UHPC design provisions for codes and specifications and design guidelines recommended by various authorities recognized globally in the professional community are described. A brief overview of the full-scale testing conducted on UHPC structural elements and their key findings is also provided. Some of the key focus areas discussed in the following sections are as follows:

- Performance of large-scale structural components utilizing UHPC under short- and long-term loading
- Implementation of UHPC in bridge structures and the related challenges and opportunities
- Code requirements and design recommendations for UHPC at the national and international levels

2.2 STRUCTURAL BEHAVIOR

2.2.1 General

The superior mechanical properties and durability of UHPC when compared to normal strength concrete (NSC) and high-strength concrete make it a suitable candidate material for innovative solutions for the bridge industry. The advantages of UHPC motivate bridge engineers to develop this material to achieve design goals that are structurally stable, ingenious, and economically feasible. This incentive of harnessing UHPC to design slender bridges with longer spans, effectively saving the cost of intermediate supporting structures, has made the study of the structural behavior of UHPC crucial for bridge construction. The material properties of UHPC have been studied carefully, and the reports are corroborated with experimental data. These properties must be assessed in conjunction with the structural behavior of the elements to identify how the material properties may be suitably enhanced to result in maximum structural performance according to the application under consideration. This section discusses the structural behavior aspects of UHPC structures.

2.2.2 Structural Behavior of UHPC

2.2.2.1 Full-Scale Testing

The work done by Graybeal (2006b) was one of many significant early studies that included testing of full-scale UHPC bridge girders. Other research studies that investigated the behavior of full-scale UHPC girders include but are not limited to Graybeal (2009), Visage et al. (2012), Crane (2012), Zhang and Graybeal (2014), Yuan and Graybeal (2016), Manning et al. (2016), Visage et al. (2019), Alahmari et al. (2021), Tadros (2021), El-Helou and Graybeal (2022b), and El-Helou and Graybeal (2022a).

2.2.2.2 UHPC Bridge Girder Construction

The Wapello County Bridge was the first bridge application of UHPC in the United States (Sritharan 2015b). The use of UHPC increased the span of the bridge from 81 ft to 111 ft, with an approximately 6 percent shallower depth UHPC girder because of the higher prestressing force that could be utilized (increasing from 22 to 49 0.6 in. diameter strands). The use of the single span bridge instead of a two-span bridge saved the large expense for construction of the intermediate support and its components, including the foundation. In light of the advantages of UHPC, more implementation of UHPC structures will be beneficial. However, acceptance and implementation of UHPC for large scale structures is limited. Sritharan (2015a) noted that standards are needed for establishing similitude models for experimental testing because it is not possible to conduct full-scale testing of the elements on a frequent basis. Standardization and simulation models would provide more data to accelerate the implementation of UHPC for structural applications.

Giesler et al. (2018) tested rectangular UHPC beams with and without a 5.5 in. deck slab. The length of the beams was 16 ft. They observed that the high-performance concrete (HPC) decked UHPC beam is much stiffer and gave relatively comparable performance to the girder without the deck. There was a slight slip between the HPC deck and UHPC channel section. The rectangular beam (15 in. deep) modeled the stem of the channel section that was to be used in the construction of a bridge tested by Alahmari et al. (2021). The bridge compared one span of shallower UHPC with a deeper HPC section and tested under standard vehicle loads. Each span length was 25 ft. They found that the performance of the UHPC section was slightly better than the HPC response

despite being shallower in depth. The bridge will continue to be monitored for long-term load impact effects.

2.2.2.3 Section Modification

Schmidt and Teichmann (2007) noted that the enhanced behavior of UHPC may be successfully implemented by adopting more slender sections, thereby reducing the cost in terms of cubic volume of UHPC used, and noted that UHPC can be significantly more expensive than normal-strength or high-strength concrete. The advantage of the structural behavior of UHPC was demonstrated in the footbridge project in Germany—the Gärtnerplatz Bridge.

Sritharan (2015a) evaluated the structural aspects of UHPC bridge projects in the state of Iowa. He noted that geometric parameters such as the thickness of members, the cover to the steel reinforcement, and the number of reinforcement bars placed per unit area of the cross-section can be optimized to develop highly economical bridge designs because of the enhanced mechanical and durability properties of UHPC.

2.2.2.4 Embedded and Development Length Testing

Steinberg and Lubbers (2003) conducted a pullout test of 0.5 in. diameter strand at 270 ksi and reported that the embedded lengths were 12, 18, and 24 in. They also reported that the strands fractured before slipping could take place. They concluded that the development length of these strands was less than 12 in. Graybeal (2006b) reported a length development of less than 37 in. for prestressing strands of the same type. The rupture of strands preceding slippage was observed by Graybeal (2006b) as well.

2.2.3 Flexure Testing of UHPC Members

2.2.3.1 Bierwagen and Abu-Hawash (2005)

Bierwagen and Abu-Hawash (2005) tested a 71 ft prestressed concrete beam with pretensioned 0.6 in. diameter strands and a depth of 3.5 ft. A prestressed concrete girder with 30 ksi compressive strength was studied without any mild steel reinforcement to develop optimized designs for highway bridges. The researchers used a proprietary UHPC mixture for the fabrication of the girder. A 71 ft beam was tested to assess flexural capacity. A deflection of 3.25 in. was observed at 264 kips of applied load in a flexure test. They also found that the observed prestressing losses

were 27 percent higher than what was estimated by design. They did not observe any cracks resulting from the high prestressing force being imparted over a short distance due to a low transfer length after the release of strands.

2.2.3.2 Graybeal (2006b)

Graybeal (2006b) reported the results of the full-scale testing of the American Association of State Highway and Transportation Officials (AASHTO) Type II prestressed girders. The girders did not contain any mild steel reinforcement, and the secondary tensile actions due to shear, shrinkage, and thermal effects were borne by UHPC alone. A typical Ductal® mix of 28 ksi was used for this testing. Figure 2.1 shows the I-girder cross-section used for this study. The compressive failure observed from the full-scale testing was found to be analogous to that of a typical fiber-reinforced concrete section. The lateral expansion due to the tensile forces is the main mode of failure of the specimens when subjected to axial compression. Under the action of shear forces, the web was observed to crush in a brittle compressive failure. This may eventually lead to the tensile pullout failure of the fibers. The authors added that the fiber pullout concentration, after the peak load is reached, leads to the formation of wider cracks that may not be held together by the prestressing strands, and the element fails because of the rupture of the highly strained strands. They concluded that structural element failure may be dominated by the pullout of fiber if mild or prestressing reinforcement is not provided.

Tests conducted by Graybeal (2006b) for studying the prestressing losses in UHPC revealed that UHPC does not seem to be highly advantageous over the conventional prestressed concrete. However, the UHPC of high compressive strengths of up to 28 ksi under thermal treatment showed a reduction in elastic shortening due to lower shrinkage strains, lower creep strains, and a higher elastic modulus.

Graybeal (2006b) tested the flexural behavior of an 80 ft long UHPC girder specimen. The load versus deflection response is illustrated in Figure 2.2. The response was compared to the predicted response of the following theoretical cases: (a) a HPC girder with a compressive strength of 8 ksi (55 MPa) and a tensile strength of 0.67 ksi (4.6 MPa), and (b) two theoretical UHPC girders with 28 ksi (193 MPa) compressive strength (one with 1.25 ksi (8.6 MPa) tensile strength and the other with 2.9 ksi (20 MPa) tensile strength). The experimental performance of UHPC was vastly

superior to that of HPC. Notably, the tensile strength of the UHPC impacted the flexural performance. The presence of steel fibers made the response more ductile than the theoretical predictions that did not account for the presence of the steel fibers.

Figure 2.3 shows the uniaxial stress-strain model developed by Graybeal (2006b). This model was applied using the assumption that the plane sections remain plane before and after bending, and it follows the strain compatibility relationships. The results from the experiments and an analytically devised model for sectional analysis of the cross-section were considered when verifying the suitability of the stress-strain model to predict the girder response.

Graybeal (2006b) also studied the cracking behavior of the girders to develop a relationship between the crack spacing and the strain, which is given as follows:

$$w = \frac{1}{25}\left(a + \frac{b}{\varepsilon^{1.5}} + \frac{c \ln \varepsilon + d}{\varepsilon^2}\right) \quad (2.1)$$

where:

w = Crack spacing, in.

a = 2.87

b = 1.82×10^6

c = -5.7210^7

d = 3.66×10^8

ε = Strain, microstrain

The effective moment of inertia, I_{eff}, of the 80 ft girder was also studied, and the researchers developed relationships to find the effective moment of inertia at different locations between the bearing and the nearest actuator load. The flexural stiffness of the girder drops only after the cracking moment is exceeded. Researchers developed a relationship between the stiffness of the girder and the applied dead and live load moment based on iterative analysis to fit to the experimental data.

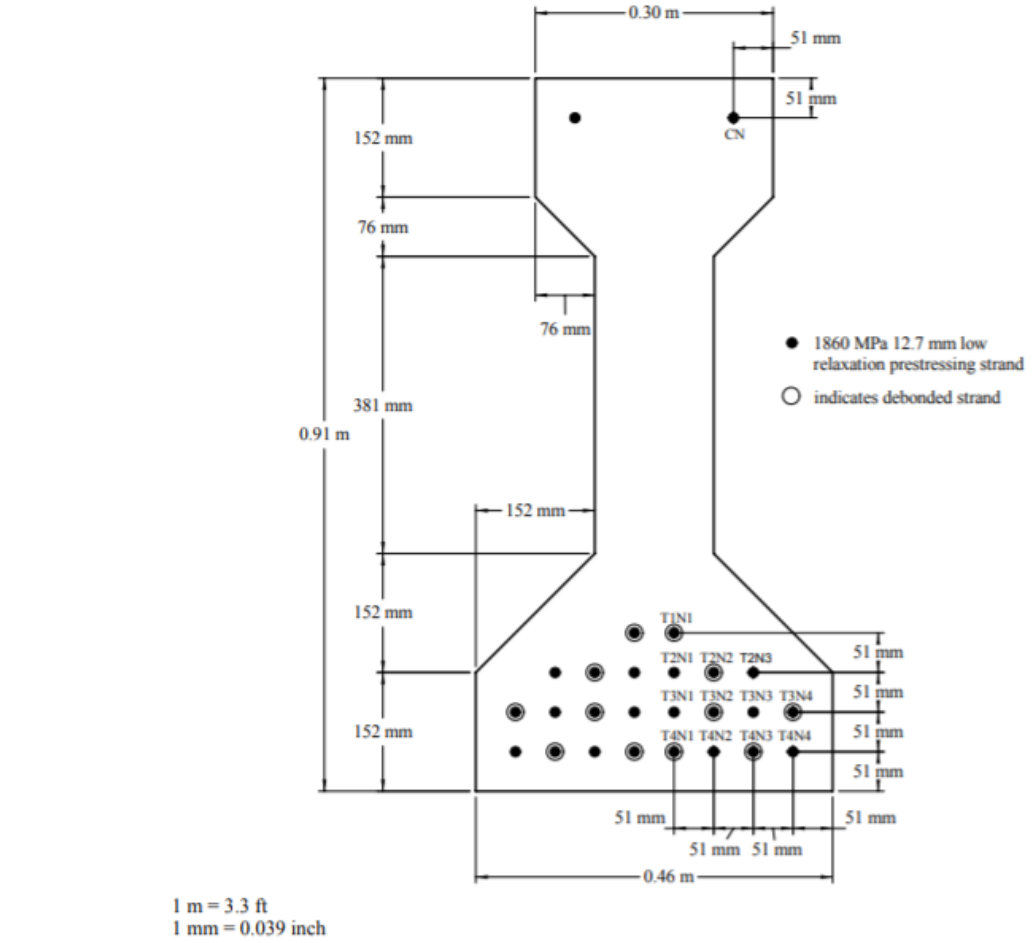

(a) Cross-section details of I-girder

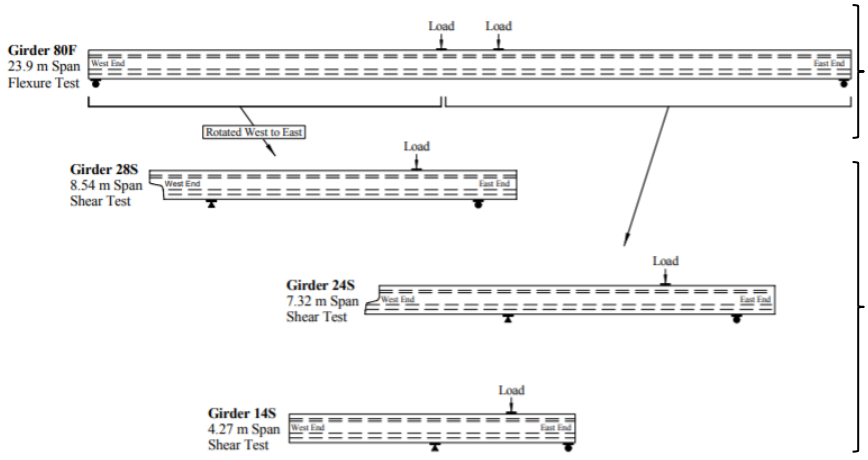

80 ft long girder for flexural testing (26 0.5 in. strands at 270 ksi).

28 ft, 24 ft, and 14 ft overall span of girders for shear testing with shear spans of 6.5 ft, 7.5 ft, and 6 ft, respectively.

(b) Elevation details of I-girders with loading arrangement

Figure 2.1. I-Girder Details Used by Graybeal (2006b).

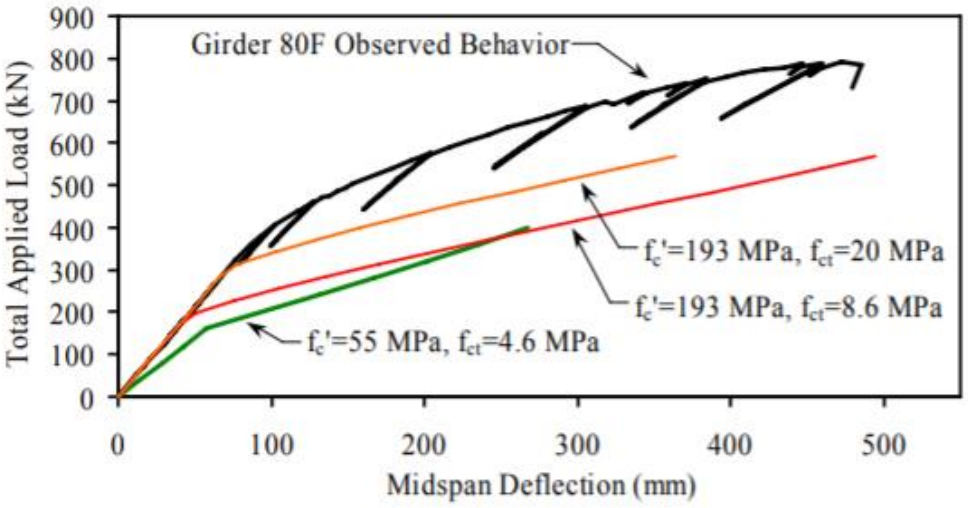

1 kN = 0.225 kip
1 MPa = 145 psi
1 mm = 0.039 inch

Figure 2.2. Comparison of Flexural Behavior of the Tested I-Girder (Graybeal 2006b).

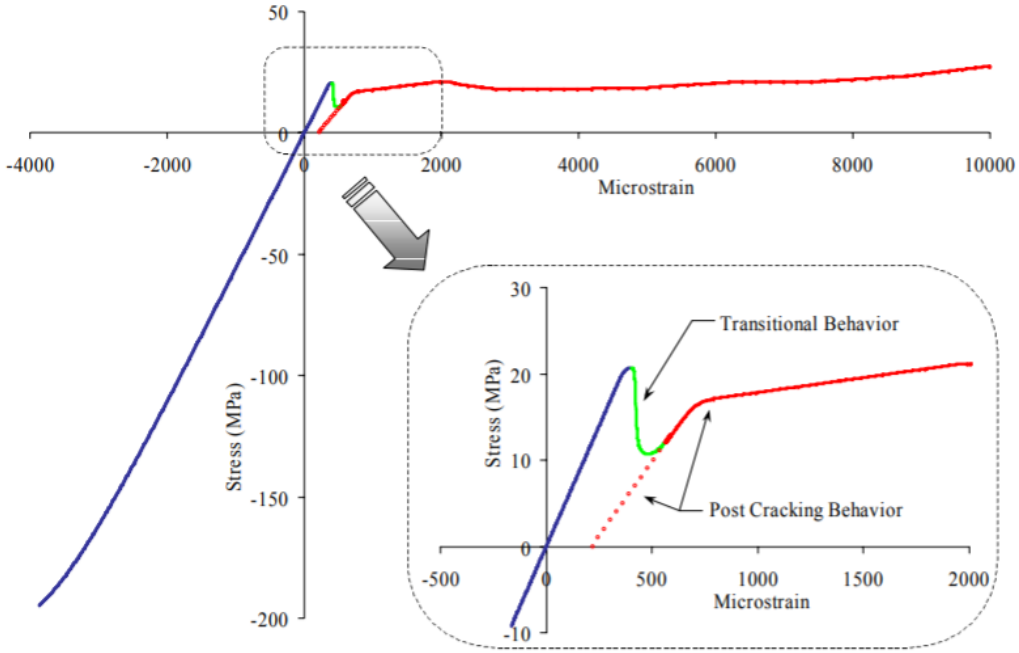

1 MPa = 145 psi

Figure 2.3. Uniaxial Stress-Strain Model (Graybeal 2006b).

2.2.3.3 Graybeal (2009)

Graybeal (2009) developed and tested a UHPC pi-girder, and that research led to experimental findings for predicting the behavior of the girder. The 70 ft long prototype girders were 33 in. deep and 96 in. wide. The average flexure strength observed from three flexure tests was slightly less than the AASHTO (2007) flexure capacity, whereas the shear capacity was 75 percent higher than the AASHTO (2007) capacity. The author reported that the deflection was also higher than the AASHTO (2007) limit.

2.2.3.4 Zhang and Graybeal (2014)

Figure 2.4 shows the cross-section of the girder and the stress-strain behavior predicted. The deck slab was of particular interest because the modified girder shape was designed to make the deck slab much shallower (4 in.). The slabs were proven to be safe in punching shear but were suspected to be affected by transverse bending (Zhang and Graybeal 2014). Therefore, the deck slab was analyzed under loading conditions defined by the AASHTO Load and Resistance Factor Design (LRFD) Bridge Design Specifications (AASHTO 2007), such that the contact area of each wheel load comprised two tires, with 20 in. perpendicular to the direction of the traffic and 10 in. parallel to the direction of traffic. The authors wanted to check the minimum achievable deck thickness for UHPC decks. For short-span bridges, such as the Jakway Park Bridge, the transverse bending may be the governing failure mode because stiffness is provided in the longitudinal direction due to the web and the bulbs of the pi-girder. Therefore, the authors used diaphragm spacing similar to the first second-generation Pi-girder bridge, Jakway Park Bridge, to run the analysis for transverse failure of the girder.

2.2.3.5 Visage et al. (2012)

Visage et al. (2012) studied the flexure behavior of UHPC beams by using moment-curvature results to understand the impact of varying the fiber content 0, 0.5, and 1.5 percent by volume for scaled experiments. Specimens were cured in ambient laboratory conditions for one day after the casting and then were demolded. A combination of steam curing and dry heat curing treatment was undertaken prior to testing. They tested 24 in. and 30 in. long beams with 6 × 6 in. cross-sections. They found that increasing the fiber content led to reduced width of cracks and better

stiffness at service conditions and higher load bearing capacity at ultimate conditions. The authors also reported that high fiber content restricted the rotation capacity due to localization of cracks.

2.2.3.6 Yoo and Yoon (2015)

Yoo and Yoon (2015) studied the impact of fibers on flexural behavior of UHPC members. The authors found that longer and twisted fibers were better for flexural performance in terms of deflection and bending than were short fibers, whereas the effect on compressive strength was negligible. Fibers, especially longer fibers dispersed nonhomogenously, showed lower first cracking load and deflection, while the post-cracking load capacity and stiffness were improved due to the bridging of cracks (showing strain hardening). Due to crack localization, ductility indices were lower for those samples with fibers. Use of K = 1.25 was recommended as the fiber orientation coefficient for the modeling of the behavior of ultra-high performance fiber-reinforced concrete (UHPFRC) with stirrups, in flexure.

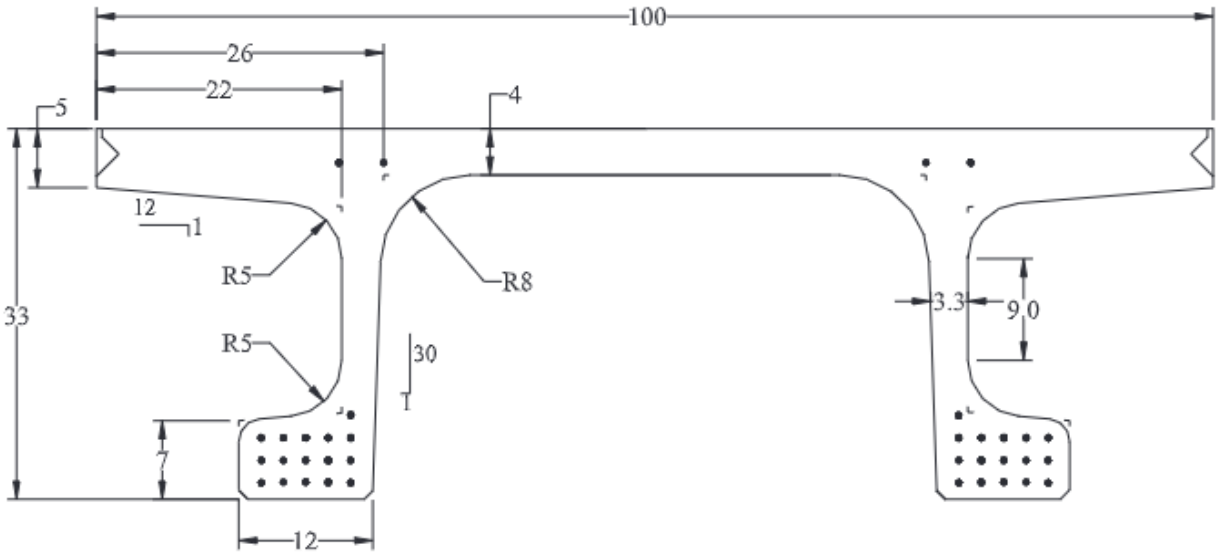

(a) Cross-section of Pi-girder (units are in in.)

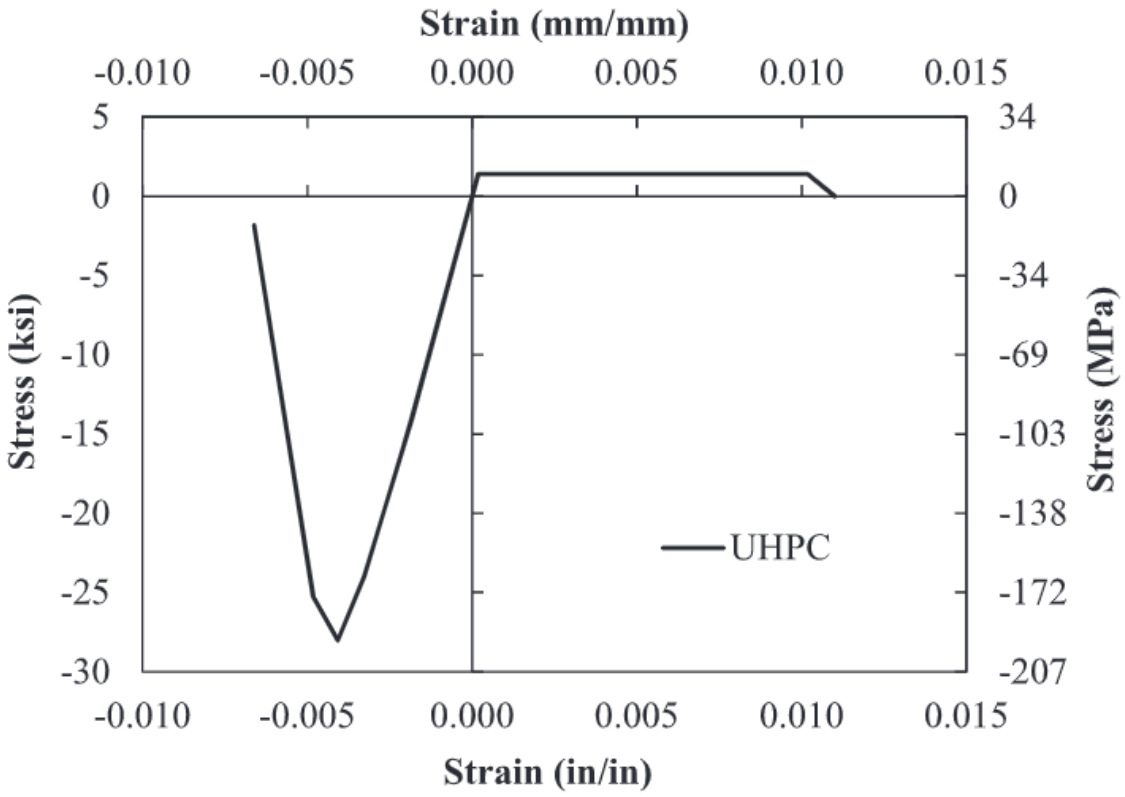

(b) Stress-strain response of girder UHPC used for FE model

Figure 2.4. Second Generation Pi-Girder (Zhang and Graybeal 2014).

2.2.3.7 Shao and Billington (2019)

Shao and Billington (2019) tested two small-scale steel reinforced UHPC beams of 6.6 ft span length to develop a design framework that utilizes the high compressive strength of UHPC by forcing failure through crushing of the concrete in compression rather than tensile failure by strain localization, which is the commonly reported failure mode of steel reinforced UHPC beams. The authors tested two beams of 6.6 ft length and varying streel reinforcement ratios, 0.96 and 2.10 percent, to induce tension-controlled and compression-controlled failures, respectively. They tested the beams in four-point bending tests. The authors recommended an idealized stress-strain distribution for computing the flexure capacity of beams in two failure models, namely failure after crack localization and failure by crushing of concrete with strain hardening of steel reinforcement, as shown in Figure 2.5. The authors reported that in the first mode, the compressive strain is fairly low (0.0014), while in the second mode, the compressive strength of UHPC is fully utilized, and the strain at failure is high (0.0065). The authors suggested that moment-curvature analysis or finite element analysis will be more accurate than manual computations in analyzing the flexure behavior.

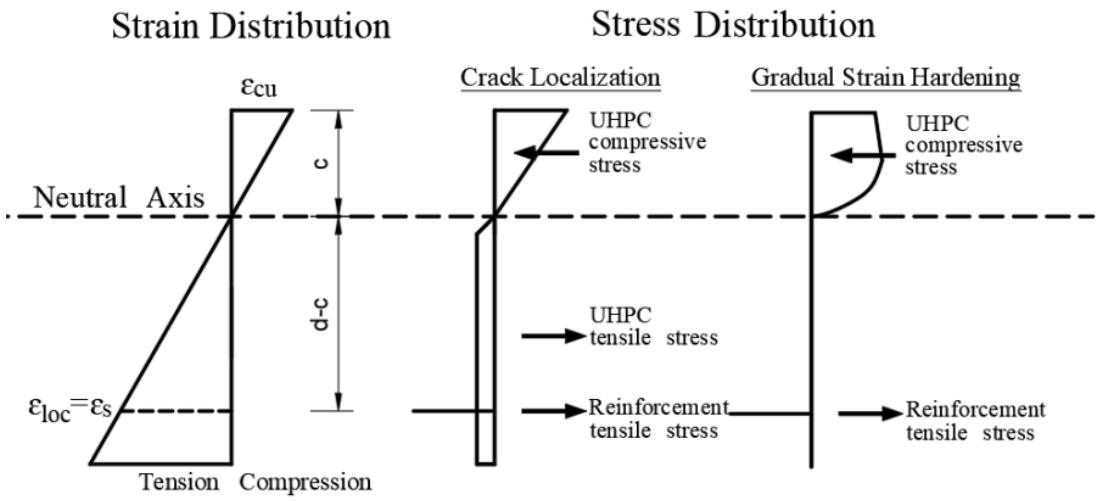

Figure 2.5. Assumed Stress-Strain Distribution for Flexure Capacity Computation (Shao and Billington 2019).

2.2.3.8 El-Helou and Graybeal (2022a)

El-Helou and Graybeal (2022a) developed design recommendations for UHPC girders under flexure based on experimental testing of full-scale prestressed UHPC girders. They tested a 62 ft long girder with 26 strands of 0.7 in. diameter. The authors assessed the reliability of the design

framework by applying it to other applicable experimental data that was available. Figure 2.6 presents the relationships proposed by El-Helou and Graybeal (2022a). The flexural design was based on linear strain distribution and stress-strain models developed for UHPC behavior. The compression model proposed was elastic-perfectly plastic and governed by the compressive strength and strain at that strength and the modulus of elasticity (MOE). The tensile model was approximated by an elastic-perfectly plastic (bilinear) model that is governed by either the stress at cracking or stress and strain at crack localization. The UHPC flexure design is largely dependent on the material properties of the mix. The strain limit at the rupture of the steel reinforcement also impacts the flexural design of a UHPC member. The authors proposed these stress-strain relationships in the UHPC AASHTO draft specifications (El-Helou and Graybeal 2022a; FHWA 2022).

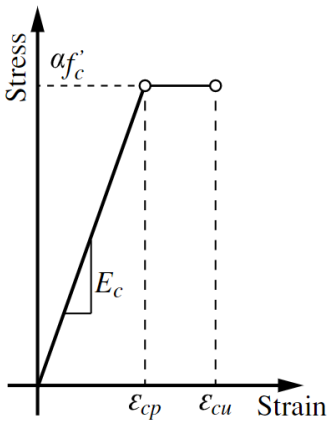

(a) Uniaxial Compression

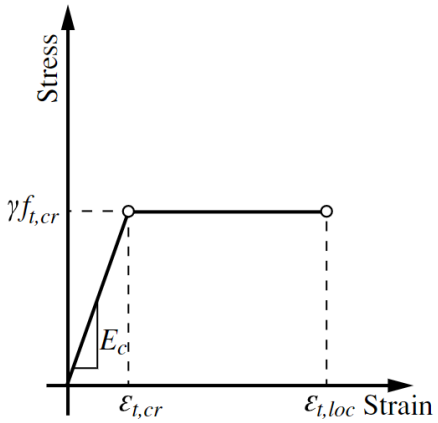

(b) Uniaxial Tension with Stress Plateau after Cracking

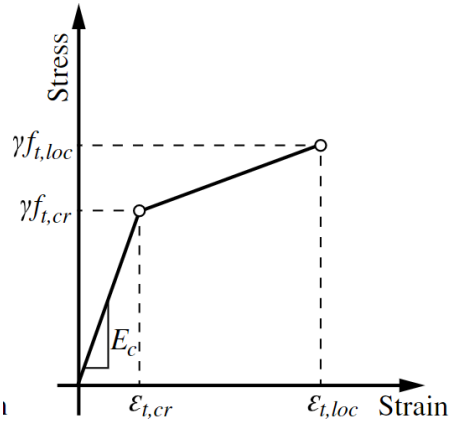

(c) Uniaxial Tension with Strain Hardening after Cracking

Figure 2.6. Idealized Stress-Strain Curves under Compression and Tension (FHWA 2022).

2.2.4 Shear Testing of UHPC Members

2.2.4.1 Cauberg et al. (2012)

Cauberg et al. (2012) tested the shear capacity of small-scale UHPC beams. The authors used 7.5 ft long beams with 6 × 10 in. cross-sections for studying behavior under shear failure for different conditions. The details of the three specimens are as follows: (a) Beam 1 contained the lowest cement content and large-sized aggregate, (b) Beam 2 was reactive powder concrete, and (c) Beam 3 had no coarse aggregate.

The ratio of the distance of the shearing force from the support at the nearest edge *a* to the effective depth of the beam *d* was denoted as the *a*/*d* ratio. The prominent failure modes for *a*/*d* = 3 are as follows:

1. A shear failure occurred for all three beams with no fibers or stirrups and for all three beams with a combination of 0.24 in. and 1.2 in. long fibers (up to 2 percent by volume).
2. A shear compression failure occurred for all three beams with stirrups alone (no fiber reinforcement).
3. A shear compression failure occurred for Beams 1 and 3 with fibers of length 0.24 in. and 1.2 in. (0.5 percent by volume), and shear failure occurred for Beam 2.
4. A shear compression failure occurred for Beam 1 with fibers of length 0.24 in. (2 percent), and flexural failure occurred for the other two beams.

The major conclusions of this study include the following: (a) the shear capacity of UHPC beams with fibers was higher than the CEB FIP Model Code (*fib* 2013) prediction; (b) for UHPC with fibers, transverse steel reinforcement may be eliminated if further study confirms this conclusion; and (c) UHPC without fibers shows lower shear resistance.

2.2.4.2 Crane (2012)

Crane (2012) tested full-scale UHPC girders subject to shear. A total of six shear tests were conducted on 32 in. deep precast prestressed UHPC girders (bulb-tee shaped) with HPC deck slabs. The first specimen was tested without the CIP slab because an interface failure occurred during a prior flexure test of the specimen. All other specimens were tested with a composite deck slab. The specimens with a deck had a shear span of 8 ft, while the first specimen had a shear span of

6 ft. The reinforcement ratio varied from 0 percent, to 0.41 percent, to 0.83 percent. Three specimens had a fluted interface surface, while the remaining two had a smooth interface surface. The authors compared the experimental shear capacity based on Mohr's circle approach using the direct tension strength measured from companion specimens and based on modified compression field theory by Bentz et al. (2006), with an additional strength component for the fiber contribution. The fiber contribution was based on AFGC/SETRA (2002), and the concrete contribution was based on recommendations for HPC in AASHTO (2010). The author reported that Mohr's circle approach is conservative, and the code-based modifications resulted in predictions that were 15 percent below the experimental shear capacity of the girder.

The author also investigated the interface shear capacity of these UHPC/HPC full-scale members. The interface surface differed for each interface shear test along the length of the girder. The parameters they considered were smooth surface (leaving the UHPC surface untreated), fluted surface (developed by form liners), partial interface reinforcement, and no interface reinforcement. The interface shear failure was identified at a jump in the shear-interface slip response or a drop in the slope of the load-deflection response. The AASHTO (2010) estimate of interface shear capacity was unconservative for smooth interface surfaces, while the American Concrete Institute (ACI) ACI 318-08 (2008) estimate with a friction coefficient of μ = 0.6 gave a conservative estimate for smooth surfaces. However, for practical design purposes, smooth surfaces for composite sections were not recommended. The code-based recommendations were found to be more suited for fluted interface surfaces and are on the conservative side. The authors reported that the equations recommended by Patnaik (1994) showed the highest agreement with the experimental results, although they were somewhat on the conservative side.

2.2.4.3 Baby et al. (2014b)

Baby et al. (2014b) also tested the shear resistance of UHPFRC I (prestressed/passive steel bars) girders. They tested I-beams of 15 in. depth and span length of 7 ft. The authors corroborated that it is important to account for the fiber orientation for the flexural and shear behavior originally suggested by AFGC/SETRA (2002). They reported that an increase of 2.5 percent of steel fibers resulted in close to a 250 percent jump in shear capacity. Testing was done with and without fiber reinforcement and stirrups for comparison. They found that the localization of shear cracks occurs after the yielding of the stirrups. Bridging of cracks due to fibers and impact of stirrups is

significant only when the yield strain of stirrups is much lower than the tensile strain capacity of the UHPFRC.

2.2.4.4 El-Helou and Graybeal (2022b)

As noted in Section 2.2.3.8, El-Helou and Graybeal (2022b) conducted shear testing of six full-scale pretensioned bridge girders made with two different proprietary UHPCs. The geometry of the girders was a modified bulb-tee, and the aim of the research was to develop the correlation between the material-level tensile strength of UHPC and the shear capacity provided by the structural members fabricated from the corresponding mix. The authors highlighted the higher shear capacity of UHPC due to the high tension-hardening behavior and post-cracking characteristics. Four 35 in. deep and two 43 in. deep girders had 26 straight prestressing strands (24 in the bottom bulb and two in the top bulb), while one 35 in. tall specimen had 20 prestressing strands, with 18 at the bottom and 2 at the top, respectively. Only one 43 in. tall girder was reinforced with transverse shear reinforcement of single-legged No. 5 bar. The prestressing strands used were low relaxation and 0.7 in. diameter. These designs included eccentric tendon layout. The steel fibers used in the mix were 0.008 in. diameter by 0.5 in. long fibers and 2 percent by volume. The authors correlated the shear capacity of the girder with the first cracking strength, which is defined as the intersection of a line with the slope of tensile MOE, offset at 0.02 percent strain, with the stress-strain curve obtained by AASHTO T 397 Draft (AASHTO 2022). The performance of the girders without transverse reinforcement was similar to the performance of the one with web reinforcement until the crack localization and shear failure. The shear capacity of the girder with transverse reinforcement had a much higher shear capacity due to the enhanced crack bridging property of the matrix. The authors reported that the shear capacity largely depends on the tensile characteristics of the mix and is not that sensitive to other parameters such as web thickness, girder depth, and number and diameter of pressing strands. Assuming that shear stress is constant within the shear depth, the principal tensile stress at ultimate failure is greater than or equal to the crack localization stress observed in a material-level direct tension test.

2.2.5 Additional Testing of UHPC Members

Several other research projects have been devoted to studying the structural behavior of UHPC elements. Table 2.1 summarizes the finding of some of these research initiatives.

Table 2.1. Summary of Research Findings for UHPC Structural Elements.

Source	Testing Focus	Findings
Fehling et al. (2008)	UHPC panels under biaxial loading	• First, the tensile loads were applied along one direction, then the compressive loads were applied in the other direction • The panels were 14 in. in the compressive direction, 20 in. and 39 in. in the tensile direction, and 3 in. thick • 0.314 in. diameter steel reinforcement bars were arranged orthogonally in two layers • Parameters such as the aggregate size, crack spacing, and the width of crack contribute to the decrease in compressive strength • The point of yielding of the reinforcement does not affect the behavior. The behavior is similar to that of NSC panels under biaxial compression
Empelmann and Oettel (2012)	UHPFRC box girders evaluated to study the torsional response	• Girder performance under torsional cracking was improved with the addition of steel fibers by 1.5 to 2.5% by volume • Higher torque at ultimate and cracking conditions, with better torsional stiffness for 2.5% fiber volume • Diagonal cracks at approximately 45 degrees during the experimental testing for all the different fiber contents
Crane and Kahn (2012)	Interface shear capacity	• The composite action of the UHPC (stem) and HPC (deck) T-beams was tested • The authors compared AASHTO (2010) and ACI 318-08 (2008) recommendations for interface shear resistance between the precast UHPC web and HPC deck • The authors varied the surface condition of the UHPC-HPC interface and the transverse reinforcement • 5 beams of 9.5 ft length were tested • The code requirements were found to be conservative for fluted interface surface and unconservative for smooth surface • The authors recommended a fluted surface for composite action despite having interface steel reinforcement

Table 2.1. Summary of Research Findings for UHPC Structural Elements (continued).

Source	Testing Focus	Findings
Yang et al. (2013)	Torsional behavior of UHPFRC beams with mild steel reinforcement	• Findings of Empelmann and Oettel (2012) were corroborated, except the diagonal cracks were observed to be affected by the longitudinal reinforcement and the number of shear reinforcement stirrups • The angle of those cracks ranged between 27 to 53 degrees
Astarlioglu and Krauthammer (2014)	Comparison between NSC and UHPFRC columns under blast loading (nonlinear behavior)	• NSC and UHPFRC columns of the same dimensions and reinforcement were numerically modeled • NSC column design did not account for blast loading. • UHPFRC is better than NSC for the columns under impulsive loading, with a resistance of up to four times the impulse load that causes failure in NSC columns • Approximately 30% reduction in displacement at peak loading conditions for UHPFRC columns
Yoo et al. (2014)	Bond behavior of embedded deformed steel bars	• 6 in. cubes with one bar vertically embedded axially were tested as per Rilem (1994) recommendations • Bond strength was not affected significantly by the fiber content or the embedment length • However, a relationship between the compressive strength and bond existed • Parameters for predicting the bond strength of steel bar by the Model Code (1993) was too conservative because it was not based on latest UHPC data • More accurate parameters were proposed based on current research data

2.3 CURRENT DESIGN GUIDELINES

2.3.1 General

Several countries, such as France, Australia, Germany, Japan, Switzerland, and South Korea, have developed design guidelines for UHPC structural elements. The Association Française de Génie Civil/French Civil Engineering Association (AFGC) published the first UHPC design guidelines in 2002 (AFGC/SETRA 2002). The Japan Society of Civil Engineers (JSCE) also published their design recommendations for UHPC based on the proprietary Ductal UHPC in 2004 (JSCE 2004). AFGC revised their design recommendations in 2013 to reflect experience and research results for 10 years after publishing their first version, and the revised version is the basis for the Association Française de Normalization NF-P-18-710 (2016) *National Addition to Eurocode 2—Design of*

Concrete Structures: Specific Rules for Ultra-High Performance Fibre-Reinforced Concrete (UHPFRC). NF-P-18-710 (2016) is the first standard for structural design of UHPC in the world, and it is organized to be a part of EN 1992 Eurocode 2 (2004) based on AFGC (2013). Because AFGC (2013) has been most widely used in the design of UHPC structures, the design method according to AFGC (2013) is discussed in the following subsection. In cases in which a difference exists between AFGC (2013) and NF-P-18-710 (2016), it has been noted. In the second subsection, JSCE's recommendations for UHPC (JSCE 2004) are introduced briefly and compared to AFGC (2013). In the last subsection, the design methods used for the UHPC bridges built in the United States are discussed.

2.3.2 AFGC Recommendations (2013)

2.3.2.1 AFGC Material Models

Gunes et al. (2012) indicated that UHPC exhibits high compressive strength and tensile strength because of the combination of a high-strength matrix and high-strength steel fibers. Especially, steel fibers carry tension after the occurrence of cracking, thus leading to the ductile behavior of UHPC. Therefore, a mechanical model of UHPC must represent these characteristics (Gunes et al. 2012). AFGC (2013) employs parameters such as fiber orientation factors and characteristic length to consider the behavior of UHPC and to craft those characteristics into constitutive laws of compression and tension.

AFGC (2013) classifies UHPC into three types based on tensile behavior: Type 1 is strain softening, Type 2 is low strain hardening, and Type 3 is high strain hardening. Types 1, 2, and 3 correspond to T1, T2, and T3, respectively, in NF-P-18-710 (2016). Because the tensile constitutive law of Type 3 is close to elastic-plastic behavior, most UHPC materials are classified into Type 1 and 2. Thus, structural design methods in this document focus on Type 1 and 2 only. In addition, all formulas in AFGC (2013) use SI units.

Although every design value should be obtained through material tests because design values such as elastic modulus or tensile strength cannot be reliably deduced from compressive strength, unlike NSC, AFGC (2013) suggests the preliminary design values shown in Table 2.2.

Table 2.2. Recommended Preliminary Design Values (AFGC 2013).

Parameter	Value
Compressive strength at 28 days, f_{ck}	150 MPa (21.7 ksi)
Ultimate compressive strain, ε_{cud}	0.0027
Elastic modulus, E_{cm}	50 GPa (7250 ksi)
Post-cracking tensile strength, f_{ctfk}	9 MPa (1.3 ksi)
Elastic tensile strength, $f_{ctfk,el}$	9 MPa (1.3 ksi)
Ultimate tensile strain, ε_{lim}	0.0025
Creep coefficient, φ	0.8
Fiber orientation factor, global, K_{global}	1.25
Fiber orientation factor, local, K_{local}	1.75

2.3.2.1.1 Fiber Orientation Factor, K

The tensile strength of UHPC can be obtained through a direct tensile test or flexural test, as suggested by AFGC (2013). Generally, the tensile strength values obtained from the material tests tend to overestimate the strength in larger structural components due to the fiber orientation of test specimens adjusting to the size of the smaller specimens that promote the preferred fiber orientation for tensile or flexural capacity where fibers near the surface tend to align in the longitudinal direction, which is called the edge effect. However, in reality, the orientation and dispersion of fibers in large elements are not aligned like the specimens for the flexural or tensile tests in the laboratory. To consider this different condition, *fib* (2013) published by Fédération internationale du béton, *fib* introduced a fiber orientation factor *K*, and AFGC (2013) adopted this concept and specified fiber orientation factors K_{global} and K_{local} (Resplendino 2014). In addition, NF-P-18-470 (2016) and Annex 6 in AFGC (2013) provided the testing method to obtain the *K* factors. Based on the recommended testing, the global fiber orientation factor K_{global} is the ratio of the mean of the peak of the stress-crack width (*f*-*w*) curves obtained with the specimens cast during the material testing to the mean of the peak of the *f*-*w* curves obtained with the sawn specimens. K_{local} is the ratio of the mean of the peak of the *f*-*w* curves obtained with the specimens cast during the material testing to the lowest value of the *f*-*w* curves obtained with the sawn specimens. *K* factors are only applied to the post-cracking regime of tensile constitutive law as shown in Figure 2.7. AFGC (2013) suggested 1.25 and 1.75 for K_{global} and K_{local}, respectively.

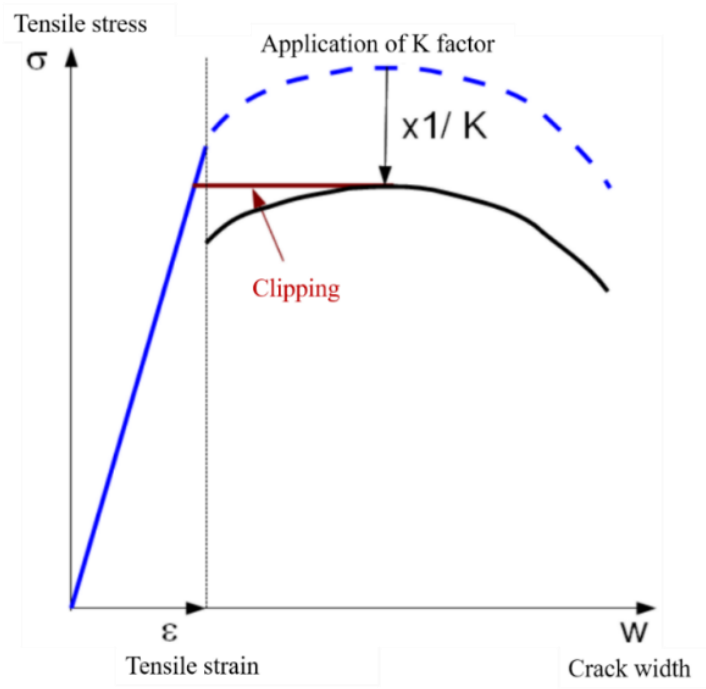

Figure 2.7. *K* Factor Application (AFGC 2013).

2.3.2.1.2 Partial Safety Factor

AFGC (2013) provided a partial safety factor γ_{cf} for fiber-reinforced concrete in tension, shown in Table 2.3, and additional partial safety factors are based on EN 1992 Eurocode 2 (2004) or NF-P-18-710 (2016). The partial safety factors are used for strength reduction, and their values depend on the design situation.

Table 2.3. Partial Safety Factors (NF-P-18-710 2016).

Design Situation	Compressive	Tension		
	Concrete	Reinforcing steel	Prestressing steel	Fiber
	γ_c	γ_s	γ_s	γ_{cf}
Persistent & Transient	1.5	1.15	1.15	1.3
Accidental	1.2	1.0	1.0	1.05

2.3.2.1.3 Characteristic Length

The characteristic length l_c is a factor to convert stress-crack width to stress-strain. Equation (2.2) and (2.3) are used for the conversion. Note that this process is used to develop the constitutive law for tension.

$$\varepsilon = \frac{f_{ct,el}}{E_{cm}} + \frac{w}{l_c} \tag{2.2}$$

$$l_c = \frac{2}{3}\, h \tag{2.3}$$

where:

ε	=	Tensile strain
$f_{ct,el}$	=	Elastic tensile stress, MPa
E_{cm}	=	Elastic modulus, MPa
w	=	Crack width, mm
l_c	=	Characteristic length, mm
h	=	Depth of section, mm

2.3.2.1.4 Constitutive Law in Compression

AFGC (2013) suggested the constitutive laws in compression for the service limit state (SLS) and ultimate limit state (ULS) shown in Figure 2.8. To draw an appropriate compressive constitutive law, f_{ck}, f_{cd}, and E_{cm} should be obtained from the material tests, and the other specific values in the compressive constitutive law can be calculated using Equations (2.4), (2.5), (2.6), and (2.7).

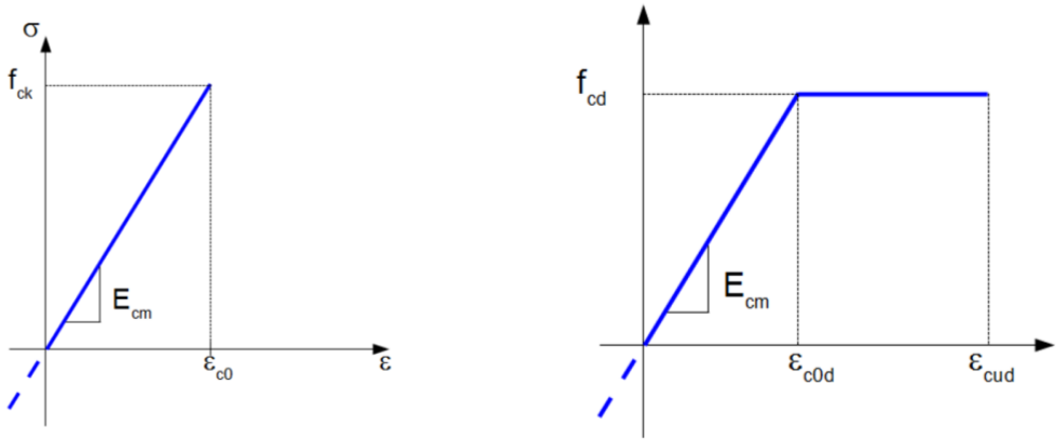

(a) SLS Constitutive Law *(b) ULS Constitutive Law*

Figure 2.8. Constitutive Laws in Compression (AFGC 2013).

$$\varepsilon_{c0} = \frac{f_{ck}}{E_{cm}} \tag{2.4}$$

$$f_{cd} = \frac{\alpha_{cc} f_{ck}}{\gamma_c} \tag{2.5}$$

$$\varepsilon_{c0d} = \frac{f_{cd}}{E_{cm}} \tag{2.6}$$

$$\varepsilon_{cud} = \left[1 + 14\left(\frac{f_{ctfm}}{f_{cm}}\right)\right] \varepsilon_{c0d} \tag{2.7}$$

where:

ε_{co} = Maximum elastic strain in compression for SLS

f_{ck} = Characteristic compressive strength for SLS, MPa

f_{cd} = Design value of compressive strength for ULS, MPa

α_{cc} = Long-term effect coefficient, 0.85

γ_c = Partial safety factor for concrete, 1.5

ε_{cod} = Design elastic strain in compression

ε_{cud} = Design ultimate compressive strain

f_{ctfm} = Maximum mean post-cracking tensile stress, MPa

f_{cm} = Maximum mean stress in compression, MPa

Although AFGC (2013) does not use global fiber orientation factor K_{global} for the ultimate compressive strain in Equation (2.7), NF-P-18-710 (2016) does use K_{global}, as shown in Equation (2.8).

$$\varepsilon_{cud} = \left[1 + 14\left(\frac{f_{ctfm}}{K_{global}\, f_{cm}}\right)\right] \varepsilon_{c0d} \tag{2.8}$$

2.3.2.1.5 Constitutive Law in Tension

The material tests for pre-cracking (elastic) strength, post-cracking strength, and fiber orientation factor are conducted to determine the constitutive laws in tension for SLS and ULS. AFGC (2013) suggested (1) a four-point bending test with an unnotched prism or a direct tensile test for pre-cracking (elastic) strength and fiber orientation factor, and (2) a three-point bending test with notched prism to obtain moment-crack width relationship or a direct tensile test for post-cracking

behavior. Parameters ε_{lim} and $\varepsilon_{u,lim}$ are also obtained from the material testing but are limited to a maximum value of 0.0025. AFGC (2013) provided the tensile constitutive law shown in Figure 2.9 and the equations for required values to develop this law.

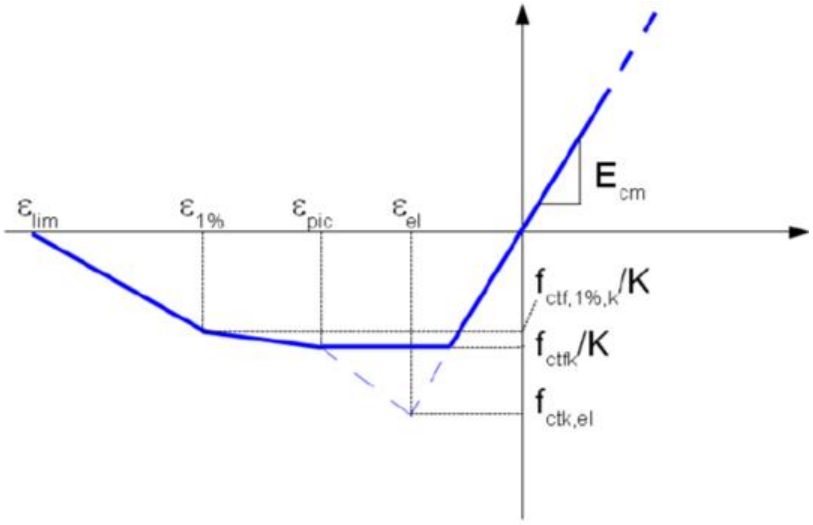

(a) SLS Constitutive Law

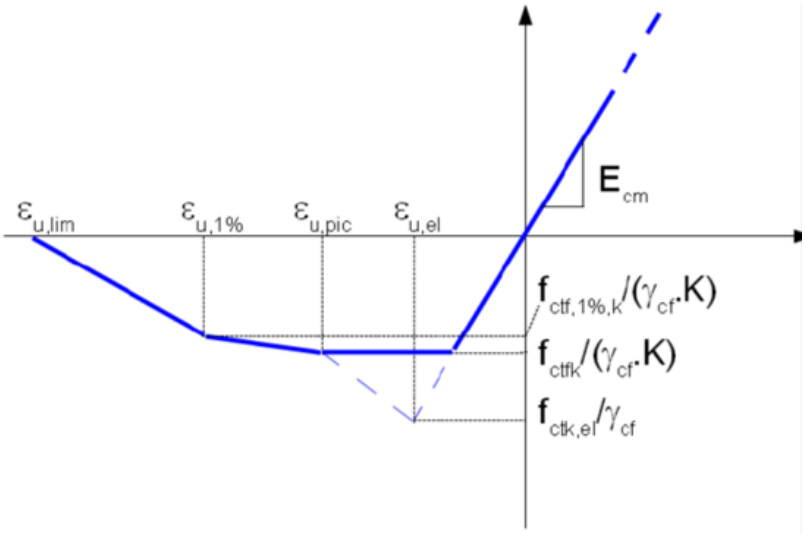

(b) ULS Constitutive Law

Figure 2.9. Constitutive Law in Tension (AFGC 2013).

$$\varepsilon_{peak} = \frac{w_{peak}}{l_c} + \frac{f_{ctk,el}}{E_{c,eff}} \text{ at SLS} \quad (2.9)$$

$$\varepsilon_{u,peak} = \frac{w_{peak}}{l_c} + \frac{f_{ctk,el}}{\gamma_{cf}\, E_{c,eff}} \text{ at ULS} \quad (2.10)$$

$$\varepsilon_{u,1\%} = \frac{w_{1\%}}{l_c} + \frac{f_{ctk,el}}{\gamma_{cf}\, E_{c,eff}} \text{ at ULS} \quad (2.11)$$

$$\varepsilon_{u,lim} = \varepsilon_{lim} = \frac{l_f}{4l_c} \quad (2.12)$$

where:

ε_{peak} = Strain corresponding to post-cracking strength

$\varepsilon_{u,peak}$ = Strain corresponding to ultimate post-cracking strength

ε_{el} = Elastic tensile strain at SLS

$\varepsilon_{u,el}$ = Elastic tensile strain at ULS

w_{peak} = Crack opening corresponding to the local peak, or 0.3 mm if there is no peak, mm

l_c = Characteristic length, $\frac{2}{3}h$, mm

$f_{ctk,el}$ = Characteristic elastic tensile strength, MPa

$E_{c,eff}$ = Effective elastic modulus, MPa

γ_{cf} = Partial safety factor for fibers, 1.3

$\varepsilon_{1\%}$ = Strain corresponding to crack width of $0.01h$

$\varepsilon_{u,1\%}$ = Ultimate strain corresponding to crack width of $0.01h$

$w_{1\%}$ = Crack opening corresponding to 0.01 h, mm

h = Height of the beam tested under flexure corresponding to the thickness of the structure, mm

ε_{lim} = Ultimate tensile strain at SLS

$\varepsilon_{u,lim}$ = Ultimate tensile strain at ULS

l_f = Fiber length, mm

For Equations (2.11) and (2.12), the maximum allowable crack opening is the minimum value between $w_{1\%}$ and $\frac{l_f}{4}$. In Equations (2.11) and (2.12), the maximum allowable crack opening is

divided by the characteristic length l_c to transform the crack opening to the strain corresponding to the maximum admissible post-cracking strength. This strain plus the reduced elastic strain in Equation (2.11) is the total allowable ultimate tensile strain. Because AFGC (2013) allows crack openings between 0.002 in. and 0.012 in. for SLS depending on the member and exposure class, Equation (2.9) contains a cracked portion. The specific allowable crack width for SLS can be found in Table 7.201 in NF-P-18-710 (2016).

2.3.2.1.6 Minimum Ductility Condition

Minimum ductility condition is called a non-brittleness condition (NF-P-18-710 2016). This condition, expressed in Equation (2.13), ensures sufficient ductility in bending.

$$\frac{1}{w_{lim}} \int_0^{w_{lim}} \frac{\sigma(w)}{K_{global}} \mathrm{d}w \geq \max(0.4 f_{ctm,el}, 3\ \mathrm{MPa}) \tag{2.13}$$

where:

w_{lim} = Maximum allowable crack opening, 0.3 mm

$\sigma(w)$ = Characteristic post-cracking stress, MPa

$f_{ctm,el}$ = Mean elastic limit stress in tension, MPa

2.3.2.2 AFGC Flexural Design

Major structural design specifications for NSC employ a rectangular compressive stress distribution and disregard the tensile strength when determining the design flexural capacity of a section. This simplified method provides a good estimate for the behavior of conventional reinforced concrete at ultimate conditions; thus, it is widely utilized in design codes, including AASHTO (2020) and ACI 318-19 (2019). However, Weldon et al. (2010) noted that this method cannot be applied to the design of UHPC members because a rectangular compressive stress distribution is not valid for UHPC since it is closer to a triangular shape. In addition, the post-cracking tensile capacity of UHPC reflects the crack bridging effect of steel fibers, while the design of CC assumes that the concrete cannot carry tensile force after cracking. Therefore, the design criteria of UHPC must be based on crack opening criteria, while the basis of NSC is a maximum material strength criteria (Gunes et al. 2012).

Even though AFGC (2013) does not provide a formula (such as one for an equivalent stress block), for flexural design, the flexural strength can be calculated by sectional analysis, as shown in Figure 2.10, using compressive and tensile constitutive laws, maximum allowable crack opening criteria for tensile strain at SLS and ULS, and maximum compressive strain (Yoo and Yoon 2016).

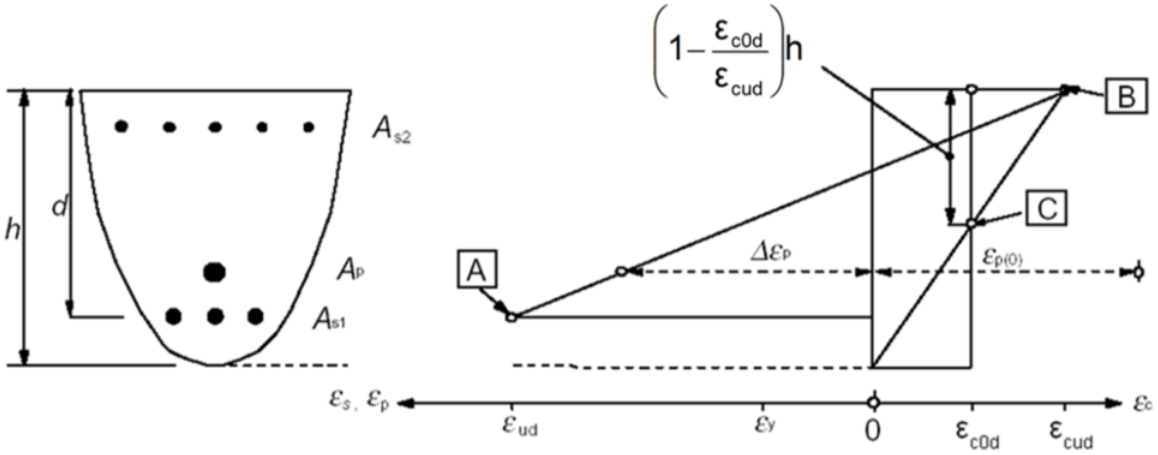

A: Reinforcing steel tension strain limit
B: UHPC compression strain limit
C: UHPC pure compression strain limit

Figure 2.10. Stress-Strain Distribution in Cross-Section (NF-P-18-710 2016).

The maximum compressive strain can be calculated using Equation (2.7). The maximum tensile strain at the ULS can be computed using Equations (2.11) and (2.12) with the maximum allowable crack opening. The maximum tensile strain at the SLS is calculated using Equation (2.9), with the allowable crack opening for w_{peak} based on Table 7.201 in NF-P-18-710 (2016).

2.3.2.3 AFGC Shear Design

Although the ultimate shear resistance of CC consists of concrete and reinforcing steel contributions, according to AFGC (2013), the ultimate shear resistance of UHPC V_{Rd} considers the additional contribution due to steel fibers, as shown in Equation (2.14).

$$V_{Rd} = V_{Rd,c} + V_{Rd,s} + V_{Rd,f} \tag{2.14}$$

where:

$V_{Rd,c}$ = UHPC contribution term, kN

$V_{Rd,s}$ = Reinforcement contribution term, kN

$V_{Rd,f}$ = Fiber contribution term, kN

AFGC (2013) specified three cases for calculating the concrete contribution $V_{Rd,c}$: (1) reinforced sections, (2) prestressed sections, and (3) non-prestressed and non-reinforced sections, as shown in Equations (2.15), (2.16), and (2.17), respectively.

$$V_{Rd,c} = \frac{0.21}{\gamma_{cf}\gamma_E} k\sqrt{f_{ck}} b_w d \tag{2.15}$$

$$V_{Rd,c} = \frac{0.24}{\gamma_{cf}\gamma_E} k\sqrt{f_{ck}} b_w z \tag{2.16}$$

$$V_{Rd,c} = \frac{0.18}{\gamma_{cf}\gamma_E} k\sqrt{f_{ck}} b_w h \tag{2.17}$$

$$k = 1 + 3(\sigma_{cp}/f_{ck}) \tag{2.18}$$

$$\sigma_{cp} = N_{Ed}/A_c \tag{2.19}$$

where:

- γ_E = Safety factor related to uncertainty, $\gamma_{cf}\gamma_E$ =1.5
- b_w = Smallest width of the cross-section in tensile area, mm
- d = Distance between the extreme compressed fiber and the longitudinal reinforcement, mm
- z = Lever arm of the internal forces for a member of constant height corresponding to the bending moment in the member considered, mm (approximate value of $z = 0.9d$)
- h = Height of the cross-section, mm
- N_{Ed} = Axial force in the cross-section due to the external loads, kN
- A_c = Gross cross-sectional area of the UHPC, mm^2

The term $V_{Rd,s}$ is the contribution of the shear reinforcement, such as stirrups. The shear capacity provided by the vertical shear reinforcement is found using Equation (2.20):

$$V_{Rd,s} = \frac{A_{sw}}{s} z f_{ywd} \cot\theta \quad (2.20)$$

where:

A_{sw} = Cross-sectional area of shear reinforcement, mm^2

s = Spacing of the stirrups, mm

f_{ywd} = Yield strength of the shear reinforcement, MPa

θ = Angle between the principal compression stress and the beam axis, a minimum value of 30 degrees is recommended, degrees

The shear resistance provided by fibers $V_{Rd,f}$ is calculated as shown in Equation (2.21):

$$V_{Rd,f} = \frac{A_{fv}\,\sigma_{Rd,f}}{\tan\theta} \quad (2.21)$$

$$\sigma_{Rd,f} = \frac{1}{K\,\gamma_{cf}} \frac{1}{w_{lim}} \int_0^{w_{lim}} \sigma_f(w)\,dw \quad (2.22)$$

where:

A_{fv} = Area of fiber effect, $A_{fv} = b_w z$, mm^2

$\sigma_{Rd,f}$ = Residual tensile strength, MPa

w_{lim} = Maximum of w_u and 0.3 mm

w_u = Ultimate crack width at the ULS for bending, mm

$\sigma_f(w)$ = Stress after crack opening, MPa

The *AFGC Guidelines* (AFGC 2013), Section 3.1, provide a tensile constitutive law indicating the maximum allowable crack opening as follows:

$$w_{\text{lim}} = \min\left(\frac{h}{100}, \frac{l_f}{4}\right) \quad (2.23)$$

where:

h = Total height of the section, in.

l_f = Fiber length, in.

Mobasher et al. (2014) recommended a reduction factor of 0.34 to account for the overestimation of the capacity measured using ASTM C1609 (inferred tension bending strength) in design

computations for fiber reinforced concrete sections. The uniaxial direct tension test for UHPC can provide a more direct alternative for measuring tensile strength to support such computations.

For UHPC exhibiting high strain hardening (Type 3), the post-cracking peak remains higher than the elastic tensile strength. The design law is then considered to be strain hardening. This type of tensile behavior is desirable per the definition of UHPC, which requires sustained post-cracking tensile strength prior to failure. This kind of behavior can be obtained for UHPC with a sufficient fiber content. For Type 3 behavior, a mean-strain constitutive law can be assumed rather than a crack width law (because of the large number of very fine and very dense cracks) but measured over a sufficient length. In the case of high strain hardening UHPC, the $\sigma_{Rd,f}$ term can be expressed in the following manner:

$$\sigma_{Rd,f} = \frac{1}{K\,\gamma_{cf}} \frac{1}{\varepsilon_{lim}-\varepsilon_{el}} \int_{\varepsilon_{el}}^{\varepsilon_{lim}} \sigma_f(\varepsilon)\,\mathrm{d}\varepsilon \tag{2.24}$$

where:

ε_{lim} = Maximum between ε_u and ε_{max}

ε_u = Ultimate tension strain attained at the ULS for bending combined with axial forces on the outer fiber under the moment exerted in the section

ε_{max} = $\varepsilon_{u,lim} = \frac{w_{lim}}{l_c}$ where $l_c = \frac{2}{3}h$

ε_{el} = Strain corresponding to elastic (first cracking) tensile strength, f_t/E_c

Then the term $\int_{\varepsilon_{el}}^{\varepsilon_{lim}} \sigma_f(\varepsilon)\,\mathrm{d}\varepsilon$ is the area under the stress-strain diagram between ε_{lim} and ε_{el}. The term $\frac{1}{\varepsilon_{lim}-\varepsilon_{el}} \int_{\varepsilon_{el}}^{\varepsilon_{lim}} \sigma_f(\varepsilon)\,\mathrm{d}\varepsilon$ results in an average value between ultimate tensile strength f'_{tu}, which corresponds to the tensile strength at ε_{lim}, and elastic tensile strength f'_t. Thus, Equation (2.24) can be rewritten as follows:

$$\sigma_{Rd,f} = \frac{1}{K\,\gamma_{cf}} \frac{f'_t + f'_{tu}}{2} \tag{2.25}$$

2.3.3 JSCE Recommendations

The significant difference between the UHPC design approach in AFGC (2013) and JSCE (2004) is that JSCE (2004) employs a bilinear stress-strain curve for compression and a bilinear tension

softening curve with material properties based on Ductal. JSCE (2004) uses the equivalent specific length, which is similar in concept to the characteristic length of AFGC (2013), to transform a crack opening displacement to a corresponding strain. JSCE (2004) recommendations provide the material models shown in Figure 2.11.

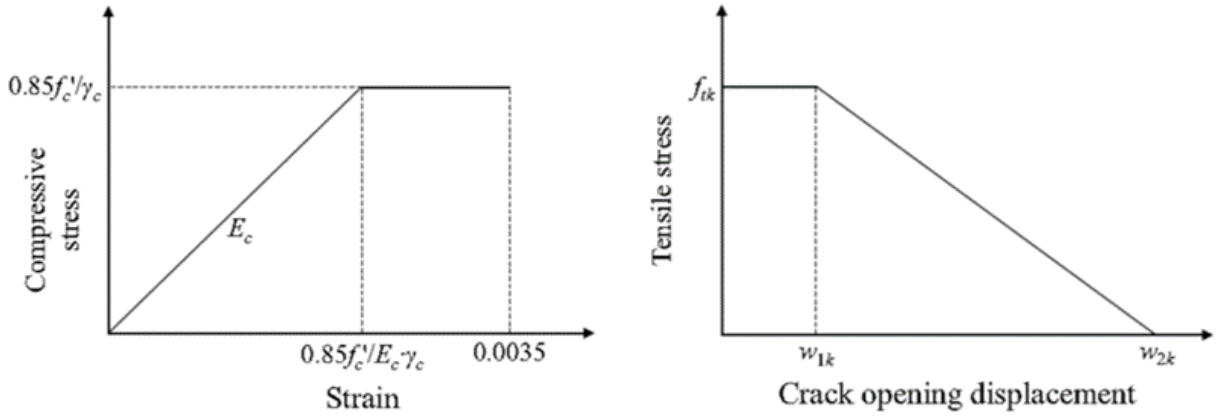

(a) Compressive Stress-Strain Curve *(b) Tension Softening Curve*

Notes:
f_c' = Compressive strength, ksi
γ_c = Partial safety factor, 1.3
E_c = Young's Modulus, ksi
f_{tk} = Characteristic value of tensile strength of UHPC
w_{1k} = Crack opening displacement at 0.5 mm (0.02 in.)
w_{2k} = Crack opening displacement at zero tensile stress, 4.3 mm (0.17 in.)

Figure 2.11. Material Models (JSCE 2004).

2.3.4 Design Methods Used for UHPC Bridges in United States

The first two UHPC road bridges in the United States, the Mars Hill Bridge and the Cat Point Creek Bridge, were designed based on AFGC/SETRA (2002) and the AASHTO LRFD Bridge Design Specifications (2002) for limit states and load calculations using a design criteria based on crack openings (Weldon et al. 2010). The approach used a material model developed by Chuang and Ulm (2002) for the tensile behavior of UHPC. The results of the modeled response versus the experimental response of a notched beam are shown in Figure 2.12. The Mars Hill Bridge in Wapello County, Iowa, was completed in 2006, with a 108 ft span length and three 42 in. deep UHPC girders that are modified standard Iowa bulb-tee Type C girders without shear reinforcement (Rouse et al. 2011). The Cat Point Creek Bridge near Warsaw, Virginia, was completed in 2008 with 10 spans—each 81.5 ft long—and five 45 in. deep prestressed concrete bulb-tee beams (Weldon et al. 2010). Weldon et al. (2010) reported that both bridges used Ductal

for the UHPC mix, with 28 ksi and 23 ksi 28-day compressive strengths for the Mars Hill Bridge and Cat Point Creek Bridge, respectively.

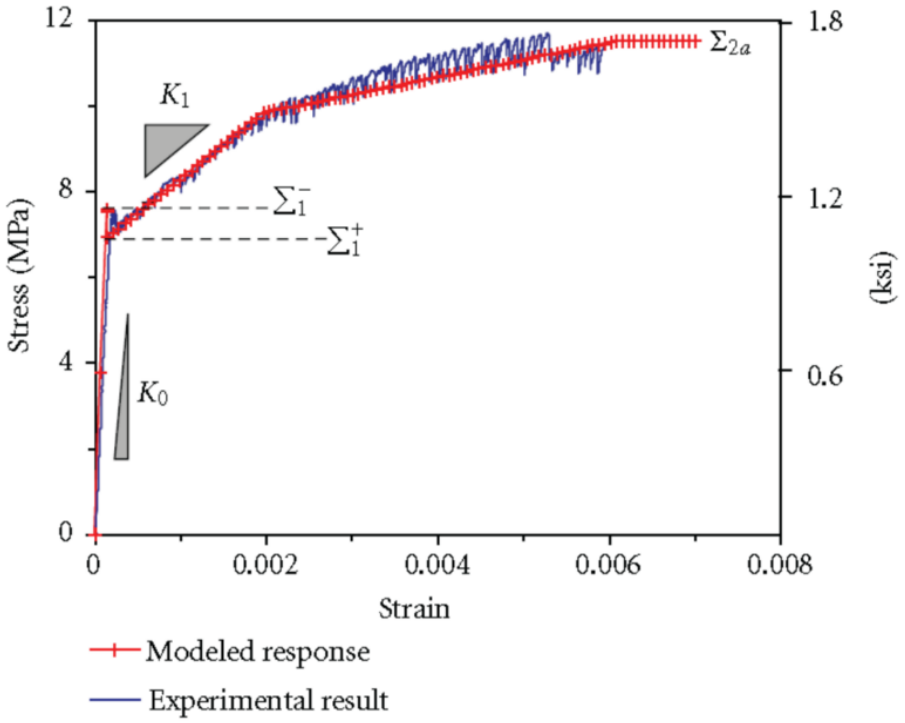

Figure 2.12. Comparison of Modeled Response versus Experimental Response (Gunes et al. 2012).

Alahmari et al. (2021) designed and constructed a two-span bridge in Anthony, New Mexico. The flexure design was based on AASHTO (2012) recommendations with modifications to account for the tensile strength of UHPC. Figure 2.13 presents the assumed UHPC behavior. Giesler et al. (2018) revealed the details of the design. Each span of the bridge was 25 ft long. One span consisted of UHPC channel-shaped girders with shallower depth, while the other span was a UHPC channel-shaped girder with a deeper section. Both were topped with a CC deck slab. Both beams were designed to sustain the same loading conditions.

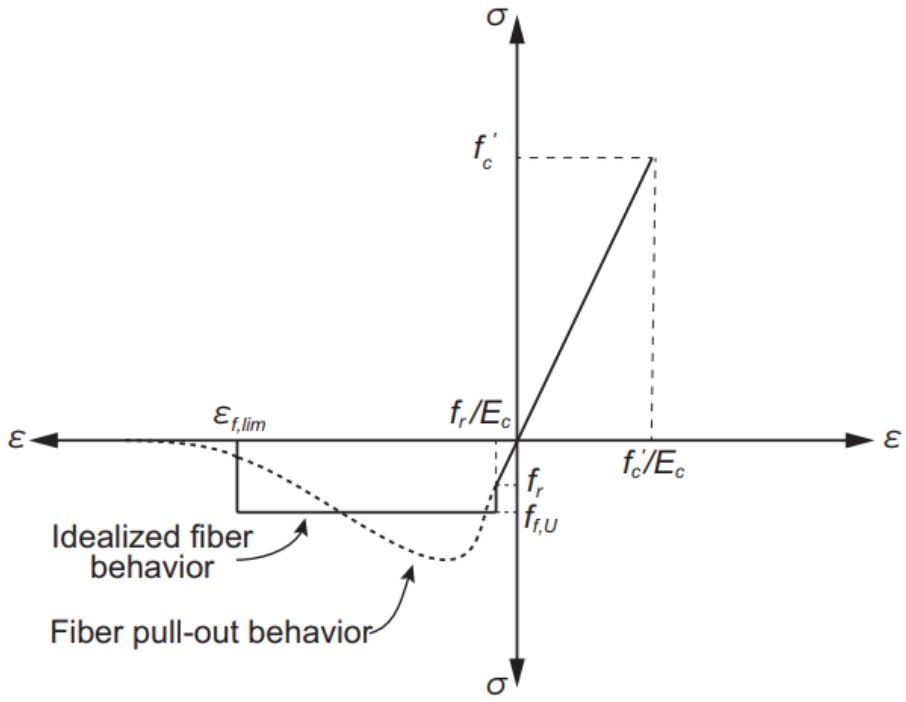

Figure 2.13. Assumed UHPC Behavior (Giesler et al. 2018).

2.3.4.1 Flexural Design

Gunes et al. (2012) reported the design principles and the calculation procedure using a design method by Chuang and Ulm (2002) for the flexural and shear section. The authors used the crack opening criteria according to AFGC/SETRA (2002) and AASHTO LRFD Bridge Design Specifications (2002) for Service III Limit State for tensile stress and Strength I Limit State for ultimate strength calculation. The authors conducted sectional analysis based on the following principles: (a) maximum tensile strain based on the allowable crack width, (b) plane section assumption (Navier-Bernoulli), (c) stress-strain model of UHPC, and (d) sectional equilibrium.

2.3.4.1.1 Maximum Tensile Strain

Cracking is not allowed for the maximum tensile strain at the SLS. Thus, the maximum allowable tensile strain at the SLS is the cracking strength Σ_1^- divided by the initial stiffness K_0, as shown in Equation (2.26). This value is the same as the elastic strain ε_{el} in Figure 2.9 from AFGC (2013).

$$\varepsilon_{SLS} = \frac{\Sigma_1^-}{K_0} \tag{2.26}$$

where:

ε_{SLS} = Maximum allowable tensile strain at SLS

Σ_1^- = Cracking strength, ksi

K_0 = Initial stiffness, ksi

The maximum allowable crack opening at ULS is the minimum value between $0.01\ h$ and $\frac{l_f}{4}$ for a reinforced structural components or 0.01 in. for an unreinforced structural component. Based on this crack opening criteria, the maximum allowable tensile strains at ULS may be calculated using Equation (2.27):

$$\varepsilon_{ULS} = \frac{\Sigma_1^-}{K_0} + \frac{w_{re}^{lim}}{l_c} \tag{2.27}$$

where:

ε_{ULS} = Maximum allowable tensile strain at ULS

l_c = Characteristic length, $\frac{2}{3}h$, in.

w_{re}^{lim} = Maximum allowable crack opening for a reinforced section at ULS, in., minimum ($0.01\ h$ and $\frac{l_f}{4}$)

Equation (2.27) becomes the same as Equation (2.10) by substitution of the maximum allowable crack opening for w_{peak} and by considering the partial safety factor.

2.3.4.1.2 Force Equilibrium

Force equilibrium is equal to that of NSC.

$$N_R = \int_A \sigma(y)\ \mathrm{d}a = 0 \tag{2.28}$$

$$M_R = \int_A y\ \sigma(y)\ \mathrm{d}a = 0 \tag{2.29}$$

where:

N_R = Normal force, kips

A = Cross-section area, in^2

$\sigma(y)$ = Longitudinal stress in the cross-section A, ksi

M_R = Moment in the cross-section A, kip-in

y = Distance from neutral axis, in.

Using the material model shown in Figure 2.12 with the material properties and the section dimensions, the flexural capacity can be calculated by sectional analysis with iterative calculation of Equations (2.28) and (2.29). Gunes et al. (2012) assumed a loss of prestress force as 20 percent and used 0.85 as a strength reduction factor for flexural design.

2.3.4.2 Shear Design

Gunes et al. (2012) also provided the shear design calculations without stirrups. The shear capacity at SLS is computed using Equation (2.30). The web area is used as the effective shear area A_w^{eff}. The maximum allowable shear stress τ_{lim} is calculated using the cracking strength Σ_1^- and the longitudinal stress from the prestressing force σ using Equation (2.31), which is found from the principal stress equation shown in Equation (2.32). The strength reduction factor ϕ is 0.85 for SLS.

$$\phi V_{SLS} = A_w^{eff} \times \tau_{lim} \tag{2.30}$$

$$\tau_{lim} = \Sigma_1^- \sqrt{1 - \frac{\sigma}{\Sigma_1^-}} \tag{2.31}$$

$$\frac{\sigma}{2} + \sqrt{\left(\frac{\sigma}{2}\right)^2 + {\tau_{lim}}^2} \leq \Sigma_1^- \tag{2.32}$$

where:

V_{SLS} = Shear capacity at SLS, kips

A_w^{eff} = Effective shear section area, in^2

τ_{lim} = Maximum allowable shear stress, ksi

σ = Longitudinal stress from the prestressing force, ksi

ϕ = Strength reduction factor for SLS, taken as 0.85

To calculate the shear capacity at ULS using Equation (2.33), the contribution of UHPC and steel fibers should be considered, as shown in Equations (2.34) and (2.35), respectively. The admissible crack opening of the web is considered to be 0.01 in. as an unreinforced section; thus, the maximum allowable strain at ULS ε_{ULS} is calculated using Equation (2.37). The residual UHPC tensile strength σ_p is calculated using Equation (2.36) with ε_{SLS} from Equation (2.26). The strength reduction factor for the concrete contribution φ_c is $2/3$. The strength reduction factor for the fiber contribution φ_f is also $2/3$ when considering a global fiber orientation factor K = 1.25 and the intrinsic variability of the material properties of 0.8 $\left(\frac{1}{K} \times 0.8 \approx \frac{2}{3}\right)$.

$$\phi V_{ULS} = \phi_c V_c \times \phi_f V_f \tag{2.33}$$

$$V_c = 0.09\sqrt{f_c'} b_w d \tag{2.34}$$

$$V_f = \frac{A\sigma_p}{\tan \beta_u} \tag{2.35}$$

$$\sigma_p = \frac{1}{\varepsilon_{ULS} - \varepsilon_{SLS}} \int_{\varepsilon_{SLS}}^{\varepsilon_{ULS}} \sigma_s \mathrm{d}s \tag{2.36}$$

$$\varepsilon_{ULS} = \frac{\Sigma_2}{K_0} + \frac{w_{un}^{lim}}{l_c} \tag{2.37}$$

where:

V_{ULS} = Shear capacity at ULS, kips

V_c = Shear capacity contributed by UHPC, kips

V_f = Shear capacity contributed by fiber, kips

f_c' = Compressive strength at 28 days, ksi

b_w = Web thickness, in.

z = Effective height (strand to top flange), in.

A = Effective area, $b_w \times z$, in^2

σ_p = Residual UHPC tensile strength, ksi

β_u = Inclination angle between a diagonal crack and the longitudinal direction of the beam, with a lower bound of β_u= 30°, degrees

ϕ_c = Design factor for UHPC, $\frac{2}{3}$

ϕ_f = Design factor for fiber, $\frac{2}{3}$

Σ_2 = Ductile strength, ksi

σ_s = Stress at a corresponding strain, ksi

w_{un}^{lim} = Maximum allowable crack opening for an unreinforced section at ULS, 0.01 in.

2.3.5 ACI 544.4R-18: Guide to Design with Fiber-Reinforced Concrete

ACI 544.4R-18 (2018) is a design guide for fiber-reinforced concrete (FRC). Even though this guide does not specifically address UHPC, it provides important recommendations regarding flexural and shear design for FRC that may have applicability to UHPC. This guideline classifies steel fibers into micro- and macro-fiber, with the fiber diameter of 0.012 in. as the separating limit. The guide focuses on the design of macro FRC because macro fibers are considered structural fibers, while micro fibers are used for crack control.

2.3.5.1 Flexural Design

ACI 544.4R-18 (2018) introduces two coupled standard test and design methods for flexural design as follows:

1. ASTM C1609/C1609M (2012) *Standard Test Method for Flexural Performance of Fiber-Reinforced Concrete (Using Beam with Third-Point Loading)* as a test method with RILEM TC 162-TDF (2002) *Test and Design Methods for Steel Fibre Reinforced Concrete* as a design method.
2. EN 14651 (2005) *Test Method for Metallic Fibered Concrete—Measuring the Flexural Tensile Strength (Limit of Proportionality (LOP), Residual)* as a test method with *fib* (2013) as a design method.

The flexural residual strength of FRC is obtained through the test methods, and these parameters are used to calculate the flexural capacity of FRC members.

2.3.5.1.1 ASTM C1609 with RILEM TC 162-TDF

ASTM C1609/C1609M (2012) measures the complete pre-and post-cracking flexural response of an unnotched beam subjected to four-point bending. The size of a specimen is 6 × 6 × 20 in., with

a span of 18 in. The test is conducted until reaching a midpoint deflection of 1/150 of the span length while measuring flexural residual loads at 1/600 and 1/150 of the span length corresponding to f_{600}^{D} and f_{150}^{D}, as shown in Figure 2.14.

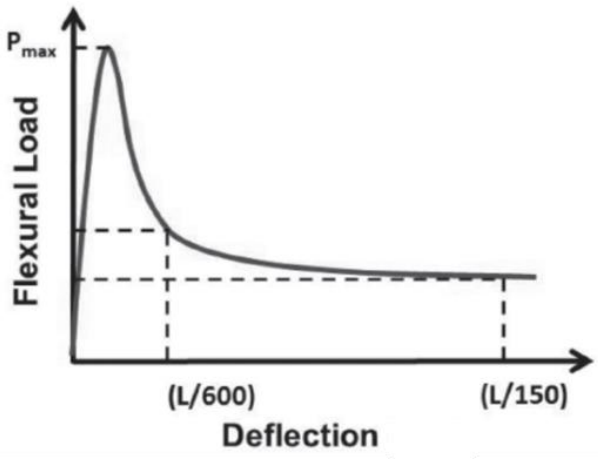

Figure 2.14. Schematics of a Typical Test Result (ASTM C1609/C1609M 2012).

RILEM TC 162-TDF (2002) uses a stress block concept similar to CC. However, the shape of the compressive stress distribution is simplified to a triangular shape, as shown in Figure 2.15.

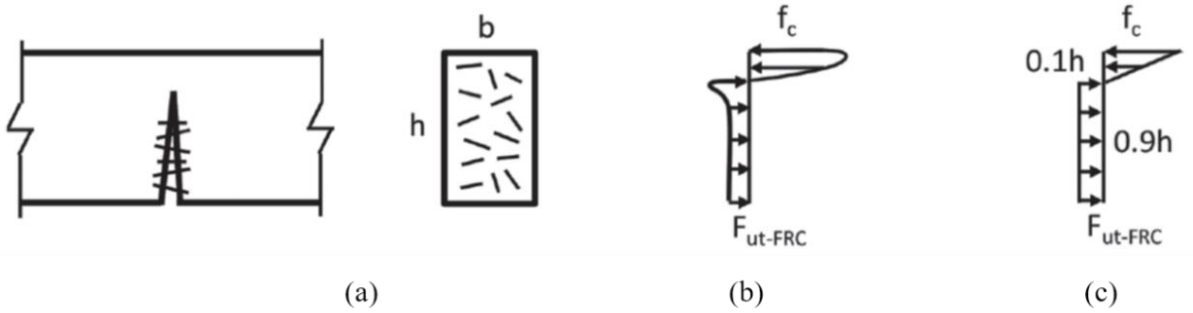

Figure 2.15. Schematics of Stress Block for a Cracked FRC Flexural Member: (a) Beam Section, (b) Actual Distribution of Normal Stresses, (c) Simplified Distribution of Normal Stresses (ACI 544.4R-18 2018).

Based on this stress block and the measured flexural response from ASTM C1609/C1609M (2012), the ultimate tensile strength of cracked FRC and the nominal bending moment for an FRC section are calculated using Equations (2.38) and (2.39), respectively. These equations are from the force equilibrium in the cross-section. The tensile strength of cracked FRC and the nominal bending moment for FRC at SLS can be also calculated by Equations (2.38) and (2.39) using f_{600}^{D} instead of f_{150}^{D} or using other design limits depending on serviceability requirements:

$$f_{ut-FRC} = 0.37 f_{150}^{D} \tag{2.38}$$

$$M_{n-FRC} = f_{150}^{D} \times \frac{bh^2}{6} \tag{2.39}$$

where:

f_{ut-FRC} = Ultimate tensile strength of cracked FRC, ksi

M_{n-FRC} = Nominal bending moment for an FRC section, kip-in.

f_{150}^{D} = FRC flexural residual strength at a deflection of $L/150$, ksi

f_{600}^{D} = FRC flexural residual strength at a deflection of $L/600$, ksi

b = Beam width, in.

h = Beam height, in.

2.3.5.1.2 EN 14651:2005 with Model Code 2010

This coupled test and design method uses a moment-crack width relationship. EN 14651 (2005) measures deflection and crack-mouth opening displacement (CMOD) of a notched beam subjected to three-point bending. The size of a specimen is 6 × 6 × 22 in., with a span of 20 in. and 1 in. depth of notch at midspan. The test is conducted until reaching a CMOD of 0.14 in. while measuring flexural residual loads at CMOD of 0.02, 0.06, 0.1, and 0.14 in. corresponding to $f_{R,1}$, f_{R2}, $f_{R,3}$, and $f_{R,4}$, respectively, as shown in Figure 2.16.

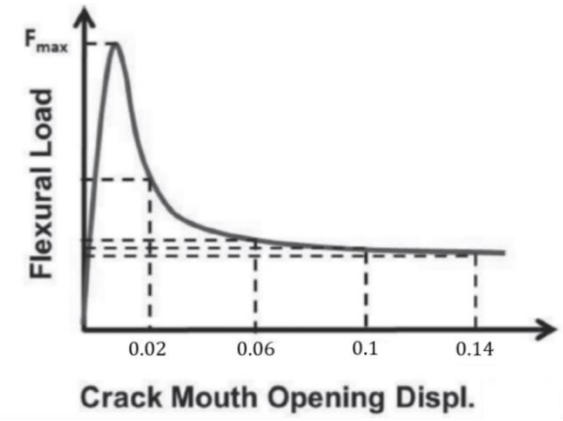

Figure 2.16. Schematics of a Typical Test Result (EN 14651 2005).

Unlike RILEM TC 162-TDF (2002), *fib* (2013) uses a constant tensile residual strength f_{FTu}, as shown in Figure 2.17(c), with the two material models for the post-crack tensile strength of FRC. The material models are simplified rigid-plastic and linear models.

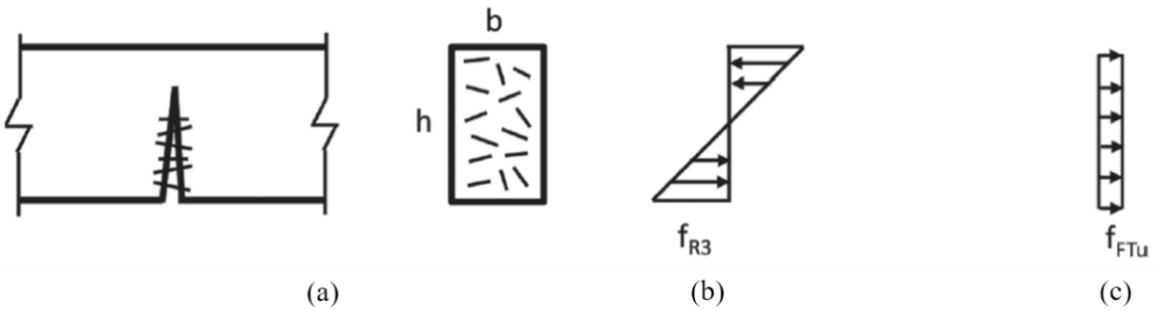

Figure 2.17. Schematics of Stress Block for a Cracked FRC Flexural Member: (a) Beam Section, (b) Distribution of Normal Stresses, (c) Simplified Distribution of Normal Stresses (ACI 544.4R-18 2018).

The simplified rigid-plastic model is used only for the ULS, as shown in Figure 2.18(a). The ultimate tensile strength of FRC $f_{Ftu-FRC}$ is one-third of the flexural residual strength $f_{R,3}$, as shown in Equation (2.40). The value of one-third is close to the 0.37 value used by RILEM TC 162-TDF (2002). The equation for the nominal bending moment shown in Equation (2.41) is consistent with RILEM TC 162-TDF (2002).

$$f_{Ftu-FRC} = \frac{1}{3} f_{R,3} \tag{2.40}$$

$$M_{nu-FRC} = f_{R,3} \times \frac{b h_{sp}^2}{6} \tag{2.41}$$

where:

$f_{Ftu-FRC}$ = Ultimate tensile strength of FRC at ULS, ksi

M_{nu-FRC} = Nominal bending moment for an FRC section at ULS, kip-in.

$f_{R,3}$ = Flexural residual strength at a CMOD of 0.1 in., ksi

b = Beam width, in.

h_{sp} = Net height of the beam (total height − notch height), in.

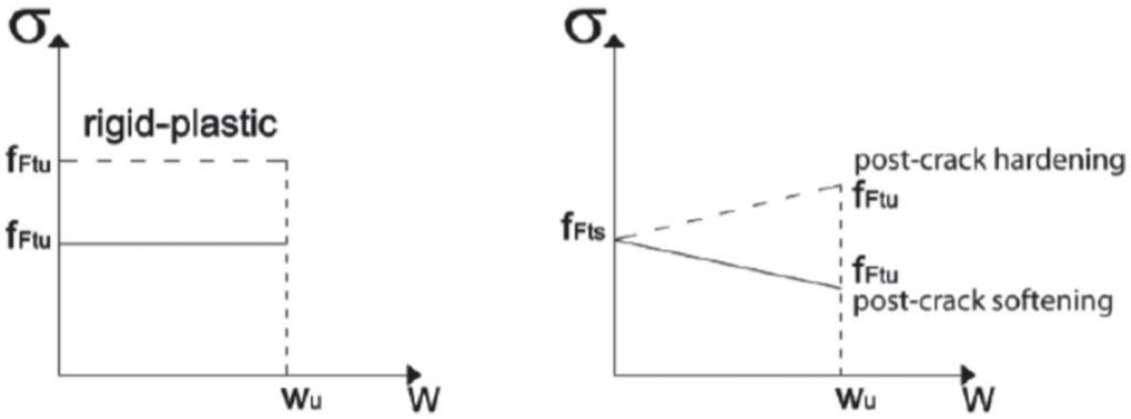

(a) Rigid-Plastic Model for ULS only *(b) Linear Model for SLS and ULS*

Figure 2.18. Simplified Post-Crack Stress-Crack Width Relationship in Model Code 2010 (*fib* 2013).

The linear model assumes that the flexural residual strength is linearly related to the crack width. This model is applied to both the SLS and ULS. The tensile strength and the nominal bending moment are calculated using Equations (2.42) and (2.44) for SLS and Equations (2.43) and (2.45) for ULS, respectively.

$$f_{Fts-FRC} = 0.45 f_{R,1} \tag{2.42}$$

$$f_{Ftu-FRC} = \left(0.45 f_{R,1}\right) - \frac{w_u}{CMOD_3}\left(0.45 f_{R,1} - 0.5 f_{R,3} + 0.2 f_{R,1}\right) \tag{2.43}$$

$$M_{ns-FRC} = f_{R,1} \times \frac{b h_{sp}^2}{6} \tag{2.44}$$

$$M_{nu-FRC} = f_{R,3} \times \frac{b h_{sp}^2}{6} \tag{2.45}$$

where:

$f_{Fts-FRC}$ = Tensile strength of FRC at SLS, ksi

M_{ns-FRC} = Nominal bending moment for an FRC section at SLS, kip-in.

$f_{R,1}$ = Flexural residual strength at a CMOD of 0.02 in., ksi

w_u = Maximum crack width, in.

$CMOD_3$ = Crack-mouth opening displacement of 0.1 in

2.3.5.2 Shear Design

ACI 544.4R-18 (2018) introduced the shear design method for steel FRC from Model Code 2010 (*fib* 2013) that provides formulas for shear capacity of steel fiber-reinforced NSC without shear reinforcement, such as stirrups, but with conventional longitudinal reinforcement.

2.3.5.2.1 Model Code 2010

Section 7.7.3.2 of Model Code 2010 (*fib* 2013) provides Equation (2.46) for the shear design of FRC. This section allows elimination of conventional shear reinforcement such as stirrups if $f_{ut-FRC} > 0.6\sqrt{f_c}$. The value of f_{ut-FRC} can be determined using Equation (2.40).

$$V_{FRC} = \left\{ \frac{27.6 \times 0.18}{\gamma_c} k_s \left[100\rho \left(1 + 7.5 \frac{f_{ut-FRC}}{f_t} \right) f_c \right]^{\frac{1}{3}} + 0.15\sigma_{cp} \right\} bd \quad (2.46)$$

$$k_s = 1 + \sqrt{\frac{8}{d}} \leq 2 \quad (2.47)$$

$$\rho = \frac{A_s}{bd} \quad (2.48)$$

where:

γ_c = Partial safety factor for concrete, 1.0
k_s = Size effect factor
ρ = Longitudinal reinforcement ratio
A_s = Area of longitudinal reinforcement, in^2
f_{ut-FRC} = Ultimate tensile residual strength of FRC from Equation (2.40), psi
f_t = Tensile strength of plain concrete, psi
f_c = Compressive strength of plain concrete, psi
σ_{cp} = Average normal stress acting on concrete cross-section due to loading or prestressing, psi
d = Effective depth, in.

2.4 ONGOING WORK FOR DESIGN CODES AND STANDARDS

2.4.1 General

European countries have led the development of guidelines and recommendations for UHPC because most of the commercial UHPC mixtures have been developed in Europe. Australia, Japan, and South Korea have also developed guidelines and recommendations. The French began to standardize UHPC guidelines in 2012, and French standards for UHPC were eventually published in 2016. ACI Committee 239C, ASTM, and the Canadian Standard Association (CSA) have developed guidelines, standards, and provisions for FRC, including UHPC. The following subsection describes and summarizes recent UHPC guidelines in Europe. The next subsection focuses on French standards—the world's first standards for UHPC. The last subsection introduces ongoing activities on codes and standards for UHPC in North America.

2.4.2 Codes and Guidelines for UHPC in Europe

Schmidt and Fröhlich (2015) indicated that four guidelines for UHPC are largely recognized and utilized for industrial applications in Europe. Those are *AFGC* (2013) in France, *Swiss Society of Engineers and Architects* (2013) in Switzerland, *DAfStb-Guideline* (2017) in Germany, and *fib Task Group 8.6* (2013). Schmidt and Fröhlich (2015) reported that French recommendations provided in AFGC (2013) focus on the design of fiber-reinforced structural members. The Swiss Society of Engineers and Architects (2013) of Switzerland mainly handles the use of UHPC with conventional reinforcement for strengthening existing concrete structures. In addition, the German DAfStb-Guideline (2017) comprehensively deals with material constituents, properties, and design. The *fib* Task Group 8.6 (2013) integrates the design guidelines of France and Switzerland with research results for material properties from a research program funded by the German Research Foundation (Schmidt and Fröhlich 2015).

AFGC (2013) is discussed in Section 2.3.2 in detail. AFGC (2013) mainly describes design methods for structural elements reinforced with steel fibers, while material constituents, mixture design, and fresh properties are briefly discussed as part of structural member design. This process is because commercial UHPC mixtures are used as a rule in France, and thus the material properties are based on identity cards that are provided by proprietary UHPC producers (Schmidt and Fröhlich 2015). Therefore, AFGC (2013) only refers to the material test methods for UHPC based

on European codes for testing concrete, such as EN 12350 for testing fresh concrete and EN 12390 for testing hardened concrete. However, because existing European codes for testing concrete are not appropriate to obtain parameters for flexural design, AFGC (2013) describes the flexural beam test for the tensile capacity and the test method for the fiber orientation factors in Annex 3 and Annex 6, respectively, to obtain the appropriate tensile constitutive law and parameters for design of fiber-reinforced UHPC.

The technical guideline of Switzerland (Swiss Society of Engineers and Architects 2013) introduces a design method for strengthening existing concrete using a thin layer of UHPC. This method is usually applied to bridge decks. The Swiss Society of Engineers and Architects (2013) includes a direct tensile test method in Annex C to classify UHPC into three performance classes depending on strain softening or hardening, and then the material models are determined depending on the performance classes from the direct tension test.

The German approach to develop recommendations for UHPC is more comprehensive than the French and Swiss guidelines. This approach starts from material constituents, which are based on locally available materials, to applicability, to precast and ready-mix plants. Therefore, the German Research Foundation funded the research program coordinated by the University of Kassel that conducted research studies on raw material, fresh and hardened properties, microstructures, durability, and design and test methods (Schmidt and Fröhlich 2015). The German Committee for Structural Concrete (Deutscher Ausschuss für Stahlbeton (DAfStb)) prepared a draft version of DAfStb-Guideline (2017). Schmidt et al. (2017) reported that DAfStb-Guideline (2017) comprise two parts. Part 1 handles design methods for UHPC, and Part 2 provides requirements for raw materials, mixture design, and quality control. Currently, the DAfStb-Guideline is in progress.

The committee members who published *Ultra High Performance Fiber Reinforced Concrete* (*fib* Task Group 8.6 2013) are experts from France, Switzerland, and Germany. The approach of this guideline was combined appropriately with the French, Swiss, and German approaches mentioned above (Schmidt and Fröhlich 2015). The *fib* Task Group 8.6 (2013) introduced performance-based design principles such as ULS, SLS, and sustainability for design of structural members by adopting the material models that are based on French and Swiss design guidelines. These technical guidelines deal with UHPC with or without steel fiber and/or conventional

reinforcement. In addition to design methods, *fib* Task Group 8.6 (2013) considered material properties and mechanical performances by reflecting the experimental results conducted as part of the German Research Program (2005-2013) and industrial experience in Europe. These guidelines, with the recommendations from Task Group 8.8 of *fib* for *Structural Design with Flowable Concrete*, have developed the effect of fiber orientation and dispersion (Grünewald et al. 2010). This concept is included in NF-P-18-710 (2016) as well as AFGC (2013). The objective of Task Group 8.6 is to incorporate design, production, and construction methods for UHPC into Model Code 2020 of *fib* as a part of the code (Matthews et al. 2018).

2.4.3 First Standards for UHPC

Although several guidelines have been developed, these guidelines have some limitations with respect to widespread application of UHPC. Therefore, the effort to standardize UHPC guidelines began in France in 2012, and the first UHPC standards in the world were published in 2016 (Toutlemonde et al. 2016). These standards consist of three parts: (1) production standard NF-P-18-470 (NF-P-18-470 2016), (2) design standard NF-P-18-710 (NF-P-18-710 2016), and (3) execution standard NF-P-18-451 (NF-P-18-451 2018). These standards are technically based on AFGC (2013) and conform to the form of European Standards (Toutlemonde et al. 2016).

2.4.3.1 NF-P-18-470

Toutlemonde et al. (2018) reported that the product standard NF-P-18-470 NF-P-18-470 (2016) substitutes for the existing CC standards. This standard includes appropriate test methods for UHPC production in annexes. The scope of NF-P-18-470 NF-P-18-470 (2016) is UHPC that has greater than 18.9 ksi characteristic compressive strength at 28 days while achieving non-brittleness condition, which is described in Section 2.3.2.1.6 of this report, due to metallic or nonmetallic fibers. However, the design standard NF-P-18-470 NF-P-18-710 (2016) does not cover UHPC with a characteristic compressive strength smaller than 21.8 ksi and nonmetallic fiber-reinforced UHPC; therefore, part of the scope in accordance with NF-P-18-470 NF-P-18-470 (2016) cannot be designed by NF-P-18-470 NF-P-18-710 (2016) (Toutlemonde et al. 2016). Toutlemonde et al. (2018) provided part of the UHPC material specifications from NF-P-18-470 NF-P-18-470 (2016), which are summarized below:

- Non-brittleness condition (which is described in Section 2.3.2.1.6)
- Nominal upper size of aggregates is not greater than 0.39 in.
- Density of UHPC ranges between 137.3 and 174.8 lb/ft^3
- Characteristic elastic tensile strength at 28 day is greater than 0.87 ksi
- Water porosity at 90 days is not greater than 9.0 percent

NF-P-18-470 (NF-P-18-470 2016) defines different classes of UHPC depending on the characteristic compressive strength at 28 days, tensile behavior, workability, and curing. The classes based on compressive strength are from *Bétons Fibrés à Ultra-Hautes Performances* (BFUP) 18.9/21.0 to BFUP 36.3/38.4. The first number in the class is the compressive strength in ksi obtained from a cylinder test, and the second number is that obtained from a cube test. The classification based on tensile strength is determined by comparing the tensile limit of elasticity $f_{ct,el}$ to post-cracking tensile strength f_{ctf} (Toutlemonde et al. 2016). The classes of workability are determined by a flow table test or slump-flow test. The classes of thermal curing are categorized as (a) STT—no heat treatment; (b) TT1—thermally-induced acceleration of hydration for obtaining earlier initial setting; (c) TT2—heat treatment after setting at about 190°F with higher humidity than 90 percent; and (d) TT1+2—both TT1 and TT2 are applied (Resplendino 2014).

NF-P-18-470 (NF-P-18-470 2016) also includes the steps for evaluation of UHPC with acceptance criteria. These steps are (1) the evaluation of constituents and mix proportions, (2) the evaluation of properties by conducting material tests, and (3) the evaluation of the quality at a fresh and hardened state (Toutlemonde et al. 2016). For the evaluation of constituents and mix proportions, selected materials must meet project requirements and NF-P-18-470 (NF-P-18-470 2016). In addition, possible deviations during the manufacturing process should be considered in this step. The evaluation for material properties must be conducted to check conformity of required mechanical properties. In this step, a trial test using prototype elements should be performed to validate transportation, placing, and the curing process. The effective fiber orientation factor should also be determined to check design results. The last evaluation is conducted during the production process. In that step, conformity of UHPC with the required fresh and hardened properties is evaluated.

2.4.3.2 NF-P-18-710

NF-P-18-710 (NF-P-18-710 2016) is a national complement to EN 1992 Eurocode 2 (2004), and thus, has the same format as EN 1992 Eurocode 2 (2004). NF-P-18-710 (NF-P-18-710 2016) is technically based on AFGC (2013). As discussed in Section 2.3.2, the main difference with the design of NSC is the contribution of tensile capacity of UHPC and the crack bridging effect of steel fibers to the tensile constitutive law. In addition, NF-P-18-710 (NF-P-18-710 2016) considers shear resistance of steel fibers. Thus, the constitutive laws are utilized for flexural and shear capacity of UHPC for the ULS as well as for crack control for the SLS.

Another difference is the non-brittleness condition that guarantees minimum ductility of UHPC instead of the minimum reinforcement ratio in the design of NSC. The non-brittleness condition requires that the post-cracking tensile capacity up to crack width of 0.012 in. should be greater than the maximum value between 40 percent of elastic tensile strength and 0.44 ksi (Toutlemonde et al. 2016).

While design parameters such as elastic modulus, tensile strength, and modulus of rupture for NSC are expressed as a function of the characteristic compressive strength at 28 days, these formulas for UHPC have not been standardized yet (Toutlemonde et al. 2018). Thus, NF-P-18-710 NF-P-18-710 (2016) provides preliminary design values for those parameters but also states that these preliminary design values, especially fiber orientation factor K, must be verified by the evaluation for material properties with the material tests and/or the trial test with a prototype according to NF-P-18-710 (NF-P-18-710 2016).

NF-P-18-710 (NF-P-18-710 2016) specifies the minimum cover thickness as 1.5 times the fiber length. The cover thickness can be reduced due to low permeability and high durability. Reduction of cover thickness increases the moment arm and thus improves the flexural section capacity. NF-P-18-710 (NF-P-18-710 2016) also provides brief fire design guidelines in Annex R and seismic verification in Annex U (Toutlemonde et al. 2016).

2.4.3.3 NF-P-18-451

The execution standard NF-P-18-451 (NF-P-18-451 2018) has the same format as NF EN 13670/CN (2013) *Execution of Concrete Structures—National Addition to NF EN 13670:2013*.

NF-P-18-451 (NF-P-18-451 2018), which covers UHPC productions that are either cast in place, precast, joint fill, or repair on existing concrete conforming to NF-P-18-470 (NF-P-18-470 2016). This standard handles a series of requirements related to execution, including storage condition of the constituents; the required power of a mixer; the device for placing fibers into the mixer; mock-up tests; transporting; placing and vibrating; duration of placing; flow of UHPC; joint treatment; and treatment of existing concrete surfaces (Toutlemonde et al. 2018).

NF-P-18-451 (NF-P-18-451 2018) also includes recommendations regarding the falsework and formwork at early ages. The shape of molds should not disturb the flow of fibers; thus, sharp edges are not preferred. To avoid restraints at early ages to prevent unintended stress, molds should be dismantled at the appropriate time (Toutlemonde et al. 2018).

2.4.4 Current Efforts for Developing UHPC Specifications in North America

Currently, there are no dedicated design codes specifically for UHPC in North America. Due to a lack of design guidelines for UHPC, structural engineers have used existing codes in the United States with conservative safety factors or have adopted guidelines from other countries. To resolve these obstacles, AASHTO, ACI, ASTM, and Canadian Standards Associations (CSA) have been working on design specifications and guidelines, standard test methods, and material and test standards.

ACI Subcommittee 239C (Structural Design of Ultra-High Performance Concrete) was organized in 2015 and published an emerging technology report on the structural design of UHPC in 2018. The emerging technology report covers production of UHPC, concrete properties, structural design of UHPC components, and applications.

For material testing of UHPC, ASTM published ASTM C1856 (2017) *Standard Practice for Fabricating and Testing Specimens of Ultra-High Performance Concrete* in 2017. This ASTM standard provides the modifications of the existing test standards to adapt to the characteristics of UHPC. ASTM C1856 (2017) includes the modified test methods shown in Table 2.4. Even though most of the material properties can be obtained using ASTM test methods, the direct tensile test method is not standardized yet. AASHTO is currently in the process of standardizing the uniaxial tension test.

Table 2.4. The Modified Test Methods Provided by ASTM C1856 (2017).

Properties	Modified ASTM Test Methods
Flow	C1437 and C230
Time of setting	C191
Curing	C31 or C192
Compressive strength	C39
Flexural strength	C1609
MOE and Poisson's ratio	C469
Creep in compression	C512
Length change	C157 or C341
Resistance to abrasion	C944
Resistance to freezing and thawing	C666
Resistance to chloride ion penetration	C1202

The Working Group on UHPC under CSA A23.1 was formed in 2015. The working group developed a new annex on UHPC materials, including classes of UHPC, constituents, mix proportioning, mixing, formwork, placing, curing, and quality control. Different classes of UHPC are defined based on mechanical properties, tensile behavior, and types of fibers, as shown in Table 2.5. This annex was published in 2019 as a part of CSA A23.1-2019. Section 8 of the latest edition of the Canadian Highway Bridge Design Code, CSA S6:19 (2019), presents the definition of tension hardening and tension softening of FRCs, including UHPC.

The Federal Highway Administration (FHWA) has delivered the proposed UHPC structural design guidelines (draft version) to the AASHTO Committee on Bridges and Structures T-10 for consideration. The draft specifications are currently under review. These specifications propose tensile and compressive stress-strain models idealized for implementation for flexure design. The parameters for the models are based on the material-level tests under tension and flexure. The computation of nominal moment and shear capacity of UHPC is explained and formulated based on the work done by several researchers in the past.

Table 2.5. Classification of UHPC in CSA A23.1 (Ahlborn et al. 2016).

Range of Mechanical Properties	Class		
	H (Strain hardening tensile properties)	**S (Strain softening tensile properties)**	**N (Non-fiber composite)**
$f_c' > 17.4$ $f_t' > 0.73$	H1	S1	N1
$f_c' > 17.4$ $0.44 < f_t' < 0.73$	H2	S2	N2
$f_c' > 17.4$ f_t' not required	N/A	N/A	N3

Note:
1. f_c' = characteristic compressive strength at 28 days, ksi; f_t' = characteristic tensile strength at 28 days, ksi.
2. N/A: Not applicable

In a collaborative effort to develop a design philosophy that can be practicable for the precasters, the Precast/Prestressed Concrete Institute (PCI) sponsored a research study to investigate the development of large-scale UHPC structural girders and develop design guidelines for the implementation of longer UHPC girders with slender sections (eConstruct 2020). The research report suggests a design philosophy largely based on AASHTO (2014), ACI 318-14 (2014), and the PCI Design Handbook (PCI 2017). The Phase II report for this project will include the details of the design guidelines and the full-scale experimental testing results.

The research conducted by PCI provides recommendations for evaluating the reinforcement required to resist splitting resistance in UHPC. Equation (2.49) presents the contribution of fibers to splitting resistance as per eConstruct (2020).

$$f_{fiber} = \frac{1}{2} f_t A_{cb} \tag{2.49}$$

where:

f_{fiber} = Contribution from fibers, ksi

f_t = Tensile strength of UHPC, ksi

A_{cb} = Concrete section area that resists the bursting force within a distance of a quarter of the overall depth of the girder, in^2

3 ANALYTICAL FEASIBILITY STUDY

3.1 INTRODUCTION

The analytical feasibility study was conducted early in the project with an objective of utilizing current TxDOT shapes to evaluate the potential benefits of using UHPC in terms of longer span lengths and/or a reduced number of girder lines. The feasibility study focused on three prestressed girder types based on the most commonly constructed bridge types in Texas and the input provided by TxDOT project team. The selected girder types were (a) PCSB with a side-by-side beam configuration for short-span bridges, (b) Tx54 prestressed concrete I-girders for medium- to long-span precast girder bridges, and (c) Tx62 prestressed concrete I-girders for long-span precast girder bridges.

Conventional PCSB bridges are the most used girder types for short-span bridges in Texas, especially when a low clearance is required. According to the TxDOT FY2017 Average Unit Cost report (TxDOT 2017b), Tx shapes constitute 55 percent of all new bridge construction, and Tx54 is one of the most commonly used Tx shapes to achieve medium to long span lengths. The Tx62 girder is also selected as an alternative to achieve longer span lengths that can be practically carried on the highways.

Several design cases for each girder type were evaluated to provide an initial assessment of the potential benefits that can be realized using UHPC and to identify required mechanical properties of UHPC to achieve longer span lengths compared to CC. The design parameters were chosen based on the common TxDOT bridge widths, girder spacings, standard girder geometries, and standard deck slab thicknesses. The specified mechanical properties for UHPC were selected based on the values identified in the literature and preliminary design values provided in *Ultra High Performance Fibre-Reinforced Concretes (Bétons Fibrés à Ultra-Hautes Performances) Recommendations* by the French Association for Civil Engineers (AFGC 2013). The design approach for the preliminary designs follows the *AASHTO LRFD Bridge Design Specifications* (AASHTO 2020) and TxDOT *Bridge Design Manual* (TxDOT 2021) with some minor modifications based on recommendations for UHPC designs in FHWA reports. TxDOT standard practices were followed to ensure that the results could be compared to typical TxDOT conventional prestressed bridges.

Note that during this research project, additional recommendations and potential requirements became available, including journal papers from FHWA (El-Helou and Graybeal 2022a; El-Helou and Graybeal 2022b; El-Helou and Graybeal 2023; El-Helou et al. 2022; Mohebbi and Graybeal 2022; Mohebbi et al. 2022; Muzenski et al. 2022), the AASHTO draft specifications for UHPC (FHWA 2022), and the PCI study on nonproprietary UHPC (eConstruct 2020; Tadros 2021). These updates will be discussed in more detail within the review of the experimental results of the full-scale girder tests (Chapters 5 and 6 of this Volume 2 report) and with respect to the suggested design guidelines and illustrative examples provided in the Volume 3 report.

AASHTO LRFD Specifications (AASHTO 2020) Article 5.5 specifies that structural components be designed to satisfy relevant service, strength, fatigue, and extreme event limit states during all stages, including construction, stressing, handling, transportation, erection, and throughout the service life of the structure.

AASHTO LRFD Specifications (AASHTO 2020) Article 1.3.3 specifies that each component and connection be designed to satisfy Equation (3.1).

$$\sum \eta_i \gamma_i Q_i \leq \phi R_n \tag{3.1}$$

where:

- η_i = Load modifier relating to ductility, redundancy, and operational classification = 1.0 for strength limit state if used for conventional designs complying with the AASHTO LRFD specifications (AASHTO 2020), conventional levels of redundancy, and for typical bridges; = 1.0 for all other limit states
- γ_i = Load factor
- Q_i = Force effect
- ϕ = Resistance factor
- R_n = Nominal resistance

3.2 SERVICE LIMIT STATES

The AASHTO LRFD Specifications (AASHTO 2020) Article 5.5.2 requires investigation of cracking, deflections, and concrete stresses under service level loading.

3.2.1 Crack Control

The AASHTO LRFD Specifications (AASHTO 2020) Article 5.6.7, control of cracking by distributing reinforcement, specifies that all concrete components, save deck slabs, having tension exceeding 80 percent of the modulus of rupture ($0.24\sqrt{f_c'}$, ksi) shall have crack control reinforcement, as indicated in the same article. For prestressed concrete members using CC, the tension stress limit at service ($0.19\sqrt{f_c'}$, ksi) guarantees the tension stresses are smaller than the 80 percent limit; thus, crack control reinforcement is not necessary. Currently, no crack control criteria for prestressed UHPC members exists in major structural design codes in the United States. However, during the feasibility study, it was noted that for the new UHPC design guidelines in development, a tensile stress limit at service of 85 percent of the tensile strength based on direct tension testing was being considered (Graybeal 2019). This limit on tensile stresses may be considered sufficient to avoid requiring crack control reinforcement. Furthermore, UHPC has steel fibers that provide additional crack control capabilities in comparison to CC.

3.2.2 Optional Deflection Check

The AASHTO LRFD Specifications (AASHTO 2020) Article 5.6.3.5 provides guidelines for calculating deflections and camber under dead load, live load, prestressing, creep, and shrinkage. Instantaneous deflections can be calculated using the gross moment of inertia I_g or effective moment of inertia I_e, as specified in the same article. For prestressed members, it is suggested more accurate creep and shrinkage coefficients be used by following the empirical expressions provided in Article 5.4.2.3 together with the MOE at the time of loading. The AASHTO LRFD Specifications (AASHTO 2020) Article 2.5.2.6 provides further guidelines for optional deflection checks, which are listed as follows:

- The vehicular load includes the dynamic load allowance, and the live load portion of the Service I load combination shall be used.
- All design lanes should be loaded, and all supporting components should be assumed to deflect equally.
- For composite design, the stiffness of the design cross-section used for the determination of deflection should include the entire width of the roadway and the structurally continuous portions of the railings, sidewalks, and median barriers.

- In the absence of other criteria, the deflection limit for vehicular loads may be considered as Span/800 for steel, aluminum, and/or concrete vehicular bridges.

The AASHTO LRFD Specifications (AASHTO 2020) Article 3.6.1.3.2 (Loading for Optional Live Load Deflection Evaluation) states that if the optional live load-deflection criteria specified in Article 2.5.2.6.2 is invoked, the deflection should be taken as the larger of (a) that resulting from the design truck alone, or (b) that resulting from 25 percent of the design truck taken together with the design lane load.

3.2.3 Concrete Stress Limits

Compressive stress limits at different stages were considered based on the criteria provided in the AASHTO LRFD Specifications (AASHTO 2020) Article 5.9.2.3, while tensile stress limits at different stages were considered as 85 percent of the elastic tensile strength based on direct tension testing (Graybeal 2019). In this section, all tensile stresses and allowable tensile stress limits use a positive sign convention, while all compressive stresses and allowable compressive stress limits use a negative sign convention. All loads are factored using the load factors provided in the AASHTO LRFD Specifications (AASHTO 2020) Table 3.4.1-1 for the Service I or Service III load combinations, as applicable. The Service I load combination uses a load factor $\gamma = 1.0$ for all dead and live loads, while the Service III load combination uses a load factor $\gamma = 0.8$ for live loads.

3.2.3.1 Compressive Stresses at Release

The compressive stress calculation at release considers the initial prestressing stress due to the applied prestressing force together with the elastic shortening loss, which results in an effective prestressing stress just after transfer of $f_{pe0} = f_{pi} - \Delta f_{pES}$, where f_{pi} is the prestressing steel stress immediately prior to transfer, and Δf_{pES} is the prestress loss due to elastic shortening. The prestressing steel stress prior to transfer, also referred to as jacking stress f_{pi}, is limited to $0.75 f_{pu}$, where f_{pu} is the specified tensile strength of the prestressing strands (TxDOT 2021). Compression stresses were calculated using the Service I load combination provided in the AASHTO LRFD Specifications (AASHTO 2020) Table 3.4.1-1. Article 5.9.2.3.1a specifies the compressive stress limit for pretensioned and post-tensioned components before losses as $0.65 f'_{ci}$. The stress limit

state for concrete compressive stresses at release gives the following design inequality for the stress check of the extreme bottom fiber of the girder a transfer length away from the girder's end.

$$-\frac{A_{ps}f_{pe0}}{A_g}-\frac{A_{ps}f_{pe0}e_{pg}}{S_b}+\frac{M_{Dt}}{S_b}\geq -0.65f'_{ci} \tag{3.2}$$

where:

A_{ps} = Total area of prestressing steel, in^2

f_{pe0} = Effective stress in prestressing steel just after release $= f_{pi}-\Delta f_{pES}$, ksi

f_{pi} = Prestressing steel stress immediately prior to transfer $= 0.75f_{pu}$, ksi

A_g = Cross-sectional area of the girder, in^2

e_{pg} = Eccentricity of prestressing force with respect to centroid of the girder, in.

S_b = Section modulus with respect to the extreme bottom fiber of the noncomposite girder section, in^3

M_{Dt} = Moment due to self-weight of the girder taken at a distance equal to the transfer length from the girder end, kip-in.

f'_{ci} = Specified compressive strength of concrete at the time of prestress release, ksi.

3.2.3.2 Tensile Stresses at Release

Similarly, tensile stress calculations are conducted using the effective stress after prestress loss due to elastic shortening and using the load factors based on the Service I load combination provided in Table 3.4.1-1 (AASHTO 2020). However, the tensile stress limit is taken as 85 percent of the specified elastic (first cracking) tensile strength of the concrete at the time of release that is measured from direct tension tests (Graybeal 2019). The stress limit state for concrete tensile stresses at release gives the following design inequality for the stress check at the extreme top fiber of the girder at a distance equal to the transfer length from the girder end.

$$-\frac{A_{ps}f_{pe0}}{A_g}+\frac{A_{ps}f_{pe0}e_{pg}}{S_t}-\frac{M_{Dt}}{S_t}\leq 0.85f'_{ti} \quad (3.3)$$

where:

S_t = Section modulus for the extreme top fiber of the noncomposite girder, in^3

f'_{ti} = Specified elastic tensile strength of concrete at the time of release, ksi

3.2.3.3 Compressive Stresses during Deck Placement

The AASHTO LRFD Specifications (AASHTO 2020) Table 5.9.2.3.2a-1 provides the compressive stress limit at SLS after losses due to effective prestress and permanent (dead) loads as $0.45f'_c$. Compressive stresses during deck placement were calculated using the effective prestress after losses, the noncomposite girder section properties, and the Service I load combination provided in the AASHTO LRFD Specifications (AASHTO 2020) Table 3.4.1-1. The stress limit state for concrete compressive stresses after losses during deck placement is then based on the following design inequality for the stress check at the midspan extreme top fiber of the girder.

$$-\frac{A_{ps}f_{pe}}{A_g}+\frac{A_{ps}f_{pe}e_{pg}}{S_t}-\frac{M_g+M_s+M_h}{S_t}\geq -0.45f'_c \quad (3.4)$$

where:

f_{pe} = Effective stress in prestressing steel after losses, ksi

S_t = Section modulus with respect to the extreme top fiber of the noncomposite girder section, in^3.

M_g = Moment at midspan due to self-weight of the girder, kip-in.

M_s = Moment at midspan due to weight of the deck slab, kip-in.

M_h = Moment at midspan due to weight of the haunch, kip-in.

f'_c = Specified compressive strength of concrete at 28 days, ksi

3.2.3.4 Tensile Stresses during Deck Placement

Tensile stresses were calculated for the noncomposite girder section using the effective prestress after losses and the permanent (dead) loads at the time of deck placement with the Service I load combination provided in the AASHTO LRFD Specifications (AASHTO 2020) Table 3.4.1-1.

Based on the recommendations provided by Graybeal (2019), 85 percent of the specified elastic (first cracking) tensile strength of the concrete at the time of release was used instead of the AASHTO LRFD Specifications (AASHTO 2020) tensile stress limit after losses. The tensile stress limit after losses during deck placement was taken as 85 percent of the specified elastic (first cracking) tensile strength of the concrete at 28 days measured from direct tension tests. The following design inequality is used to check the stress limit for concrete tensile stresses during deck placement at the midspan extreme bottom fiber of the girder.

$$-\frac{A_{ps}f_{pe}}{A_g}-\frac{A_{ps}f_{pe}e_{pg}}{S_b}+\frac{M_g+M_s+M_h}{S_b}\leq 0.85f_t' \tag{3.5}$$

where:

f_t' = Specified elastic tensile strength of concrete at 28 days, ksi

3.2.3.5 Compressive Stresses at Service Limit State after Losses

Compressive stresses were calculated for the composite section using the effective prestress after losses and the Service I load combination provided in the AASHTO LRFD Specifications (AASHTO 2020) Table 3.4.1-1. The AASHTO LRFD Specifications (AASHTO 2020) Table 5.9.2.3.2a-1 provides two separate compressive stress limits for the SLS after losses depending on the loading condition: (1) the compressive stress limit due to the sum of effective prestress and permanent (dead) loads shall be taken as $0.45f_c'$; (2) the compressive stress limit due to the sum of effective prestress, permanent loads, and transient loads as well as during shipping and handling shall be taken as $0.60\phi_w f_c'$, where ϕ_w is the reduction factor for the slenderness effect of the web and flanges (taken as 1.0 if the slenderness ratios are smaller than 15.0). The two stress limit states for concrete compressive stresses after losses at the final load stage gives the following design inequalities for the stress check at the extreme top fiber of the girder at midspan:

$$-\frac{A_{ps}f_{pe}}{A_g}+\frac{A_{ps}f_{pe}e_{pg}}{S_t}-\frac{M_g+M_s+M_h}{S_t}-\frac{M_{ws}+M_r}{S_{tg}}\geq -0.45f_c' \quad (3.6)$$

where:

S_{tg} = Section modulus with respect to the extreme top fiber of the girder calculated for the composite section, in^3

M_{ws} = Moment at midspan due to weight of the wearing surface, kip-in.

M_r = Moment at midspan due to weight of the railing, kip-in.

$$-\frac{A_{ps}f_{pe}}{A_g}+\frac{A_{ps}f_{pe}e_{pg}}{S_t}-\frac{M_g+M_s+M_h}{S_t}-\frac{M_{ws}+M_r+M_L}{S_{tg}}\geq -0.60f_c' \quad (3.7)$$

where:

M_L = Moment at midspan due to live loads, kip-in.

3.2.3.6 Tensile Stresses at Final

Tensile stresses were calculated for the composite section using the effective prestress after losses and the Service III load combination provided in the AASHTO LRFD Specifications (AASHTO 2020) Table 3.4.1-1. The difference between the Service I and Service III load combinations is that the Service III load combination uses a 0.8 load factor for live loads. The tensile stress limit after losses at the final load stage was taken as 85 percent of the specified elastic (first cracking) tensile strength measured from direct tension tests of the concrete at 28 days (Graybeal 2019). The stress limit state for concrete tensile stresses after losses at the final load stage gives the following design inequality for the stress check at the midspan extreme bottom fiber of the girder.

$$-\frac{A_{ps}f_{pe}}{A_g}-\frac{A_{ps}f_{pe}e_{pg}}{S_b}+\frac{M_g+M_s+M_h}{S_b}+\frac{M_{ws}+M_r+0.8M_L}{S_{bc}}\leq 0.85f_t' \quad (3.8)$$

where:

S_{bc} = Section modulus with respect to the extreme bottom fiber of the girder calculated for the composite section, in^3

3.3 FATIGUE LIMIT STATE

The AASHTO LRFD Specifications (AASHTO 2020) Article 5.5.3 provides specifications for checking the fatigue in prestressed components. Fatigue checks are not required for the

reinforcement in prestressed components that are designed to have tensile stresses due to the Service III load combination within the tensile stress limit for concrete at SLS after losses.

The AASHTO LRFD Specifications (AASHTO 2020) specifies the stress limit for concrete compressive stresses due to the Fatigue I load combination and one-half of the sum of the unfactored effective prestress and permanent loads as $0.4f_c'$ after losses. The stress limit state for concrete compressive stresses after losses at the final load stage gives the following design inequality for the stress check at the midspan extreme top fiber of the girder.

$$\frac{1}{2}\left(-\frac{A_{ps}f_{pe}}{A_g}+\frac{A_{ps}f_{pe}e_{pg}}{S_t}-\frac{M_g+M_s+M_h}{S_t}-\frac{M_{ws}+M_r}{S_{tg}}\right)-\frac{1.75M_L}{S_{tg}}\geq -0.40f_c' \qquad (3.9)$$

3.4 STRENGTH LIMIT STATE

The appropriate design methodologies specified in the AASHTO LRFD Specifications (AASHTO 2020) have been partially adopted, along with the design guidelines developed by Graybeal (2008) for calculating the flexural resistance of UHPC sections. The AFGC Guidelines (AFGC 2013) were used for computing the shear resistance of UHPC sections. The reduced nominal resistance was calculated as the product of nominal resistance multiplied by the resistance factors provided in the AASHTO LRFD Specifications (AASHTO 2020) Article 5.5.4.2. The resistance factor ϕ for tension-controlled prestressed concrete members with bonded strands is taken as 1.0.

All loads are factored using the load factors γ provided in the AASHTO LRFD Specifications (AASHTO 2020) Table 3.4.1-1 for the Strength I load combination. Load factors for the Strength I load combination are listed below:

γ_{DC} = Load factor for dead load of structural components = 1.25
γ_{DW} = Load factor for dead load of wearing surface and utilities = 1.50
γ_{LL} = Load factor for vehicular live load = 1.75

3.4.1 Flexural Resistance at Strength Limit State

The uniaxial stress-strain behavior of UHPC is significantly different than the CC because the shape of the compression zone is closer to a triangular stress block rather than a rectangular one. Therefore, the rectangular stress block assumption for the compression region may not be

appropriate. In addition, the flexural resistance calculations for CC neglects the concrete contribution in the tension zone for simplifying the analysis, while UHPC exhibits significant sustained tensile strength prior to tensile failure (Graybeal 2008).

The nominal flexural resistance of UHPC girders was calculated using the design guidelines provided by Graybeal (2008), which is similar to the methodology provided in the AFGC Guidelines (AFGC 2013). The recommended approximate uniaxial stress-strain response of the UHPC section must satisfy the following criteria:

1. Compressive strength corresponds to 85 percent of the specified compressive strength of the UHPC.
2. Tensile strength corresponds to 50 percent of the specified sustained post-cracking tensile strength of UHPC. (UHPC should maintain the post-cracking tensile strength at least up to a strain of 0.007 in./in. based on direct tension tests.)
3. Limiting tensile strain of 0.007 in./in is used, such that the tensile strength is neglected for higher strain values.

Figure 3.1 shows a graphical representation of the proposed stress-strain behavior and corresponding strain diagram for a composite UHPC I-girder and CC deck slab section. The resistance factor ϕ for calculating flexural resistance is taken as 1.0.

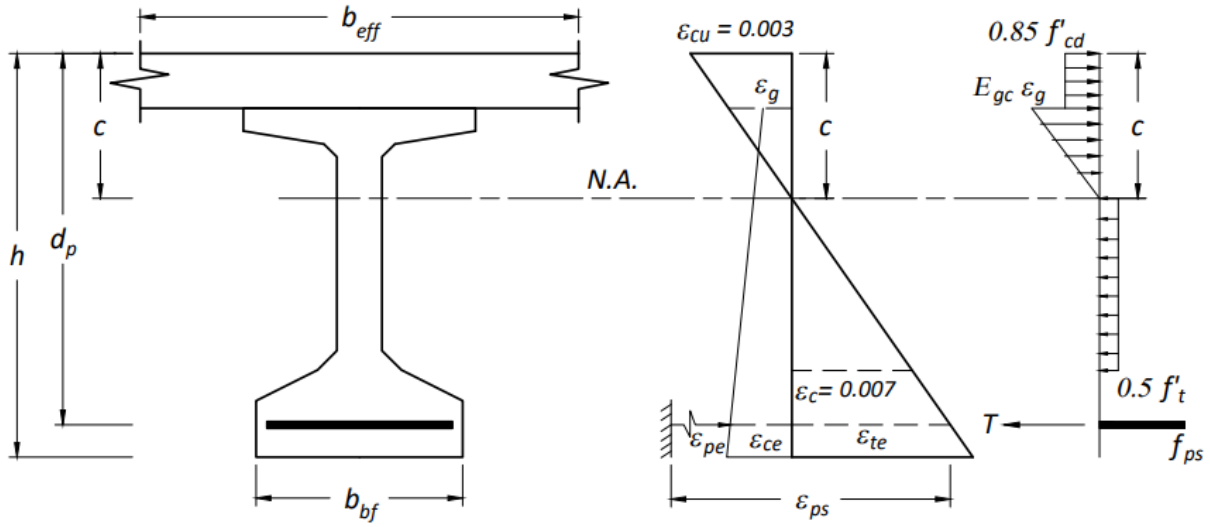

Figure 3.1. Typical Strain Diagram and Stress Distribution for a Composite Section with Prestressing Strands.

In Figure 3.1 the parameters are defined as follows:

b_{eff} = Effective width of the deck slab, in.

c = Distance from the extreme compression fiber to the neutral axis, in.

d_p = Distance from the extreme compression fiber to the centroid of the prestressing strands, in.

h = Overall depth of the member, in.

b_{bf} = Width of the bottom flange, in.

ε_{cu} = Failure strain of deck concrete in compression, in./in.

ε_g = Concrete strain at the top fiber of the girder, in./in.

ε_{pe} = Strain in the prestressing strands due to the effective prestressing force, in./in.

ε_{ce} = Decompression strain (tension strain in prestressing needed to reduce the compression strain in the concrete at the centroid of the prestressing to zero), in./in.

ε_{te} = Tensile strain in concrete at the centroid of the prestressing strands beyond the decompression strain and up to nominal conditions for flexure, in./in.

ε_{ps} = Strain in prestressing steel corresponding to the nominal flexural resistance of the member, in./in.

E_{gc} = MOE of the girder concrete, ksi

f_{ps} = Average stress in prestressing steel corresponding to the nominal flexural resistance of the member, ksi

3.4.2 Shear Resistance at Strength Limit State

The ultimate shear resistance of UHPC considers the contribution of the steel fibers in addition to the shear strength attributed to the concrete and reinforcing steel as follows:

$$V_{Rd} = V_{Rd,c} + V_{Rd,s} + V_{Rd,f} \tag{3.10}$$

where:

$V_{Rd,c}$ = Concrete term, kips

$V_{Rd,s}$ = Shear reinforcement term, kips

$V_{Rd,f}$ = Fiber contribution term, kips

The AFGC Guidelines (AFGC 2013) explains the contribution of each component, and Equations (2.15) to (2.22) documented in Chapter 2 provide these relationships.

3.5 DESIGNS FOR 5SB15 SLAB BEAMS

One of the longest possible span lengths using 5SB15 slab beams was selected from the TxDOT standard bridge drawings as the base bridge geometry to allow comparison of UHPC designs. The bridge geometry, material properties (except the concrete compressive strength of the slab beams), and section properties were kept the same as the selected standard slab beam design. The following research questions are addressed by investigating the following design objectives:

1. Is it possible to achieve a 60 ft span length for a 30 ft wide bridge using six 5SB15 UHPC slab beams? What would be the required concrete compressive strength at release and at 28 days to achieve this span length?
2. Is it possible to achieve a 70 ft span length for a 30 ft wide bridge using six 5SB15 UHPC slab beams? What would be the required concrete compressive strength at release and at 28 days to achieve this span length?

3. What is the maximum achievable span length for a 30 ft wide bridge using 5SB15 UHPC slab beams with a 14 ksi compressive strength at release and a 22 ksi compressive strength at 28 days?

Note that the design elastic tensile strength from direct tension testing of UHPC was assumed to be 0.75 ksi at release and 1.0 ksi at 28 days for all design cases based on values obtained from the literature (Graybeal 2006a; Haber et al. 2018; Wille et al. 2014a; Wille et al. 2014b). The empirical square root relation between tensile strength and compressive strength is different from CC. Currently, limited data are available to derive such a relationship; thus, design tensile strength based on direct tension testing is considered. The tensile stress limit is taken as 85 percent of the elastic tensile strength based on the material reduction factor in tension recommended by Graybeal (2019).

3.5.1 Geometry of Slab Beam Bridge

Figure 3.2 shows the cross-sectional details of the selected prestressed bridge using 5SB15 slab beams. Six 5SB15 PCSB are spaced at 5 ft ¼ in. on center across a 30 ft 1 in. overall bridge width topped with 5 in. CIP reinforced concrete deck slab. An average 2 in. constant haunch thickness was assumed along the entire span length as part of permanent dead loads. However, the haunch contribution to stiffness of the composite section was neglected because the haunch thickness varies along the length and may be very small at the midspan. The assumed superimposed dead loads consist of an average 2 in. thick asphalt overlay and T551 rails, one of the heaviest railing types used by TxDOT. The weight of the rails was distributed to three girders closest to each of the bridge's edges, as recommended by the *TxDOT Bridge Design Manual* (TxDOT 2021). Table 3.1 summarizes these key geometric design parameters for the selected typical standard bridge cross-section using 5SB15 prestressed slab beams.

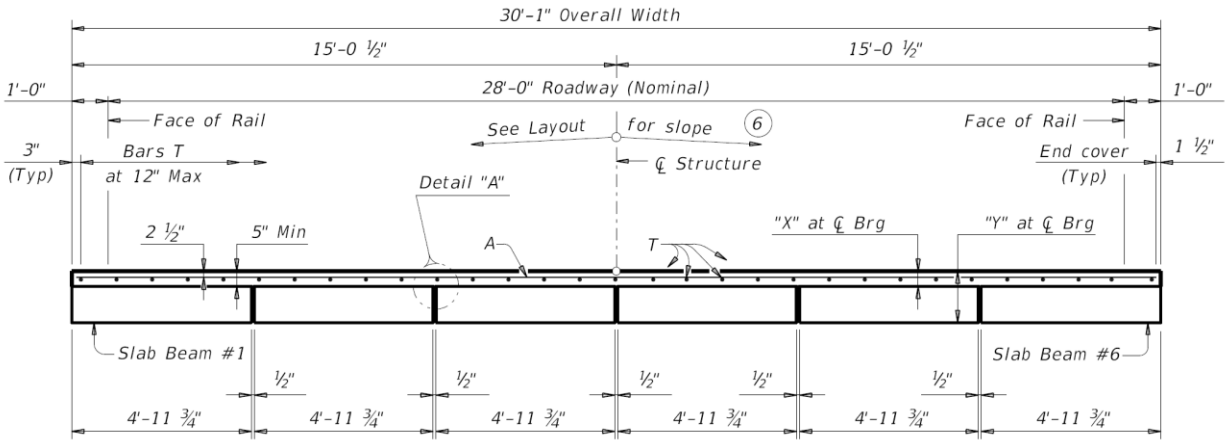

Figure 3.2. Typical Bridge Cross-Section Using 5SB15 Slab Beams (TxDOT 2019).

Table 3.1. Geometric Properties of 5SB15 Slab Beam Bridge.

Parameter	Description/Value
Bridge Width, W	30'-1"
Girder Spacing, S	5'-0¼"
Number of Girders, n	6
Deck Thickness, t_s	5 in.
Wearing Surface Thickness, t_{ws}	2 in. asphalt
Haunch Thickness, t_h	2 in. for weight calculation only
Railing	T551 (0.382 kip/ft)

3.5.2 Girder Details and Section Properties of 5SB15 Slab Beam Girder

Figure 3.3 shows geometric and reinforcement details and the strand layout of the standard 5SB15 prestressed slab beam girder. The 4 ft 11¾ in. wide and 15 in. deep 5SB15 slab beams can hold a maximum of 56 strands located at the bottom two rows of a 2 × 2 in. grid. Section properties of the noncomposite 5SB15 slab beam girder, including area, centroid location, moment of inertia, and the weight per unit length, were calculated based on the standard cross-section geometry. Table 3.2 lists the calculated section properties that are consistent with the values provided in the structural drawing files from *TxDOT Bridge Standards* (TxDOT 2019).

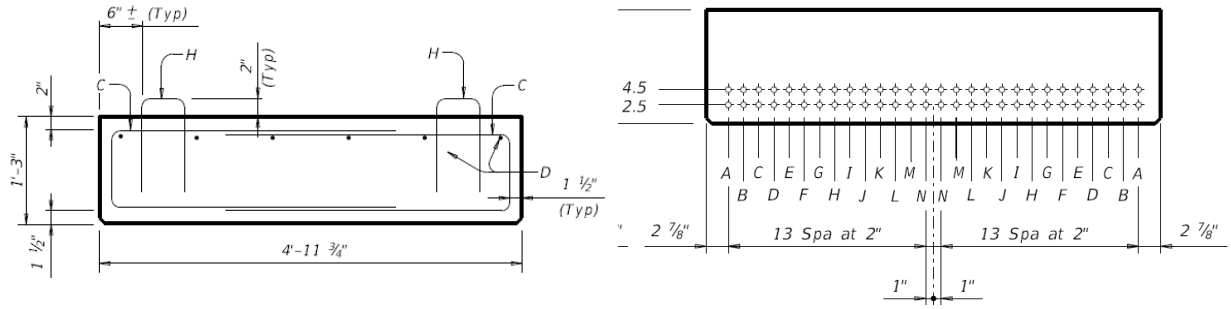

(a) Reinforcement details *(b) Strand layout*

Figure 3.3. Section Geometry of 5SB15 Slab Beam.

Table 3.2. Section Properties of 5SB15 Slab Beam.

Parameter	Value
Area, A (in^2)	896.25
Centroid Distance from Top, y_t (in.)	7.5
Centroid Distance from Bottom, y_b (in.)	7.5
Moment of Inertia, I_g (in^4)	16,805
Girder Weight, w_g (kip/ft)	0.996

Note: Unit weight of the UHPC slab beam girder with reinforcement is taken as 0.160 kcf.

3.5.3 Material Properties for Slab Beam Bridges

Table 3.3 lists the material properties used for the design of 5SB15 prestressed slab beam bridges that were kept the same for all alternative design cases investigated in this study. The unit weight of concrete for the CC deck was taken as 0.145 kcf to compute the MOE, while the unit weight of conventional deck concrete with reinforcement was considered to be 0.150 kcf to compute the dead load of the deck slab. The unit weight of UHPC is 0.155 kcf (Graybeal 2006a), which is slightly higher than CC due to the presence of fibers. Therefore, the unit weight of the UHPC slab beam with reinforcement was taken as 0.165 kcf.

The design compressive strength of CIP deck concrete was taken as 4 ksi based on the structural drawings provided in the *TxDOT Bridge Standards* (TxDOT 2019). Design compressive and tensile strengths of UHPC slab beams at release and at 28 days are key properties for the design of prestressed concrete girders. Allowable stress design criteria for CC only considers the design compressive strength as a parameter, and tensile stress limits are typically calculated using empirical square root relationships between compressive and tensile strength. However, for

UHPC, the tensile strength is not formulated as a function of compressive strength; therefore, the design tensile strengths at release and at 28 days were considered based on common values in the literature. The concrete tensile strength of UHPC slab beams was assumed to be 0.75 ksi at release and 1.0 ksi at service, and kept the same for all alternative UHPC design cases, whereas the concrete compressive strengths of UHPC slab beams at release and at 28 days were kept as a variable for different design cases, which are listed in the following subsection. For the cases that determine the maximum achievable span length, the compressive strength of UHPC slab beams was taken as 14 ksi at release and 22 ksi at service.

The AASHTO LRFD Specifications (AASHTO 2020) Article 5.4.2.4 provides an empirical relationship for calculating the MOE of normal weight concrete, with a design compressive strength up to 15 ksi and with unit weight between 0.090 and 0.155 kcf, as given in Equation (3.11). This equation was used to compute the MOE of the CIP deck concrete E_{cd}.

$$E_{cd} = 120{,}000 K_1 w_c^{2.0} {f'_{cd}}^{0.33} \tag{3.11}$$

where:

E_{cd} = MOE of concrete, ksi

K_1 = Correction factor for source of aggregate, to be taken as 1.0 unless determined by physical testing

w_c = Unit weight of CC = 0.145 kcf

f'_{cd} = Compressive strength of deck concrete, ksi

The MOE expression provided in the AASHTO LRFD Specifications (AASHTO 2020) is limited to concrete compressive strengths up to 15 ksi and thus should not be used for UHPC. Graybeal (2014) provided a MOE expression—shown in Equation (3.12)—for UHPC that was developed based on the test results of steel fiber-reinforced UHPC with compressive strengths between 14 and 26 ksi. Therefore, the following empirical relationship was used for calculating the MOE of UHPC girders E_{cg}:

$$E_c = 1550\sqrt{f_c'} \quad (3.12)$$

where:

E_c = MOE of UHPC, ksi

f_c' = Compressive strength of UHPC, ksi

The MOE of the prestressed UHPC girders can be much higher than the MOE of the CIP deck concrete. Therefore, transformed section properties of the composite deck-girder section are calculated using the modular ratio between the prestressed UHPC girder and CIP deck slab. The modular ratio is $\eta = E_{cg}/E_{cd}$.

Table 3.3. Material Properties for 5SB15 Slab Beam Bridges.

Parameter	Description/Value
Compressive strength of deck concrete, f_{cd}'	4.0 ksi
Elastic tensile strength of UHPC girder at release, f_{ti}'	0.75 ksi
Elastic tensile strength of UHPC girder at 28 days, f_t'	1.0 ksi
Compressive strength of UHPC girder at release, f_{ci}'	14 ksi or varies*
Compressive strength of UHPC girder at 28 days, f_c'	22 ksi or varies*
Unit weight of CC (used to compute E_{cd}), γ_{cc}	0.145 kcf
Unit weight of CC with reinforcement (to compute dead load of deck)	0.150 kcf
Unit weight of UHPC (used to compute E_{cg}), γ_{UHPC}	0.155 kcf
Unit weight of UHPC slab beam with reinforcement (to compute dead load of beam)	0.165 kcf
Unit weight of asphalt overlay, γ_{ws}	0.140 kcf
Weight of T551 rail, w_r	0.382 klf (dist. to 3 girders)
Ultimate strength of prestressing strands, f_{pu}	270 ksi
MOE of prestressing strands, E_{ps}	28,500 ksi

*Varies for the design cases that consider a target span length and corresponding required UHPC strength.

3.5.4 Alternative Design Cases for Slab Beam Bridges

Table 3.4 provides the main design parameters for the alternative design cases explored for the prestressed UHPC slab beam bridges. Three design cases were explored, as follows:

- Case 1 determines the required UHPC slab beam f_{ci}' and f_c' for a target span length of 60 ft, which is 20 percent longer than what the conventional slab beam girder can achieve.

- Case 2 determines the required UHPC slab beam f'_{ci} and f'_c for a target span length of 70 ft, which is 40 percent longer than what the conventional slab beam girder can achieve.
- Case 3 explores the maximum achievable span length based on the specified compressive and tensile strength of UHPC slab beams.

For all three design cases, bridge width, girder spacing, number of girders, deck thickness, and elastic tensile strength of UHPC slab beams are kept constant.

Table 3.4. Main Design Parameters for Alternative Designs Using 5SB15 Girders.

Parameter	CC-TxDOT	UHPC-Case 1	UHPC-Case 2	UHPC-Case 3
Span Length (ft)	50	**60**	**70**	**Maximum**
Bridge Width	30'-1"	30'-1"	30'-1"	30'-1"
Girder Spacing	5'-0¼"	5'-0¼"	5'-0¼"	5'-0¼"
Number of Girders	6	6	6	6
Overhang	2'-5⅞"	2'-5⅞"	2'-5⅞"	2'-5⅞"
Deck thickness (in.)	5.0	5.0	5.0	5.0
Span/Depth Ratio	30	36	42	TBD
f'_{ci} (ksi)	4.0	TBD	TBD	14
f'_c (ksi)	5.0	TBD	TBD	22
f'_{ti} (ksi)	–	0.75	0.75	0.75
f'_t (ksi)	–	1.0	1.0	1.0
Strand Diameter (in.)	0.6	0.6	0.6	0.6 or 0.7
Number of Strands	22	TBD	TBD	TBD
Debonded Strands	6	TBD	TBD	TBD

Notes:
1. CC-TxDOT (TxDOT 2019) indicates CC for comparison
2. – : Not available
3. TBD = To Be Determined

3.5.5 Flexural Stress Design at Service Limit State for Slab Beam Bridges

The three alternative design cases listed in the previous section were investigated using the design methodology described in Sections 3.2 and 3.3 to determine the optimum number of strands and maximum achievable span length.

Figure 3.4 shows an example chart in which the curves shown with solid lines indicate a lower bound eccentricity solution for the limit state considered and the physical limits of the girder geometry. The considered SLSs include the following:

- The SLSs for allowable tensile and compressive stresses at *release*, which produce upper bound eccentricity solutions.
- The allowable tensile and compressive stresses for flexure at the *time of deck casting* and at *service*.
- The *fatigue* limit state for allowable compressive stress at service.
- The allowable tensile and compressive stresses at release when some strands are debonded (included for the cases that requires debonding).

For all the analyzed cases, the service tension stress limit and tension stress limit at release (sometimes with debonding) control the solution domain. The optimum eccentricity and number of strands is indicated by a red asterisk.

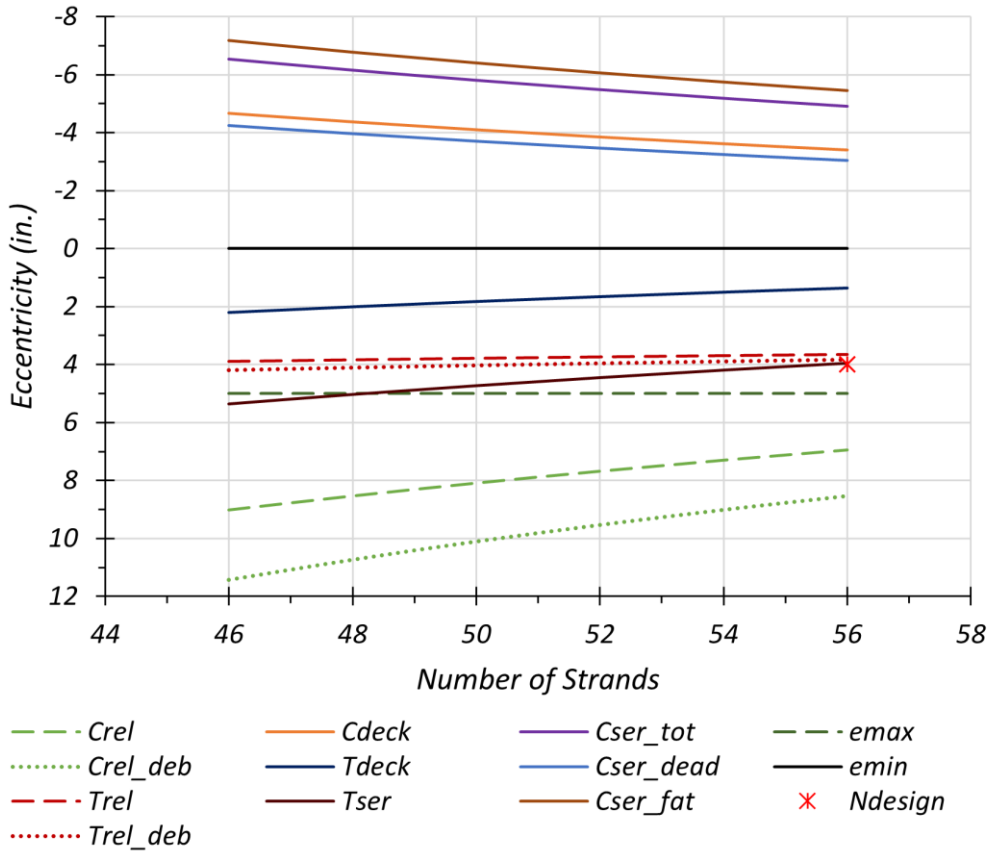

Notes:

1. Solid lines = minimum eccentricity, dashed lines = maximum eccentricity
2. Allowable stress limits at release after elastic shortening losses at the end of transfer length:
   Crel = Compression stress limit = $0.65f'_{ci}$
   Trel = Tension stress limit = $0.85f'_{ti}$
   Crel_deb = Compression stress limit when some of the strands are debonded = $0.65f'_{ci}$
   Trel_deb = Tension stress limit when some of the strands are debonded = $0.85f'_{ti}$
3. Allowable stress limits at the time of deck placement after losses for the noncomposite girder:
   Cdeck = Compression stress limit at midspan = $0.45f'_c$
   Tdeck = Tension stress limit at midspan = $0.85f'_t$
4. Allowable stress limits at service after losses for the composite girder at midspan:
   Cser_tot = Compression stress limit for stresses due to total load plus effective prestress = $0.60f'_c$
   Cser_dead = Compression stress limit for stresses due to effective prestress plus permanent (dead) loads = $0.45f'_c$
   Cser_fat = compression stress limit for stresses due to Fatigue I live loads plus one-half of the sum of stresses due to prestress and permanent (dead) loads = $0.40f'_c$
   Tser = tension stress limit considering Service III load combination = $0.85f'_t$
5. Physical limits due to girder geometry:
   emax = Maximum possible eccentricity based on the cg of the section
   Emin = Minimum eccentricity considered to be fully concentric prestress
6. *Ndesign* = Selected number of strands and corresponding eccentricity

Figure 3.4. Sample Eccentricity Solution Domain for UHPC 5SB15 Girders—70 ft Bridge.

3.5.5.1 Case 1 Design

Figure 3.5 shows the solution domain for the feasible eccentricity based on the eight limit states considered. The Case 1 design uses the same bridge cross-section as one of the current TxDOT standard designs (CC-TxDOT in Table 3.4) and explores the possibility of extending the span length to 60 ft, compared to 50 ft when CC is used. Researchers investigated this design case to find the optimum number of strands and required concrete compressive strength to achieve the target span length. It is possible to achieve a 60 ft span length by using 40 strands with four in. eccentricity using compressive strength at release $f'_{ci} = 7.0$ ksi and compressive strength at service $f'_c = 12.0$ ksi.

Figure 3.6 shows the strand layout for a standard 5SB15 slab beam girder where the green filled locations show the 40 strands used for the Case 1 design to achieve a 60 ft span length. The applied prestressing force using 40 strands and a 4 in. eccentricity for a 60 ft span causes a 3.3 in. camber for the noncomposite girder just before deck placement, which was assumed to be at 40 days. The camber calculations consider the creep effect using the empirical creep equations provided in the AASHTO LRFD Specifications (AASHTO 2020) at 40 days and a 1 day release. The camber of the noncomposite girder just after deck placement was calculated to be 2.1 in. under the weight of deck concrete.

Live load deflections were also calculated and compared to the optional live load-deflection limit using the optional deflection check criteria provided in Section 3.2.2 of this report. Live load deflections were calculated to be 0.99 in., while the live load-deflection limit is 0.87 in. The estimated live load deflections are 14 percent higher than the limit values using the optional deflection check.

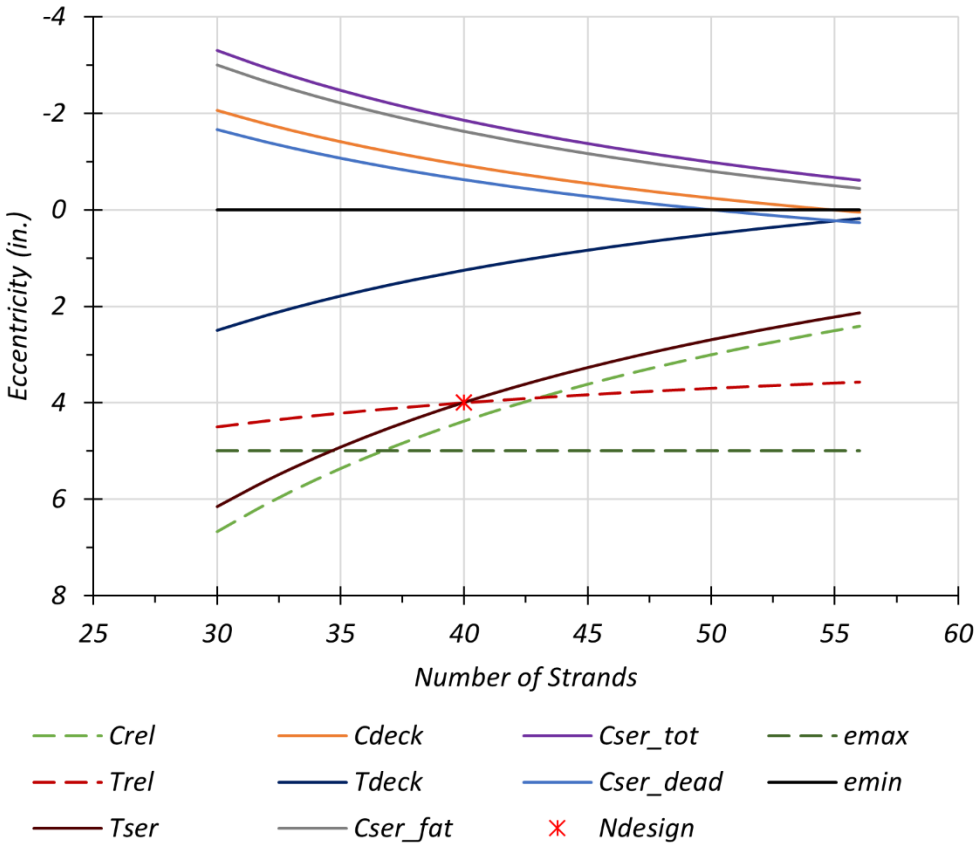

Notes:

1. Solid lines = minimum eccentricity, dashed lines = maximum eccentricity
2. $f'_{ci} = 7.0$ ksi, $f'_c = 12.0$ ksi

Figure 3.5. Eccentricity Solution Domain for UHPC 5SB15 Girders—60 ft Bridge.

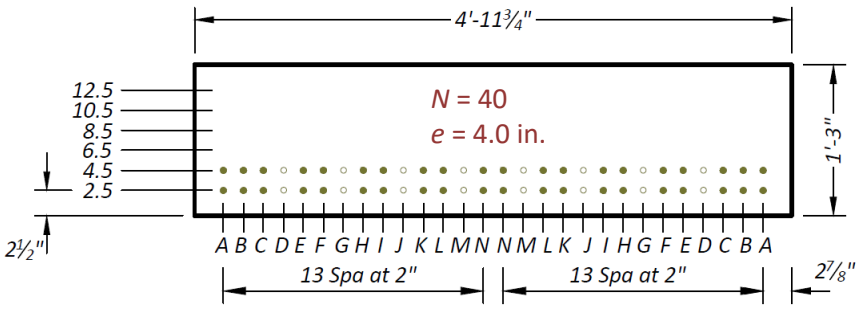

Notes:

1. N = Number of strands, e = eccentricity
2. Camber = 3.3 in. just before deck placement, Camber = 2.1 in. just after deck placement

Figure 3.6. Optimum Strand Design for UHPC 5SB15 Girders—60 ft Bridge.

3.5.5.2 Case 2 Design

Figure 3.7 shows the eccentricity solution domain for a 70 ft bridge based on the eight limit states considered. The Case 2 design uses the same bridge cross-section as one of the current TxDOT standard designs (CC-TxDOT in Table 3.4) and explores the possibility of extending the span length to 70 ft, as opposed to 50 ft when CC is used. Researchers investigated this design case to find the optimum number of strands and required concrete compressive strength to achieve the target span length. The tensile stress limit at release at the girder ends (red dashed line) requires a smaller eccentricity than the minimum eccentricity required to satisfy the tensile stress limit at service at the girder midspan (maroon solid line). Therefore, it is not possible to achieve a 70 ft span length without debonding. It is possible to achieve a 70 ft span length by using 56 strands and debonding eight strands from the bottom row up to 3 ft and using a compressive strength at release of $f'_{ci} = 14.0$ ksi and a compressive strength at service of $f'_c = 22.0$ ksi. The proposed strand layout results in a 4 in. midspan eccentricity and a 3.83 in. end eccentricity.

Figure 3.8 shows the strand layout for a standard 5SB15 slab beam girder in which the green filled locations show straight bonded strands and orange filled locations show the straight strands debonded up to 3 ft from both ends. All 56 strand locations were used for the Case 2 design to achieve 70 ft span length. The applied prestressing force using 56 strands with a 4 in. midspan eccentricity for a 70 ft span causes a 4.1 in. camber for the noncomposite girder just before deck placement, which was considered to be at 40 days. The camber calculations consider the creep effect using the AASHTO LRFD Specifications' (AASHTO 2020) empirical creep equations for a 40-day-old girder when the prestress is applied at one day. The camber of the noncomposite girder just after deck placement was calculated to be 2.4 in. due to the additional weight of the deck concrete.

Live load deflections were calculated using the optional deflection check criteria provided in Section 3.2.2 of this report and compared with the optional live load-deflection limit. Live load deflections were calculated to be 1.4 in., while the live load-deflection limit is 1.0 in. The estimated live load deflections are 40 percent higher than the limit values based on optional deflection check provided in the AASHTO LRFD Specifications (AASHTO 2020).

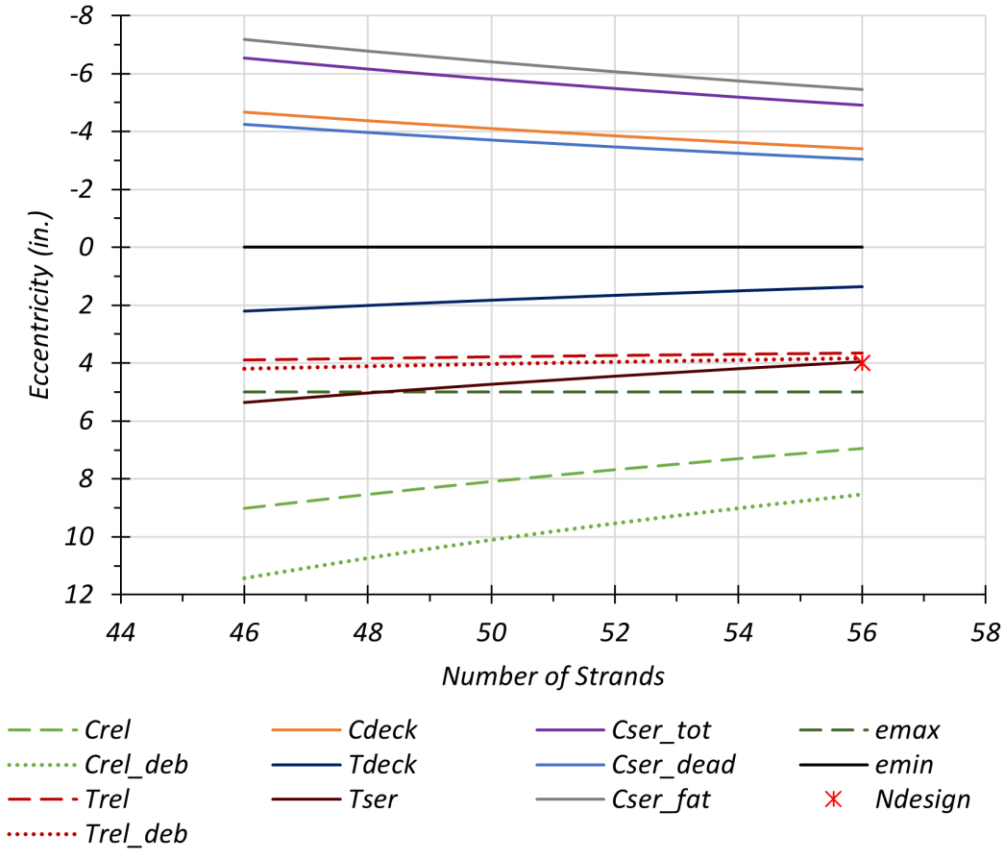

Notes:

1. Solid lines = minimum eccentricity, dashed lines = maximum eccentricity
2. $f'_{ci} = 14.0$ ksi, $f'_c = 22.0$ ksi

Figure 3.7. Eccentricity Solution Domain for UHPC 5SB15 Girders—70 ft Bridge.

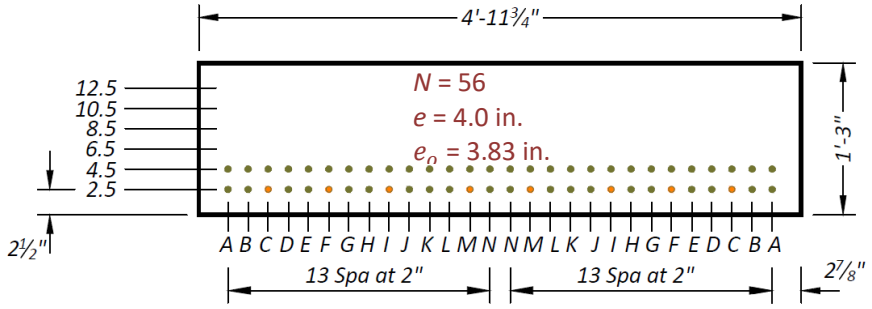

Notes:

1. N = Number of strands, e = eccentricity
2. Camber = 4.1 in. just before deck placement, Camber = 2.4 in. just after deck placement
3. 8 strands debonded at locations shown as orange fill

Figure 3.8. Optimum Strand Design for UHPC 5SB15 Girders—70 ft Bridge.

3.5.5.3 Case 3 Designs

Unlike the Case 1 and 2 designs, the Case 3 designs investigate the maximum achievable span length for target compressive strength at release of $f'_{ci} = 14.0$ ksi and a target compressive strength at service of $f'_c = 22.0$ ksi using an inverse design approach that calculates span length for given material properties. Figure 3.9 shows the maximum span length solution domains based on eight concrete stress limits. The optional deflection limit (green solid line) is also shown on the graphs but is not used as a limitation on the maximum achievable span length. For both designs using 0.6 in. or 0.7 in. strands, the optional deflection limit actually controls the design but is not applied in this investigation.

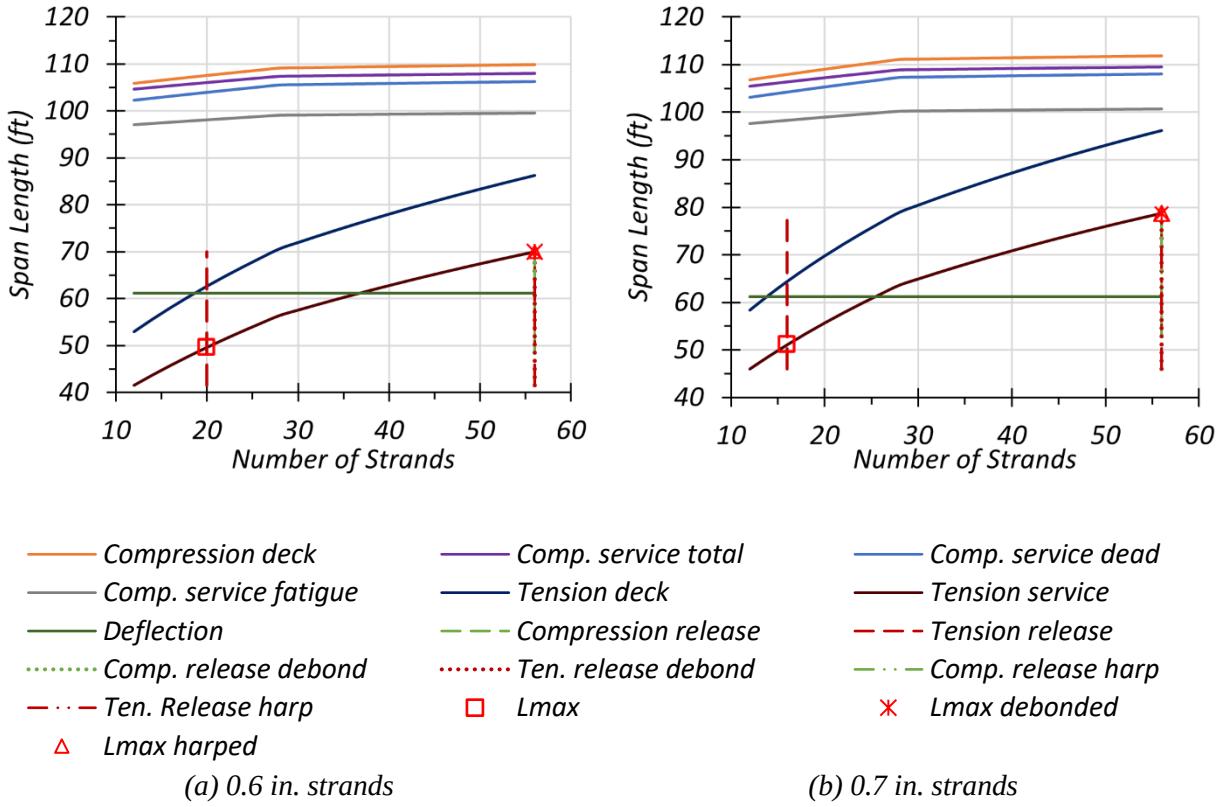

(a) 0.6 in. strands *(b) 0.7 in. strands*

Note: Solid lines = maximum span, dashed lines = maximum number of strands.

Figure 3.9. Span Length Solution Domain for UHPC 5SB15 Girder.

For 0.6 in. diameter strands (Figure 3.9a), the maximum achievable span length is 70 ft when eight strands are debonded or four strands are harped. This design case results in the same design as Case 2. It is necessary to debond or harp strands to satisfy the tensile stress limit at release at the

girder ends; otherwise, only 20 strands can be utilized, which means only a 50 ft span length can be achieved.

For 0.7 in. diameter strands (Figure 3.9b), the maximum achievable span length is 78 ft when 18 strands are debonded or 8 strands are harped. It is necessary to debond or harp to satisfy the tensile stress limit at release at the girder ends; otherwise only 16 strands can be utilized, and then only a 51 ft span length can be achieved.

Table 3.5 summarizes the maximum achievable span lengths, number of required strands, and debonding or harping information for different strand diameters. For the harped case, the hold-down points are taken as $L/20$ ft from the midspan of the girder.

Table 3.5. Maximum Achievable Span Length for UHPC 5SB15 Girders.

Strand Diameter (in.)	Total No. of Strands	No. of Debonded Strands	No. of Harped Strands	Maximum Achievable Span (ft)
0.6	20	0	0	50
	56	8	0	70
	56	0	4	70
0.7	16	0	0	51
	56	18	0	78
	56	0	8	78

Notes:
1. Debonded case using 0.6 in. strands: 8 strands up to 3 ft
2. Debonded case using 0.7 in. strands: 18 strands up to 3.5 ft and 4 strands up to 6.5 ft
3. Harped case: Hold-down point is at $L/20$ ft from the midspan

Optimum eccentricity and number of strand requirements were calculated like the Case 1 and Case 2 designs by using the maximum achievable span length values. Figure 3.10(a) shows the eccentricity solution domain for a 70 ft long bridge based on the eight limit states considered when 0.6 in. diameter strands are used. The tensile stress limit at release at the girder ends (red dashed line) requires a smaller eccentricity than the minimum eccentricity required to satisfy the tensile stress limit at service at the girder midspan (maroon solid line). Therefore, it is not possible to achieve a 70 ft span length without debonding. It is possible to achieve a 70 ft span length by using 56 strands and debonding 8 strands from the bottom row up to 3 ft. The proposed strand layout results in a 4 in. midspan eccentricity and a 3.83 in. end eccentricity. Figure 3.10(b) shows the eccentricity solution domain for a 78 ft long bridge based on the eight limit states considered when 0.7 in. diameter strands are used. Similarly, the tensile stress limit at release requires a smaller

eccentricity than the minimum eccentricity required to satisfy the tensile stress limit at service. Therefore, 18 strands debonded up to 3.5 ft and 6 strands debonded up to 6.5 ft are used. The proposed strand layout results in a 4 in. midspan eccentricity and a 3.95 in. end eccentricity.

Figure 3.11 shows the strand layout for a standard 5SB15 slab beam girder where the green filled locations show straight bonded strands and orange filled locations show the straight debonded strands from both ends. All 56 strand locations were used for both designs using 0.6 in. and 0.7 in. strands to achieve 70 ft and 78 ft span lengths, respectively. The camber calculations considered the creep coefficient using the AASHTO LRFD Specifications (AASHTO 2020) empirical creep equations for a 40-day-old girder when prestress is applied at one day. For the design case using 0.6 in. strands, the applied prestressing force using 56 strands and a 4 in. midspan eccentricity for a 70 ft span causes a 4.1 in. camber for a noncomposite girder just before deck placement. For the design case using 0.7 in. strands, the applied prestressing force using 56 strands and a 4 in. midspan eccentricity for a 78 ft span causes a 7.5 in. camber for a noncomposite girder just before deck placement. Table 3.6 lists the estimated camber results for both debonded and harped options for both design cases using 0.6 in. or 0.7 in. strands. It is possible to achieve more balanced deflections by having less initial camber when some strands are harped instead of using debonding.

Live load deflections were calculated using the optional deflection check criteria provided in Section 3.2.2 of this report and compared with the optional live load deflection limit. For the design case using 0.6 in. diameter strands, live load deflections were calculated to be 1.4 in., while the live load-deflection limit is 1.0 in. For the design case using 0.7 in. diameter strands, live load deflections were calculated to be 2.0 in., while the live load-deflection limit is 1.1 in. For both design cases using 0.6 in. or 0.7 in. diameter strands, the estimated live load deflections are higher than the limit values based on the optional deflection check provided in the AASHTO LRFD Specifications (AASHTO 2020).

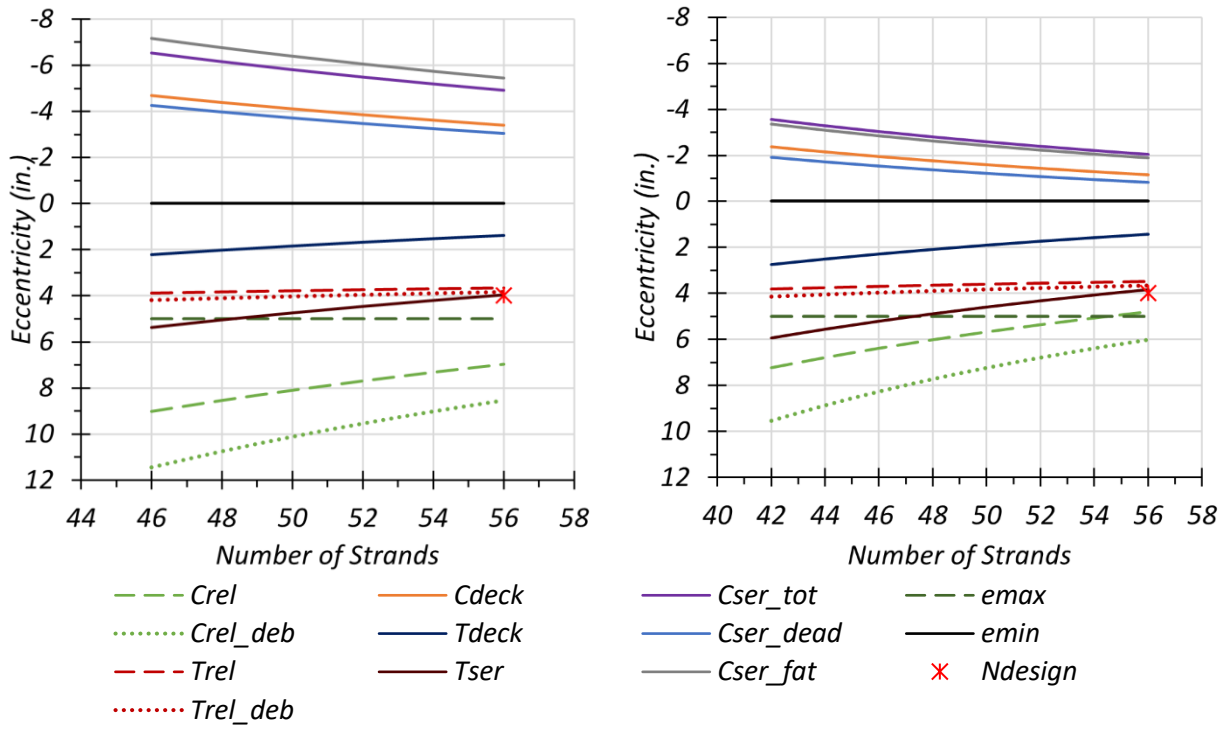

(a) 70 ft bridge with 0.6 in. strands *(b) 78 ft bridge with 0.7 in. strands*

Notes:

1. Solid lines = minimum eccentricity, dashed lines = maximum eccentricity
2. $f'_{ci} = 14.0$ ksi, $f'_c = 22.0$ ksi

Figure 3.10. Eccentricity Solution Domain for UHPC 5SB15 Girders.

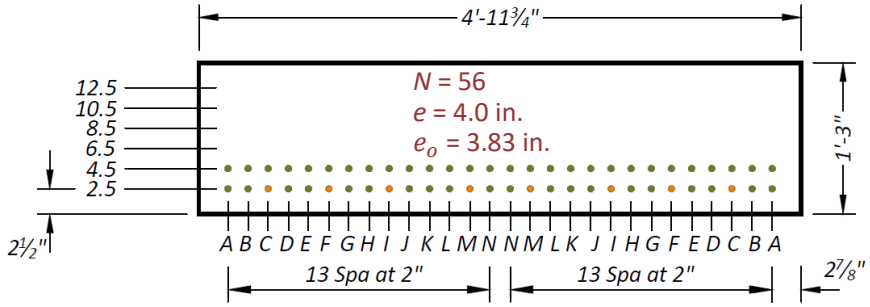

(a) 70 ft bridge with 0.6 in. strands

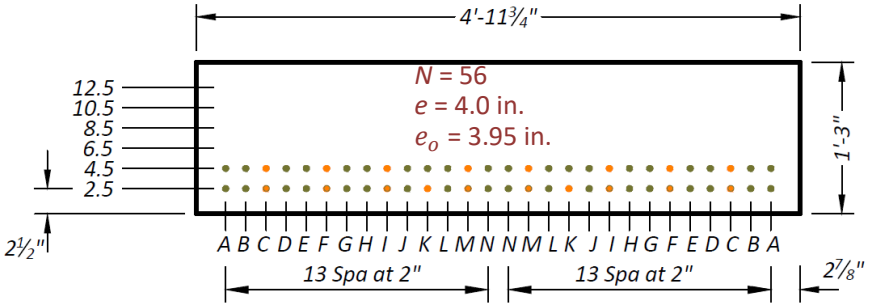

(b) 78 ft bridge with 0.7 in. strands

Notes:

1. N = Number of strands, e = eccentricity at midspan, e_o = end eccentricity
2. Green fill = bonded straight strands, orange fill = debonded strands

Figure 3.11. Optimum Strand Design for UHPC 5SB15 Girders.

Table 3.6. Estimated Camber for UHPC 5SB15 Girders.

Strand Diameter (in.)	No. of Debonded Strands	No. of Harped Strands	Time of Camber	Camber (in.)
0.6	8	0	Just before deck placement	4.1
			Just after deck placement	2.4
	0	4	Just before deck placement	3.7
			Just after deck placement	2.0
0.7	18	0	Just before deck placement	7.5
			Just after deck placement	4.8
	0	8	Just before deck placement	6.1
			Just after deck placement	3.4

Notes:

1. Debonded case using 0.6 in. strands: 8 strands up to 3 ft
2. Debonded case using 0.7 in. strands: 18 strands up to 3.5 ft and 4 strands up to 6.5 ft
3. Harped case: Hold-down point is at L/20 ft away from the centerline

3.5.5.4 Summary of Flexural Stress Designs for UHPC 5SB15 Girder

For all three design cases investigated, the tension stress limit at service and release controls the optimum number of strands and eccentricity. The maximum achievable span length was found to be 70 ft when 0.6 in. diameter strands are used and 78 ft when 0.7 in. diameter strands are used. Table 3.7 summarizes design parameters and the results of the parametric feasibility study. Case 3a and 3b are subcategories for differentiating debonded and harped design solutions when 0.6 in. diameter strands are used. Similarly, Case 3c and 3d are subcategories for differentiating debonded and harped design solutions when 0.7 in. diameter strands are used.

Table 3.7. Summary of Flexural Stress Designs for 5SB15 Girder.

Parameter	Case 1	Case 2	Case 3a	Case 3b	Case 3c	Case 3d
Span Length, ft	60	70	70	70	78	78
Total Width	30'-1"	30'-1"	30'-1"	30'-1"	30'-1"	30'-1"
Girder Spacing	5'-0¼"	5'-0¼"	5'-0¼"	5'-0¼"	5'-0¼"	5'-0¼"
No. of Girders	6	6	6	6	6	6
Overhang	2'-5⅞"	2'-5⅞"	2'-5⅞"	2'-5⅞"	2'-5⅞"	2'-5⅞"
CIP Deck Thickness, in.	5.0	5.0	5.0	5.0	5.0	5.0
Span/Depth	36	42	42.6	42.6	47.5	47.5
f'_{ci} (ksi)	7.0	14.0	14.0	14.0	14.0	14.0
f'_c (ksi)	12.0	22.0	22.0	22.0	22.0	22.0
f'_{ti} (ksi)	0.75	0.75	0.75	0.75	0.75	0.75
f'_t (ksi)	1.0	1.0	1.0	1.0	1.0	1.0
Strand Diameter (in.)	0.6	0.6	0.6	0.6	0.7	0.7
No. of Strands	40	56	56	56	56	56
Debonded Strands	0	8	8	0	18	0
Harped Strands	0	0	0	4	0	8
Camber Before Deck (in.)	3.3	4.1	4.1	3.7	7.5	6.1
Camber After Deck (in.)	2.1	2.4	2.4	2.0	4.8	3.4

Figure 3.12 provides a bar chart comparison for the maximum achievable span lengths using 0.6 in. and 0.7 in. diameter strands. Compared to the standard slab beam girder design using CC,

the designs using 0.6 in. diameter strands can provide around a 40 percent longer span length, while the designs using 0.7 in. diameter strands can provide around a 55 percent increase in span length. The full potential of UHPC can be leveraged by using large diameter (0.7 in.) strands. However, using 0.7 in. diameter strands leads to larger camber values that can potentially be mitigated by harping strands. In addition, the optional live load-deflection check might be a concern for these longer span lengths.

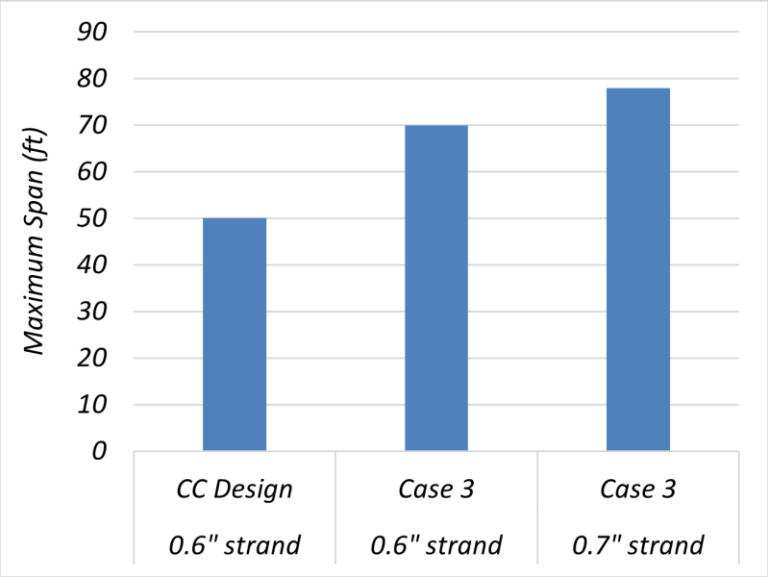

Figure 3.12. Comparison of Maximum Span Lengths for UHPC 5SB15 Girder.

3.5.6 Flexural Resistance at Strength Limit State

The flexural resistance ϕM_n of the slab beams must be greater than the factored flexural demand M_u using the Strength I load combination provided in the AASHTO LRFD Specifications (AASHTO 2020) Table 3.4.1-1. Section 3.4 of this report provides the load and resistance factors and the design approach for calculating the flexural resistance using a triangular stress block approach. The flexural resistance of slab beams was also calculated using the traditional rectangular stress block approach following the guidelines and assumptions provided in the AASHTO LRFD Specifications (AASHTO 2020) Article 5.6.2.1.

Table 3.8 summarizes the factored flexural demand M_u and reduced nominal flexural resistance ϕM_n results for both Case 3 designs using 0.6 in. and 0.7 in. diameter strands. Figure 3.13 shows a bar chart comparing the factored flexural demands for Case 3 designs with the reduced nominal flexural resistance computed using both the rectangular and triangular stress block approach. The

details about Case 3 designs may be found in the previous section. Both the rectangular and triangular stress block approach suggest that the reduced nominal flexural resistance is greater than the factored flexural demand. Using triangular stress distribution results in a slightly lower flexural resistance estimate than using rectangular stress block distribution results.

Table 3.8 Flexural Demand and Resistance Results for 5SB15 UHPC Slab Beam—Case 3.

Nominal Strand Diameter	Factored Flexural Demand M_u, kip-ft	Reduced Nominal Flexural Resistance ϕM_n, kip-ft	
		Rectangular stress block	Triangular stress block
0.6 in.	2424	2747	2729
0.7 in.	2934	3439	3270

Note: The resistance factor ϕ for tension-controlled prestressed concrete members with bonded strands is taken as 1.0 based on AASHTO LRFD Specifications (AASHTO 2020).

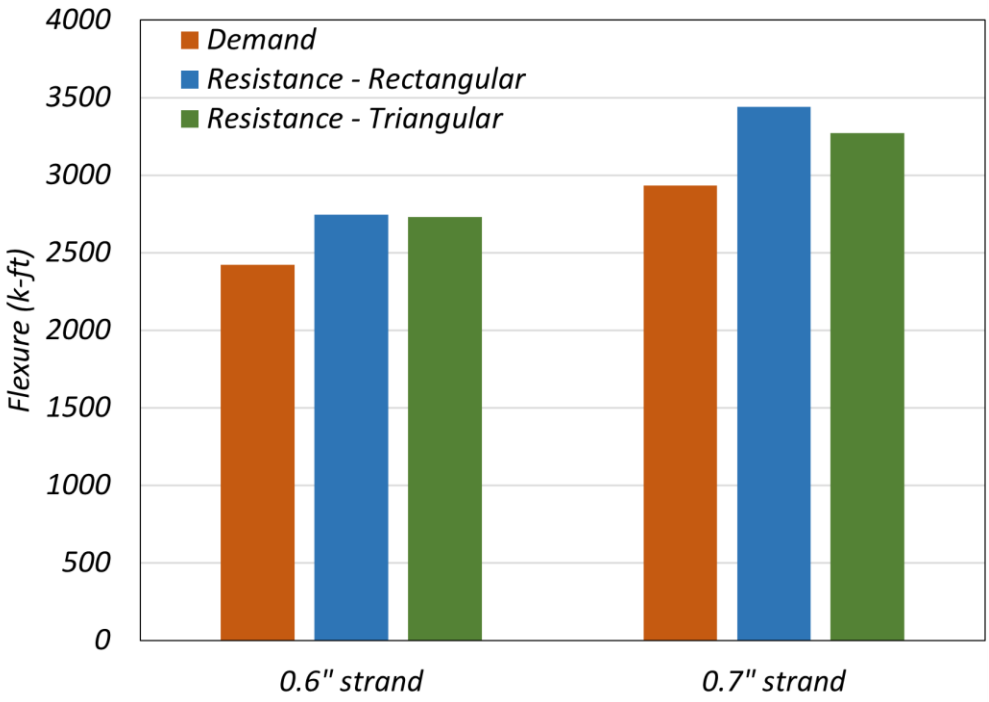

Figure 3.13. Comparison of Flexural Resistance for UHPC 5SB15 Slab Beam—Case 3.

3.5.7 Shear Resistance at Strength Limit State

The nominal shear resistance V_n of slab beams will be greater than the factored shear demand V_u when using the Strength I load combination provided in AASHTO LRFD Specifications (AASHTO 2020) Table 3.4.1-1. Section 3.4 of this report provides the load and resistance factors

and the design approach for calculating the shear resistance. The AFGC Guidelines (AFGC 2013) shear design methodology has been used for calculating shear resistance.

Table 3.9 summarizes the factored shear demand V_u and shear resistance V_n results using 0.6 in. and 0.7 in. diameter strands for both Case 3 designs. Figure 3.14 shows a bar chart comparing the factored shear demands for Case 3 designs. Two different shear resistance values were calculated based on the AFGC method used for calculating the shear depth, which depends on the lever arm of the internal forces corresponding to the bending moment. Both shear resistance values using the shear depth from the rectangular and triangular stress block approach suggest that the factored shear resistance is much greater than the factored shear demand. Using the triangular stress distribution for calculating the shear depth results in a 40 percent lower shear resistance estimate than when using the rectangular stress block. Even if the triangular stress block approach is used for calculating the shear depth, the factored shear demand V_u is less than one-half of V_n. This indicates that minimum shear reinforcement may not be necessary. Note that the nominal shear resistance is calculated by considering only the concrete contribution and fiber contribution. The concrete contribution is a function of elastic tensile strength of the concrete, the shear area $b_w z$, and the applied prestressing force. The fiber contribution is a function of shear area $b_w z$ and the residual tensile strength of fiber-reinforced section, which depends on the fiber content.

Table 3.9 Shear Demand and Resistance Results for 5SB15 UHPC Slab Beam—Case 3.

Nominal Strand Diameter	Factored Shear Demand V_u, kips	Nominal Shear Resistance V_n, kips	
		Rectangular stress block	Triangular stress block
0.6 in.	139	1023	701
0.7 in.	150	985	738

Note: The shear resistance is calculated using AFGC Guidelines (AFGC 2013), which include safety factors in nominal shear resistance equations rather than in a resistance factor ϕ.

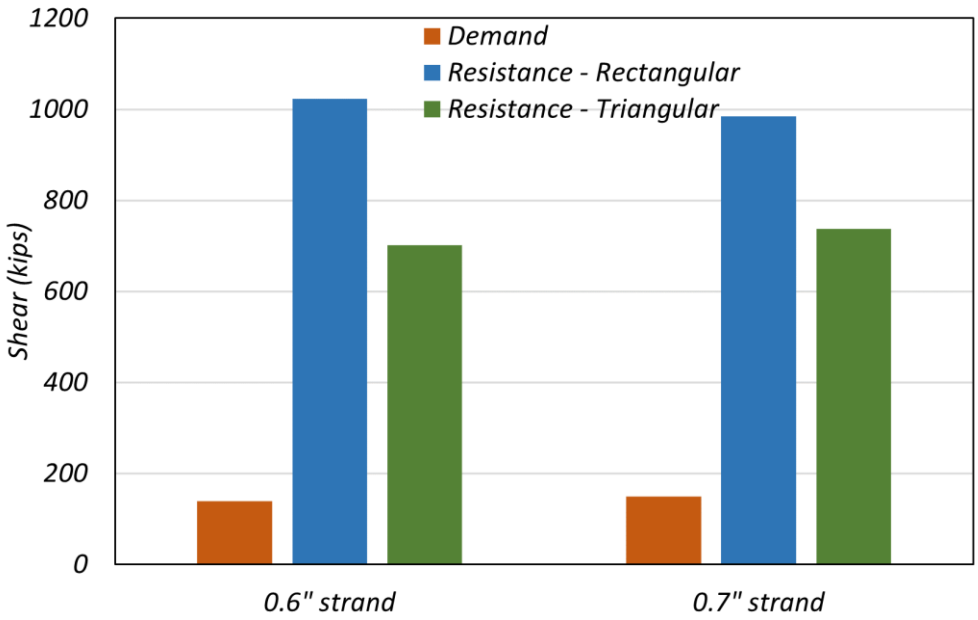

Figure 3.14. Comparison of Shear Resistance for UHPC 5SB15 Girder—Case 3 Designs.

3.6 DESIGNS FOR TX54 I-GIRDERS

One of the longest possible span lengths using Tx54 prestressed concrete I-girders was selected from the TxDOT standard bridge drawings as the base bridge geometry to allow comparison of UHPC designs. The bridge cross-section, girder spacing, material properties (except girder concrete strength), and section properties of the girder were kept the same as the selected standard Tx54 girder design for main design cases. Several subcases were explored by considering a different deck thickness and a different girder spacing. A 7.0 in. thick deck was also considered to determine the potential benefit of using thinner 2.5 in. thick UHPC precast concrete panels (PCPs) as stay-in-place formwork, with the remainder of the deck composed of the standard 4.5 in. thick CIP concrete. A reduced deck thickness option was included to evaluate the effect of reduced superstructure weight to the tension strength requirement. Note that the CIP deck thickness remains the same and provides the same minimum cover. Only the thickness of the PCPs was modified to 2.5 in., which maintained the cover for the reinforcement within the 4.5 in. (minimum) CIP deck.

The following research questions were addressed by investigating the three main design cases, which have several subcases:

1. Is it possible to achieve a 160 ft span length for a 46 ft wide bridge using:
    a) Six Tx54 UHPC I-girders?
    b) Five Tx54 UHPC I-girders?

    What would be the required concrete compressive strength at release and at 28 days to achieve this span length?
2. Is it possible to achieve a 170 ft span length for a 46 ft wide bridge using:
    a) Six Tx54 UHPC I-girders?
    b) Six Tx54 UHPC I-girders and a 7 in. thick deck?
    c) Five Tx54 UHPC I-girders and a 7 in. thick deck?

    What would be the required concrete compressive strength at release and at 28 days to achieve such a span length?
3. What is the maximum achievable span length for a 46 ft wide bridge using Tx54 UHPC I-girders that have 14 ksi compressive and 0.75 ksi elastic tensile strength at release, and 22 ksi compressive and 1.0 ksi elastic tensile strength at 28 days for:
    a) Six Tx54 UHPC I-girders?
    b) Six Tx54 UHPC I-girders and a 7 in. thick deck?
    c) Five Tx54 UHPC I-girders and a 7 in. thick deck?

Note that the design elastic tensile strength from direct tension testing of UHPC was assumed to be 0.75 ksi at release and 1.0 ksi at 28 days for all design cases based on the values obtained from the literature (Graybeal 2006a; Haber et al. 2018; Wille et al. 2014a). The tensile stress limit is taken as 85 percent of the elastic tensile strength based on the material reduction factor in tension that was recommended by Graybeal (2019).

3.6.1 Geometry of Tx54 I-Girder Bridge

Figure 3.15 shows the cross-section details of the selected prestressed bridge using Tx54 I-girders. For the main design cases, six Tx54 prestressed concrete I-girders are spaced at 8 ft on center across a 46 ft overall bridge width topped with an 8.5 in. thick deck slab (4 in. PCPs plus 4.5 in. CIP reinforced concrete deck). For the subcases, five girders at 10 ft spacing and a 7 in. thick deck option were also considered. An average 2 in. constant haunch thickness was assumed along the entire span length as part of permanent dead loads. However, the haunch contribution to the stiffness of the composite section was neglected because the haunch thickness varies along the

length and may be as small as 0.5 in. at the midspan. The assumed superimposed dead loads consist of an average 2 in. thick asphalt overlay and T551 rails, one of the heaviest railing types used by TxDOT. The weight of the rails was distributed to the three girders closest to each of the bridge's edges, as recommended by the *TxDOT Bridge Design Manual* (TxDOT 2021). Table 3.10 summarizes these key geometric design parameters for the selected typical standard bridge cross-section using Tx54 prestressed I-girders.

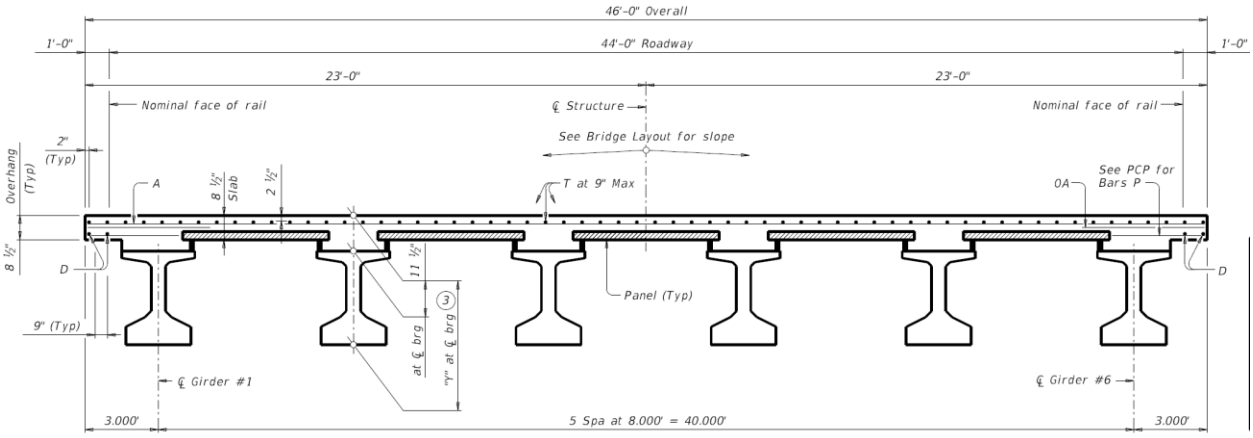

Figure 3.15. Typical Bridge Cross-Section Using Tx54 Girders (TxDOT 2019).

Table 3.10. Geometric Properties of Tx54 Bridge.

Parameter	Description/Value
Bridge Width, W	46 ft
Girder Spacing, S	8 ft or 10 ft
Number of Girders, n	5 or 6
Deck Thickness, t_s	8.5 in. or 7 in.
Wearing Surface Thickness, t_{ws}	2 in. asphalt
Haunch Thickness, t_h	2 in. for weight calculation only
Railing	T551 (0.382 kip/ft)

3.6.2 Girder Details and Section Properties of Tx54 I-Girder

Figure 3.16 shows geometric and reinforcement details and strand layout of the standard Tx54 prestressed I-girder. The 54 in. deep Tx54 prestressed I-girders have a 32 in. wide bottom bulb that can hold a maximum of 66 strands in six rows of a 2 × 2 in. grid, while the 7 in. wide web can hold 38 strands in 19 rows of a 2 × 2 in. grid. Section properties of the noncomposite Tx54 I-girder, including area, centroid location, moment of inertia, and the weight per unit length were calculated

based on the standard cross-section geometry. Note that the unit weight of the conventional Tx54 I-girder with reinforcement is taken as 0.155 kcf, while the UHPC Tx54 I-girder with reinforcement is taken as 0.165 kcf because the UHPC is about 10 lb/ft^3 heavier than the CC due to the presence of fibers. Table 3.11 lists the calculated section properties, which are consistent with the values provided in the structural drawing files from *TxDOT Bridge Standards* (TxDOT 2019).

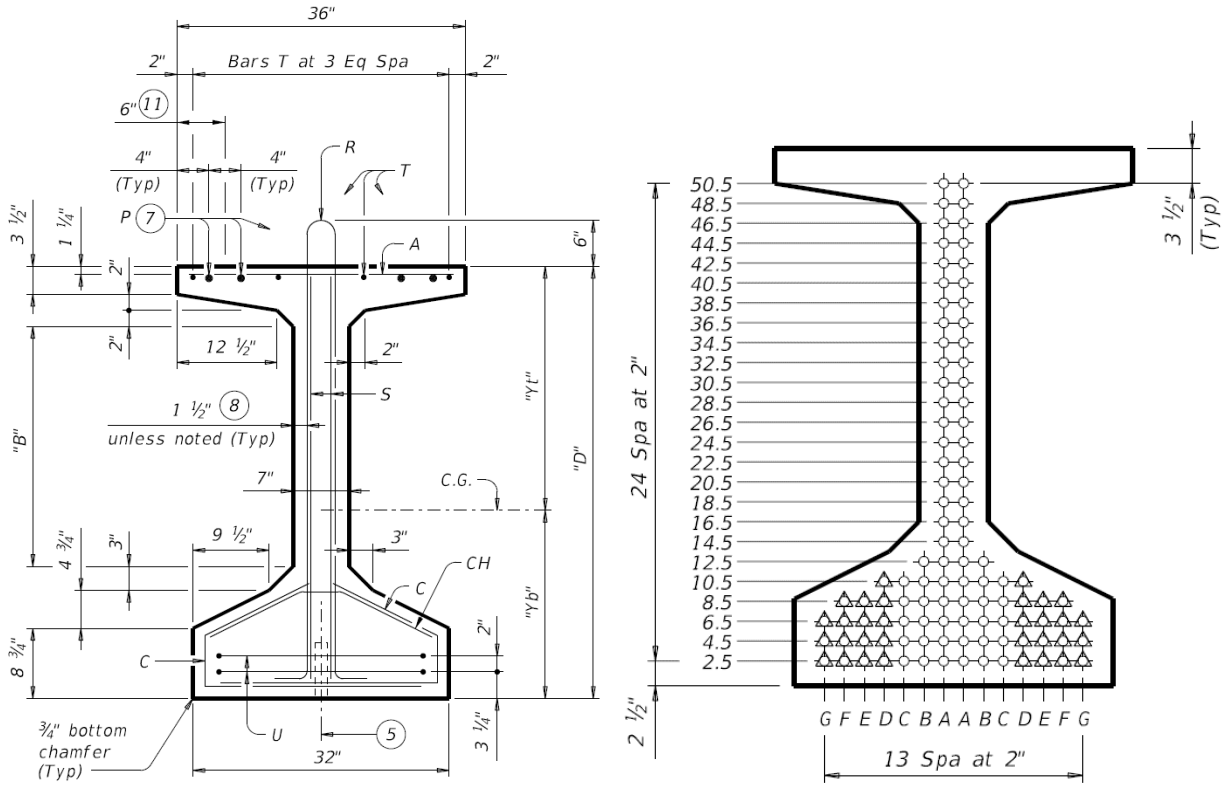

(a) Reinforcement Details *(b) Strand Layout*

Figure 3.16. Section Geometry of Tx54 Girder (TxDOT 2019).

Table 3.11. Section Properties of Tx54 Girder.

Parameter	Value
Area, A (in^2)	817
Centroid Distance from Top, y_t (in.)	30.49
Centroid Distance from Bottom, y_b (in.)	23.51
Moment of Inertia, I_g (in^4)	299,740
Girder Weight, w_g (kip/ft)	0.936

Note: Unit weight of the UHPC Tx54 girder with reinforcement is taken as 0.165 kcf.

3.6.3 Material Properties for Tx54 I-Girder Bridge

Table 3.12 lists the material properties used for the design of Tx54 prestressed I-girder bridges that were used for all alternative design cases investigated in this study. The design compressive strength of CIP deck concrete was taken as 4 ksi based on the structural drawings provided in the *TxDOT Bridge Standards* (TxDOT 2019). The unit weight of concrete for CC deck was taken as 0.145 kcf to compute MOE, while the unit weight of conventional deck concrete with reinforcement was taken as 0.150 kcf to compute the dead load of the deck slab. The unit weight of UHPC is 0.155 kcf, which is slightly higher than CC due to the presence of fibers. Therefore, the unit weight of a UHPC Tx54 I-girder with reinforcement was 0.165 kcf.

Design compressive and tensile strengths of concrete at release and at 28 days are key properties for the design of prestressed concrete girders. Allowable stress design criteria for CC only considers design compressive strength as a parameter, and tensile stress limits are generally calculated using the empirical square root relationships between the compressive and tensile strength. However, for UHPC, the tensile strength is not formulated as a function of compressive strength; thus, the design elastic tensile strengths at release and at 28 days were considered based on common values in the literature. The elastic tensile strength of UHPC Tx54 girders was assumed to be 0.75 ksi at release and 1.0 ksi at service and kept the same for all alternative UHPC design cases for maximum achievable span length. For these cases, the compressive strength of UHPC girders was taken as 14 ksi at release and 22 ksi at service.

For the design cases that consider a target span length and determine the concrete strength, the elastic tensile strength was increased to 1.0 ksi at release and up to 3.0 ksi at service to achieve the target span length. Note that although some design cases consider an elastic tensile strength as high as 3.0 ksi, it is not practical to achieve elastic tensile strength values above 1.5 ksi based on the direct tension test results seen in the literature. The concrete compressive strength of UHPC Tx54 I-girders at release and at 28 days were kept as a variable for these design cases.

The MOE of CC of the deck slab was calculated using the AASHTO LRFD Specifications (AASHTO 2020) equation, and MOE of the UHPC slab beam girder was calculated using the MOE equation provided by Graybeal (2014). Section 3.5.3 provides both equations.

Table 3.12. Material Properties for Tx54 Girder Bridges.

Parameter	Description/Value
Compressive strength of deck concrete, f'_{cd}	4.0 ksi
Tensile strength of UHPC girder at release, f'_{ti}	0.75 or 1.0 ksi
Tensile strength of UHPC girder at 28 days, f'_{t}	1.0 to 3.0 ksi
Compressive strength of UHPC girder at release, f'_{ci}	14 ksi or varies*
Compressive strength of UHPC girder at 28 days, f'_{c}	22 ksi or varies*
Unit weight of CC (used to compute E_c), γ_{cc}	0.145 kcf
Unit weight of CC with reinforcement (to compute dead load)	0.150 kcf
Unit weight of UHPC, γ_{UHPC}	0.155 kcf
Unit weight of UHPC Tx54 girder with reinforcement (to compute dead load)	0.165 kcf
Unit weight of asphalt overlay, γ_{ws}	0.140 kcf
Weight of T551 rail, w_r	0.382 kip/ft (distributed to three girders)
Ultimate strength of prestressing strands, f_{pu}	270 ksi
MOE of strands, E_{ps}	28,500 ksi

*Varies for the design cases that consider a target span length and designs for UHPC strength.

3.6.4 Alternative Design Cases for Tx54 Girder Bridges

Table 3.13 provides the main design parameters for the alternative design cases explored for the prestressed UHPC Tx54 I-girders. Three main design cases with several subcases were explored, as described in the beginning of Section 3.6.

Table 3.13. Main Design Parameters for Alternative Designs Using Tx54 Girders.

Parameter	CC-TxDOT	UHPC Case 1a	UHPC Case 1b	UHPC Case 2a	UHPC Case 2b	UHPC Case 2c	UHPC Case 3a	UHPC Case 3b	UHPC Case 3c
Span Length (ft)	120	160	160	170	170	170	Max.	Max.	Max.
Bridge Width (ft)	46	46	46	46	46	46	46	46	46
Girder Spacing (ft)	8	8	10	8	8	10	8	8	10
Number of Girders	6	6	5	6	6	5	6	6	5
Overhang (ft)	3	3	3	3	3	3	3	3	3
Deck Thickness (in.)	8.5	8.5	8.5	8.5	7.0	7.0	8.5	7.0	7.0
Span/Depth Ratio	23.0	30.7	30.7	32.6	33.4	33.4	TBD	TBD	TBD
f'_{ci} (ksi)	5.7	TBD	TBD	TBD	TBD	TBD	14	14	14
f'_{c} (ksi)	6.9	TBD	TBD	TBD	TBD	TBD	22	22	22
f'_{ti} (ksi)	–	TBD	TBD	TBD	TBD	TBD	0.75	0.75	0.75
f'_{t} (ksi)	–	TBD	TBD	TBD	TBD	TBD	1.0	1.0	1.0
Strand Diameter (in.)	0.6	TBD	TBD	TBD	TBD	TBD	TBD	TBD	TBD
Number of Strands	44	TBD	TBD	TBD	TBD	TBD	TBD	TBD	TBD
Debonded Strands	6	TBD	TBD	TBD	TBD	TBD	TBD	TBD	TBD

Notes:
1. CC-TxDOT indicates CC for comparison
2. - : Not available
3. TBD = To Be Determined

3.6.5 Flexural Stress Design at Service Limit State for Tx54 Girder Bridges

The design cases listed in the previous section were investigated using the design methodology described in Sections 3.2 and 3.3 to determine the optimum number of strands and maximum achievable span length. The feasible eccentricity and number of strands design space has been explored for eight stress limit states. Section 3.5.5 provides a sample chart and detailed descriptions of each plotted limit state.

3.6.5.1 Case 1 Designs

Figure 3.17 shows the eccentricity solution domains for a 160 ft bridge based on the eight limit states considered for both six-girder and five-girder configurations. Case 1 design uses the same bridge cross-section as one of the current TxDOT standard designs (CC-TxDOT in Table 3.13) and explores the possibility of extending the span length to 160 ft, compared to 120 ft when CC is used. This design case was investigated to find the optimum number of strands and required concrete compressive strength to achieve the target span length.

The tensile stress limit at release at the girder ends (red dashed line) and the tensile stress limit at service at the girder midspan (maroon solid line) control the Case 1 designs. The required elastic (first cracking) tensile strength of UHPC increased to 1.5 ksi for six-girder and 2.6 ksi for five-girder configurations to achieve a 160 ft span length. Such high elastic tensile strength values may not be achievable in routine production. The required compressive strength at release was $f'_{ci} = 14$ ksi, and compressive strength at service was $f'_c = 22$ ksi. The six-girder bridge requires 84 strands with a 13.63 in. midspan eccentricity, while the five-girder bridge requires 82 strands with a 14.13 in. midspan eccentricity to achieve a 160 ft span length without debonding or harping. Figure 3.18 shows the strand layout for six-girder and five-girder configurations using a standard Tx54 I-girder in which the green filled locations show straight bonded strands.

The camber calculations considered the creep coefficient using the AASHTO LRFD Specifications (AASHTO 2020) empirical creep equations at 40 days when prestress is applied at one day. For the six-girder configuration, the applied prestressing force using 84 strands and 13.63 in. midspan eccentricity causes a 5.9 in. camber for a noncomposite girder just before deck placement. For the five-girder configuration, the applied prestressing force using 82 strands and 14.13 in. midspan eccentricity causes a 6.3 in. camber for a noncomposite girder just before deck placement. Table 3.14 lists the estimated camber of the noncomposite girder for both six- and five-girder configurations before and after deck placement. Live load deflections were calculated using the optional deflection check criteria provided in Section 3.2.2 and compared to the optional live load deflection limit. Live load deflections for both configurations were found to be within the deflection limits.

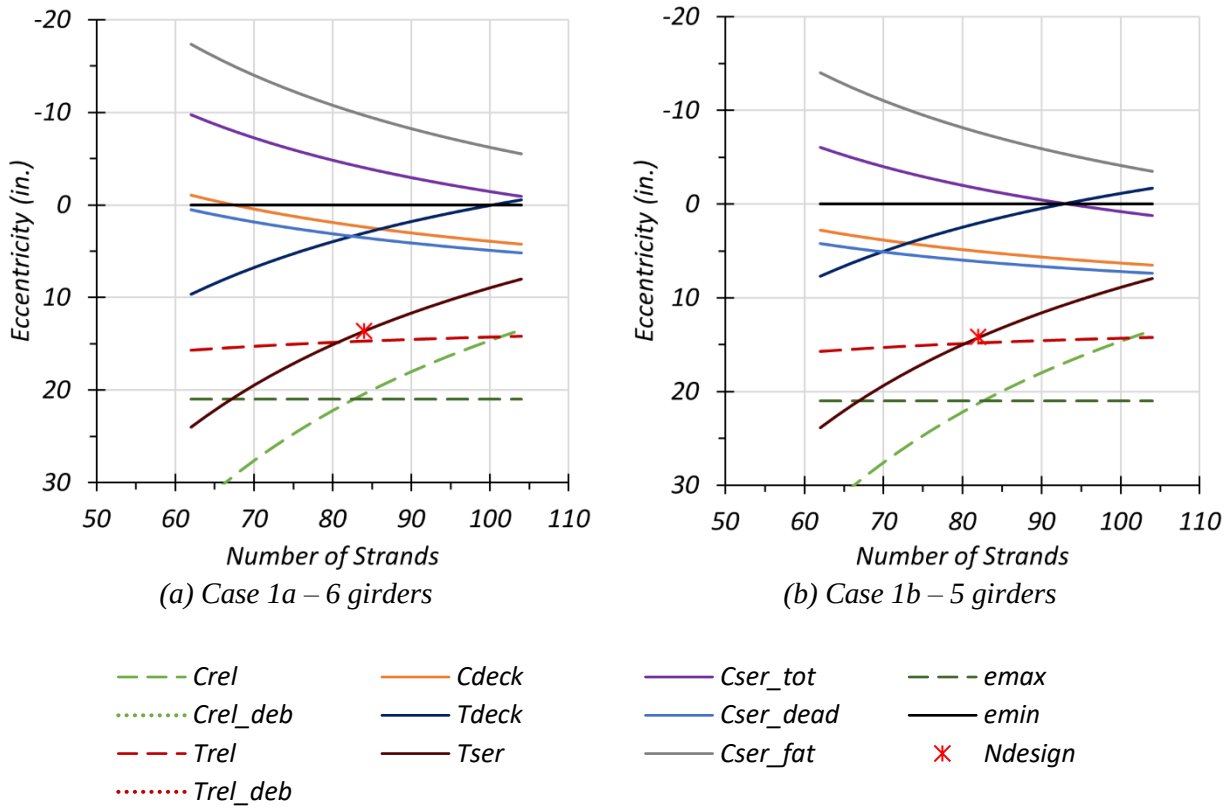

(a) Case 1a – 6 girders

(b) Case 1b – 5 girders

Notes:

1. Solid lines = minimum eccentricity, dashed lines = maximum eccentricity
2. $f_t' = 1.5$ ksi for Case 1a, $f_t' = 2.6$ ksi for Case 1b
3. $f_{ci}' = 14.0$ ksi, $f_c' = 22.0$ ksi

Figure 3.17. Eccentricity Solution Domain for UHPC Tx54 Girders—160 ft Bridge.

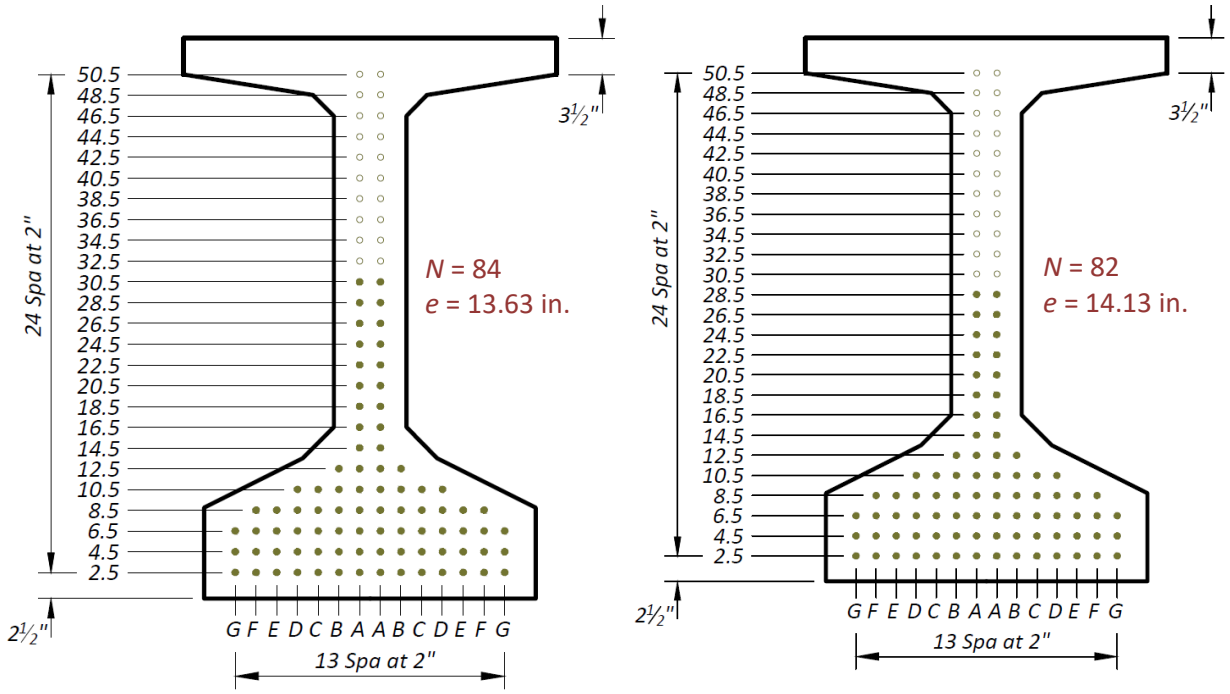

(a) Case 1a – 6 girders *(b) Case 1b – 5 girders*

Notes:
1. N = Number of strands, e = eccentricity at midspan
2. Green fill = bonded straight strands

Figure 3.18. Optimum Strand Design for UHPC Tx54 Girders—160 ft Bridge.

Table 3.14. Estimated Camber for UHPC Tx54 Girders—160 ft Bridge.

Design Case	Number of Strands	Eccentricity (in.)	Time of Camber	Camber (in.)
Case 1a (6 girders)	84	13.63	Just before deck placement	5.9
			Just after deck placement	0.0
Case 1b (5 girders)	82	14.13	Just before deck placement	6.3
			Just after deck placement	−1.1

3.6.5.2 Case 2 Designs

Figure 3.19 shows the eccentricity solution domains for a 170 ft bridge based on the eight limit states considered for three different subcategories: (1) Case 2a uses six girders and an 8.5 in. deck, (2) Case 2b uses six girders and a 7.0 in. deck, and (3) Case 2c uses five girders and a 7.0 in. deck. Case 2 designs use a similar bridge cross-section as one of the current TxDOT standard designs (CC-TxDOT in Table 3.13) and explore the possibility of extending the span length to 170 ft, as opposed to 120 ft when CC is used. This design case was investigated to find the optimum number of strands and required concrete compressive strength to achieve the target span length of 170 ft.

The tensile stress limit at release at the girder ends (red dashed line) and the tensile stress limit at service at the girder midspan (maroon solid line) controls the Case 2 designs. The elastic (first cracking) tensile strength of UHPC increased to 2.6 ksi for Case 2a, 2.3 ksi for Case 2b, and 3.4 ksi for Case 2c to achieve a 170 ft span length. Such high elastic tensile strength values can be difficult to achieve in routine production. Cases 2a and 2b requires 82 strands with a 14.13 in. midspan eccentricity, while Case 2c requires 80 strands with a 14.61 in. midspan eccentricity to achieve a 170 ft span length without debonding or harping and uses a compressive strength of 14 ksi at release and 22 ksi at service. Figure 3.20 shows the strand layout for all three subcategories of Case 2 using a standard Tx54 I-girder in which the green filled locations show straight bonded strands.

The camber calculations considered the creep coefficient using the AASHTO LRFD Specifications (AASHTO 2020) empirical creep equations at 40 days when prestress was applied at one day. For Case 2a and 2b, the applied prestressing force using 82 strands and a 14.13 in. midspan eccentricity for a 170 ft span causes a 5.4 in. camber for the noncomposite girder just before deck placement. For Case 2c, the applied prestressing force using 80 strands and a 14.61 in. midspan eccentricity for a 170 ft span causes a 5.6 in. camber for the noncomposite girder just before deck placement. Table 3.15 lists the estimated camber of the noncomposite girder for all three subcategories of Case 2 before and after deck placement. Live load deflections were also calculated using the optional deflection check criteria provided in Section 3.2.2 of this report and compared with the optional live load deflection limit. Live load deflections were found to be within the deflection limits for all considered Case 2 designs.

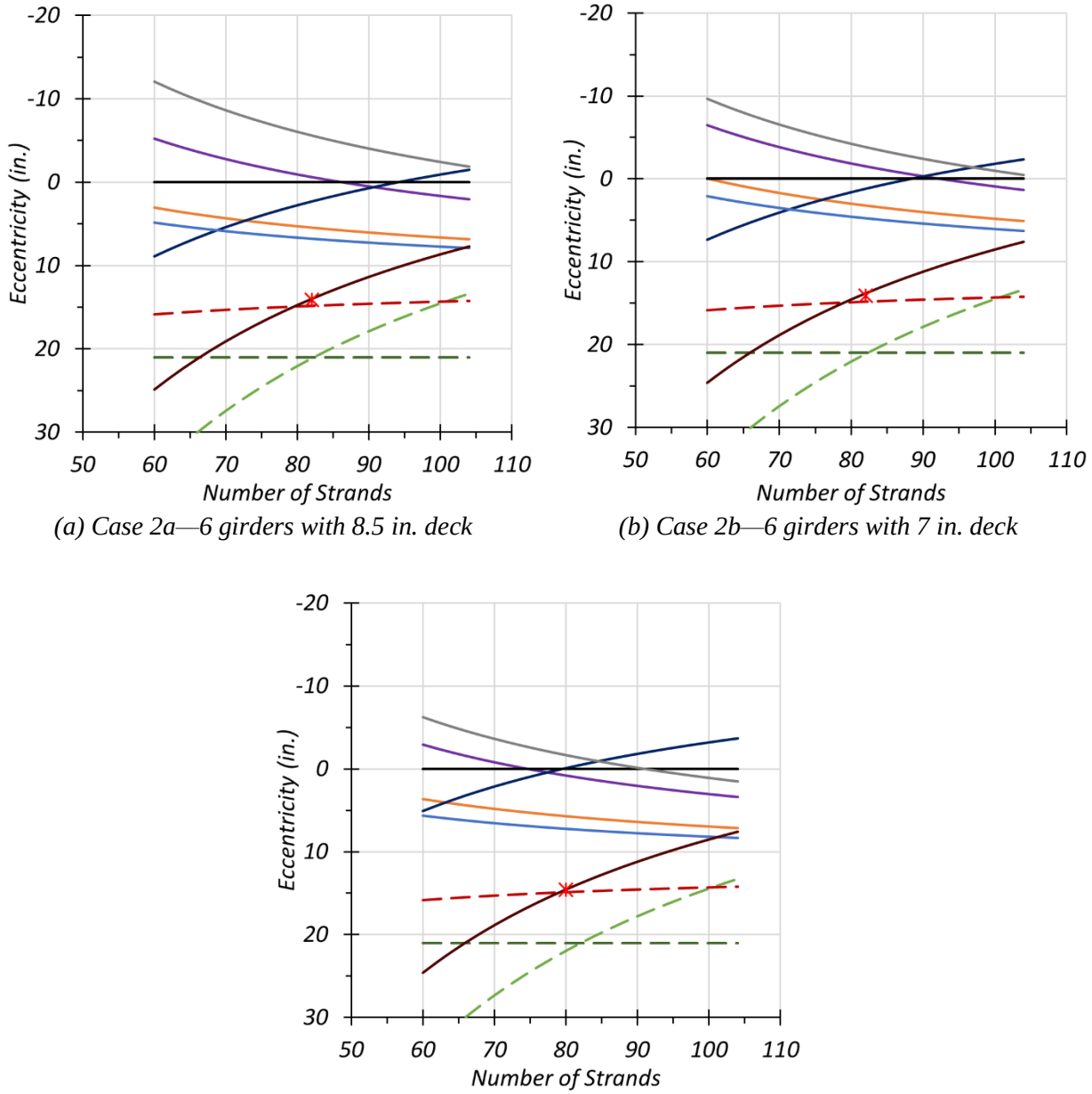

(a) Case 2a—6 girders with 8.5 in. deck

(b) Case 2b—6 girders with 7 in. deck

(c) Case 2c—5 girders with 7 in. deck

Notes:

1. Solid lines = minimum eccentricity, dashed lines = maximum eccentricity
2. $f_t' = 2.6$ ksi for Case 2a, $f_t' = 2.3$ ksi for Case 2b, $f_t' = 3.4$ ksi for Case 2c
3. $f_{ci}' = 14.0$ ksi, $f_c' = 22.0$ ksi

Figure 3.19. Eccentricity Solution Domain for UHPC Tx54 Girders—170 ft Bridge.

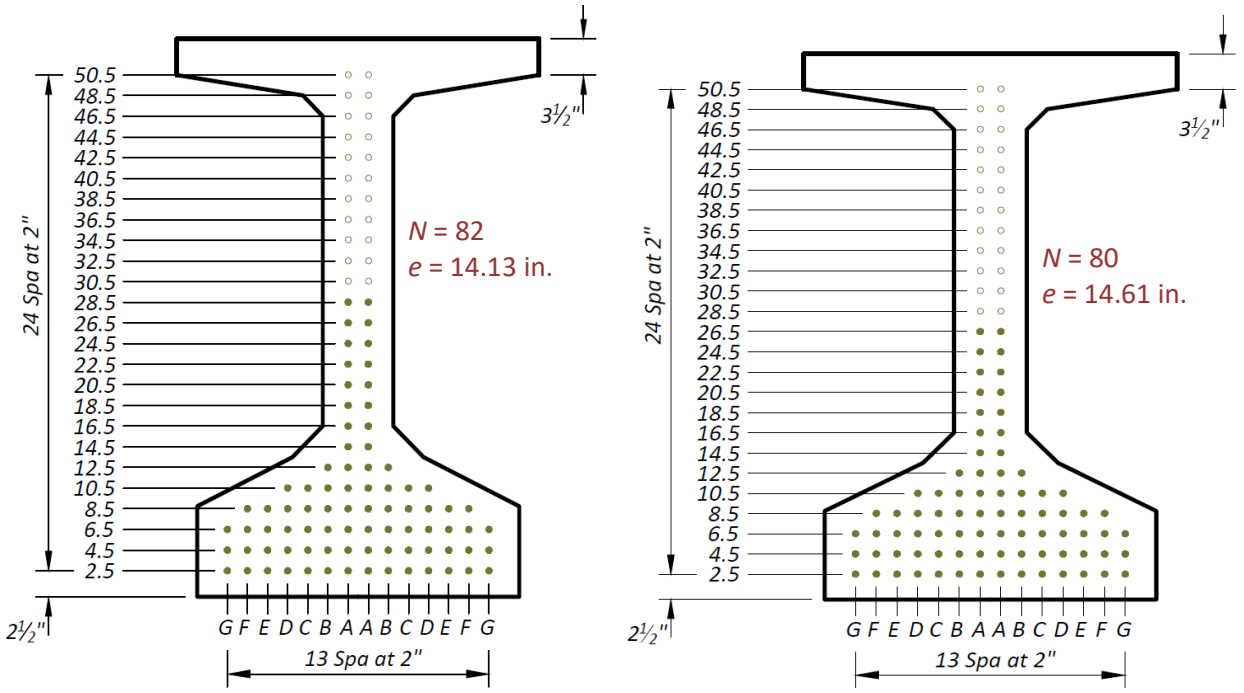

(a) Case 2a and 2b *(b) Case 2c*

Notes:
1. N = Number of strands, e = eccentricity at midspan
2. Green fill = bonded straight strands

Figure 3.20. Optimum Strand Design for UHPC Tx54 Girders—170 ft Bridge.

Table 3.15. Estimated Camber for UHPC Tx54 Girders—170 ft Bridge.

Design Case	No. of Strands	Eccentricity (in.)	Time of Camber	Camber (in.)
Case 2a (6 girders, 8.5" deck)	82	14.13	Just before deck placement	5.4
			Just after deck placement	−2.2
Case 2b (6 girders, 7" deck)	82	14.13	Just before deck placement	5.4
			Just after deck placement	−1.0
Case 2c (5 girders, 7" deck)	80	14.61	Just before deck placement	5.6
			Just after deck placement	−2.2

3.6.5.3 Case 3a Designs (6 Girders and 8.5 in. Deck)

Case 3 designs have the same subcategory designs as Case 2. Those subcategories (3a, 3b, and 3c) are organized in separate sections because each investigates the use of both 0.6 in. and 0.7 in. diameter strands, while Case 1 and Case 2 designs consider only 0.6 in. diameter strands. Although 0.7 in. strands are not currently available in Texas precast plants, this feasibility study included an evaluation of the potential benefit of using 0.7 in. strands in UHPC girders to further increase the possible span lengths.

Unlike Case 1 and Case 2 designs, Case 3a focuses on determining the maximum achievable span length for a bridge having six Tx54 UHPC I-girders with an 8.5 in. CC deck. The UHPC strength is set to a target compressive strength $f'_{ci} = 14$ ksi at release and $f'_c = 22$ ksi at service. An inverse design approach is used, which calculates the possible span length for the specified given material properties. Figure 3.21 shows the maximum span length solution domains based on eight concrete stress limits. The optional deflection limit (green solid line) is also shown on the graphs but does not control the design cases considered for Tx54 girders.

For the design case using 0.6 in. diameter strands (Figure 3.21a), the maximum achievable span length is 155 ft, using 84 strands based on the tensile stress limit at service. This span length can be achieved without debonding or harping. The dashed red line indicates the minimum number of strands to satisfy the tensile stress limit at the girder ends at release, and the dashed green line is the maximum number of strands to satisfy the compression stress limit at the girder ends at release. Therefore, the span length solution domain is between the red and green dashed lines and the maroon solid line.

For the design case using 0.7 in. diameter strands (Figure 3.21b), the maximum achievable span length is 172 ft with 82 strands when four strands are debonded or six strands are harped. It is necessary to debond or harp some strands to satisfy the compression stress limit at release at the girder ends; otherwise, there is no design solution because the compressive stress limit at release (green dashed) requires a smaller number of strands than the minimum number of strands necessary to satisfy tensile stress limit at release (red dashed line). The red dotted line indicates the minimum number of strands and the green dotted line indicates the maximum number of strands when four strands are debonded. Therefore, the span length solution domain falls between the red and green dotted lines and the maroon solid line for the debonded case. Similarly, the red dashed-dotted line indicates the minimum number of strands, and the green dashed-dotted line indicates the maximum number of strands when six strands are harped. Therefore, the span length solution domain is between the red and green dashed-dotted lines and the maroon solid line for the harped case.

Table 3.16 summarizes the maximum achievable span lengths, number of required strands, and debonding or harping information for different strand diameters. For the harped case, the hold-down points are taken as $L/20$ ft away from the midspan of the girder.

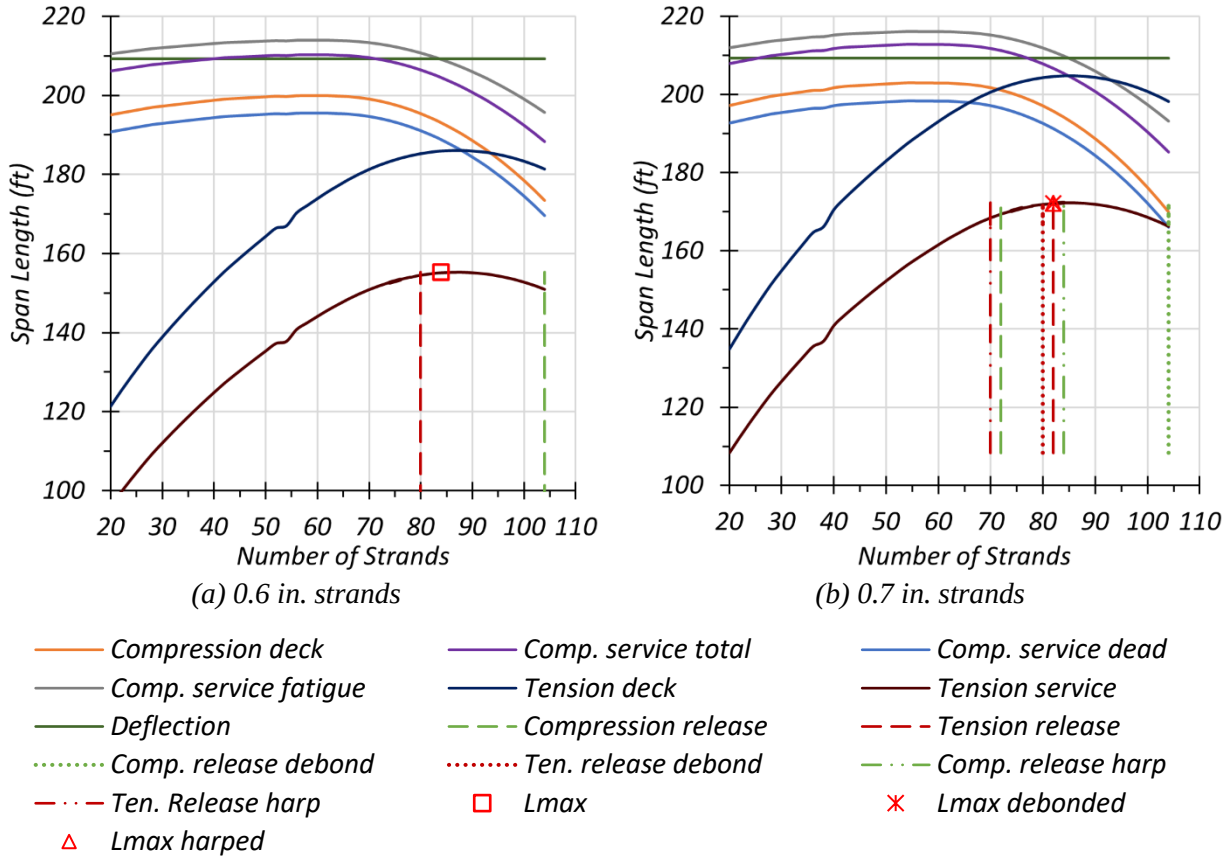

Note: Solid lines = maximum span, dashed red lines = minimum number of strands, dashed green lines = maximum number of strands.

Figure 3.21. Span Length Solution Domain for UHPC Tx54 Girder—Case 3a.

Table 3.16. Maximum Achievable Span Length for UHPC Tx54 Girder—Case 3a.

Strand Diameter (in.)	Total No. of Strands	No. of Debonded Strands	No. of Harped Strands	Maximum Achievable Span (ft)
0.6	84	0	0	155
0.7	82	4	0	172
	82	0	6	172

Notes:
1. Debonded case using 0.7 in. strands: 4 strands up to 3.5 ft and 2 strands up to 9.5 ft from girder ends
2. Harped case: hold-down point is at *L*/20 ft away from the girder midspan location

Optimum eccentricity and number of strand requirements were calculated like Case 1 and Case 2 designs using the maximum achievable span length values. Figure 3.22(a) shows the eccentricity

solution domain for a 155 ft bridge based on the eight limit states considered when 0.6 in. diameter strands are used. The optimal solution requires 84 strands having a 13.63 in. midspan eccentricity to achieve a 155 ft span length. Figure 3.22(b) shows the eccentricity solution domain for a 172 ft bridge based on the eight limit states considered when 0.7 in. diameter strands are used. The compressive stress limit at release at the girder ends (green dashed line) requires a smaller eccentricity than the minimum eccentricity required to satisfy tensile stress limit at service at the girder midspan (maroon solid line). It is not possible to achieve a 172 ft span length without debonding or harping. Therefore, the optimal design requires 82 strands having a 14.13 in. midspan eccentricity with four debonded strands or six harped strands. For I-girders, harping provides a more viable method to resolve stress exceedance issues at girder ends because it provides more balanced deflections by reducing the amount of camber. The proposed strand layout for the harped case results in a 14.13 in. midspan eccentricity and 12.52 in. end eccentricity.

Figure 3.23 shows the strand layout for a standard Tx54 I-girder where the green filled locations show straight bonded strands and red filled locations show the harped strands from both ends. The camber calculations considered the creep coefficient using the AASHTO LRFD Specifications (AASHTO 2020) empirical creep equations for 40 days when prestress was applied at one day. For the design case using 0.6 in. strands, the applied prestressing force (using 84 strands and a 13.63 in. midspan eccentricity for a 155 ft span) causes a 6.2 in. camber for the noncomposite girder just before deck placement. For the design case using 0.7 in. strands, the applied prestressing force (using 82 strands—six of which are harped—having a 14.13 in. midspan eccentricity and a 12.52 in. end eccentricity) creates a 10.3 in. camber for the noncomposite girder just before deck placement. Table 3.6 lists the estimated camber estimations for debonded and harped options for both design cases using 0.6 in. or 0.7 in. strands. Although 0.7 in. strands provide the potential to increase span lengths, camber values are increased significantly. Using harped strands rather than debonding can provide more balanced deflections by reducing the initial camber. It may be possible to achieve fully balanced final deflection just after deck placement by harping more strands and/or adjusting the hold-down location.

Live load deflections were also calculated using the optional deflection check criteria provided in Section 3.2.2 of this report and compared with the optional live load deflection limit. The estimated live load deflections for Case 3a were found to be smaller than the deflection limit.

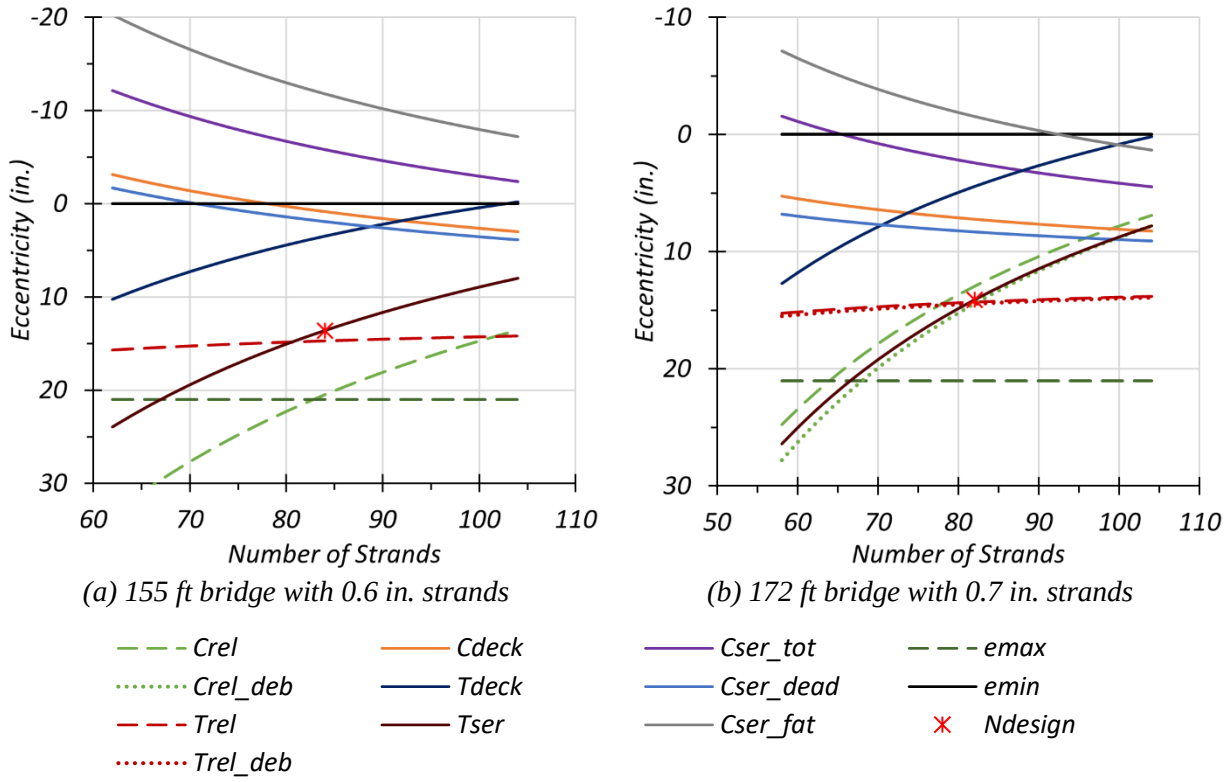

(a) 155 ft bridge with 0.6 in. strands

(b) 172 ft bridge with 0.7 in. strands

Note: Solid lines = minimum eccentricity, dashed lines = maximum eccentricity.

Figure 3.22. Eccentricity Solution Domain for UHPC Tx54 Girders—Case 3a.

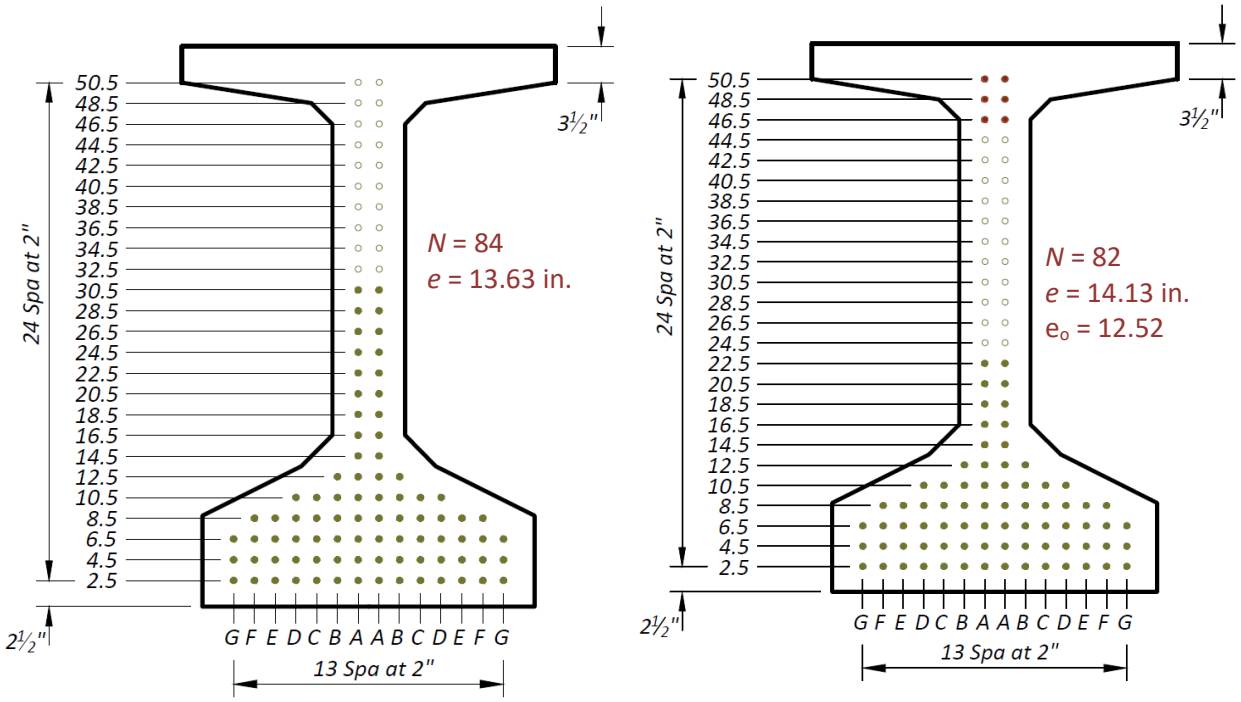

(a) 155 ft bridge with 0.6 in. strands *(b) 172 ft bridge with 0.7 in. strands*

Notes:
1. N = Number of strands, e = eccentricity at midspan, e_o = end eccentricity
2. Green fill = bonded straight strands, red fill = harped strands

Figure 3.23. Optimum Strand Design for UHPC Tx54 Girders—Case 3a.

Table 3.17. Estimated Camber for UHPC Tx54 Girders—Case 3a.

Strand Diameter (in.)	No. of Debonded Strands[1]	No. of Harped Strands[2]	Time of Camber	Camber (in.)
0.6	0	0	Just before deck placement	6.2
			Just after deck placement	1.0
0.7	4	0	Just before deck placement	11.2
			Just after deck placement	3.2
	0	6	Just before deck placement	10.3
			Just after deck placement	2.3

Notes:
1. Debonded case: 4 strands up to 3.5 ft and 2 strands up to 9.5 ft from the girder ends
2. Harped case: hold-down point is at L/20 ft away from the girder midspan location

3.6.5.4 Case 3b Designs (6 Girders and 7.0 in. Deck)

For Case 3b designs, researchers investigated to find the maximum achievable span length for a bridge having six Tx54 UHPC I-girders with a 7.0 in. CC deck for a target compressive strength of 14 ksi at release and 22 ksi at service by using an inverse design approach that calculates span length for given material properties. Figure 3.24 shows maximum span length solution domains

based on eight concrete stress limits. The optional deflection limit (green solid line) is also shown on the graphs and does not control the Case 3b designs.

For the design case using 0.6 in. diameter strands (Figure 3.24a), based on the tensile stress limit at service, the maximum achievable span length is 158 ft using 86 strands and can be achieved without debonding or harping. The dashed red line indicates the minimum number of strands to satisfy tensile stress limit at the girder ends at release, and the dashed green line is the maximum number of strands to satisfy the compression stress limit at girder ends at release. Therefore, the span length solution domain lies between the red and green dashed lines and maroon solid line.

For the design case using 0.7 in. diameter strands (Figure 3.24b), the maximum achievable span length is 175.5 ft with 82 strands when four strands are debonded or six strands are harped. To achieve the maximum span length based on the tensile stress limit at service (maroon solid line), it is necessary to debond or harp because the compressive stress limit at release (green dashed line) requires a smaller number of strands than the minimum number of strands necessary to satisfy the tensile stress limit at release (red dashed line). The red dotted line indicates the minimum number of strands, and the green dotted line indicates the maximum number of strands when four strands are debonded. Therefore, the span length solution domain lies between the red and green dotted lines and maroon solid line (tension limit for service) for the debonded case. Similarly, the red dashed-dotted line indicates the minimum number of strands, and the green dashed-dotted line indicates the maximum number of strands when six strands are harped. Therefore, the span length solution domain lies between the red and green dashed-dotted lines and maroon solid line (tension limit for service) for the harped case.

Table 3.18 summarizes the maximum achievable span lengths, number of required strands, and debonding or harping information for different strand diameters. For the harped case, the hold-down points are taken as $L/20$ ft away from the centerline of the girder.

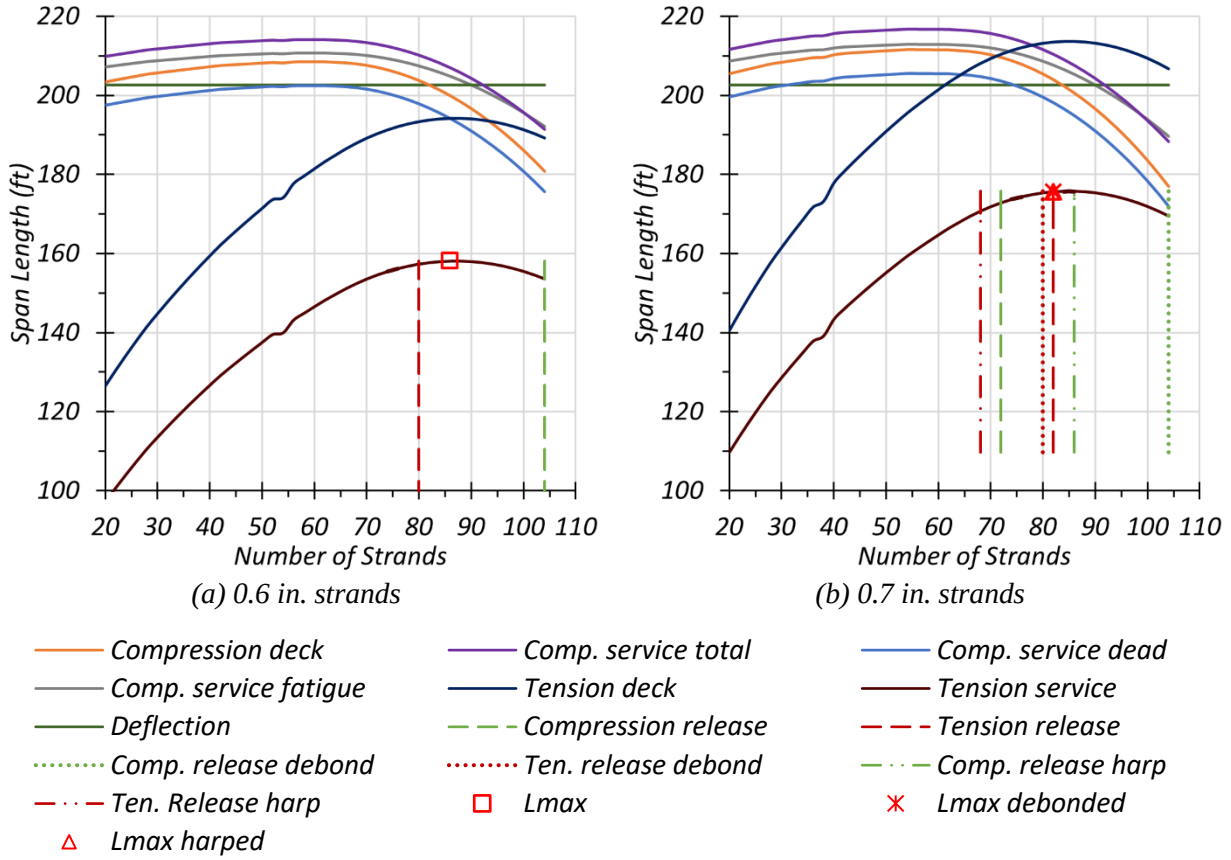

Note: Solid lines = maximum span, dashed red lines = minimum number of strands, dashed green lines = maximum number of strands.

Figure 3.24. Span Length Solution Domain for UHPC Tx54 Girder—Case 3b.

Table 3.18. Maximum Achievable Span Length for UHPC Tx54 Girder—Case 3b.

Strand Diameter (in.)	Total Number of Strands	Number of Debonded Strands	Number of Harped Strands	Maximum Achievable Span Length (ft)
0.6	84	0	0	158
0.7	82	4	0	175.5
	82	0	6	175.5

Notes:
1. Debonded case using 0.7 in. strands: 4 strands up to 3.5 ft and 2 strands up to 9.5 ft
2. Harped case: Hold-down point is at *L*/20 ft away from the centerline

The optimum eccentricity and number of strand requirements were calculated for the maximum achievable span length values obtained for Case 3b designs. Figure 3.25(a) shows the eccentricity solution domain for a 158 ft bridge based on the eight limit states considered when 0.6 in. diameter strands are used. The optimal solution requires 86 strands having 13.10 in. midspan eccentricity to achieve a 158 ft span length. Figure 3.25(b) shows the eccentricity solution domain for a 175.5 ft bridge based on the eight limit states considered when 0.7 in. diameter strands are used. The

compressive stress limit at release for girder ends (green dashed line) requires smaller eccentricity than the minimum eccentricity required to satisfy tensile stress limit at service at the girder midspan (maroon solid line). It is not possible to achieve a 175.5 ft span length without debonding or harping. Therefore, the optimal design requires 82 strands having 14.13 in. midspan eccentricity with four debonded strands or six harped strands. For I-girders, harping provides a more viable method to resolve stress exceedance issues at girder ends because it provides more balanced deflections by reducing the amount of camber. The proposed strand layout for the harped case results in 14.13 in. midspan eccentricity and 12.52 in. end eccentricity.

Figure 3.26 shows the strand layout for a standard Tx54 I-girder in which the green filled locations show straight bonded strands, and the red filled locations show the harped strands from both ends. Table 3.19 lists the camber estimations for debonded and harped options for both design cases using 0.6 in. or 0.7 in. strands. The camber calculations considered the creep coefficient using the AASHTO LRFD Specifications (AASHTO 2020) empirical creep equations for a 40-day-old girder when prestress was applied at one day. For the design case using 0.6 in. strands, the applied prestressing force using 86 strands and 13.10 in. midspan eccentricity for a 158 ft span causes a 5.8 in. camber for noncomposite girders just before deck placement. For the design case using 0.7 in. strands, the applied prestressing force using 82 strands—six of which are harped—having 14.13 in. midspan eccentricity and 12.52 in. end eccentricity creates 10.1 in. camber for noncomposite girders just before deck placement. Using the harping option rather than debonding can provide more balanced deflections by having less initial camber. It may be possible to achieve fully balanced final deflection just after deck placement by harping more strands and/or adjusting hold-down locations.

Live load deflections were also calculated using the optional deflection check criteria provided in Section 3.2.2 of this report and compared with the optional live load deflection limit. Estimated live load deflections for Case 3b designs were found to be smaller than the deflection limit.

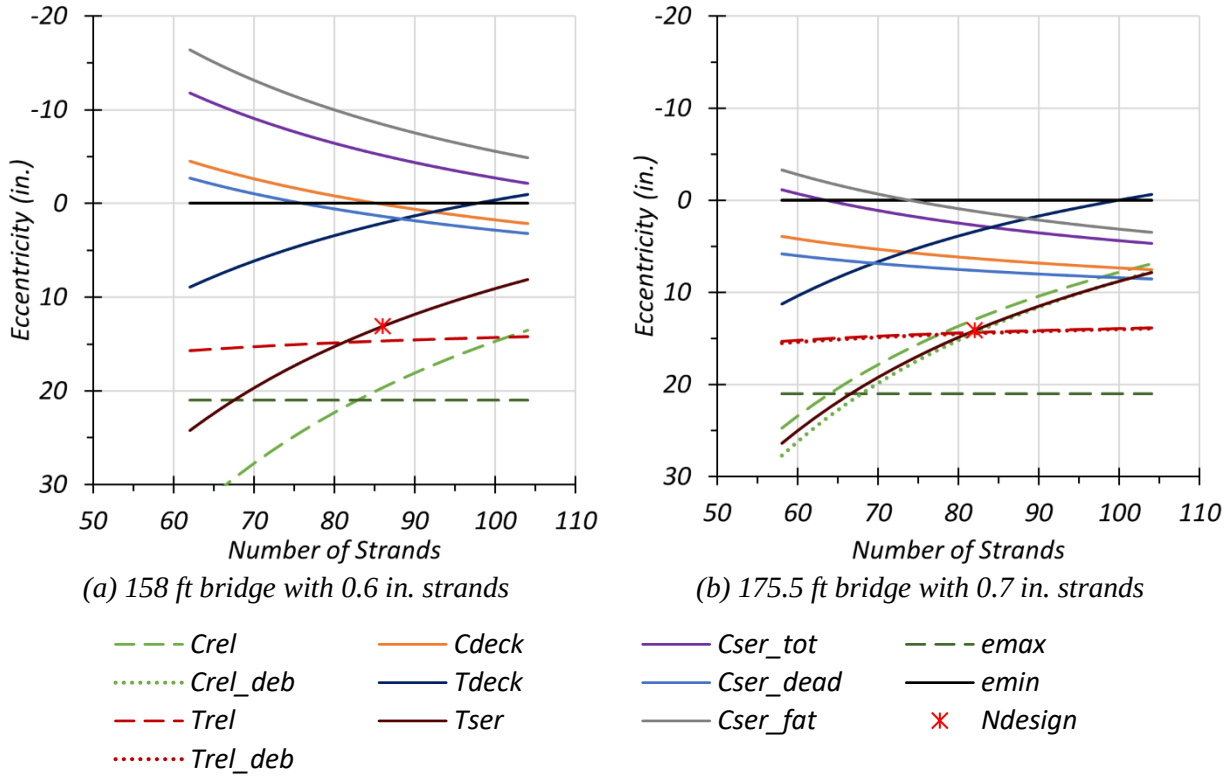

(a) 158 ft bridge with 0.6 in. strands

(b) 175.5 ft bridge with 0.7 in. strands

Note: Solid lines = minimum eccentricity, dashed lines = maximum eccentricity.

Figure 3.25. Eccentricity Solution Domain for UHPC Tx54 Girders—Case 3b.

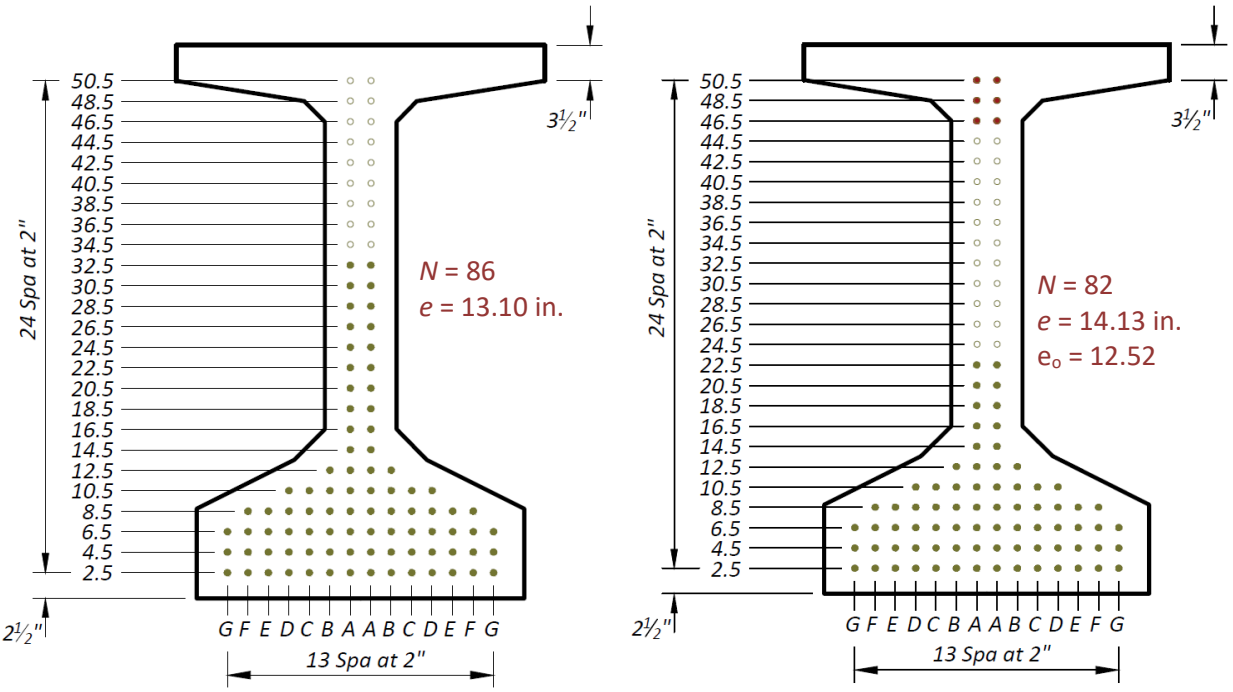

(a) 158 ft Bridge with 0.6 in. Strands *(b) 175.5 ft Bridge with 0.7 in. Strands*

Notes:
1. N = Number of strands, e = eccentricity at midspan, e_o = end eccentricity
2. Green fill = bonded straight strands, red fill = harped strands

Figure 3.26. Optimum Strand Design for UHPC Tx54 Girders—Case 3b.

Table 3.19. Estimated Camber for UHPC Tx54 Girders—Case 3b.

Strand Diameter (in.)	Number of Debonded Strands	Number of Harped Strands	Time of Camber	Camber (in.)
0.6	0	0	Just before deck placement	5.8
			Just after deck placement	1.0
0.7	4	0	Just before deck placement	11.0
			Just after deck placement	3.8
	0	6	Just before deck placement	10.1
			Just after deck placement	2.9

Notes:
1. Debonded case using 0.7" strands: 4 strands up to 3.5 ft and 2 strands up to 9.5 ft
2. Harped case: Hold-down point is at L/20 ft away from the centerline

3.6.5.5 Case 3c Designs (5 Girders and 7.0 in. Deck)

For Case 3c designs, researchers investigated the maximum achievable span length for a bridge having five Tx54 UHPC I-girders with a 7.0 in. CC deck for a target compressive strength of 14 ksi at release and 22 ksi at service using an inverse design approach that calculates span length for given material properties. Figure 3.27 shows maximum span length solution domains based on

eight concrete stress limits. The optional deflection limit (green solid line) is also shown on the graphs and does not control the Case 3c designs.

For the design case using 0.6 in. diameter strands (Figure 3.27a), based on the tensile stress limit at service, the maximum achievable span length is 148.5 ft using 86 strands and can be achieved without debonding or harping. The dashed red line indicates a minimum number of strands to satisfy tensile stress limit at the girder ends at release, and the dashed green line is the maximum number of strands to satisfy the compression stress limit at girder ends at release. Therefore, the span length solution domain lies between the red and green dashed lines (compressive and tensile stress limit at release) and under the maroon solid line (tensile stress limit at service).

For the design case using 0.7 in. diameter strands (Figure 3.27b), the maximum achievable span length is 165.0 ft with 82 strands when four strands are debonded or six strands are harped. To achieve maximum span length based on the tensile stress limit at service (maroon solid line), it is necessary to debond or harp because the compressive stress limit at release (green dashed line) requires a smaller number of strands than the minimum number of strands necessary to satisfy the tensile stress limit at release (red dashed line). The red dotted line indicates the minimum number of strands, and the green dotted line indicates the maximum number of strands when four strands are debonded. Therefore, the span length solution domain is bounded by the red and green dotted lines and the maroon solid line for the debonded case. Similarly, the red dashed-dotted line indicates the minimum number of strands and the green dashed-dotted line indicates the maximum number of strands when six strands are harped. Therefore, the span length solution domain is bounded by the red and green dashed-dotted lines and the maroon solid line for the harped case.

Table 3.20 summarizes the maximum achievable span lengths, number of required strands, and debonding or harping information for different strand diameters. For the harped case, the hold-down points are taken as L/20 ft away from the centerline of the girder.

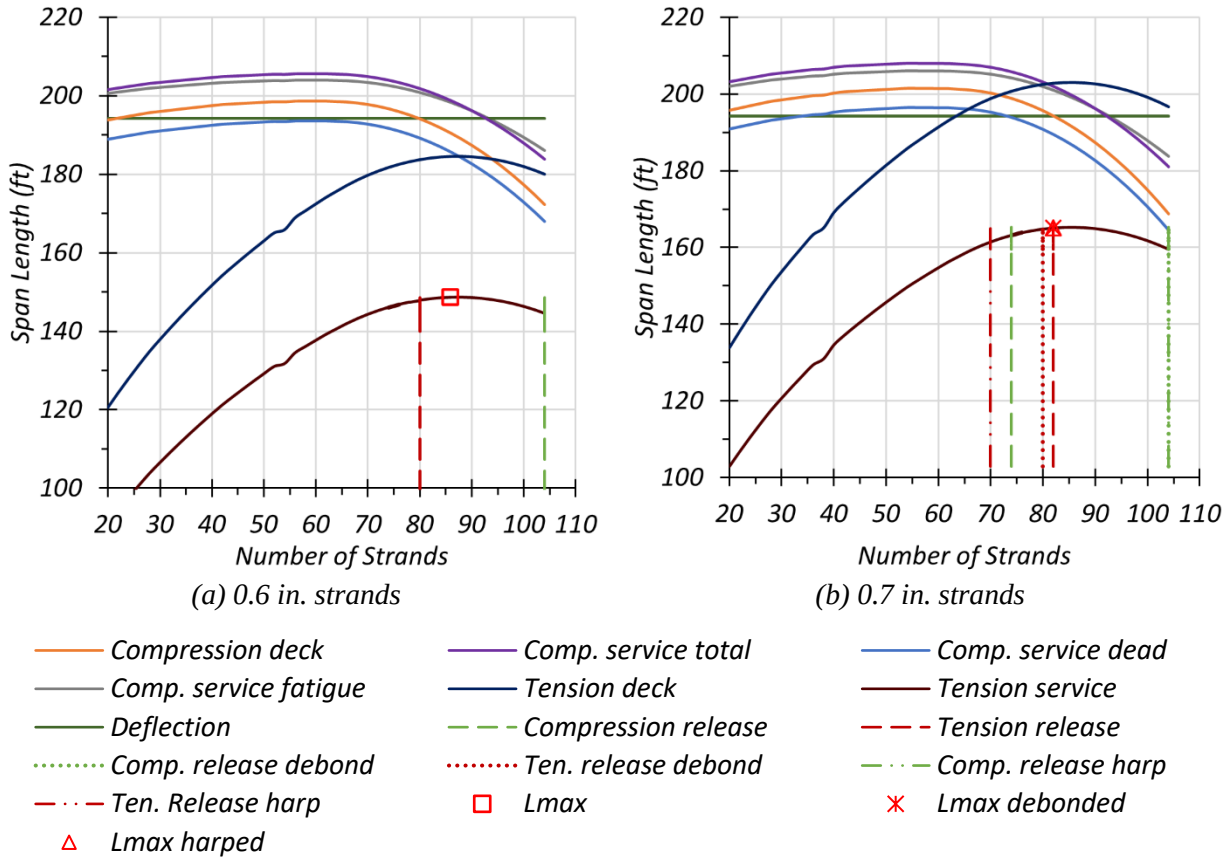

Note: Solid lines = maximum span, dashed red lines = minimum number of strands, dashed green lines = maximum number of strands.

Figure 3.27. Span Length Solution Domain for UHPC Tx54 Girder—Case 3c.

Table 3.20. Maximum Achievable Span Length for UHPC Tx54 Girder—Case 3c.

Strand Diameter (in.)	Total Number of Strands	Number of Debonded Strands	Number of Harped Strands	Maximum Achievable Span Length (ft)
0.6	86	0	0	148.5
0.7	82	4	0	165
	82	0	6	165

Notes:
1. Debonded case using 0.7" strands: 4 strands up to 3.5 ft and 2 strands up to 9.5 ft
2. Harped case: Hold-down point is at L/20 ft away from the centerline

The optimum eccentricity and number of strand requirements were calculated for the maximum achievable span length values obtained for Case 3c designs. Figure 3.28(a) shows the eccentricity solution domain for a 148.5 ft bridge based on the eight limit states considered when 0.6 in. diameter strands are used. The optimal solution requires 86 strands having a 13.10 in. midspan eccentricity to achieve a 148.5 ft span length. Figure 3.28(b) shows the eccentricity solution domain for a 165.0 ft bridge based on the eight limit states considered when 0.7 in. diameter strands

are used. The compressive stress limit at release at the girder ends (green dashed line) requires smaller eccentricity than the minimum eccentricity required to satisfy tensile stress limit at service at the girder midspan (maroon solid line). It is not possible to achieve a 165.0 ft span length without debonding or harping. Therefore, the optimal design requires 82 strands having 14.13 in. midspan eccentricity with four debonded strands or six harped strands. For I-girders, harping provides a more viable method to resolve stress exceedance issues at girder ends because it provides more balanced deflections by reducing the amount of camber. The proposed strand layout for the harped case results in 14.13 in. midspan eccentricity and 12.52 in. end eccentricity.

Figure 3.29 shows the strand layout for a standard Tx54 I-girder in which the green filled locations show straight bonded strands and red filled locations show the harped strands from both ends. Table 3.21 lists the camber estimations for debonded and harped options for both design cases using 0.6 in. or 0.7 in. strands. The camber calculations considered the creep coefficient using the AASHTO LRFD Specifications (AASHTO 2020) empirical creep equations for a 40-day-old girder when prestress was applied at one day. For the design case using 0.6 in. strands, the applied prestressing force using 86 strands and a 13.10 in. midspan eccentricity for a 148.5 ft span causes a 6.2 in. camber for noncomposite girders just before deck placement. For the design case using 0.7 in. strands, the applied prestressing force using 82 strands—six of which are harped—having 14.13 in. midspan eccentricity and 12.52 in. end eccentricity creates a 10.6 in. camber for noncomposite girders just before deck placement. Using the harping option rather than debonding can provide more balanced deflections by having less initial camber. It may be possible to achieve a fully balanced final deflection just after deck placement by harping more strands and/or adjusting hold-down location.

Live load deflections were also calculated using the optional deflection check criteria provided in Section 3.2.2 of this report and compared with the optional live load deflection limit. Estimated live load deflections for Case 3c designs were found to be smaller than the deflection limit.

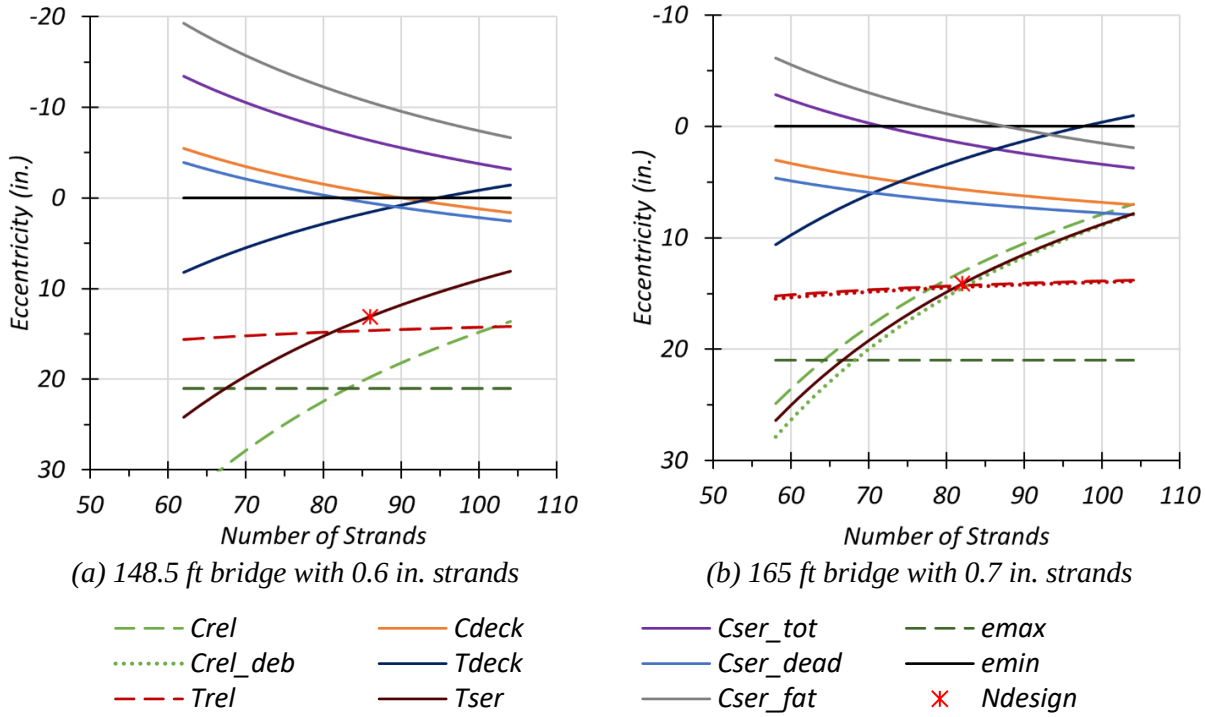

(a) 148.5 ft bridge with 0.6 in. strands *(b) 165 ft bridge with 0.7 in. strands*

Note: Solid lines = minimum eccentricity, dashed lines = maximum eccentricity.

Figure 3.28. Eccentricity Solution Domain for UHPC Tx54 Girders—Case 3c.

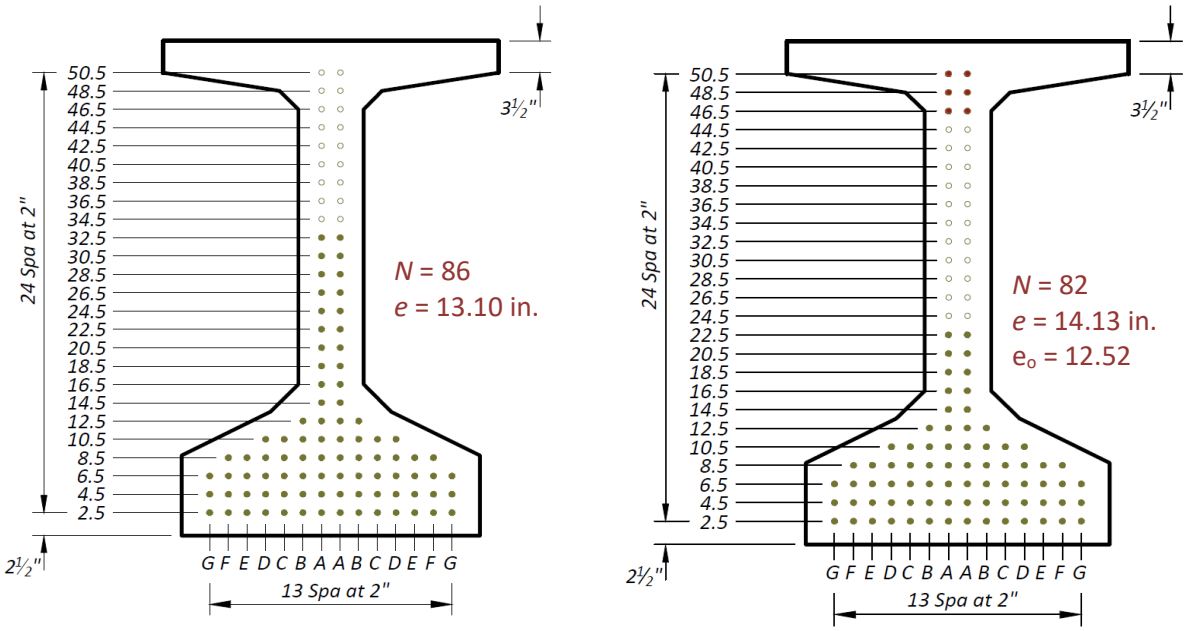

(a) 148.5 ft Bridge with 0.6 in. Strands *(b) 165 ft Bridge with 0.7 in. Strands*

Notes:

1. N = Number of strands, e = eccentricity at midspan, e_o = end eccentricity
2. Green fill = bonded straight strands, red fill = harped strands

Figure 3.29. Optimum Strand Design for UHPC Tx54 Girders—Case 3c.

Table 3.21. Estimated Camber for UHPC Tx54 Girders—Case 3c.

Strand Diameter (in.)	Number of Debonded Strands	Number of Harped Strands	Time of Camber	Camber (in.)
0.6	0	0	Just before deck placement	6.2
			Just after deck placement	1.7
0.7	4	0	Just before deck placement	11.3
			Just after deck placement	4.4
	0	6	Just before deck placement	10.6
			Just after deck placement	3.7

Notes:
1. Debonded case using 0.7 in. strands: 4 strands up to 3.5 ft and 2 strands up to 9.5 ft
2. Harped case: Hold-down point is at $L/20$ ft away from the centerline

3.6.5.6 Summary of Flexural Stress Designs for UHPC Tx54 Girder

All three design cases and the subcases were investigated with 0.6 in. diameter strands to explore the optimum eccentricity and maximum achievable span length. Table 3.22 summarizes design parameters and the results of the parametric feasibility study for the design cases using 0.6 in. diameter strands. The tension stress limit at service and release controls the optimum number of strands and eccentricity for all design cases using 0.6 in. diameter strands.

For Case 3 designs using 0.6 in. diameter strands, the tension stress limit at service controls the maximum achievable span length that can be achieved without debonding or harping any strands. The maximum achievable span length was found to be 155 ft for Case 3a, 158 ft for Case 3b, and 148.5 ft for Case 3c design. Reducing the deck thickness from 8.5 in. to 7.0 in. (Case 3a versus Case 3b) provides a relatively small increase (only 3 ft, less than 2 percent) in the maximum achievable span length. Reducing the number of girder lines from six girders to five girders for a bridge having 7.0 in. deck thickness (Case 3b vs. Case 3c) decreases the maximum achievable span length by around 10 ft, which is more than a 6 percent reduction.

Case 1 designs explored the required concrete strength to achieve a 160 ft span length. The required elastic tensile strength was found to be 1.5 ksi for the Case 1a design, which uses six girder lines. Typical elastic tensile strength values for UHPC range between 1.0 and 1.5 ksi based on the literature review. Although the required tensile strength of 1.5 ksi is relatively high, a 160 ft span length can be achieved using six girder lines. However, tensile strength values greater than 1.5 ksi would be difficult to achieve on a routine basis and are not considered practical. The Case 1b design, which explores the possibility of using five girder lines for a 160 ft span length, requires a

2.6 ksi elastic tensile strength; thus, it is not practical. Similarly, Case 2 designs, which explore the possibility of achieving 170 ft span lengths, require elastic tensile strengths ranging between 2.3 and 3.4 ksi. Such high elastic tensile strength values are above the practical limits for the expected elastic tensile strength of current UHPC mixtures.

A 160 ft span length can be achieved using six Tx54 UHPC girders when the elastic tensile strength is increased to 1.5 ksi. However, it is very difficult and impractical to obtain a 170 ft span length using Tx54 UHPC girders since this process leads to a required elastic tensile strength that is higher than typical UHPC limits.

Table 3.22. Summary of Flexural Stress Designs for Tx54 Girder Using 0.6 in. Strands.

Parameter	Case 1a	Case 1b	Case 2a	Case 2b	Case 2c	Case 3a	Case 3b	Case 3c
Span Length, ft	160.0	160.0	170.0	170.0	170.0	155.0	158.0	148.5
Total Width, ft	46	46	46	46	46	46	46	46
Girder Spacing, ft	8	10	8	8	10	8	8	10
No. of Girders	6	5	6	6	5	6	6	5
Overhang, ft	3	3	3	3	3	3	3	3
Deck Thickness, in.	8.5	8.5	8.5	7.0	7.0	8.5	7.0	7.0
Span/Depth	30.7	30.7	32.6	33.4	33.4	29.8	31.1	29.2
f'_{ci} (ksi)	14.0	14.0	14.0	14.0	14.0	14.0	14.0	14.0
f'_{c} (ksi)	22.0	22.0	22.0	22.0	22.0	22.0	22.0	22.0
f'_{ti} (ksi)	0.75	0.75	0.75	1.0	1.0	0.75	0.75	0.75
f'_{t} (ksi)	1.5	2.6	2.6	2.3	3.4	1.0	1.0	1.0
Strand Diameter (in.)	0.6	0.6	0.6	0.6	0.6	0.6	0.6	0.6
No. of Strands	84	82	82	82	80	84	86	86
Debonded Strands	0	0	0	0	0	0	0	0
Harped Strands	0	0	0	0	0	0	0	0
Camber Before Deck (in.)	5.90	6.3	5.4	5.4	5.6	6.2	5.8	6.2
Camber After Deck (in.)	−0.02	−1.1	−2.2	−1.0	−2.2	1.0	1.0	1.7

Case 3 designs were also investigated considering the use of 0.7 in. diameter strands to explore the maximum achievable span length and the corresponding optimum number of strands and eccentricity. Table 3.23 summarizes the design parameters and the results of the parametric feasibility study for all Case 3 designs using 0.7 in. diameter strands. For Case 3 designs using 0.7 in. diameter strands, the tension stress limit at service controls the maximum achievable span length, and four strands must be debonded or six strands must be harped to pass all stress limits. The maximum achievable span length was found to be 172 ft for Case 3a, 175.5 ft for Case 3b, and 165 ft for Case 3c designs.

Table 3.23. Summary of Flexural Stress Designs for Tx54 Girder Using 0.7 in. Strands.

Parameter	Case 3a.1	Case 3a.2	Case 3b.1	Case 3b.2	Case 3c.1	Case 3c.2
Span Length, ft	172.0	172.0	175.5	175.5	165.0	165.0
Total Width, ft	46	46	46	46	46	46
Girder Spacing, ft	8	8	8	8	10	10
No. of Girders	6	6	6	6	5	5
Overhang, ft	3	3	3	3	3	3
Deck Thickness, in.	8.5	8.5	7.0	7.0	7.0	7.0
Span/Depth	33.0	33.0	34.5	34.5	30.6	30.6
f'_{ci} (ksi)	14.0	14.0	14.0	14.0	14.0	14.0
f'_{c} (ksi)	22.0	22.0	22.0	22.0	22.0	22.0
f'_{ti} (ksi)	0.75	0.75	0.75	0.75	0.75	0.75
f'_{t} (ksi)	1.0	1.0	1.0	1.0	1.0	1.0
Strand Diameter (in.)	0.7	0.7	0.7	0.7	0.7	0.7
No. of Strands	82	82	82	82	82	82
Debonded Strands	4	0	4	0	4	0
Harped Strands	0	6	0	6	0	6
Camber Before Deck (in.)	11.2	10.3	11.0	10.1	11.3	10.6
Camber After Deck (in.)	3.2	2.3	3.8	2.9	4.4	3.7

Figure 3.30 provides a bar chart comparison for the maximum achievable span lengths using 0.6 in. and 0.7 in. diameter strands. In comparison to the standard Tx54 I-girder design using CC,

the designs using 0.6 in. diameter strands can provide around a 30 percent longer span length, while the designs using 0.7 in. diameter strands can provide around a 50 percent longer span length. Thus, the full potential of UHPC can best be leveraged by using large diameter (0.7 in.) strands.

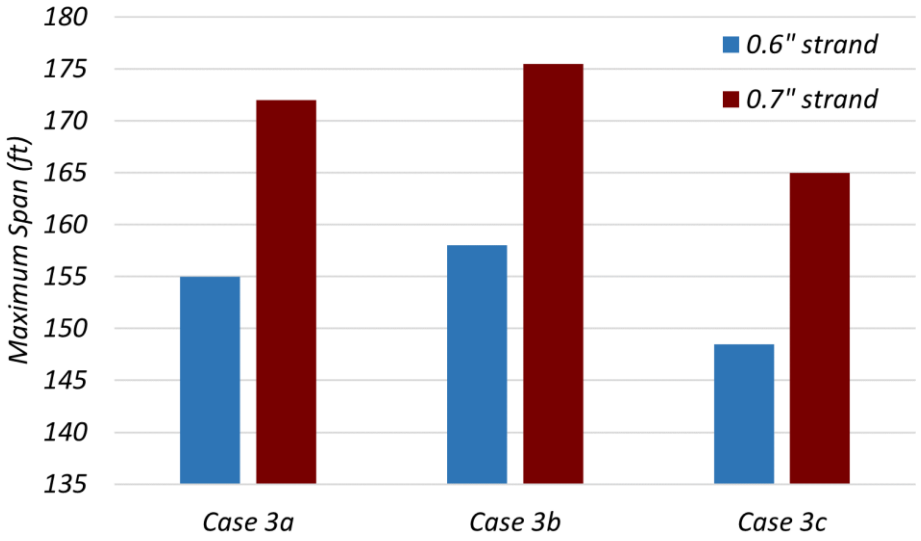

Figure 3.30. Comparison of Maximum Span Lengths for UHPC Tx54 Girders.

3.6.6 Flexural Resistance at Strength Limit State

The reduced nominal flexural resistance ϕM_n of Tx54 girders must be greater than the factored flexural demand M_u using the Strength I load combination provided in the AASHTO LRFD Specifications (AASHTO 2020) Table 3.4.1-1. Section 3.4 of this report provides the load and resistance factors and the design approach for calculating flexural resistance using a triangular stress block approach. The flexural resistance of Tx54 girders was also calculated using the conventional rectangular stress block approach following the guidelines and assumptions provided in the AASHTO LRFD Specifications (AASHTO 2020) Article 5.6.2.1.

Table 3.24 summarizes the factored flexural demand M_u, and reduced nominal flexural resistance ϕM_n results for both Case 3 designs using 0.6 in. and 0.7 in. diameter strands. Figure 3.31 shows a bar chart comparing the factored flexural demands for Case 3 designs with the reduced nominal flexural resistance computed using both the rectangular and triangular stress block approach. The details about Case 3 designs may be found in the previous section. Both the rectangular and

triangular stress block approach suggest that the reduced nominal flexural resistance is greater than the factored flexural demand. When compared to rectangular stress distribution, using triangular stress distribution to calculate the flexural resistance of Tx54 UHPC girders results in 1–2 percent higher estimate for design cases using 0.6 in. diameter strands, while providing 2–4 percent lower estimates for design cases using 0.7 in. diameter strands. Note that using the triangular stress distribution method is more complicated than the rectangular stress block approach, especially when applying it to I-girder shapes.

Table 3.24. Flexural Demand and Resistance Results for Tx54 Girders—Case 3.

Nominal Strand Diameter	Design Case	Factored Flexural Demand M_u, kip-ft	Reduced Nominal Flexural Resistance ϕM_n, kip-ft	
			Rectangular stress block	Triangular stress block
0.6 in.	Case 3a	13,630	17,410	17,659
	Case 3b	13,788	17,038	17,113
	Case 3c	14,171	17,559	17,827
0.7 in.	Case 3a	16,260	22,261	21,368
	Case 3b	16,440	20,954	20,539
	Case 3c	16,860	22,415	21,569

Note: The resistance factor ϕ for tension-controlled prestressed concrete members with bonded strands is taken as 1.0 based on the AASHTO LRFD Specifications (AASHTO 2020).

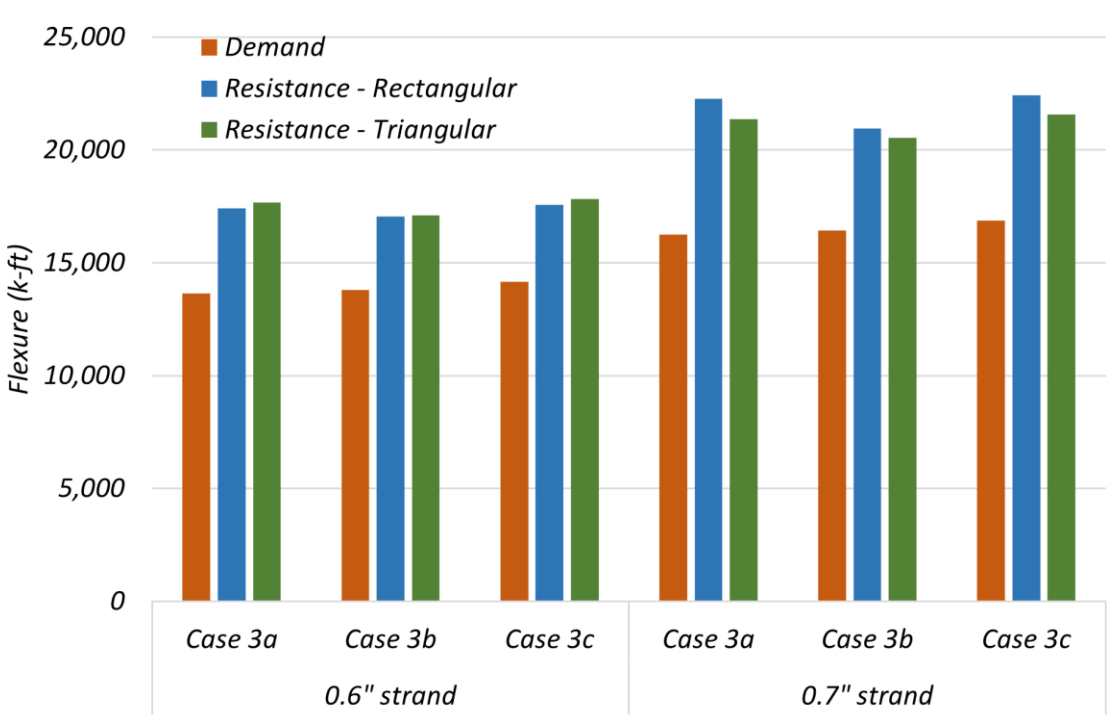

Figure 3.31. Comparison of Flexural Resistance for UHPC Tx54 Girder.

3.6.7 Shear Resistance at Strength Limit State

The shear resistance of Tx54 UHPC girders must be greater than the factored shear demand using the Strength I load combination provided in AASHTO LRFD Specifications (AASHTO 2020) Table 3.4.1-1. Section 3.4 of this report provides the load and resistance factors and the design approach for calculating shear resistance. The AFGC Guidelines' (AFGC 2013) shear design methodology has been used for calculating shear resistance.

Table 3.25 summarizes the factored shear demand V_u and shear resistance V_n results for both Case 3 designs using 0.6 in. and 0.7 in. diameter strands. Figure 3.32 shows a bar chart comparing the factored shear demands for Case 3 designs with the factored shear resistance computed using the AFGC Guidelines (AFGC 2013). Two different shear resistance values were calculated based on the method used for calculating the shear depth, which depends on the lever arm of the internal forces corresponding to the bending moment. Both shear resistance values using the shear depth from the rectangular and triangular stress block approach suggest that the factored shear resistance is greater than the factored flexural demand for most design cases. Design cases using five girders have slightly lower shear resistance when the triangular stress block approach is used for

calculating the shear depth. Using a triangular stress distribution for calculating the shear depth results in a 15 percent lower shear resistance estimate than when using a rectangular stress block.

If the shear reinforcement guidelines from the AASHTO LRFD Specifications (AASHTO 2020) Article 5.7.2.3 are adopted, the regions having a factored shear force greater than half of the factored shear resistance provided by concrete and fibers requires minimum shear reinforcement. Whether the triangular stress block or rectangular stress block approach is used for calculating the shear depth, half of the shear resistance provided by concrete and fibers ($0.5(V_{Rd,c} + V_{Rd,f})$) is smaller than the factored shear demand at the critical shear section. This finding indicates that the five-girder designs would need some shear reinforcement in the critical shear regions. The empirical equation to calculate the minimum required transverse shear reinforcement is provided in the AASHTO LRFD Specifications (AASHTO 2020) Article 5.7.2.5. The minimum shear reinforcement is likely be required for the first quarter of the girder length for most cases.

Table 3.25. Shear Demand and Resistance Results for Tx54 Girders—Case 3.

Nominal Strand Diameter	Design Case	Factored Shear Demand V_u, kips	Nominal Shear Resistance V_n, kips	
			Rectangular stress block	Triangular stress block
0.6 in.	Case 3a	385	481	407
	Case 3b	378	463	392
	Case 3c	412	471	401
0.7 in.	Case 3a	417	479	421
	Case 3b	408	468	411
	Case 3c	445	476	421

Note: The shear resistance is calculated using AFGC Guidelines (AFGC 2013), which includes safety factors in nominal shear resistance equations rather than a resistance factor ϕ.

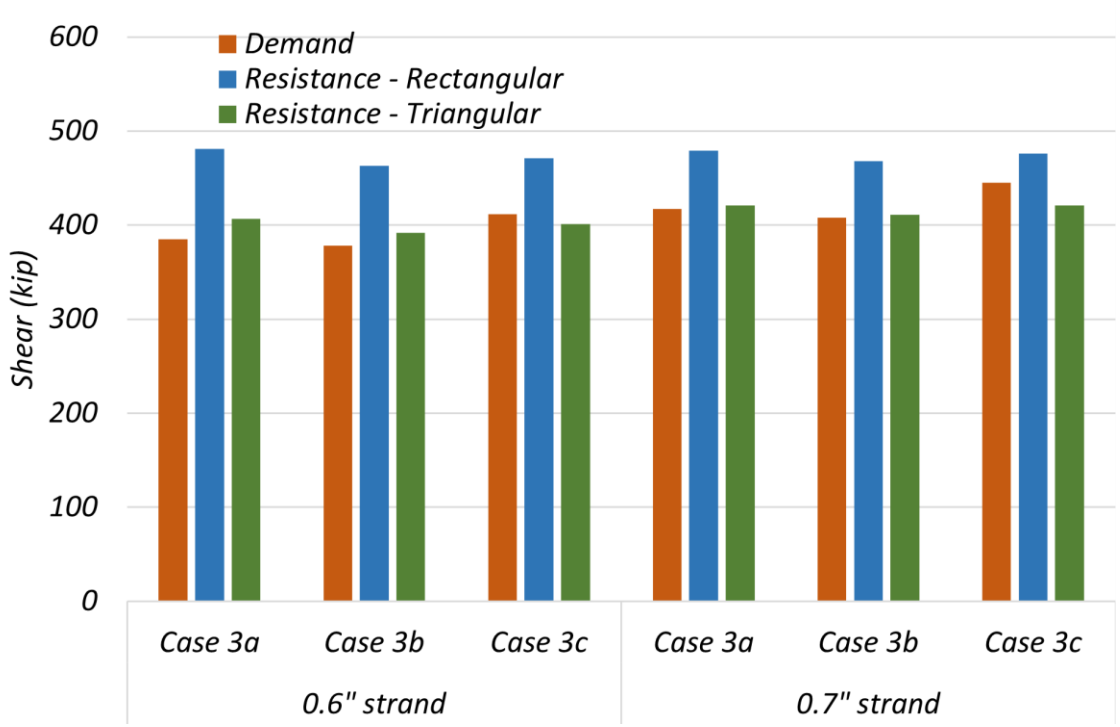

Figure 3.32. Comparison of Shear Resistance for UHPC Tx54 Girder.

3.7 DESIGNS FOR TX62 I-GIRDERS

One of the longest possible span lengths using Tx62 prestressed concrete I-girders was selected from the TxDOT standard bridge drawings as the base bridge geometry to allow comparison of UHPC designs. The bridge cross-section, girder spacing, material properties (except girder concrete strength), and section properties of the girder were kept the same as the selected standard Tx62 girder design for the main design cases. Several subcases were explored by considering a different deck thickness and a different girder spacing. A 7.0 in. thick deck was considered to determine the potential benefit of using thinner 2.5 in. thick UHPC PCPs as stay-in-place formwork, with the remainder of the deck composed of the standard 4.5 in. thick CIP concrete. The reduced deck thickness option was included to evaluate the effect of reduced superstructure weight with respect to the tension strength requirement. Note that the CIP concrete deck thickness remains the same and provides the same minimum cover. Only the thickness of the PCPs was modified to 2.5 in., which would maintain the cover for the reinforcement within the 4.5 in. (minimum) CIP deck. The following research questions were addressed by investigating the following three main design cases, which have several subcases.

1. Is it possible to achieve a 160 ft span length for a 46 ft wide bridge using:
    a) Six Tx62 UHPC I-girders?
    b) Five Tx62 UHPC I-girders?

    What would be the required concrete compressive strength at release and at 28 days to achieve this span length?
2. Is it possible to achieve a 170 ft span length for a 46 ft wide bridge using:
    a) Six Tx62 UHPC I-girders?
    b) Six Tx62 UHPC I-girders and a 7 in. thick deck?
    c) Five Tx62 UHPC I-girders and a 7 in. thick deck?

    What would be the required concrete compressive strength at release and at 28 days to achieve this span length?
3. What is the maximum achievable span length for a 46 ft wide bridge using Tx62 UHPC I-girders that have 14 ksi compressive and 0.75 ksi elastic tensile strength at release, and 22 ksi compressive and 1.0 ksi elastic tensile strength at 28 days for:
    a) Six Tx62 UHPC I-girders?
    b) Six Tx62 UHPC I-girders and a 7 in. thick deck?
    c) Five Tx62 UHPC I-girders and a 7 in. thick deck?

Note that the design elastic tensile strength from direct tension testing of UHPC was assumed to be 0.75 ksi at release and 1.0 ksi at 28 days for all design cases based on the values obtained from the literature (Graybeal 2006a; Haber et al. 2018; Wille et al. 2014a). The tensile stress limit was considered as 85 percent of the elastic tensile strength based on the material reduction factor in tension that was recommended by Graybeal (2019).

3.7.1 Geometry of Tx62 I-Girder Bridge

Figure 3.33 shows the cross-section details of the selected prestressed bridge using Tx62 I-girders. For the main design cases, six Tx62 prestressed concrete I-girders are spaced at 8 ft centers across a 46 ft overall bridge width topped with an 8.5 in. deck slab (4 in. PCPs plus 4.5 in. CIP reinforced concrete deck). For the subcases, five girders at 10 ft spacing and 7 in. thick deck options were also considered. An average 2 in. constant haunch thickness was assumed along the entire span length as part of permanent dead loads. However, the haunch contribution to the stiffness of the composite section was neglected because the haunch thickness varies along the length and may be

as small as 0.5 in. at the midspan. The assumed superimposed dead loads consist of an average 2 in. thick asphalt overlay and T551 rails, one of the heaviest railing types used by TxDOT. The weight of the rails was distributed to three girders closest to each of the bridge's edges, as recommended by the *TxDOT Bridge Design Manual* (TxDOT 2021). Table 3.26 summarizes these key geometric design parameters for the selected typical standard bridge cross-section using prestressed Tx62 I-girders.

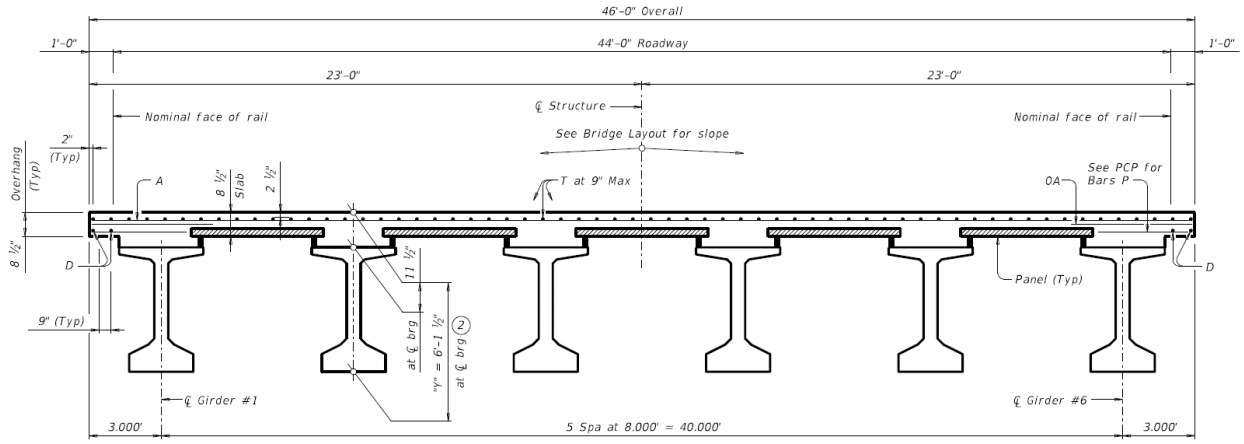

Figure 3.33. Typical Bridge Cross-Section Using Tx62 I-Girders (TxDOT 2019).

Table 3.26. Geometric Properties of Tx62 I-Girder Bridge.

Parameter	Description/Value
Bridge Width, W	46 ft
Girder Spacing, S	8 or 10 ft
Number of Girders, n	5 or 6
Deck Thickness, t_s	8.5 or 7.0 in.
Wearing Surface Thickness, t_{ws}	2 in. asphalt
Haunch Thickness, t_h	2 in. for weight calculation only
Railing	T551 (0.382 kip/ft)

3.7.2 Girder Details and Section Properties of Tx62 I-Girder

Figure 3.34 shows geometric and reinforcement details and strand layout of the standard Tx62 prestressed I-girder. The 62 in. deep Tx62 prestressed I-girders have a 32 in. wide bottom bulb that can hold a maximum of 66 strands in six rows of a 2 × 2 in. grid, while the 7 in. wide web can hold 46 strands in 23 rows of a 2 × 2 in. grid. Section properties of the noncomposite Tx62 I-girder—including area, centroid location, moment of inertia, and the weight per unit length—

were calculated based on the standard cross-section geometry. Note that the unit weight of the conventional Tx62 I-girder with reinforcement is 0.155 kcf, while the UHPC Tx62 I-girder with reinforcement is considered to be 0.165 kcf since UHPC is about 10 lb/ft^3 heavier than the CC due to the presence of fibers. Table 3.27 lists the calculated section properties, which are consistent with the values provided in the structural drawing files from *TxDOT Bridge Standards* (TxDOT 2019).

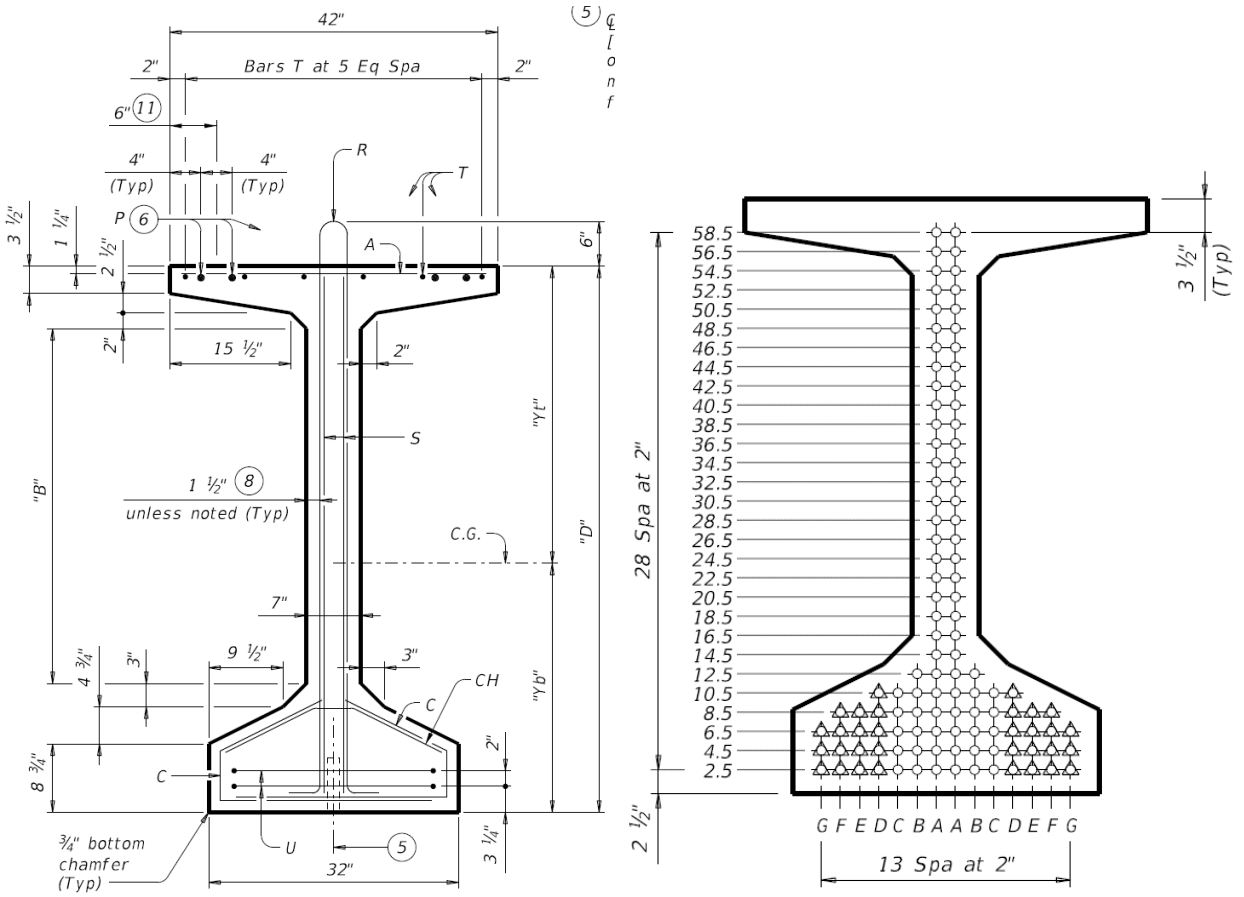

(a) Reinforcement details *(b) Strand layout*

Figure 3.34. Section Geometry of Tx62 I-Girder (TxDOT 2019).

Table 3.27. Section Properties of Tx62 I-Girder.

Parameter	Value
Area, A (in^2)	910
Centroid Distance from Top, y_t (in.)	33.72
Centroid Distance from Bottom, y_b (in.)	28.28
Moment of Inertia, I_g (in^4)	463,072
Girder Weight, w_g (kip/ft)	0.980

Note: Unit weight of the UHPC Tx62 girder with reinforcement is taken as 0.165 kcf.

3.7.3 Material Properties for Tx62 I-Girder Bridge

Table 3.28 lists the material properties used for the design of Tx62 prestressed I-girder bridges that were used for all alternative design cases investigated in this study. The design compressive strength of the CIP deck concrete was taken as 4 ksi based on the structural drawings provided in the *TxDOT Bridge Standards* (TxDOT 2019). The unit weight of concrete for the CC deck slab was taken as 0.145 kcf to compute MOE. To compute the dead load of the deck slab, the unit weight of the conventional deck concrete with reinforcement was considered to be 0.150 kcf. The unit weight of UHPC was taken as 0.155 kcf, which is slightly higher than CC due to the presence of fibers. Therefore, the unit weight of UHPC Tx62 I-girder with reinforcement was taken as 0.165 kcf.

Design compressive and tensile strengths of concrete at release and at 28 days are key properties for the design of prestressed concrete girders. Allowable stress design criteria for CC only considers design compressive strength as a parameter, and tensile stress limits are generally calculated using the empirical square root relationships between the compressive and tensile strength. However, for UHPC, the tensile strength is not formulated as a function of compressive strength; thus, the design elastic tensile strengths at release and at 28 days were considered based on common values in the literature. The elastic tensile strength of UHPC Tx62 girders was assumed to be 0.75 ksi at release and 1.0 ksi at service and kept the same for all alternative UHPC design cases that were designed for maximum achievable span length. For the design cases that consider a target span length and designs for the concrete strength, elastic tensile strength was increased up to 1.7 ksi at service to achieve the target span length. The concrete compressive strength of UHPC Tx62 I-girders at release and at 28 days were kept as a variable for the design cases that consider a target span length and design for the concrete strength. For the cases that

design for maximum achievable span length, the compressive strength of UHPC girders was taken as 14 ksi at release and 22 ksi at service.

The MOE of CC of the deck slab was calculated using the AASHTO LRFD Specifications (AASHTO 2020) expression, and MOE of the UHPC slab beam girder was calculated using the MOE equation provided by Graybeal (2014). Section 3.5.3 provides both equations.

Table 3.28. Material Properties for Tx62 Girder Bridge.

Parameter	Description/Value
Compressive strength of deck concrete, f'_{cd}	4.0 ksi
Tensile strength of girder concrete at release, f'_{ti}	0.75 ksi
Tensile strength of girder concrete at 28 days, f'_{t}	1.0 to 1.7 ksi
Compressive strength of UHPC girder at release, f'_{ci}	14 ksi or varies*
Compressive strength of UHPC girder at 28 days, f'_{c}	22 ksi or varies*
Unit weight of CC (used to compute E_c), γ_{cc}	0.145 kcf
Unit weight of CC with reinforcement (to compute dead load)	0.150 kcf
Unit weight of UHPC, γ_{UHPC}	0.155 kcf
Unit weight of UHPC Tx62 girder with reinforcement (to compute dead load)	0.165 kcf
Unit weight of asphalt overlay, γ_{ws}	0.140 kcf
Weight of T551 rail, w_r	0.382 kip/ft (distributed to three girders)
Ultimate strength of prestressing stands, f_{pu}	270 ksi
MOE of strands, E_{ps}	28,500 ksi

*Varies for the design cases that consider a target span length and designs for UHPC strength.

3.7.4 Alternative Design Cases for UHPC

Table 3.29 provides the main design parameters for the alternative design cases explored for the prestressed UHPC Tx62 I-girders. Three main design cases with several subcases were explored, as described in the beginning of Section 3.7.

Table 3.29. Main Design Parameters for Alternative Designs Using Tx62 I-Girders.

Parameter	CC-TxDOT	UHPC Case 1a	UHPC Case 1b	UHPC Case 2a	UHPC Case 2b	UHPC Case 2c	UHPC Case 3a	UHPC Case 3b	UHPC Case 3c
Span Length (ft)	130	160	160	170	170	170	Max.	Max.	Max.
Bridge Width (ft)	46	46	46	46	46	46	46	46	46
Girder Spacing (ft)	8	8	10	8	8	10	8	8	10
Number of Girders	6	6	5	6	6	5	6	6	5
Overhang (ft)	3	3	3	3	3	3	3	3	3
Deck Thickness (in.)	8.5	8.5	8.5	8.5	7.0	7.0	8.5	7.0	7.0
Span/Depth Ratio	22.1	27.2	27.2	28.9	29.6	29.6	TBD	TBD	TBD
f'_{ci} (ksi)	5.8	TBD	TBD	TBD	TBD	TBD	14	14	14
f'_{c} (ksi)	6.7	TBD	TBD	TBD	TBD	TBD	22	22	22
f'_{ti} (ksi)	–	0.75	0.75	0.75	0.75	0.75	0.75	0.75	0.75
f'_{t} (ksi)	–	TBD	TBD	TBD	TBD	1.0	1.0	1.0	1.0
Strand Diameter (in.)	0.6	TBD	TBD	TBD	TBD	TBD	TBD	TBD	TBD
Number of Strands	42	TBD	TBD	TBD	TBD	TBD	TBD	TBD	TBD
Debonded Strands	6	TBD	TBD	TBD	TBD	TBD	TBD	TBD	TBD

Notes:
1. CC-TxDOT indicates CC for comparison
2. – : Not available
3. TBD: To Be Determined

3.7.5 Flexural Stress Design at Service Limit State

The design cases listed in Section 3.7 were investigated using the design methodology described in Sections 3.2 and 3.3 to determine the optimum number of strands and maximum achievable span length. Feasible eccentricity and number of strand design space have been explored for eight stress limit states. Section 3.5.5 provides a sample chart and detailed descriptions of each plotted limit state.

3.7.5.1 Case 1 Designs

Figure 3.35 shows the eccentricity solution domains for a 160 ft bridge based on the eight limit states considered for both six-girder and five-girder configurations. Case 1 designs use the same bridge cross-section as one of the current TxDOT standard designs (CC-TxDOT in Table 3.29) and explore the possibility of extending the span length to 160 ft as opposed to 130 ft when CC is used. Researchers investigated this design case to find the optimum number of strands and required concrete compressive strength to achieve the target span length. The tensile and compressive stress

limit at release at the girder ends (red and green dashed lines) and the tensile stress limit at service at the girder midspan (maroon solid line) control the Case 1 designs. The required elastic (first cracking) tensile strength of UHPC increased to 1.2 ksi for the five-girder configuration, while the compressive strengths of UHPC at release were 10.2 ksi for the six-girder and 11.6 ksi for the five-girder configurations to achieve a 160 ft span length. The six-girder bridge requires 76 strands with a 19.31 in. midspan eccentricity, while the five-girder bridge requires 90 strands with a 16.76 in. midspan eccentricity to achieve a 160 ft span length that uses compressive strength of 22 ksi at service without debonding or harping.

Figure 3.36 shows the strand layout for six-girder and five-girder configurations using a standard Tx62 I-girder in which the green filled locations show straight bonded strands. The camber calculations considered the creep coefficient using the AASHTO LRFD Specifications (AASHTO 2020) empirical creep equations at 40 days when prestress was applied at one day. For the six-girder configuration, the applied prestressing force using 76 strands and 19.31 in. midspan eccentricity for a 160 ft span causes a 6.7 in. camber for a noncomposite girder just before deck placement. For the five-girder configuration, the applied prestressing force using 90 strands and 16.76 in. midspan eccentricity for a 160 ft span causes a 7.2 in. camber for a noncomposite girder just before deck placement. Table 3.30 lists the estimated camber of the noncomposite girder for both six- and five-girder configurations before and after deck placement. Live load deflections were also calculated using the optional deflection check criteria provided in Section 3.2.2 of this report and compared to the optional live load deflection limit. Live load deflections for both configurations were found to be within the deflection limits.

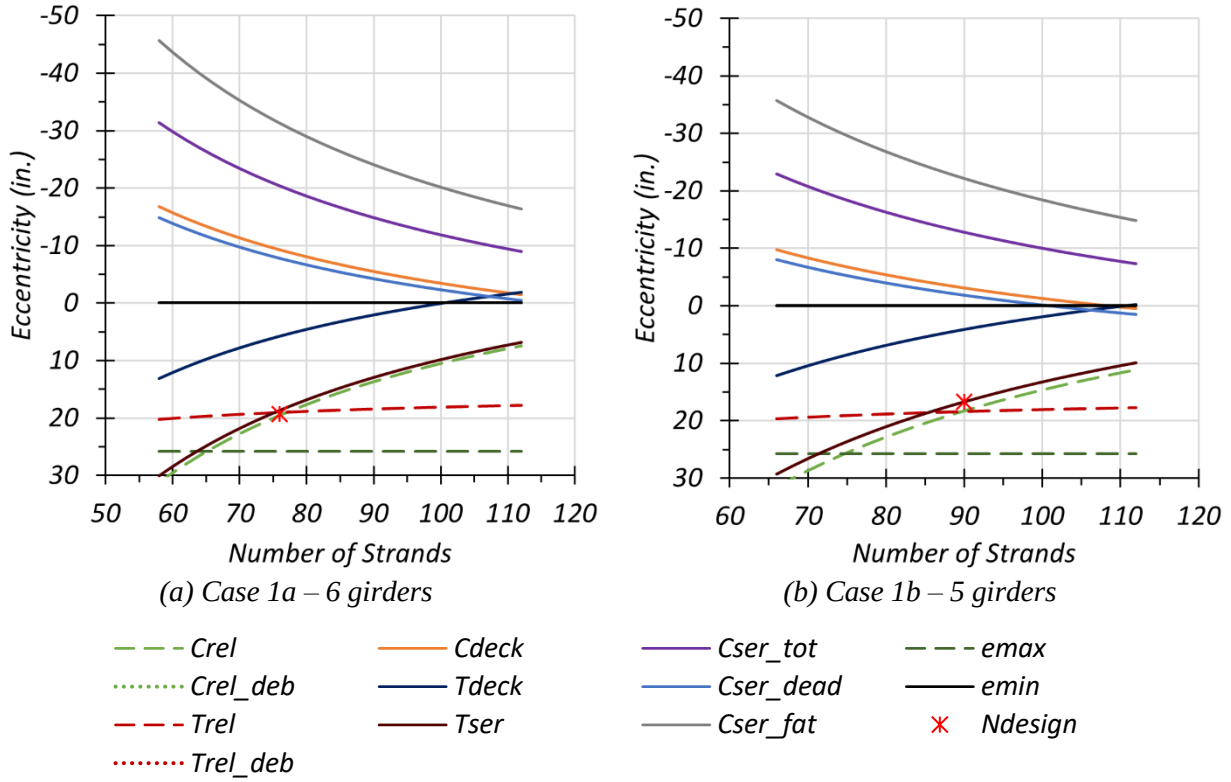

Notes:

1. Solid lines = minimum eccentricity, dashed lines = maximum eccentricity
2. $f_t' = 1.0$ ksi, for Case 1a, $f_t' = 1.2$ ksi for Case 1b
3. $f_{ci}' = 10.2$ ksi, for Case 1a, $f_{ci}' = 11.6$ ksi for Case 1b

Figure 3.35. Eccentricity Solution Domain for UHPC Tx62 Girders—160 ft Bridge.

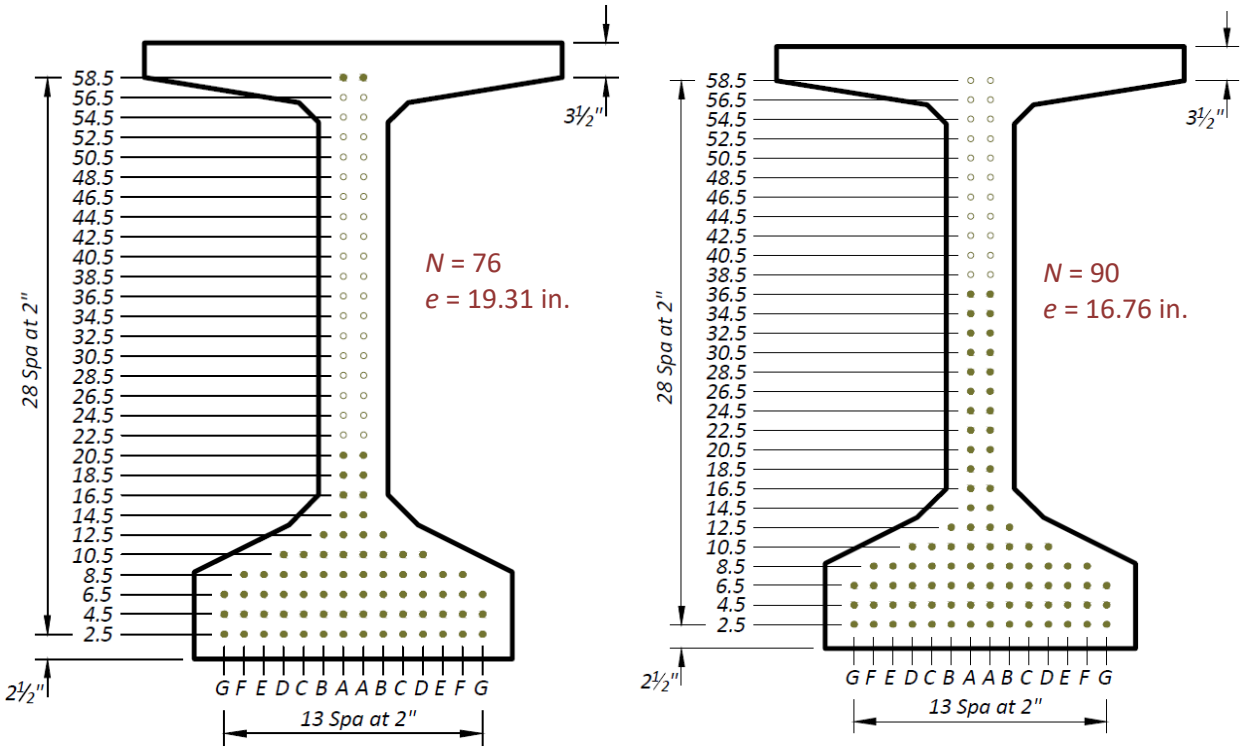

(a) Case 1a – 6 girders *(b) Case 1b – 5 girders*

Notes:

1. *N* = Number of strands, *e* = eccentricity at midspan
2. Green fill = bonded straight strands

Figure 3.36. Optimum Strand Design for UHPC Tx62 Girders—160 ft Bridge.

Table 3.30. Estimated Camber for UHPC Tx62 Girders—160 ft Bridge.

Design Case	No. of Strands	Eccentricity (in.)	Time of Camber	Camber (in.)
Case 1a (6 girders)	76	19.31	Just before deck placement	6.7
			Just after deck placement	2.8
Case 1b (5 girders)	90	16.76	Just before deck placement	7.2
			Just after deck placement	2.5

3.7.5.2 Case 2 Designs

Figure 3.37 shows the eccentricity solution domains for a 170 ft bridge based on the eight limit states considered for three different subcategories: (1) Case 2a, which uses six girders and an 8.5 in. deck, (2) Case 2b, which uses six girders and a 7.0 in. deck, and (3) Case 2c, which uses five girders and a 7.0 in. deck. Case 2 designs use similar bridge cross-sections as one of the current TxDOT standard designs (CC-TxDOT in Table 3.29) to explore the possibility of extending the span length to 170 ft, as opposed to 130 ft when CC is used. Researchers investigated this design

case to find the optimum number of strands and required concrete compressive strength to achieve the target span length of 170 ft. The tensile and compressive stress limit at release at the girder ends (red and green dashed lines) and the tensile stress limit at service at the girder midspan (maroon solid line) control the Case 2 designs. The elastic (first cracking) tensile strength of UHPC increased to 1.2 ksi for Case 2a, and 1.9 ksi for Case 2c, while the compressive strengths of UHPC at release were 11.5 ksi for Case 2a and 11.2 ksi for Case 2b and 2c to achieve a 170 ft span length. All Case 2 designs require 88 strands with a 17.33 in. midspan eccentricity to achieve a 170 ft span length without debonding or harping.

Figure 3.38 shows the strand layout for all three subcategories of Case 2 using the standard Tx62 I-girder in which the green filled locations show straight bonded strands. Table 3.31 lists the estimated camber of the noncomposite girder for all three subcategories of Case 2 designs before and after deck placement. The camber calculations considered the creep coefficient using the AASHTO LRFD Specifications (AASHTO 2020) empirical creep equations at 40 days when prestress was applied at one day. For Case 2a, the applied prestressing force using 88 strands and a 17.33 in. midspan eccentricity for a 170 ft span causes a 7.1 in. camber for the noncomposite girder just before deck placement. For 2b and 2c, the applied prestressing force using 88 strands and a 17.33 in. midspan eccentricity for a 170 ft span causes a 7.2 in. camber for the noncomposite girder just before deck placement. Live load deflections were also calculated using the optional deflection check criteria provided in Section 3.2.2 of this report and compared with the optional live load deflection limit. Live load deflections were found to be within the deflection limits for all considered Case 2 designs.

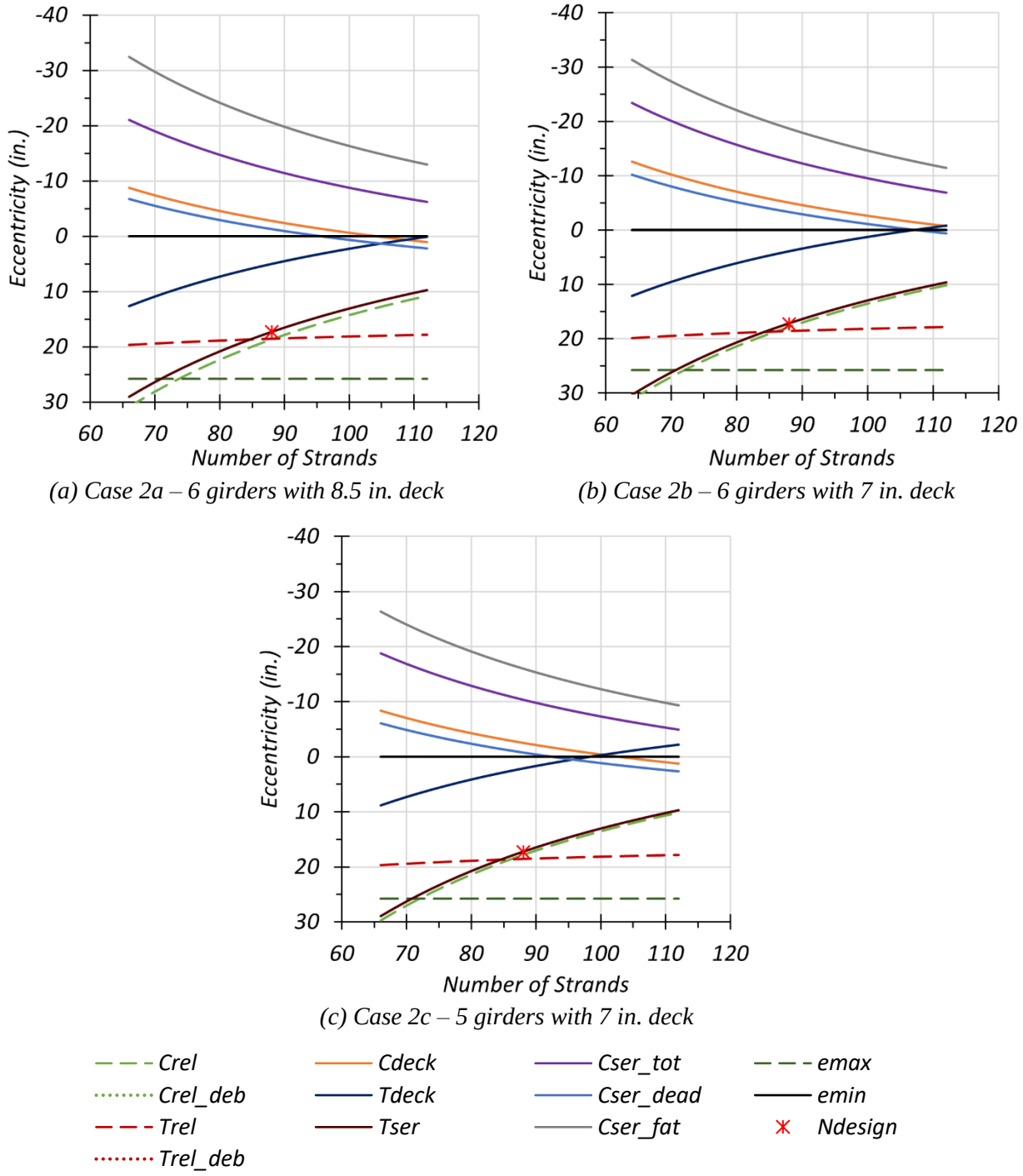

(a) Case 2a – 6 girders with 8.5 in. deck

(b) Case 2b – 6 girders with 7 in. deck

(c) Case 2c – 5 girders with 7 in. deck

Notes:

1. Solid lines = minimum eccentricity, dashed lines = maximum eccentricity
2. $f_t' = 1.2$ ksi for Case 2a, $f_t' = 1.0$ ksi for Case 2b, $f_t' = 1.9$ ksi for Case 2c
3. $f_{ci}' = 11.5$ ksi, for Case 2a, $f_{ci}' = 11.2$ ksi for Case 2b and 2c

Figure 3.37. Eccentricity Solution Domain for UHPC Tx62 Girders—170 ft Bridge.

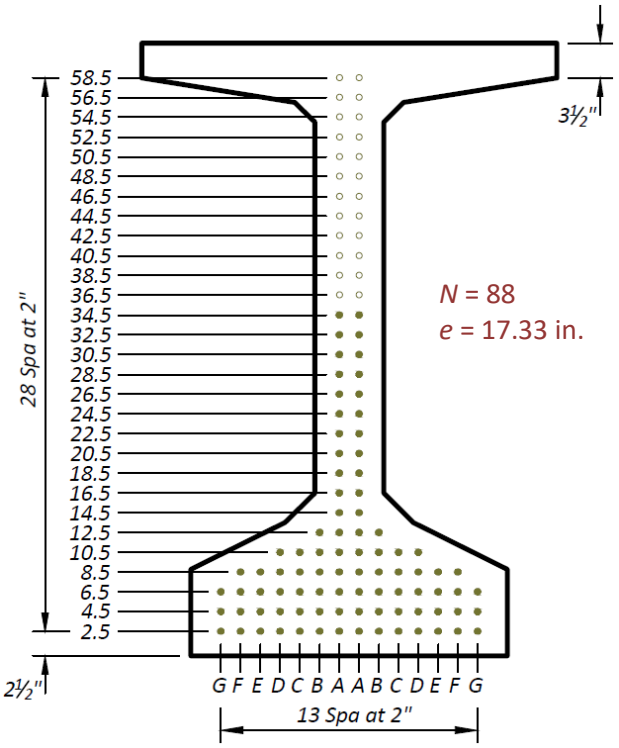

Notes:

1. N = Number of strands, e = eccentricity at midspan
2. Green fill = bonded straight strands

Figure 3.38. Optimum Strand Design for UHPC Tx62 Girders—Case 2 Designs.

Table 3.31. Estimated Camber for UHPC Tx62 Girders—170 ft Bridge.

Design Case	No. of Strands	Eccentricity (in.)	Time of Camber	Camber (in.)
Case 2a (6 girders, 8.5" deck)	88	17.33	Just before deck placement	7.1
			Just after deck placement	2.1
Case 2b (6 girders, 7" deck)	88	17.33	Just before deck placement	7.2
			Just after deck placement	3.0
Case 2c (5 girders, 7" deck)	88	17.33	Just before deck placement	7.2
			Just after deck placement	2.1

3.7.5.3 Case 3a Designs (6 Girders and 8.5 in. Deck)

Case 3 designs have the same subcategory designs as Case 2, and for each one researchers investigated the use of 0.6 in. and 0.7 in. diameter strands, while Case 1 and Case 2 designs consider only 0.6 in. diameter strands. Although 0.7 in. strands are not currently available in Texas precast plants, this feasibility study included an evaluation of the potential benefit of using 0.7 in. strands in UHPC girders to further increase possible span lengths.

For Case 3a designs, researchers investigated the maximum achievable span length for a bridge having six Tx62 UHPC I-girders with an 8.5 in. CC deck. The UHPC strength is set to a target compressive strength $f'_{ci} = 14$ ksi at release and $f'_c = 22$ ksi at service. An inverse design approach was used, which calculates the possible span length for the specified material properties. Figure 3.39 shows the maximum span length solution domains based on eight concrete stress limits. The optional deflection limit (green solid line) is also shown on the graphs but does not control the design cases considered for Tx62 girders.

For the design case using 0.6 in. diameter strands (Figure 3.39a), the maximum achievable span length based on the tensile stress limit at service is 171 ft and uses 90 strands. This span length can be achieved without debonding or harping. The dashed red line indicates the minimum number of strands to satisfy the tensile stress limit at release, and the dashed green line is the maximum number of strands to satisfy the compression stress limit at release. Therefore, the span length solution domain lies between the red and green dashed lines (compressive and tensile limits at release) and the maroon solid line (tensile stress limit at service).

For the design case using 0.7 in. diameter strands (Figure 3.39b), the maximum achievable span length with 90 strands is 190.5 ft when four strands are debonded or eight strands are harped. To achieve the maximum span length based on the tensile stress limit at service (maroon solid line), it is necessary to debond or harp some strands because the compressive stress limit at release (green dashed line) requires a smaller number of strands than the minimum number of strands necessary to satisfy the tensile stress limit at release (red dashed line). The red dotted line indicates the minimum number of strands and the green dotted line indicates the maximum number of strands when four strands are debonded. Therefore, the span length solution domain lies between the red and green dotted lines and the maroon solid line for the debonded case. Similarly, the red dashed-dotted line indicates the minimum number of strands and the green dashed-dotted line indicates the maximum number of strands when eight strands are harped. Therefore, the span length solution domain is between the red and green dashed-dotted lines and the maroon solid line for the harped case.

Table 3.32 summarizes the maximum achievable span lengths, number of required strands, and debonding or harping information for different strand diameters. For the harped case, the hold-down points are taken as *L*/20 ft away from the midspan of the girder.

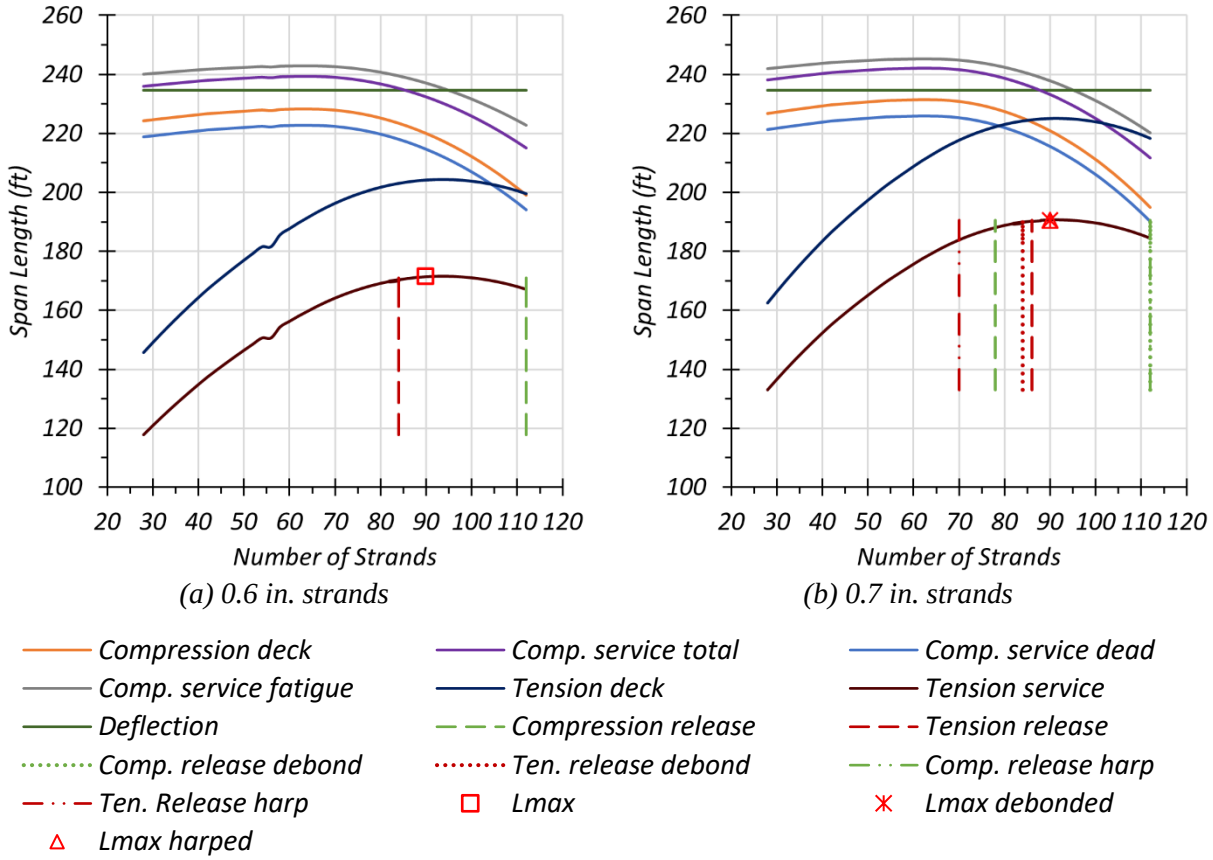

Note: Solid lines = maximum span, dashed red lines = minimum number of strands, dashed green lines = maximum number of strands.

Figure 3.39. Span Length Solution Domain for UHPC Tx62 Girder—Case 3a.

Table 3.32. Maximum Achievable Span Length for UHPC Tx54 Girder—Case 3a.

Strand Diameter (in.)	Total No. of Strands	No. of Debonded Strands	No. of Harped Strands	Maximum Achievable Span (ft)
0.6	90	0	0	171
0.7	90	4	0	190.5
	90	0	8	190.5

Notes:
1. Debonded case using 0.7 in. strands: 4 strands up to 3.5 ft and 2 strands up to 9.5 ft
2. Harped case: Hold-down point is at *L*/20 ft away from the midspan

The optimum eccentricity and number of strand requirements were calculated for the maximum achievable span length values obtained for Case 3a designs. Figure 3.40(a) shows the eccentricity solution domain for a 171 ft bridge based on the eight limit states considered when 0.6 in. diameter

strands are used. The optimal solution requires 90 strands having 16.76 in. midspan eccentricity to achieve a 171 ft span length. Figure 3.40(b) shows the eccentricity solution domain for a 190.5 ft bridge based on the eight limit states considered when 0.7 in. diameter strands are used. The compressive stress limit at release at the girder ends (green dashed line) requires a smaller eccentricity than the minimum eccentricity required to satisfy the tensile stress limit at service at the girder midspan (maroon solid line). It is not possible to achieve a 190.5 ft span length without debonding or harping. Therefore, the optimal design requires 90 strands having a 16.76 in. midspan eccentricity with four debonded strands or eight harped strands. For I-girders, harping provides a more viable method to resolve stress exceedance issues at girder ends because it provides more balanced deflections by reducing the amount of camber. The proposed strand layout for the harped case results in a 16.76 in. midspan eccentricity and a 14.80 in. end eccentricity.

Figure 3.41 shows the strand layout for a standard Tx62 I-girder in which the green filled locations show straight bonded strands, and the red filled locations show the harped strands from both ends. Table 3.33 lists the camber estimations for debonded and harped options for both design cases using 0.6 in. or 0.7 in. strands. The camber calculations consider the creep coefficient using the AASHTO LRFD Specifications (AASHTO 2020) empirical creep equations at 40 days when prestress is applied at one day. For the design case using 0.6 in. strands, the applied prestressing force using 90 strands and 16.76 in. midspan eccentricity for a 171 ft span causes a 6.2 in. camber for the noncomposite girder just before deck placement. For the design case using 0.7 in. strands, the applied prestressing force (using 90 strands—eight of which are harped—having a 16.76 in. midspan eccentricity and a 14.80 in. end eccentricity) creates a 9.9 in. camber for the noncomposite girder just before deck placement. Using harped strands rather than debonding can provide more balanced deflections by reducing the initial camber. It may be possible to achieve a fully balanced final deflection just after deck placement by harping more strands and/or adjusting the hold-down location.

Live load deflections were also calculated using the optional deflection check criteria provided in Section 3.2.2 of this report and compared to the optional live load deflection limit. The estimated live load deflections for Case 3a were found to be smaller than the deflection limit.

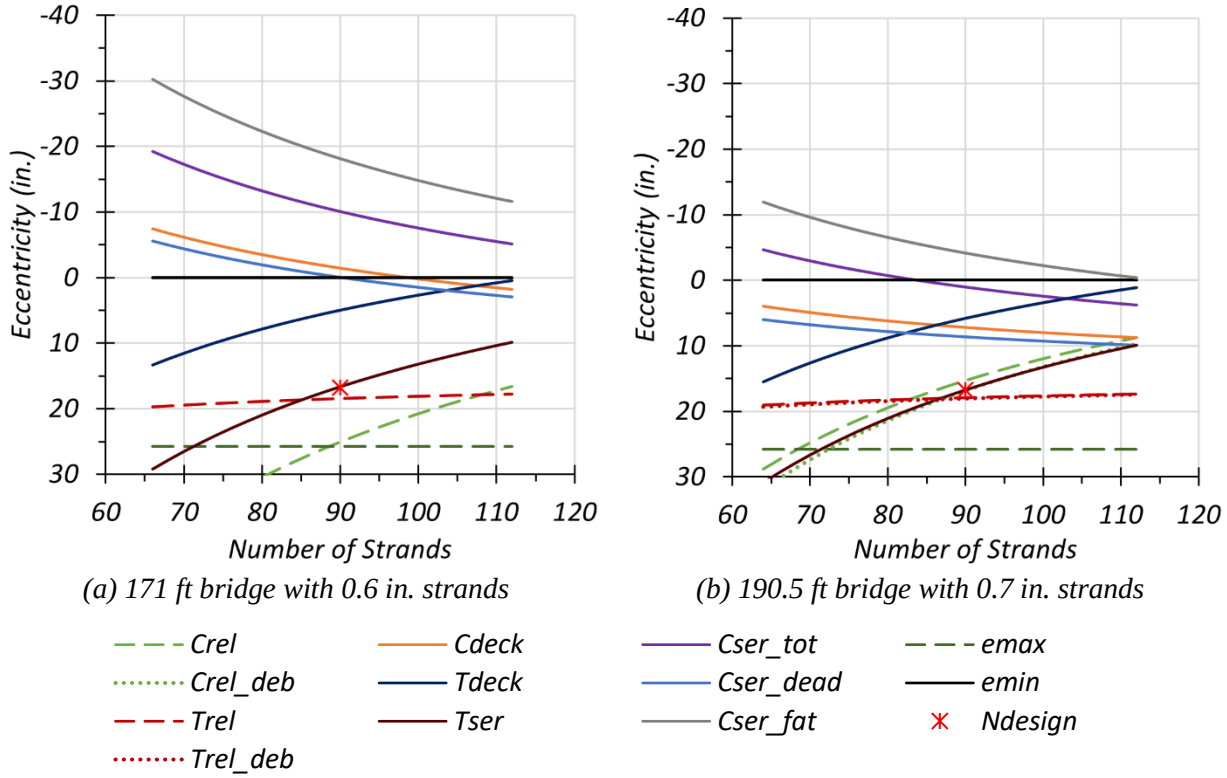

(a) 171 ft bridge with 0.6 in. strands

(b) 190.5 ft bridge with 0.7 in. strands

Note: Solid lines = minimum eccentricity, dashed lines = maximum eccentricity.

Figure 3.40. Eccentricity Solution Domain for UHPC Tx62 Girders—Case 3a.

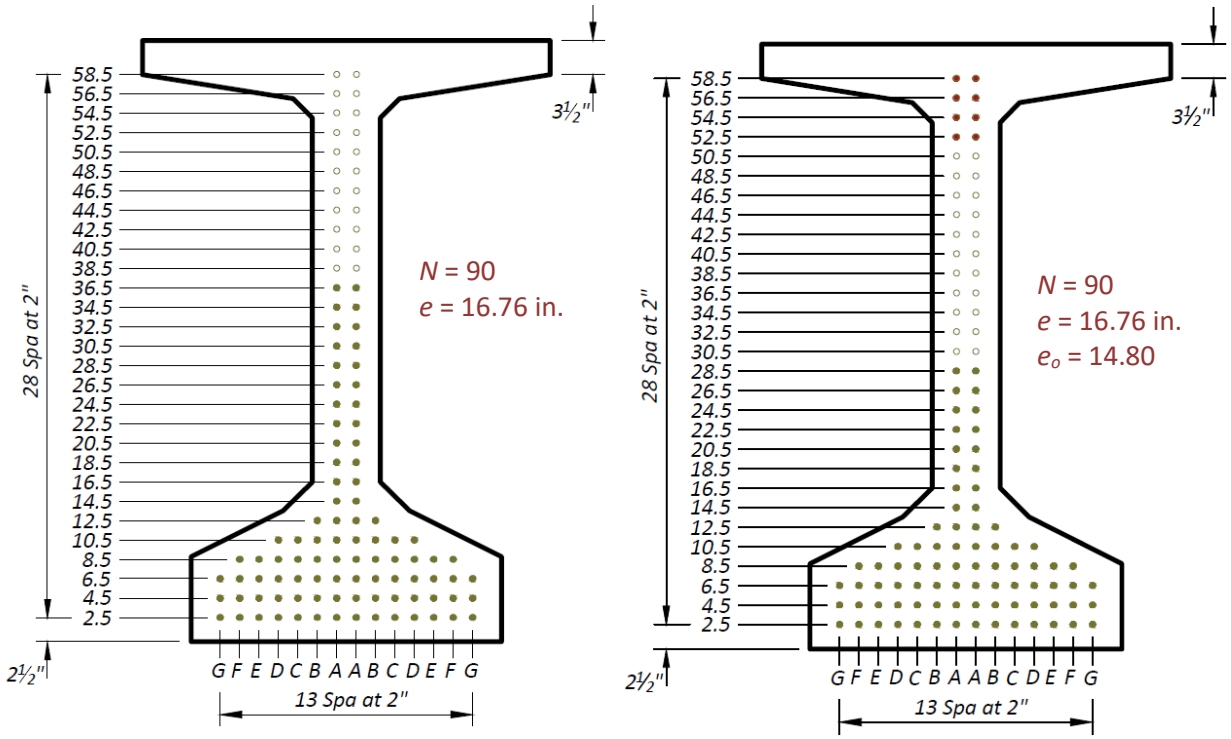

(a) 171 ft bridge with 0.6 in. strands *(b) 190.5 ft bridge with 0.7 in. strands*

Notes:
1. N = Number of strands, e = eccentricity at midspan, e_o = end eccentricity
2. Green fill = bonded straight strands, red fill = harped strands

Figure 3.41. Optimum Strand Design for UHPC Tx62 Girders—Case 3a.

Table 3.33. Estimated Camber for UHPC Tx62 Girders—Case 3a.

Strand Diameter (in.)	No. of Debonded Strands	No. of Harped Strands	Time of Camber	Camber (in.)
0.6	0	0	Just before deck placement	6.2
			Just after deck placement	1.1
0.7	4	0	Just before deck placement	10.8
			Just after deck placement	2.9
	0	8	Just before deck placement	9.9
			Just after deck placement	2.0

Notes:
1. Debonded case using 0.7 in. strands: 4 strands up to 3.5 ft and 2 strands up to 9.5 ft
2. Harped case: Hold-down point is at $L/20$ ft away from the midspan

3.7.5.4 Case 3b Designs (6 Girders and 7.0 in. Deck)

For Case 3b designs, researchers investigated the maximum achievable span length for a bridge having six Tx62 UHPC I-girders with a 7.0 in. CC deck for a target compressive strength of 14 ksi at release and 22 ksi at service using an inverse design approach that calculates span length for

given material properties. Figure 3.42 shows the maximum span length solution domains based on eight concrete stress limits. The optional deflection limit (green solid line) is also shown on the graphs and does not control the design cases considered for Tx62 girders.

For the design case using 0.6 in. diameter strands (Figure 3.42(a)), the maximum achievable span length based on the tensile stress limit at service is 174.5 ft using 92 strands and can be achieved without debonding or harping. The dashed red line indicates the minimum number of strands to satisfy the tensile stress limit at release, and the dashed green line is the maximum number of strands to satisfy the compression stress limit at release. Therefore, the span length solution domain is between the red and green dashed lines (compressive and tensile limit at release) and the maroon solid line (tensile stress limit at service).

For the design case using 0.7 in. diameter strands (Figure 3.42(b)), the maximum achievable span length is 194 ft with 88 strands when four strands are debonded or eight strands are harped. To achieve the maximum span length based on the tensile stress limit at service (maroon solid line), it is necessary to debond or harp some strands because the compressive stress limit at release (green dashed line) requires a smaller number of strands than the minimum number of strands necessary to satisfy the tensile stress limit at release (red dashed line). The red dotted line indicates the minimum number of strands, and the green dotted line indicates the maximum number of strands when four strands are debonded. Therefore, the span length solution domain is between the red and green dotted lines and the maroon solid line for the debonded case. Similarly, the red dashed-dotted line indicates the minimum number of strands and the green dashed-dotted line indicates the maximum number of strands when eight strands are harped. Therefore, the span length solution domain is between the red and green dashed-dotted lines and the maroon solid line for the harped case.

Table 3.34 summarizes the maximum achievable span lengths, number of required strands, and debonding or harping information for different strand diameters. For the harped case, the hold-down points are taken as $L/20$ ft away from the midspan of the girder.

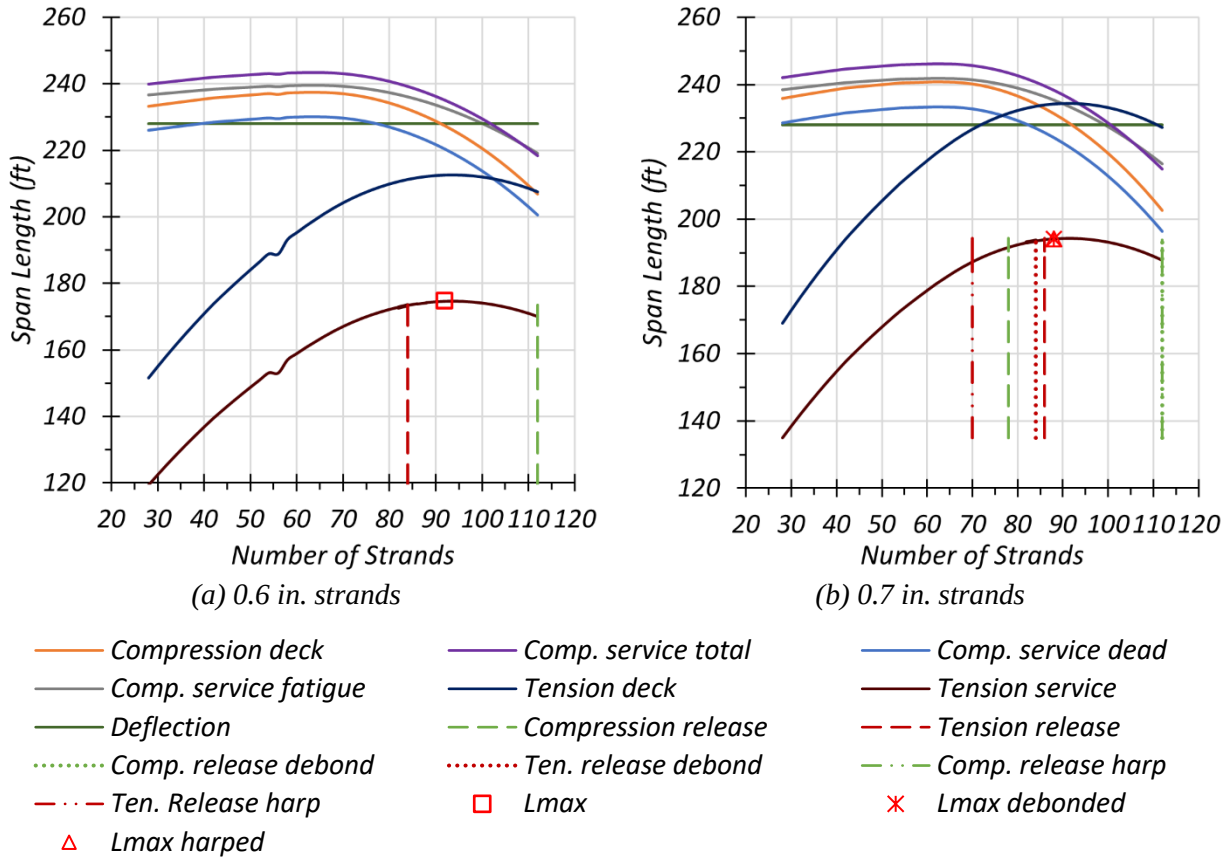

Note: Solid lines = maximum span, dashed red lines = minimum number of strands, dashed green lines = maximum number of strands.

Figure 3.42. Span Length Solution Domain for UHPC Tx62 Girder—Case 3b.

Table 3.34. Maximum Achievable Span Length for UHPC Tx62 Girder—Case 3b.

Strand Diameter (in.)	Total No. of Strands	No. of Debonded Strands	No. of Harped Strands	Maximum Achievable Span Length (ft)
0.6	92	0	0	174.5
0.7	88	4	0	194.0
	88	0	8	194.0

Notes:
1. Debonded case using 0.7 in. strands: 4 strands up to 3.5 ft and 2 strands up to 9.5 ft
2. Harped case: Hold-down point is at *L*/20 ft away from the midspan

The optimum eccentricity and number of strand requirements were calculated for the maximum achievable span length values obtained for Case 3b designs. Figure 3.43(a) shows the eccentricity solution domain for a 174.5 ft bridge based on the eight limit states considered when 0.6 in. diameter strands are used. The optimal solution requires 92 strands having a 16.17 in. midspan eccentricity to achieve a 174.5 ft span length. Figure 3.43(b) shows the eccentricity solution domain for a 194.0 ft bridge based on the eight limit states considered when 0.7 in. diameter strands are used. The compressive stress limit at release at the girder ends (green dashed line) requires

smaller eccentricity than the minimum eccentricity required to satisfy tensile stress limit at service at the girder midspan (maroon solid line). It is not possible to achieve a 194.5 ft span length without debonding or harping. Therefore, the optimal design requires 88 strands having a 17.33 in. midspan eccentricity with four debonded strands or eight harped strands. For I-girders, harping provides a more viable method to resolve stress exceedance issues at girder ends because it provides more balanced deflections by reducing the amount of camber. The proposed strand layout for the harped case results in a 17.33 in. midspan eccentricity and a 15.14 in. end eccentricity.

Figure 3.44 shows the strand layout for a standard Tx62 I-girder in which the green filled locations show straight bonded strands, and the red filled locations show the harped strands from both ends. Table 3.35 lists the camber estimations for debonded and harped options for both design cases using 0.6 in. or 0.7 in. strands. The camber calculations considered the creep coefficient using the AASHTO LRFD Specifications (AASHTO 2020) empirical creep equations at 40 days when prestress was applied at one day. For the design case using 0.6 in. strands, the applied prestressing force (using 92 strands and a 16.17 in. midspan eccentricity for a 174.5 ft span) causes a 5.7 in. camber for the noncomposite girder just before deck placement. For the design case using 0.7 in. strands, the applied prestressing force (using 88 strands—eight of which are harped—having a 17.33 in. midspan eccentricity and a 15.14 in. end eccentricity) creates a 10.0 in. camber for the noncomposite girder just before deck placement. Using harped strands rather than debonding can provide more balanced deflections by reducing the initial camber. It may be possible to achieve fully balanced final deflection just after deck placement by harping more strands and/or adjusting the hold-down location.

Live load deflections were also calculated using the optional deflection check criteria provided in Section 3.2.2 of this report and compared to the optional live load deflection limit. Estimated live load deflections for Case 3b designs were found to be smaller than the deflection limit.

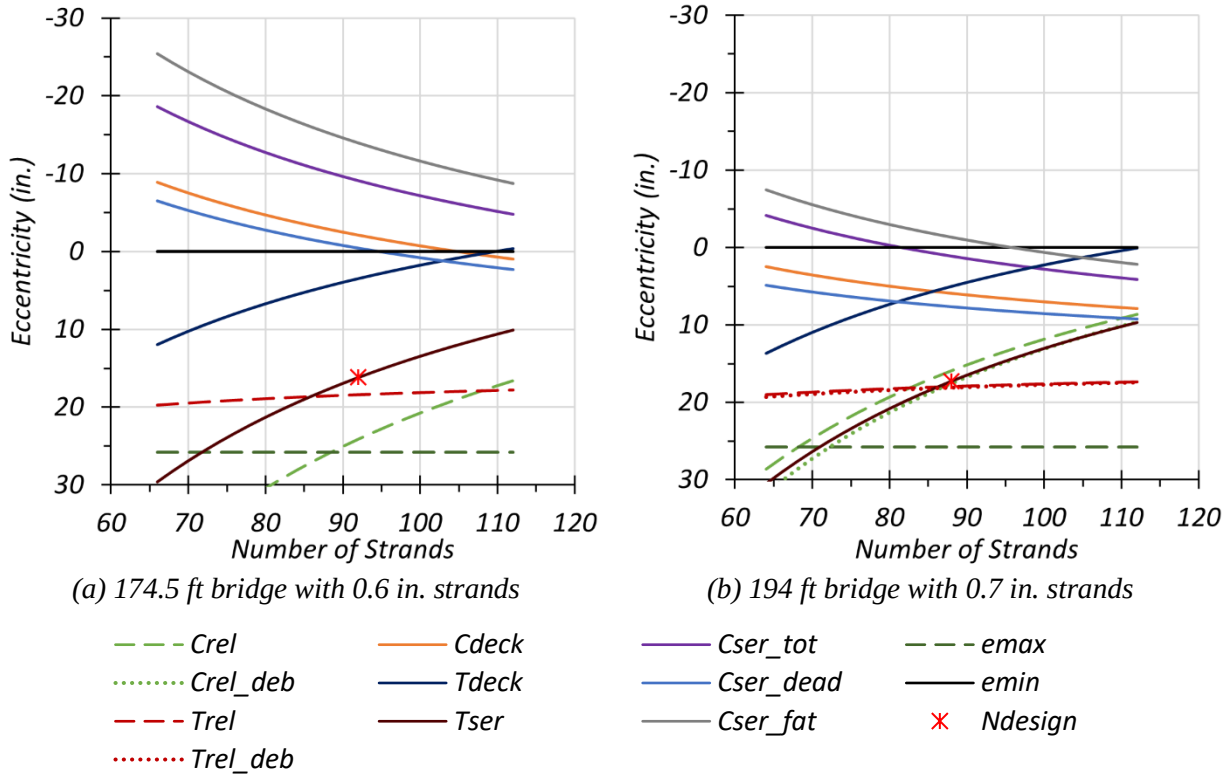

(a) 174.5 ft bridge with 0.6 in. strands

(b) 194 ft bridge with 0.7 in. strands

Note: Solid lines = minimum eccentricity, dashed lines = maximum eccentricity.

Figure 3.43. Eccentricity Solution Domain for UHPC Tx62 Girders—Case 3b.

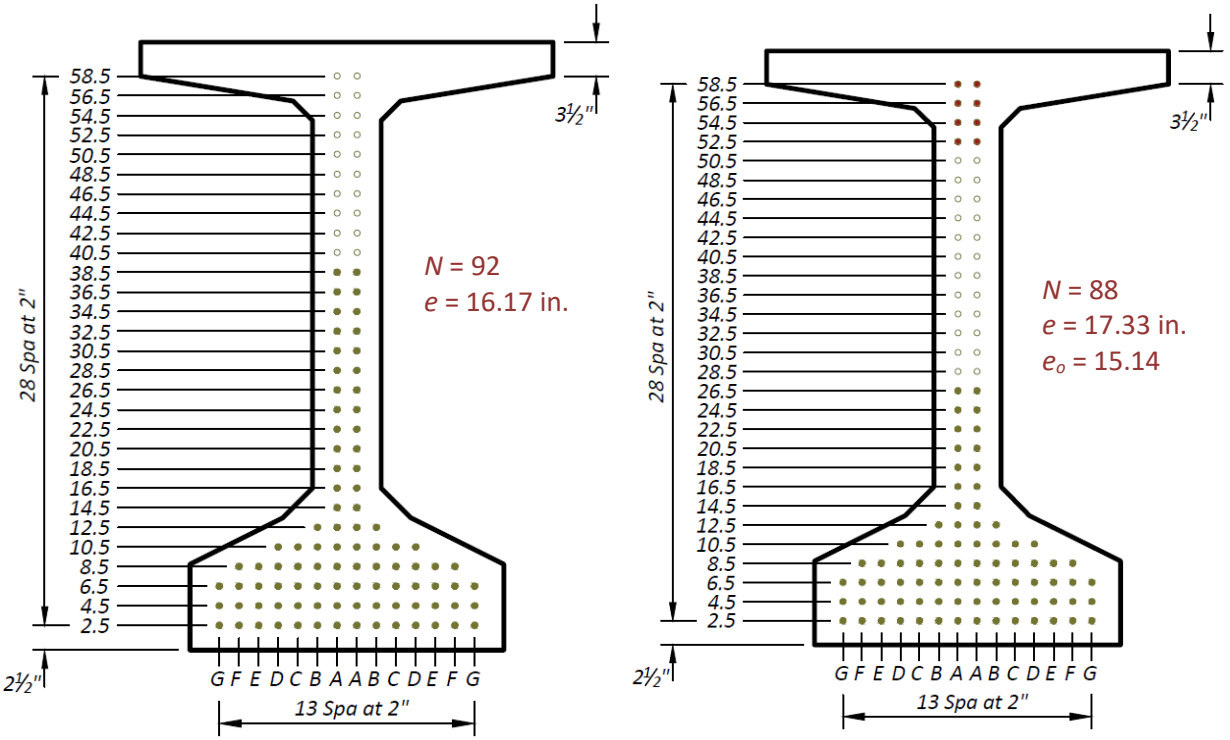

(a) 174.5 ft bridge with 0.6 in. strands *(b) 194 ft bridge with 0.7 in. strands*

Notes:
1. N = Number of strands, e = eccentricity at midspan, e_o = end eccentricity
2. Green fill = bonded straight strands, red fill = harped strands

Figure 3.44. Optimum Strand Design for UHPC Tx62 Girders—Case 3b.

Table 3.35. Estimated Camber for UHPC Tx62 Girders—Case 3b.

Strand Diameter (in.)	No. of Debonded Strands	No. of Harped Strands	Time of Camber	Camber (in.)
0.6	0	0	Just before deck placement	5.7
			Just after deck placement	1.1
0.7	4	0	Just before deck placement	11.0
			Just after deck placement	3.8
	0	8	Just before deck placement	10.0
			Just after deck placement	2.8

Notes:
1. Debonded case using 0.7 in. strands: 4 strands up to 3.5 ft and 2 strands up to 6.5 ft
2. Harped case: Hold-down point is at L/20 ft away from the midspan

3.7.5.5 Case 3c Designs (5 Girders and 7.0 in. Deck)

For Case 3c designs, researchers investigated the maximum achievable span length for a bridge having five Tx62 UHPC I-girders with 7.0 in. CC deck for a target compressive strength of 14 ksi at release and 22 ksi at service using an inverse design approach that calculates span length for

given material properties. Figure 3.45 shows the maximum span length solution domains based on eight concrete stress limits. The optional deflection limit (green solid line) is also shown on the graphs but does not control the design cases considered for Tx62 girders.

For the design case using 0.6 in. diameter strands (Figure 3.45(a)), the maximum achievable span length based on the tensile stress limit at service is 164.0 ft using 88 strands and can be achieved without debonding or harping. The dashed red line indicates the minimum number of strands to satisfy the tensile stress limit at release, and the green dashed line is the maximum number of strands to satisfy the compression stress limit at release. Therefore, the span length solution domain is between the red and green dashed lines (compressive and tensile limit at release) and the maroon solid line (tensile stress limit at service).

For the design case using 0.7 in. diameter strands (Figure 3.45(b)), the maximum achievable span length is 183 ft with 90 strands when four strands are debonded or eight strands are harped. To achieve the maximum span length based on the tensile stress limit at service (maroon solid line), it is necessary to debond or harp some strands because the compressive stress limit at release (green dashed line) requires a smaller number of strands than the minimum number of strands necessary to satisfy the tensile stress limit at release (red dashed line). The red dotted line indicates the minimum number of strands and the green dotted line indicates the maximum number of strands when four strands are debonded. Therefore, the span length solution domain is between the red and green dotted lines and the maroon solid line for the debonded case. Similarly, the red dashed-dotted line indicates the minimum number of strands and the green dashed-dotted line indicates the maximum number of strands when eight strands are harped. Therefore, the span length solution domain is between the red and green dashed-dotted lines and the maroon solid line for the harped case.

Table 3.36 summarizes the maximum achievable span lengths, number of required strands, and debonding or harping information for different strand diameters. For the harped case, the hold-down points are taken as $L/20$ ft away from the midspan of the girder.

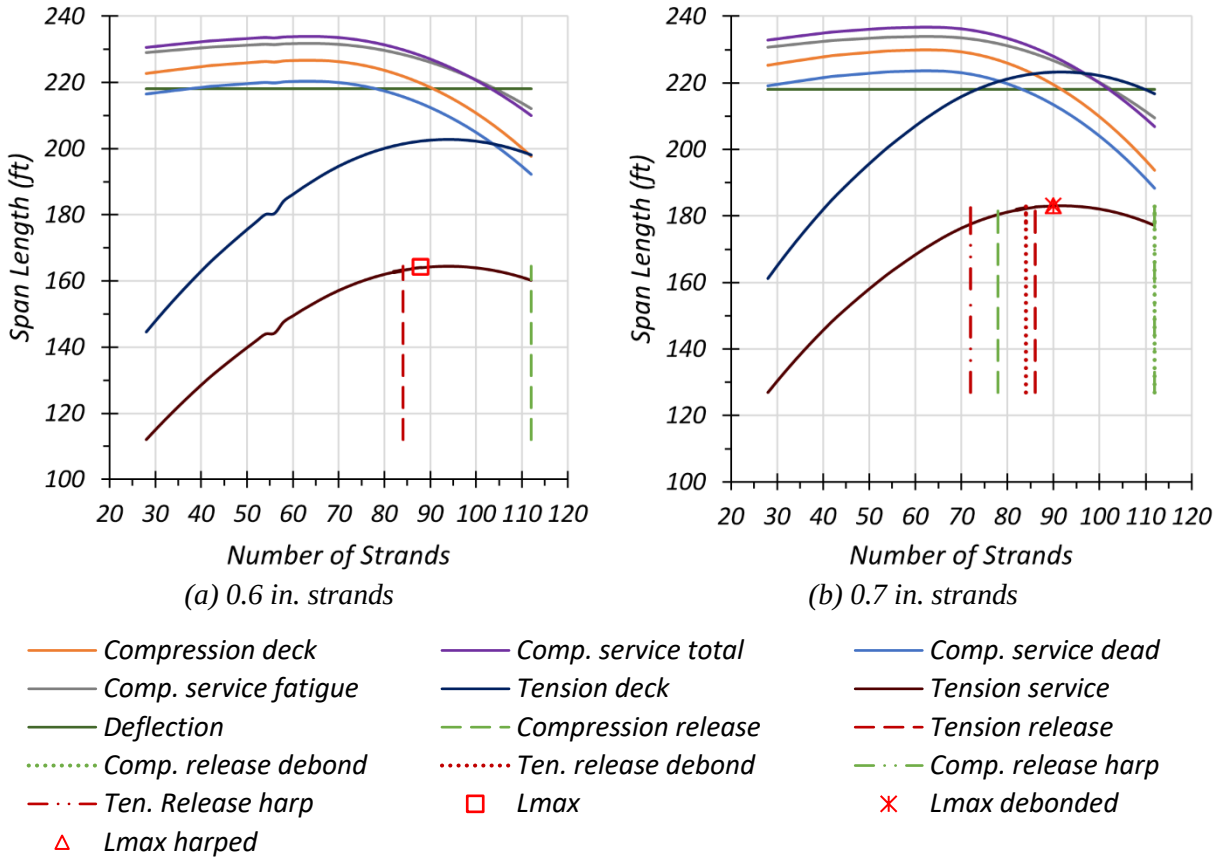

Note: Solid lines = maximum span, dashed red lines = minimum number of strands, dashed green lines = maximum number of strands.

Figure 3.45. Span Length Solution Domain for UHPC Tx62 Girder—Case 3c.

Table 3.36. Maximum Achievable Span Length for UHPC Tx62 Girder—Case 3c.

Strand Diameter (in.)	Total No. of Strands	No. of Debonded Strands	No. of Harped Strands	Maximum Achievable Span (ft)
0.6	88	0	0	164
0.7	90	4	0	183
	90	0	8	183

Notes:
1. Debonded case using 0.7 in. strands: 4 strands up to 3.5 ft and 2 strands up to 9.5 ft
2. Harped case: Hold-down point is at *L*/20 ft away from the midspan

The optimum eccentricity and number of strand requirements were calculated for the maximum achievable span length values obtained for the Case 3c designs. Figure 3.46(a) shows the eccentricity solution domain for a 163 ft bridge based on the eight limit states considered when 0.6 in. diameter strands are used. The optimal solution requires 88 strands having 17.33 in. midspan eccentricity to achieve a 163 ft span length. Figure 3.46(b) shows the eccentricity solution domain for a 183 ft bridge based on the eight limit states considered when 0.7 in. diameter strands

are used. The compressive stress limit at release at the girder ends (green dashed line) requires smaller eccentricity than the minimum eccentricity required to satisfy the tensile stress limit at service at the girder midspan (maroon solid line). It is not possible to achieve a 183 ft span length without debonding or harping. Therefore, the optimal design requires 90 strands having 16.76 in. midspan eccentricity with four debonded strands or eight harped strands. For I-girders, harping provides a more viable method to resolve stress exceedance issues at girder ends because it provides more balanced deflections by reducing the amount of camber. The proposed strand layout for the harped case results in 16.76 in. midspan eccentricity and 14.80 in. end eccentricity.

Figure 3.47 shows the strand layout for a standard Tx62 I-girder in which the green filled locations show straight bonded strands, and the red filled locations show the harped strands from both ends. Table 3.37 lists the camber estimations for debonded and harped options for both design cases using 0.6 in. or 0.7 in. strands. The camber calculations considered the creep coefficient using the AASHTO LRFD Specifications (AASHTO 2020) empirical creep equations for a 40-day-old girder when prestress was applied at one day. For the design case using 0.6 in. strands, the applied prestressing force (using 88 strands and a 17.33 in. midspan eccentricity for a 164.0 ft span) causes a 6.6 in. camber for the noncomposite girder just before deck placement. For the design case using 0.7 in. strands, the applied prestressing force (using 90 strands—eight of which are harped—having a 16.76 in. midspan eccentricity and a 14.80 in. end eccentricity) creates a 10.3 in. camber for the noncomposite girder just before deck placement. Using harped strands rather than debonding can provide more balanced deflections by reducing the initial camber. It may be possible to achieve fully balanced final deflection just after deck placement by harping more strands and/or adjusting the hold-down location.

Live load deflections were also calculated using the optional deflection check criteria provided in Section 3.2.2 of this report and compared to the optional live load deflection limit. Estimated live load deflections for Case 3c designs were found to be smaller than the deflection limit.

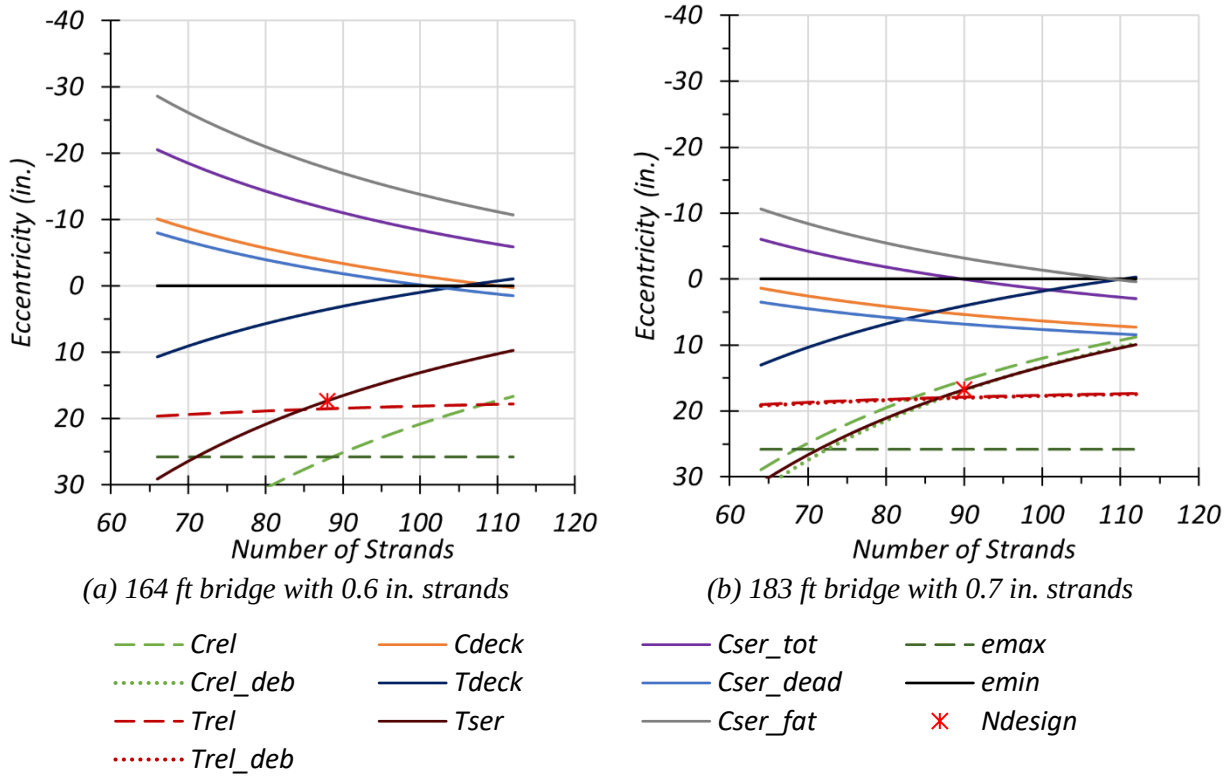

(a) 164 ft bridge with 0.6 in. strands

(b) 183 ft bridge with 0.7 in. strands

Note: Solid lines = minimum eccentricity, dashed lines = maximum eccentricity.

Figure 3.46. Eccentricity Solution Domain for UHPC Tx62 Girders—Case 3c.

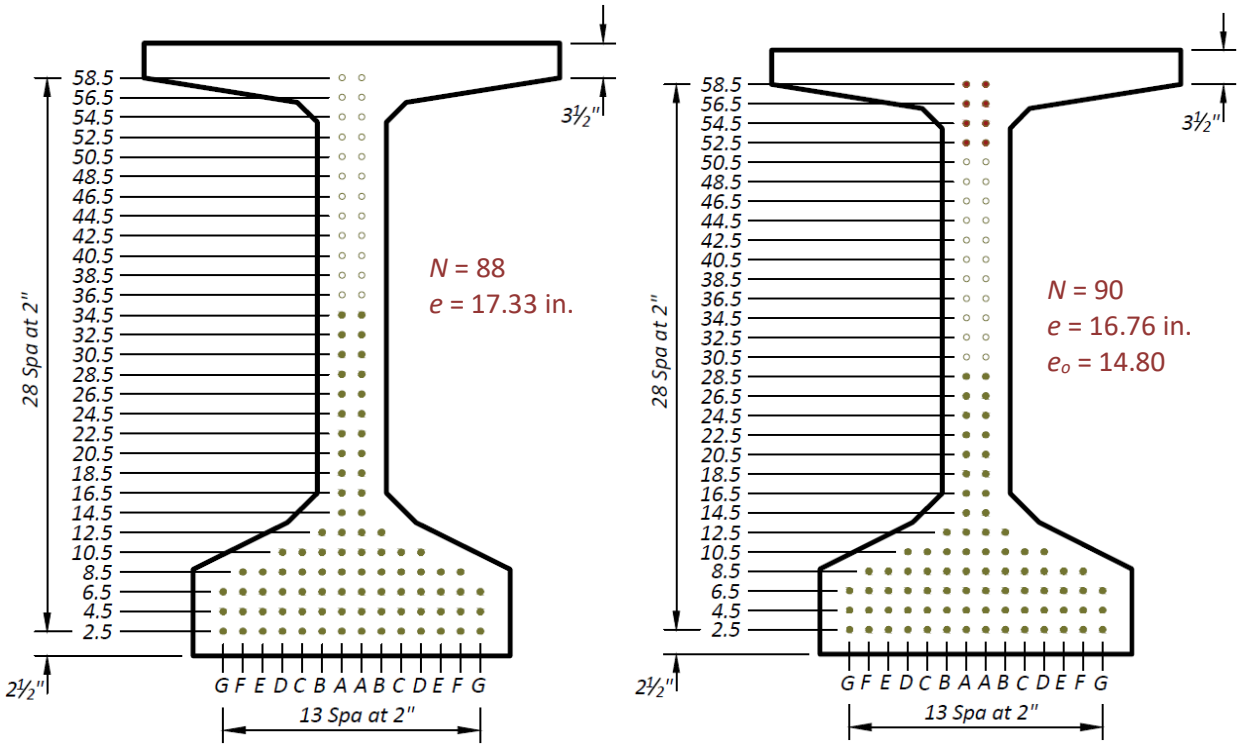

(a) 164 ft bridge with 0.6 in. strands *(b) 183 ft bridge with 0.7 in. strands*

Notes:
1. N = Number of strands, e = eccentricity at midspan, e_o = end eccentricity
2. Green fill = bonded straight strands, red fill = harped strands

Figure 3.47. Optimum Strand Design for UHPC Tx62 Girders—Case 3c.

Table 3.37. Estimated Camber for UHPC Tx62 Girders—Case 3c.

Strand Diameter (in.)	No. of Debonded Strands	No. of Harped Strands	Time of Camber	Camber (in.)
0.6	0	0	Just before deck placement	6.6
			Just after deck placement	2.2
0.7	4	0	Just before deck placement	11.1
			Just after deck placement	4.2
	0	8	Just before deck placement	10.3
			Just after deck placement	3.4

Notes:
1. Debonded case using 0.7 in. strands: 4 strands up to 3.5 ft and 2 strands up to 9.5 ft
2. Harped case: Hold-down point is at L/20 ft away from the midspan

3.7.5.6 Summary of Flexural Stress Designs for UHPC Tx62 Girder

All three design cases and the subcases were investigated with 0.6 in. diameter strands to explore the optimum eccentricity and maximum achievable span length. Table 3.38 summarizes design parameters and the results of the parametric feasibility study for the design cases using 0.6 in.

diameter strands. The tension stress limit at service and release and compression stress limit at release controls the optimum number of strands and eccentricity for all design cases using 0.6 in. diameter strands.

Case 1 designs were explored for the required concrete strength to achieve a 160 ft span length. The required elastic tensile strength was found to be 1.2 ksi for the Case 1b design, which uses five girder lines. The initial compressive strength can be as low as 10.2 ksi for Case 1a and 11.6 ksi for Case 1b design. Case 2 designs were explored for the possibility of achieving 170 ft span lengths, and an elastic tensile strength of 1.2 ksi was required for Case 2a and of 1.9 ksi for Case 2c design. Typical elastic tensile strength values for UHPC ranges between 1.0 and 1.5 ksi based on the literature review. The required tensile strength of 1.9 ksi is relatively high; thus, extending the span length to 170 ft may not be practical for a five-girder configuration. The required initial compressive strength for Case 2 designs ranges between 11.2 and 11.5 ksi.

For Case 3 designs using 0.6 in. diameter strands, tension stress limit at service controls the maximum achievable span length that can be achieved without debonding or harping any strands. The maximum achievable span length was found to be 171 ft for Case 3a, 174.5 ft for Case 3b, and 164.0 ft for Case 3c design. Reducing the deck thickness from 8.5 in. to 7.0 in. (Case 3a versus Case 3b) provides a relatively small increase (only 3.5 ft, 2 percent) in the maximum achievable span length. Reducing the number of girder lines from six girders to five girders for a bridge having 7.0 in. deck thickness (Case 3b vs. Case 3c) decreases the maximum achievable span length by around 10 ft, which is a more than 6 percent reduction.

A 160 ft span length can be achieved using only five Tx62 UHPC girders when the elastic tensile strength is increased to 1.2 ksi. However, it is very difficult and not practical to build a 170 ft span length using five Tx62 UHPC girders because it requires elastic tensile strengths that are higher than typical UHPC limits.

Table 3.38. Summary of Flexural Stress Designs for Tx62 Girder Using 0.6 in. Strands.

Parameter	Case 1a	Case 1b	Case 2a	Case 2b	Case 2c	Case 3a	Case 3b	Case 3c
Span Length, ft	160	160	170	170	170	171.0	174.5	164
Total Width, ft	46	46	46	46	46	46	46	46
Girder Spacing, ft	8	10	8	8	10	8	8	10
No. of Girders	6	5	6	6	5	6	6	5
Overhang, ft	3	3	3	3	3	3	3	3
Deck Thickness, in.	8.5	8.5	8.5	7.0	7.0	8.5	7.0	7.0
Span/Depth	27.2	27.2	28.9	29.6	29.6	29.1	30.3	28.5
f'_{ci} (ksi)	10.2	11.6	11.5	11.2	11.2	14.0	14.0	14.0
f'_c (ksi)	22.0	22.0	22.0	22.0	22.0	22.0	22.0	22.0
f'_{ti} (ksi)	0.75	0.75	0.75	0.75	0.75	0.75	0.75	0.75
f'_t (ksi)	1.0	1.2	1.2	1.0	1.9	1.0	1.0	1.0
Strand Diameter (in.)	0.6	0.6	0.6	0.6	0.6	0.6	0.6	0.6
No. of Strands	76	90	88	88	88	90	92	88
Debonded Strands	0	0	0	0	0	0	0	0
Harped Strands	0	0	0	0	0	0	0	0
Camber Before Deck (in.)	6.7	7.2	7.1	7.2	7.2	6.2	5.7	6.6
Camber After Deck (in.)	2.8	2.5	2.1	3.0	2.1	1.1	1.1	2.2

Case 3 designs were also investigated in regard to the use of 0.7 in. diameter strands to explore the maximum achievable span length and the optimum eccentricity for the maximum span length. Table 3.39 summarizes design parameters and the results of the parametric feasibility study for all Case 3 designs using 0.7 in. diameter strands. For Case 3 designs using 0.7 in. diameter strands, the tension stress limit at service controls the maximum achievable span length, which requires debonding four strands or harping eight strands. The maximum achievable span length was found to be 190.5 ft for Case 3a, 194.0 ft for Case 3b, and 183 ft for Case 3c.

Table 3.39. Summary of Flexural Stress Designs for Tx62 Girder Using 0.7 in. Strands.

Parameter	Case 3a.1	Case 3a.2	Case 3b.1	Case 3b.2	Case 3c.1	Case2 3c.2
Span Length, ft	190.5	190.5	194.0	194.0	183	183
Total Width, ft	46	46	46	46	46	46
Girder Spacing, ft	8	8	8	8	10	10
No. of Girders	6	6	6	6	5	5
Overhang, ft	3	3	3	3	3	3
Deck Thickness, in.	8.5	8.5	7.0	7.0	7.0	7.0
Span/Depth	32.4	32.4	33.7	33.7	31.8	31.8
f'_{ci} (ksi)	14.0	14.0	14.0	14.0	14.0	14.0
f'_{c} (ksi)	22.0	22.0	22.0	22.0	22.0	22.0
f'_{ti} (ksi)	0.75	0.75	0.75	0.75	0.75	0.75
f'_{t} (ksi)	1.0	1.0	1.0	1.0	1.0	1.0
Strand Diameter (in.)	0.7	0.7	0.7	0.7	0.7	0.7
No. of Strands	90	90	88	88	90	90
Debonded Strands	4	0	4	0	4	0
Harped Strands	0	8	0	8	0	8
Camber Before Deck (in.)	10.8	9.9	11.0	10.0	11.1	10.3
Camber After Deck (in.)	2.9	2.0	3.8	2.8	4.2	3.4

Figure 3.48 provides a bar chart comparison for the maximum achievable span lengths using 0.6 in. and 0.7 in. diameter strands. Compared to the standard Tx62 I-girder design using CC, the designs using 0.6 in. diameter strands can provide around 30 percent longer span length, while the designs using 0.7 in. diameter strands can provide around 50 percent longer span length. Thus, the full potential of UHPC can be best leveraged by using large diameter (0.7 in.) strands.

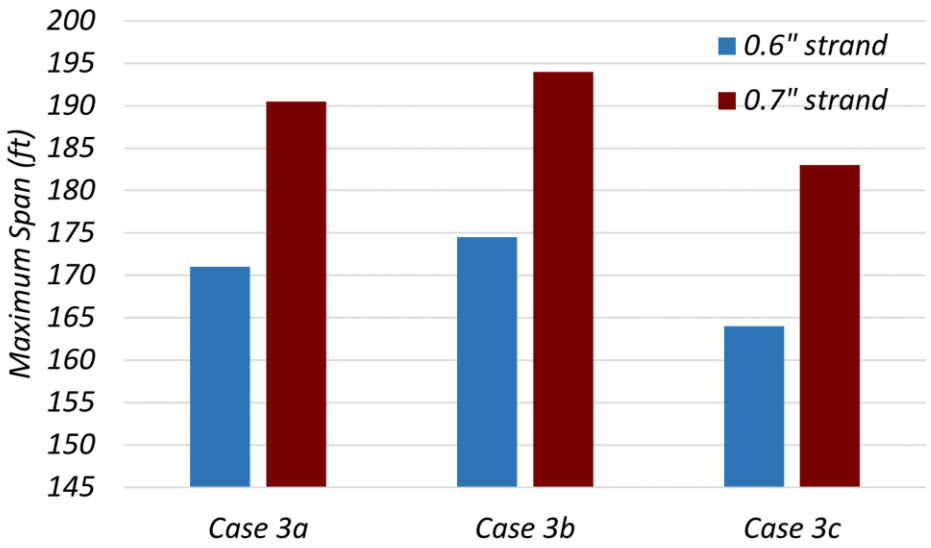

Figure 3.48. Comparison of Maximum Span Lengths for UHPC Tx62 Girders.

3.7.6 Flexural Resistance at Strength Limit State

The flexural resistance of Tx62 girders must be greater than the factored flexural demand given in the Strength I load combination provided in the AASHTO LRFD Specifications (AASHTO 2020) Table 3.4.1-1. Section 3.4 of this report provides the load and resistance factors and the design approach for calculating the flexural resistance using the triangular stress block approach. The flexural resistance of Tx62 girders was also calculated using the conventional rectangular stress block approach following the guidelines and assumptions provided in the AASHTO LRFD Specifications (AASHTO 2020) Article 5.6.2.1.

Table 3.40 summarizes the factored flexural demand M_u and reduced nominal flexural resistance ϕM_n results for Case 3 designs using 0.6 in. and 0.7 in. diameter strands. Figure 3.49 shows a bar chart comparing the factored flexural demands for Case 3 designs with the reduced nominal flexural resistance computed using both the rectangular and triangular stress block approach. Details about Case 3 designs may be found in the previous section. Both the rectangular and triangular stress block approach suggest that the reduced nominal flexural resistance is greater than the factored flexural demand. Compared to rectangular stress distribution, using triangular stress distribution for calculating the flexural resistance of Tx62 UHPC girders results in a 1–2 percent higher estimate for design cases using 0.6 in. diameter strands, while providing 2–4 percent lower estimates for design cases using 0.7 in. diameter strands. Note that using the triangular stress

distribution method is more complicated than using the rectangular stress block approach when applied to I-girder shapes.

Table 3.40. Flexural Demand and Resistance Results for Tx62 Girders—Case 3.

Nominal Strand Diameter	Design Case	Factored Flexural Demand M_u, kip-ft	Reduced Nominal Flexural Resistance ϕM_n, kip-ft	
			Rectangular stress block	Triangular stress block
0.6 in.	Case 3a	16,809	21,275	21,593
	Case 3b	17,032	20,955	21,157
	Case 3c	17,396	21,149	21,044
0.7 in.	Case 3a	20,238	27,741	26,579
	Case 3b	20,392	26,189	25,728
	Case 3c	20,900	27,935	26,840

Note: The resistance factor ϕ for tension-controlled prestressed concrete members with bonded strands is taken as 1.0 based on the AASHTO LRFD Specifications (AASHTO 2020).

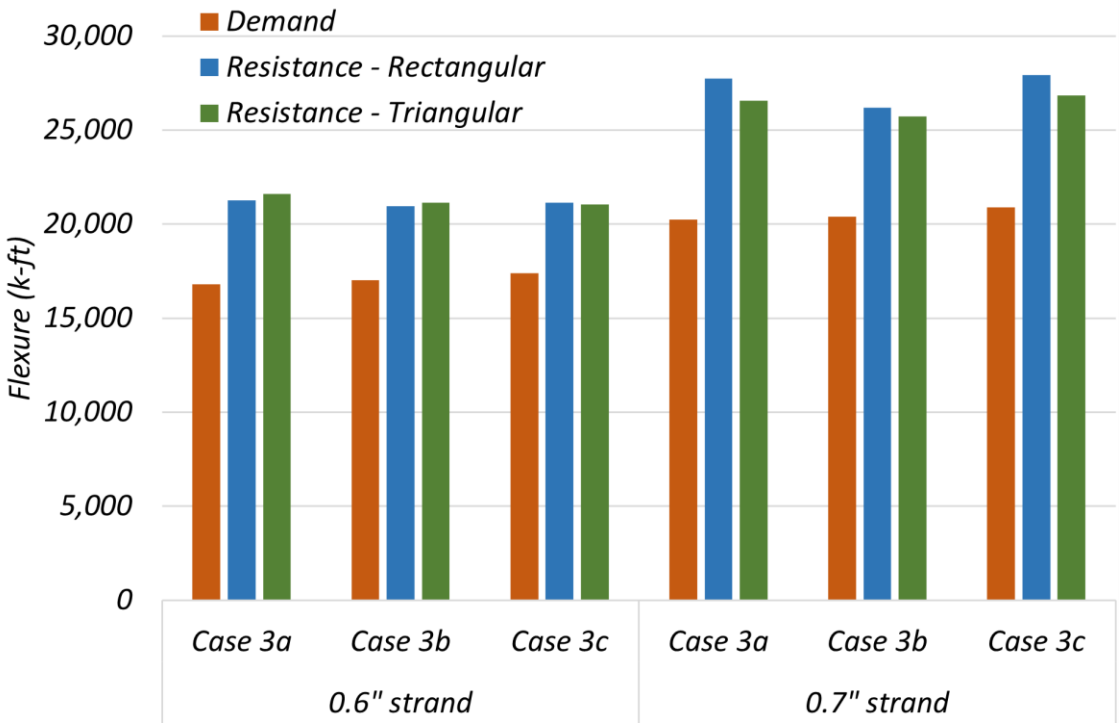

Figure 3.49. Comparison of Flexural Resistance for UHPC Tx62 Girder.

3.7.7 Shear Resistance at Strength Limit State

The shear resistance of Tx62 UHPC girders must be greater than the factored shear demand given by the Strength I load combination provided in the AASHTO LRFD Specifications (AASHTO 2020) Table 3.4.1-1. Section 3.4 of this report provides the load and resistance factors and the design approach for calculating the shear resistance. The AFGC Guidelines (AFGC 2013) shear design methodology has been used for calculating shear resistance.

Table 3.41 summarizes the factored shear demand V_u and shear resistance V_n results for both Case 3 designs using 0.6 in. and 0.7 in. diameter strands. Figure 3.50 shows a bar chart comparing the factored shear demands for Case 3 designs with the factored shear resistance computed using the AFGC Guidelines (AFGC 2013). Two different shear resistance values were calculated based on the method used for calculating the shear depth, which depends on the lever arm of the internal forces corresponding to the bending moment. Both shear resistance values using the shear depth from the rectangular and triangular stress block approach suggest that the factored shear resistance is greater than the factored flexural demand for most design cases. Design cases using five girders have slightly lower shear resistance when the triangular stress block approach is used for calculating the shear depth and may need shear reinforcement at critical shear regions only. Using a triangular stress distribution for calculating the shear depth results in a 10–15 percent lower shear resistance estimate than when using the rectangular stress block.

If the shear reinforcement guidelines from the AASHTO LRFD Specifications (AASHTO 2020) Article 5.7.2.3 are adopted, the regions having factored shear force greater than the half of the factored shear resistance provided by concrete and fibers requires minimum shear reinforcement. Whether the triangular stress block or rectangular stress block approach is used for calculating the shear depth, half of the shear resistance provided by concrete and fibers ($0.5(V_{Rd,c} + V_{Rd,f})$) is smaller than the factored shear demand at the critical shear section. The empirical equation to calculate the minimum required transverse shear reinforcement is provided in the AASHTO LRFD Specifications (AASHTO 2020) Article 5.7.2.5. The minimum shear reinforcement is likely to be required for the first quarter of the girder length for most cases.

Table 3.41. Shear Demand and Resistance Results for Tx62 Girders—Case 3.

Nominal Strand Diameter	Design Case	Factored Shear Demand V_u, kips	Nominal Shear Resistance V_n, kips	
			Rectangular stress block	Triangular stress block
0.6 in.	Case 3a	423	543	464
	Case 3b	415	525	446
	Case 3c	451	545	501
0.7 in.	Case 3a	461	536	474
	Case 3b	451	533	469
	Case 3c	490	533	474

Note: The shear resistance is calculated using AFGC Guidelines (AFGC 2013), which includes safety factors in nominal shear resistance equations rather than a resistance factor ϕ.

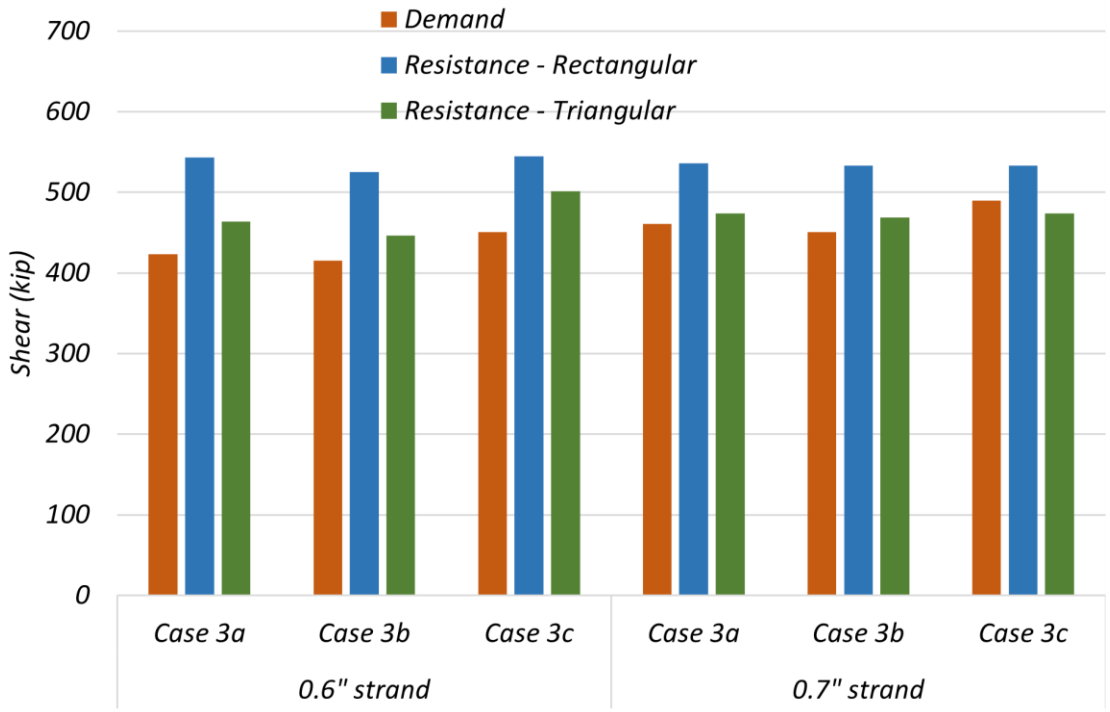

Figure 3.50. Comparison of Shear Resistance for UHPC Tx62 Girder.

3.8 SUMMARY

The analytical feasibility study was the first step toward identifying the potential designs that could be optimized with UHPC. The existing literature on the structural design of UHPC served as the basis of the design considerations for the trial designs. The trial designs—namely (1) 5SB16 PCSB with a side-by-side configuration for short-span bridges, (2) Tx54 prestressed concrete I-girders for medium- to long-span bridges, and (3) Tx62 for prestressed concrete I-girders for long-span

bridges—were developed using the strength values of UHPC noted in the literature. The potential benefits of utilizing precast, pretensioned UHPC bridge girders were determined based on the AASHTO design approach with slight modifications for UHPC. The material target properties, especially for the tension and compression limit states, are based on the design assumptions noted in Chapter 3. Various parameters, including number of girders, girder spacing, strand diameter, deck thickness, and compressive and tensile strength of concrete were varied to optimize the UHPC girder designs and to study the following research questions:

- What is the maximum possible span length for a given bridge type with specific geometric and material properties?
- What is the possible extension of span length beyond the current standard design when using UHPC girders?
- Is it possible to remove a girder line to optimize a bridge design when using UHPC girders?

The following key findings are noted based on the results of the feasibility study:

1. *Development of potential UHPC design options.* Based on the published range of UHPC properties, such as the unit weight, compressive and tensile strengths, and prestress losses, UHPC girder designs were developed for the above-mentioned shapes:
    - For 5SB15 slab beam girders, in comparison to the standard slab beam girder design using CC, the designs using 0.6 in. diameter strands can provide around a 40 percent longer span length, while the designs using 0.7 in. diameter strands can provide around a 55 percent increase in span length. However, the camber is higher for the 0.7 in. diameter strands; harping the strands is beneficial for controlling the camber.
    - For Tx54 girders, longer span lengths were evaluated for varying material strengths of UHPC, using different girder spacing, using a 7.0 in. deck with 2.5 in. UHPC PCPs, and varying the strand layout. Increasing span lengths beyond 30–40 percent longer is not practically feasible due to the high compressive and tensile strength requirements for the UHPC mixture. Approximately a 29 percent increase in span length is possible for a Tx54 girder with 0.6 in. strand diameters versus using an 8.5 in. CC deck.
    - For Tx62 shape girders, longer span lengths were analyzed for different girder spacing, varying strand diameters, different compressive and tensile strengths of UHPC, and

varying strand layouts. For 0.6 in. diameter strands, an approximately 30 percent increase in span length can be achieved with conventional deck thickness and with a thinner deck, while the designs using 0.7 in. diameter strands can provide up to 50 percent longer span length.

2. *Impact of strand diameter*. The full potential of UHPC can be leveraged by using larger diameter (0.7 in.) strands. However, using 0.7 in. diameter strands leads to larger camber values that can potentially be mitigated by harping strands. In addition, the optional live load-deflection check might be a concern for these longer span lengths. To maximize the benefits of UHPC, 0.7 in. diameter strands can be considered for future designs.
3. *Recommendations for nonproprietary UHPC mixture.* Based on the findings of the analytical feasibility study, the potential benefits of implementing UHPC for bridge structures instead of using CC were highlighted. The target strengths for the nonproprietary UHPC mixture to be developed in this research were set as follows: 14 ksi compressive strength and 0.75 ksi tensile strength at release, and 22 ksi compressive strength and 1.0 ksi tensile strength at service.
4. *Recommendations for full-scale testing program*. Following review of the results and discussions with the TxDOT team, it was decided to test two Tx34 girder shapes for a medium span length bridge case and one Tx54 girder shape for a longer span bridge case with no change to the strand diameter (0.6 in.) or deck thickness.

Table 3.42 presents a summary of successful design options when using 5SB15 girders for standard CC design and UHPC designs. Case 1 and Case 2 investigate the target material properties for 60 ft and 70 ft span lengths, respectively. Case 3d explores the maximum length that can be achieved for specific target properties but requires the use of 0.7 in. strands.

Table 3.42. Summary of Design Options for 5SB15 Girders.

Parameter	CC - TxDOT	Case 1	Case 2	Case 3d
Span Length, ft	50	60	70	78
Total Width	30'-1"	30'-1"	30'-1"	30'-1"
Girder Spacing	5'-0¼"	5'-0¼"	5'-0¼"	5'-0¼"
No. of Girders	6	6	6	6
Overhang	2'-5⅞"	2'-5⅞"	2'-5⅞"	2'-5⅞"
CIP Deck Thickness, in.	5.0	5.0	5.0	5.0
Span/Depth	30	36	42	47.5
f'_{ci} (ksi)	4.0	7.0	14.0	14.0
f'_{c} (ksi)	5.0	12.0	22.0	22.0
f'_{ti} (ksi)	–	0.75	0.75	0.75
f'_{t} (ksi)	–	1.0	1.0	1.0
Strand Diameter (in.)	0.6	0.6	0.6	0.7
No. of Strands	22	40	56	56
Debonded Strands	6	0	8	0
Harped Strands	–	0	0	8
Camber Before Deck (in.)	–	3.3	4.1	6.1
Camber After Deck (in.)	–	2.1	2.4	3.4

Table 3.43 presents a summary of successful design options when using Tx54 I-beams for standard CC design and UHPC designs. Case 1 and Case 2 investigate the target material properties for 160 ft and 170 ft span lengths, respectively. Case 3a and Case 3a.2 explore the maximum length that can be achieved for specific target properties using 0.6 in. and 0.7 in. diameter strands, respectively.

Table 3.43. Summary of Design Options for Tx54 Girders.

Parameter	CC-TxDOT	Case 1a	Case 2a	Case 3a	Case 3a.2
Span Length, ft	120	160	170	155	172
Total Width, ft	46	46	46	46	46
Girder Spacing, ft	8	8	8	8	8
No. of Girders	6	6	6	6	6
Overhang, ft	3	3	3	3	3
Deck Thickness, in.	8.5	8.5	8.5	8.5	8.5
Span/Depth	23.0	30.7	32.6	29.8	33.0
f'_{ci} (ksi)	5.7	14.0	14.0	14.0	14.0
f'_{c} (ksi)	6.9	22.0	22.0	22.0	22.0
f'_{ti} (ksi)	–	0.75	0.75	0.75	0.75
f'_{t} (ksi)	–	1.5	2.6	1.0	1.0
Strand Diameter (in.)	0.6	0.6	0.6	0.6	0.7
No. of Strands	44	84	82	84	82
Debonded Strands	6	0	0	0	0
Harped Strands	–	0	0	0	6
Camber Before Deck (in.)	–	5.90	5.4	6.2	10.3
Camber After Deck (in.)	–	−0.02	−2.2	1.0	2.3

Table 3.44 presents a summary of successful design options when using Tx62 I-beams for standard CC design and UHPC designs. Case 1 and Case 2 investigate the target material properties for 160 ft and 170 ft span lengths respectively. Case 3a and Case 3a.2 explore the maximum length that can be achieved for specific target properties using 0.6 in. and 0.7 in. diameter strands, respectively.

Table 3.44. Summary of Design Options for Tx62 Girders.

Parameter	CC-TxDOT	Case 1b	Case 2a	Case 3a	Case 3a.2
Span Length, ft	130.0	160	170	171.0	190.5
Total Width, ft	46	46	46	46	46
Girder Spacing, ft	8	10	8	8	8
No. of Girders	6	5	6	6	6
Overhang, ft	3	3	3	3	3
Deck Thickness, in.	8.5	8.5	8.5	8.5	8.5
Span/Depth	22.1	27.2	28.9	29.1	32.4
f'_{ci} (ksi)	5.8	11.6	11.5	14.0	14.0
f'_c (ksi)	6.7	22.0	22.0	22.0	22.0
f'_{ti} (ksi)	–	0.75	0.75	0.75	0.75
f'_t (ksi)	–	1.2	1.2	1.0	1.0
Strand Diameter (in.)	0.6	0.6	0.6	0.6	0.7
No. of Strands	42	90	88	90	90
Debonded Strands	6	0	0	0	0
Harped Strands	–	0	0	0	8
Camber Before Deck (in.)	–	7.2	7.1	6.2	9.9
Camber After Deck (in.)	–	2.5	2.1	1.1	2.0

4 FULL-SCALE TEST PROGRAM

4.1 INTRODUCTION

To establish a better understanding of the structural behavior of UHPC precast, pretensioned bridge girders for potential implementation in Texas, frequently used standard TxDOT bridge girder sections (Tx34 and Tx54) were selected for plant casting and structural testing in this research project. The structural behavior of the full-scale girder specimens topped with a standard CC deck slab was investigated in flexure and shear under both service and ultimate load conditions. Design values and analytical predictions of the structural response of these girders were compared with the experimental performance of the girders to support the assessment and development of design recommendations for UHPC precast, pretensioned bridge girders.

Two Tx34 girders and one Tx54 girder were fabricated at a precast plant in Texas from the nonproprietary mix developed as a part of this research. The Volume 1 report documents the development of the nonproprietary UHPC mixture design along with fabrication of the girder specimens, including production and placing UHPC at the precast plant. Section 4.2 lists the geometric details of the prototypes and the specimens. This section also illustrates the as-built details of the specimens that were used in the full-scale test program. Section 4.3 describes the construction of the deck. Section 4.4 elaborates on the full-scale testing program. Section 4.5 summarizes the average short-term hardened properties measured from material-level tests for all three girder specimens. Chapter 6 of the Volume 1 report includes more details on the fabrication, UHPC mixture design, and fresh and hardened properties.

4.2 PROTOTYPE AND SPECIMEN DETAILS

Based on the feedback from the TxDOT Project Monitoring Committee after the review of the analytical feasibility study, two Tx34 specimens and one Tx54 specimen were designed for laboratory testing. The specimen designs are based on prototype bridge designs; however, the girder specimen lengths were reduced to allow for laboratory testing. Table 4.1 summarizes the prototype and specimen details of the three girder specimens.

Table 4.1. Details of Prototype and Specimen.

	Parameters			Tx34-1	Tx34-2	Tx54
Prototype	Backwall-to-Backwall Length, ft			77	85	121
	Span Length, ft			75	83	119
	Strand Diameter, in.			0.6	0.6	0.6
	Total No. of Strands			30	38	48
	Number of Strands	℄	Bot.	26	34	44
			Top	4	4	4
		End	Bot.	26	28	36
			Top	4	10	12
	Eccentricity, in.	℄		8.61	8.80	15.10
		End		8.61	5.64	8.76
	Nominal Moment Capacity (M_n), k-ft			4609	5688	11,131
	Neutral Axis Depth for M_n (from top of deck), in.			6.03	7.55	10.00
Specimen	Length between Seats, ft			48.5	48.5	68. 5
	Nominal Moment Capacity (M_n), k-ft			4609	5688	11,131

Note: The strand layout is the same for the prototype and specimen.

Note that the two Tx34 girder designs were based on a backwall-to-backwall girder length of 77 ft and 85 ft, while the Tx54 prototype design has a 121 ft length. The backwall-to-backwall length is defined as the total span length between the two abutment backwalls. The span length is defined as the center-to-center distance of the bearings of the girder. The girder spacing was 8 ft center-to-center, and an 8.5 in. thick CC deck was considered in the design of the prototypes. Tx34-1 used an eccentric strand design with all straight strands, while the Tx34-2 and Tx54 girder specimens had some harped strands. The center of the bearing pads of the girder were located 9 in. from the girder ends. The bearing pads used were 1 ft 9 in. wide, 8 in. long (in the direction of the girder axis), and 2.03 in. thick.

The total number of 0.6 in. diameter prestressing strands of 270 ksi ultimate strength for each of the prototypes are listed in Table 4.1. Of the total strands provided, four were located at the top of the girder section to facilitate the tying of interface shear bars, henceforth referred to as U-composite bars (UC-bars) (#5). Tx34-1 had an eccentric strand layout with 26 strands at the bottom, while the Tx34-2 and Tx54 girders had harped strand layouts with six and eight harped strands, respectively. The same strand arrangement is maintained for the prototypes. Eccentricity

is defined as the location of the center of gravity of the strands to the centroid of the cross-section of the girder. Table 4.1 provides the eccentricities of the prestressing at the ends and midspan for each girder specimen. Since compression is primarily in the deck, the nominal moment strengths of the girders were determined based on the AASHTO (2020) rectangular stress block model. One-half of each girder span was provided with minimum transverse reinforcement, hereafter termed "reinforced end," and the other half was not provided with any transverse reinforcement in the web; thus, it is hereafter referred to as "unreinforced end." Chapter 3 details the capacity and the limit states for which the girders were designed.

Figure 4.1, Figure 4.2, and Figure 4.3 show the as-built drawings for the three girder specimens. The appendix includes the drawings that were delivered to the precaster prior to the fabrication. Note that typical mild steel reinforcement that is standard in the Tx-girder bottom flange (C-, CH- and U-bars) was omitted on the unreinforced end to utilize the enhanced tensile properties of UHPC. Therefore, the unreinforced end did not have any confinement reinforcement or bursting reinforcement at that end. The reinforced end included standard confinement reinforcement in addition to the minimum shear reinforcement with the spacing as per AASHTO (2020) design requirements. The fiber contribution was determined as per eConstruct (2020) and Tadros (2021). Section 2.4.4 of this report provides this information. Other reinforcement details at the reinforced end were also reduced to the minimum requirement. For the Tx34-2 specimen, there were additional transverse R-bars placed at the reinforced end (shown as orange bars). These extra bars were added as a result of a miscommunication arising at the plant prior to the installation of the instrumented R-bars in the girder. The shear testing of the specimens was slightly modified to account for the extra shear strength imparted by those additional bars and to evaluate the portion of the girder with the desired R-bar spacing. The Tx54 specimen drawing shows the dimensions of the hold-down points measured in the field during the fabrication process. The theoretical hold-down locations used for design purposes were at 5 ft on either side of the midspan for both the Tx34-2 and Tx54 specimens.

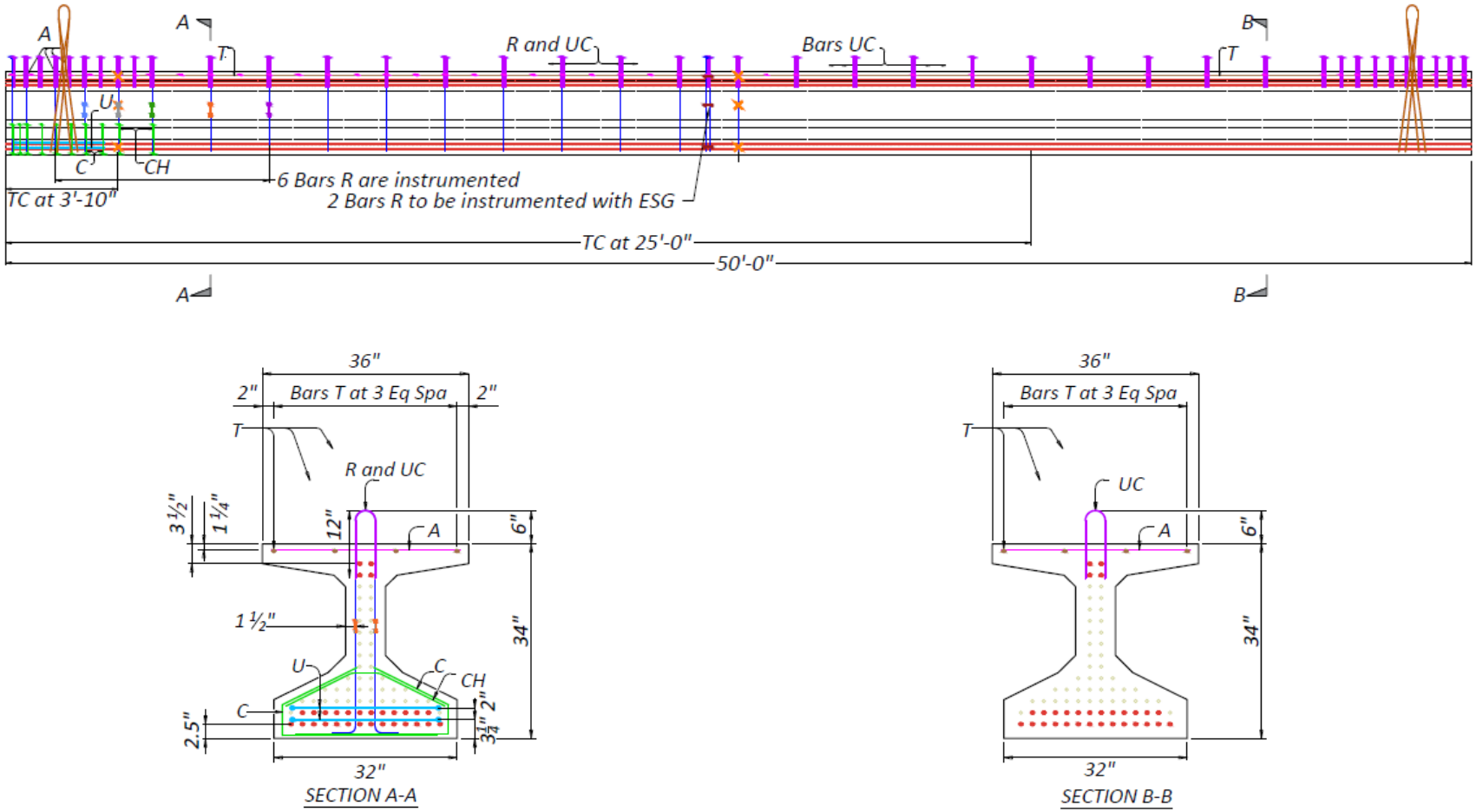

Note: Thermocouple (TC) and Embedded Strain Gage (ESG) are the sensors installed in the field.

Figure 4.1. Tx34-1 Structural Design Drawing of Elevation and Cross-Sections.

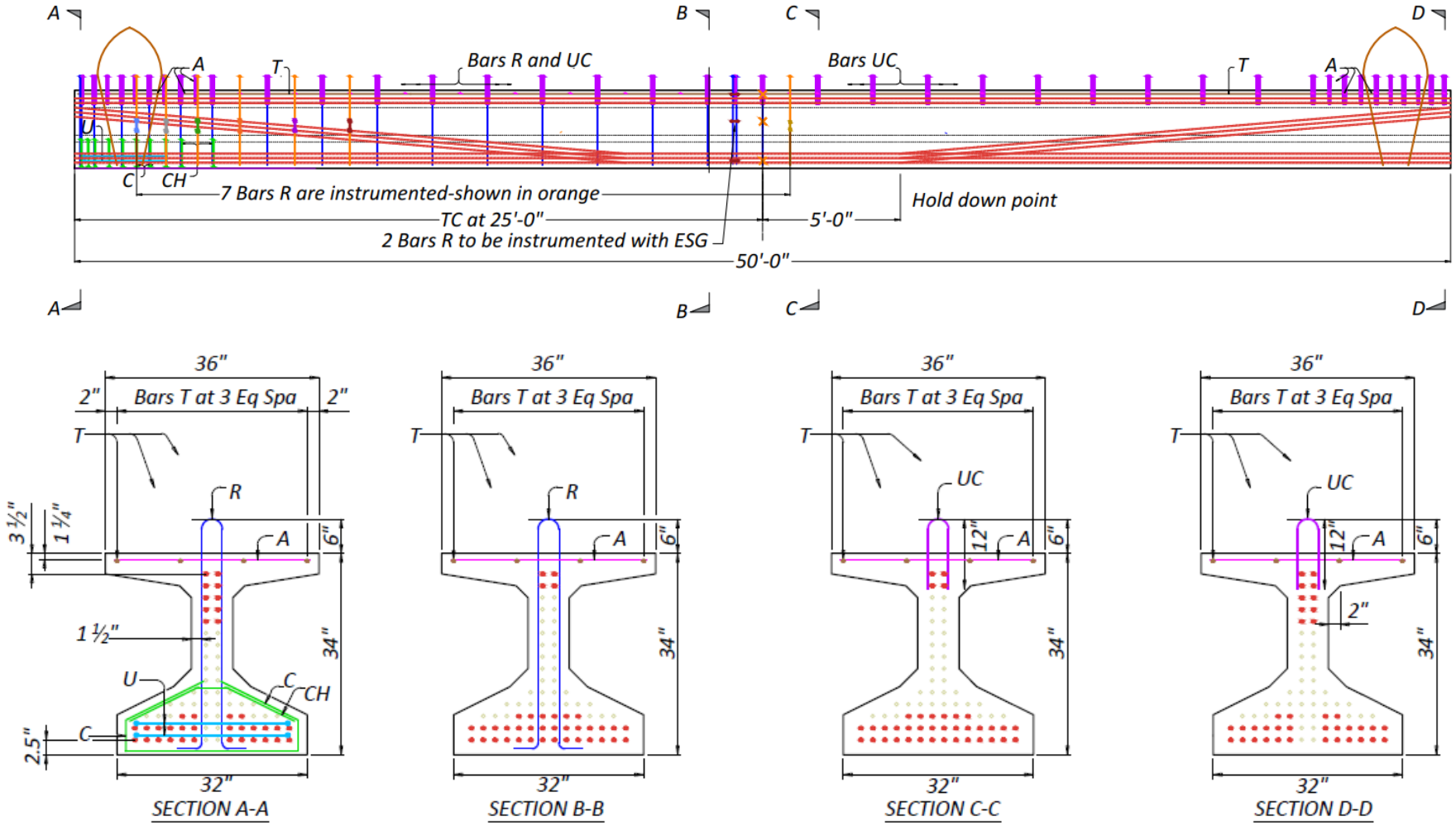

Notes:
1. TC and ESG are the sensors installed in the field
2. Hold-down locations for design are 5' 0" from the midspan

Figure 4.2. Tx34-2 Structural Design Drawing of Elevation and Cross-Sections.

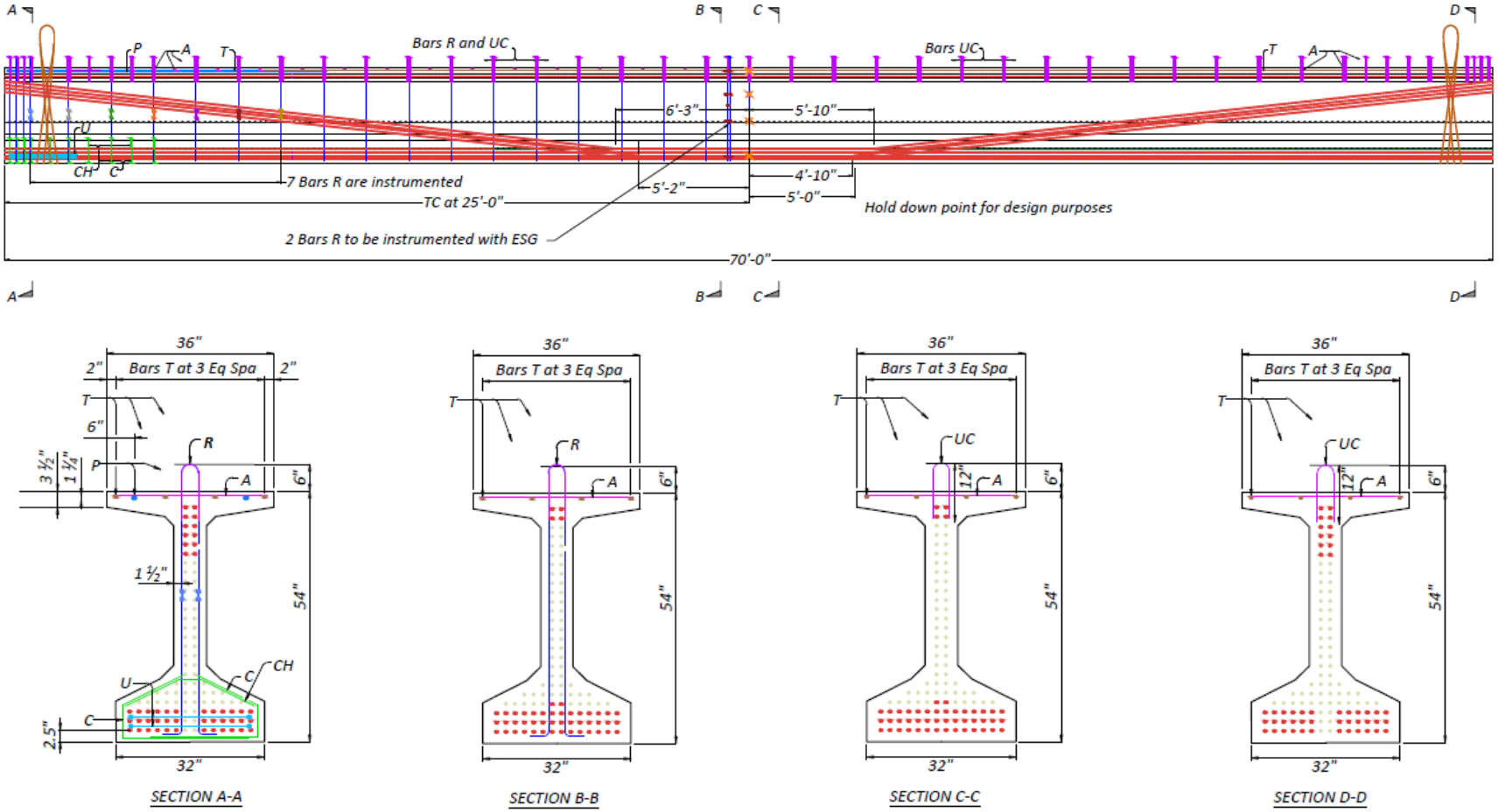

Notes:
1. TC and ESG are the sensors installed in the field
2. Hold-down locations for design are 5' 0" from the midspan. The dimensions of the hold-down points were measured during girder fabrication

Figure 4.3. Tx54 Structural Design Drawing of Elevation and Cross-Sections.

4.3 DECK SLAB CONSTRUCTION

One of the primary objectives of this research project was to study the performance of UHPC bridge girders with a CIP reinforced CC deck slab for implementation in Texas. Therefore, a CC bridge deck with an effective width of 96 in., corresponding to the prototype girder spacing, was proposed for construction in the High Bay Structures and Material Testing Laboratory (HBSMTL) prior to girder testing. Because the space available between the columns for the actuators was limited, the width of the slab was reduced to 92 in.

All three girders were topped with a CC deck slab. A Class S concrete with a specified 4 ksi design compressive strength at 28 days in accordance with TxDOT standard specifications item 421 was considered for design purposes when estimating the composite section properties for all three specimens. The formwork for the deck was fabricated and assembled in the HBSMTL to construct a 92 in. wide and 8.5 in. thick deck slab. The reinforcement details of the deck slab were based on TxDOT Bridge Design Manual (TxDOT 2023). The deck reinforcement consisted of No. 4 (0.5 in. diameter) Grade 60 mild steel bars placed with a top and bottom mesh having 9 in. center-to-center spacing between parallel longitudinal and transverse bars. The bottom clear cover to the transverse reinforcement was 1.25 in., while the top clear cover to longitudinal reinforcement was 2.5 in. Figure 4.4 presents the CC deck details for the UHPC girder specimens. Figure 4.5 presents the photos of the various stages of the deck construction, such as the deck formwork, the reinforcement mesh, slump testing and preparation of the companion compressive strength samples, and the deck slab after concrete pour.

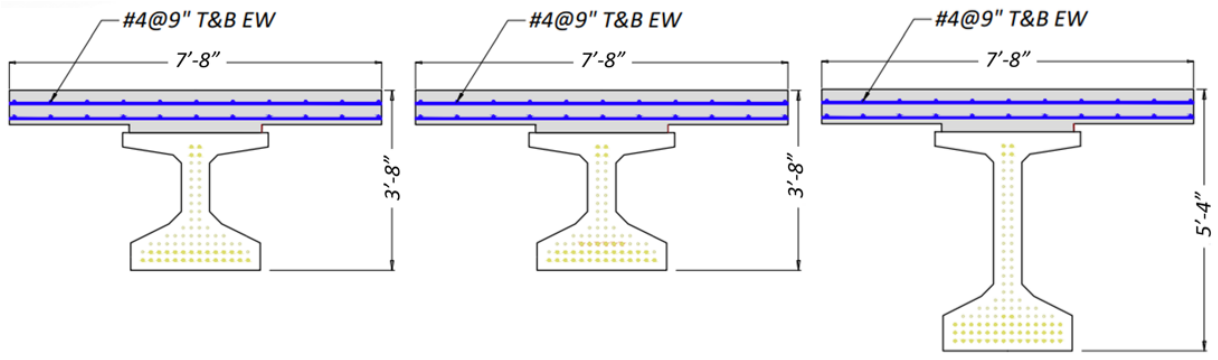

(a) Tx34-1 *(b) Tx34-2* *(c) Tx54*

Figure 4.4. CC CIP Deck Slab with UHPC Girders.

Tx34-1 Deck Formwork and Reinforcement Mesh

Reinforcement Mesh

Slump Testing and Sample Preparation

CC Deck Slab after Finishing

Figure 4.5. CIP Deck Slab Construction.

(a) Tx34-1

Figure 4.6. Girder Specimens with Finished Deck Slab.

(b) Tx34-2

(c) Tx54

Figure 4.6. Girder Specimens with Finished Deck Slab. (Cont.).

4.4 FULL-SCALE TEST PROGRAM AND INSTRUMENTATION

The properties of camber and transfer length were continuously monitored from the stage of release of prestressing strands to the final testing of the girders. The full-scale test matrix included a

flexure and shear test for each girder. To evaluate the impact of the superior tensile strength on the shear resistance of the girder, one-half of the girder span was provided with minimum transverse reinforcement, while the shear reinforcement was eliminated in the other half. Table 4.2 shows the proposed test matrix on the girder specimens.

Table 4.2. Test Parameters of the Full-Scale Tests.

Specimen No.	Specimen Name	Tendon Profile	Trans. Reinf. Ratio[1]	Test
1	Tx34-1	Eccentric	N/A	Flexure
			0	Shear 1
			$\rho_{v,min}$	Shear 2
2	Tx34-2	Harped	N/A	Flexure
			0	Shear 1
			$\rho_{v,min}$	Shear 2
3	Tx54	Harped	N/A	Flexure
			0	Shear 1
			$\rho_{v,min}$	Shear 2

Notes:
1. Transverse reinforcement ratio is varied, where indicated, within the end region (1/2 of the span length)
2. $\rho_{v,min}$ = minimum transverse shear reinforcement. Based on the preliminary designs in outlined in Chapter 3, minimum transverse shear reinforcement generally provides sufficient transverse shear resistance of UHPC Tx Shapes
3. Inverted U-shaped #5) bars, which extend 6 in. above the top flange, will be used as interface shear reinforcement to provide composite action between the UHPC girder and CC deck slab
4. N/A: Not applicable

The flexure capacity of the prototypes was tested by conducting a four-point bending test on the girder. The moment capacity at the midspan was evaluated for all three girders, and the shear capacity of each end of the specimen ends was tested to capture the shear capacity of the prototype. The performance of the specimens was monitored through a wide range of sensors. The type of instrument, abbreviations used for the instruments in this report, and the purpose of each instrument are shown in Table 4.3. Table 4.4 summarizes the number instruments of each type.

Table 4.3. Details of Instrumentation for Full-Scale Tests.

Instrument Type	Instrument Type	Abbreviation	Measurement Purpose
Thermocouple	Provided by precast plant.	TC	Internal Temperature
String Potentiometer	TE Connectivity	SP	Deflection profile and strains on the surface on UHPC and CC
Surface Concrete Strain Gage	PL-60-11-3LJCT-F	SG	Strains on the surface on UHPC and CC
Surface Mounted Concrete Strain Gage	KM-100B	KSG	Strains on the surface of UHPC
Embedded Concrete Gage	KM-100B	ESG	Strains within the volume of concrete at midspan
Surface Steel Strain Gage	FLAB-5-350-11-5LJCT-F	SSG	Strain in transverse steel rebar
Linear Variable Displacement Transducer (LVDT)		LVDT (also denoted as LV)	Shear strain and interface shear slip
Demountable Mechanical (DEMEC) Gages		DM	Transfer length measurement

Table 4.4. Number of Instruments for Full-Scale Tests.

	Number of Instruments		
Instrument Type	**Tx34-1**	**Tx34-2**	**Tx54**
Thermocouples (TC)	6	3	3
String Potentiometer (SP)	18	19	25
Surface Concrete Strain Gage (SG)	8	8	8
Surface Mounted Concrete Strain Gage (KSG)	4	4	4
Embedded Concrete Gage (ESG)	4	4	6
Surface Steel Strain Gage (SSG)	12	14	14
Linear Variable Displacement Transducer (LVDT/LV)	16	16	16
Demountable Mechanical (DEMEC) Gages	60	38	18

The locations of the instruments were selected to measure strains, deflections, and temperature at key locations of interest. The overall instrumentation plan focused on the midspan for the flexure test and on the region near the girder ends for the shear tests. The sensor locations were streamlined after testing the first girder specimen based on the lessons learned from the results. The sensor locations were also modified for each test—depending on the type of girder and locations of interest to be monitored—to obtain the optimal information for studying the behavior of the composite girder shapes. The overall instrumentation plan for each specimen along with the test setup are discussed in Chapters 5 and 6. The following sections describe the purpose and locations of the instruments.

4.4.1 Thermocouples

TCs were installed by precast plant personnel at the girder midspan for all three girders and at the midspan and the unreinforced end of the Tx34-1 specimen. The TCs were installed at different depths over the height of the girder, such as at the centroid of the top flange, the web, and the bottom flange to monitor the temperature changes of each batch of UHPC. For the deeper Tx54 girder, two TCs were installed in the web at equal spacing. Figure 4.7 presents the specified locations of the TC over the depth of each girder specimen.

4.4.2 String Potentiometers

SPs were used to measure the vertical deflections of the girder and to determine horizontal strains in the constant bending moment region. The SPs used to measure vertical deflection were installed along the span and below the girder. Two SPs were installed at the girder ends to measure any upward movement of the girder end. Based on the predicted deflections, 4 in. and 12 in. stroke SPs were placed to obtain optimal accuracy and allow for a longer range of deflections. SPs were arranged such that they were 3 ft center-to-center, with additional SPs placed under the actuators and at the midspan. Figure 4.8 presents the SP arrangement for the specimens for the flexure test. The arrangement is similar for the testing of the shear spans. Chapter 6 presents the specific instrumentation arrangements for the shear tests. Table 4.5 and Table 4.6 present the location of vertical deflection measuring SPs for Tx34-1, Tx34-2 flexure tests, and Tx54, respectively.

Table 4.5. Locations of SPs for Tx34-1 and Tx34-2.

SP ID		SP-1	SP-2	SP-3	SP-4	SP-5	SP-6	SP-7	SP-8	SP-9	SP-10	SP-11	SP-12	SP-13	SP-14	SP-15	SP-16	SP-17	SP-18	SP-19
Stroke, in.		4	4	4	4	4	4	4	4	12	4	4	4	4	4	4	4	4	4	N/A
Tx34-1	Distance, ft	−0.75	1.5	3	6	7.5	9	12	18	19.5	21	22	30	33	36	39	42	45	49.25	N/A
Tx34-2	Distance, ft	−0.75	1.5	4.5	7.5	10.5	13.5	16.5	19.5	24.5	26.5	29	32	35	43	41	44	47	48	49.25

Notes:
1. The distance is measured from the centerline of the east bearing pad
2. The direction from east to west is considered positive
3. The SPs at the ends record the uplift (if any) of the girder ends
4. N/A: Not applicable

Table 4.6. Locations of SPs for Tx54.

Tx54	SP ID	SP-1	SP-2	SP-3	SP-4	SP-5	SP-6	SP-7	SP-8	SP-9	SP-10	SP-11	SP-12	SP-13
	Stroke, in.	4	4	4	4	4	4	4	4	4	4	4	12	12
	Distance, ft	−0.75	2.5	4.5	7.5	10.5	13.5	16.5	19.5	22.5	25.5	28.5	32.5	34
	SP ID	SP-14	SP-15	SP-16	SP-17	SP-18	SP-19	SP-20	SP-21	SP-22	SP-23	SP-24	SP-25	N/A
	Stroke, in.	4	4	4	4	4	4	4	4	4	4	4	4	N/A
	Distance, ft	36.5	41.5	43.5	46	49	52.5	56	58.5	61.5	64.5	66.5	69.25	N/A

Notes:
1. The distance is measured from the centerline of the east bearing pad
2. The direction from east to west is considered positive
3. The SPs at the ends record the uplift (if any) of the girder ends
4. N/A: Not applicable

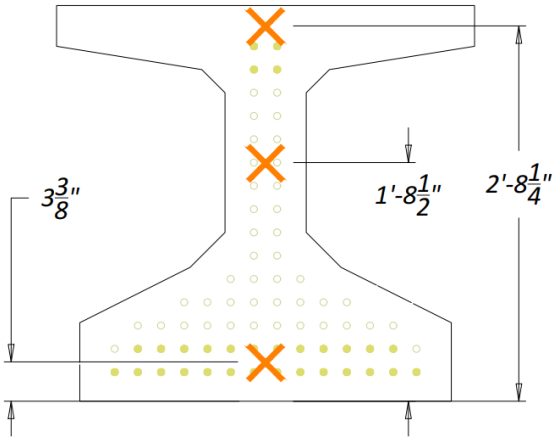

(a) Tx34-1 and Tx34-2 Cross-Section

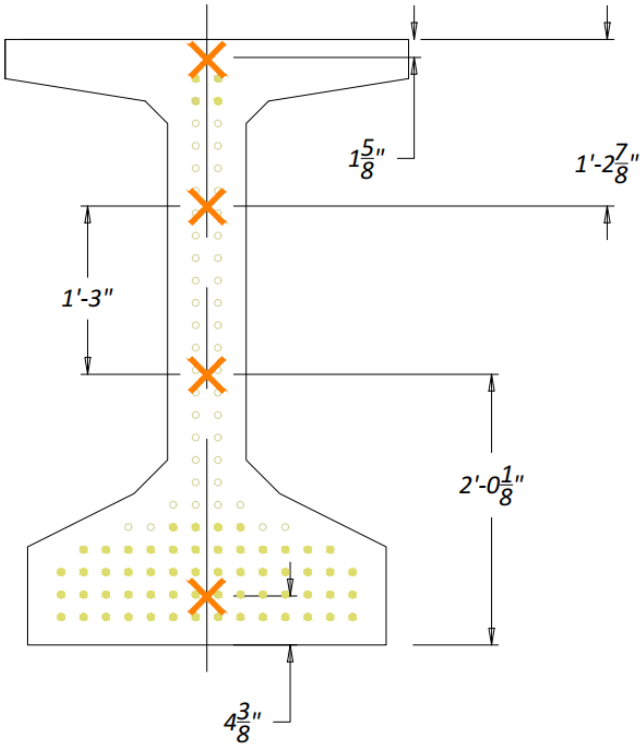

(b) Tx54-1 Cross-Section

Figure 4.7. Specified TC Arrangement.

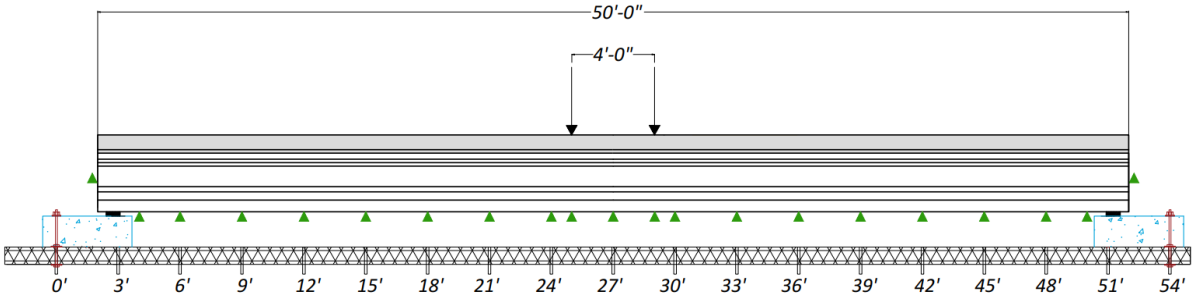

(a) Tx34-1 and Tx34-2

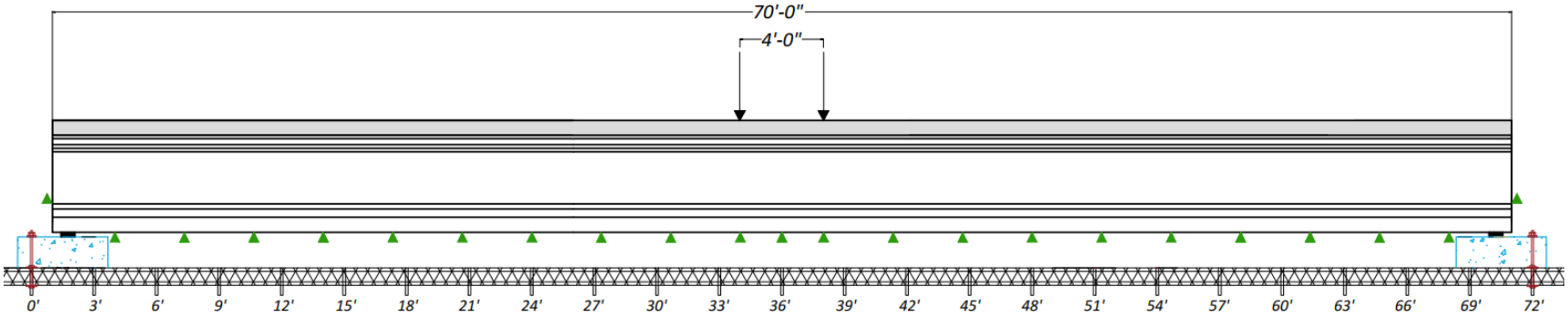

(b) Tx54

Figure 4.8. SPs for Vertical Deflection.

Figure 4.9 and Figure 4.10 present the arrangement of SPs for horizontal strain measurements during flexural testing. The SPs dedicated to measuring the horizontal displacements of the girder had a maximum 2 in. stroke because more sensitivity was desired for low range deformation measurements. A set of five SPs were installed at the top of the CC deck, and a pair of two were installed at the underside of the UHPC girder. Extra SPs were provided to ensure redundancy in the measurements. SPs were also installed on the vertical face of the specimen, over the girder depth, and at mid-height of the deck, top flange, web, and bottom flange. Similar to the TCs, the web of the Tx54 girder had two SPs on the face of the web, with equal spacing between them. Chapters 5 and 6 present the results of the horizontal strain measurements.

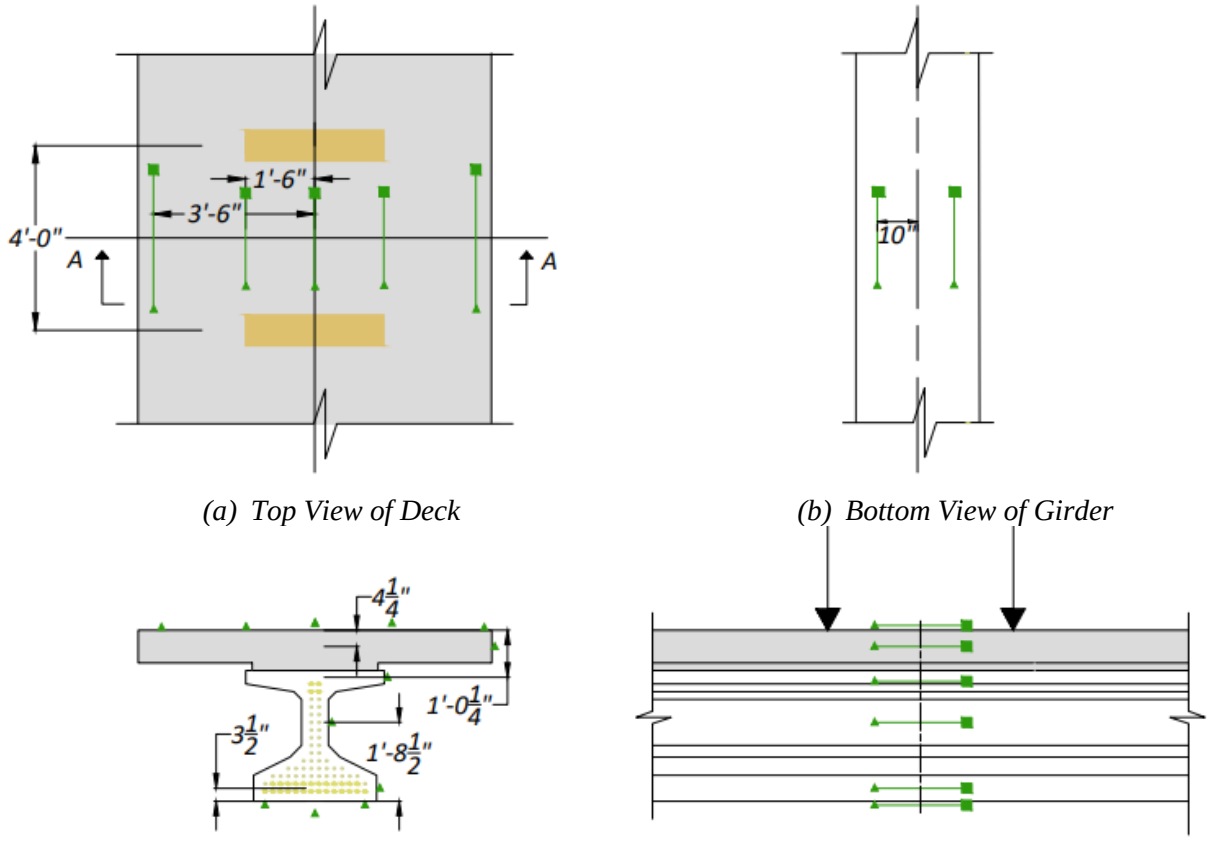

(a) Top View of Deck

(b) Bottom View of Girder

(c) Section A-A

(d) Elevation View of Girder

Figure 4.9. Tx34-1 and Tx34-2 SPs between Actuators at Midspan.

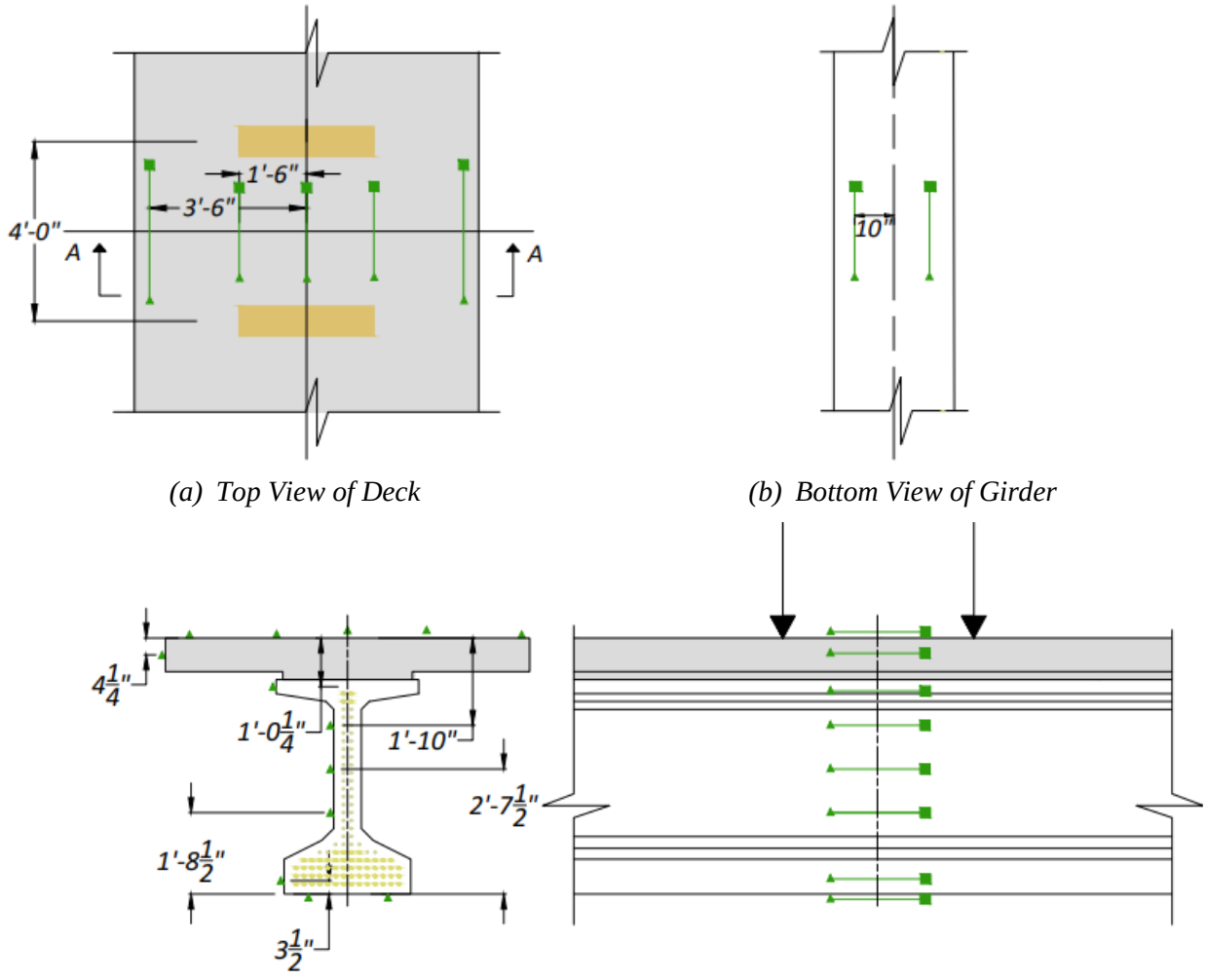

(a) Top View of Deck *(b) Bottom View of Girder*

(c) Section A-A *(d) Elevation View of Girder*

Figure 4.10. Tx54-2 SPs between Actuators at Midspan.

4.4.3 Surface Concrete Strain Gages

SGs were also installed at the top and bottom of the CC deck and UHPC girder, respectively, to measure normal strains between the actuators during the flexure and shear testing. Figure 4.11 presents the strain gages installed at midspan of Tx34-1. The strain gages, as observed from the first flexure test, showed the most meaningful data, particularly in the small strain range, in comparison to the SPs and LVDTs. All the strain gages across the girder width were quite consistent at the midspan locations and could be reduced to two gages at the top of the deck and bottom of the girder. The remaining strain gages were better utilized by installing them at the shear ends to monitor shear strains. Therefore, for subsequent testing, the strain gages located between the actuators used to measure the normal strain were reduced. Figure 4.12 and Figure 4.13 present

the updated strain gage instrumentation for the Tx34-2 and Tx54 girder specimens. Chapters 5 and 6 present the results of the strain measurements.

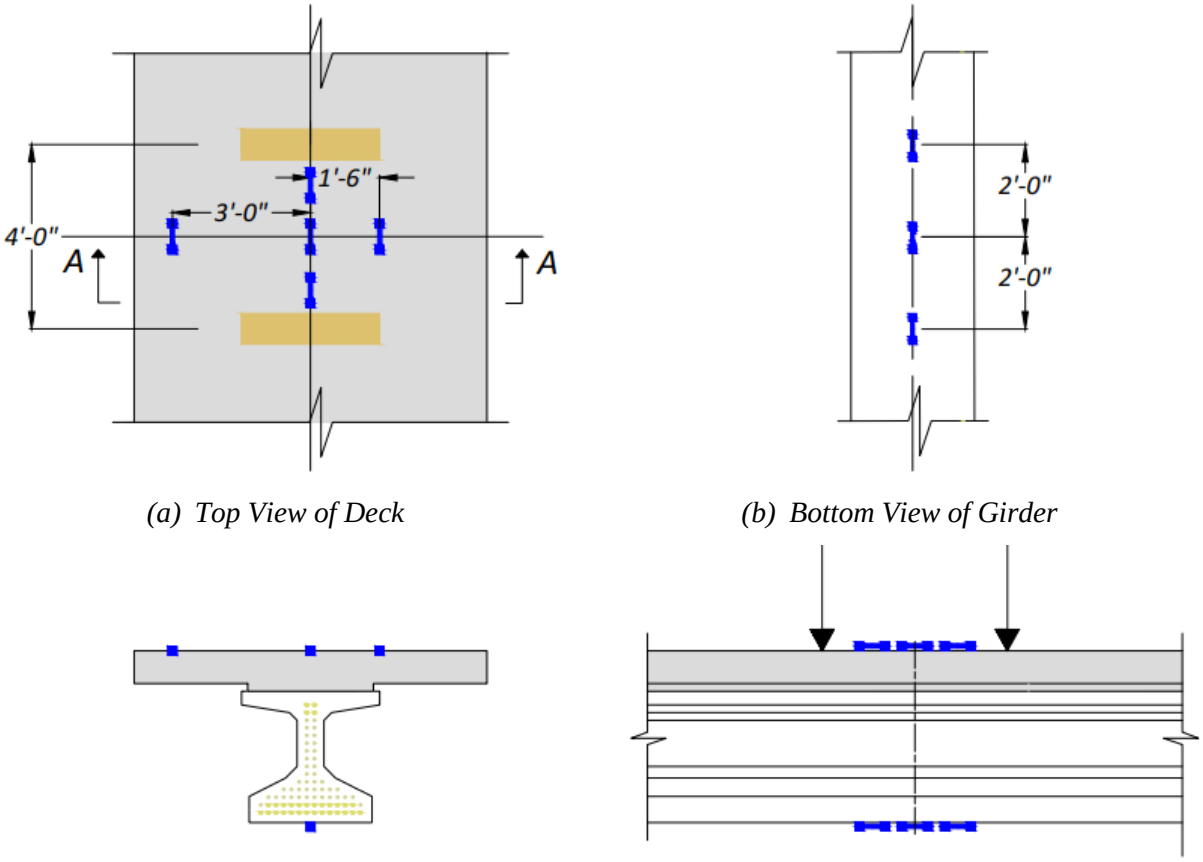

(a) Top View of Deck

(b) Bottom View of Girder

(c) Section A-A

(d) Elevation View of Girder

Figure 4.11. Tx34-1 SG between Actuators.

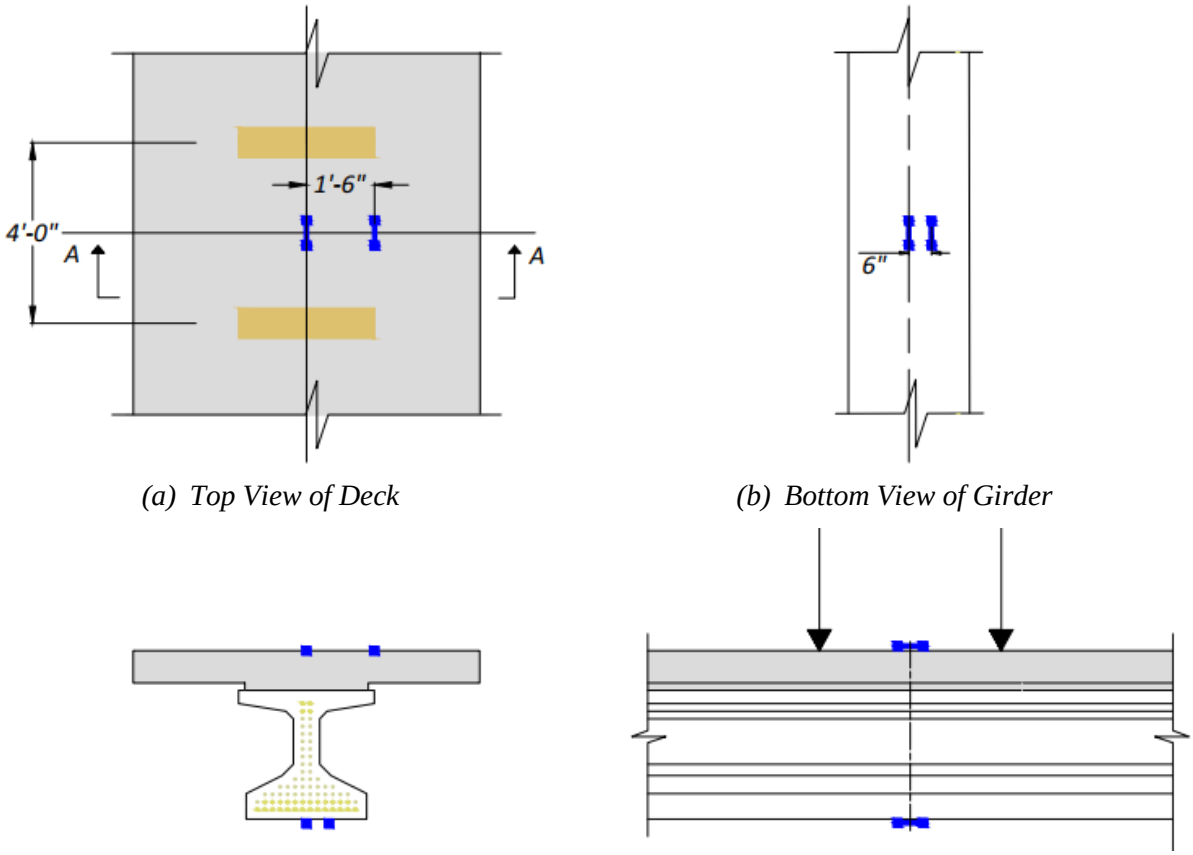

(a) Top View of Deck

(b) Bottom View of Girder

(c) Section A-A

(d) Elevation View of Girder

Figure 4.12. Tx34-2 SG between Actuators.

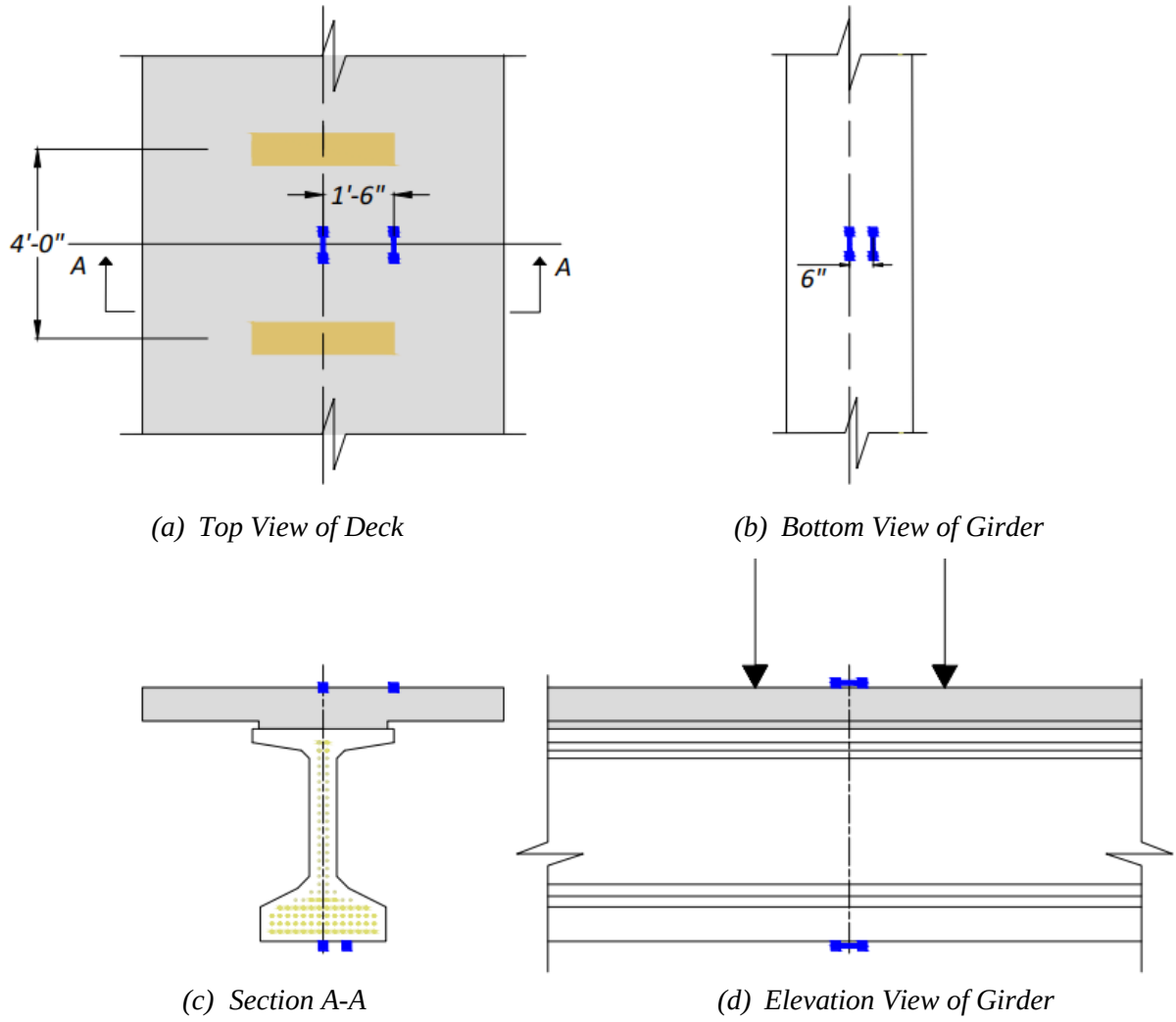

(a) Top View of Deck

(b) Bottom View of Girder

(c) Section A-A

(d) Elevation View of Girder

Figure 4.13. Tx54 SGs between Actuators.

The performance of the LVDTs for measuring small strains was poor compared to that of the strain gages. Therefore, SGs were installed in the web of the girder to monitor the strains near the cracks in the web. The strain gages were installed in pairs to measure the strains parallel and transverse to the shear cracks. Figure 4.14 presents a pair of SGs installed at existing or probable shear crack locations. The existing cracks were those arising from the flexure test conducted prior to testing the shear ends. Chapter 6 contains more details for the instrumentation locations and the results of the shear strain measurements.

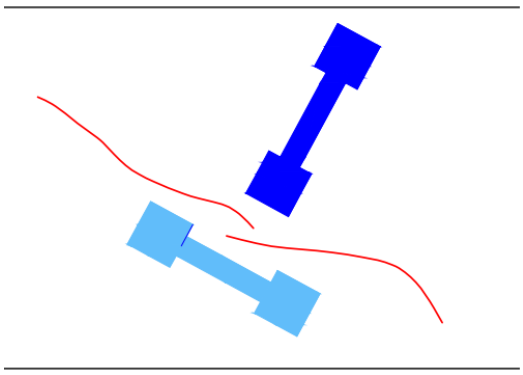

Figure 4.14. SGs in Web at Shear Cracks.

4.4.4 Surface-Mounted Concrete Strain Gages

KM-B100 gages were mounted on the surface of the girder to measure shear cracks in the shear regions. The strain gages were first installed in the bottom flange of the girder at the shear ends for strain monitoring. After the results of the first test, it was determined that a better use for the KSG was to serve as an additional pair to monitor the shear strains in the web parallel and transverse to the crack. Figure 4.15 presents the locations KSGs were installed for all the girder specimens. Chapter 6 presents the results of the KSGs.

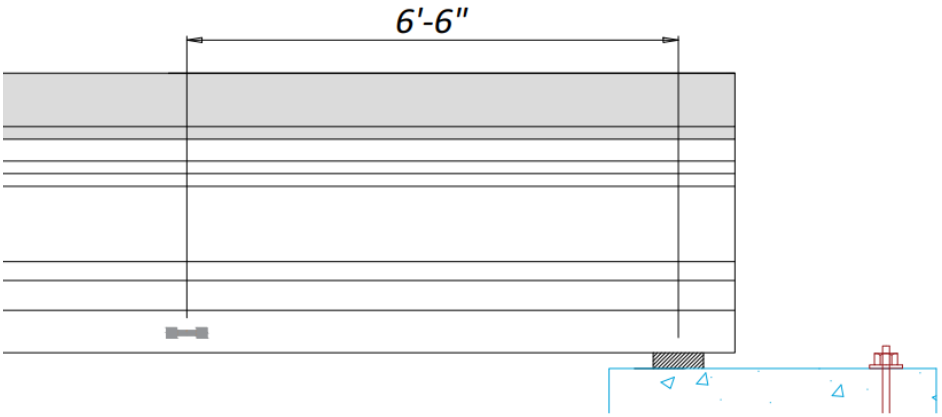

(a) KSG Installed at Bottom Flange during Flexure Test of Tx34-1

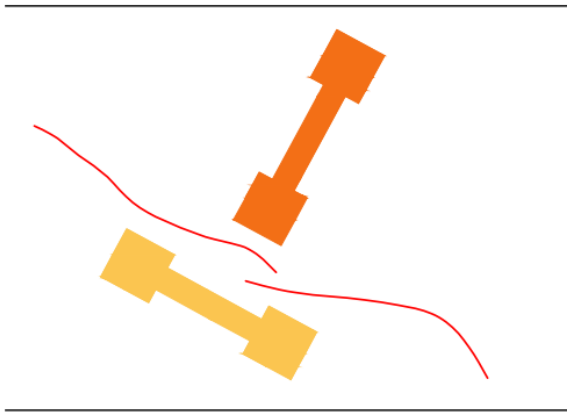

(b) KSG Installed at Shear Crack in the Web for All Shear Tests

Figure 4.15. KSG at Ends.

4.4.5 Embedded Strain Gages

Embedded KM-B100 strain gages were installed at the midspan of the specimen prior to casting the girder and deck. For the flexure test of each girder, the ESGs were located at the centroid of the deck, top flange, web, and the bottom flange in the constant bending moment region. Two equally spaced gages were installed in the web of the Tx54 specimen because of the deeper web. Some gages were damaged during the UHPC pour, which may have been due to the damage to the body of the gage itself or damage to the cable. One gage from Tx34-1, two gages from Tx34-2, and two gages from Tx54 were damaged. Figure 4.16 presents the ESG arrangement at midspan for the three girder specimens. Chapter 5 presents the results of the strain profile measured using the ESGs.

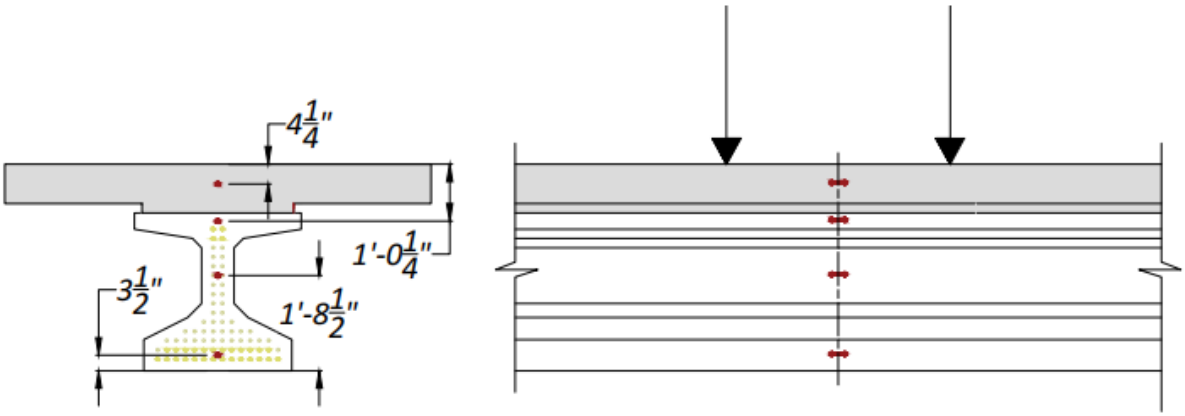

(a) Tx34-1 and Tx34-2

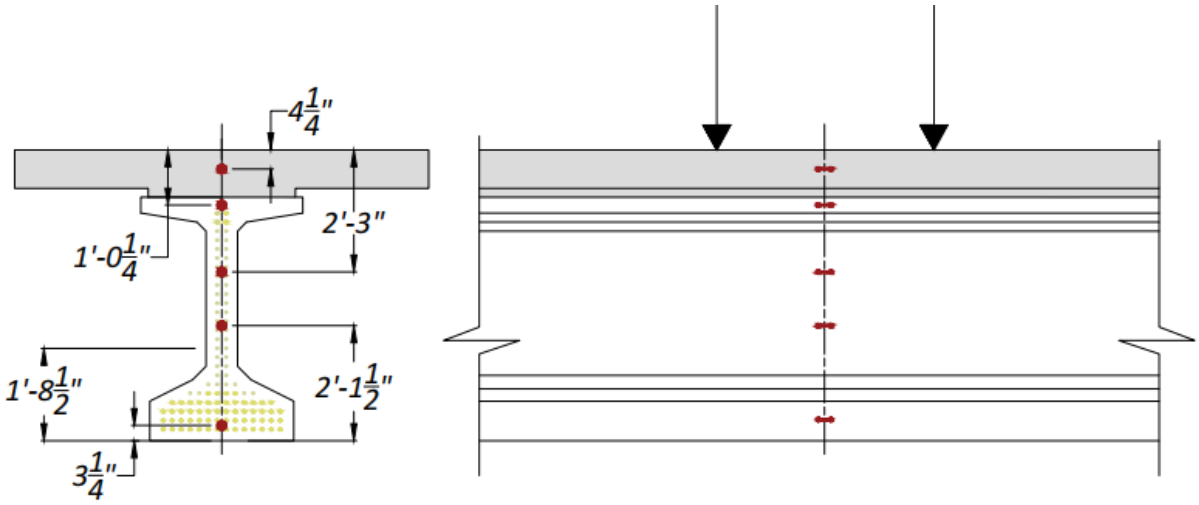

(b) Tx54

Figure 4.16. Tx54 ESGs at Midspan.

4.4.6 Surface Steel Strain Gages

The SSGs were installed on the legs of the transverse web R-bars such that they were located at the centroid of the web of the specimens. The instrumented R-bars were installed at one end of each girder. These gages were used to measure the strain in the transverse R-bars during the shear testing. Figure 4.17 presents the placement of the instrumented R-bars with respect to the other R-bars in all three specimens. For the Tx34-2, the placement of the R-bars at the plant was earlier than planned. Therefore, the instrumented R-bars had to be inserted between the design transverse reinforcement. One extra instrumented R-bar was placed 1 ft from the midspan in the unreinforced end as well. The gages were preinstalled on the R-bars in the controlled conditions of the laboratory

prior to transporting the gages to the field for installation. The surface of the R-bar was marked and ground at the plant to remove the ribs of the steel bars at both legs in the place of installation. The surface was cleaned using acetone, neutralizer 5, and M-prep Conditioner A. The cleaned surface was left to dry before the application of the gage; adhesive tape was used to carefully place the gage at the desired location. The tape was applied and removed along the circumference of the steel bar to avoid hoop stress being induced in the gage. The adhesive M bond 200 and M coat J coating was used for bonding the gage and protecting the gage from damage, respectively. The gages were wrapped in protective foam after installation to prevent damage during transportation.

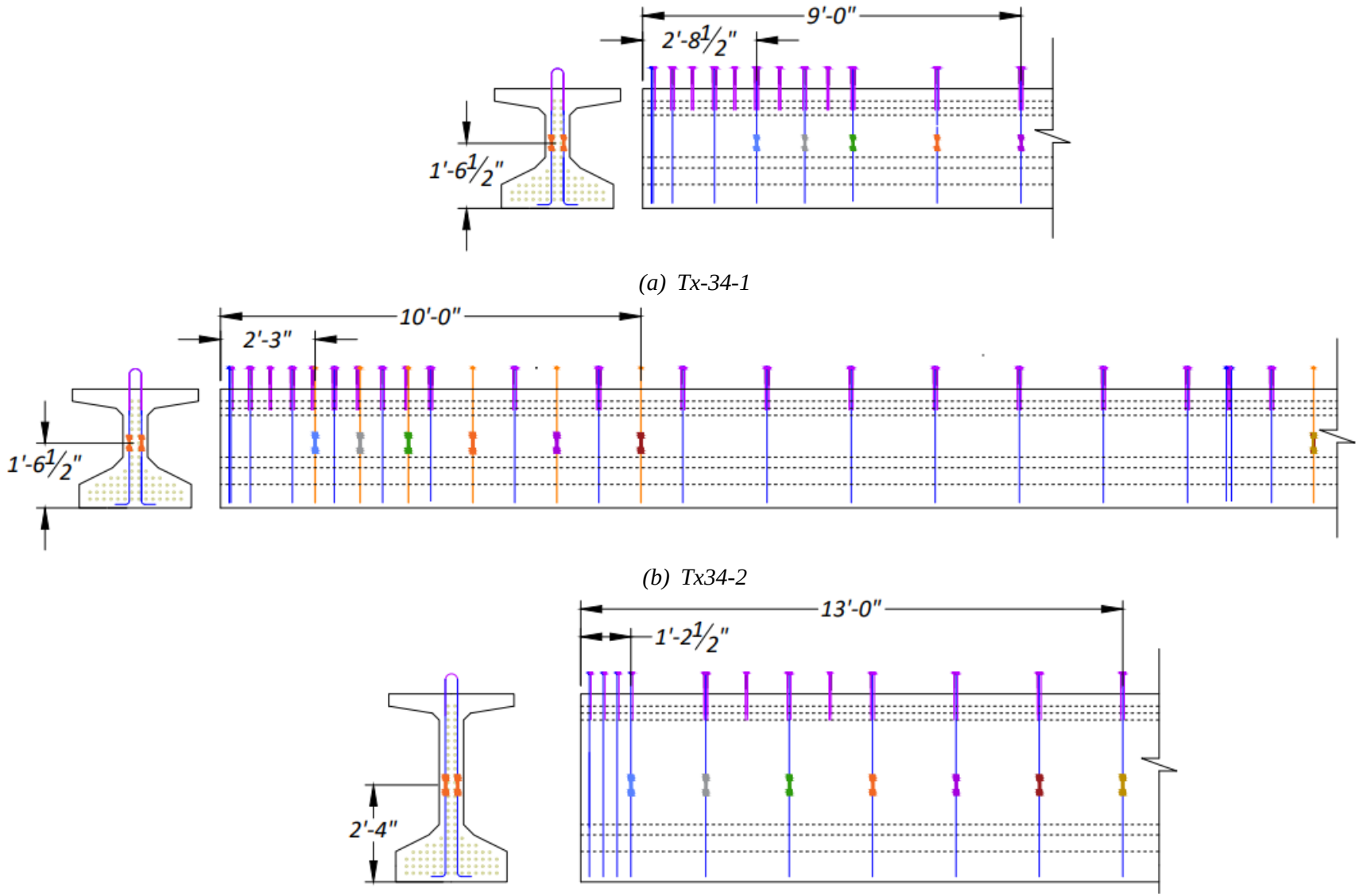

(a) Tx-34-1

(b) Tx34-2

(c) Tx54

Figure 4.17. Surface Steel Strain Gages (SSGs).

4.4.7 Linear Variable Displacement Transducers

A frame of six LVDTs was installed at the shear ends to form a rosette to determine the shear crack angle base on the shear strains measured across the shear cracks. The LVDTs were installed at 0, 30, and 120 degrees to the horizontal directions. One frame was installed at each end of the girder. Figure 4.18(a) presents the configuration of the LVDT frame installed on the girder web. The frame was assembled from aluminum bars of 1 in. width and 0.25 in. thickness and varying lengths. The lengths of the bars for Tx34-1 and Tx34-2 were 10 in., 17 in., and 19.5 in. The bar lengths for Tx54 were 18.5 in., 31.5 in., and 36 in. The bars had slots for the movement of the LVDTs at one end to record the displacements, while the other end had holes to fix the LVDT at one end. Holes were drilled into the concrete using a hammer drill to provide grooves for the threaded rods that held the bars in place. The LVDTs were installed on the frame with brackets. Chapter 6 presents the details of measuring strains from the LVDT frame with the results of shear testing. Figure 4.19 presents the photos of the LVDT setup.

LVDTs were installed for measuring the horizontal slip between the deck and girder. These were installed at 5.5 ft from the east and west ends of the girder at both the north and south face. LVDTs were also used to measure the horizontal interface slip between the CC deck and the UHPC girder. LVDTs were installed at 5.5 ft from the ends of the girder at the east and west ends on the north and south faces. Chapter 6 presents the results of the LVDT slip.

4.4.8 Demountable Mechanical Gages

DEMEC points were installed every 2 in. along the bottom flange at both ends of the girder and on both faces. These points were monitored before and after the release of strands to measure the transfer length. Figure 4.20 presents the ends with DEMEC gages installed for all the girder specimens. Chapter -2075909280.□ details the instrumentation and measurements.

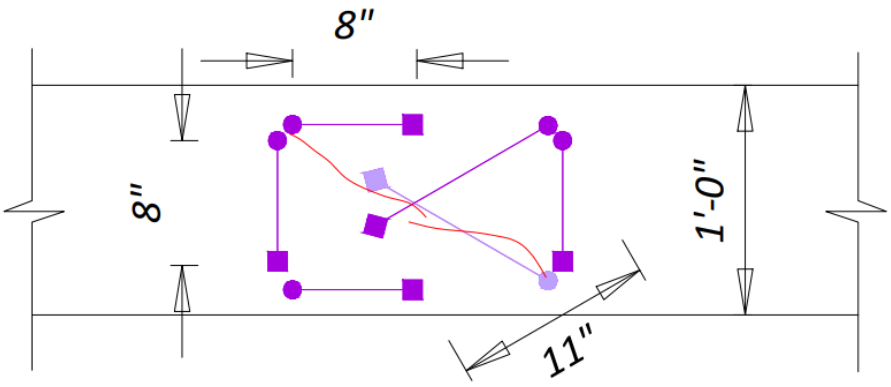

(a) LVDT Frame Installed in the Web at Shear Cracks for Tx34-1 and Tx34-2

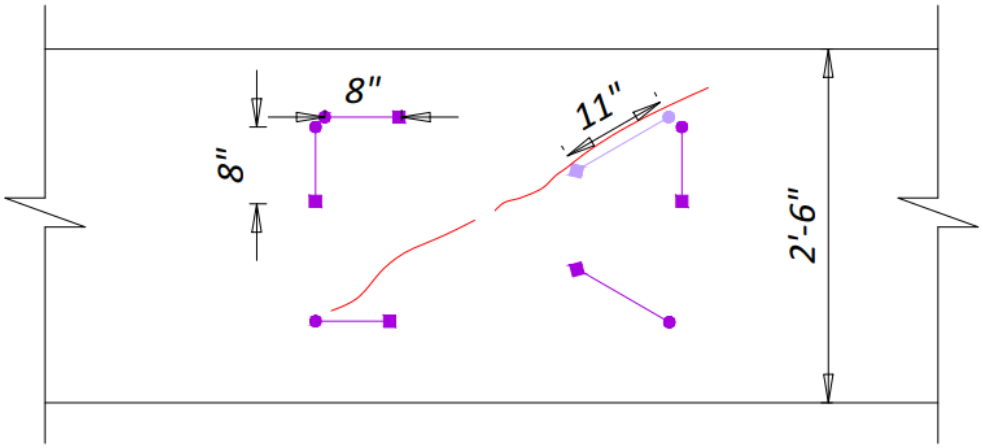

(b) LVDT Frame Installed in the Web at Shear Cracks for Tx54

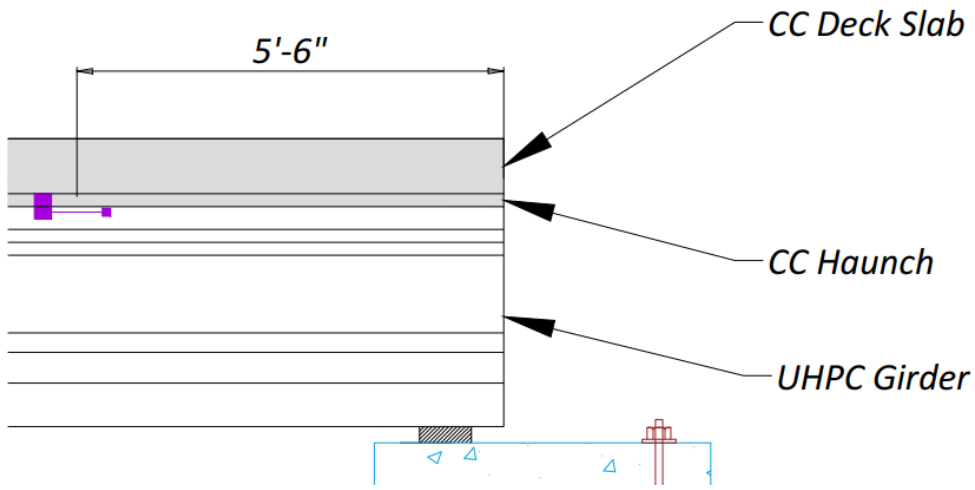

(c) LVDTs for Measuring Interface Shear Slip for All Specimens

Figure 4.18. LVDTs.

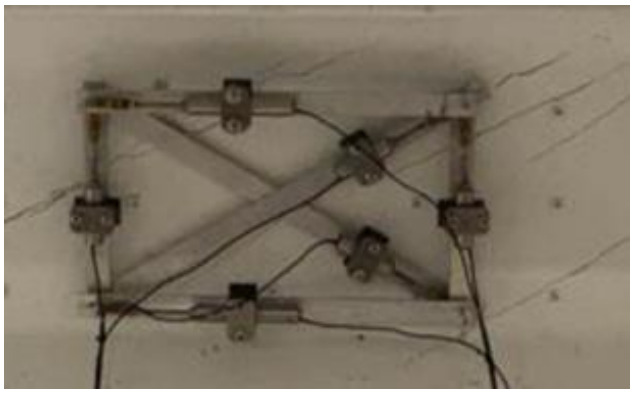

(a) Photo of LVDT Setup for Tx34-1

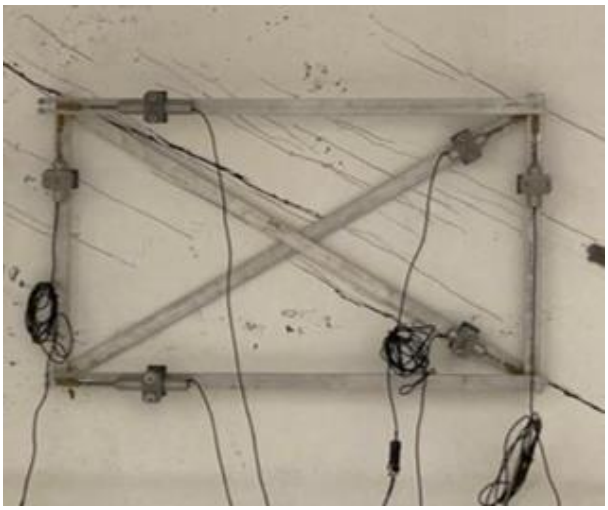

(b) Photo of LVDT Setup for Tx54

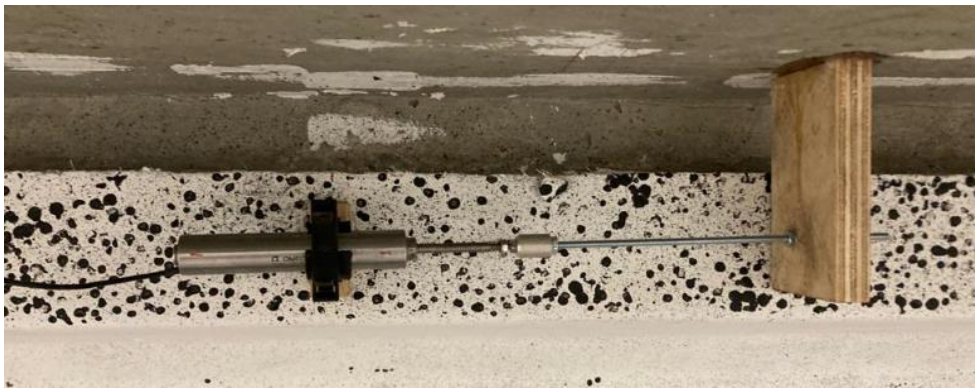

(c) LVDTs for Measuring Interface Shear Slip for Tx34-1

Figure 4.19. Photos of LVDT Setups.

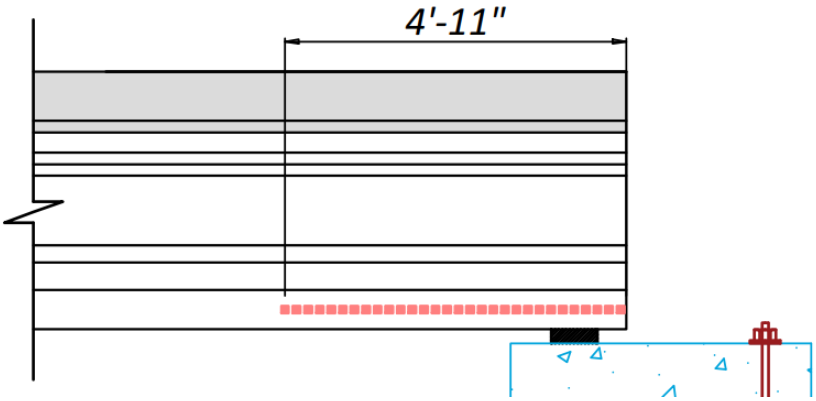

(a) Tx34-1 – 30 DEMEC Points at 2 in. Spacing

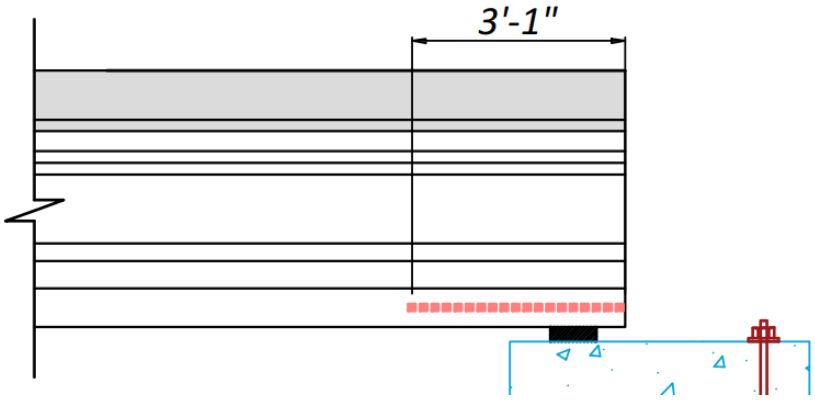

(b) Tx34-2 – 19 DEMEC Points at 2 in. Spacing

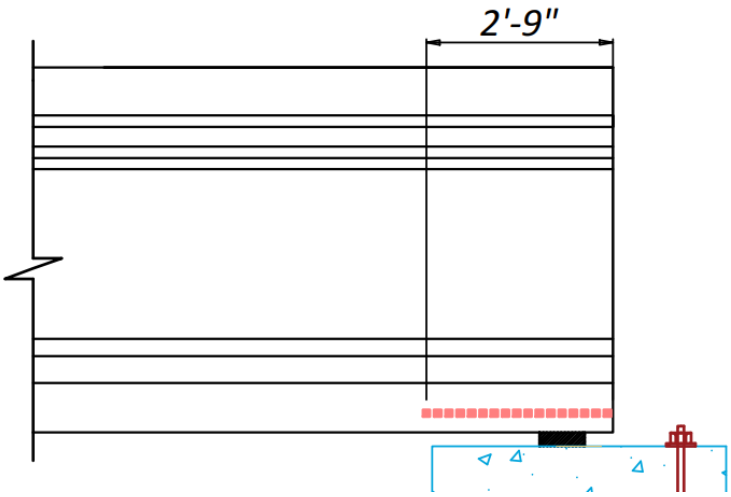

(c) Tx54 – 9 DEMEC Points at 4 in. Spacing

Figure 4.20. DEMEC Gages for Transfer Length Monitoring at Girder Ends.

4.5 SHORT-TERM HARDENED PROPERTIES OF COMPANION SPECIMENS

This section summarizes the measured short-term hardened properties of the companion specimens cast with the full-scale specimens. Chapter 6 of the Volume 1 report documents the material-level test matrix of the companion specimens and the detailed results of the fresh and hardened properties with individual specimen results. This section summarizes the hardened property results of the representative specimens that influence the full-scale behavior of the UHPC girders. These material-level properties were used for the prediction of the flexure and shear response of the composite girder specimens. These predictions guided the loading protocol, test setup, and identification of regions of interest to study the flexure and shear behavior of the girder specimens during flexure and shear testing. The measured hardened property values gave insight into the potential adjustments needed to the original design assumptions used for the girder specimens.

4.5.1 Compressive Strength

Table 4.7 presents the average compressive strength results of the three girder specimens at various ages. The average compressive strength of the girders at 1 day and 28 days was used for the moment-curvature analysis for flexure testing and shear testing. These values were used in the UHPC models that predict the moment-curvature response for the girders. The data from the moment-curvature analysis are then used for the load-deflection analysis. Table 4.8 presents the average compressive strength results of the CC CIP deck slab on the three girder specimens at various ages.

Table 4.7. Average Compressive Strength of UHPC Girder Specimens.

Girder ID	1 Day	7 Days	28 Days	56 Days	Day of Flexure Test	Day of Shear Test
Tx34-1	15.5	19.1	18.9	18.9	19.1 (159 days)	19.8 (187 days)
Tx34-2	15.2	16.4	18.0	18.9	18.9 (165 days)[1]	18.9 (165 days)[2]
Tx54	16.1	15.6	16.5	18.8	18.1 (33 days)[3,4]	17.0 (45 days)[5]

Notes:
1. Tx34-2 flexure test was conducted at the age of 156 days
2. Tx34-2 Shear 1 and 2 tests were conducted at the age of 167 and 184 days, respectively
3. The compression test corresponding to the Tx54 flexure test was conducted using 4 × 8 in. Surecure samples
4. Tx54 flexure test was conducted at the age of 34 days
5. Tx54 Shear 1 and 2 tests were conducted at the age of 40 and 45 days, respectively
6. Unit: ksi

Table 4.8. Average Compressive Strength of the CC Deck.

Girder ID	1 Day	28 Days	Day of Flexure Test	Day of Shear Test
Tx34-1	2.8	5.5	6.1 (111 days)	6.3 (139 days)
Tx34-2	2.6	6.6	7.0 (98 days)[1]	7.0 (98 days)[2]
Tx54	2.6	5.1	5.1 (16 days)	5.1 (28 days)

Notes:
1. Tx34-2 flexure test was conducted at the deck concrete age of 89 days
2. Tx34-2 shear test was conducted at the deck concrete age of 100 days
3. The deck concrete age at the time of compression testing is given in parentheses
4. Unit: ksi

4.5.2 Modulus of Elasticity

The average MOE value measured at the time of testing was used for the prediction of the moment-curvature and load-deflection response of the specimens. The test day age indicates the age at which the companion specimens were tested. The material tests were performed during the period in which the full-scale girder tests were conducted. In some cases, this test occurred 1–2 days before or after the full-scale girder testing. Table 4.9 presents the average MOE data of the three girders at various ages, including the test days.

Table 4.9. Average MOE of UHPC Girder Specimens.

Girder ID	3 days	7 days	28 days	56 days	Test day
Tx34-1	6662	6044	6330	6455	6628 (184)[1]
Tx34-2	6446	-	7163	-	6498 (166)[1]
Tx54	6742	7107	7423	-	7446 (45)[1]

Notes:
1. Testing age in parentheses
2. - : Not available
3. Unit: ksi

4.5.3 Direct Uniaxial Tension Test

The direct uniaxial tension test results are used for the flexure and shear predictions. The early age tensile strength and the later age tensile strength are used for the moment-curvature analysis for modeling of UHPC stress-strain behavior in tension. These data are based on the 7 day and 28 day tensile strength of the companion specimens and is tabulated in Table 4.10. The 7 day and 28 day test results for Tx34-2 prisms did not perform as per the requirement of the test, and most of the specimens developed cracks outside the gage length, possibly due to bending of the specimen during the tension test. The specimens with the most viable data were selected for the average tensile test data computation. The shear capacity predictions rely on the first cracking tensile stress

and those data were taken from the material-level tests conducted during the period of full-scale testing, as tabulated in Table 4.10. The value of the MOE from the direct tension test is also provided. The first cracking tensile stress was computed based on the recommendations from AASHTO T 397 Draft (AASHTO 2022). The details are documented in Section 6.4.4 of the Volume 1 report. The first cracking strength is the intersection of the line with the MOE of the elastic part of the stress-strain curve passing through 0.02 percent strain and the stress-strain curve. The maximum stress is denoted by the peak stress. Figure 4.21 illustrates the first cracking strength, the peak strength, and the 0.02 percent offset line. In addition, the recommended PCI (eConstruct 2020) limit of 0.004 strain and 0.75 ksi stress for a typical uniaxial tensile stress-strain plot is shown.

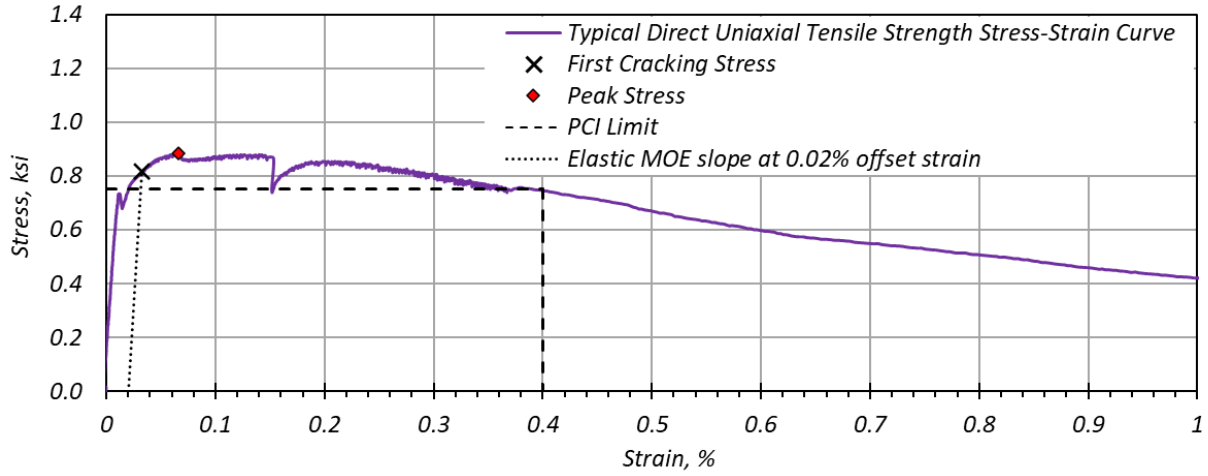

Figure 4.21. Typical Uniaxial Tensile Strength Stress-Strain Curve.

Table 4.10. Average Uniaxial Tension Test Data.

Girder	Age (days)	First Cracking		Peak Stress		MOE, ksi
		Strain, με	Stress, ksi	Strain, με	Stress, ksi	
Tx34-1	7	250	0.55	120	0.64	6256
Tx34-2	7	177	0.56	419	0.63	6176
Tx54	7	162	0.81	374	0.88	6024
Tx34-1	28	87	0.31	486	0.45	4899
Tx34-2	28	157	0.62	168	0.67	6332
Tx54	28	234	0.83	515	0.92	6231
Tx34-1	187	319	0.53	491	0.60	4871
Tx34-2	165	544	0.62	779	0.70	7036
Tx54	46	389	0.95	265	1.16	7000

Note: Tx34-1 and Tx34-2 showed low tensile strength due to potential fiber settlement.

The relative tensile strength of the two Tx34 girder specimens (approximately 0.65 ksi) was lower than the Tx54 girder specimen (1.16 ksi) for full-scale test days. The average tensile strengths for early ages and later ages of the companion samples for the Tx54 girder specimen are comparable to the laboratory trial batches. This difference may be due to the settlement of fibers in the first two girder specimens due to higher flow spread values, which may be more pronounced in the smaller scale samples used for tension testing. The details of the differences of the tensile strength based on the fiber settlement is explained in the Volume 1 report, Chapter 6. The details of the impact of the tensile strength of the flexure and shear performance are documented in Chapters 5 and 6 of the Volume 2 report.

4.6 SUMMARY

Based on the target values identified from the analytical feasibility study, the nonproprietary UHPC mixtures were developed, and the most promising UHPC mixture was selected for precast, pretensioned UHPC girder fabrication, as documented in the Volume 1 report. In consultation with the TxDOT committee, two Tx34 girder specimens and one Tx54 girder specimen were selected for full-scale testing under shear and flexure. The list below summarizes the key aspects of the full-scale testing program.

1. *Details of UHPC girder specimens.* The material properties of the selected mixture design from various trials conducted in the laboratory and the precast plant were used as design inputs for the prototype designs (compressive strength of 14 ksi at release and 18.9 ksi at service, and a direct uniaxial tensile strength of 0.75 ksi at release and 1.0 ksi at service). The precast plant facility had certain limitations on the capacity and availability of casting beds because of the production schedule. Therefore, limitations on the number of strands were considered in the final design of the prototype girders and girder specimens. For example, the prototype girders were limited in span length because of the restriction on the number of prestressing strands. Because the flexure and shear behavior of the UHPC girders and their interaction with a CC deck under standard traffic loads were the primary objective of the research project, the three specimens were designed to evaluate the flexure, shear, and transfer length properties of the corresponding prototype bridge girder designs. The specimens were of reduced span length to accommodate limitations in the laboratory. Two Tx34 specimens (50 ft long) and one Tx54 specimen (70 ft long) were produced with

UHPC at the precast plant, and a CIP CC deck was constructed for each girder specimen in the laboratory. The main parameters for each girder specimen are as follows: (a) Tx34-1 had 30 eccentric strands with a protype bridge span length of 77 ft, (b) Tx34-2 had 38 strands with 6 harped strands and a protype bridge span length of 85 ft, and (c) Tx54 had 48 strands with 8 harped strands and a protype bridge span length of 121 ft.

2. *Instrumentation, measurements, and inspection at the precast plant.* The girders were instrumented with embedded gages at the midspan to monitor the flexure strain profile along the height of the girder. TCs were also installed along the height of the girder to monitor the temperature development during the first 16 hours at the midspan and the end. The details of the temperature development are documented in Section 6.3.3 of the Volume 1 report. Several instrumented R-bars were installed at the shear end to monitor the strain of the transverse reinforcement under shear loading. Camber and transfer length readings were taken in the field. The surface of the girders was evaluated to document any defects or cracks. The details of the surface evaluation can be found in Section 6.2.2.3, 6.2.3.3, and 6.2.4.3 of the Volume 1 report.
3. *Hardened properties.* Companion material-level test specimens were cast for monitoring the material properties of the UHPC girder specimens and the CIP deck slab of CC. The average values of the material properties that were used for the analysis of the specimens prior to testing are as shown in Table 4.11.

Table 4.11. Summary of Short-Term Hardened Properties.

Description	Tx34-1, ksi	Tx34-2, ksi	Tx54, ksi
Compressive Strength (CIP deck slab), 28 days	5.5	6.5	5.1
Compressive Strength (UHPC), 28 days	18.9	18.0	16.5
Compressive Strength (UHPC), test day	19.1 (187 days)	18.9 (165 days)	18.1 (45 days)
Direct Uniaxial Tensile Strength at First Cracking, test day	0.53 (187 days)	0.62 (165 days)	0.95 (45 days)
MOE, 3 days	6662	6446	6742
MOE, 28 days	6330	7163	7446

Note: The test days are noted in parentheses where applicable.

4. *Instrumentation and measurements in the laboratory.* Embedded gages installed in the field were used to monitor internal strains due to flexure at midspan. The SPs and surface strain gages were installed at the midspan to monitor strains due to flexure at the girder surface. These surface strain measuring instruments were also located in between the actuators

during the shear tests. SGs, KSGs, and LVDTs were installed at the shear ends to monitor the shear strains. LVDTs were also utilized to monitor the interface slip between the CC deck and the UHPC girder. Finally, SPs were installed along the span length of the specimens to obtain the vertical deflection profile of the specimens under loading conditions. With respect to the instrumentation, the following observations were made:

- The SPs were consistently effective for vertical measurements of larger magnitude for all the tests. However, their effectiveness in capturing strains of low magnitude was not consistent for all the tests, possibly because the sensitivity and the resolution were not effective capturing some smaller horizontal strains occurring during some flexure and shear tests, particularly those resulting in very small deformations at the instrument.
- The transfer length was monitored using a detachable mechanical (DEMEC) strain gauge at the girder ends. The use of stainless steel contact seats were found to provide more consistent measurements than punched aluminum plates.
- The surface strain gages were observed to be very sensitive to small strains and were the most consistent instruments.
- K-gages that were cast in the UHPC girder were less reliable, possibly due to damage during the casting process. The K-gages installed on the surface were more effective in recording data.
- The LVDTs were less sensitive than the strain gages in the range of strains of small magnitude but effective in capturing strains of large magnitude, particularly for wide shear cracks.
- Overall, the use of LVDTs, K-gages, and strain gages provided sufficient redundancy to monitor small and large strains.

5 FULL-SCALE FLEXURE TESTS OF UHPC GIRDERS

5.1 INTRODUCTION

The flexural capacity of the UHPC girder specimens made composite with a CC deck was tested by loading each girder specimen under four-point bending. The original design and analysis of the girders from prototype bridges was initially based on an idealized stress-strain relationship available from the literature at the time of the design of the specimens, as described in Chapter 3. A detailed moment-curvature analysis of the girder sections was then conducted using nonlinear material stress-strain models. This analysis utilized computational programming to conduct a sectional fiber analysis of the girder cross-sections. The design values assumed prior to the fabrication were based on the material-level test properties at the laboratory and from the precast plant trial batch specimens. The analysis was then further revised based on the material-level tests conducted on the companion specimens cast with the girder specimens in the precast plant. Section 4.5 documents the details of the material-level tests of the companion specimens.

Chapter 4 provided details related to the full-scale test program for both flexure and shear, including the specimen details and material properties. This chapter describes the flexural testing program for the three full-scale UHPC girder specimens. Section 5.2 provides the flexural test setup for each girder and the details of the specimen loading. Section 5.3 explains the analysis conducted to predict the moment-curvature and load-deflection response of each girder specimen. The experimental test details and response of the specimens are individually documented for each girder specimen in Sections 5.5, 5.7, and 5.8. The results of the three specimens are then compared in Section 5.9, and general conclusions and key findings are noted.

5.2 TEST SETUP, LOADING, AND INSTRUMENTATION DETAILS

A total of three flexure tests were conducted, one for each girder specimen. The flexural capacity was evaluated at the midspan of the specimens. The performance of the UHPC girder with a CC deck under flexure was assessed in comparison with the service and factored demand loads that would be applied to an equivalent prototype bridge, as detailed in Chapter 4. The *ultimate condition* is defined for this study as the condition at which the specimen is loaded until failure or to a specified design limit corresponding to the strength limit state. The test setup and loading were selected to simulate the design loads on a highway bridge in terms of the moment demand at

midspan, and the testing was carried out to ultimate conditions, while limiting damage to allow subsequent testing for shear at the girder ends.

5.2.1 Test Setup and Loading of the Composite Girder Specimens

Figure 5.1 shows the test setup with the actuators for the flexure test of the Tx34-1 and Tx34-2 girders, and Figure 5.4 presents the setup for Tx54. The test setup and loading for the flexure test used two 600-kip hydraulic actuators to load the specimens under four-point bending. The 300-ton actuators have a 48 in. stroke at 10,000 psi and were manufactured by SPX Power Team. A constant bending moment region of 4 ft was considered at the midspan to simulate the tandem load conditions for a highway bridge. Figure 5.2, Figure 5.3, and Figure 5.5 present the photographs of the flexure test setup of the three girders prior to testing in the HBSMTL.

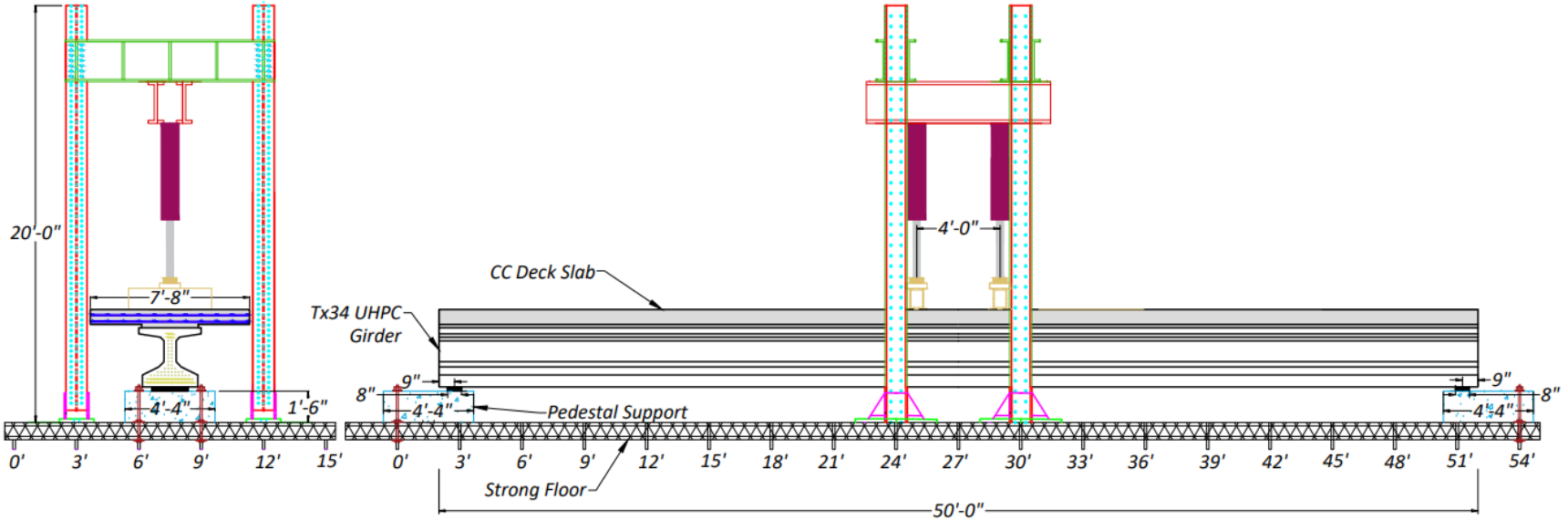

(a) Section View *(b) Elevation View*

Figure 5.1. Flexure Test Setup for Tx34-1 and Tx34-2 Girder Specimens.

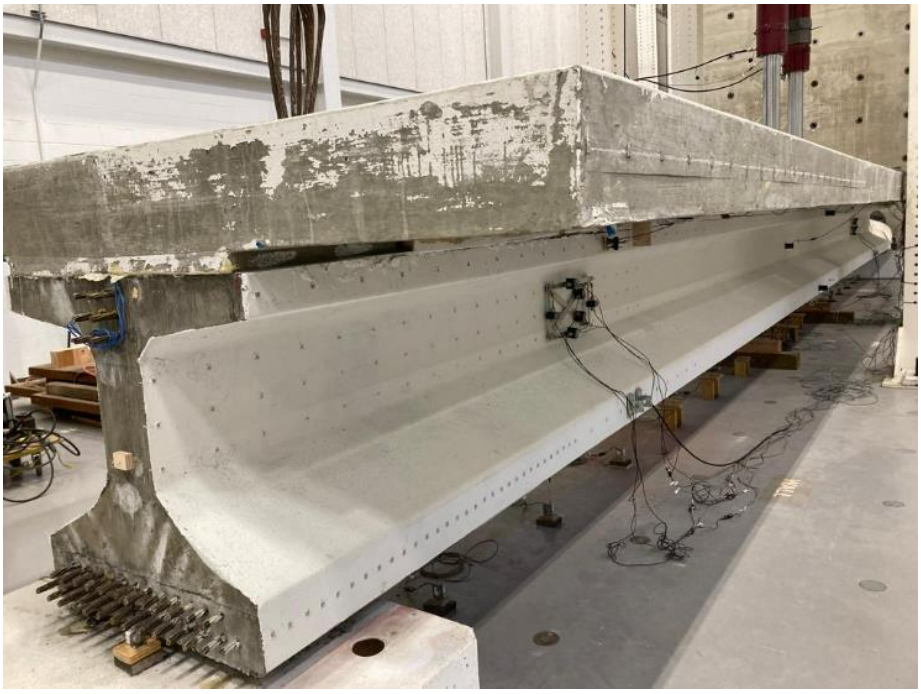

(a) Tx34-1 Test Setup (North Elevation)

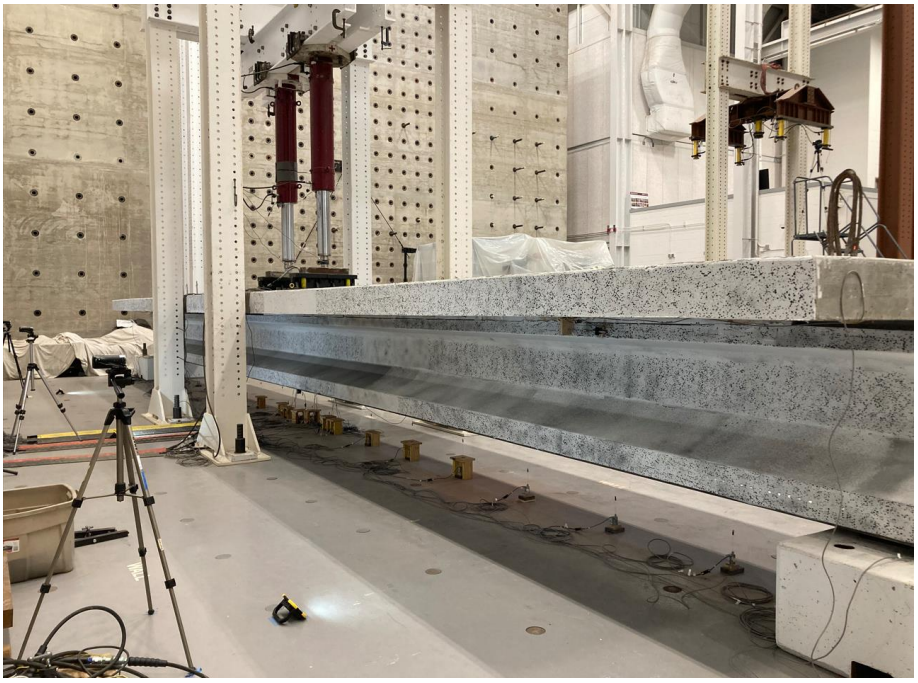

(b) Tx34-1 Test Setup (South Elevation)

Figure 5.2. Flexure Test Setup for Tx34-1 Girder.

(a) Tx34-2 Test Setup (North Elevation)

(b) Tx34-2 Test Setup (South Elevation)

Figure 5.3. Flexure Test Setup for Tx34-2 Girder.

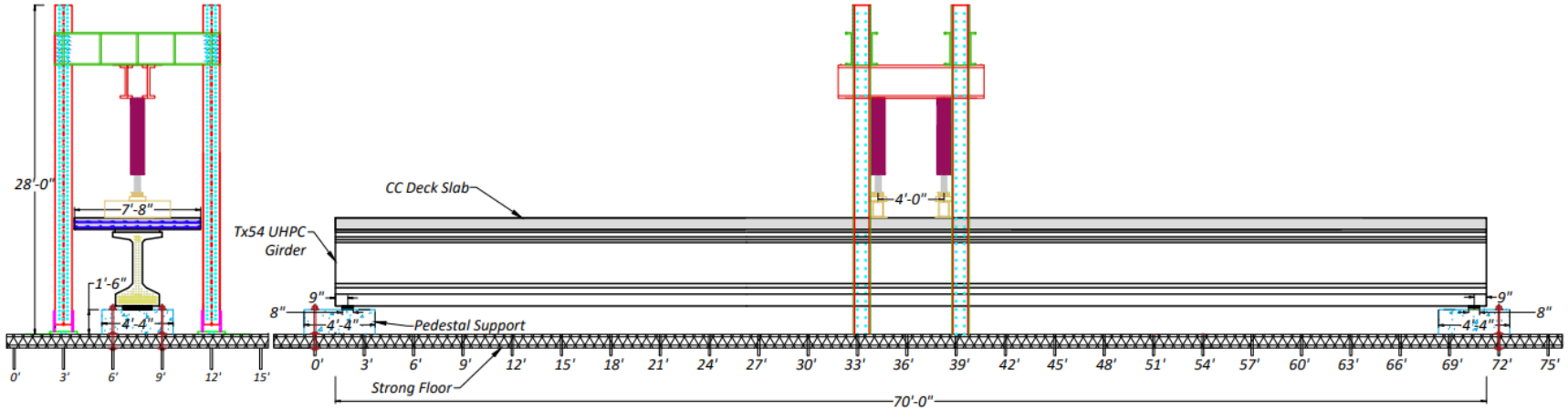

(a) Section view *(b) Elevation view*

Figure 5.4. Flexure Test Setup for Tx54 Girder.

(a) Tx54 Test Setup (Overhead View)

(b) Tx54 Test Setup (Floor Level View)

Figure 5.5. Flexure Test Setup for Tx34-2 Girder (North Elevation).

5.2.2 Instrumentation for Flexure Testing of Composite Girder Specimens

The instrumentation plan was revised slightly after the first flexure test based on the post-processing of the results of the first test. The arrangement of the instruments was modified slightly to maximize the monitoring of the regions of interest. Figure 5.6, Figure 5.7, and Figure 5.8 show the overall instrumentation for the flexure tests for Tx34-1, Tx34-2, and Tx54. The vertical

deflection of the beams was monitored by a series of SPs placed at 3 ft intervals, with additional SPs under each actuator, at girder ends, and at the midspan.

The 4 in. SPs had the advantage of higher accuracy in the smaller deflection range, while the 12 in. SPs had more stroke to record larger deflections. In case the deflection of the girder was larger than the stroke of the 4 in. SP, SPs of both 4 in. and 12 in. strokes were used. The strains at the midspan in the constant bending moment region were also of interest. These strains were measured with surface concrete strain gages (SG) mounted on the top of the slab and on the bottom surface of the girder. The strains along the elevation profile of the girder were measured by SPs (installed externally) and by embedded concrete gages (embedded within the deck and girder) at the mid-height of each component of the elevation, namely the deck, top flange, web, and the bottom flange of the girder. Because the web of the Tx54 girder is deeper than the Tx34 girders, there were additional sensors distributed along the web height of this specimen. Chapter 4 provides additional details for the instrumentation used in the full-scale testing.

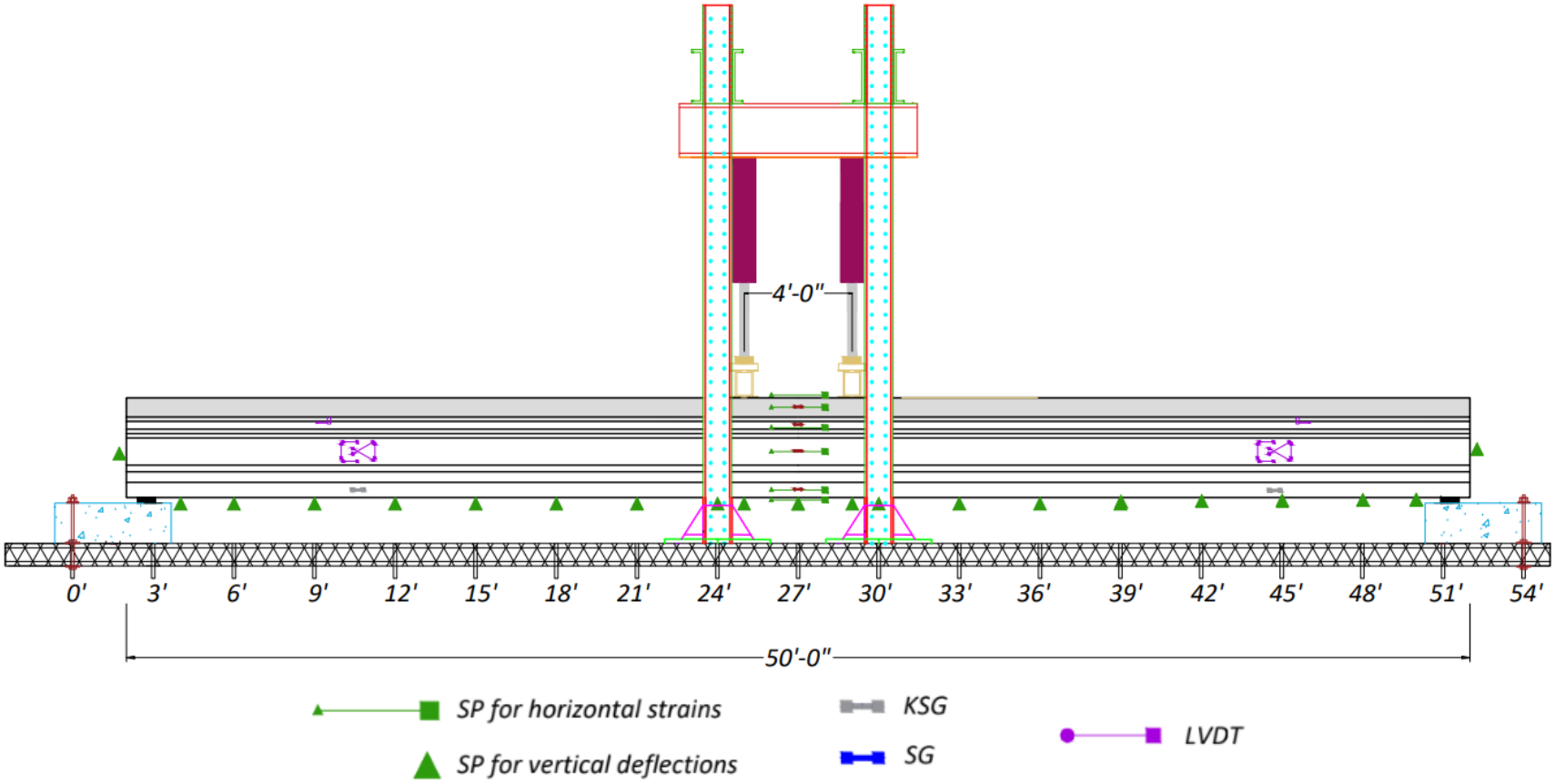

Figure 5.6. Instrumentation for Flexure Test of Tx34-1.

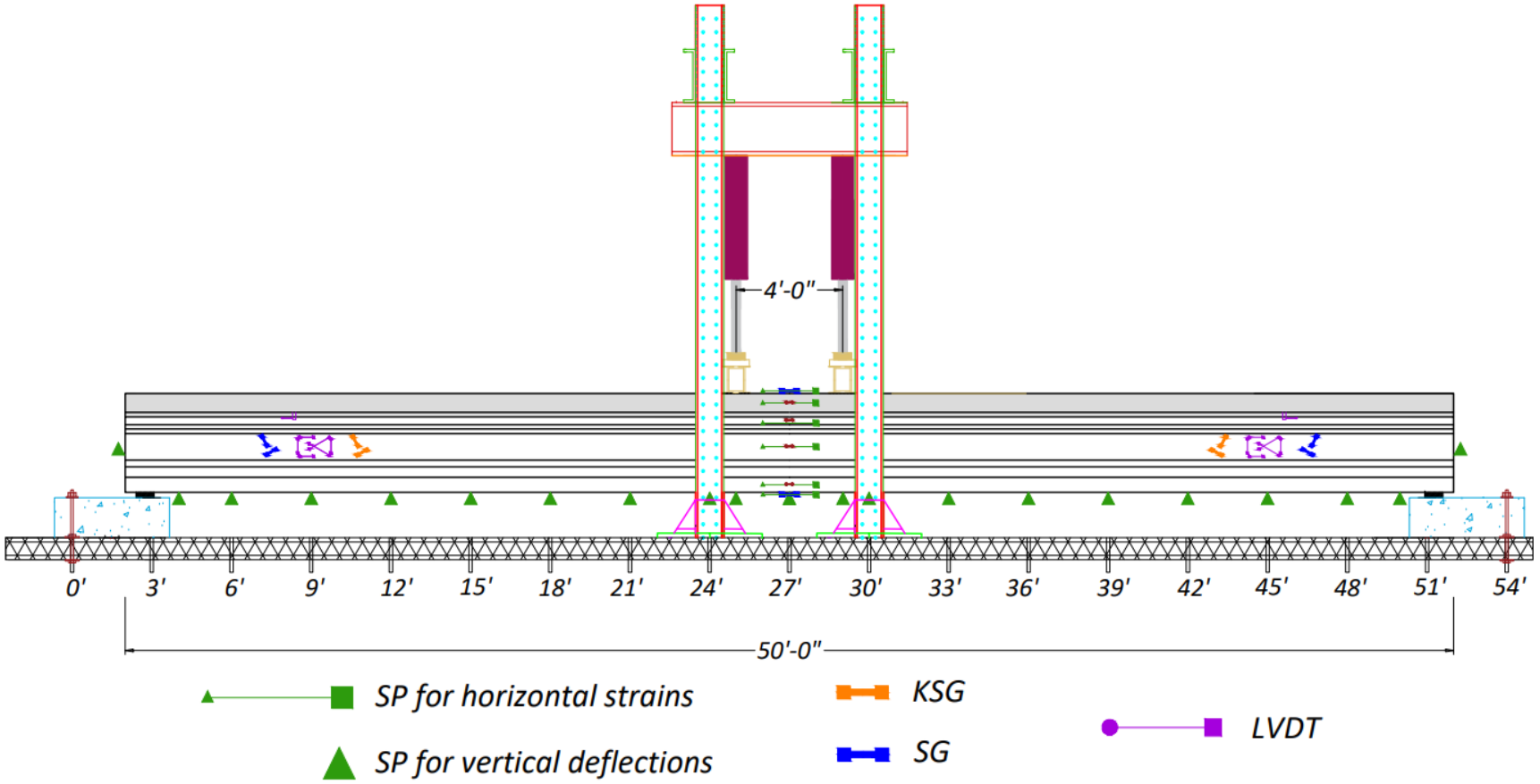

Figure 5.7. Instrumentation for Flexure Test of Tx34-2.

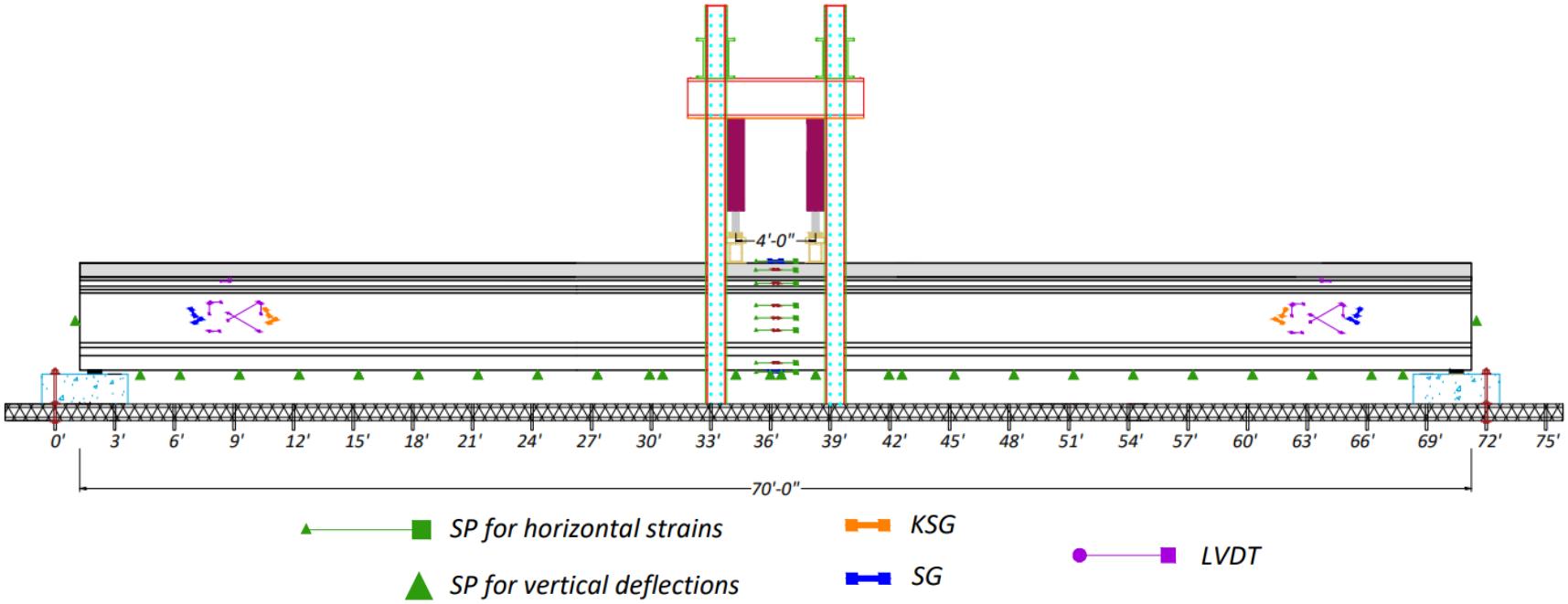

Figure 5.8. Instrumentation for Flexure Test of Tx54.

5.3 THEORETICAL MOMENT-CURVATURE ANALYSIS

Based on the material properties of the components of the composite section, namely UHPC, CC, prestressing strands, and mild steel reinforcement, the respective component stress-strain plots were computed. For this analysis, the CC deck was modeled based on the Karthik and Mander (2011) model to capture the compressive and tensile behavior of the unconfined concrete of the deck slab. The mild steel reinforcement used in the CC deck was modeled based on a realistic steel stress-strain model that was simplified and defined in Karthik and Mander (2011). The model developed by Gunasekaran (2020) was used to define the compressive and tensile behavior of UHPC. The Devalapura and Tadros (1992) model was used to capture the behavior of the prestressing strands used in the UHPC girder. The material-level testing for the UHPC for the girders and the CC for the decks was conducted in the HBSMTL. Section 4.5 summarizes the material-level test results used for the girder analysis. The Volume 1 report contains detailed test results of the companion specimens from the girder and the deck slab.

5.3.1 Material Models

Figure 5.9 shows the stress-strain plots for each of the material models used for the moment-curvature analysis of the composite specimen section. Table 5.1 presents the input values used to define the models for the moment-curvature analysis of the specimens. The compressive strength of the CC deck and the compressive strength, tensile strength, and MOE of the UHPC girders at service were experimentally tested using the companion specimens fabricated with the girder specimen. All the other parameters in the models are based on the standard values recommended by the respective models or AASHTO (2020) provisions. Table 5.1 presents the details. A layer-by-layer (fiber) analysis was conducted based on the strain of each fiber of the cross-section at different loading stages. The fiber analysis is based on the procedure developed and articulated in Mander (1983), which was later extended by Karthik and Mander (2011), Urmson and Mander (2012), and Gunasekaran (2020). Further details of each material model are provided below.

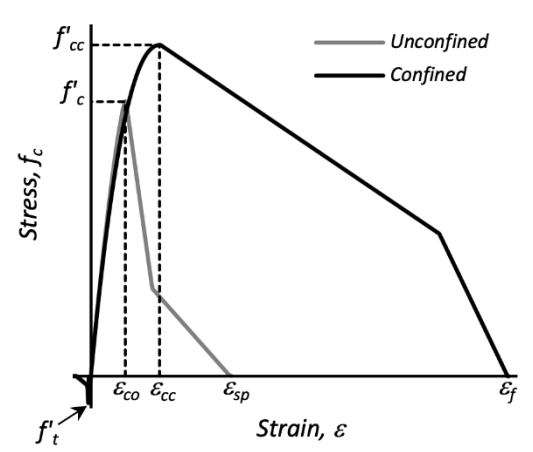

(a) CC

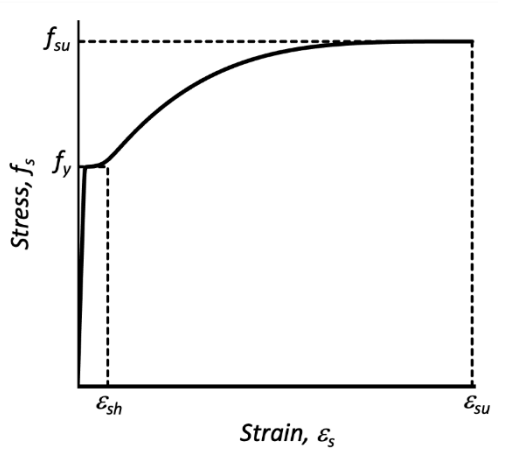

(b) Mild Steel

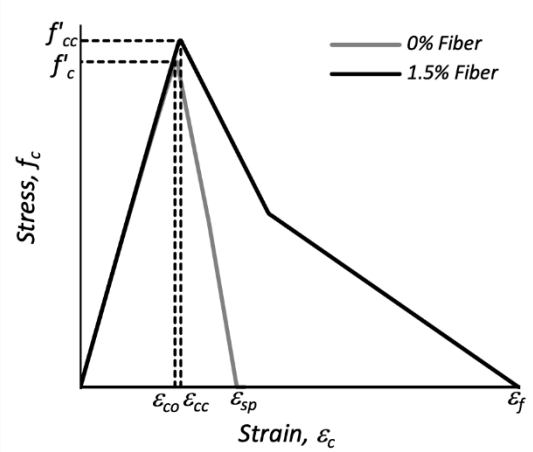

(c) UHPC (Compression)

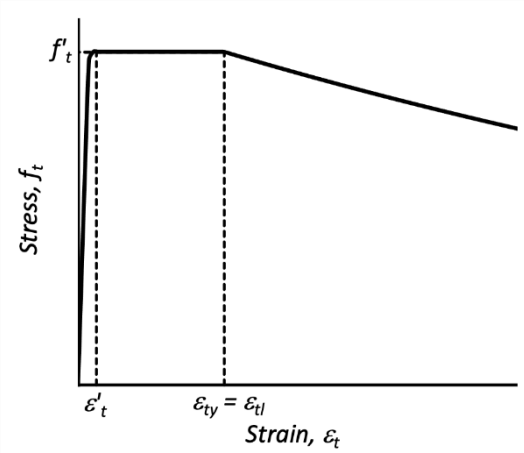

(d) UHPC (Tension)

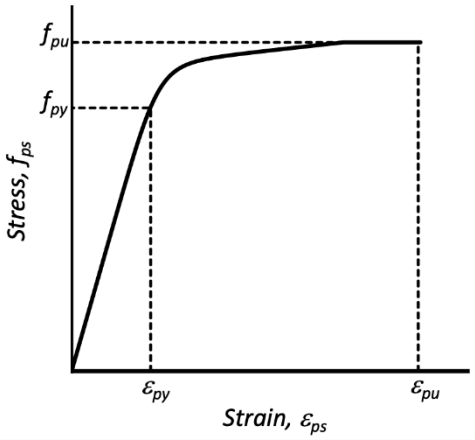

(e) Prestressing Strands

Figure 5.9. Stress-Strain Models Adopted for Different Materials.

Table 5.1. Input Data for Defining Material Models.

Parameter			Tx34-1	Tx34-2	Tx54	Remark
Conventional Concrete		f'_c, ksi	5.5			Experimental
		E_c, ksi	4459			AASHTO (2020)
		$f'_{cc} = f'_c$, ksi,	5.5			Karthik and Mander (2011)
		$f_{cu} = f_{c1}$, ksi,	1.74			
		f'_t, ksi	0.56			
		$\varepsilon_{cc} = \varepsilon_{co}$	0.002			
		$\varepsilon_{cu} = \varepsilon_{c1}$	0.0036			
		$\varepsilon_f = \varepsilon_{sp}$	0.0082			
Reinforcing Steel		f_y, ksi	63			Karthik and Mander (2011)
		f_{su}, ksi	94.3			
		ε_{sh}	0.008			
		ε_{su}	0.12			
		E_s, ksi	29,000			
		E_{sh}, ksi	1160			
UHPC	Compression	V_f	1.50%			Experimental
		f'_c, ksi	18.9	18.9	18.8	
		E_g, ksi	6330	7091	7423	
		f'_{cc}, ksi	20.0	20.0	19.9	Gunasekaran (2020)
		ε_{co}	0.0031	0.0027	0.0026	
		ε_{cc}	0.0032	0.0028	0.0027	
		ε_{sp}	0.005			
		ε_f	0.014			
	Tension	$f'_t = f'_{tp}$, ksi	0.53	0.62	0.95	Experimental
		ε'_t	0.00008	0.00009	0.00013	Gunasekaran (2020)
		$\varepsilon_{ty} = \varepsilon_{tl}$	0.002			
		c	0.0153			
Prestressing Steel		f_{pu}, ksi	270			Devalapura and Tadros (1992)
		ε_{pu}	0.035			
		A	887			
		B	27613			
		C	112.4			
		D	7.360			

5.3.1.1 Conventional Concrete (Karthik and Mander 2011)

The following equations define the model for the unconfined CC used in the deck:

$$0 \le x < 1 \qquad f_c = Kf'_c(1 - |1 - x|^n) \tag{5.1}$$

$$1 \le x < x_u \qquad f_c = Kf'_c - \left(\frac{Kf'_c - f_{cu}}{x_u - 1}\right)(x - 1) \tag{5.2}$$

$$x_u \le x < x_f \qquad f_c = f_{cu}\left(\frac{x - x_f}{x_u - x_f}\right)(x - 1) \tag{5.3}$$

where:

f_c = Stress in concrete, ksi

ε_c = Strain in concrete

K = Confinement ratio, taken as 1.0 for the deck slab

f'_c = Characteristic strength of concrete, ksi

f_{cu} = Ultimate stress, ksi.

ε_{cc} = Peak strain = $0.0015 + {f'_c\,(ksi)}/{10^4}$

ε_{cu} = Ultimate strain

ε_f = Failure strain = $0.012 - {7\,f'_c\,(ksi)}/{10^4}$

x = Normalized strain = ${\varepsilon_c}/{\varepsilon_{cc}}$

x_u = ${\varepsilon_{cu}}/{\varepsilon_{cc}}$

x_f = ${\varepsilon_f}/{\varepsilon_{cc}}$

E_c = MOE of concrete, ksi = $120{,}000 K_1 w_c{}^{2.0} f'_c{}^{0.33}$

K_1 = Correction factor for source of aggregate = 1

w_c = Unit weight of concrete, kcf

n = ${E_c \varepsilon_{co}}/{f'_c}$

5.3.1.2 Mild Steel (Karthik and Mander 2011)

The model to describe the mild steel, which was used as deck reinforcement and drawn from Karthik and Mander (2011), is as follows:

$$f_s = \frac{E_s \varepsilon_s}{\left\{1+\left|\frac{E_s \varepsilon_s}{f_y}\right|^{20}\right\}^{0.05}} + \left(f_{su} - f_y\right)\left[1 - \frac{|\varepsilon_{su}-\varepsilon_s|^P}{\{|\varepsilon_{su}-\varepsilon_{sh}|^{20P}+|\varepsilon_{su}-\varepsilon_s|^{20P}\}^{0.05}}\right] \quad (5.4)$$

where:

f_s = Stress in steel, ksi

ε_s = Strain in steel

P = $\frac{E_{sh}(\varepsilon_{su}-\varepsilon_{sh})}{(f_{su}-f_y)}$

E_s = MOE, ksi

E_{sh} = Strain hardening modulus, ksi

f_y = Yield strength, ksi

f_{su} = Ultimate strength, ksi

ε_{sh} = Strain hardening strain

ε_{su} = Ultimate strain

5.3.1.3 UHPC (Gunasekaran 2020)

The UHPC model in compression and tension developed by Gunasekaran (2020) was used because the experimental data closely fit this model. Figure 5.10 presents the tensile model versus the experimental data from material-level testing. The precaster mix from the trial batch was used to verify the fit of the model with the experimental data. The compression behavior is defined as follows:

$0 \leq x < 1$ $$f_c = f'_c(1 - |1 - x|^n) \quad (5.5)$$

$1 \leq x < x_1$ $$f_c = f'_c - \left(\frac{f'_c - f_{c1}}{x_1 - 1}\right)(x - 1) \quad (5.6)$$

$x_1 \leq x < x_f$ $$f_c = f_{c1}\left(\frac{x - x_f}{x_1 - x_f}\right) \quad (5.7)$$

where:

f_c = Compressive stress in UHPC, ksi

ε_c = Compressive strain in UHPC

f'_c = Characteristic peak stress, ksi

f_{c1} = Ultimate stress, ksi

E_g = MOE of UHPC, ksi

ε_{co} = Peak strain = $1.25\left(f'_c / E_g\right) - 0.0006$

ε_{c1} = Ultimate strain = 0.0041

ε_{sp} = Failure strain = 0.005

x = Normalized strain = $\varepsilon_c / \varepsilon_{co}$

x_{c1} = $\varepsilon_{c1} / \varepsilon_{co}$

x_f = $\varepsilon_{sp}/\varepsilon_{co}$

n = $E_g\varepsilon_{co}/f'_c$

Control parameters for compressive stress-strain relation for UHPC with fibers are defined as follows:

f'_{cc} = Peak stress = $f'_c(1+4V_f)$, ksi

ε_{cc} = Peak strain = $\varepsilon_{co}(1+2.5V_f)$

ε_{c2} = Ultimate strain = $\varepsilon_{c1}(1+31V_f)$

f_{c2} = Ultimate stress = $f_{c1}(1+3.8V_f)$, ksi

ε_f = Failure strain = $\varepsilon_{sp}(1+120V_f)$

V_f = 1.5% of fiber by volume

The tension behavior is defined as follows:

$$f_t = \frac{E_g\varepsilon_t}{\left(1+\left(\frac{\varepsilon_t}{\varepsilon'_t}\right)^{20}\right)^{0.05} e^{\langle\frac{\varepsilon_t-\varepsilon_{tl}}{c}\rangle}} + 4\left(f'_{tp}-f'_t\right)\frac{\langle\varepsilon'_{ty}-\varepsilon_t\rangle\langle\varepsilon_t-\varepsilon'_t\rangle}{\left(\varepsilon'_{ty}-\varepsilon'_t\right)^2} \quad (5.8)$$

where:

f_t = Tensile stress in UHPC, ksi

ε_t = Tensile strain in UHPC

ε_t = Axial strain in tension

f'_t = Tensile stress at first crack, ksi

f'_{tp} = Maximum tensile stress, ksi

E_g = MOE of UHPC, ksi

ε'_t = Tensile strain at first crack = f'_t/E_c

ε'_{ty} = Strain at start of stress plateau

ε_{tl} = Strain at the end of stress plateau

c = A constant that depends on UHPC material mix property

The Macaulay's brackets used in the equation renders the negative terms enclosed within the brackets 0 and while the positive values unchanged.

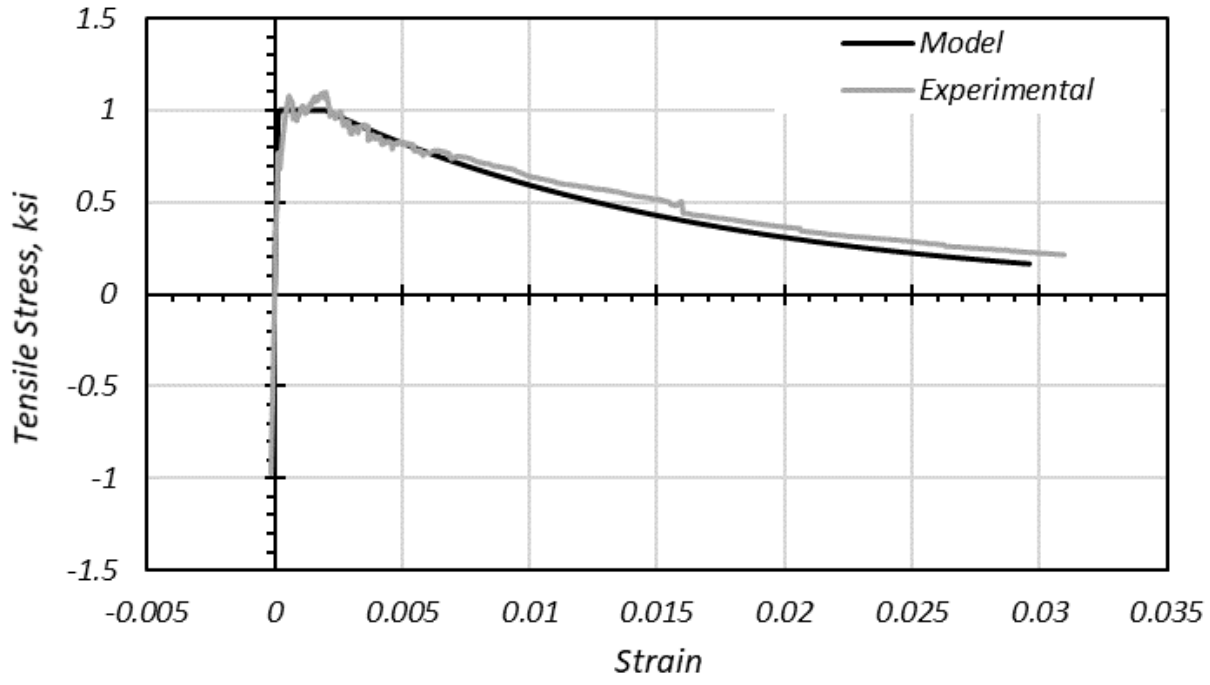

Figure 5.10. Uniaxial Tension Test: Experimental Data versus Model.

5.3.1.4 Prestressing Strands (Devalapura and Tadros 1992)

The model for stress in prestressing strands is shown in the following equation:

$$f_{ps} = \varepsilon_{ps}\left[A + \frac{B}{\left\{1+\left(C\varepsilon_{ps}\right)^{D}\right\}^{1/D}}\right] \leq f_{pu} \tag{5.9}$$

where:

f_{ps} = Stress in prestressing strands, ksi

ε_{ps} = Strain in prestressing strands

A, B, C, D = Constants for low-relaxation prestressing strands

5.3.2 Analysis Methodology

If the curvature, centroidal strain, and the distance of the layers from the centroidal axis are known, the strain at the center of each layer (or fiber) may be determined using the following expression:

$$\varepsilon_{y,j} = \varepsilon_{0,j} + \phi_j y \tag{5.10}$$

where:

$\varepsilon_{y,j}$ = Strain at a fiber

$\varepsilon_{0,j}$ = Centroidal strain

y = Distance from the centroidal axis to the center of the fiber

ϕ_j = Curvature that may be calculated by adding the curvature increment to the curvature obtained in the preceding sectional analysis.

Further,

$$\phi_j = \phi_{j-1} + \Delta\phi \tag{5.11}$$

in which

ϕ_{j-1} = Curvature of the previous sectional analysis, and $\Delta\phi$ = increment in curvature

To ensure the compatibility of strain and equilibrium of forces, an incremental relationship is used to couple the axial force and bending moment as follows:

$$\begin{Bmatrix} \Delta P_j \\ \Delta M_j \end{Bmatrix} = \begin{bmatrix} \partial P/\partial \varepsilon_0 & \partial P/\partial \phi \\ \partial M/\partial \varepsilon_0 & \partial M/\partial \phi \end{bmatrix} \begin{Bmatrix} \Delta \varepsilon_{0j} \\ \Delta \phi_j \end{Bmatrix} \tag{5.12}$$

where:

ΔP_j = Axial force change

ΔM_j = Bending moment change

$\Delta \varepsilon_{0j}$ = Incremental change in strain of small magnitude

$\Delta \phi_j$ = Incremental change in curvature of small magnitude

The partial differential parameters in the matrix are computed as follows:

$$\partial P/\partial \varepsilon_0 = \frac{P_{i+} - P_i}{\varepsilon_{0i+} - \varepsilon_{0i}} \tag{5.13}$$

$$\partial P/\partial \phi = \frac{P_{i+} - P_i}{\phi_{i+} - \phi_i} \tag{5.14}$$

$$\partial M/\partial \varepsilon_0 = \frac{M_{i+} - M_i}{\varepsilon_{0i+} - \varepsilon_{0i}} \tag{5.15}$$

$$\partial M/\partial \phi = \frac{M_{i+} - M_i}{\phi_{i+} - \phi_i} \tag{5.16}$$

The change in centroidal axis strain was obtained by determining the out-of-balance axial force, $\Delta P = P_i - N$, along with the incremental curvature, as follows:

$$\Delta\varepsilon_{0,j} = \frac{\Delta P - \left(\partial P/\partial \phi\right)_{j-1} \Delta\phi}{\left(\partial P/\partial \varepsilon_0\right)_{j-1}} \tag{5.17}$$

The new centroidal axis strain was obtained by adding the change in centroidal axis strain $\Delta\varepsilon_{0j}$ to the centroidal axis strain value obtained in the previous analysis $\Delta\varepsilon_{0,j-1}$ as follows:

$$\varepsilon_{0,j} = \varepsilon_{0,j-1} + \Delta\varepsilon_{0,j} \tag{5.18}$$

The out-of-balance force obtained must be within the tolerance limit for iterating the curvature using the incremental curvature. If the out-of-balance force is not within tolerance, then the incremental curvature is set to zero, and Equations (5.11) to (5.18) are repeated until the force is within the tolerance value. Using the fiber level strain values and corresponding material stress-strain models, the corresponding forces were computed, and thereby the forces and moments were determined. This procedure is repeated for different curvature values until the failure strain value is obtained. Typically, the failure strain is defined by either the girder bottom (UHPC tensile) strain or the deck top (CC compressive) strain. For the preliminary analysis based on previous material-level testing conducted prior to the full-scale girder fabrication, a failure tensile strain value of 0.01 was adopted for UHPC, and a failure compressive strain value of 0.005 was adopted for CC.

The decompression limit is marked by the stage at which the strain in the bottom fiber reaches zero. The composite section is considered to have cracked when the stress in the bottom fiber of the concrete reaches the cracking strength of UHPC, f_t. The yielding stage is considered when the prestressing strands closest to the extreme tension fiber reach their yield strain, which is considered as the strain at which the stress reaches 80 percent of ultimate prestress. The service and factored demands are considered as per AASHTO (2020) and are elaborated on in Section 3.2 and 3.4. The

neutral axis shift is the stage at which the neutral axis moves out of the UHPC girder and enters the CC haunch.

5.4 LOAD-DEFLECTION ANALYSIS

The deflection for different loading stages of the specimen was evaluated by extending the load-deflection analysis performed on an aramid fiber-reinforced polymer prestressed member (Pirayeh Gar et al. 2018). This analysis accounted for the nonlinear behavior of the specimen by incorporating the curvature, moment of inertia, and the MOE of the specimen at different stages of loading. The initial response within the linear region operates on the elastic material properties of the specimens. As the stiffness of the specimen reduces with the load after cracking, the curvature increase is nonlinear, resulting in larger deflections. This process is captured by a step-wise computation of the stiffness of the composite beam at different stages. The moment-curvature developed is decoupled to obtain the moment and curvature diagram at various load stages. The curvature input is taken from the moment-curvature analysis of the specimen described in Section 5.3.

Figure 5.11 illustrates the different stages of the computation and the impacts of higher curvature and loss of stiffness on the deflection of the section in the nonlinear phase of the loading. The different loading stages considered include elastic loading phase up to cracking, cracking to yielding of the prestressing strands, yielding to the peak moment, and peak to ultimate. The cracking load was determined using the stress at the first crack measured from the companion specimen subjected to uniaxial tension. The yield point was designated as the stage at which the stress in the bottom prestressing strands is at 80 percent of the ultimate prestress f_{pu}.

The moment-curvature graph can be divided into different stages such as elastic stage, post-crack stage, and post-yield stage. The flexural rigidity of the component of interest varies at different stages due to the presence of cracks. The total curvature is thus defined as the summation of curvatures before and after cracking (Pirayeh Gar et al. 2018).

$$\phi = \phi_g + \phi^* \tag{5.19}$$

where:

ϕ_g = Elastic curvature $= \frac{M}{E}\left(\frac{1}{I_g}\right)$

ϕ^* = Inelastic curvature $= \left(\frac{M-M_{cr}}{E}\right)\left(\frac{1}{I_{cr}} - \frac{1}{I_g}\right)$

The inelastic component of the curvature includes the post-crack and post-yield stages. The equivalent moment of inertia of the post-yield stage is determined and is used to find the post-yield curvature component. Conjugate beam theory is then used to determine the elastic and inelastic deflection components using the elastic and inelastic curvatures.

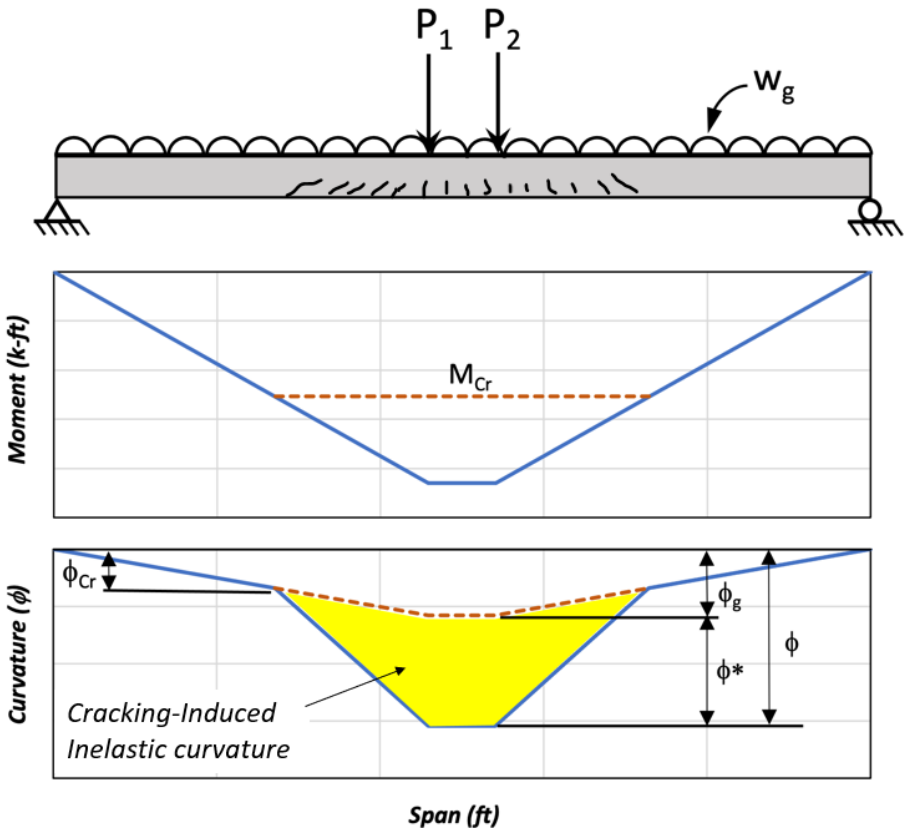

Figure 5.11. Post-Cracking Load-Deflection Analysis.

5.5 NOMINAL MOMENT STRENGTH FOR DESIGN

The nominal moment strength for design of the UHPC girders was computed based on the rectangular stress block method recommended by AASHTO (2020). The depth of the neutral axis is taken as the distance of the neutral axis from the extreme compression fiber. The neutral axis is determined by iterating along the depth of the cross-section until the tensile and compressive forces

are in equilibrium. The magnitude of the rectangular stress block is governed by the compressive strengths for CC deck and UHPC respectively, depending on the location of the neutral axis. The method recommended by FHWA (2022) is based on the triangular stress block explained in Section 3.4.1. The rectangular method used in AASHTO (2020) is suggested because it is simple and conservative in the case of a UHPC I-girder with a composite CC deck. Equation (5.20) presents the nominal moment capacity of the specimen:

$$M_n = NA_p f_{ps}\left(d_p - \frac{a}{2}\right) \tag{5.20}$$

where:

N = Number of prestressing strands

A_p = Area of each prestressing strand, in^2

f_{ps} = Average stress in prestressing steel at the time for which the nominal resistance of the member is determined, ksi

d_p = Distance from extreme compression fiber to the centroid of the prestressing strands, in.

a = Depth of equivalent rectangular stress block, in.

The depth of the equivalent rectangular stress block a is β_1 times the depth of the neutral axis from the compressive fiber, where the factor β_1 is dependent on the compressive strength of the concrete. According to AASHTO (2020) a value of 0.85 is adopted for the CC deck and a value of 0.65 for the UHPC girder. Table 5.2 presents the design nominal flexure capacity computed based on the rectangular stress block (AASHTO 2020) and the triangular stress block (FHWA 2022) for the portion of the UHPC girder in compression with the experimental results for all three girder specimens. The difference in capacity computed by the two methods differs from one another by 3 percent and are both conservative when compared to the experimental capacity. The majority of the compression force is resisted by the CC deck, which reduced the impact of the compression model selected for the UHPC girder when determining M_n.

Table 5.2. Nominal Moment Capacity Comparison—Calculated versus Experimental.

	Tx34-1		Tx34-2		Tx54	
Description	**Moment, k-ft**	**Percent Difference**	**Moment, k-ft**	**Percent Difference**	**Moment, k-ft**	**Percent Difference**
Experimental	5020	N/A	6562	N/A	12,860	N/A
AASHTO (2020)	4750	−5.4%	5906	−10.0%	11,131	−13.4%
FHWA (2022)	4861	−3.2%	6044	−7.9%	11,211	−12.8%

Note: N/A: Not applicable.

5.6 TX34-1 FLEXURE TEST RESULTS

5.6.1 Flexure and Shear Capacity Analysis

The moment-curvature analysis and shear capacity analysis were conducted with the measured material properties for the companion samples taken during girder fabrication. There was a decrease in the tensile strength of the Tx34-1 girder versus the original design assumptions, which may be due to the higher flow spread value of 11.3 in. for Batches 2 and 3 (see the Volume 1 report). Therefore, the girder shear capacity was computed based on the experimental uniaxial tensile strength that was lower than the design strength. The specimen was then reanalyzed for the flexure test setup. The analytical predictions prior to testing indicated that flexure-shear interaction could lead to a shear crack in the Tx34-1 girder specimen at the unreinforced end if the cracking strain limit of the UHPC girder is similar to the direct tension strength of the companion specimens.

At a total actuator load of 380 kips, the shear force occurring at the end without stirrups exceeded the reanalyzed predicted shear capacity at a uniaxial tensile strength of 0.53 ksi (from experimental data), as shown in Figure 5.12(a). The bending moment at this stage does not reach the predicted live load flexural capacity of the specimen, as shown in Figure 5.12(b). Therefore, it was anticipated that a premature shear failure at the unreinforced end may occur prior to the flexure failure of the beam during the flexure test. Beyond this point, the load on the actuator closest to the unreinforced end was disengaged, and only the actuator closest to the reinforced end was used to continue loading the girder and further test the flexure capacity of the girder at the midspan. This transition between the loading setup marks the end of Phase I loading and the beginning of Phase II loading.

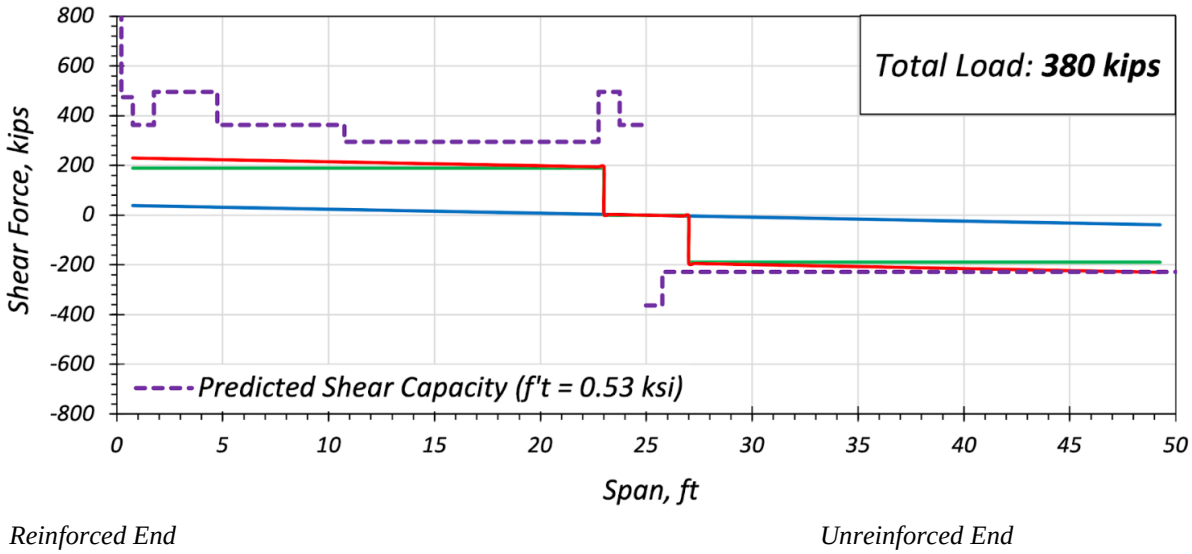

(a) Shear Force Diagram

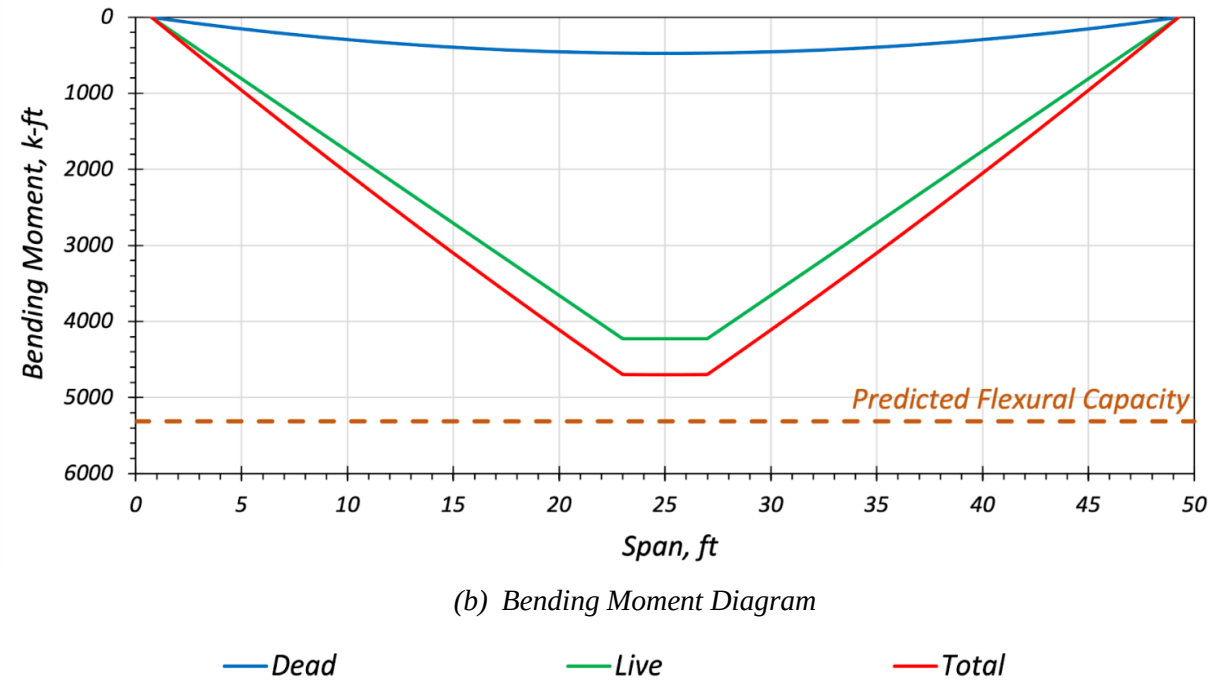

(b) Bending Moment Diagram

Figure 5.12. Tx34-1 Flexure and Shear Analysis—Phase I Loading.

5.6.2 Flexural Response and Observations

The flexure test for the Tx34-1 girder specimen was conducted on November 12, 2021. A trial run was conducted a day prior within the elastic limit of the girder (to avoid permanent deformations) so that all instruments were ensured to be working properly. During flexure testing, the specimen

was loaded at 0.5 kip per second per actuator under force control. The first stop for crack monitoring was conducted at the service demand. The service and factored moment demands were based on the prototype bridge girder used to design the girder specimen.

Figure 5.13 presents the moment-curvature response and load-deflection response of the girder specimen. The moment capacity is plotted against the dimensionless curvature ϕD, obtained by multiplying the curvature with the total depth D, of the specimen. Phase I of the test closely followed the predicted trend. Phase II showed deviation from the prediction, with the experimental results being less than the prediction by approximately 6 percent due to the permanent deformations occurring in the specimen after Phase I. Different significant milestones, such as the decompression limit, yielding stage, and the service and factored demand during the loading are marked with gray dashed lines in the figure. Figure 5.14 presents the deflection profile of the Tx34-1 girder in Phase I, with 406 kips total actuator load, and at Phase II, with 450 kips total actuator load.

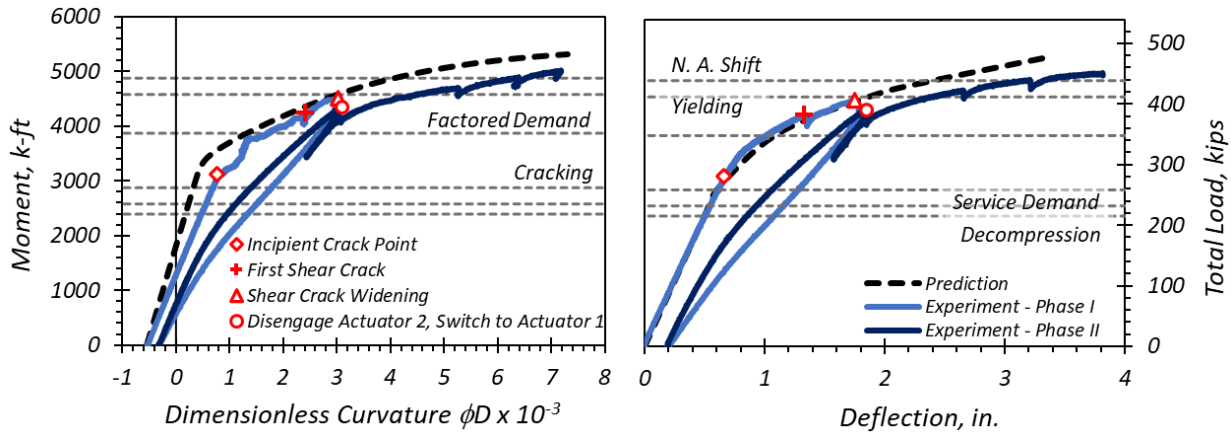

(a) Moment-Curvature Response *(b) Load-Deflection Curve*

Note: Phase I loading and unloading (light blue) is followed by Phase II loading (dark blue).

Figure 5.13. Tx34-1 Flexure Test Response.

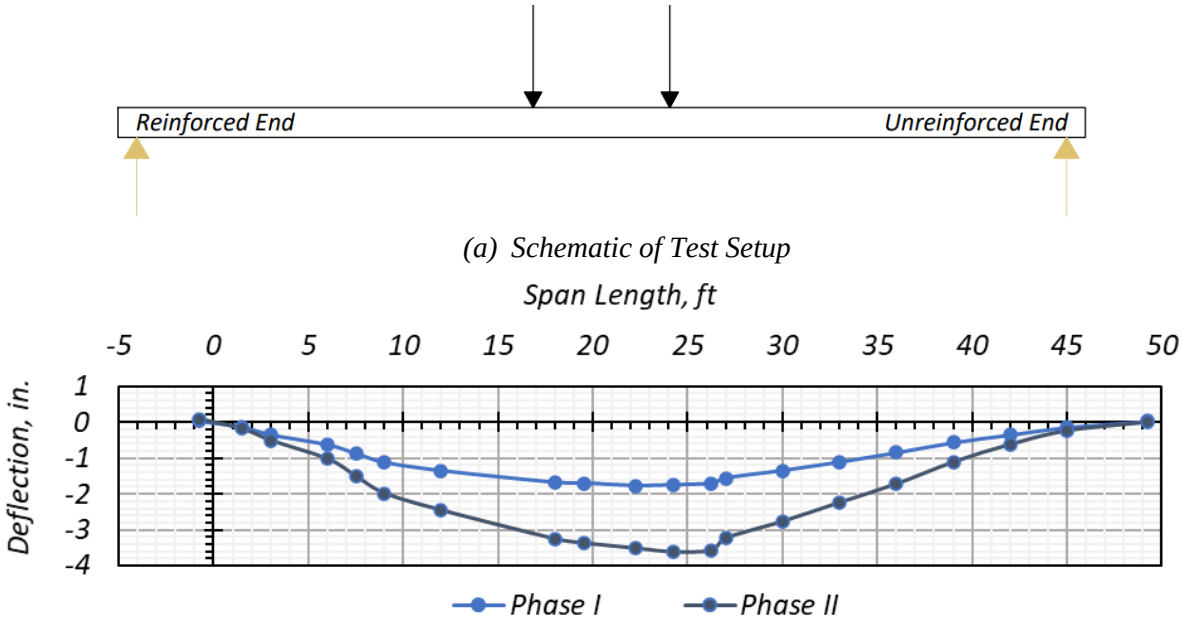

(a) Schematic of Test Setup

(b) Deflection Profile

Figure 5.14. Tx34-1 Deflection Profile.

Some key observations noted during flexure testing of this girder are as follows:

- The service moment demand of 2580 k-ft at midspan was attained at 232 kips total load. The specimen showed linear elastic behavior when the service limit was reached.
- During the flexure test, linear behavior was observed without any visible cracking up to a total load of 300 kips.
- The factored demand moment of 3870 k-ft was attained at a total load of 348 kips. The girder exhibited nonlinear behavior at this stage of loading. Cracking sounds were heard as the load was increased.
- At a total load of 380 kips, the cracking sounds increased, and visible shear cracks (hairline) were observed in the web at the unreinforced end.
- At a total load of 392 kips, flexure cracks with widths smaller than 0.004 in. were visible in the bottom flange. The girder stiffness reduced slightly, as depicted by the nonlinearity of the load-deflection curve.
- As the load was increased, cracks began to propagate and widen. The shear cracks at the unreinforced end started widening to around 0.01 in. at a total load of 406 kips. This marked the end of Phase I of the flexure test of the Tx34-1 specimen, which was terminated

due to the shear cracks in the unreinforced end of the specimen. The load on the specimen was reduced to a service load, and cracks were documented. After the documentation, the girder was completely unloaded.

- The flexure test was resumed in Phase II by loading the two actuators to the load of 203 kips on each actuator (total load of 406 kips), to get the specimen to the termination point of Phase I. Beyond this point, the actuator nearer to the unreinforced end was disengaged gradually, and the other actuator, away from the unreinforced end, continued to be loaded until flexure crack localization was observed. This process was done to assess the specimen for higher moments at midspan and allow for a subsequent shear test at the reinforced end of the specimen.
- Cracking sounds at the midspan started growing more frequent and intense, and flexure cracks began to propagate from the web into the top flange, while new cracks continued to form at the bottom flange and web. These cracks ranged from hairline to 0.008 in. The behavior of the girder became more nonlinear during this loading stage.
- At 422 kips on the engaged actuator near the reinforced end, the cracks at the midspan widened to 0.01 in. At that stage, the crack at the unreinforced end widened to 0.06 in. while the reinforced end had predominantly hairline cracks, with a few 0.006 in. wide cracks.
- At 450 kips on the engaged actuator near the reinforced end, three low-pitched loud sounds were heard, and crack localization was observed at a crack under that actuator. At that stage, it appeared that the crack bridging property of the fibers was lost, and there may have been a slip of the prestressing strands. The crack under the actuator was approximately 0.19 in. wide. At that stage, the crack widths at the unreinforced and reinforced ends were 0.08 in. and 0.008 in., respectively. The test was terminated at this point to preserve the specimen for the shear test at the reinforced end. The specimen had a maximum applied moment of 5050 k-ft, and the unreinforced end resisted a shear force of 202 kips.

Figure 5.15 presents the cracks observed at different stages of loading, including factored demand, yield, and termination point of the test. At the factored demand load, no visible cracks were seen. Figure 5.16 presents images of the shear cracks at the unreinforced end. Figure 5.17(a) and (b) present images of the flexure cracks at the constant bending moment region.

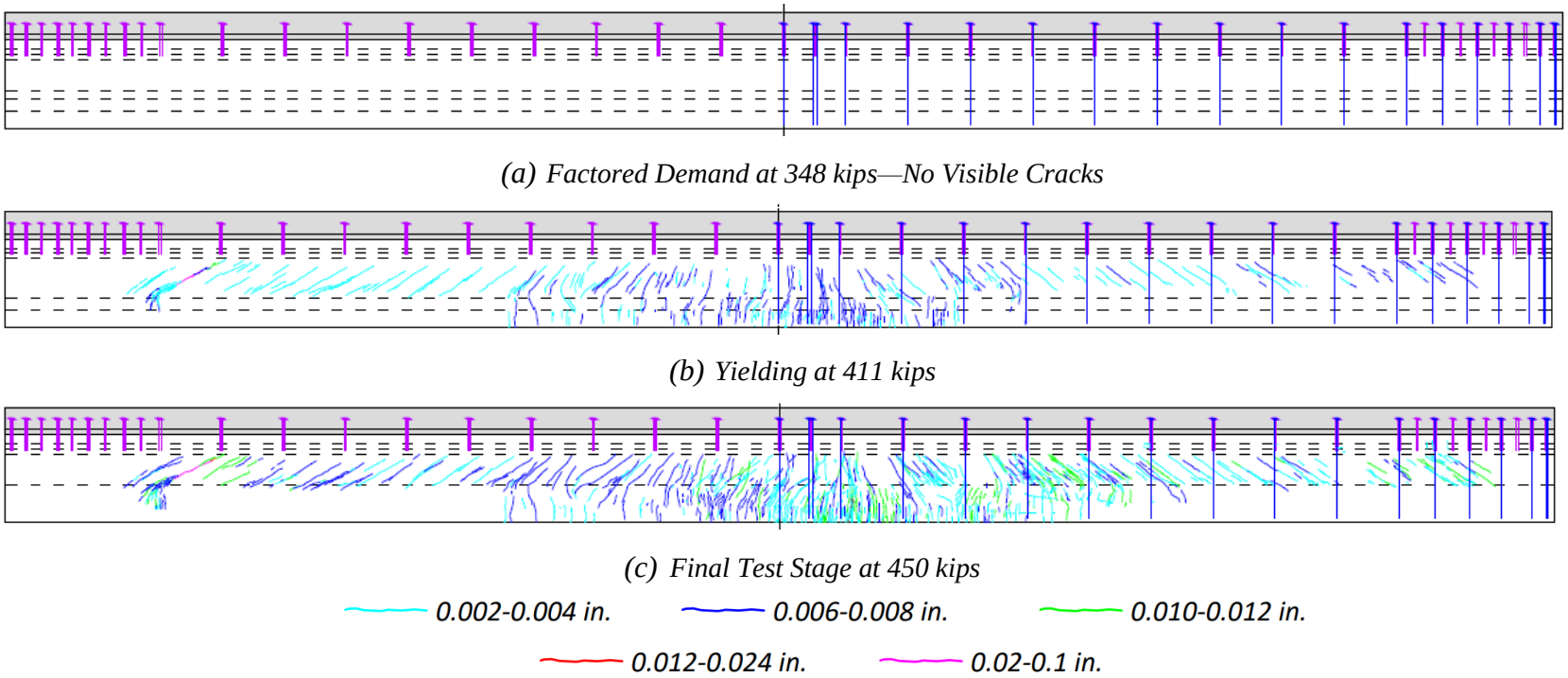

Figure 5.15. Tx34-1 Flexure Cracks at Different Stages of Loading.

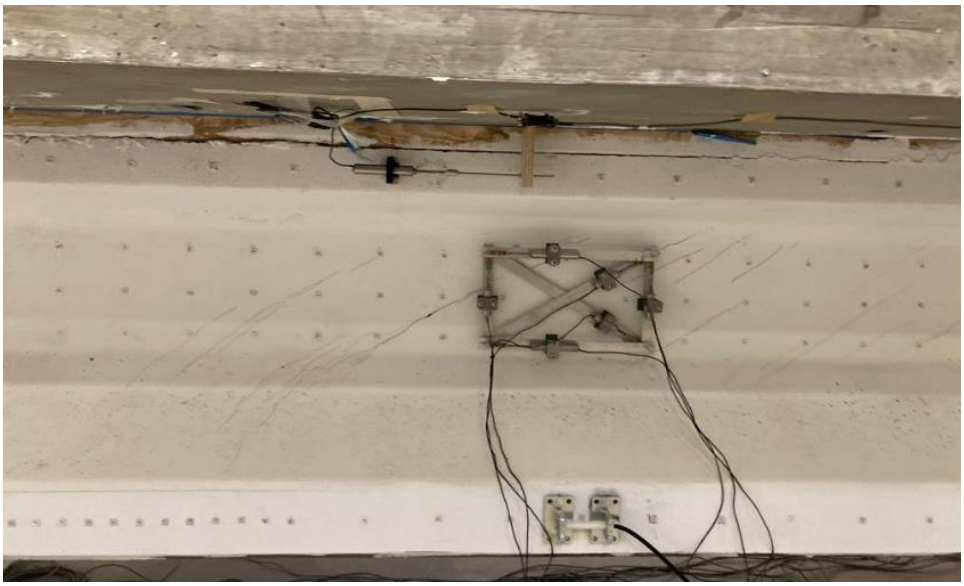

Figure 5.16. Tx34-1 Shear Cracks at Unreinforced End at 450 Kips.

(a) Cracks Formed at Midspan

(b) Underside of the Girder Soffit

Figure 5.17. Tx34-1 Flexure Cracks in Constant Bending Moment Region at 450 Kips.

5.6.3 Experimental and Predicted Strain Results

Figure 5.18 illustrates the SPs and the strain gages located at the top of the CC deck slab and at the bottom of the UHPC girder soffit. Figure 5.19 presents the comparison of experimental strains with the predicted theoretical strains. Figure 5.19(a) presents the strain data determined from the

SPs' measurements and the SGs at the top of the CC deck and at the bottom of the UHPC girder. The top SP data are presented in shades of orange and red, while the corresponding top SG data are presented in shades of blue. The bottom SP data are indicated by shades of gray, while the corresponding SG data are indicated by shades of green. The top SP data (orange and red) did not provide reliable measurements, which could be due to potential slip of the SPs or due to the sensors not picking up the small changes in strain.

The remaining experimental data from the Phase I portion of the test were close to the prediction. There was a slight offset from the prediction for the Phase II test results, which can be attributed to the creep-induced permanent deformations after the nonlinear loading of the specimen in Phase II. Figure 5.19(b) presents only the data measured by strain gages compared with the prediction. The strain gage data appear to be more reliable during testing due to greater sensitivity of the sensors.

The test was terminated at a compressive strain of 0.0016 at the top of the deck slab and a tensile strain of 0.006 strain. This localization strain under tension was considered as a termination point because the crack at the underside of the soffit had widened, and the girder was to be used for subsequent shear performance testing. This is similar to the strain results of the direct uniaxial tension test and the localization crack value reported by El-Helou and Graybeal (2022a).

The strain profile at key stages of loading was plotted using the data from the strain gages at the top and bottom of the composite section, from the SPs at the top and bottom of the cross-section, and along the elevation of the composite specimen cross-section. Figure 5.20 presents the strain profile at decompression, cracking, yielding, neutral axis shift, and termination point of the test. The prediction (solid black line) is based on theoretical strains obtained from the moment-curvature analysis of Section 5.3.

The ESG did not perform well, and some may have been damaged during the pour of UHPC. For the Tx34-1 girder specimen, the SP at the bottom performed well, whereas those on the top did not seem to capture the strains well. The strains were higher than the predicted strains at and after yielding, which could be attributed to the loss in crack bridging capability of the matrix due to widening of cracks.

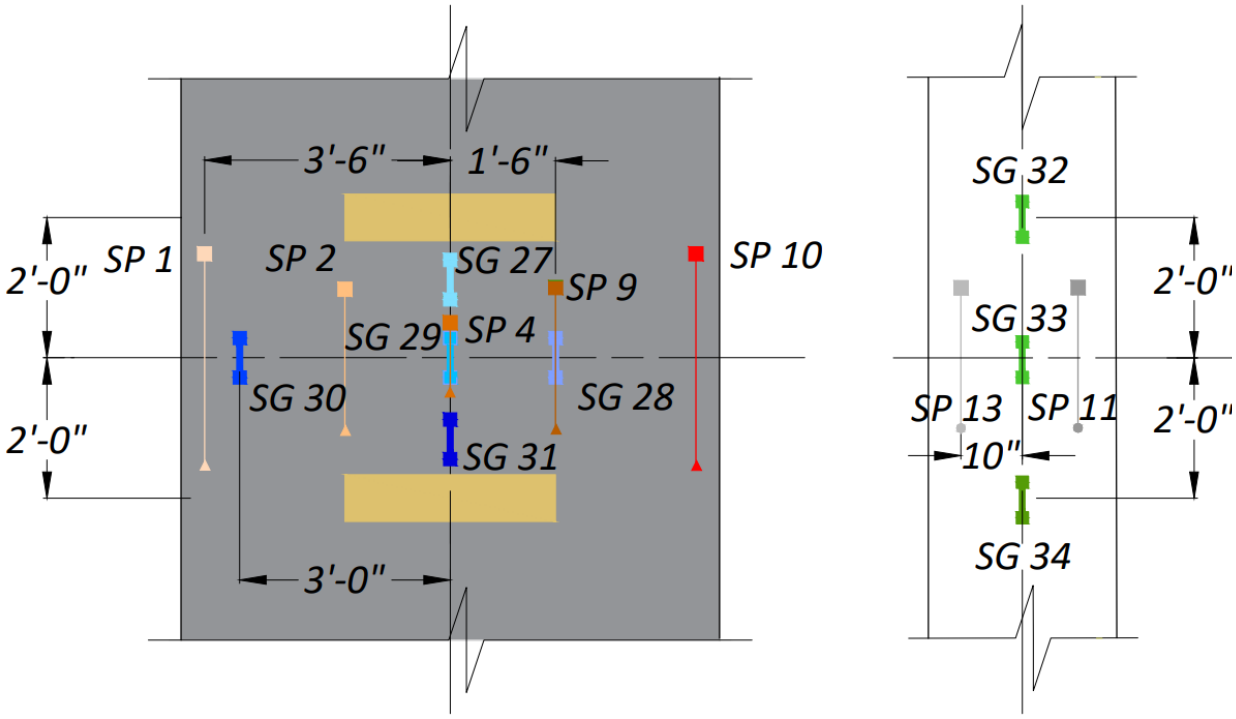

(a) Top of CC deck slab *(b) Underside of UHPC girder soffit*

Figure 5.18. Top and Bottom Instruments at Midspan for Tx34-1.

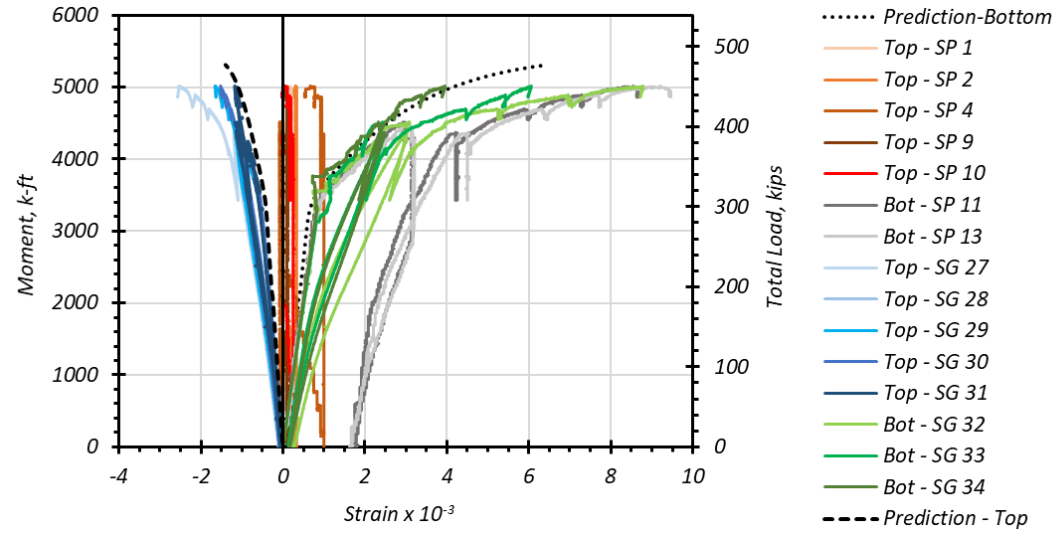

(a) Top and Bottom Strains (SP and SG)

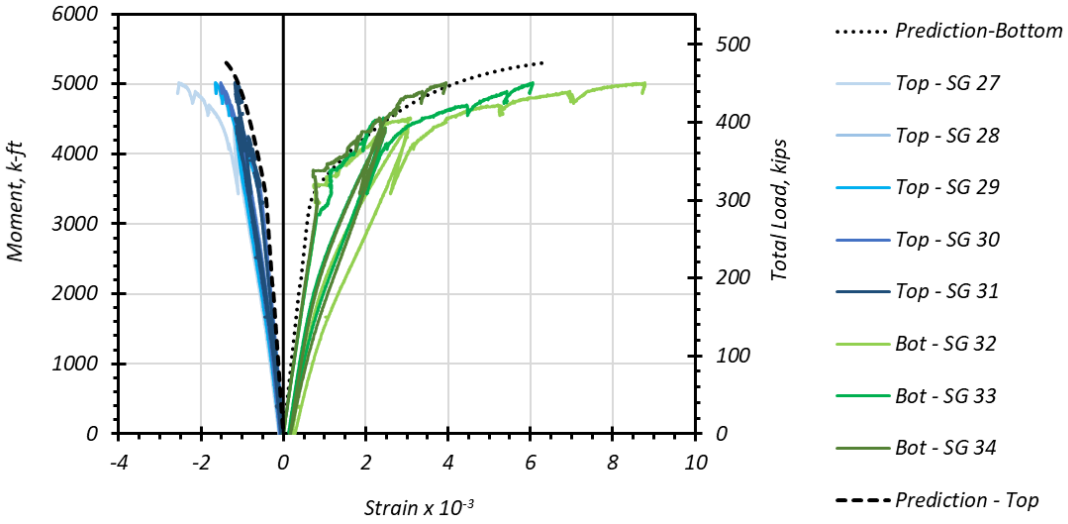

(b) Top and Bottom Strains (SG only)

Figure 5.19. Top and Bottom Strains at Midspan for Tx34-1.

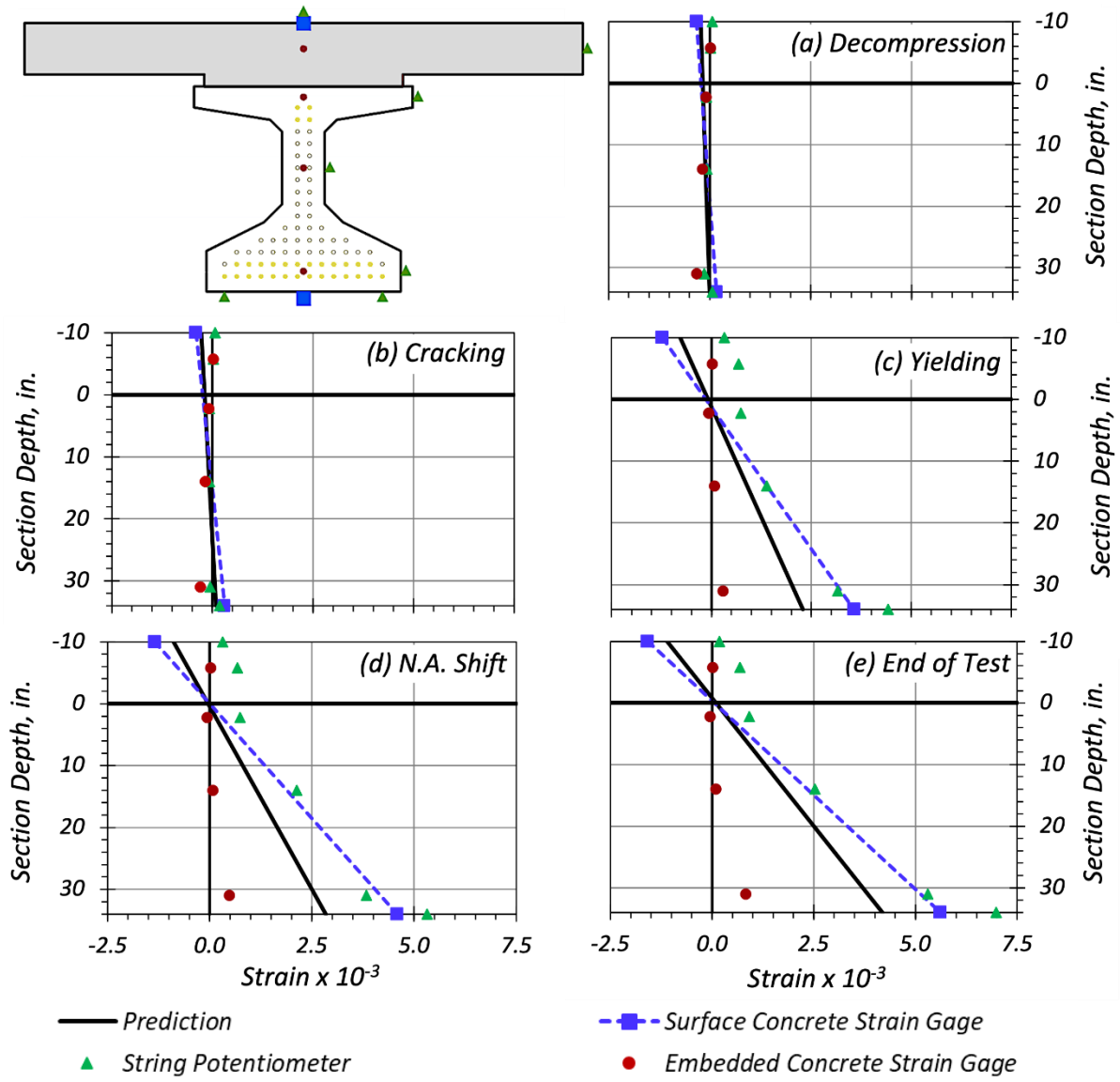

Notes:
1. The horizontal line at 0 in. depth marks the UHPC girder–CC haunch interface
2. Decompression: 216 kips (total actuator load)
3. Cracking: 258 kips (total actuator load)
4. Yielding: 412 (total actuator load)
5. Neutral Axis Shift: 438 kips (total actuator load)
6. End of Test: 478 kips (total actuator load)

Figure 5.20. Strain Profiles for Tx34-1.

5.7 TX34-2 FLEXURE TEST RESULTS

5.7.1 Flexure and Shear Capacity Analysis

The second Tx34 specimen was also fabricated during the summer months. The experience casting the first girder specimen and the lessons learned helped the research team and the precast plant personnel to improve control over the mix and casting process. This specimen had improved tensile strength when compared to the first specimen based on the material-level test results. Six strands were harped in this design, which further improved the shear capacity of the girder ends. Based on the pretest analysis, no premature shear failure was expected while the beam was being tested in flexure. Figure 5.21 presents the shear force and bending moment diagrams for the flexure test of the Tx34-2 girder. It was analytically predicted that the shear capacity would not be exceeded during the flexure-shear interaction when loading the midspan of the girder, and therefore, premature shear failure of the ends was not anticipated.

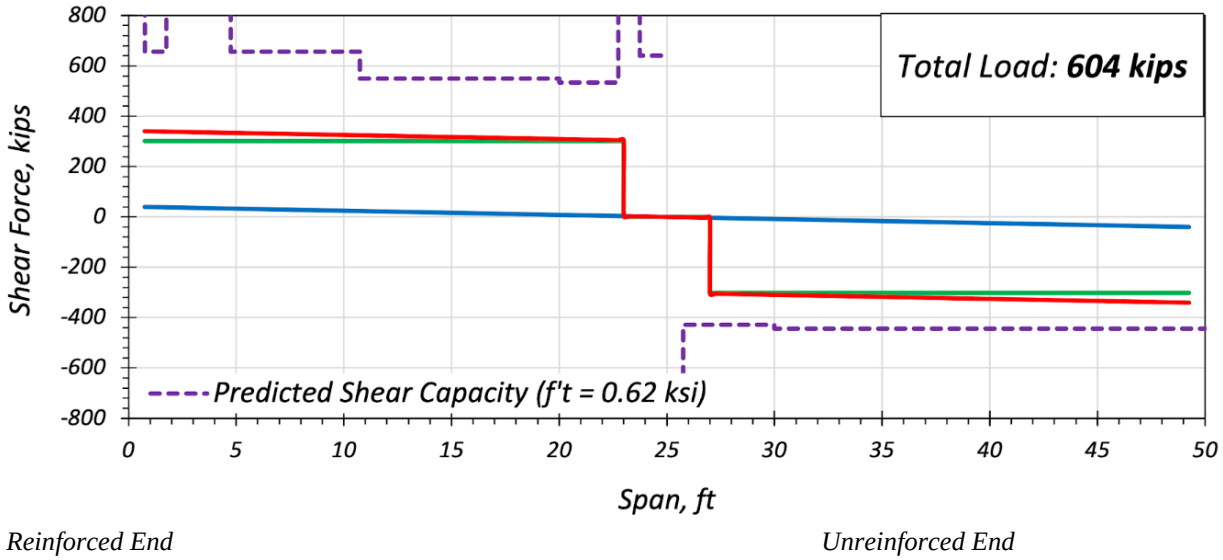

(a) Shear Force Diagram

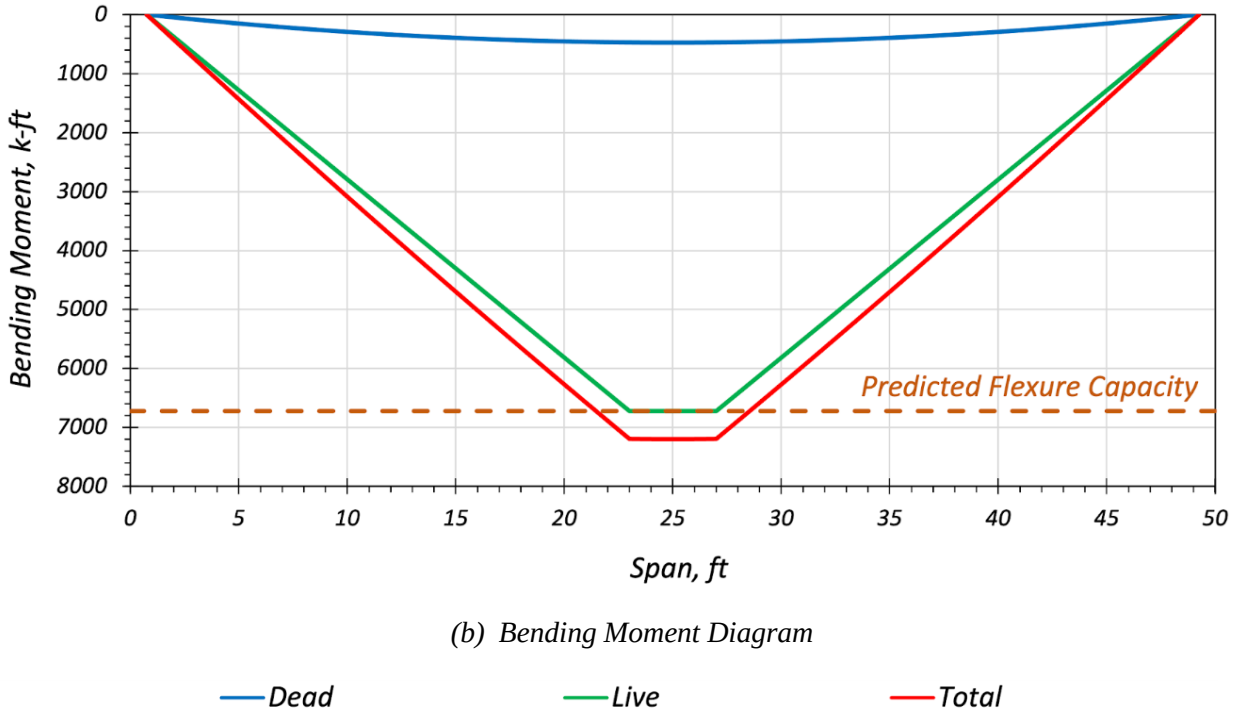

(b) Bending Moment Diagram

Figure 5.21. Tx34-2 Flexure-Shear Analysis.

5.7.2 Flexural Response and Observations

The flexure test for the Tx34-2 girder was conducted on January 21, 2022. The specimen was loaded under elastic conditions a day prior to the testing to ensure that the instruments and

equipment were working properly. Figure 5.22 presents the moment-curvature response and load-deflection response of the Tx34-2 girder specimen. The moment capacity computed from the analysis is plotted against the iterative curvature multiplied by the total depth of the specimen D. The moment-curvature curve and the load-deflection curve closely track the predicted capacities. Figure 5.23 presents the deflection profile of the Tx34-2 girder specimen at the maximum total actuator load of 604 kips.

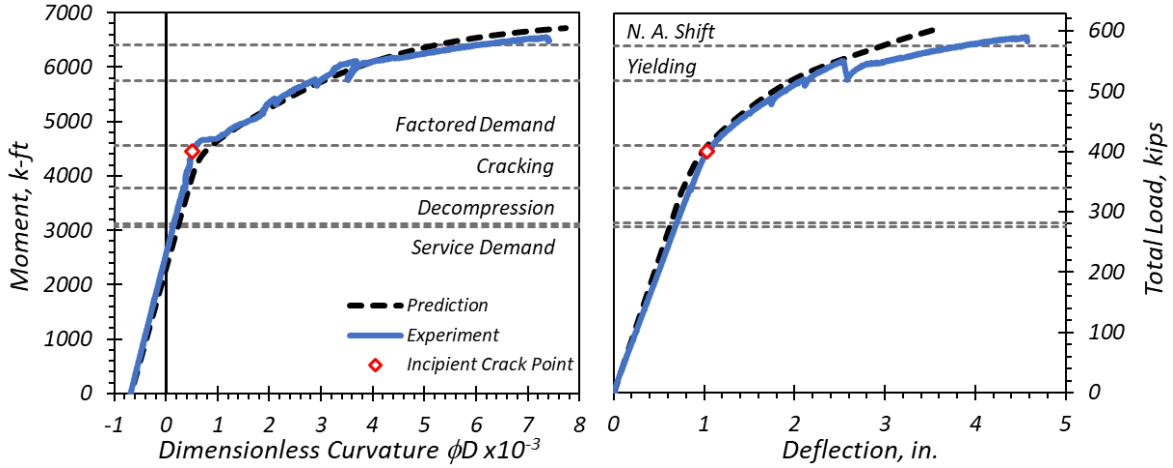

(a) Moment-Curvature Response *(b) Load-Deflection Curve*

Figure 5.22. Tx34-2 Flexure Test Response.

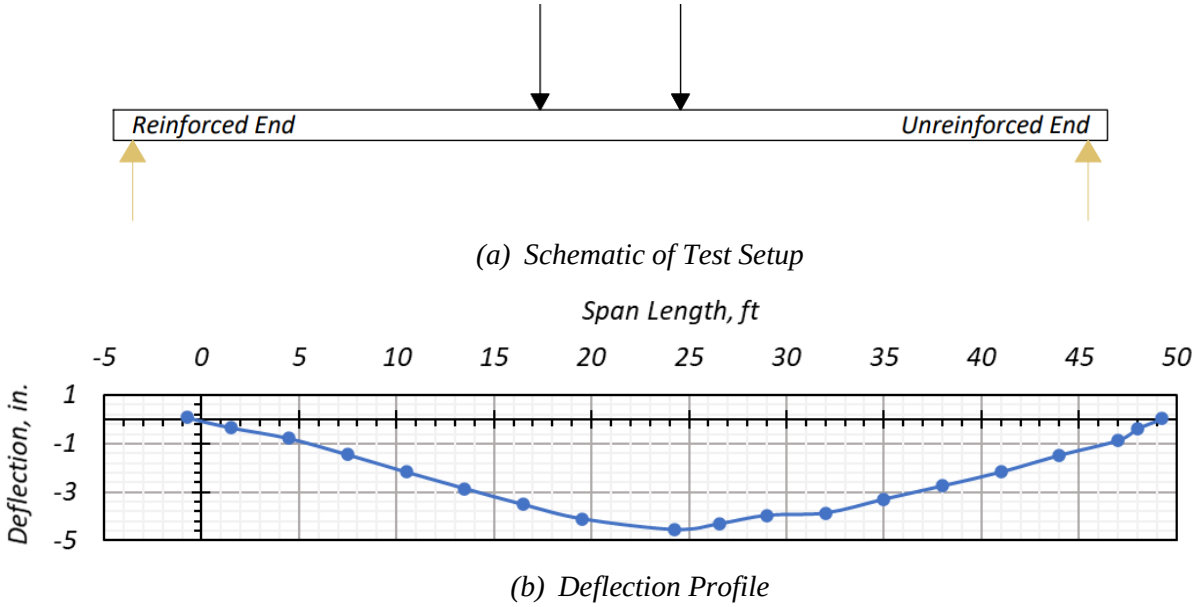

(a) Schematic of Test Setup

(b) Deflection Profile

Figure 5.23. Tx34-2 Deflection Profile.

Some key observations noted during flexure testing of this girder are as follows:

- The specimen showed linear elastic behavior until the service moment demand of 3065 k-ft at midspan was attained at 275 kips total load with no visible cracking.
- The specimen continued to show linear behavior until 400 kips total actuator load occurred.
- There was incipient cracking heard at 410 kips total load (factored demand load with 4560 k-ft moment); however, no cracks were visible.
- At a total load of 440 kips, the cracking sound grew louder, and hairline flexure cracks were observed at the bottom flange at the midspan.
- At a total load of 460 kips, hairline shear cracks were noticed at the unreinforced end.
- At a total of 486 kips, shear cracks $\leq$ 0.004 in. wide were visible in the web at the unreinforced end of the specimen, and hairline cracks at the midspan region were observed.
- As the total load was increased, nonlinearity became more pronounced, and the cracks began propagating into the web at the midspan.
- At a total load of 513 kips, the flexure and shear cracks multiplied.
- At a total load of 550 kips, cracks < 0.004 in. wide were observed at the midspan, while the cracks at the unreinforced end in the web were $\leq$ 0.006 in. wide, and those cracks at the reinforced end were $\leq$ 0.004 in. wide.
- A loud dull sound was heard at a total load of 550 kips, followed by loading up to 580 kips. It is suspected that the sound could be due to a slip at the girder to haunch interface or due to a slip of prestressing strands. Some spalling of the CC haunch was observed, with a 0.16 in. wide spalled concrete observed.
- Crack localization was observed at the bottom flange under the actuator near the reinforced end, with a crack width of 0.005 in., and the crack at the underside of the soffit was 0.12 in. wide.
- This specimen was loaded to a maximum moment of 6562 k-ft. The test was terminated to preserve the specimen for subsequent shear tests at the ends.

Figure 5.24 presents the cracks observed at several key load stages. No visible cracking was observed during the service and factored load conditions of the flexure test, as shown in Figure 5.24(a). Figure 5.24(b) and Figure 5.24(c) present the cracks observed at yield and the final

stage of testing, respectively. Figure 5.25 presents images of the flexure crack at the underside of the soffit of Tx34-2.

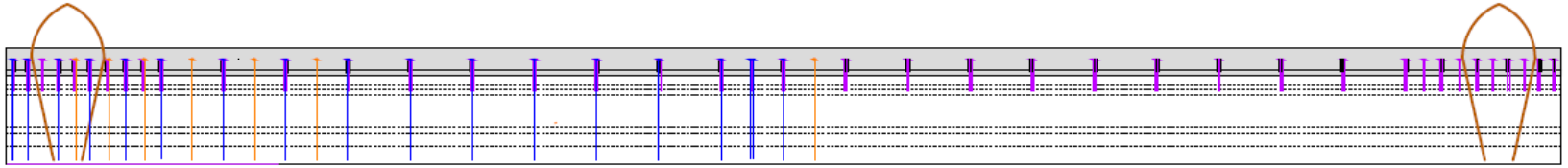

(a) Factored demand at 410 kips—No visible cracks

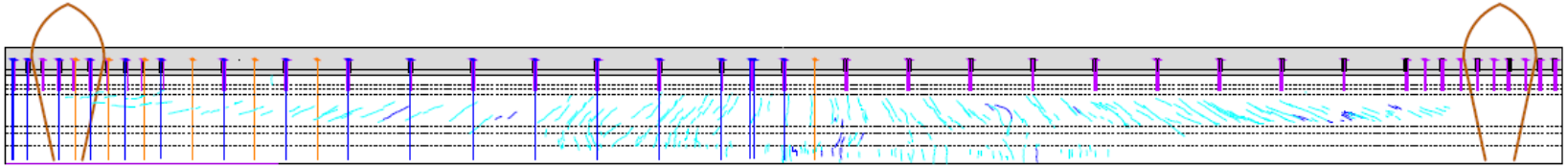

(b) Yielding at 517 kips

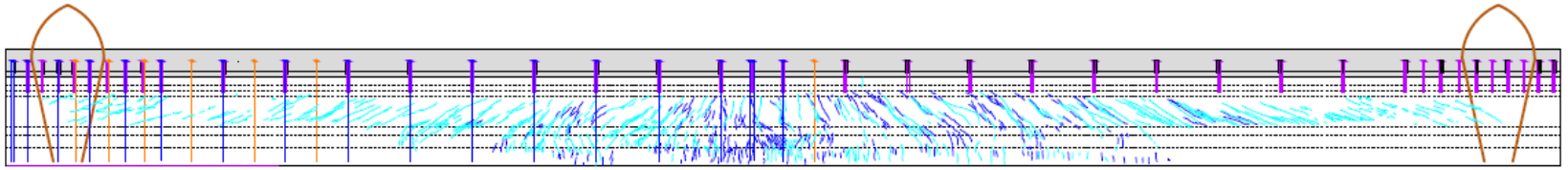

(c) Final test stage for crack mapping at 590 kips

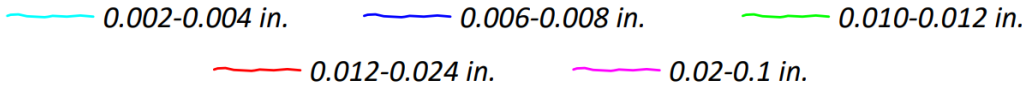

Figure 5.24. Tx34-2 Flexure Cracks at Different Stages of Loading.

Figure 5.25. Fibers Bridging the Crack at the Underside of the Soffit of Tx34-2.

5.7.3 Experimental and Predicted Strain Results

Figure 5.26 illustrates the arrangement of SPs and SGs at the top and bottom of the specimen. The arrangement was changed slightly based on the results of Tx34-1 because redundancy of sensors was needed more for SP due to their lower sensitivity when compared to the SG. Therefore, the number of SGs used was reduced and instead allocated to the shear regions to monitor shear strains. The SGs were installed in the shear regions during the flexure test because of their performance from Tx34-1 girder testing and also to monitor the strains in the shear regions with a sensor more sensitive than LVDTs in case there was any activity occurring due to flexure-shear interaction.

Figure 5.27 presents the experimental strain data at the top and bottom of the specimen cross-section in the constant bending moment region. The SP and SG data for this specimen were quite consistent with each other and with the predictions. Figure 5.27(a) presents the top SP data in varying shades of orange and red, while the top SG data are represented in shades of green. The bottom SP data are in shades of gray, while the bottom SG data are indicated by shades of blue. Figure 5.27(b) highlights only the strain gage data for a clearer comparison of the experimental and predicted data. The top SGs and top SPs were observed to be very close to the prediction. The bottom SGs were close to the prediction. Although the bottom SPs followed the same trend of the

prediction and the bottom SGs, there was a slight offset in the data of the SPs and SGs, potentially due to the difference in the sensitivity of the instruments or some imperfection in the signal.

Figure 5.28 presents the strain profile measured experimentally through SPs and SGs at key stages of the test. The strains measured by the SGs are close to the predictions until yielding. The top and bottom strains based on the SP measurements were relatively close, while at intermediate heights, the measurements were not as close to the prediction. The embedded concrete strain gages did not give meaningful results. The post-yield behavior indicates strains greater than the predicted deformation under tension, which could be the result of the loss in tensile strength after crack localization.

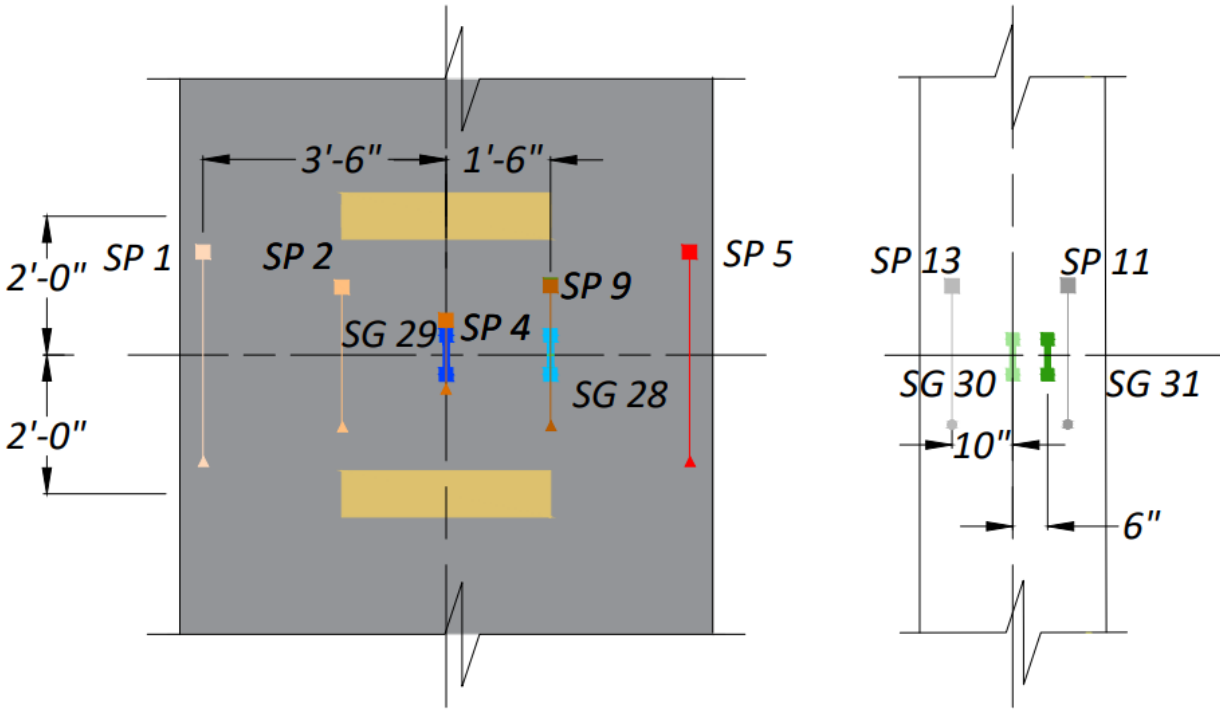

(a) Top of CC deck slab *(b) Underside of UHPC soffit*

Figure 5.26. Top and Bottom Instruments at Midspan for Tx34-2.

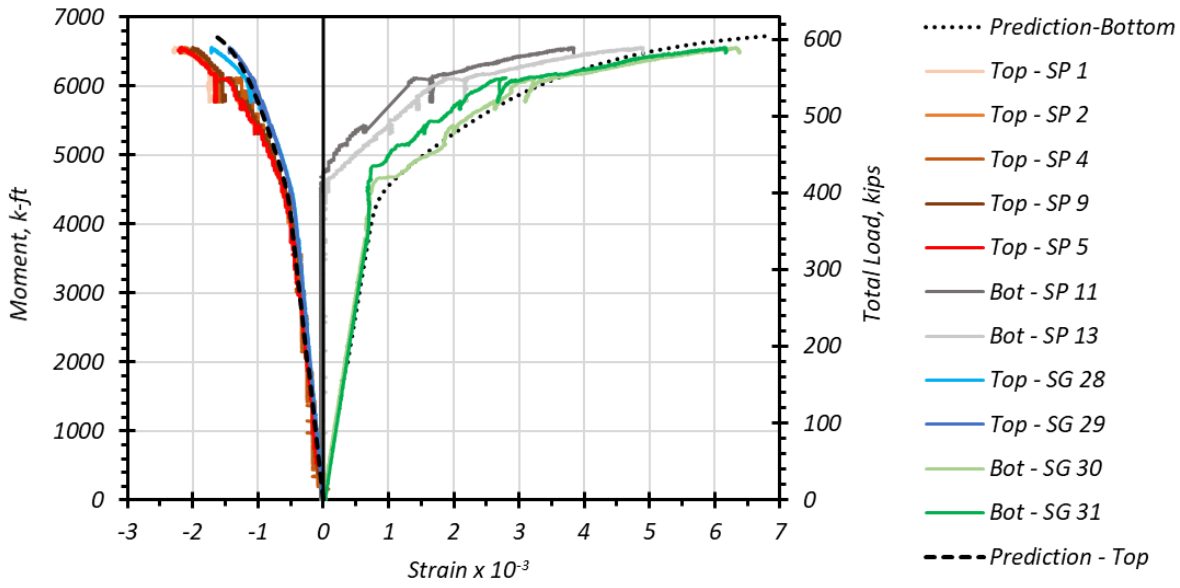

(a) Top and bottom strains (SP and SG)

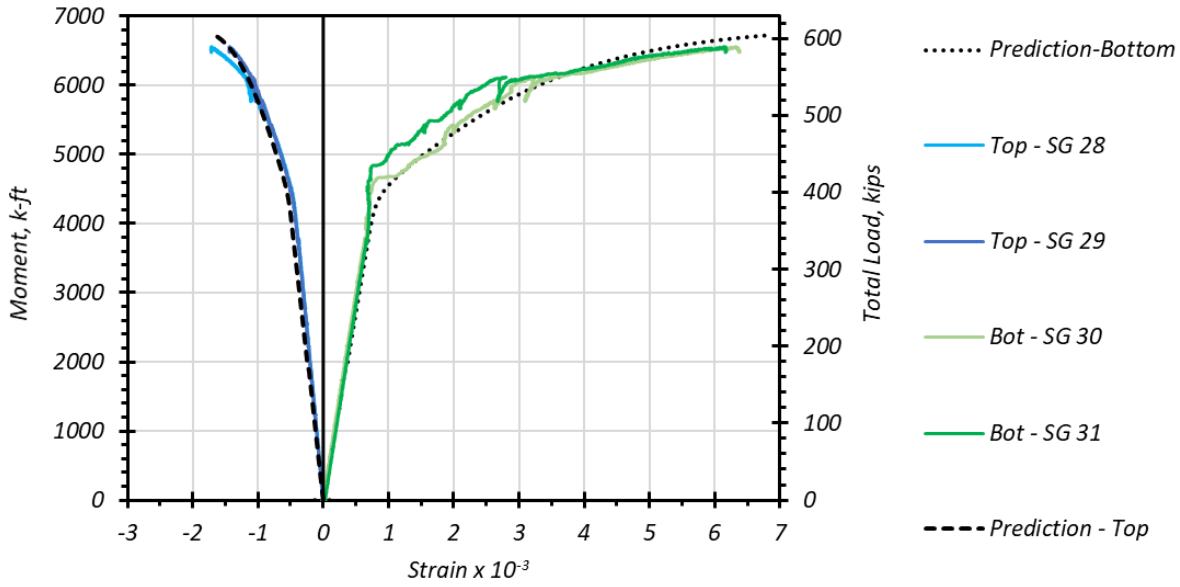

(b) Top and bottom strains (SG)

Figure 5.27. Top and Bottom Strains at Midspan for Tx34-2.

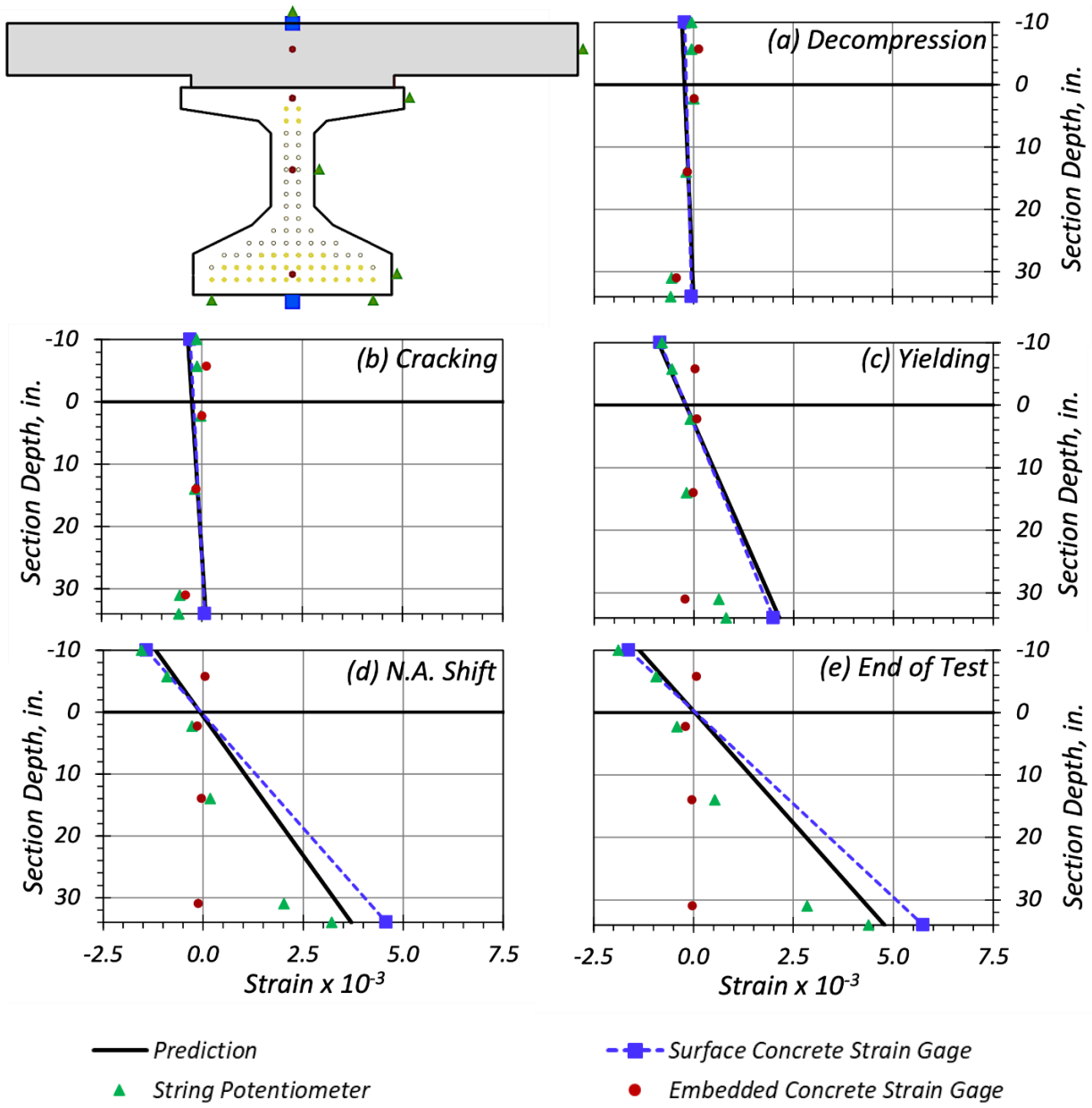

Notes
1. The horizontal line at 0 in. depth marks the UHPC girder–CC haunch interface
2. Decompression: 280 kips (total actuator load)
3. Cracking: 340 kips (total actuator load)
4. Yielding: 516 (total actuator load)
5. Neutral Axis Shift: 576 kips
6. End of Test: 604 kips (total actuator load)

Figure 5.28. Strain Profiles for Tx34-2.

5.8 TX54 FLEXURE TEST RESULTS

5.8.1 Flexure and Shear Capacity Analysis

The Tx54 girder specimen was also designed with six harped strands, similar to the Tx34-2 specimen, to take advantage of the improved shear strength of the unreinforced end and to avoid any premature shear cracks. The Tx54 girder companion specimens had a measured tensile capacity comparable to the mix developed at the lab and for the precast plant trial batch. The deeper web, improved tensile strength relative to the first two girder specimens, and the use of harped tendons were considered in estimating the expected girder response. The Tx54 specimen was not expected to fail in shear due to flexure-shear interaction when conducting the flexure test. Figure 5.29 presents the shear force and bending moment diagrams of the Tx54 girder specimen when loading the girder to its flexure capacity. From the analysis prior to testing, the shear force capacity was higher than the shear demand on the girder during the flexure test. Therefore, a shear failure was not expected during the flexure testing, unlike the Tx34-1 girder specimen.

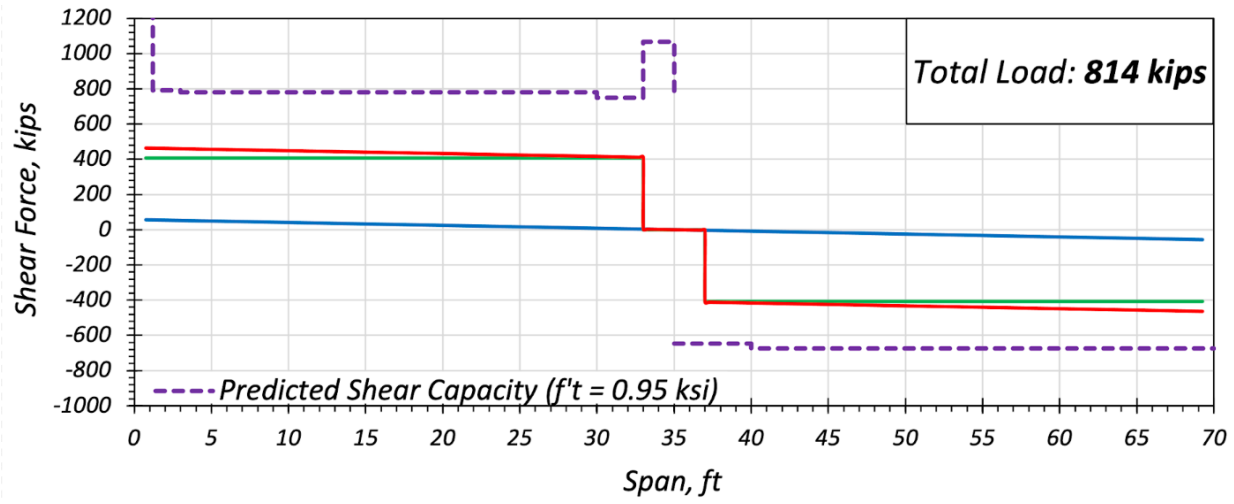

(a) Shear Force Diagram

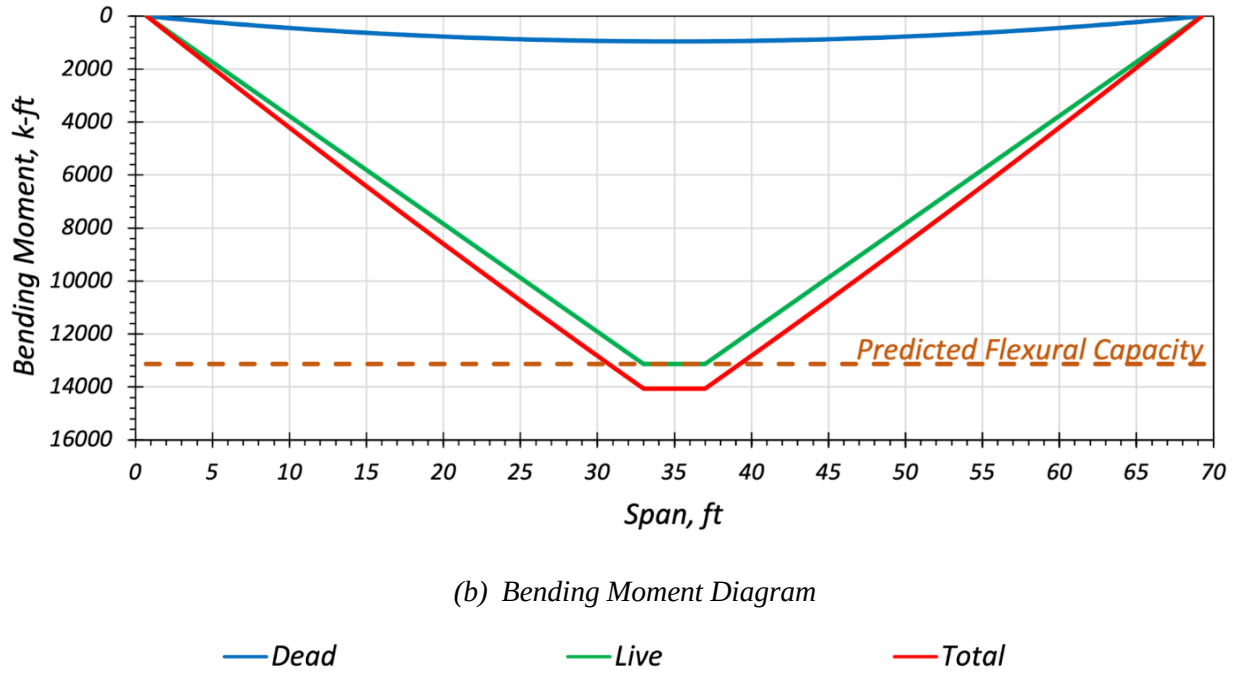

(b) Bending Moment Diagram

Figure 5.29. Flexure-Shear Analysis Tx54.

5.8.2 Flexural Response and Observations

The Tx54 girder specimen was tested in flexure on May 12, 2022. An elastic loading test was conducted a day prior to ensure that the instruments and equipment were working properly. The specimen was loaded at the same rate as the previous specimens (0.5 kip per second per actuator). Quick pauses were made at the service and factored demand limit states to check for cracks.

Figure 5.30 presents the moment-curvature and load-deflection capacity of the Tx54 girder specimen, with a maximum applied moment of 12,860 k-ft. The moment capacity is plotted against the product of the iterative curvature and the total depth *D* of the specimen. The predicted response of this girder specimen also closely matches the experimental results. Figure 5.31 presents the deflection profile of Tx54 when loaded to a maximum load of 800 kips.

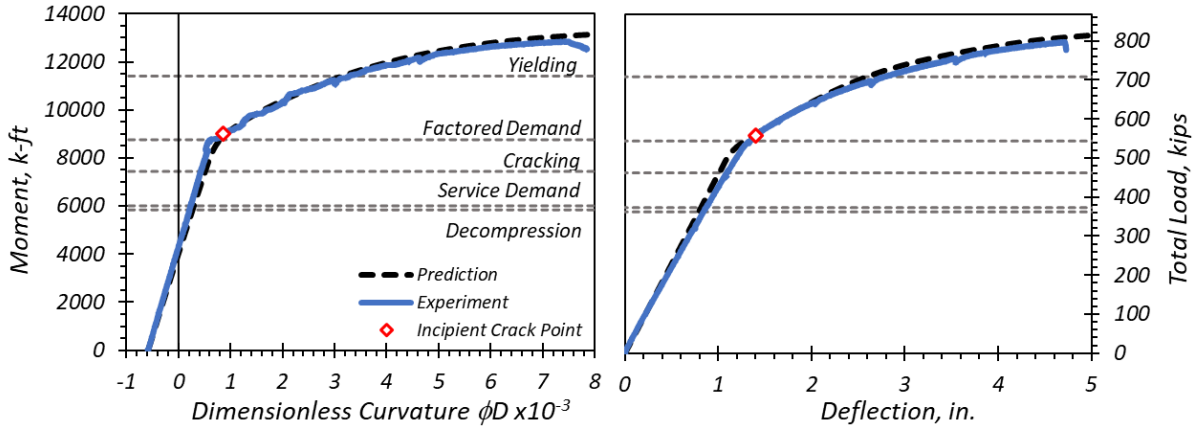

(a) Moment-Curvature Response *(b) Load-Deflection Curve*

Figure 5.30. Tx54 Flexure Test Response.

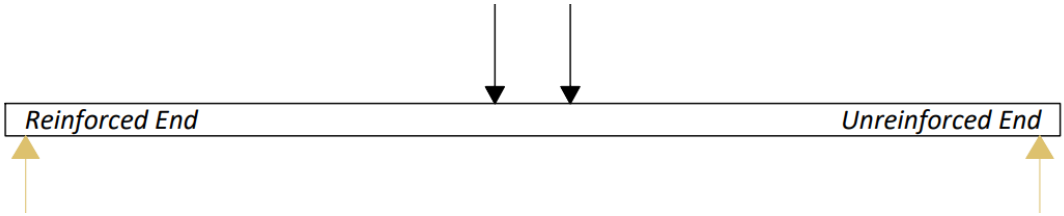

(a) Schematic of Test Setup

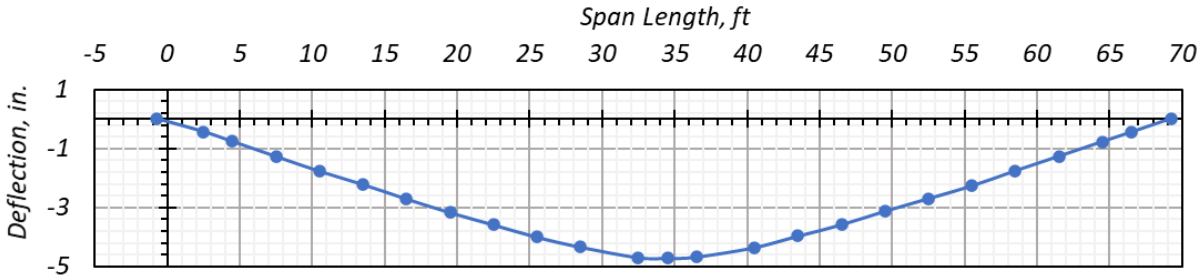

(b) Deflection Profile

Figure 5.31. Tx54 Deflection Profile.

Some key observations noted during flexure testing of the Tx54 girder specimen are as follows:

- The service moment demand for the prototype bridge of 6012 k-ft at midspan was attained at a total load of 373 kips total load. The factored moment demand limit of 8763 k-ft was attained at a total actuator load of 543 kips. No cracks were observed at either loading level when the test was paused for crack monitoring.
- The specimen response showed linear behavior until a total actuator load of 558 kips, slightly above the design-factored moment.
- At 560 kips total load, incipient microcracks were observed at the midspan bottom flange.
- At 590 kips total load, cracking at the midspan increased, with crack propagation into the bottom of the web. Hairline flexure cracks were marked, and the loading was continued.
- At 698 kips total load, the cracks propagated up to the top of the web to the top flange. The cracks were less than or equal to 0.012 in. wide.
- At 720 kips total load, cracking was more pronounced in the flexure-shear region (15 to 22 ft from the ends).
- At 748 kips total load, a dull sound was heard followed by two more loud sounds at 780 kips. The cracking sound intensified, and the cracks at the midspan widened to less than or equal to 0.024 in.
- At 800 kips total load, the cracks at midspan appeared to propagate faster and exhibited intensified cracking sounds. A post-cracking strain of 0.006 was selected as the localization strain based on the material-level tests of the companion specimens. Therefore, the test was terminated when this strain was reached at the bottom flange (measured by the SG) at a total load of 800 kips to preserve the specimen for the shear tests at the girder ends.
- This specimen exhibited the best flexure performance based on its better crack bridging property of fibers, strength, and ductility among all three girder specimens.

Figure 5.32 presents the observed cracks at three loading stages: (1) the factored demand loading stage when there was no cracking, (2) yielding, and (3) the final loading stage of the test after the load was reduced to allow for safe documentation of crack observations. Figure 5.33 presents a photograph of the cracks in the constant bending moment region for Tx54. The flexure capacity of this girder was quite high due to the high tensile strength of UHPC, larger cross-section of the girder, and more prestressing strands. Though the cracks did not widen as much as the previous

specimens at the soffit, the test was terminated when the tensile strain at the bottom was recorded as 0.006 to be consistent with the previous tests and to preserve the specimen for subsequent shear testing.

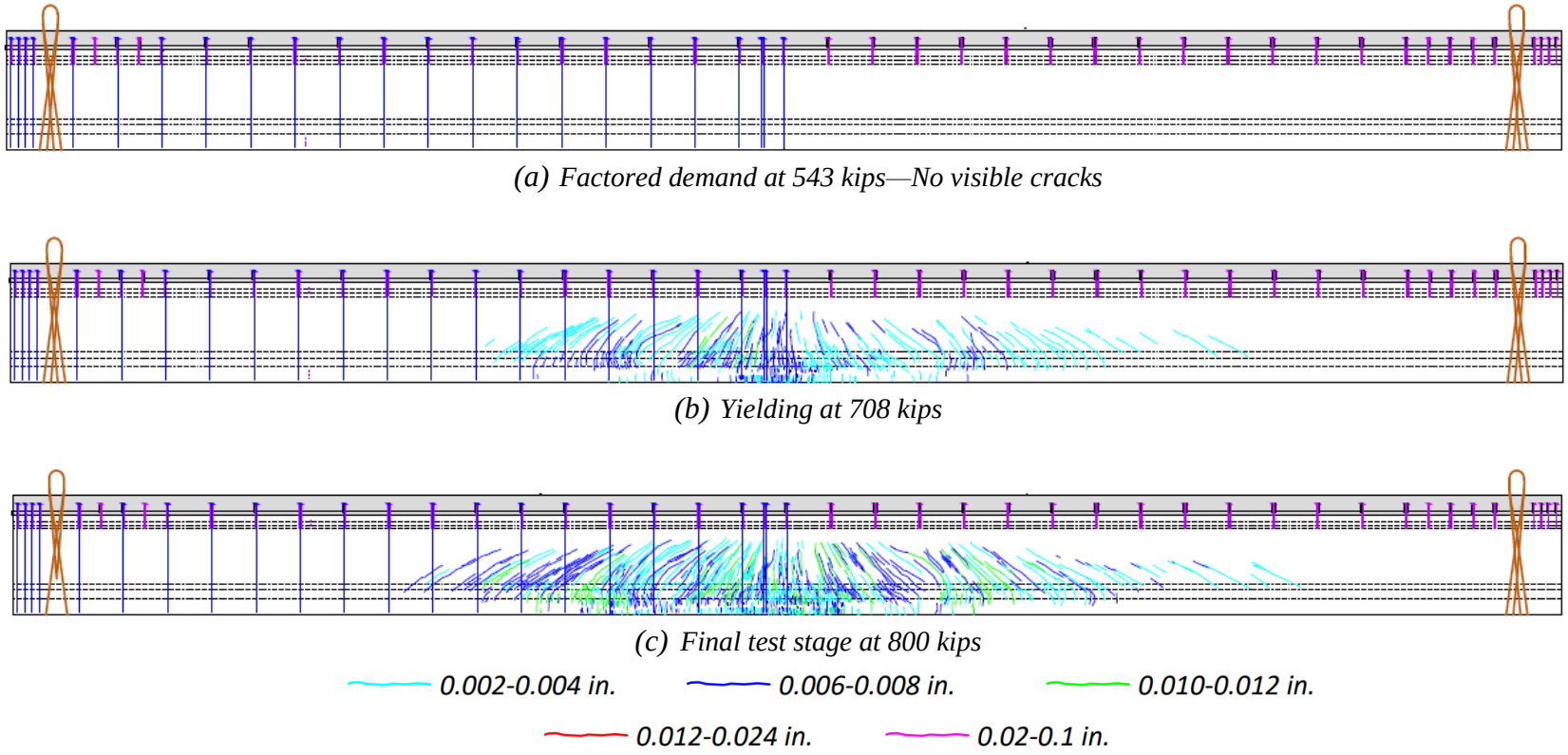

Figure 5.32. Tx54 Flexure Cracks at Different Stages of Loading.

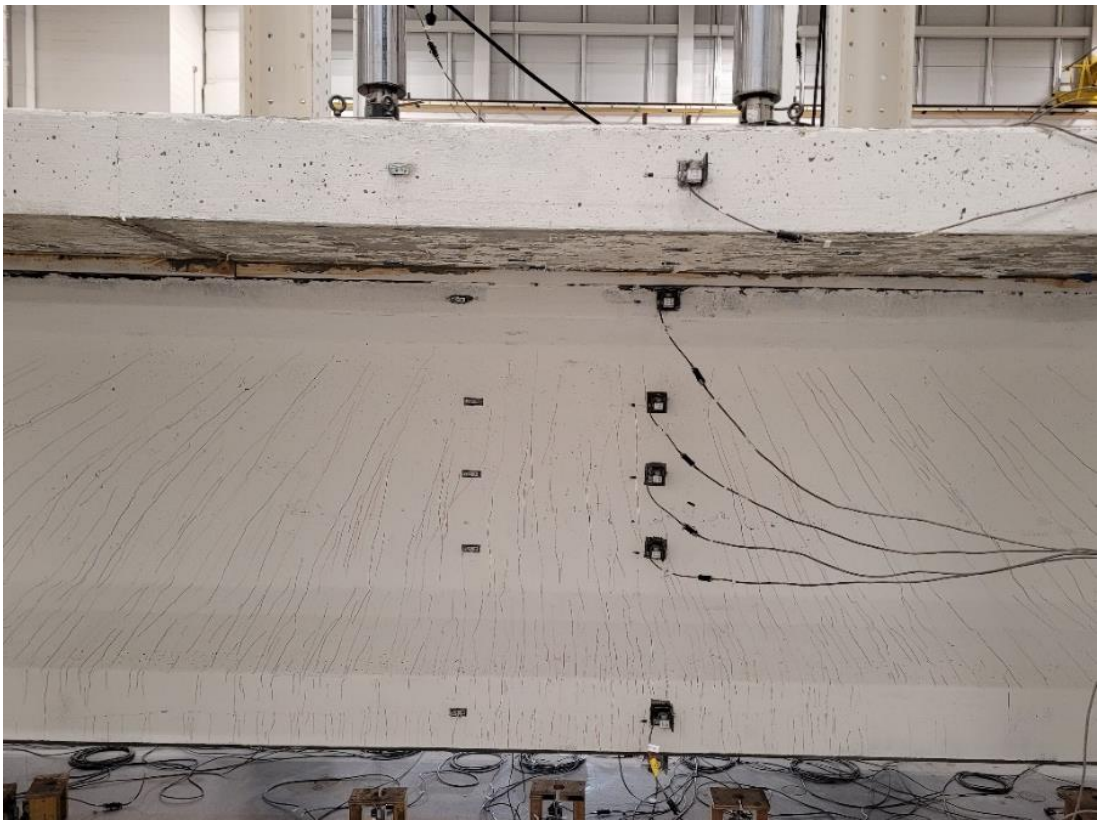

Figure 5.33. Cracks in Constant Bending Moment Region Tx54.

5.8.3 Experimental and Predicted Strain Results

Figure 5.34 illustrates the SPs and SGs installed and located at the top of the CC deck slab and the bottom of the UHPC girder soffit. Figure 5.35 presents the top and bottom strains from the flexure test of the Tx54 specimen. Figure 5.35(a) includes the data from both the SGs and SPs. The top SPs are indicated by shades of orange and red, while the bottom SPs are indicated by shades of gray. The top SGs are represented by shades of green, while the bottom SGs are represented by shades of blue. In this test, the bottom SPs show some slipping when compared to the SGs, whereas the top SPs and SG are quite consistent with each other and the prediction. The method of attachment of the SP and the SG was consistent for all three girder specimens. The SG are directly glued to the concrete surface, while the SPs are mounted on fixtures. The strain range of the SGs better captured small change in strains, especially those taking place in the initial phase of the test, than the SPs. Figure 5.35(b) shows the data for the top and bottom SGs only.

Figure 5.36 presents the strain profile measured experimentally through SPs and SGs at key stages of the test. The strains measured by the SGs are close to the predictions up to yielding. The top

and bottom strains based on the SP measurements were relatively close, while at intermediate heights, the measurements were not as close to the prediction. The embedded concrete strain gages did not provide meaningful results. The post-yield behavior indicates strains greater than the predicted deformation under tension, which could be the result of the loss in tensile strength after crack localization at the bottom of the girder.

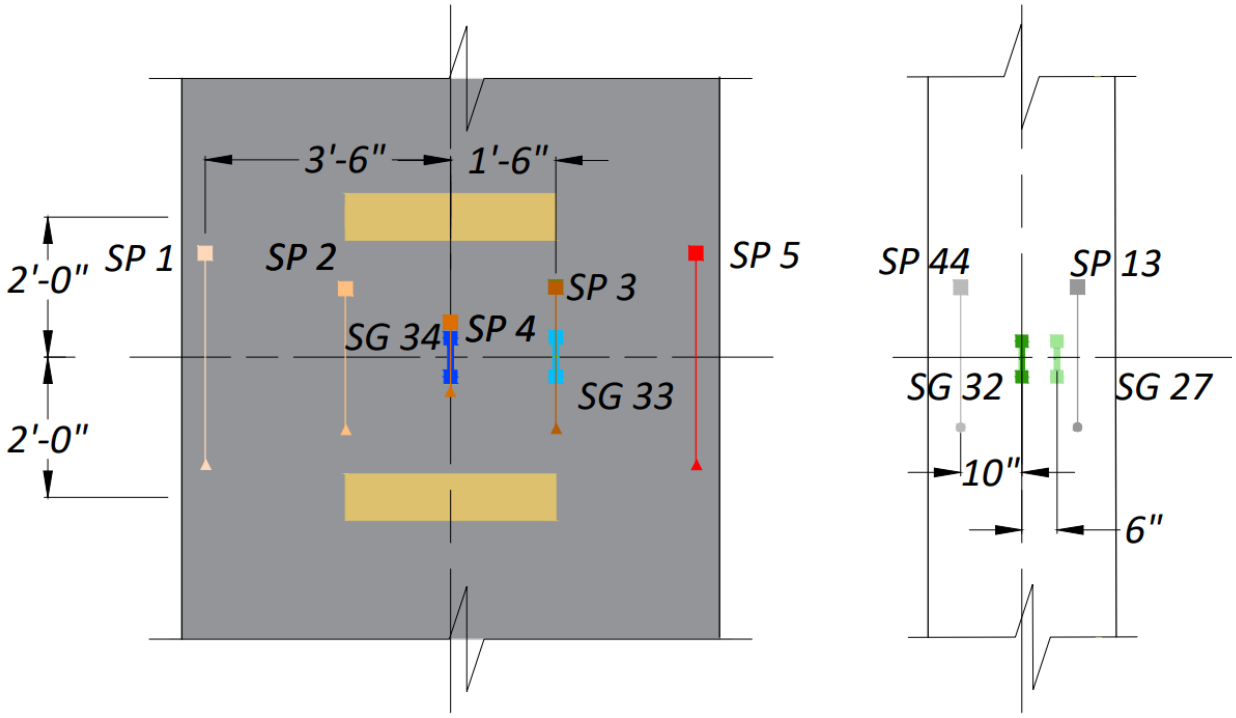

(a) Top of CC deck slab *(b) Underside of UHPC soffit*

Figure 5.34. Top and Bottom Instruments at Midspan for Tx54.

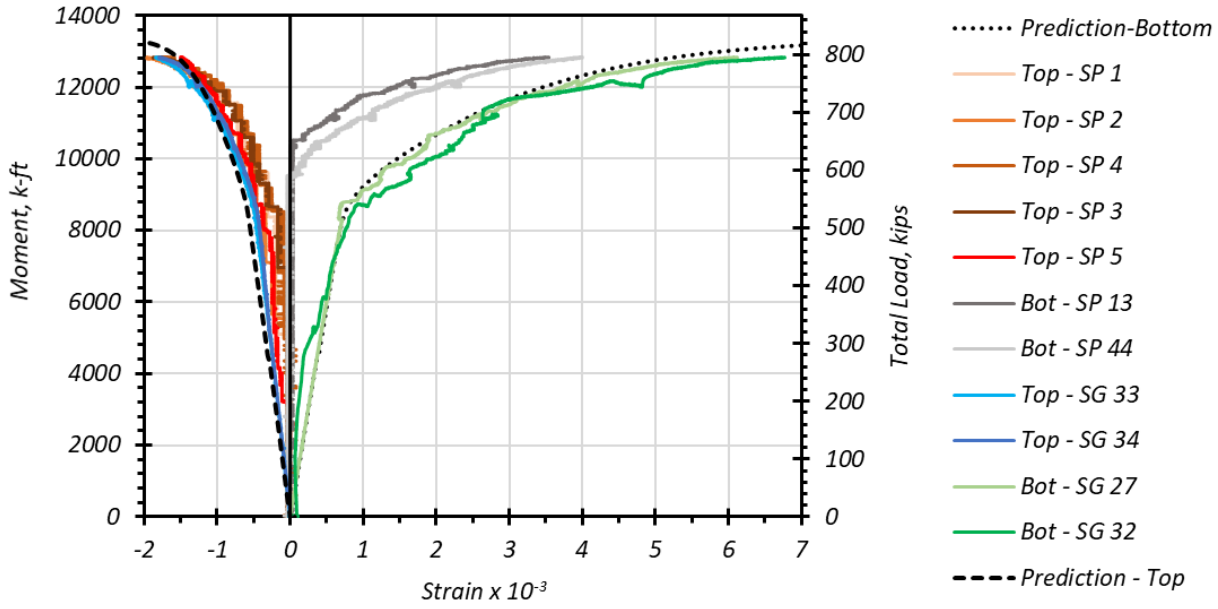

(a) Top and bottom strains (SP and SG)

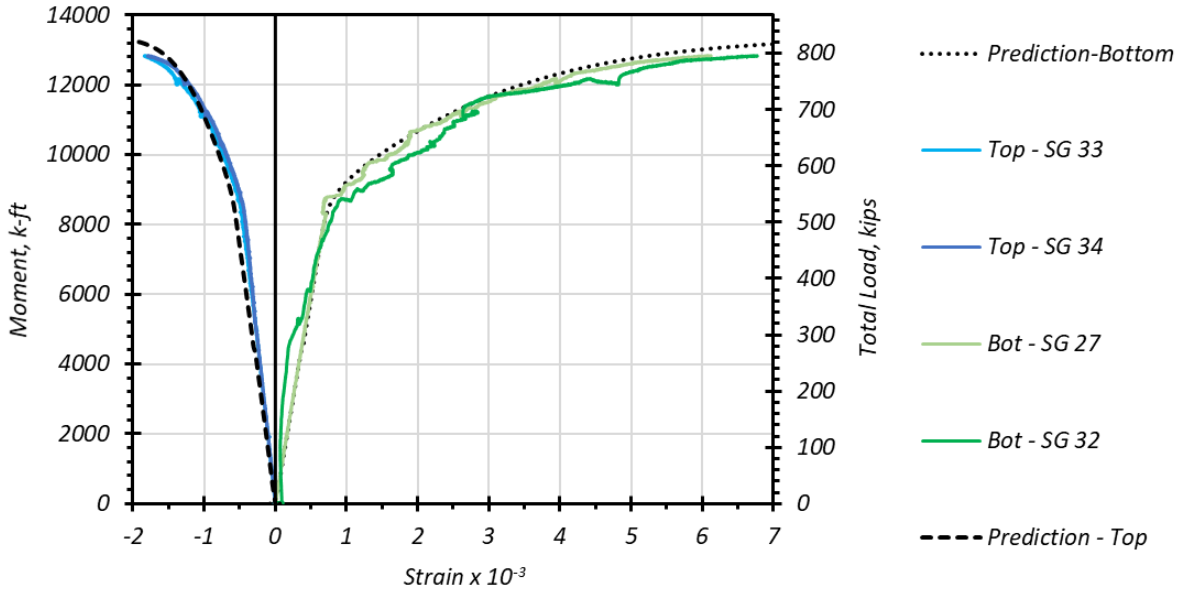

(b) Top and bottom strains (SG only)

Figure 5.35. Top and Bottom Strains at Midspan for Tx54.

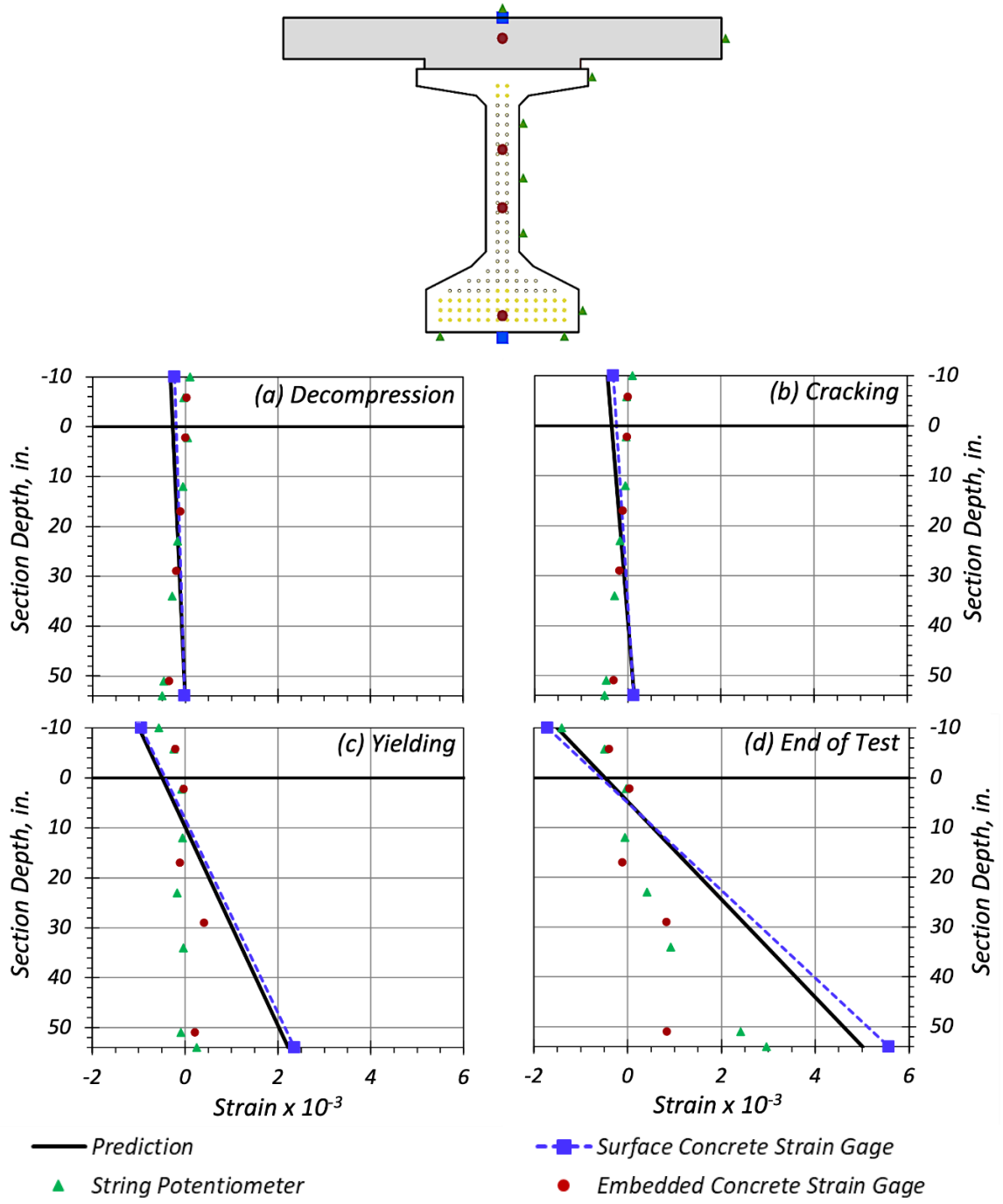

Notes:
1. The horizontal line at 0 in. depth marks the UHPC girder–CC haunch interface
2. Decompression: 362 kips (total actuator load)
3. Cracking: 462 kips (total actuator load)
4. Yielding: 708 (total actuator load)
5. End of Test: 800 (total actuator load)

Figure 5.36. Strain Profile for Tx54.

5.9 COMPARISON OF FLEXURE TEST RESULTS

The data from the flexure tests of Tx34-1, Tx34-2, and Tx54 girders specimens are further compared in this section. The flexural strength and the top and bottom strains in the constant bending moment region were selected as primary parameters of interest for the flexure test. The midspan deflections with the total actuator load were also documented.

5.9.1 Comparison of Moment Capacity and Demands

The service and factored demands based on the corresponding prototype bridge designed as per AASHTO (2020) are tabulated in Table 5.3. The nominal moment capacity values based on AASHTO (2020) for the design of the prototype are also listed in Table 5.3. The nominal capacity based on idealized and simplified stress-strain models, the experimental capacity, and the predicted capacity based on an iterative moment-curvature analysis using nonlinear stress-strain models are compared. Figure 5.37 presents a comparison of the flexure capacity of the three girders. The following observations are noted:

- The moment strength based on the maximum applied moment during testing was well above the service and factored load moments for the prototype bridges considered for each specimen. The average ratio of M/M_{test} for service was 0.48, while the average ratio of M/M_{test} for factored loading was 0.72.
- The nominal moment capacity values determined according to AASHTO (2020) were lower than the experimental capacities observed in full-scale testing, with an average ratio of M/M_{test} of 0.90.
- The predicted moment capacities based on Section 5.3 were slightly higher than the experimental capacities, with an average ratio of M/M_{test} of 1.03, indicating the approach used provides good estimates of the actual flexure strength.
- The flexure capacity was tested until a tensile strain of 0.009, 0.006, and 0.007, respectively, for Tx34-1, Tx34-2, and Tx54. Strain at the bottom of the girder was monitored by the strain gages installed at the bottom of the girder.
- Tx34-1, with 30 strands, showed the lowest capacity in flexure because of the lower prestressing force and lower tensile strength (0.53 ksi) of the mixture.

- Tx34-2 had more prestressing force (38 strands) than Tx34-1 and a slightly improved tensile strength (0.62 ksi). This specimen had a 31 percent higher experimental flexural capacity than Tx34-1.
- Tx54 had the highest prestressing force (48 strands) and the highest tensile strength among the three girder specimens (0.95 ksi).

Table 5.3. Summary of Moment Values for Girder Specimens.

Description of Moment	Tx34-1		Tx34-2		Tx54		Avg. M/M_{test}
	Moment, k-ft	M/M_{test}	Moment, k-ft	M/M_{test}	Moment, k-ft	M/M_{test}	
Service Load	2580	0.51	3065	0.47	6012	0.47	0.48
Factored Load	3870	0.77	4560	0.69	8763	0.68	0.72
Nominal	4750	0.95	5906	0.90	11,131	0.87	0.90
Predicted	5314	1.06	6720	1.02	13,140	1.02	1.03
M_{test}	5020	N/A	6562	N/A	12,860	N/A	N/A

Note: M_{test} is the maximum moment applied to the girder during flexure testing.
N/A: Not applicable.

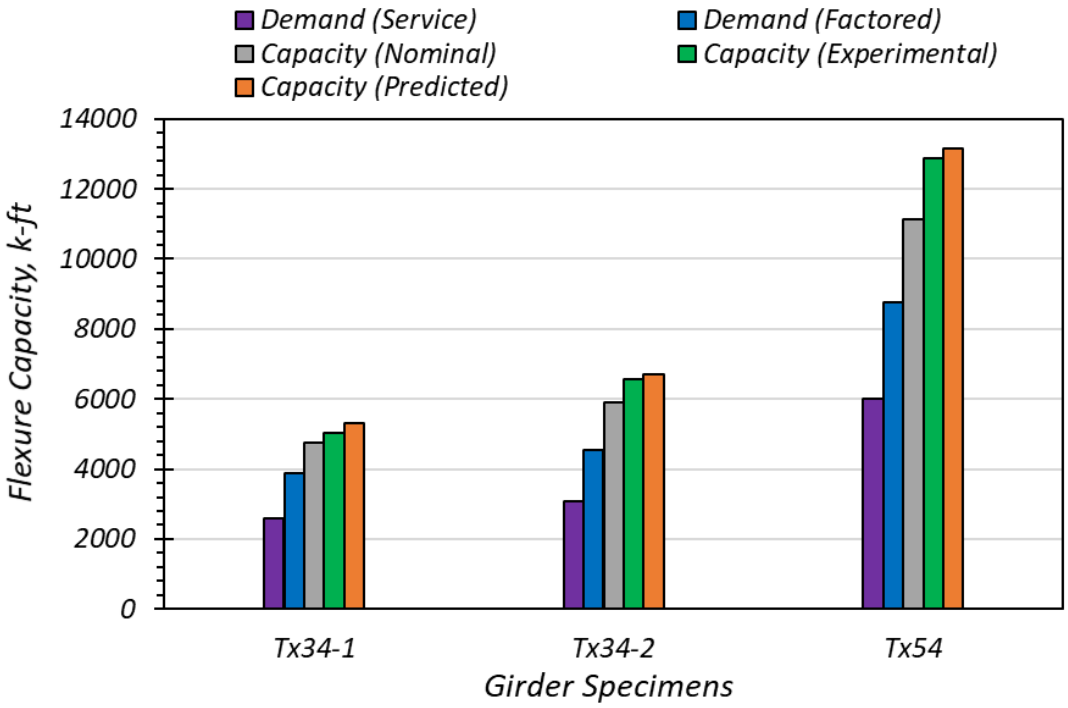

Figure 5.37. Flexure Capacity of Girder Specimens.

5.9.2 Moment-Curvature and Load-Deflection Response

Figure 5.38 presents a comparison of the moment-curvature and load-deflection plots for each of the girder specimens (Tx34-1, Tx34-2, and Tx54). The curvature progression through the testing

was computed from the top and bottom strains measured by strain gages and is expressed as a dimensionless ratio of the curvature and the total depth of the section (inclusive of the CC deck and haunch). The analytical predictions are based on the companion specimen material-level tests and plotted with experimental data using dashed lines for the moment-curvature and load-deflection plots. The analysis is explained in Sections 5.3 and 5.4.

For Tx34-1, the first cracking occurred prior to the factored demand being reached at the midspan. Due to the test being terminated after the widening of the shear crack, the plots of Tx34-1 also show an unloading branch of Phase I and a loading branch of Phase II. The disengaging of the actuator near the unreinforced end is indicated by a circle. The cracks observed at the service and factored demand stage were within serviceable limits (0.016 in.) recommended by Patnaik et al. (2017) under dry air exposure conditions.

All three specimens showed nearly linear elastic behavior for the midspan moment corresponding to service load demands for the prototype bridge with no cracking. Shear cracks did not develop prior to the factored demand load except for Tx34-1, upon which a premature shear crack occurred in the unreinforced region, and the initial visible cracking occurred a little over the factored demand load (at 32 kips higher than factored demand load).

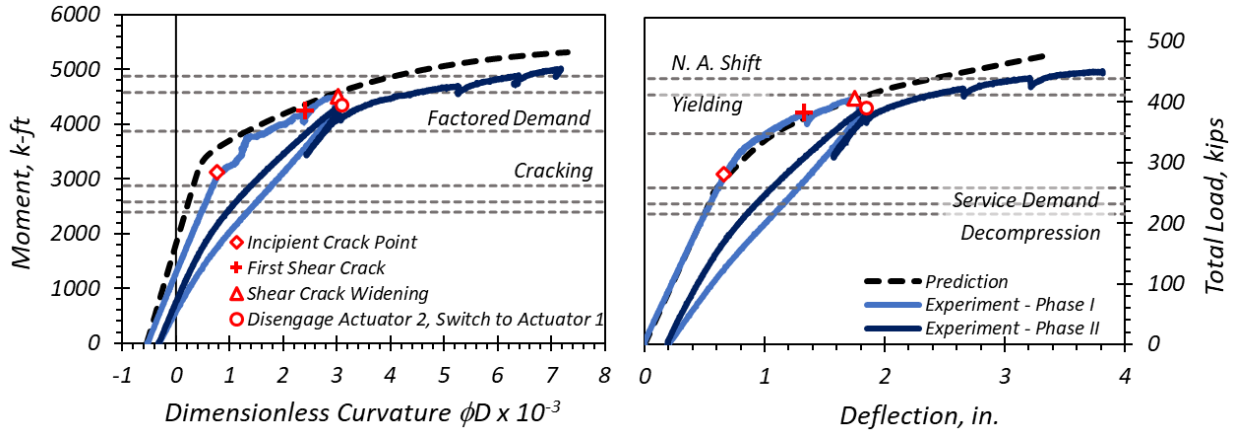

Phase I loading and unloading (light blue) followed by Phase II loading (dark blue).

(a) Tx34-1

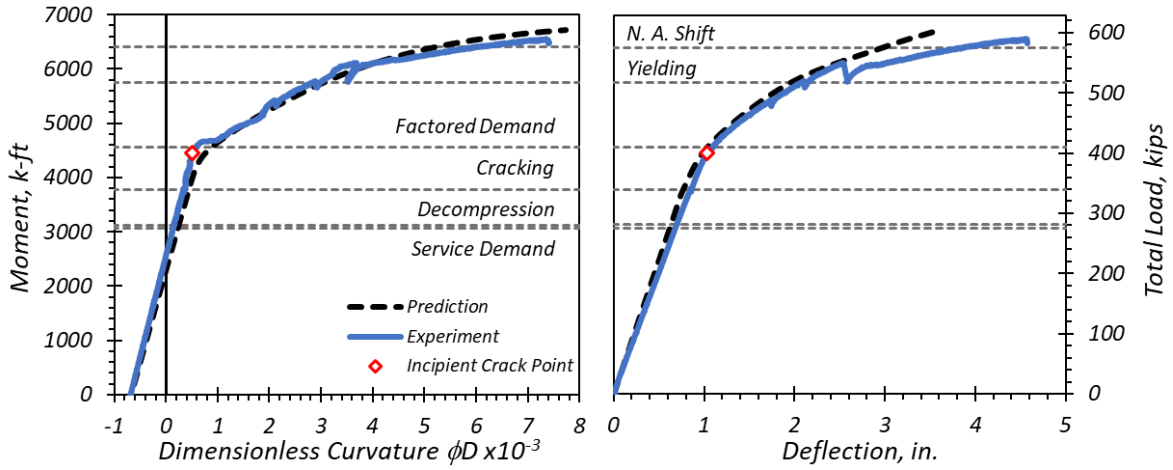

(b) Tx34-2

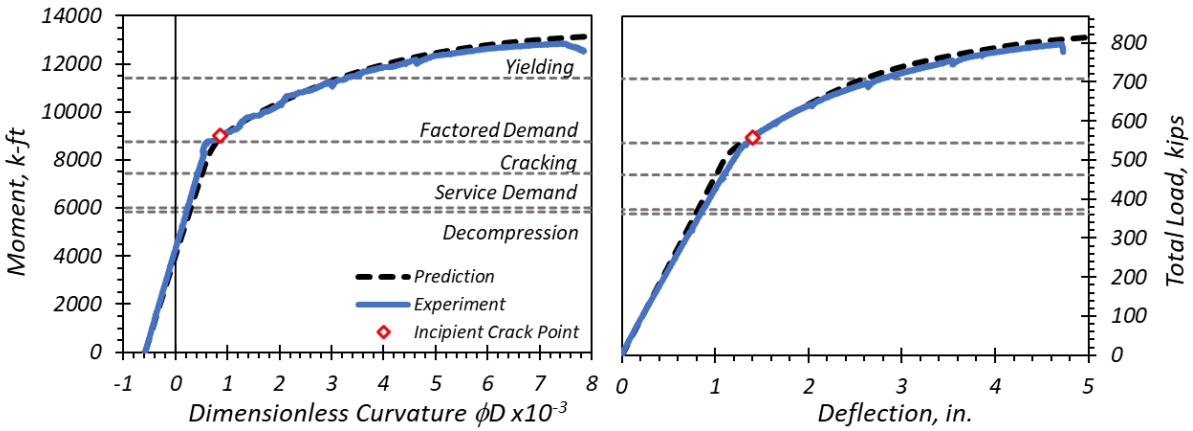

(c) Tx54

Figure 5.38. Moment-Curvature and Load-Deflection Plots under Flexure Test.

5.9.3 Comparison of Crack Widths

Table 5.4 presents the crack width range for all three girders at termination of testing. The cracks were mostly hairline cracks (0.004 in.), with some widening to 0.008 in., 0.010 in., and 0.012 in. for Tx34-1, Tx34-2, and Tx54 girders, respectively. The cracks on the underside of the girders widened upon crack localization to 0.019 in., 0.018 in., and 0.060 in. for Tx34-1, Tx34-2, and Tx54 girders, respectively. Crack widths in the range of 0.010–0.015 in. are considered to be within the aesthetic acceptable limits under service conditions as per Patnaik et al. (2017). When the structure is subjected to service loads, under dry conditions the acceptable crack width is 0.016 in., and in humid conditions, the acceptable crack width is 0.012 in. (ACI 224R-08 2001). ACI 224R-08 (2001) also recommends a 0.007 in. limit on crack width for bridge decks subjected to deicing chemicals and a limit of 0.006 in. when subjected to spraying of sea water or cycles of wetting and drying. The widest cracks at the soffit for the flexure test of Tx34-1 had the maximum width when compared to the other two specimens, which may be due to the lower tensile strength of the Tx34-1.

Table 5.4. Crack Widths at Termination of Flexure Tests.

Description	Tx34-1	Tx34-2	Tx54
Crack Width Range at Maximum Load, in.	0.004–0.008	0.004–0.010	0.004–0.012
Maximum Crack Width at Girder Soffit, in.	0.19	0.12	0.060
Load Stage, kips	478	604	800

5.10 SUMMARY

A four-point bending full-scale test was conducted on each of the three UHPC girder specimens to simulate the prototype load conditions at the midspan. The response of the specimens in the constant bending moment region was monitored by a suite of sensors. The responses included the strains and deflections to compute the moment-curvature and load-deflection of the specimen through the progression of load. Based on the analysis conducted as per the procedures elaborated on in Section 5.3 and 5.4 and the full-scale testing observations documented in Sections 5.5, 5.7, and 5.8, the following conclusions were drawn:

1. *General flexural performance of girder specimens*. The following general observations were made with respect to the flexural response and behavior of the girder specimens.

- Overall, the flexure performance of the three specimens was adequate for the design loads of the corresponding prototype bridge, and the behavior of all the specimens in flexure was ductile even at the peak loads.
- The maximum flexure capacity of the specimens under flexure prior to destructive damage to the beam was recorded. The girders were to be preserved for subsequent shear tests of both the ends. Therefore, the tests were terminated after crack localization was observed in the constant bending moment region. Tensile strains of approximately 0.009, 0.006, and 0.007 were observed at the peak loads for Tx34-1, Tx34-2, and Tx54, respectively.
- There was no cracking observed at service and factored demand conditions.
- Up to service level demand, all three specimens showed linear response without cracking. The service load was lower than the experimental capacity by 49 percent, 53 percent, and 53 percent for Tx34-1, Tx34-2, and Tx54, respectively.
- At factored level demand, some nonlinearity was observed accompanied by incipient cracking. However, the cracks were well within serviceable widths. The factored demand load was lower than the experimental capacity by 23 percent, 31 percent, and 32 percent for Tx34-1, Tx34-2, and Tx54, respectively.
- The flexural performance of the girder was significantly impacted by the material properties of the girder, especially the tensile strength of UHPC. This finding was consistent with the analytical evaluation that showed a direct relationship between the performance of a specimen and the material strength of each of its components. In addition to the material test properties of the components of the specimen, the flexure capacity is also dependent on the span length, type of girder shape, and the type (harped or eccentric) and number of prestressing strands.

2. *Individual girder flexural performance*. With respect to the flexural response and behavior of the individual girder specimens, the following observations were made:
    - *Tx34-1*. This girder specimen had an eccentric strand layout with the lowest prestressing force. The tensile strength (first cracking strength of 0.53 ksi and peak strength of 0.6 ksi) of the companion samples for the girder specimen was lower than the design assumption for the specimen, which led to a shear failure at the girder end without transverse reinforcement before the flexure failure. Therefore, after the shear

crack widening at the unreinforced end, the actuator at the end near the unreinforced end was disengaged, and the actuator near the reinforced end continued to be loaded until flexure crack localization occurred. The specimen had a maximum measured flexure capacity of 5020 k-ft. Based on the companion prototype bridge design, the service demand was 49 percent lower than the experimental capacity, and the factored demand load was 23 percent lower than the experimental capacity. The crack widths ranged from hairline to 0.008 in., and the localized flexure crack that occurred at the underside of the girder was 0.19 in. wide. Overall, the flexural performance was ductile due to the crack bridging property of the fibers. Because of the slightly higher flow of the Tx34-1 UHPC mixture, fiber settlement was observed in the material-level companion specimens. There may have been similar settlement at the bottom of the Tx34-1 girder, which would tend to enhance the girder flexure performance despite the low tensile strength of the companion material-level specimens.

- *Tx34-2.* This specimen had more prestressing force than Tx34-1, a harped strand layout, and improved tensile strength (first cracking strength of 0.62 ksi and peak strength of 0.7 ksi). The maximum measured flexure strength of this specimen was 6562 k-ft. Based on the companion prototype bridge design, the service demand was 53 percent lower than the experimental capacity, and the factored demand load was 31 percent lower than the experimental capacity. The crack widths at maximum loading ranged from hairline to 0.01 in., with a localized flexure crack at the soffit widening to 0.12 in. at maximum loading. Because the tensile capacity of this specimen was slightly better than the Tx34-1 girder and there was shear resistance due to harping of strands, there was no premature shear failure.
- *Tx54.* This specimen exhibited enhanced performance in flexure relative to the first two girder specimens. The Tx54 specimen had the highest prestressing force, a harped strand layout, and tensile strength comparable to the strengths achieved in the laboratory mixture (first cracking strength of 0.95 ksi and peak strength of 1.16 ksi). There was no damage to the shear ends while conducting the flexure test. The maximum measured flexure strength of this specimen was 12,860 k-ft. Based on the companion prototype bridge design, the service demand was 53 percent lower than the experimental capacity, and the factored demand load was 32 percent lower than the

experimental capacity. The cracks in the flexure region ranged from hairline to 0.012 in. at maximum loading. The localized crack at the soffit was 0.06 in. wide at maximum loading. The behavior of the girder was ductile, and the test was terminated at a tensile strain on the bottom soffit of 0.006 to preserve the girder for further testing.

3. *Analysis and design.* With respect to analysis and design for flexure, the following observations were made based on the design and predicted response versus the measured response:
    - The standard first principles of mechanics were found to be effective in predicting the behavior of the UHPC girder specimens with a composite CC deck.
    - Nonlinear stress-strain models were used for the CC deck and UHPC to run an iterative moment-curvature analysis to predict the behavior of the girder specimens under flexure. Load-deflection analysis was conducted to predict the elastic and post-cracking deflection behavior of the specimens:
        - The predictions were largely dependent on the material properties of the girders. The material models used for the analysis had to be modified to account for the assumptions needed to model the behavior of UHPC with higher tensile strength from the steel fibers.
        - The standard analytical methods for the moment-curvature and load-deflection were found to be applicable to the standard TxDOT composite bridge section with a UHPC girder. The predictions of the flexural capacity were within 90 percent of the maximum measured flexure strength of the girders.
    - The flexural design based on AASHTO LRFD Bridge Design Specifications (AASHTO 2020) is adequate for the standard service and factored demand loads that a prototype bridge would be subjected to in the field. More details regarding the suitability of these assumptions are explained in Section 5.5 and in the recommendations provided in the Volume 3 report.

6 FULL-SCALE SHEAR TESTS OF UHPC GIRDERS

Full-scale shear tests were conducted for the three precast, pretensioned UHPC girder specimens tested in flexure (Chapter 5). The shear analysis and design of the prototype and specimen were based on the standard shear capacity computations with modifications made to account for the enhanced tensile capacity of UHPC from the added steel fibers. The shear design values assumed prior to girder fabrication were determined using the material-level test properties of the laboratory and the precast plant trial batch specimens. The analysis was conducted again after the fabrication of the specimens using the tensile and compressive strengths measured from material-level tests conducted using companion specimens cast with the girder at the precast plant.

Chapter 4 details the girder specimens. Section 4.5 documents the details of the material-level testing of the companion specimens. Section 6.1 elaborates on the shear capacity analysis that was implemented for the analysis prediction. The shear capacity of the prototype bridge girders was tested by loading the shear span at the ends of the girder specimens. Section 6.2 contains the test setup, loading details, and instrumentation. The shear tests were conducted for the Tx34-1, Tx34-2, and Tx54 girder specimens, and the details and observations are documented in Sections 6.3, 6.4, and 6.5, respectively. Section 6.5.2 compares the results of the shear tests. Section 6.7 summarizes the overall conclusions drawn from the full-scale UHPC girder shear tests.

6.1 SHEAR CAPACITY ANALYSIS

6.1.1 General

The analysis of the shear capacity of the girder specimens, consisting of full-scale composite precast, pretensioned UHPC girders with a CC deck, was based on the first principles of mechanics. The parameters used to predict the expect shear strength are consistent with the most recent research findings available at the time of the design and analysis of the prototype and specimens (Graybeal and El-Helou 2021; Tadros 2021).

The literature and existing code provisions supports the intuitive notion that the shear capacity will be directly dependent on the tensile strength of UHPC imparted by the presence of the steel fibers (AFGC 2013; Baby et al. 2014a; Voo et al. 2010). The crack bridging capacity of the UHPC fibers enhances the shear strength of the UHPC, enabling a more ductile failure as opposed to the brittle

failure of CC. Therefore, the shear capacity of UHPC differs from that of CC in that there is an additional parameter—the tensile strength of concrete. In this study, the tensile strength of concrete was taken as the measured first cracking strength of UHPC companion specimens that were cast along with the respective girder specimens for the purpose of shear capacity computations.

6.1.2 Related Design Codes and Recommendations

Design codes and research studies in the recent past such as AFGC (2013), El-Helou and Graybeal (2022b), and Tadros (2021) computed the shear capacity of UHPC girders as a combination of the shear resistance provided by the concrete, steel fibers, and transverse steel.

6.1.2.1 AFGC (2013)

The ultimate shear resistance of UHPC considers the contribution of the steel fibers in addition to the shear strength attributed to the concrete and reinforcing steel, as shown in Equation (6.1), as per AFGC (2013).

$$V_{Rd} = V_{Rd,c} + V_{Rd,s} + V_{Rd,f} \tag{6.1}$$

where:

$V_{Rd,c}$ = Concrete term, kips

$V_{Rd,s}$ = Shear reinforcement term, kips

$V_{Rd,f}$ = Fiber term, kips

Section 3.4.2 of Chapter 3 elaborates on the detailed method and definition of the terms.

6.1.2.2 AASHTO Draft Specifications (2022)

FHWA (2022) recommended—based on research by FHWA and other studies (Baby et al. 2014a; El-Helou and Graybeal 2022b; El-Helou and Graybeal 2023; Vecchio and Collins 1986)—the following expression for the shear capacity of UHPC when the contribution of the fiber and the concrete matrix is taken into consideration as a single term.

$$V_{UHPC} = \gamma_u \, f_{t,loc} \, b_v \, d_v \cot(\theta) \quad (6.2)$$

where:

γ_u = Reduction factor that adjusts the variability arising from the UHPC direct uniaxial tensile strength test parameters, ≤0.85.

$f_{t,loc}$ = Crack localization strength, ksi

b_v = Width of web section, in.

d_v = Effective shear depth, in.

θ = Shear crack angle, degrees

FHWA (2022) and El-Helou and Graybeal (2023) recommended the use of $f_{t,cr}$ if $f_{t,loc} < 1.20 f_{t,cr}$, where $f_{t,cr}$ is the effective cracking strength.

6.1.2.3 PCI Recommendations

Tadros (2021) presented the following expression for the shear capacity computation developed as part of the PCI design guidance for UHPC (further information and details are to be released following Phase II of the PCI study on UHPC):

$$V_{cf} = (4/3) f_{rr} b_v d_v \cot(\theta) \quad (6.3)$$

where:

f_{rr} = Cracking tensile strength, ksi assumed as 1 ksi

b_v = Width of web section, in.

d_v = Effective shear depth, in.

θ = Shear crack angle, degrees, computed according to AASHTO (2020)

6.1.3 Shear Strength Prediction for This Research

6.1.3.1 Components of Shear Capacity

For the present research, the total shear capacity or nominal shear resistance V_n of the UHPC section was computed by evaluating the shear resistance provided by UHPCV_{UHPC}, transverse steel reinforcement V_S, and the prestressing force component in the shear force direction V_P. It can be expressed as follows:

$$V_n = V_{UHPC} + V_S + V_P \quad (6.4)$$

where:

V_n = Nominal shear resistance, kips

V_{UHPC} = Nominal shear resistance of UHPC, kips

V_S = Shear resistance provided by transverse steel reinforcement, kips

V_P = Prestressing force component in the direction of the shear force (vertical component), kips

The three components of the shear capacity are computed using the following expressions:

$$V_{UHPC} = f'_t b_w d_v \cot(\theta) \quad (6.5)$$

$$V_S = \frac{A_v f_y d_v \cot(\theta)}{s} \quad (6.6)$$

$$V_P = N_h A_p f_{pe} \sin(\alpha) \quad (6.7)$$

where:

f'_t = First cracking tensile strength of UHPC, ksi

b_w = Width of web section, in.

d_v = Effective shear depth, in.

θ = Shear crack angle, degrees

A_v = Area of transverse steel reinforcement, in^2

f_y = Yield strength of transverse steel reinforcement, ksi

s = Vertical spacing of transverse steel reinforcement, in.

N_h = Number of harped strands

A_p = Cross-sectional area of an individual prestressing strand, in^2.

f_{pe} = Effective stress in prestressing strands after losses, ksi

α = Angle of harping, degrees

The depth of the specimen cross-section d_v was assumed to be 80 percent of the overall depth h of the section in accordance with ACI 318-19 Section 22.5.2.1 (ACI Committee 318 2019). The overall depth h was taken in this study to include the deck slab and haunch because the composite

deck depth tends to provide a slightly increased shear resistance to that of a noncomposite girder section. For example, the shear capacity with the inclusion of the slab in the shear depth for the Tx54 unreinforced end (without the shear contribution from harped tendons) is 597 kips, while the capacity without the inclusion of the deck slab is 573 kips. Therefore, the difference in the shear capacity based on the shear depth alone is 24 kips.

6.1.3.2 First Cracking Tensile Strength

The first cracking tensile strength of UHPC f'_t for the girder specimens was obtained as measured from the material-level tests. Estimates were made based on the average first cracking strength for each girder taken from the material-level tests (direct uniaxial tensile strength test). In addition, because the tensile strength of the UHPC in the web of the UHPC girder could vary among the samples tested at the material-level, upper bound and lower bound predictions—depending on the maximum and minimum measured tensile strength at first cracking—were also developed for the shear capacity.

6.1.3.3 Shear Crack Angle for Experimental Predictions

The crack angle was computed using a Mohr's circle analysis to predict the angle of the first crack in the web. The crack angle is developed based on the shearing stress and axial compressive stress (Lin and Burns 2010). The shearing unit stress distribution across the cross-section of the specimen can be determined using Equation (6.8).

$$v = \frac{VQ}{Ib} \tag{6.8}$$

where:

V = Shear force carried by the section under consideration, kips

Q = Statical moment of cross-sectional area above that level about the centroidal axis, in^3

I = Moment of inertia of the cross-section, in^4

b = Width of the cross-section at that level, in.

By using the shearing unit stress and axial compressive stress, the maximum principal tensile stress can be calculated from Equation (6.9).

$$f''_t = \sqrt{v^2 + \left(f_c/2\right)^2} - \left(f_c/2\right) \quad (6.9)$$

where:

f_c = Axial compressive stress, ksi

The crack angle θ can be obtained from the Mohr's circle as shown in Equation (6.10):

$$\theta = \frac{1}{2}\tan^{-1}\left(\frac{2v_{max}}{f_c}\right) \quad (6.10)$$

where:

v_{max} = Maximum shear stress, ksi

A fiber analysis was conducted to determine the shear stress distribution along the depth of the section using a computer-generated program, and the maximum shear stress was computed for the nominal shear force capacity of the respective girder specimens. The initial nominal shear force for this calculation was computed using the method recommended by AFGC (2013). For the method explained, the shear force used to compute the shear stress is the shear demand at the time when shear cracks were developed during the flexure test. This analysis was conducted to accurately predict the likely shear capacity of the girder ends to plan the actuator load and position such that the shear ends could be tested to failure. Table 6.1 presents the cracks angles computed for the three girders for the initial analysis for the cracks.

Table 6.1. Analytical Crack Angle versus Measured Crack Angle.

Specimen	Transverse Reinforcement	Measured Crack Angle	Crack Angle Based on Mohr's Circle	Percent Difference
Tx34-1	None	32°	25.3°	−21%
Tx34-1	Minimum	34°	28.7°	−16%
Tx34-2	None	20°	24.1°	21%
Tx34-2	Minimum	26°	27.1°	4%
Tx54	None	28°	29°	4%
Tx54	Minimum	29.5°	31°	5%

Based on the computed crack angles, the shear capacity of the girder specimens was predicted to plan the test setup, loading, and instrumentation. At the termination of the flexure tests, the shear

cracks formed were measured to compute the refined shear capacity of the girder to estimate the load required for testing the girder specimens for each shear test. The experimentally measured crack angles were within 20 percent of the analytically computed crack angles, with the exception of Tx34-1 (no transverse reinforcement end), for which the experimental results were within 27 percent of the analytical value.

6.1.3.4 Shear Crack Angle for Design

Based on the mechanics approach, the crack angle can be computed as per the Mohr's circle for the initial design purposes. A modified version of Equation (6.10) may be used for computing this angle as follows:

$$cot(\theta) = \sqrt{1 + \left|\frac{f_c}{f_t'}\right|} \tag{6.11}$$

where:

f_c = Axial compressive stress, ksi = F/A
f'_t = Uniaxial tensile stress, ksi
F = Prestressing force after losses, kips
A = Area of the girder, in^2

The design shear capacity of UHPC is computed using the following equation:

$$V_{UHPC} = f'_t b_v \, d_v \cot(\theta) \tag{6.12}$$

where:

f'_t = Uniaxial tensile stress, ksi
b_v = Width of web section, in.
d_v = Effective shear depth, in.
θ = Shear crack angle, degrees

The shear design capacity was computed for the three girder specimens using the methods explained in Section 6.1.2 and this section. The capacities (inclusive of contribution from UHPC, transverse steel, and harped tendons where applicable) are compared to the experimental capacity for the unreinforced and reinforced ends in Table 6.2 and Table 6.3, respectively. The

computations based on AFGC (2013) are observed to be conservative, while the FHWA (2022) results and predictions based on the shear crack angle for design explained in Section 6.1.3.4 are less conservative and simpler to use. The PCI method presented to the AASHTO T-10 Committee by Tadros (2021) used the assumption that the tensile strength was 1 ksi due to the limited information on this term. FHWA (2022) results and predictions based on Mohr's circle relate the contribution of shear from UHPC to the first cracking tensile strength of UHPC measured from the uniaxial direct tension test.

Table 6.2. Unreinforced End—Shear Capacity Comparison.

	Tx34-1		Tx34-2		Tx54	
Unreinforced End	**Shear Capacity, kips**	**Percent Difference**	**Shear Capacity, kips**	**Percent Difference**	**Shear Capacity, kips**	**Percent Difference**
Experimental	202	N/A	449	N/A	761	N/A
AFGC (2013)	221	9%	263	−41%	542	−29%
FHWA (2022)	337	67%	395	−12%	607	−20%
Tadros (2021)	426	111%	438	−2%	660	−13%
Prediction	266	32%	334	−26%	631	−17%

Note: N/A: Not applicable.

Table 6.3. Reinforced End—Shear Capacity Comparison.

	Tx34-1		Tx34-2		Tx54	
Method	**Shear Capacity, kips**	**Percent Difference**	**Shear Capacity, kips**	**Percent Difference**	**Shear Capacity, kips**	**Percent Difference**
Experimental	413	N/A	592	N/A	777	N/A
AFGC (2013)	284	−31%	325	−45%	636	−18%
FHWA (2022)	398	−4%	464	−22%	713	−8%
Tadros (2021)	492	19%	504	−15%	757	−3%
Prediction	344	−17%	413	−30%	729	−6%

Note: N/A: Not applicable.

6.1.3.5 Predicted Shear Strengths

Prior to testing the full-scale girder, the shear strength for each girder end was predicted; the goal was to estimate the actual shear strength in the test as closely as possible. Table 6.4 summarizes the parameters used to determine the shear strength predictions. The predicted shear strength is provided based on the average measured tensile strength at first cracking from the material-level direct uniaxial tension tests of the companion samples. In addition, Table 6.5 provides the upper and lower bound measurements used to provide upper and lower bound predictions of strength for

each girder. The effective stress after losses f_{pe} was calculated based on the long-term prestress losses, which include loss due to shrinkage, creep, and relaxation of steel. Angle α is the angle of inclination of the harped strands with respect to the horizontal longitudinal axis of the girder. The prestress losses for the design and analysis of the specimen are based on the recommendations from eConstruct (2020). Chapter -2075909280.□ documents the prestressed losses estimated from the findings of this research.

Table 6.4. Parameters and Predictions of Shear Capacity.

Parameter		Tx34-1	Tx34-2	Tx54
UHPC	f'_t, ksi	0.53	0.625	0.95
	b_w, in.	7	7	7
	d_v, in.	35.6	35.6	51.6
	θ, degrees	32	20	28
	V_{UHPC}, kips	211	428	645
Reinforcing Steel	A_v, in^2	0.4	0.4	0.4
	f_y, ksi	65	65	65
	s, in.	24	24	24
	V_S, kips	62	106	105
Prestressing Strand	N_h	0	6	8
	A_p, in^2	0.217	0.217	0.217
	f_{pe}, ksi	156.5	150.3	155.1
	α, degrees	0	4.8	6.0
	V_P, kips	0.00	16.24	28.24
Total	$V_{n,Unreinf}$, kips	**211**	**444**	**674**
	$V_{n,Reinf}$, kips	**273**	**550**	**779**

Table 6.5. Upper Bound and Lower Bound Shear Capacity.

Specimen	Type	First Cracking Tensile Strength	Shear Force, kips	
			Unreinforced	Reinforced
Tx34-1	Upper Bound	0.625	249	311
	Prediction	0.53	211	273
	Lower Bound	0.4	160	221
Tx34-2	Upper Bound	0.75	530	636
	Prediction	0.625	444	550
	Lower Bound	0.55	393	499
Tx54	Upper Bound	1.1	775	881
	Prediction	0.95	674	779
	Lower Bound	0.8	572	677

Section 6.5.2 provides a quantitative comparison of the shear capacity using different approaches of the code-based provisions.

6.2 TEST SETUP, LOADING DETAILS, AND INSTRUMENTATION

Each of the three full-scale UHPC precast, pretensioned girder specimens with CIP deck slabs were first tested in flexure, as documented in Chapter 5. After completing the flexural testing, the load setup was adjusted to further evaluate the girder response and capacity in shear by testing each girder end. The shear test of the two ends also allowed a comparison of the shear capacity through the web with and without the use of minimum transverse steel reinforcement. The effect of harping some of the prestressing tendons was also compared. Tx34-1 is designed with all eccentric tendons, while the Tx34-2 and Tx54 specimens have some harped prestressing strands. The following sections describe the test setup, loading details, and the instrumentation plan for the shear tests. Chapter 4 provides additional information, including reinforcement details and dimensions for the girder specimens, along with additional instrumentation details.

6.2.1 Overall Description

Testing to determine the shear response and capacity of the unreinforced end (without transverse reinforcement hoops) and the reinforced end (with transverse reinforcement hoops) of each girder was conducted after testing the specimens in flexure. In cases when prominent cracking occurred after the flexure test, the span length of the specimens for the shear test was modified as necessary by adjusting the position of the pedestals to avoid any possible impacts on the shear capacity

occurring due to the cracks that formed during the flexural testing. Two 600-kip actuators were used to load the girder specimens in shear. The loading arrangement was determined depending on the damage during flexure testing and the expected shear strength at each girder end. Each girder specimen was loaded at 0.5 kip per second under force control during load testing. The goal while planning the test setup was to maintain a span-to-depth ratio greater than 2:1 for each shear test. Each end of a girder specimen differed in terms of the presence of transverse reinforcement and other minimum end reinforcement such as bursting reinforcement and bottom flange reinforcement, which were absent in the unreinforced end. Chapter 4 provides the reinforcement details.

The instrumentation and test setup were adjusted as appropriate after each test based on the lessons learned, maximum actuator capacity, and the state of damage and cracking after prior load testing of the specimen under flexure or shear. The location of the actuators and the spacing between the actuators were decided based on shear analysis of the specimens prior to testing to ensure shear failure occurred in the region of interest. This step was done to ensure that the capacity of the specimen found experimentally was representative of the shear critical regions of the bridge span length and that the capacity being measured was not overestimated due to a strut-mechanism forming at the support. The location of the actuators and the spacing were also somewhat limited by the physical constraints of installing the frames from which the actuators were suspended, which was governed by the location of the tie-down holes located at 3 ft spacing in the laboratory strong floor.

6.2.2 Instrumentation and Crack Angle Measurement Using LVDTs

Based on the observed shear cracks at the unreinforced and the reinforced ends following flexure testing, the locations for the instruments for further testing of each girder end were determined. Surface strain gages and KSG were installed such that one gage was located parallel to the existing cracks, and the other gage was located transverse to the existing cracks. These sets of parallel and transverse gages were installed at the ends of interest, and the locations of these gages were influenced by (a) the location of cracks formed due to prior testing, (b) the intact surface area available to mount the gage fixtures and LVDT fixtures, and (c) the most probable location estimated for shear failure during the pretest analysis. These locations were modified for each specimen to optimize the information obtained from the sensors.

Similar to the flexure test, to provide redundancy, SPs of 4 in. stroke and 12 in. stroke were used. The strains in the region between the actuators were also measured with the use of SG and SPs mounted on the top of the slab and at the bottom surface of the girder.

At the probable crack location, a set of LVDTs were installed in the vertical and horizontal direction and in the direction parallel and perpendicular to the shear cracks. The strains measured by the LVDTs horizontal, vertical, and parallel to the crack were used to compute the crack angle based on Mohr's circle principle using the following equations:

$$\theta = \frac{1}{2}\tan^{-1}\left(\frac{\gamma_{xy}}{\varepsilon_y - \varepsilon_x}\right) \tag{6.13}$$

where:

θ = Shear crack angle, degrees

ε_x = Strain component in the *x*-direction

ε_y = Strain component in the *y*-direction

γ_{xy} = Shear strain

The strain components were calculated by resolving the strain rosette measurements as follows:

$$\begin{bmatrix}\varepsilon_a \\ \varepsilon_b \\ \varepsilon_c\end{bmatrix} = \begin{bmatrix}\cos^2(\theta_a) & \sin^2(\theta_a) & \sin(\theta_a)\cos(\theta_a) \\ \cos^2(\theta_b) & \sin^2(\theta_b) & \sin(\theta_b)\cos(\theta_b) \\ \cos^2(\theta_c) & \sin^2(\theta_c) & \sin(\theta_c)\cos(\theta_c)\end{bmatrix}\begin{bmatrix}\varepsilon_x \\ \varepsilon_y \\ \gamma_{xy}\end{bmatrix} \tag{6.14}$$

where:

ε_a = Strain obtained from horizontal LVDT

ε_b = Strain obtained from LVDT parallel to the crack

ε_c = Strain obtained from vertical LVDT.

θ_a = Angle of horizontal LVDT to the horizontal axis, 0 degrees

θ_b = Angle of diagonal LVDT to the horizontal axis, 30 degrees

θ_c = Angle of vertical LVDT to the horizontal axis, 90 degrees

The above system of equations is solved for ε_x, ε_y, and γ_{xy}, and these parameters are used in Equation (6.14) to determine the crack angle for each data point. The crack angle computed from the LVDT rosette installed in the shear span is reported in Section 6.5.2.

6.2.3 Tx34-1 Girder Specimen

For the first girder specimen tested, Tx34-1, the unreinforced end developed shear cracks during flexural testing prior to the flexure failure. Therefore, the test setup for the shear test of the unreinforced end was the same as for that of the flexure test of Tx34-1 presented in Section 5.2.1 and Figure 5.1. The ends were instrumented with an LVDT frame to obtain the strain rosette data for computing the principal strain and crack angle. The LVDTs were located based on the estimated flexure-shear interaction analysis prior to testing. Figure 6.1 shows the test setup and instrumentation for the shear test of the reinforced end of Tx34-1. Figure 6.2 presents the photos of the shear test setup of the reinforced end of the Tx34-1 specimen. The crack localization at the midspan after the first flexure test led to the formation of a wide crack at the bottom flange, and a pedestal was inserted such that the center of the bearing pad was 9 in. from the crack to ensure an intact span for the shear testing of the reinforced end. Table 6.6 presents the location of the SPs as the end of the girder being tested.

Table 6.6. Location of SPs for Tx34-1 Shear Tests.

SP ID	SP-1	SP-2	SP-3	SP-4	SP-5	SP-6	SP-7	SP-8	SP-9	SP-10
Stroke, in.	4	4	4	4	4	12	12	4	4	4
Distance, ft	−0.75	1.2	2.8	5.8	8.5	8.8	10.2	11.8	13.2	14.8

Notes:

1. The distance is measured from the centerline of the west-bearing pad
2. The direction from west to east is considered positive
3. The SPs at the ends record the uplift (if any) of the girder ends

6.2.4 Tx34-2 Girder Specimen

Figure 6.3 and Figure 6.5 present the test setup and instrumentation for Tx34-2 Shear Test 1 and Shear Test 2, respectively. Figure 6.4 and Figure 6.6 present the photos of the test setup. The first test setup was targeted at maintaining a span-to-depth ratio greater than 2:1, while forcing shear failure simultaneously at two ends. The unreinforced end failed under this setup; however, the reinforced end had a much higher shear capacity that required an additional shear test at that end using two actuators. This specimen was estimated to have slightly higher tensile strength than

Tx34-1 based on material testing of companion specimens and had harped tendons that improved the shear capacity of the specimen.

In addition to the minimum transverse reinforcement needed by design, the reinforced end had additional instrumented transverse bars that increased the shear capacity of the reinforced end. As previously mentioned in Chapter 4, the precast plant personnel had installed R-bars without instruments in the locations where the instrumented R-bars were originally planned. Because it was not possible to remove the extra R-bars, the instrumented R-bars had to be installed in between the preinstalled R-bars, thereby increasing the shear capacity of the reinforced end. To ensure the shear capacity of the reinforced end was not largely impacted by the additional bars, the span length of the specimen for the reinforced end shear test was modified to avoid the closely spaced transverse bar end. The pedestal at the reinforced end was moved 10 ft inwards to avoid testing the closely spaced transverse bar end, and the other end was adjusted by installing an additional pedestal to exclude the end damaged under the previous shear test.

Table 6.7 and Table 6.8 provide the arrangement of SPs for the shear tests conducted for the Tx34-2 girder.

Table 6.7. Location of SPs for Tx34-2 Shear Test 1.

SP ID	**SP-1**	**SP-2**	**SP-3**	**SP-4**	**SP-5**	**SP-6**	**SP-7**	**SP-8**	**SP-9**	**SP-10**
Stroke, in.	4	4	4	4	4	4	4	4	12	4
Distance, ft	−0.75	2.5	5.5	8.5	11.5	13	14.5	17.5	20.5	23.5
SP ID	SP-11	SP-12	SP-13	SP-14	SP-15	SP-16	SP-17	SP-18	SP-19	N/A
Stroke, in.	4	4	4	4	4	4	4	4	4	N/A
Distance, ft	26.5	29.5	32.5	35.5	38.5	41.25	44.25	47.25	50.25	N/A

Notes:
1. The distance is measured from the centerline of the east-bearing pad
2. The direction from east to west is considered positive
3. The SPs at the ends record the uplift (if any) of the girder ends
4. N/A: Not applicable

Table 6.8. Location of SPs for Tx34-2 Shear Test 2 (Reinforced End).

SP ID	**SP-1**	**SP-2**	**SP-3**	**SP-4**	**SP-5**	**SP-6**	**SP-7**	**SP-8**	**SP-9**	**SP-10**
Stroke, in.	4	4	4	4	12	12	4	4	4	4
Distance, ft	0	3.5	6.5	9.5	12.5	15.5	18.5	21.5	24. .5	28

Notes:
1. The distance is measured from the centerline of the east-bearing pad
2. The direction from east to west is considered positive
3. The SPs at the ends record the uplift (if any) of the girder ends

6.2.5 Tx54 Girder Specimen

Figure 6.7 and Figure 6.9 show the test setup and overall instrumentation for the shear tests of the Tx54 specimen at the reinforced and unreinforced ends, respectively. Figure 6.8 and Figure 6.10 present the photos of the test setup for Tx54 girder specimens. The Tx54 specimen has a deeper section than the first two girders, along with a higher tensile strength based on the companion material tests and more prestressing and harped strands; therefore, each girder end was loaded with two actuators at a time, much like the reinforced end testing of the Tx34-2 specimen.

Shear Test 1 was conducted on the reinforced end of the Tx54 girder after conducting the flexure test. This step allowed a longer span length to be leveraged to force shear failure in the stronger reinforced end of the girder. This result would not be possible if the unreinforced end was tested first because the significant damage would prompt a span length reduction for the subsequent shear test at the reinforced end. After the shear test of the reinforced end, the full span length of the specimen was utilized for Shear Test 2 of the unreinforced end. During Shear Test 2, the load on the damaged reinforced end of the specimen was monitored to ensure sufficient capacity during testing. The unreinforced end was tested under the same test setup as the reinforced end. Table 6.9 and Table 6.10 present the arrangement of SPs for Shear Tests 1 and 2 for the Tx54 girder.

Table 6.9. Location of SPs for Tx54 Shear Test 1 (Reinforced End).

SP ID	SP-1	SP-2	SP-3	SP-4	SP-5	SP-6	SP-7	SP-8	SP-9	SP-10	SP-11	SP-12	SP-13	SP-14
Stroke, in.	4	4	4	4	12	12	4	4	4	4	4	4	4	4
Distance, ft	−0.75	2	3	5	7.5	11	14	17	20	23	26	29	32	35
SP ID	**SP-15**	**SP-16**	**SP-17**	**SP-18**	**SP-19**	**SP-20**	**SP-21**	**SP-22**	**SP-23**	**SP-24**	**SP-25**	**SP-26**	**SP-27**	—
Stroke, in.	12	12	4	4	4	4	4	12	12	4	4	4	4	—
Distance, ft	37.5	41	44	47	50	53	55	56	59	62	65	67	70	—

Notes:
1. The distance is measured from the centerline of the east-bearing pad
2. The direction from east to west is considered positive
3. The SPs at the ends record the uplift (if any) of the girder ends

Table 6.10. Location of SPs for Tx54 Shear Test 2 (Unreinforced End).

SP ID	SP-1	SP-2	SP-3	SP-4	SP-5	SP-6	SP-7	SP-8	SP-9	SP-10	SP-11	SP-12
Stroke, in.	4	4	4	4	12	12	4	4	4	4	4	12
Distance, ft	−0.75	2.5	5	10.5	13	14.5	16.5	19.5	22.5	25.5	28.5	31.5
SP ID	**SP-13**	**SP-14**	**SP-15**	**SP-16**	**SP-17**	**SP-18**	**SP-19**	**SP-20**	**SP-21**	**SP-22**	**SP-23**	**SP-24**
Stroke, in.	12	4	4	4	4	4	4	4	4	4	4	4
Distance, ft	34.5	37.5	41	43.5	46.5	51	56	58.5	61.5	64.5	67.5	70.25

Notes:
1. The distance is measured from the centerline of the east-bearing pad
2. The direction from east to west is considered positive
3. The SPs at the ends record the uplift (if any) of the girder ends

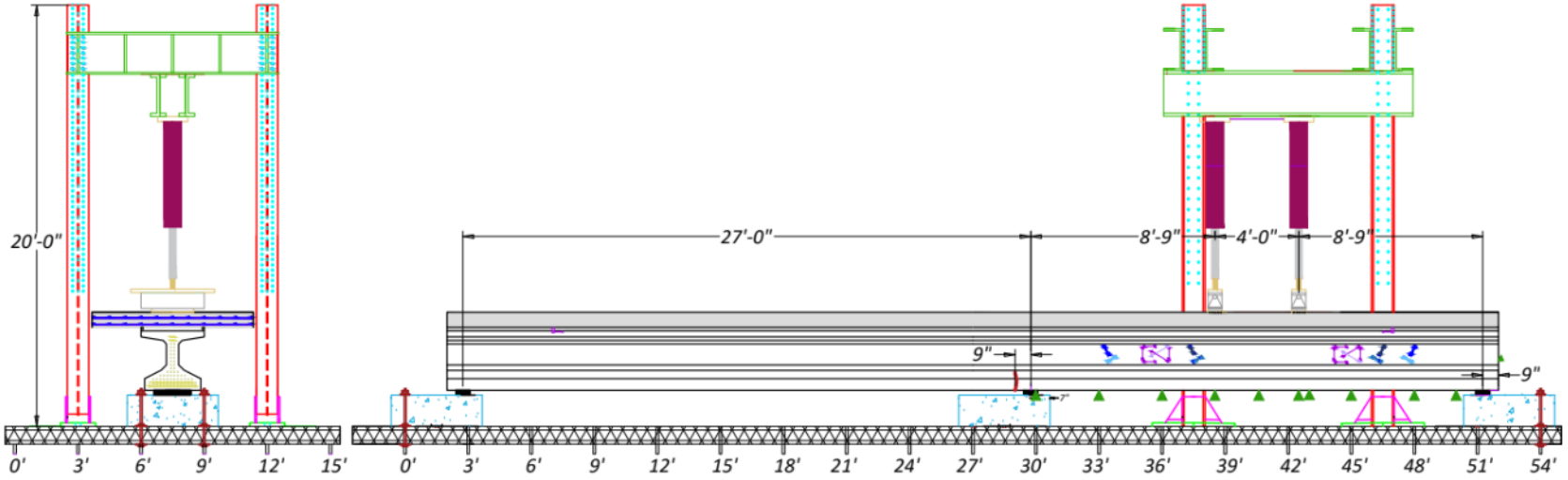

(a) Test Setup: North Face

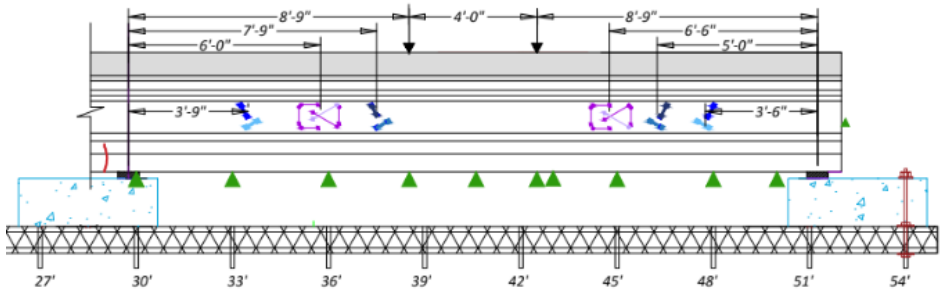

(b) North Face with LVDT and SG (West End with Hoops)

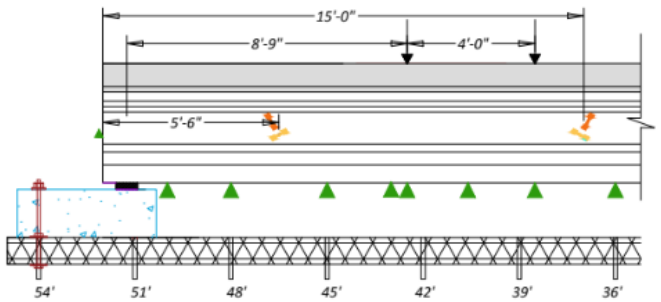

(c) South Face with KSG (West End with Hoops)

Note: KSG: Surface Mounted Concrete Strain Gage, LVDT: Linear Variable Displacement Transducer, SG: Surface Concrete Strain Gage, SP: String Potentiometer.

Figure 6.1. Tx34-1 Test Setup and Instrumentation for Shear Test 1 (Load at Reinforced End).

(a) North Face with LVDT and SG (Reinforced West End)

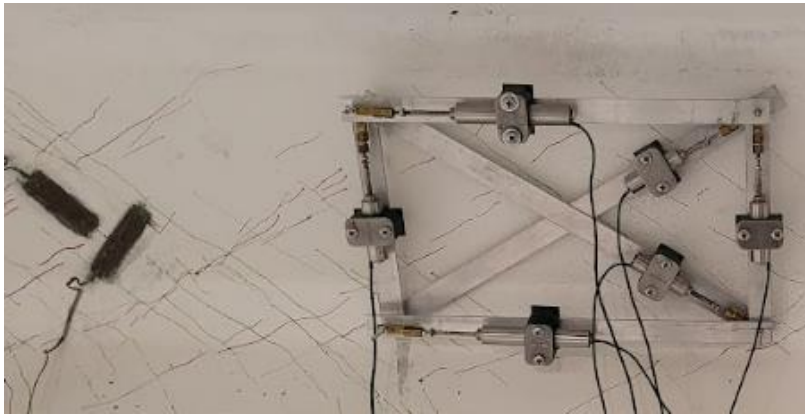

(b) LVDT and SG in the Web

(c) South Face with KSG (Reinforced West End)

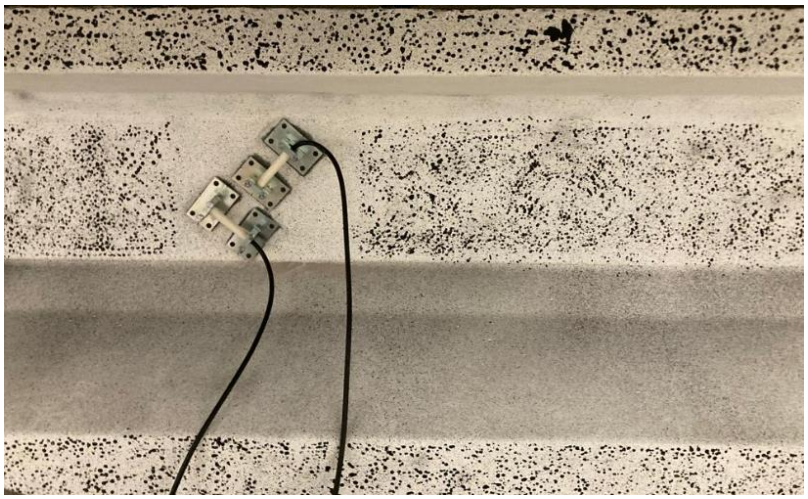

(d) KSG in the Web

Figure 6.2. Photos of Tx34-1 Test Setup and Instrumentation for Shear Test 1 (Load at Reinforced End).

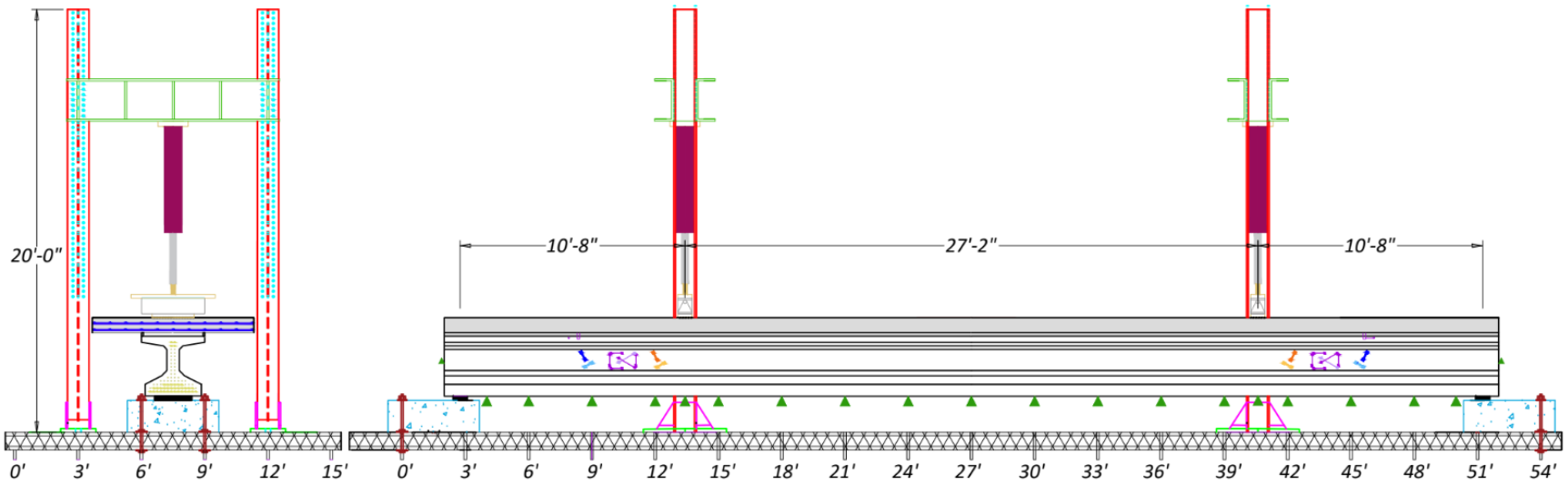

(a) Test Setup: North Face

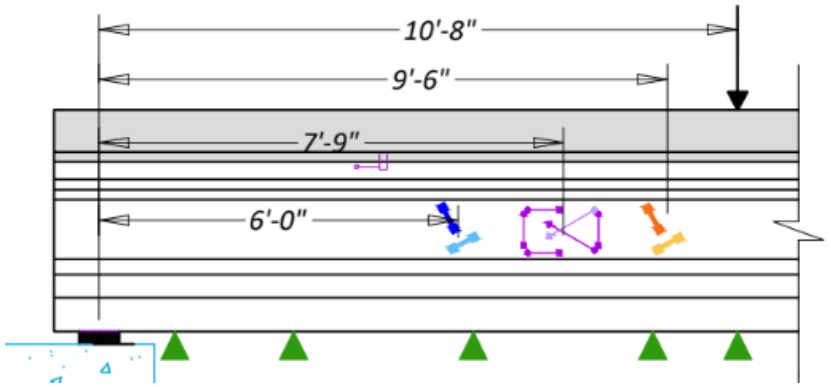

(b) North Face with SG, LVDT, and KSG (East End with Hoops)

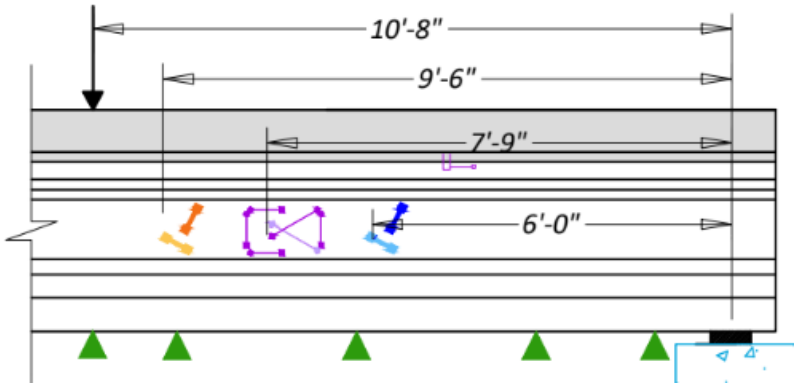

(c) North Face with SG, LVDT, and KSG (West End without Hoops)

Figure 6.3. Tx34-2 Test Setup and Instrumentation for Shear Test 1.

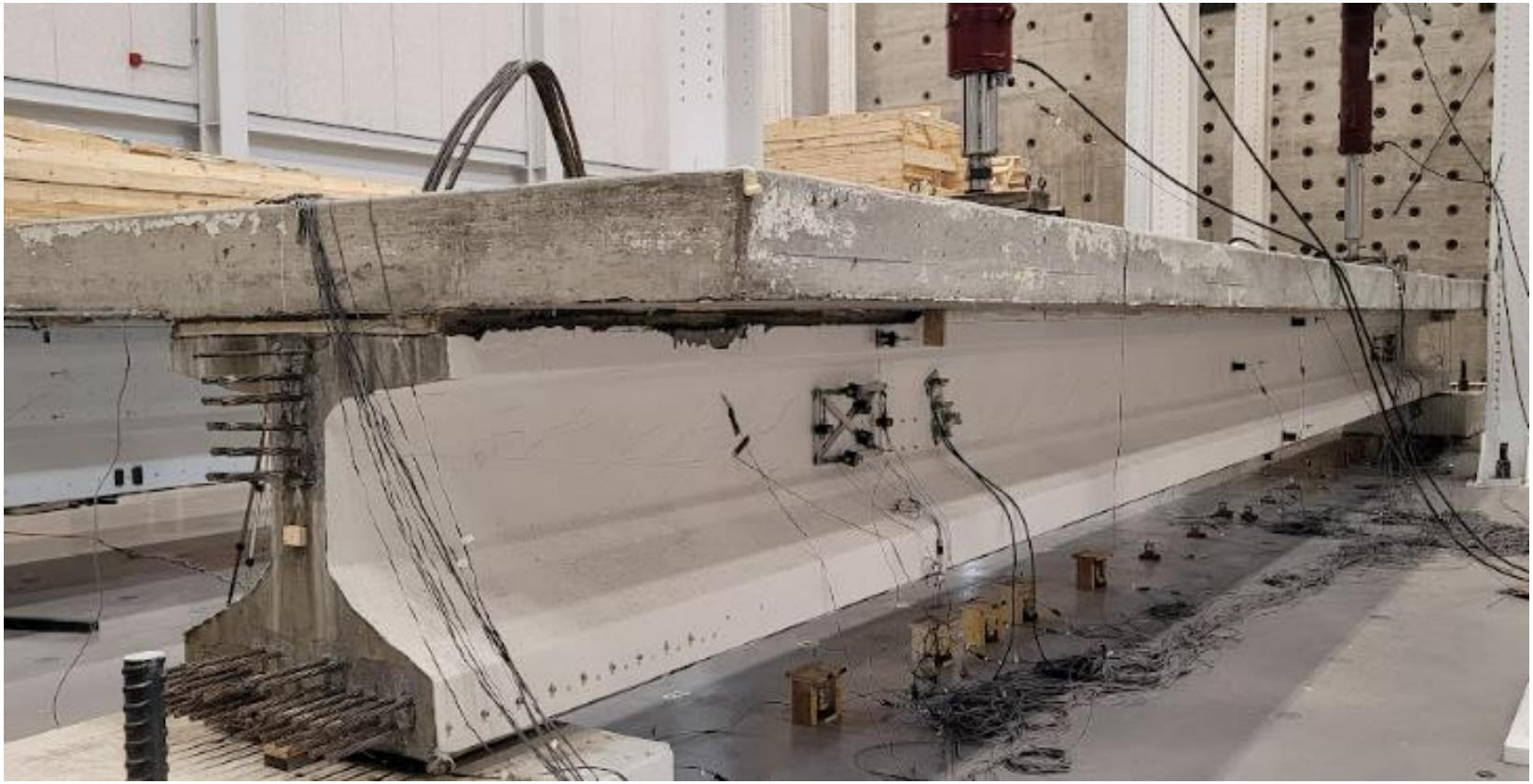

Figure 6.4. Tx34-2 Test Setup and Instrumentation for Shear Test 1 (North Face).

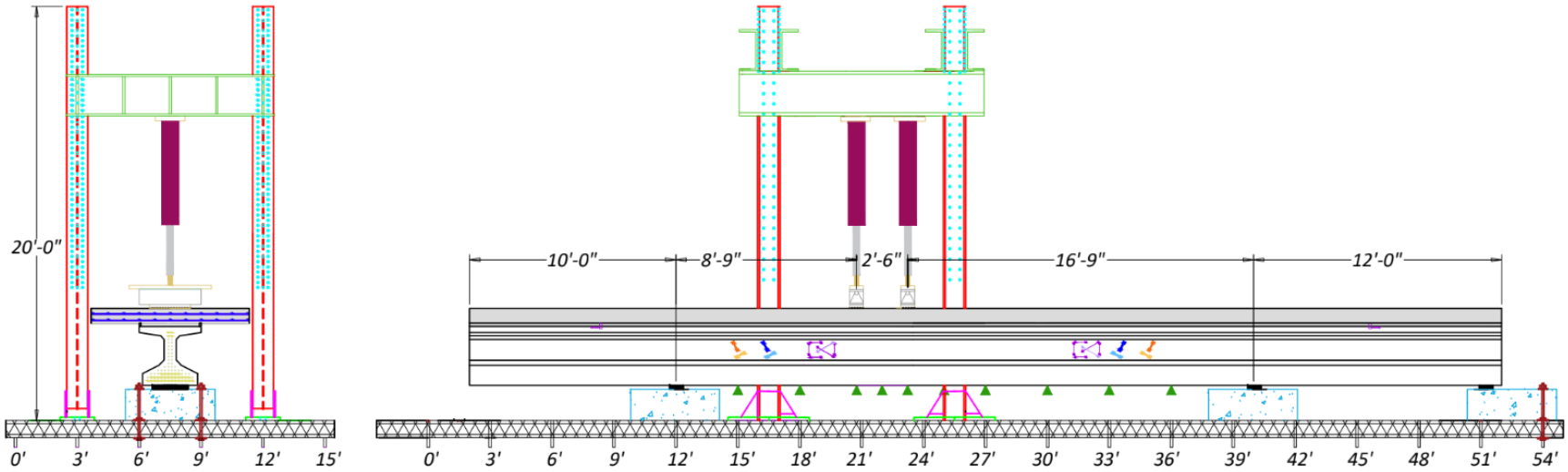

(a) Test Setup: North Face

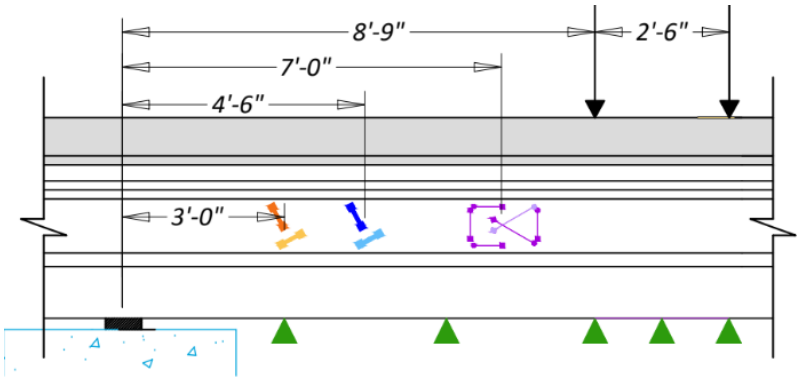

(b) North Face with SG, LVDT, and KSG (East End with Hoops)

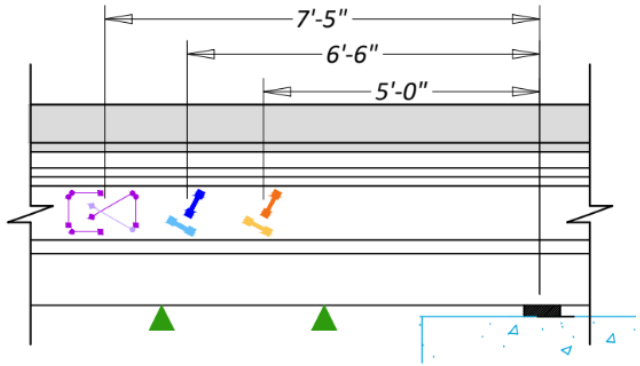

(c) North Face with SG, LVDT, and KSG (West End without Hoops)

KSG LVDT SG SP

Figure 6.5. Tx34-2 Test Setup and Instrumentation for Shear Test 2 (Load near the Reinforced End).

Figure 6.6. Tx34-2 Test Setup and Instrumentation for Shear Test 2 (North Face, Load near the Reinforced End).

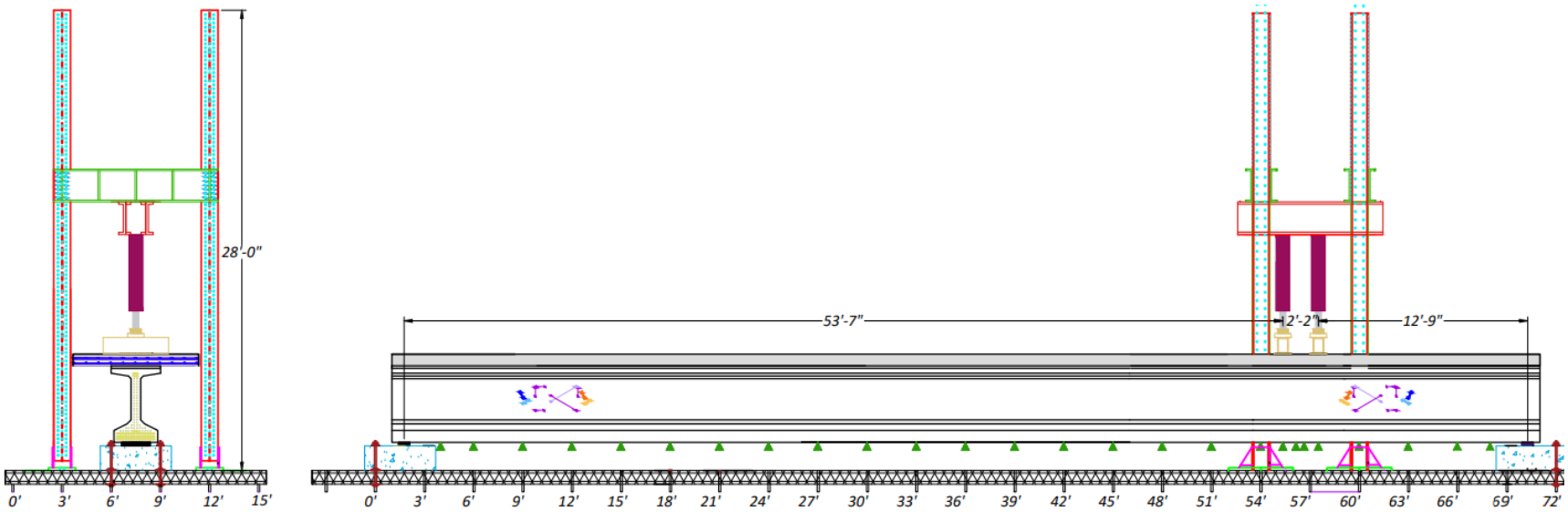

(a) Test Setup: South Face

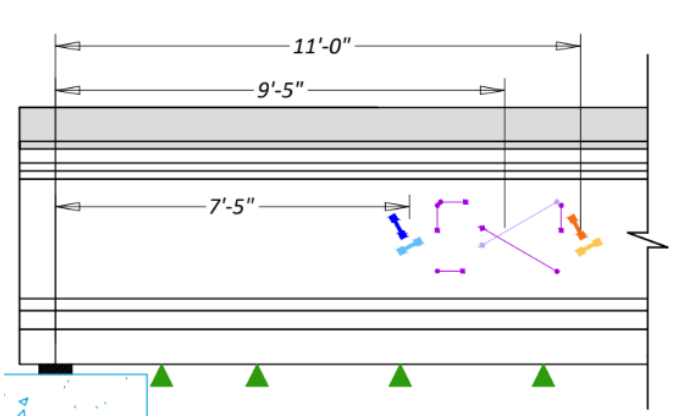

(b) West End with SG, LV, and KSG (without Hoops)

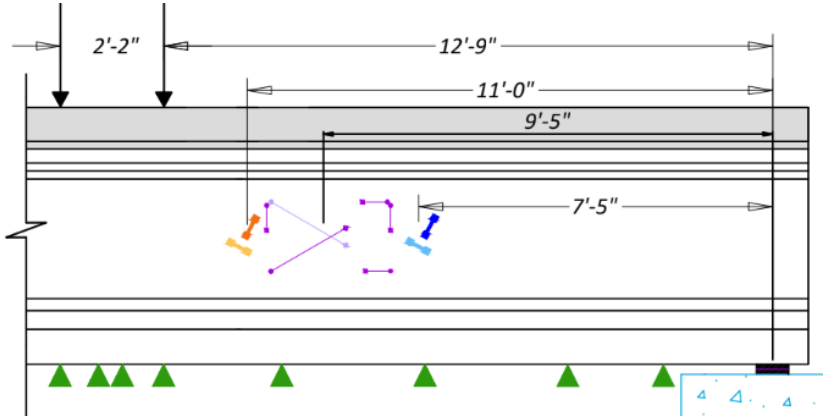

(c) East End with SG, LV, and KSG (with Hoops)

Figure 6.7. Tx54 Setup and Instrumentation for Shear Test 1 (Load at Reinforced End).

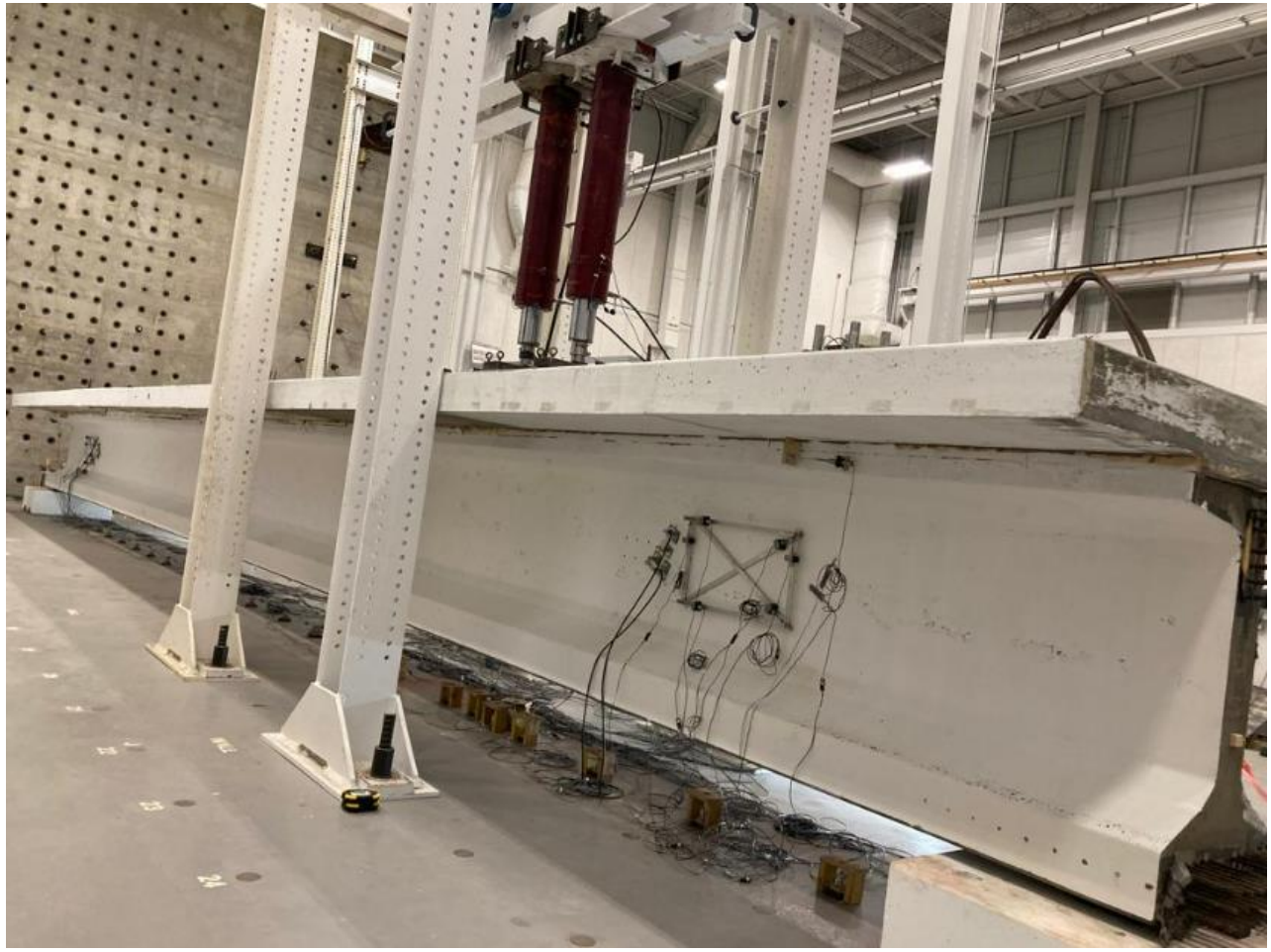

Figure 6.8. Tx54 Test Setup and Instrumentation for Shear Test 1 (Load at Reinforced End).

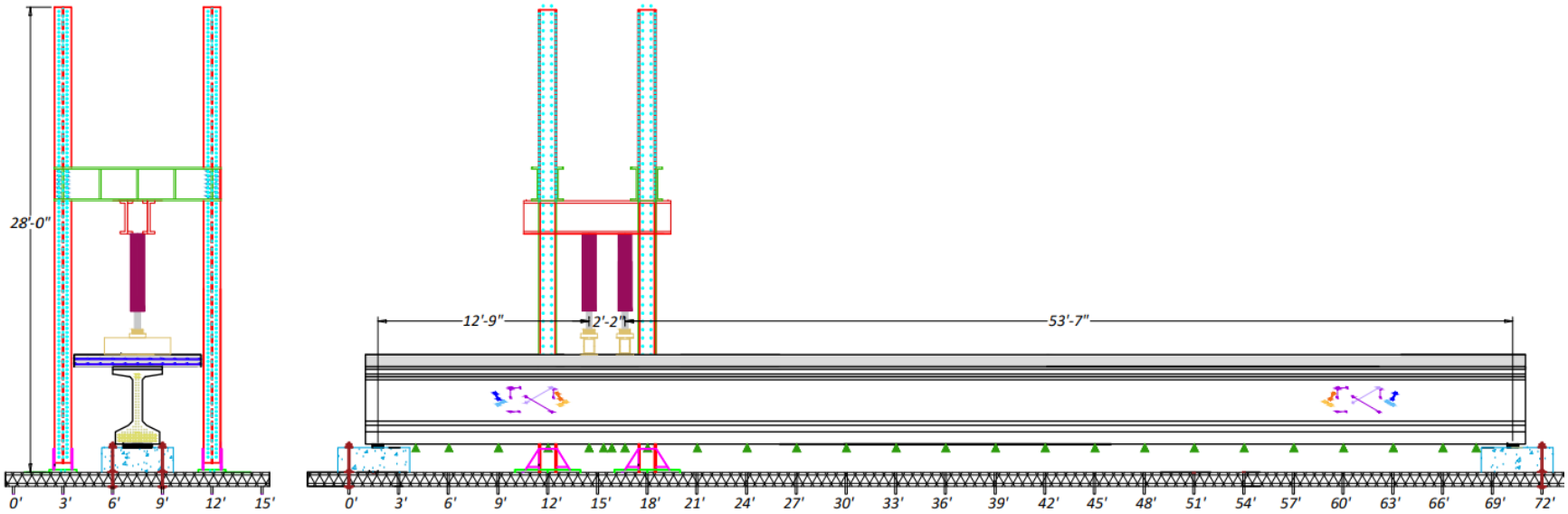

(a) Test Setup: South Face

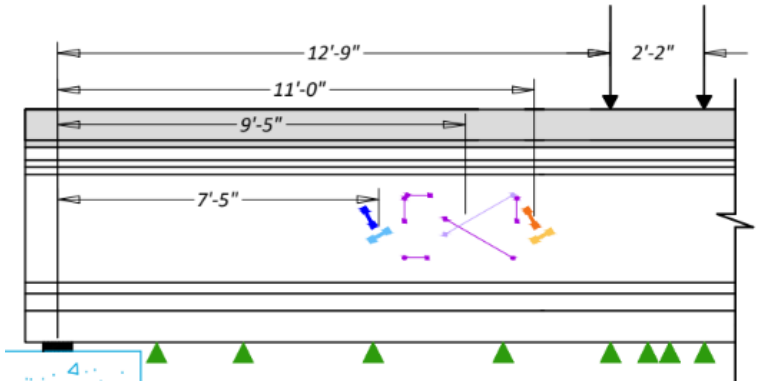

(b) South Face with SG, LV, and KSG (West End without Hoops)

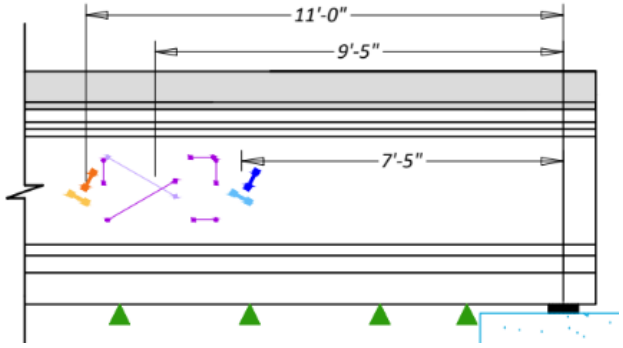

(c) South Face with SG, LV, and KSG (East End with Hoops)

KSG LVDT SG SP

Figure 6.9. Tx54 Setup and Instrumentation for Shear Test 2 (Load at Unreinforced End).

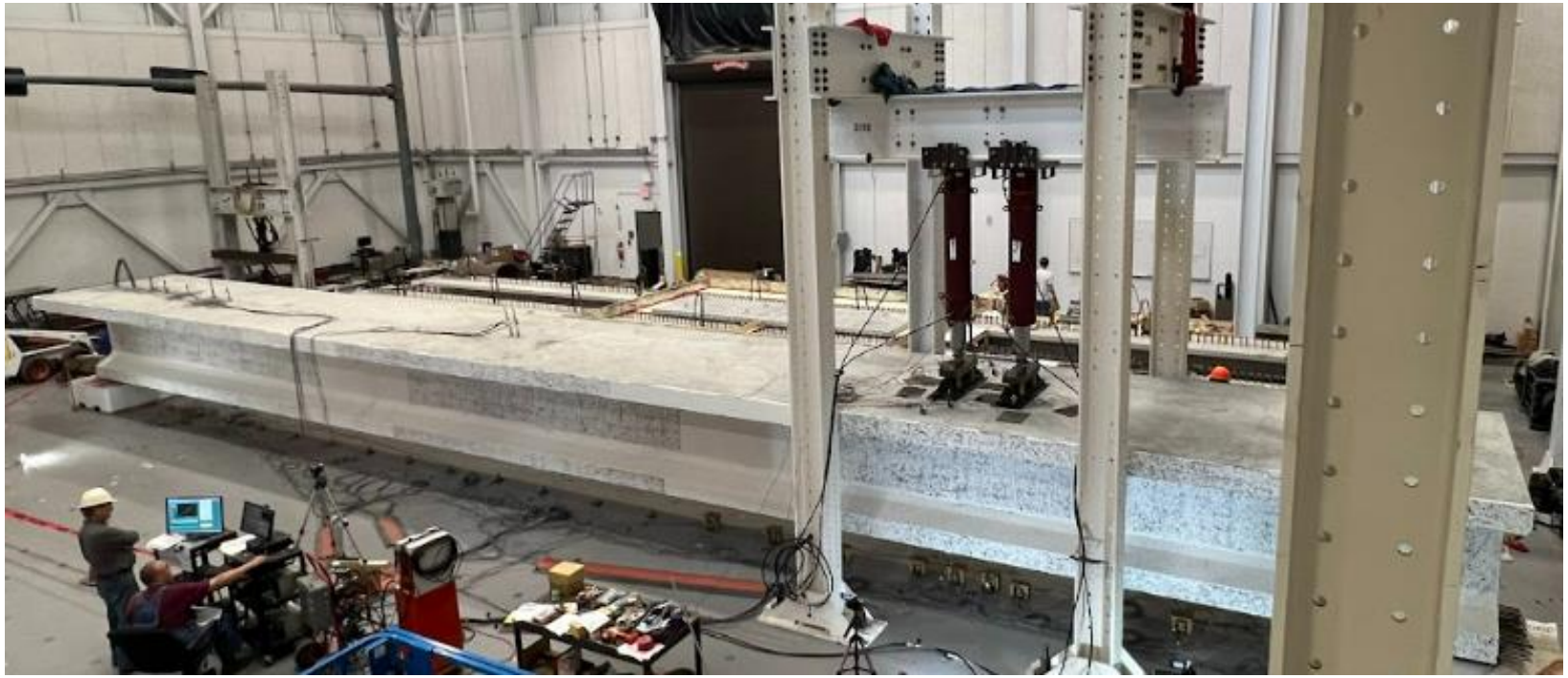

Figure 6.10. Tx54 Test Setup and Instrumentation for Shear Test 2 (North Face, Load at Unreinforced End).

6.3 TX34-1 SHEAR TEST RESULTS

The first specimen tested, Tx34-1, had the lowest tensile strength determined from the material-level testing, and this result impacted the shear capacity of the specimen, particularly the unreinforced end, significantly. Therefore, the capacity of the unreinforced end was lower than the original expected design capacity, and this trait triggered shear cracking at the unreinforced end during the flexure test. After the flexure test, the reinforced end of Tx34-1 was tested by reducing the span at that end. This step was achieved by adding a support just to one side of the widest flexural crack. The reduced span length for the reinforced end shear test was 21.5 ft, providing a span-to-depth ratio of 2.91:1. The average first cracking strength obtained from direct uniaxial tensile strength test for the Tx34-1 girder was taken as 0.53 ksi based on the material-level tests.

6.3.1 Shear Test 1: Unreinforced End

Figure 5.1 shows the test setup that led to the formation of shear cracks in the unreinforced end of the Tx34-1. Phase I of the Tx34-1 flexure test was terminated due to the observed shear cracks at a load of 380 kips on each actuator. The shear force was computed at the location of the formation of the major shear damage. This site was located 6.5 ft from the centerline of the bearing pad situated at the unreinforced end of the girder. Notable events during testing are as follows:

- *Phase I loading*. Flexure crack localization took place at a total actuator load of 406 kips. At this point, the shear cracks widths at the unreinforced end widened, varying from 0.03–0.04 in.
- *Phase II loading*. Beyond this stage, the load at the actuator near the unreinforced end was disengaged, and the second actuator closer to the reinforced end continued to be loaded. At a single actuator load of 450 kips, the cracks at the unreinforced end widened to a maximum of 0.08 in. The cracks ranged from 0.006–0.08 in., with a maximum of the 0.08 in. crack width.

Figure 6.11 shows the shear cracks in the web of the girder at the end of the flexure test. Figure 6.12 also presents the schematic shear cracks marked on the surface of the unreinforced girder end at the end of the flexure test. Although an LVDT frame was installed at both ends, the LVDTs did not pick up the small strain range data. Based on this experience, the shear ends were then

instrumented with strain gages for later tests to monitor the smaller strain values. The reinforced end exhibited residual load carrying capacity even after larger shear cracks developed at the unreinforced end at the point of termination of the test. Table 6.11 presents the range of typical crack widths observed at the unreinforced end (noted as Shear Test 1 for this discussion). The crack widths are recorded at the maximum loads of Phase I and Phase II.

Table 6.11. Range of Crack Widths for Tx34-1 Shear Test 1: Unreinforced End.

Shear Force, kips	Total Actuator Load, kips	Minimum Width, in.	Maximum Width, in.	Typical Width, in.
198	406	< 0.004	0.04	0.006
202	450	< 0.006	0.08	0.01

Figure 6.11. Tx34-1 Shear Test 1: Unreinforced End at Termination of Phase II Flexure Test.

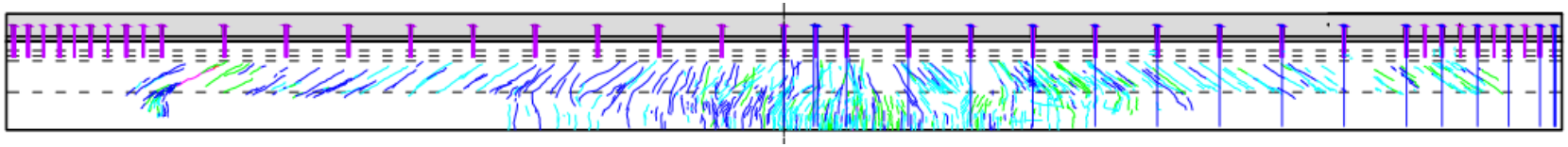

Note: End of Flexure Test (Phase II) and Shear Damage at 450 kips.

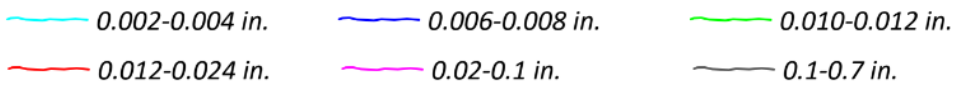

Figure 6.12. Tx34-1 Flexure Test Crack Map (Note Shear Damage at Unreinforced End).

6.3.1.1 Transverse Reinforcement Strains

Figure 6.13(a) and Figure 6.14(a) present the setup of the flexure test, which also provides the test of the Tx34-1 unreinforced girder end in shear (Shear Test 1). The strain gages installed on the transverse hoops at the reinforced end are presented and color-coded with the corresponding plots of data in the companion figures. The gages on two legs of the same R-bar are shown in one color, and different colors are used to distinguish between the location of the bars. Figure 6.13(b) and Figure 6.14(b) present the SSG data for each of the two test phases. The graphs show the strains measured by the SSG gages and plotted against the shear force at the critical crack location at the ends. The shear force in the graph includes the shear due to the self-weight. The total applied actuator load is shown on the secondary vertical axis of the plot. The instrumented gages are located at the reinforced end, while the shear force presented is at the critical crack location of the unreinforced end, located 17.5 ft from the centerline of the girder specimen (6.75 ft from the support centerline).

The transverse reinforcement begins to gain strain in tension at approximately 180 kips of shear force. The yield strain of the Grade 60 transverse reinforcement was taken as 0.00224, corresponding to a yield strength of 65 ksi, which was used to provide a more realistic estimate of the actual material properties. During Phase I, at the maximum applied shear at the unreinforced end, strain gages SSG 5 thru SSG 8 on the reinforced end exceeded the yield strain. However, the transverse reinforcement does not reach yield strain during Phase II loading. The compressive strain in SSGs 1 and 2, which are installed on the first instrumented R-bar, could be due to the action of a compressive strut at the support.

The shear capacity of the specimen due to UHPC V_{UHPC} and the combined shear capacity due to the transverse steel reinforcement and UHPC $V_{UHPC} + V_s$ are indicated with horizontal lines on the graphs. These capacities are predicted values based on the material-level test data from the companion specimens. The plot shows that the transverse steel was engaged at a shear force slightly lower than the predicted UHPC capacity for the Tx34-1 girder specimen.

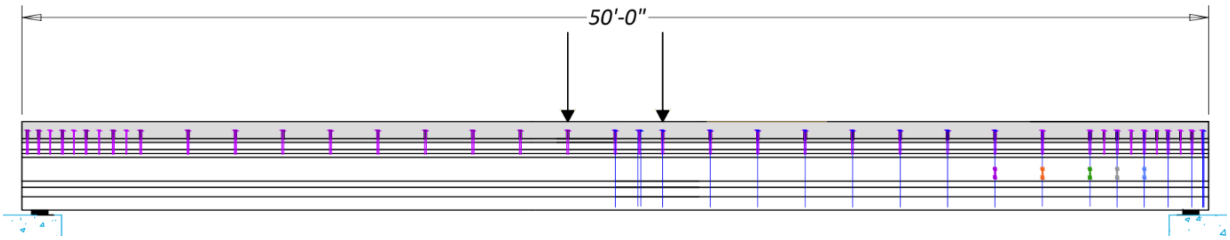

(a) Surface Steel Gages Installed on R-bars

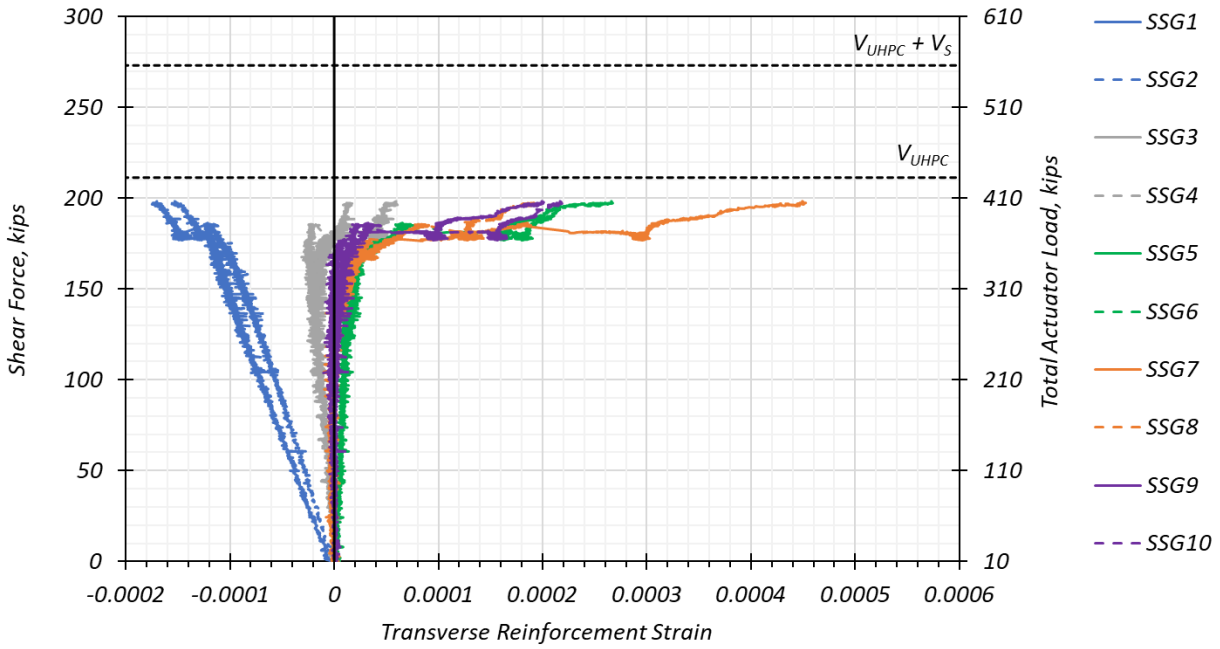

(b) Strains in Transverse Reinforcement Gages during Phase I Flexure Test

Figure 6.13. Tx34-1 Phase I Flexure Test: Transverse Reinforcement Strain Gages.

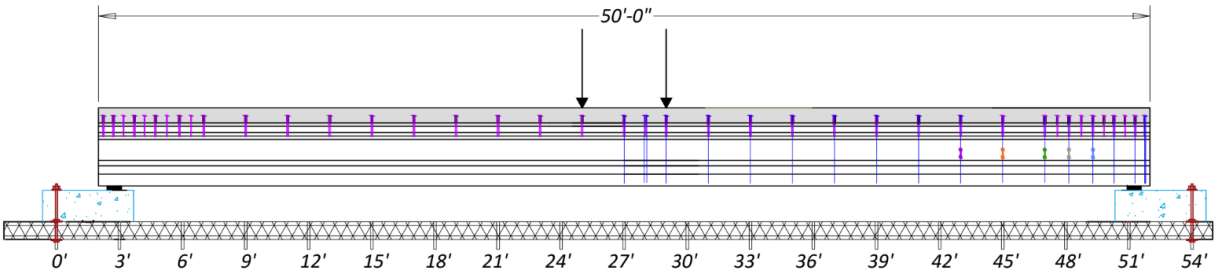

(a) Surface Steel Gages Installed on R-bars

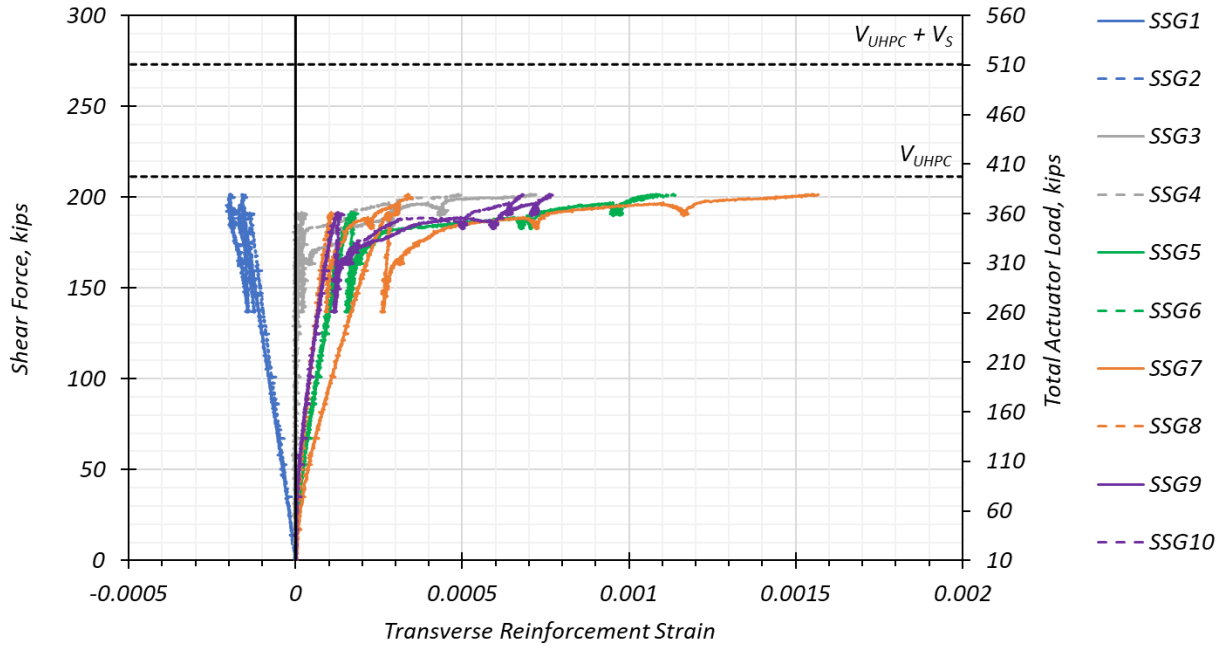

(b) Strains in Transverse Reinforcement Gages during Phase II Flexure Test

Figure 6.14. Tx34-1 Phase II Flexure Test: Strain Gages at Transverse Reinforcement.

6.3.1.2 Additional Strain Measurements and Crack Angle

Figure 6.15(a) shows the arrangement of the LVDT rosette. The photo was taken at the maximum applied load during flexural testing of the Tx34-1. As noted earlier, significant shear cracks formed in the web of the unreinforced end. Figure 6.15(b) shows the schematic of the LVDT rosette on the web and the KSG strain gage on the bottom flange. Figure 6.15(c) presents the shear force at the region of major crack development plotted against the strains measured by the LVDT rosette. The LVDT rosette and KSG did not capture the strains of low magnitude, and therefore, for the subsequent shear tests, it was decided to install bonded surface SGs in addition to LVDTs and KSGs. Only LV 6 data are presented.

Based on the computation explained in Section 6.2.1, crack angles of the major developed cracks were to be computed using the strains measured by the LVDT rosette at that location. However, the crack angles could not be computed from the LVDT rosette data because the data were insufficient; that is, one or more of the LVDTs forming the rosette did not read any data. This breakdown could be because some of the LVDTs forming the strain rosette may have malfunctioned during the crack widening. The assumed crack angle based on Mohr's circle analysis was 25.3 degrees. The crack angle physically measured 32 degrees.

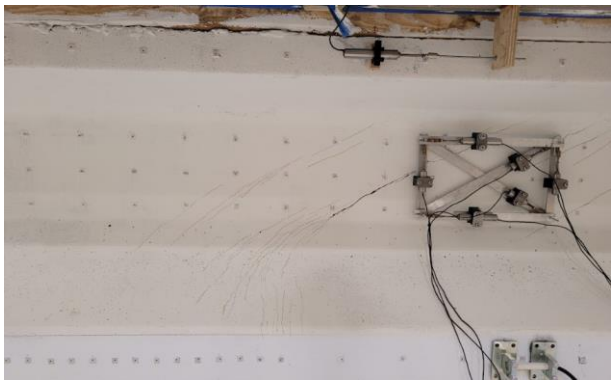

(a) Unreinforced End at Peak Load

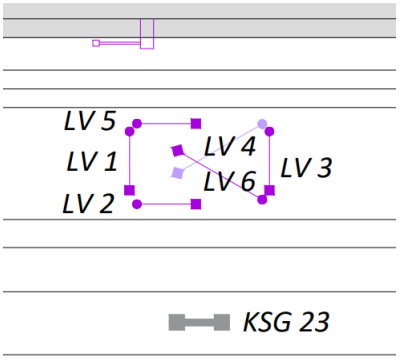

(b) Instrumentation Schematic

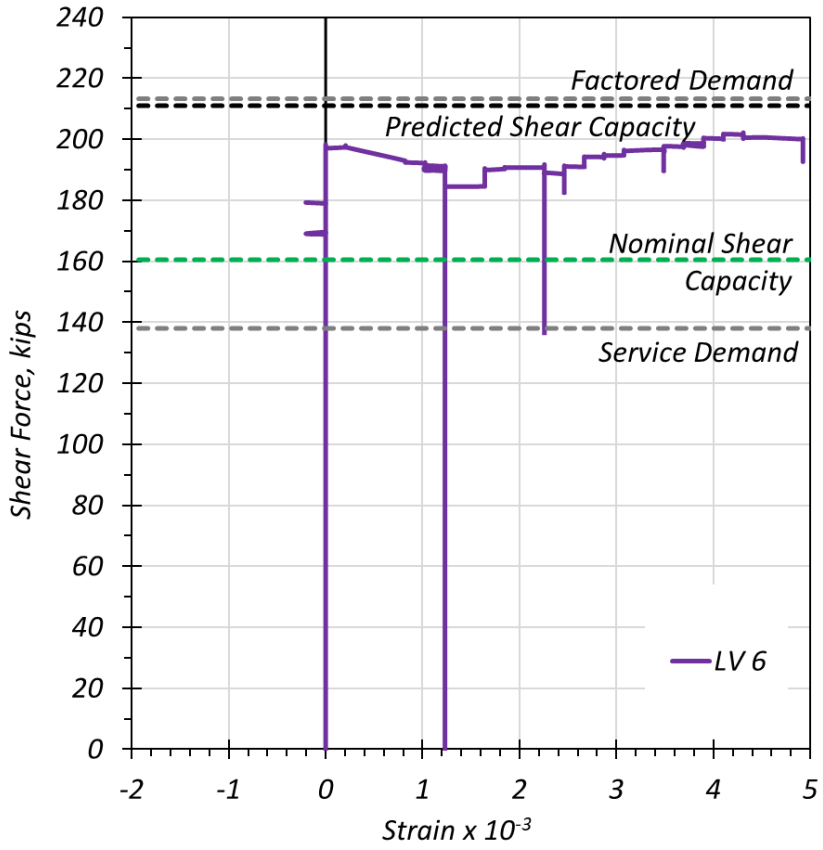

(c) Shear Force versus Strain

Figure 6.15. Tx34-1 Phase II Flexure Test: Web Strains (Unreinforced End).

6.3.1.3 Shear Force versus Deflection

The shear force at the location of the most prominent shear crack was plotted against the maximum deflection observed in the shear span and presented in Figure 6.16. The maximum applied shear force at the unreinforced end was higher than the nominal shear capacity (based on FHWA (2022)) and the service demand. However, it was less than the predicted shear capacity and the factored

shear demand. Shear force was maintained despite the damage occurring at the unreinforced end and at the midspan.

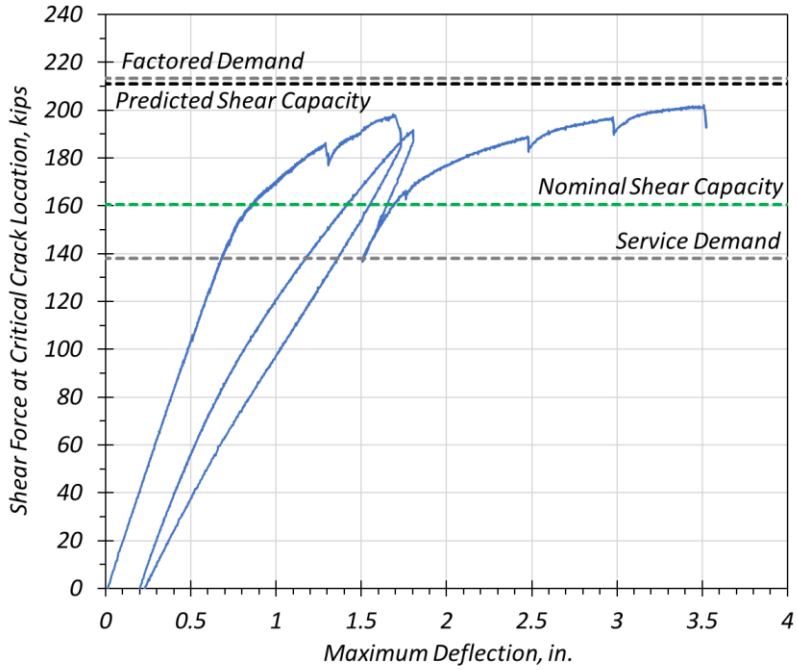

Figure 6.16. Tx34-1 Shear Test 1: Shear Force versus Maximum Deflection (Unreinforced End at Termination of Phase II Flexure Test).

6.3.1.4 Deflection Profile

Figure 5.23 presents the deflection profile at the end of the flexure test, which coincided with the end of the shear test of the unreinforced end.

6.3.1.5 Interface Shear between UHPC Girder and CC Deck

Composite reinforcement was used at the interface of the UHPC girder and CC deck to resist interface shear and provide composite action. Figure 6.17(a) presents the plan view of the layout of the four LVDTs near the ends of the girder specimens (one on each side of the web). These LVDTs were intended to measure the slip between the CC deck slab and the UHPC girder and were located 5.5 ft from each end. Figure 6.17(b) shows a photo of one of these instruments installed at the unreinforced end of the Tx34-1 specimen.

Figure 6.18(a) and (b) present the LVDT slip measured during the flexure test Phases I and II, respectively. The following observations were made:

- The occurrence of shear cracking at the end of Phase I coincided with a slight slip at both girder ends. The slip was less than 0.017 in.
- The end of Phase II that marked the widening of the shear cracks at the unreinforced end and the flexure failure at the midspan showed a slip of approximately 0.087 in. at the reinforced end and a slip of approximately 0.0225 in. at the unreinforced end.

The measured slip during Phase II may indicate that the interface shear strength at the unreinforced end is higher than the reinforced end. This result could be attributed to the higher area of interface steel present at the unreinforced end in comparison to the reinforced end. The R-bars (minimum shear reinforcement) present at the reinforced end are #4 bars (and are bundled with two #5 UC-bars), while the UC-bars at the unreinforced end are bundles of 3-#5 bars. Therefore, although the pattern of the reinforcement is maintained symmetrically, the larger amount of interface shear reinforcement at the unreinforced end improved the interface shear resistance. However, it should also be noted that when testing the reinforced end, a higher shear force is applied, which can also explain the additional slip at that end.

Researchers attempted to increase composite action by abrading the surface of UHPC after casting the girder with a sharp, pointed device throughout the span length once the UHPC began to harden on the top surface. Given the self-consolidating nature of UHPC, the roughening by abrasion method was not effective immediately after casting, and most of the abraded surface tended to chip off during the process of removing laitance before placing the CIP CC deck slab. Therefore, no further modification of the UHPC surface was employed for the remaining two specimens.

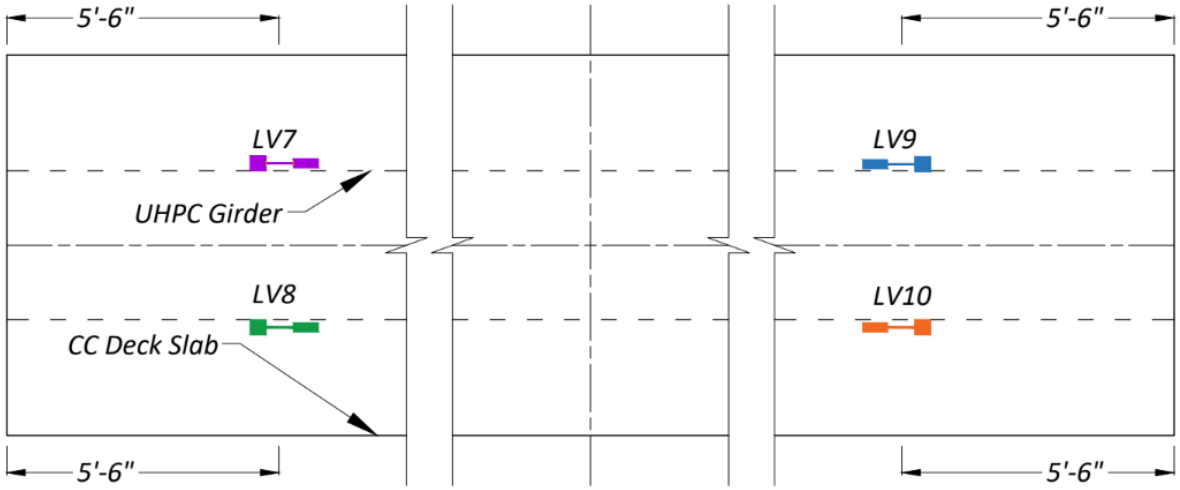

(a) Layout of LVDTs Measuring Interface Slip (Plan View)

[Note: LVDTs are located at interface of UHPC girder and deck.]

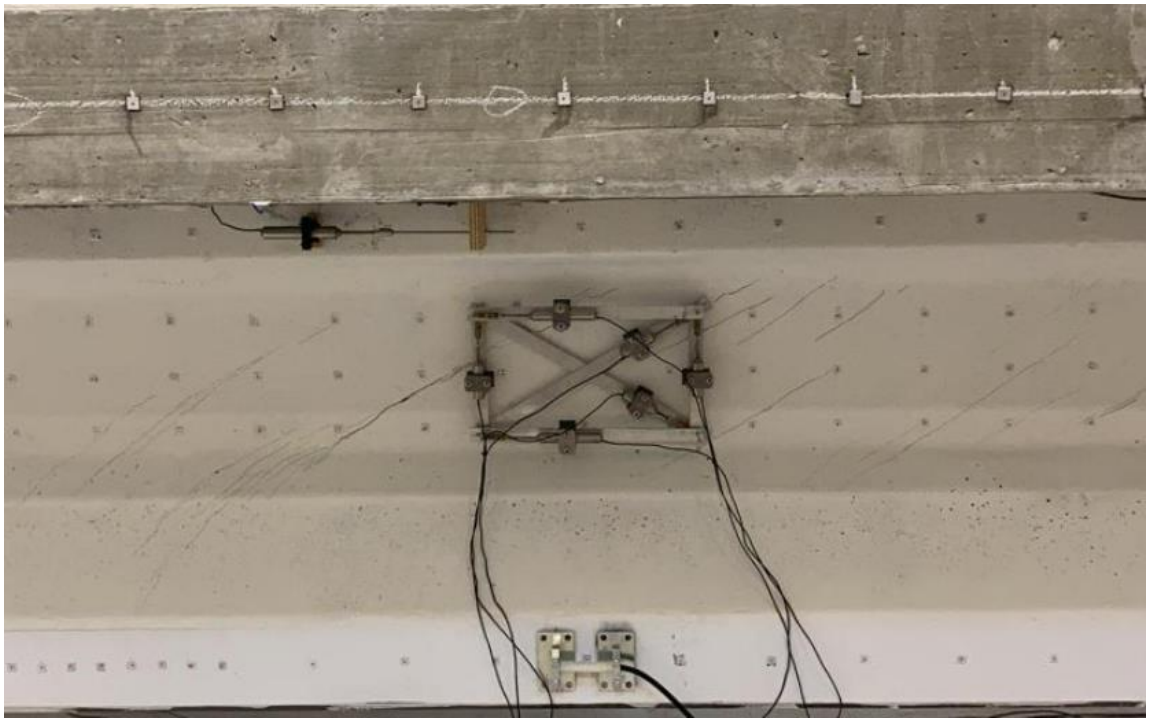

(b) LV8 at the Interface of CC Deck and UHPC Girder (Unreinforced End)

Figure 6.17. Tx34-1 Flexure Test: Interface Slip Measurements Instrumentation.

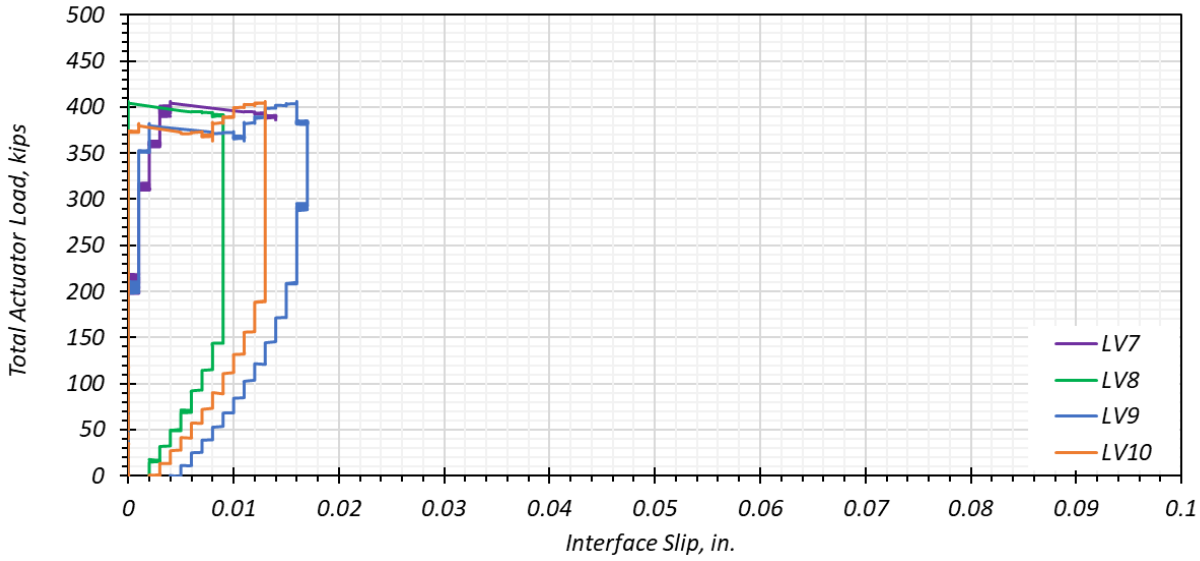

(a) Interface Slip During Phase I Testing

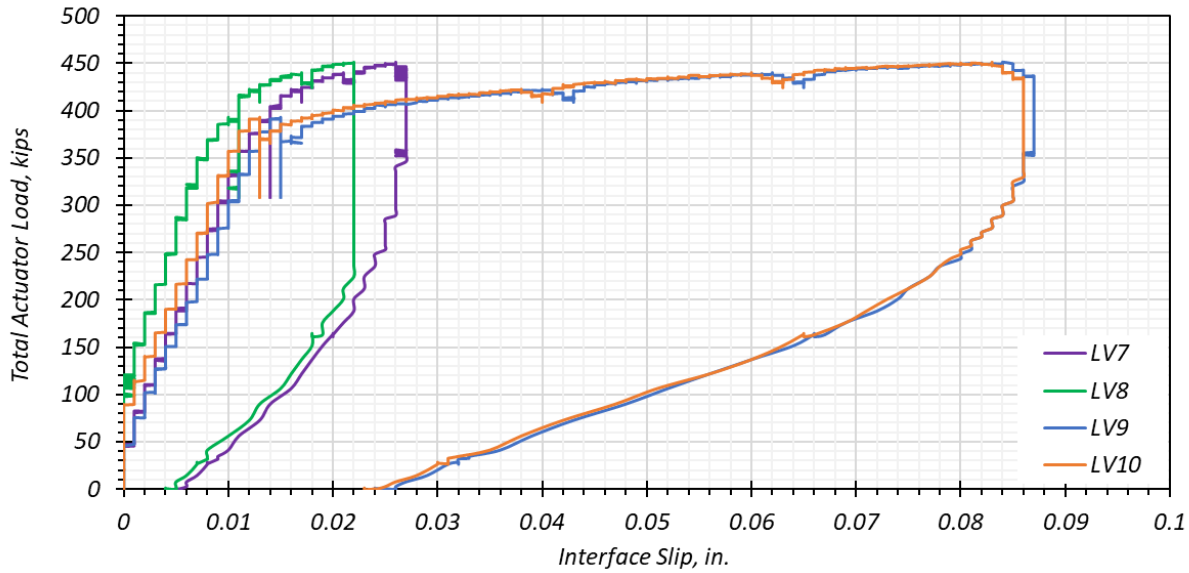

(b) Interface Slip During Phase II Testing

Figure 6.18. Tx34-1 Flexure Test with Unreinforced End Shear Failure: Interface Slip Measurements.

6.3.2 Shear Test 2: Reinforced End

Figure 6.1 describes the shear test setup for the Tx34-1 end containing minimum shear reinforcement. The span-to-depth ratio for the Tx34-1 shear test at the reinforced end was 2.4:1. The two actuators were located 30 in. apart to create the necessary shear for the predicted maximum shear capacity. These actuators were differentially loaded with the actuator near the

reinforced end being loaded with a higher load to force the shear failure to occur closer to the end support and away from the interior support added for this setup. The load on the actuator closest to the interior support was deliberately maintained at less than 50 percent of the load on the other actuator to prevent a premature failure of the region that was already damaged from flexure-shear interaction cracks. These cracks were formed during the flexure test. Notable events during shear testing are bulleted below. The shear forces noted are due to the applied loads and self-weight. The shear forces are computed at the location of the most prominent shear damage, which was 6.5 ft from the centerline of the bearing situated at the reinforced end of the girder:

- At a shear force of 270 kips in the region of major cracking (between the support and nearest actuator), minor cracks of 0.004 in. width were detected (typical).
- As the loads were increased incrementally to a shear force of 400 kips, the cracks at the reinforced end began to widen to 0.006 in.
- At a shear force of 417 kips, the cracks further widened and propagated. This step marked the end of shear testing of the first specimen. At the end near the interior support, the cracks ranged from 0.004–0.024 in. At the reinforced end, the cracks ranged from 0.006–0.022 in.

Table 6.12 presents the typical, minimum, and maximum crack widths observed at load steps when testing was paused to measure the crack widths. Figure 6.19 presents the schematic of the cracks formed at the end of the shear test.

Table 6.12. Range of Crack Widths for Tx34-1 Shear Test 2: Reinforced End.

Shear Force, kips	Total Actuator Load, kips	Minimum Width, in.	Maximum Width, in.	Typical Width, in.
270	515	< 0.004	0.004	0.0025
400	768	< 0.004	0.006	0.003
417	813	0.006	0.022	0.009

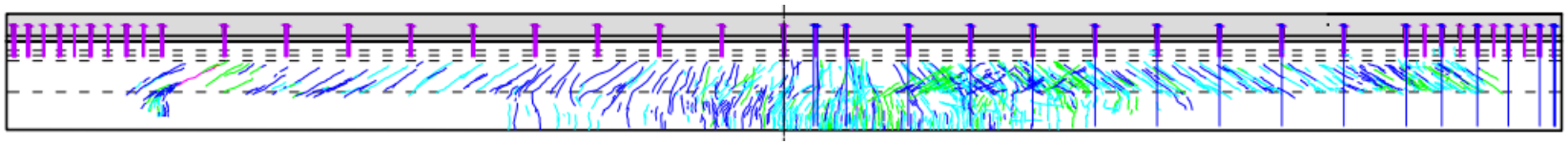

Note: Total actuator load is 813 kips.

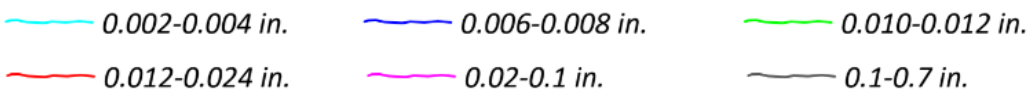

Figure 6.19. Tx34-1 Shear Test 2: Shear Cracks at End of Test.

As noted earlier, the LVDTs did not capture the small shear strain in the unreinforced region of the web during flexural testing; therefore, strain gages were installed to monitor the small strains developed at cracking for the test at the reinforced end. Figure 6.20 presents the LVDTs and the concrete surface strain gages that were installed after the flexure test. The location of the strain gages was governed by the presence of cracks developed during the flexure test. Cracks were avoided for the strain gage installation. The shear cracks were dominant at the ends, within 7 ft from the bearing. The damage at the interior support was in a crisscross pattern due to shear cracks at the interior support being perpendicular to the existing cracks after the previous flexure test.

(a) Cracks at LVDTs

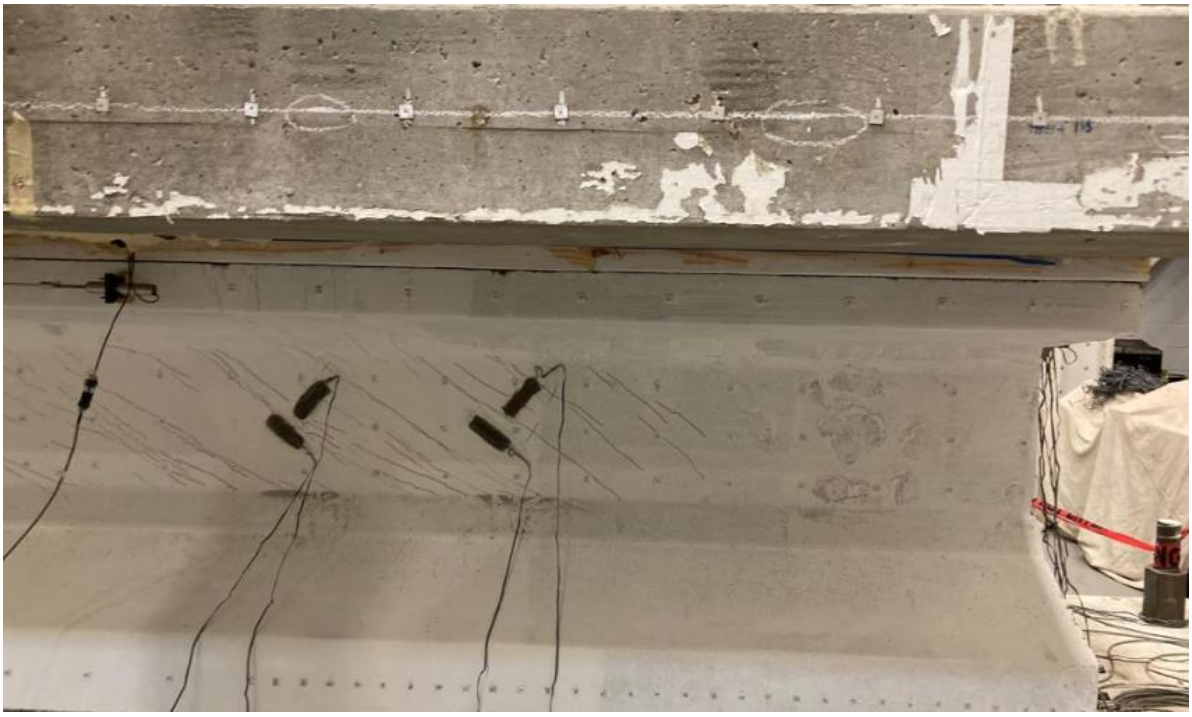

(b) Cracks at Strain Gages

Figure 6.20. Tx34-1 Shear Test 2: Shear Span of Reinforced End at Failure.

6.3.2.1 Transverse Reinforcement Strains

Figure 6.21(a) presents the schematic of the strain gages installed on the R-bars (transverse web reinforcement) at the reinforced end of the Tx34-1 girder specimen. As mentioned in Section 6.3.1.1, one strain gage was installed on each leg of the transverse reinforcement R-bar. Figure 6.21(b) shows the strains measured by these gages plotted versus shear force at the critical crack location at 3 ft from the nearest actuator load. The total actuator load is also presented as the secondary axis for reference.

There is a large difference between the strain gage SSG7 and SSG8 despite being on the same R-bar. There is also a small difference between SSG3 and SSG4 as well. This finding may be due to differential internal deformation of the two legs of the R-bars at the crack locations, or it could also be due to a bonding imperfection between the strain gage and the steel surface. SSG7 shows that the corresponding R-bar leg approached yielding, while the other R-bars did not yield at the shear failure. The yield strain for the 65 ksi bars was considered as 0.00224 for the transverse R-bars used in this research project. The strains increased with an increase in shear force being applied at the location of the respective R-bars. The first R-bar closest to the support showed negative strain, possibly due to compressive strut action close to the bearing. The other gages installed at R-bars away from the bearing pad showed tensile strain.

The shear capacity of the specimen was greater than 50 percent of the predicted shear capacity, which may have been due to higher tensile capacity of the UHPC matrix at the reinforced end. The fiber distribution was possibly denser with less fiber segregation compared to the unreinforced end, resulting in higher tensile strength. This hypothesis can be verified by the higher fiber distribution observed in the cores of the reinforced end of Tx34-1 when compared to its unreinforced end. The details are documented in the Volume 1 report, Section 8.4.1.1.

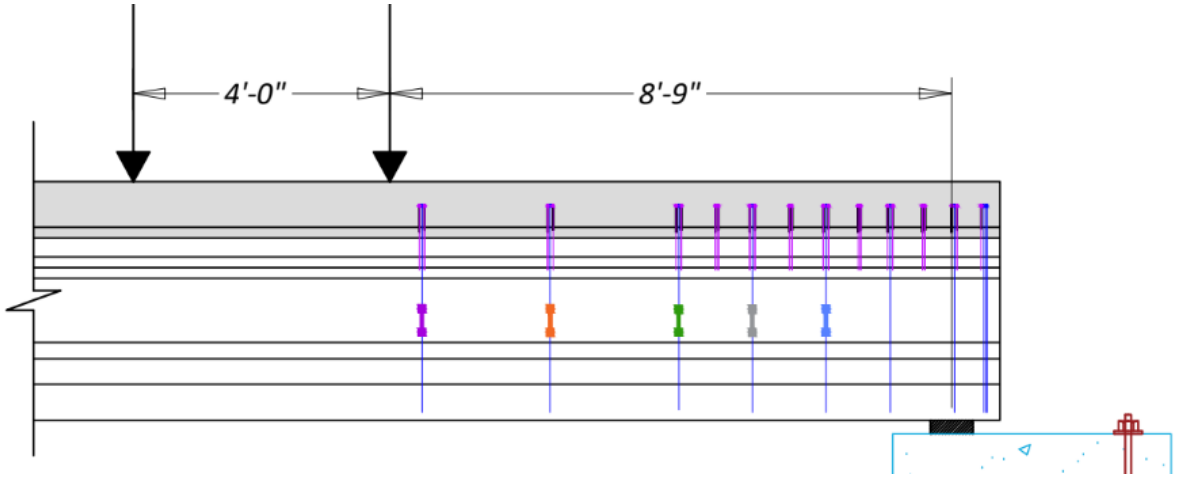

(a) Surface Steel Gages Installed on R-bars

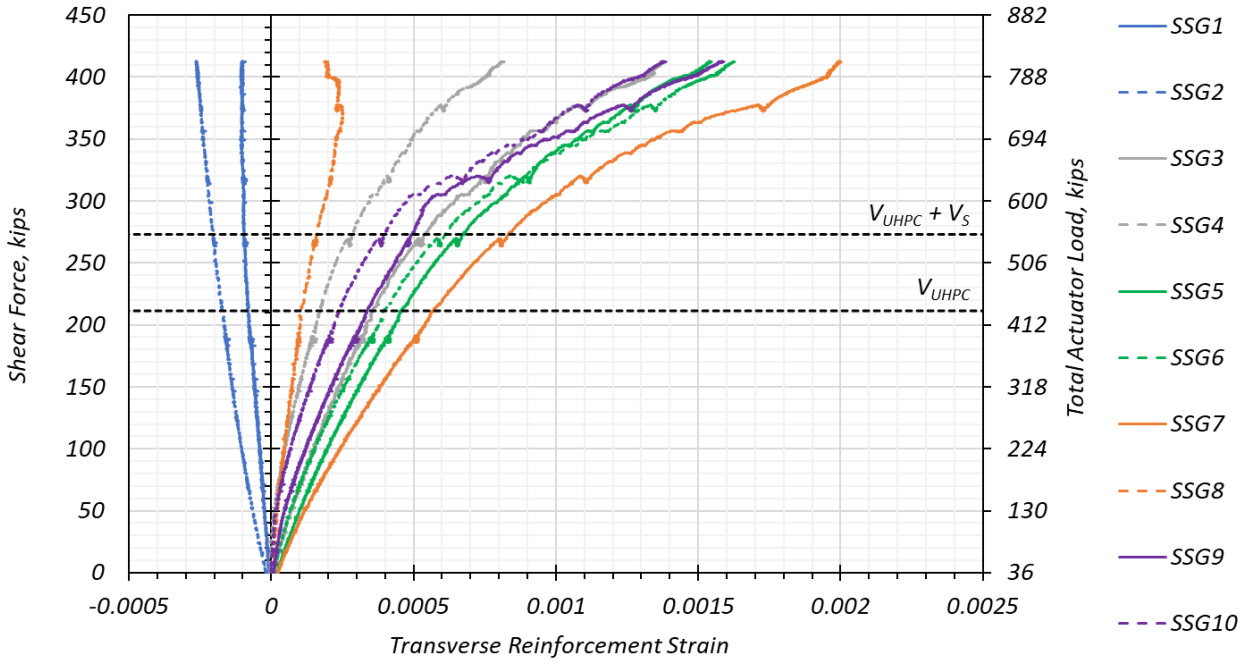

(b) Strains in Transverse Reinforcement Gages

Figure 6.21. Tx34-1 Shear Test 2: Transverse Reinforcement Strain Gages.

6.3.2.2 Additional Strain Measurements and Crack Angle

The LVDTs and SGs were located on the north face of the girder, while KSGs were located at the south face at approximately a similar location to the SGs. Figure 6.22(a) shows the arrangement of the LVDT rosette and the SGs. Figure 6.22(b) shows the schematic of the LVDT rosette and the SGs on the web. The KSGs are located on the other face of the girder behind the SGs, as shown in Figure 5.1 and Figure 6.2. Figure 6.22(c) presents the shear force at the region of major crack

development plotted against the strains measured by the LVDTs, SGs, and KSGs installed in the directions parallel and perpendicular to existing cracks. The analytically computed crack angle was 28.7 degrees. The crack angle computed from the LVDT rosette data was 29.5 degrees, while the physically measured crack angle was 34 degrees.

(a) Photograph of Tx34-1 at Peak Load

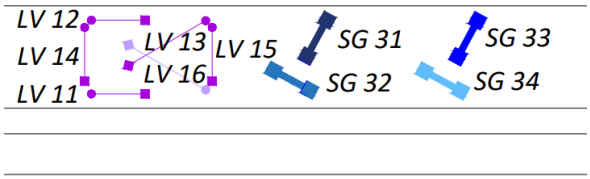

(b) Instrumentation Schematic of Shear End

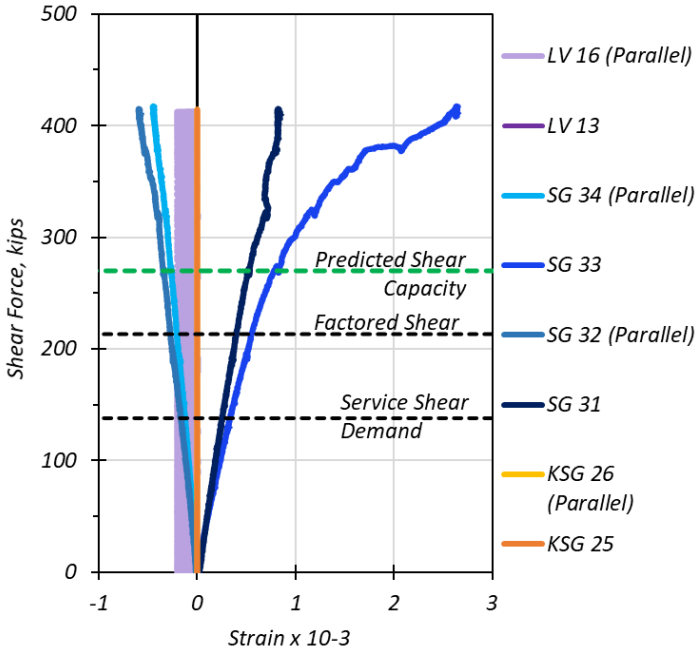

(c) Shear Force Versus Strain

Figure 6.22. Tx34-1 Shear Test 2: Web Strains (Reinforced End).

6.3.2.3 Shear Force versus Deflection

The shear force at the location of the most prominent crack was plotted against the maximum deflection observed in the shear span. Figure 6.23 presents the shear force versus the maximum deflection.

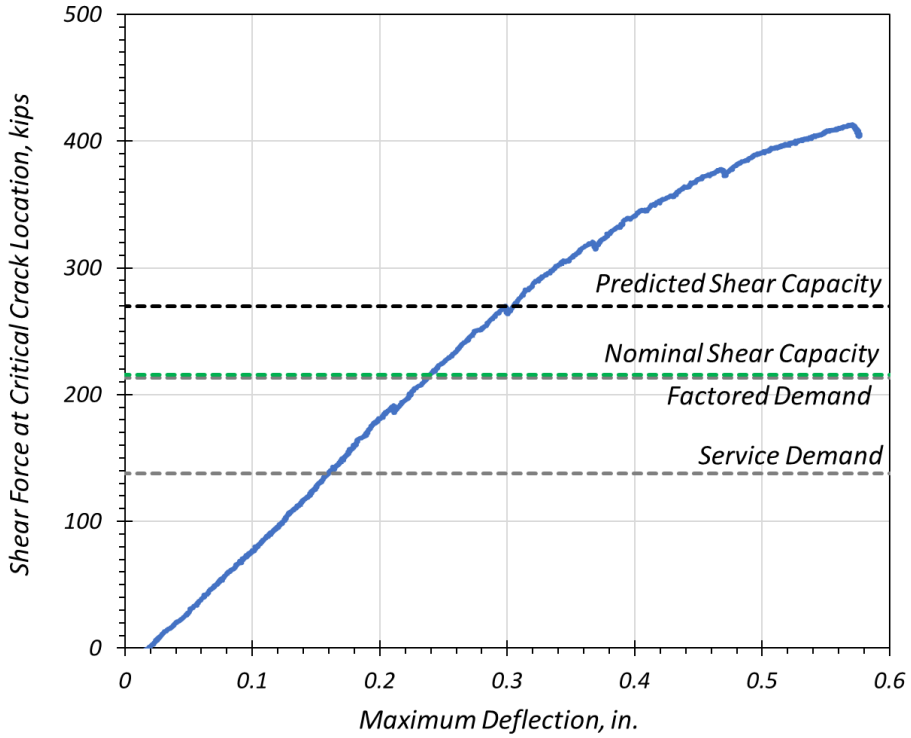

Figure 6.23. Tx34-1 Shear Test 2: Shear Force versus Maximum Deflection (Reinforced End).

6.3.2.4 Flexure Strains between the Actuators

Figure 6.24 presents the layout of the SPs in between the actuators. Figure 6.25 shows the strains recorded at the top of the CC deck and at the bottom of the UHPC girder between the actuators during Shear Test 2. These measurements are from a series of SPs across the width of the top surface of the deck. The bottom spring potentiometers were located on the bottom soffit of the UHPC girder to measure the bottom tension fiber strain. The SPs showed data trends similar to the prediction at the bottom of the specimen. The top SPs showed close to zero readings at the top of the CC deck. The SPs did not adequately detect strains of very small magnitudes in the prior flexure test and in this shear test. Therefore, surface concrete gages were installed between the actuators for subsequent shear tests to monitor the smaller magnitude strains at the top and bottom of the specimen.

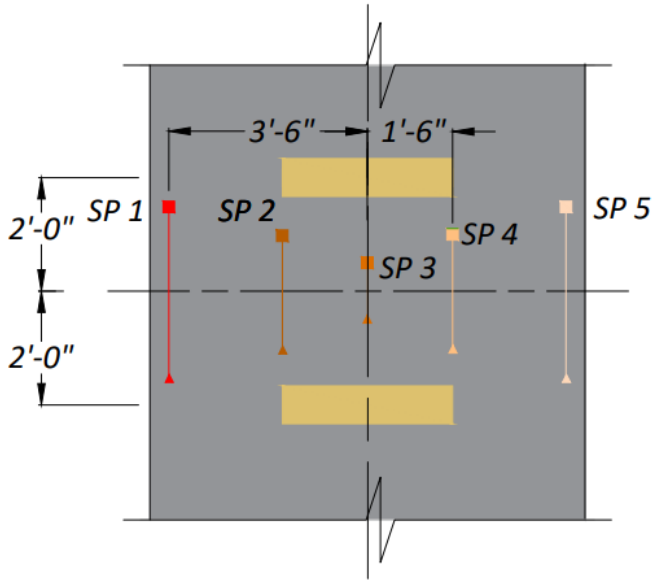

(a) Top of CC Deck Slab

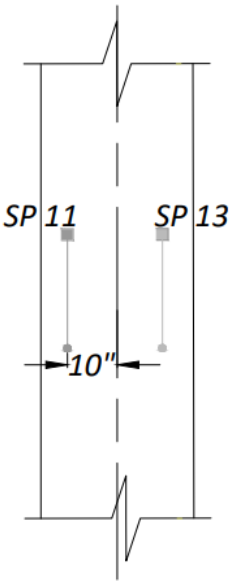

(b) Underside of UHPC Girder Soffit

Figure 6.24. Tx34-1 Shear Test 2: Layout of SPs (between Actuators).

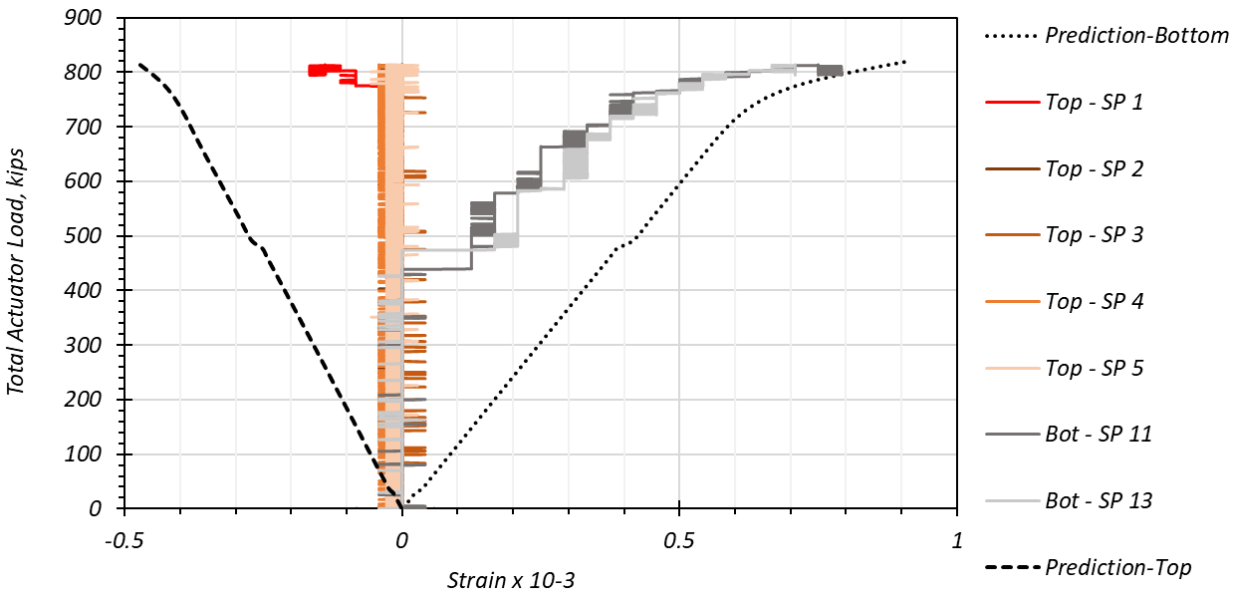

Figure 6.25. Tx34-1 Shear Test 2: Strains at Top of Deck and Bottom of Girder (between Actuators).

6.3.2.5 Deflection Profile

Figure 6.26(a) presents the schematic of the test setup when the reinforced end of Tx34-1 girder specimen was being tested. Figure 6.26(b) presents the deflection profile measured by an array of SPs along the tested span length.

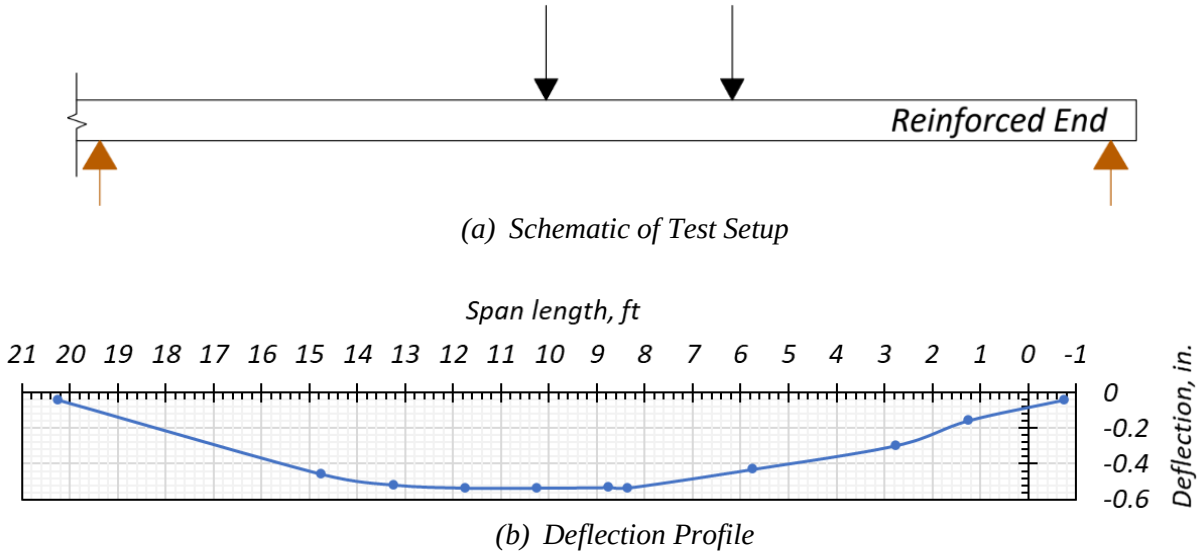

(a) Schematic of Test Setup

(b) Deflection Profile

Figure 6.26. Tx34-1 Shear Test 2: Deflection Profile.

6.3.2.6 Interface Shear between UHPC Girder and CC Deck

Figure 6.27(a) presents a schematic of the LVDTs used to measure the interface slip between the girder and the deck slab. Figure 6.27(b) provides the interface slip between the deck and the girder recorded at 5.5 ft from each girder end. There was a slip on the reinforced end of the girder, while no slip was measured at the unreinforced end of the girder. The shear slip at the reinforced end could potentially be due to the low coefficient friction between the UHPC girder and the CC deck. Roughening of the top surface can potentially reduce this slip. Increasing the interface reinforcement would also improve the interface shear resistance. The unreinforced end reads zero interface slip because it was not engaged during the testing as much as the reinforced end. The reinforced end was loaded with a higher force due to the higher capacity, and this factor could also have prompted the greater slip. A maximum slip of 0.034 in. was observed at the reinforced end.

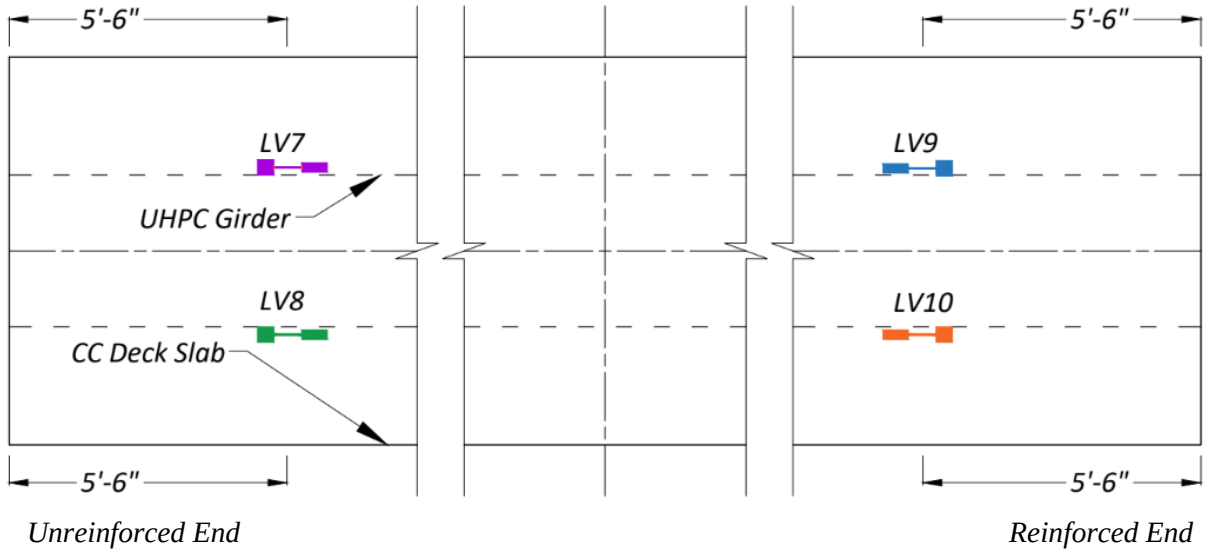

(a) Layout of LVDTs Measuring Interface Slip

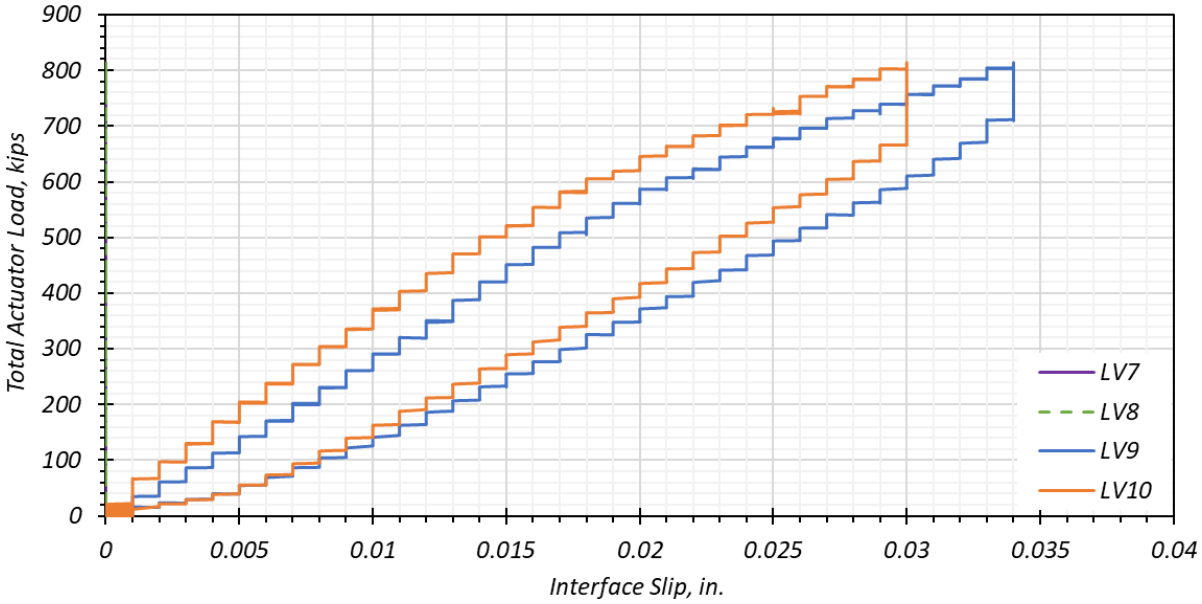

(b) Total Actuator Load versus Interface Slip

Note: LV7 and LV8 read zero data, which is interpreted as meaning zero slip at the unreinforced end.

Figure 6.27. Tx34-1 Shear Test 2: Interface Slip Measurements.

6.4 TX34-2 SHEAR TEST RESULTS

The second specimen, Tx34-2, was expected to have improved shear performance relative to the first specimen in shear due to the slightly better tensile strength determined for the small-scale samples, along with added transverse reinforcement at the reinforced end and the use of harped tendons. The unreinforced end was tested to failure using the capacity of one actuator at each end.

Each actuator was located 10.67 ft from each end. However, the as-built reinforced end was predicted to be much stronger than designed due to the presence of additional transverse bars placed by the precast plant personnel. The reinforced end was tested with two actuators placed 26 in. apart, with the actuator nearer to the bearing located 8.75 ft from the centerline of the bearing. Both the reinforced and unreinforced ends were symmetrical in terms of the test setup and instrumentation. The key events during the testing are documented and linked to the shear force occurring at the locations of major crack development. The shear forces noted are due to the applied loads and self-weight. The average first cracking strength obtained from direct uniaxial tensile strength tests for the Tx34-2 girder was taken as 0.63 ksi based on the material-level tests.

6.4.1 Shear Test 1

Figure 6.3 shows the test setup for this test. The span-to-depth ratio of this setup was 2.9:1. Both ends were loaded simultaneously with one actuator at each end. The unreinforced end developed shear cracks prior to the reinforced end, as expected. The LVDT, KSG, and SG sensors were used to monitor the locations of possible shear crack development. The shear force was computed at the location of the most prominent shear crack, which occurred 7.5 ft from the centerline of the bearing pad situated at the unreinforced end of the girder.

- At a shear force of 321 kips, hairline cracks were observed at the unreinforced end, with approximately 0.008 in. cracks appearing at the shear span. At this stage, spalling of the haunch concrete was observed.
- At a shear force of 380 kips, the cracking sound intensified at both ends.
- At a shear force of 436 kips, there was a loud sound emanating from the reinforced end.
- At a shear force of 488 kips, the cracks in the reinforced end widened, which marked the termination of the test.
- Finally, there was significant widening of the shear crack to approximately 0.7 in. There was another wide crack (0.50 in.) spanning around 4 ft from the end in the bottom flange of the unreinforced shear span that exposed a prestressing strand.

Table 6.13 presents the typical, minimum, and maximum crack widths observed at selected load steps when testing was paused to measure the crack widths at the unreinforced end.

Table 6.13. Range of Crack Widths for Tx34-2 Shear Test 1: Unreinforced End.

Shear Force, kips	Total Actuator Load, kips	Minimum Width, in.	Maximum Width, in.	Typical Width, in.
321	590	< 0.004	0.008	0.006
448	840	< 0.008	0.7	0.05

Figure 6.28 presents the schematic of the shear cracks at the end of Shear Test 1 of the unreinforced end of Tx34-2. Figure 6.29 presents the web shear cracking with the widest crack of 0.7 in. and the slip in the bottom flange at the interface of the prestressing strand. The figure also shows the exposed prestressing strand.

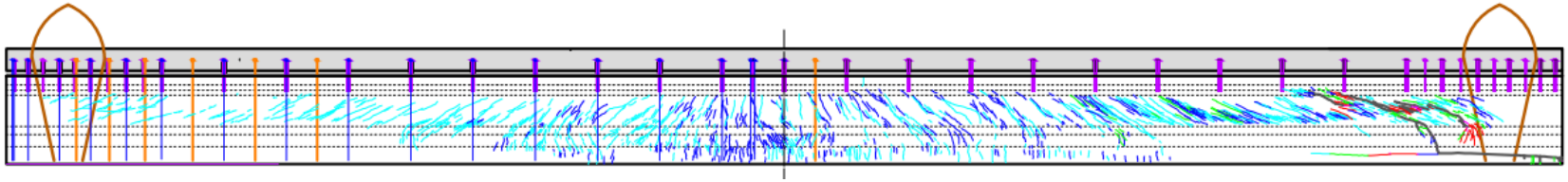

Note: Total actuator load = 840 kips.

0.002-0.004 in. 0.006-0.008 in. 0.010-0.012 in.
0.012-0.024 in. 0.02-0.1 in. 0.1-0.7 in.

Figure 6.28. Tx34-2 Shear Test 1: Shear Cracks at End of Test.

(a) Unreinforced End of Tx34-2 after Shear Failure

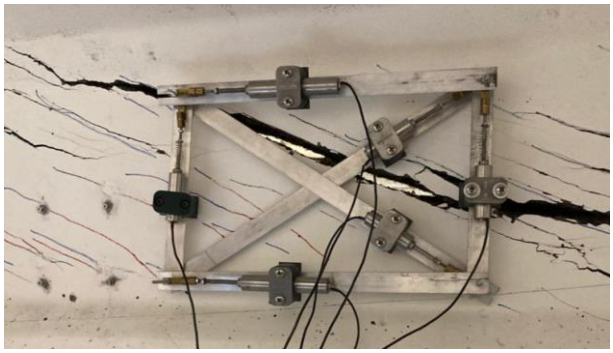

(b) Shear Crack in the Web

(c) Exposed Prestressing Strand

Figure 6.29. Tx34-2 Shear Test 1: Unreinforced End Photos of Damage.

6.4.1.1 Transverse Reinforcement Strains

Figure 6.30(a) presents a schematic of the strain gages installed in the transverse stirrups of the Tx34-2 girder at the reinforced end. Figure 6.30(b) provides the measured strains during Shear Test 1, which resulted in the failure of the unreinforced end without the hoops. The shear force was determined at the critical crack location, which is 4 ft from the nearest actuator load at the unreinforced end. The plot of the shear force versus the transverse steel strain at the reinforced end shows that the strains were highest for the R-bars located at 5.75 to 8.75 ft from the support centerline located nearest to the transverse reinforcement. The R-bars showed measured strain at

a shear force of 440 kips without yielding of the bars (assuming 0.00224 yield strain corresponds to a more realistic expected yield strength of 65 ksi for Grade 60 reinforcement).

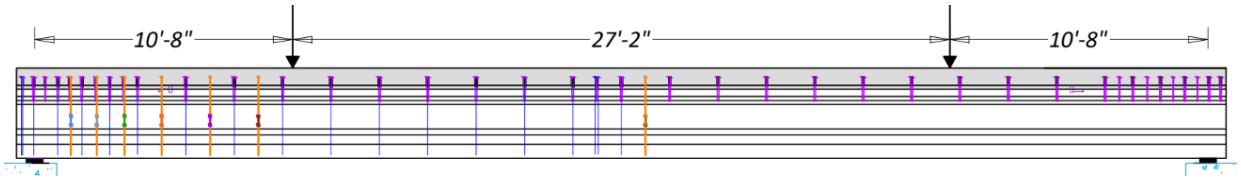

(a) Surface Steel Gages Installed on R-bars

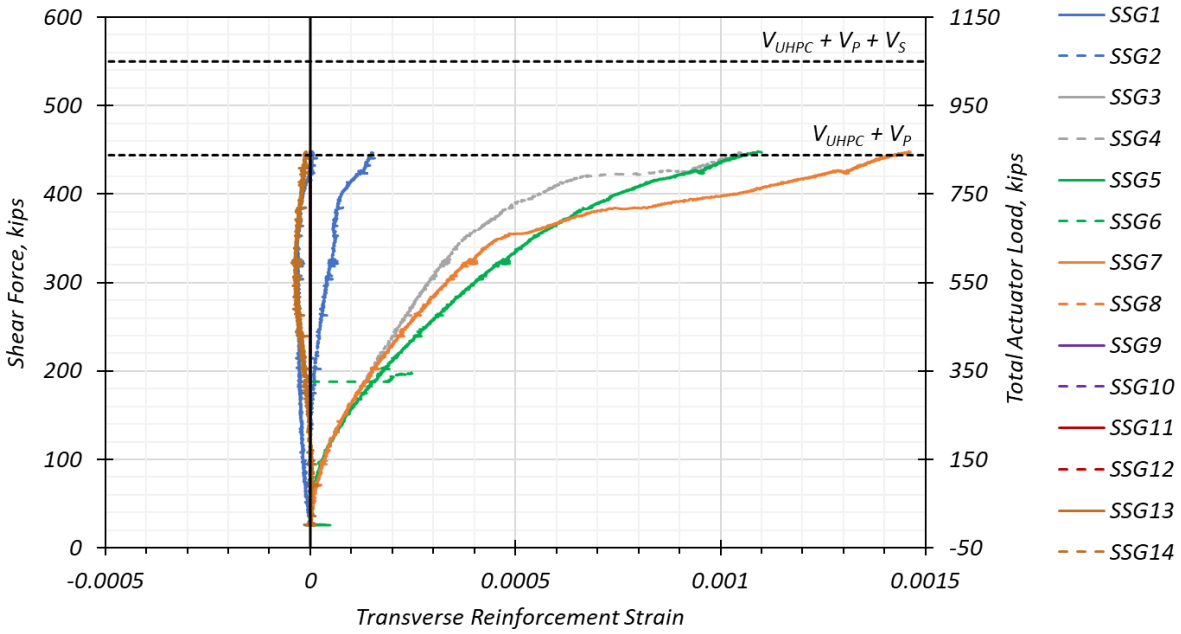

(b) Strains in Transverse Reinforcement Gages

Figure 6.30. Tx34-2 Shear Test 1: Transverse Reinforcement Strain Gages.

6.4.1.2 Additional Strain Measurements and Crack Angle

Similar to the LVDT, KSG, and SG arrangement for the testing of Tx34-1, one LVDT rosette, one pair of KSGs, and one pair of SGs were installed at each end of the girder specimen. Figure 6.31(a) shows the arrangement of the LVDT rosette, KSGs, and SGs. Figure 6.31(b) shows the schematic of the LVDT rosette, KSGs, and the SGs on the web. Figure 6.22(c) presents the shear force at the region of major crack development plotted against the strains measured by the LVDTs, SGs, and KSGs installed in the directions parallel and perpendicular to existing cracks. The analytically computed crack angle was 24.1 degrees. The crack angle could not be computed from the LVDT rosette because the measured data were insufficient to compute the angle. The physically measured angle was 20 degrees.

(a) Photograph of Tx34-2 at Peak Load

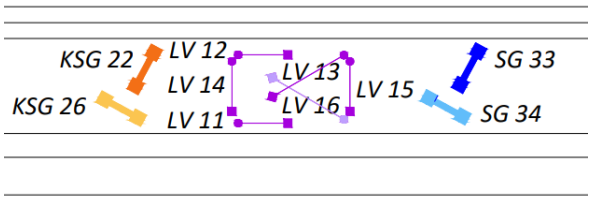

(b) Instrumentation at Shear End

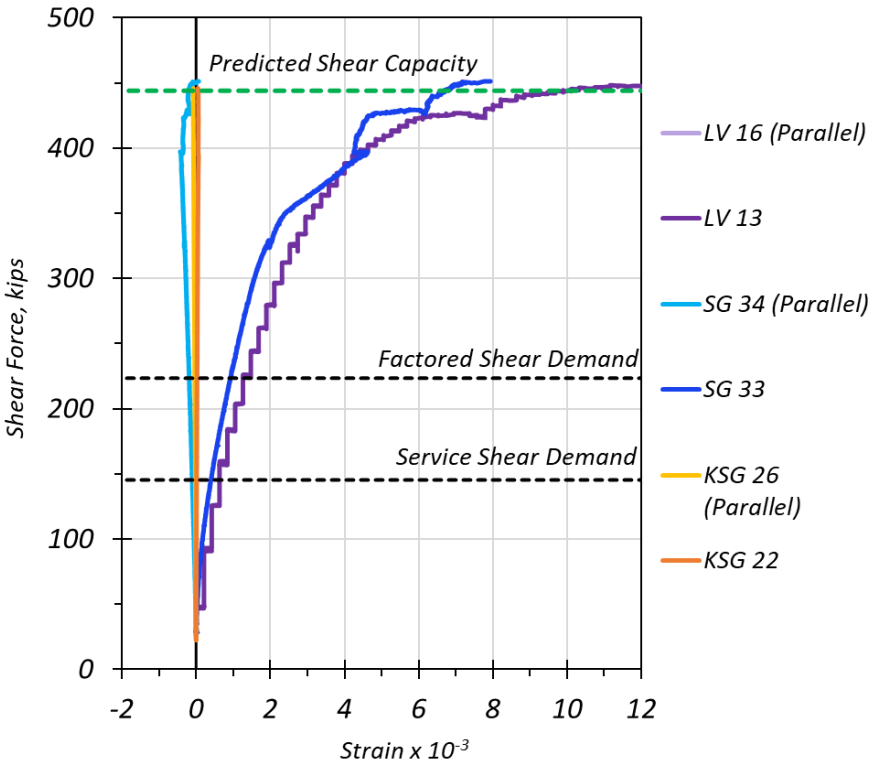

(c) Shear Force Versus Strain

Figure 6.31. Tx34-2 Shear Test 1: Web Strains (Unreinforced End).

6.4.1.3 Shear Force versus Deflection

The shear force at the location of the most prominent crack (7.5 ft from the centerline of the bearing pad situated at the unreinforced end of the girder) was plotted against the maximum deflection observed in the shear span. Figure 6.32 presents the shear force versus the maximum deflection. Note that the nominal shear capacity and predicted shear capacity correspond to the unreinforced end.

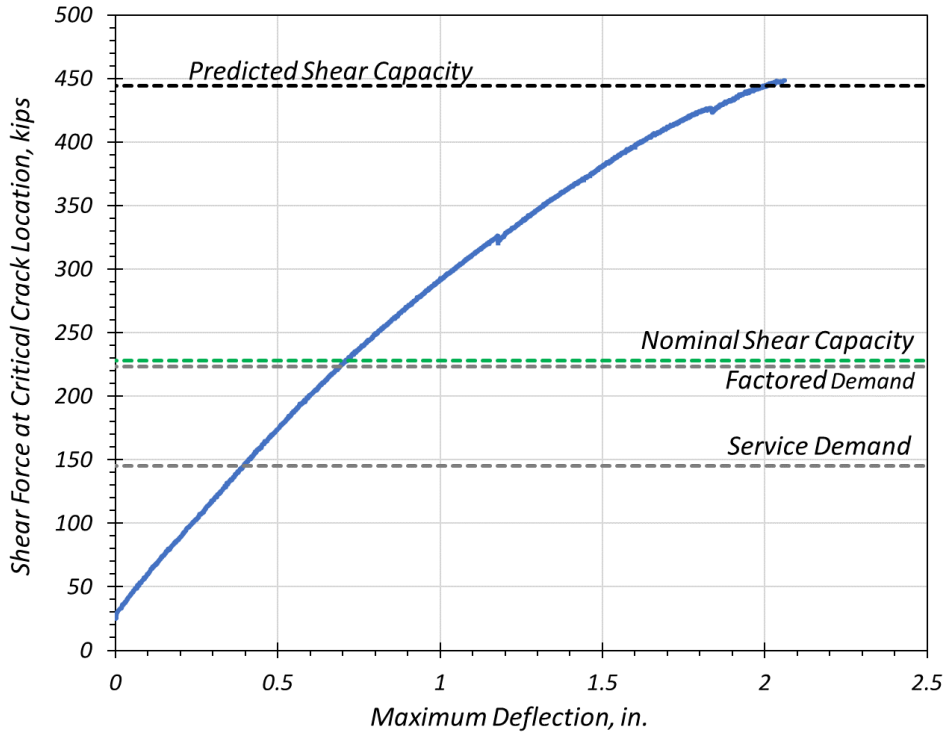

Figure 6.32. Tx34-2 Shear Test 1: Shear Force versus Maximum Deflection (Unreinforced End).

6.4.1.4 Flexure Strains between the Actuators

Figure 6.33 presents the layout of the SPs and SGs installed at the top of the CC deck and the bottom of the UHPC girder. Based on the observations of the previous flexure and shear tests, SGs were added to monitor the top and bottom strains. Figure 6.34 shows the strains measured by the strain gages and SPs located at the top and bottom of the composite girder in between the two actuators. These strains were compared with the predicted top and bottom strains computed from the moment-curvature analysis described in Section 5.3.2. The top strains from both SGs and SPs follow the same trend as the prediction. The strain at the bottom of the girder was more than the predicted strain, as shown by the larger strains on the SPs and the SGs. This result could potentially be due to not fully capturing the cracking of the girder after the flexure test in the assumptions used to compute the predicted strains.

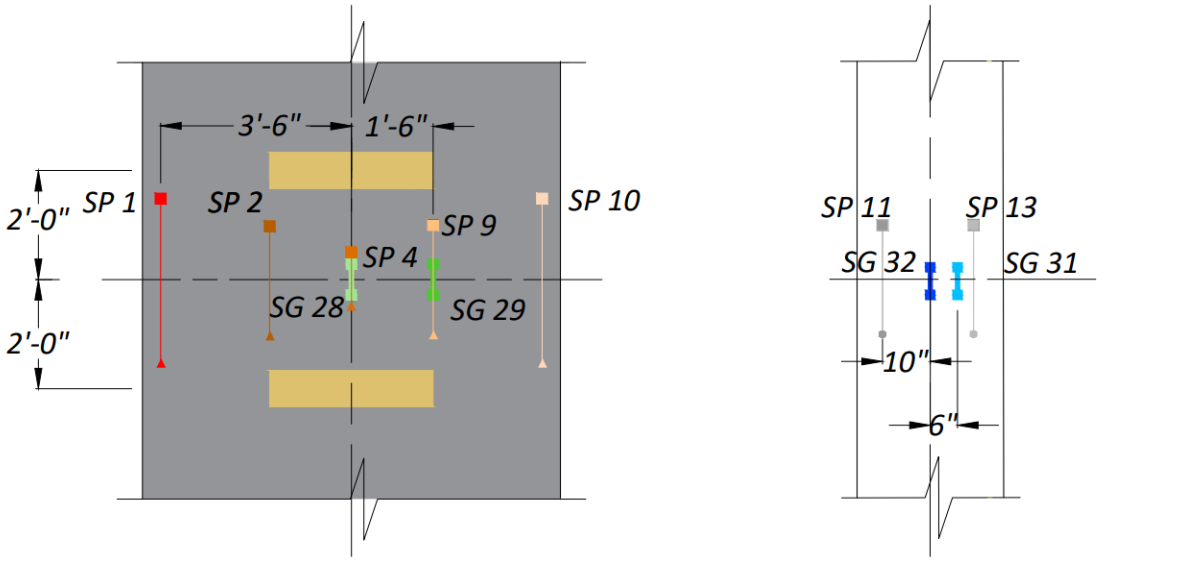

(a) Top of CC Deck Slab *(b) Underside of UHPC Girder Soffit*

Figure 6.33. Tx34-2 Shear Test 1: Layout of SPs (between Actuators).

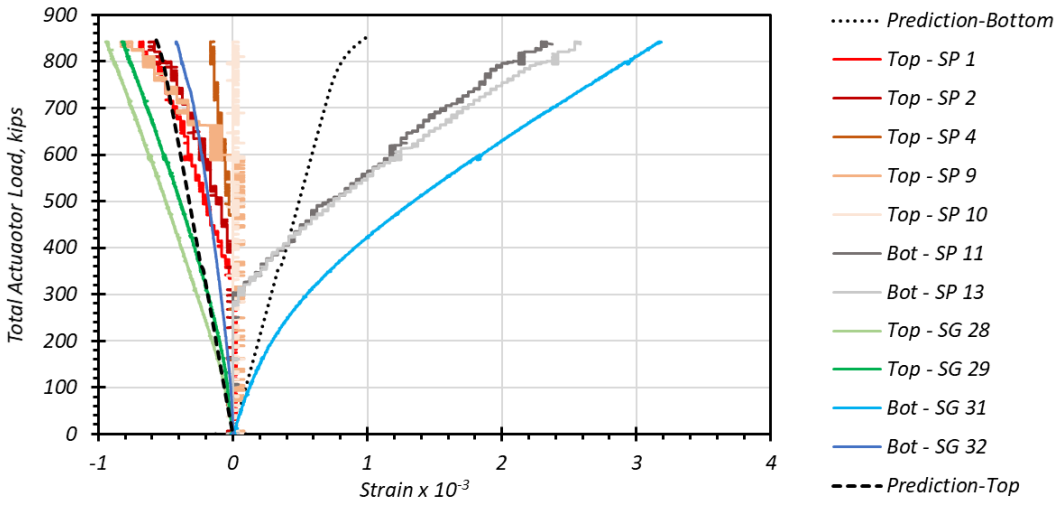

(a) Top and Bottom Strains (SP and SG)

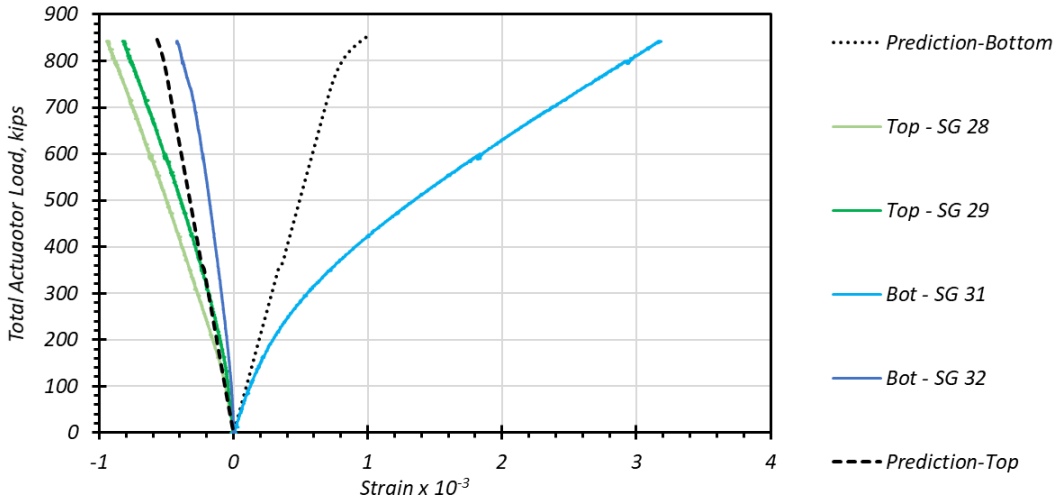

(b) Top and Bottom Strains (SG only)

Figure 6.34. Tx34-2 Shear Test 1: Strains at Top of Deck and Bottom of Girder (between Actuators).

6.4.1.5 Deflection Profile

Figure 6.35(a) and(b) present a schematic of the test setup and the deflection profile measured by vertical SPs installed along the span length.

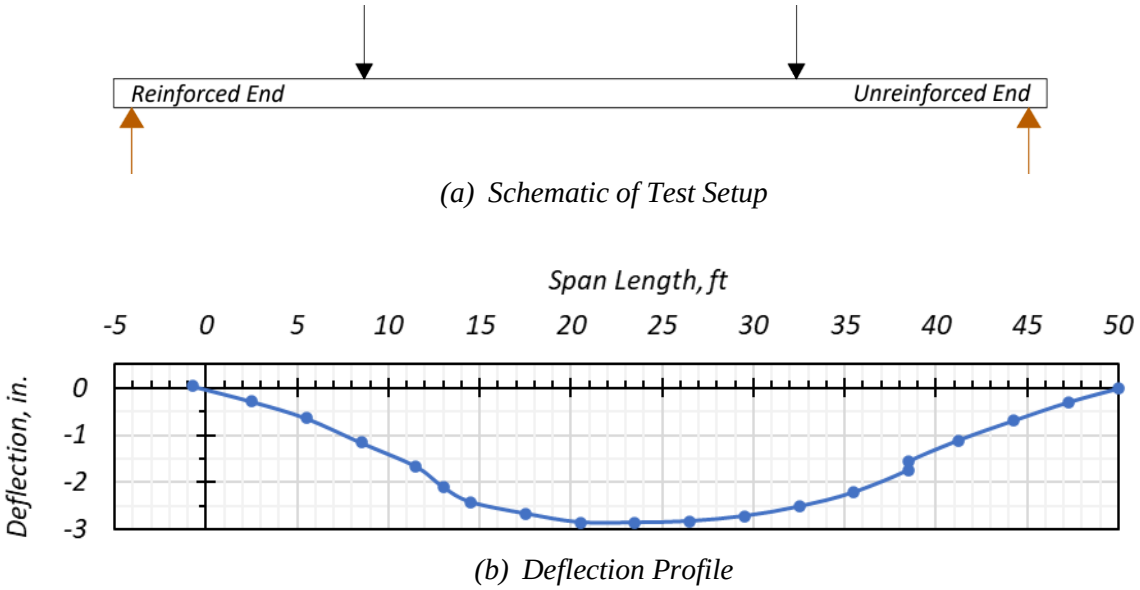

(a) Schematic of Test Setup

(b) Deflection Profile

Figure 6.35. Tx34-2 Shear Test 1: Deflection Profile.

6.4.1.6 Interface Shear between UHPC Girder and CC Deck

Figure 6.36(a) presents a schematic of the LVDTs installed at the CC deck and UHPC girder interface to measure interface slip. Figure 6.36(b) presents the interface slip measured between the deck and the girder at 5.5 ft from each girder end. The unreinforced end showed slightly less slip than the reinforced end. A maximum interface slip of 0.098 in. was observed at the reinforced end, while a maximum slip of 0.075 in. was observed at the unreinforced end. Although this difference is very small, note that the unreinforced end does have slightly more reinforcement across the interface due to the use of only #5 UC bars, while the reinforced end includes #5 UC bars and smaller diameter #4 R-bars.

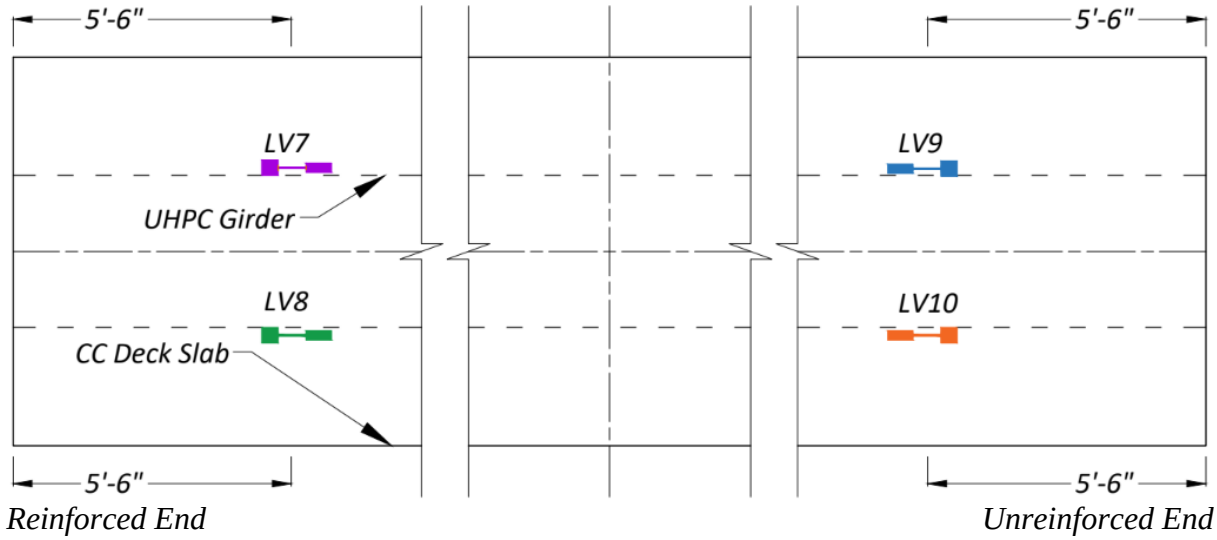

(a) Layout of LVDTs Measuring Interface Slip
[Note: LVDTS are located at interface of UHPC girder and deck.]

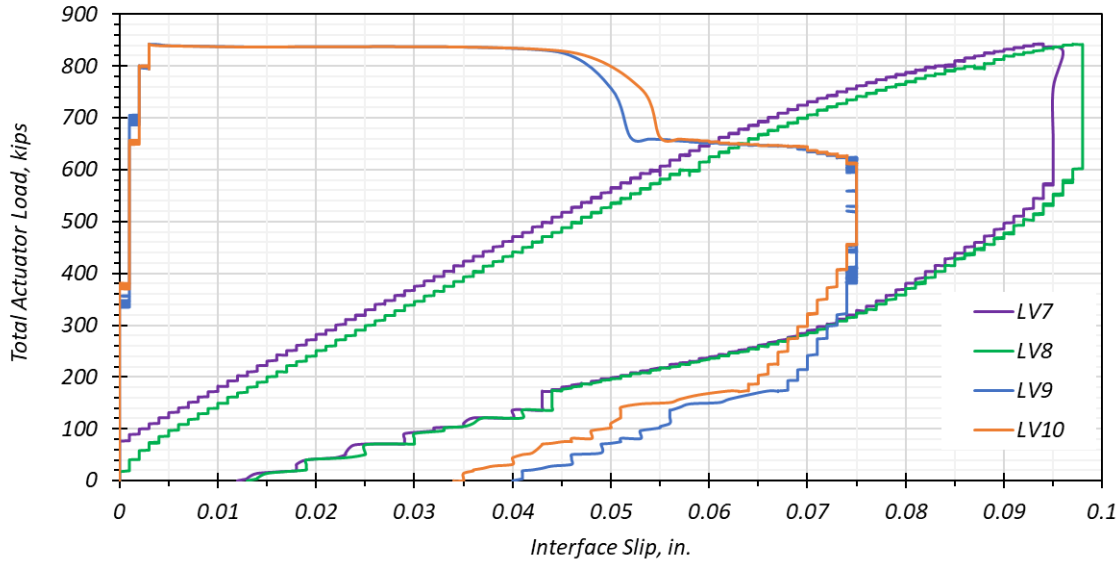

(b) Total Actuator Load versus Interface Slip

Figure 6.36. Tx34-2 Shear Test 1: Interface Slip Measurements.

6.4.2 Shear Test 2: Reinforced End

Figure 6.5 shows the test setup for the Tx34-2 Shear Test 2, which was used to more fully evaluate the shear capacity of the reinforced end. The span-to-depth ratio for this end was 2.4:1. Due to the extra transverse bars in the reinforced end, the span length of the shear test was altered. The closely spaced transverse R-bars were excluded from the testing span, and part of the unreinforced end

that was damaged under the previous shear test was also excluded from the testing span, thereby giving a reduced span length of 28 ft. The reinforced end was loaded with two actuators. The shear force was computed at the location of the major shear damage, which was 7 ft from centerline of the bearing pad at the reinforced end of the girder specimen. Key observations during testing include the following:

- At 228 kips shear force, the first cracking sounds were heard and progressively increased as the shear force went up to around 289 kips at the reinforced end.
- As the shear force increased to 308 kips at the unreinforced end, hairline cracking increased within the unreinforced shear span. This occurrence prompted the research team to hold the position of the actuator at the unreinforced end while continuing to increase the load on the actuator at the reinforced end.
- At around 309 kips shear force, the cracking of the reinforced end intensified. As the load on the reinforced end actuator peaked to 506 kips, the unreinforced end actuator dropped to 354 kips. There was a loud sound at a shear force of 312 kips, followed by another sound at 317 kips shear force. The widest shear crack observed was 0.3 in., with branching cracks varying from 0.004–0.24 in.

Figure 6.37 presents the schematic of the shear cracks at the end of Shear Test 2 of the reinforced end of Tx34-2. Figure 6.38 presents the damage after the shear failure of the reinforced end of the specimen. Table 6.14 presents the typical, minimum, and maximum crack widths observed at load steps when testing was paused to measure the crack widths.

Table 6.14. Range of Crack Widths for Tx34-2 Shear Test 2: Reinforced End.

Shear Force, kips	Total Actuator Load, kips	Minimum Width, in.	Maximum Width, in.	Typical Width, in.
228	600	< 0.004	0.008	0.006
312	860	< 0.008	0.3	0.24

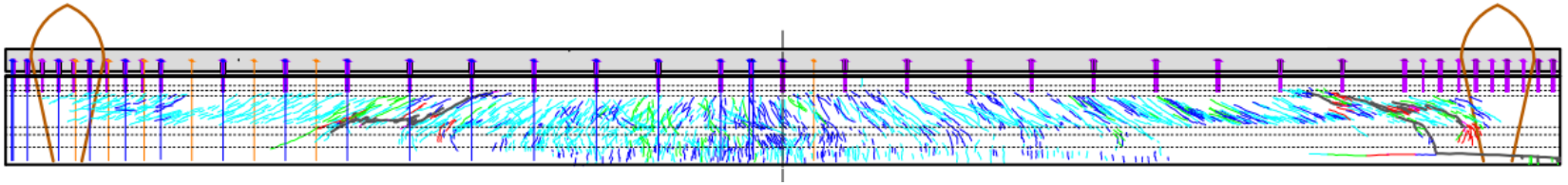

Note: Total actuator load = 860 kips.

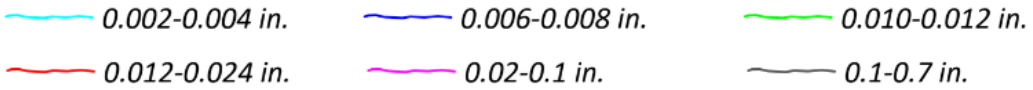

Figure 6.37. Tx34-2 Shear Test 2: Shear Cracks at End of Test (Load near Reinforced End).

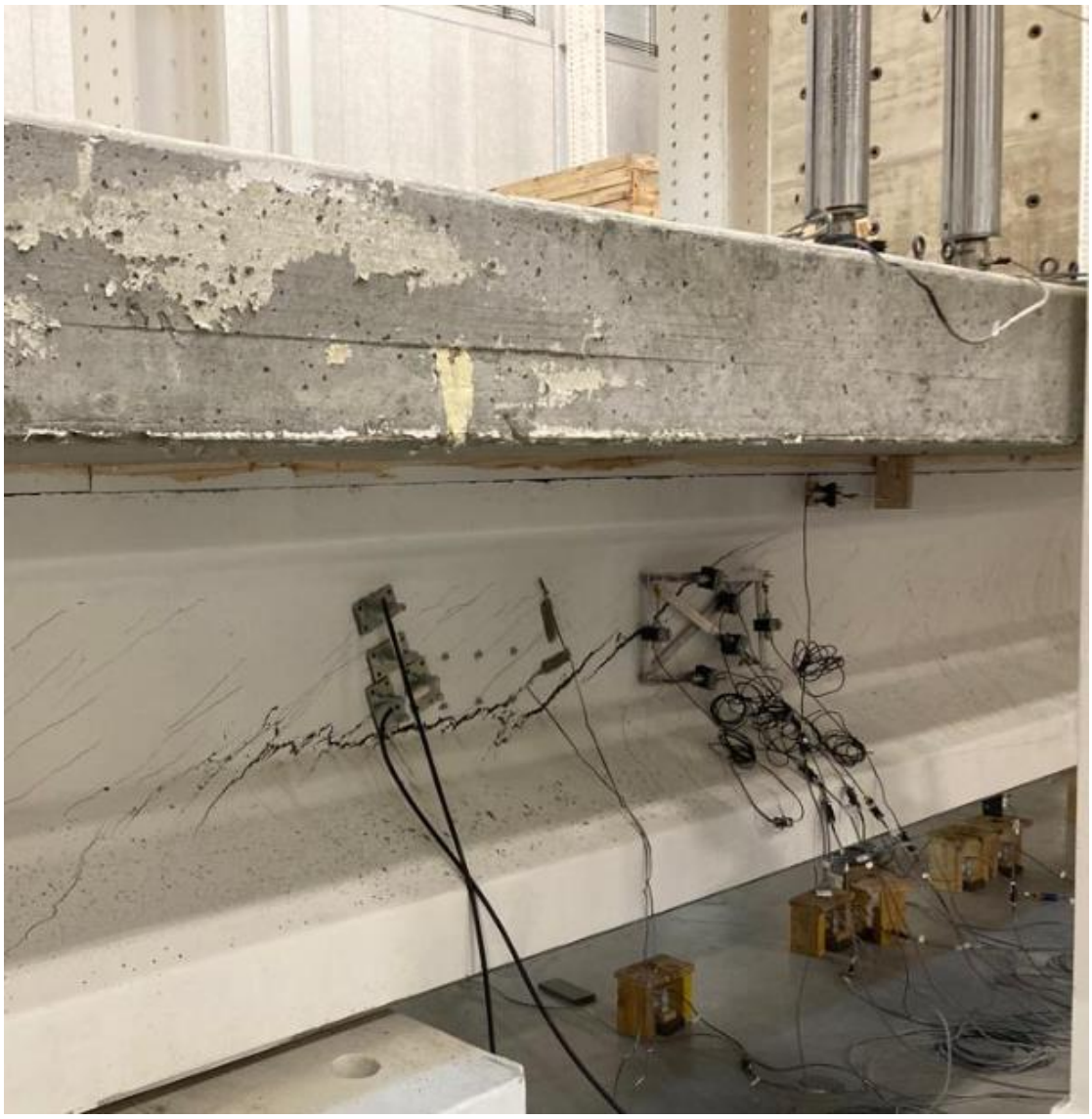

Figure 6.38. Tx34-2 Shear Test 2: Shear Span of Reinforced End at Failure.

6.4.2.1 Transverse Reinforcement Strains

Figure 6.39(a) and (b) illustrate the instrumented R-bars in Tx34-2 and the strains measured by those strain gages during the test. The shear force plotted versus the steel strain was computed at the critical crack location at 2.5 ft from the nearest actuator at the reinforced end.

As mentioned earlier, the end with minimum transverse reinforcement had more web reinforcement than the designed capacity. This capacity was predicted to be higher than the total shear force that could be generated by a shear setup utilizing the full capacity of the actuators in the lab. To test the capacity of the end with minimum web reinforcement of 24 in. spacing between

the stirrups, the additionally placed transverse bars were excluded from the tested shear span length by adjusting the location of the pedestals suitably. The steel strain gages located on the R-bar near the midspan shows the maximum strain recorded. One of the strain gages on this R-bar yielded.

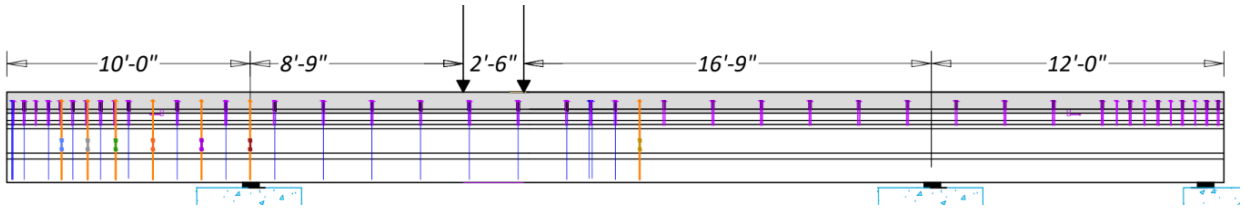

(a) Surface Steel Gages Installed on R-bars

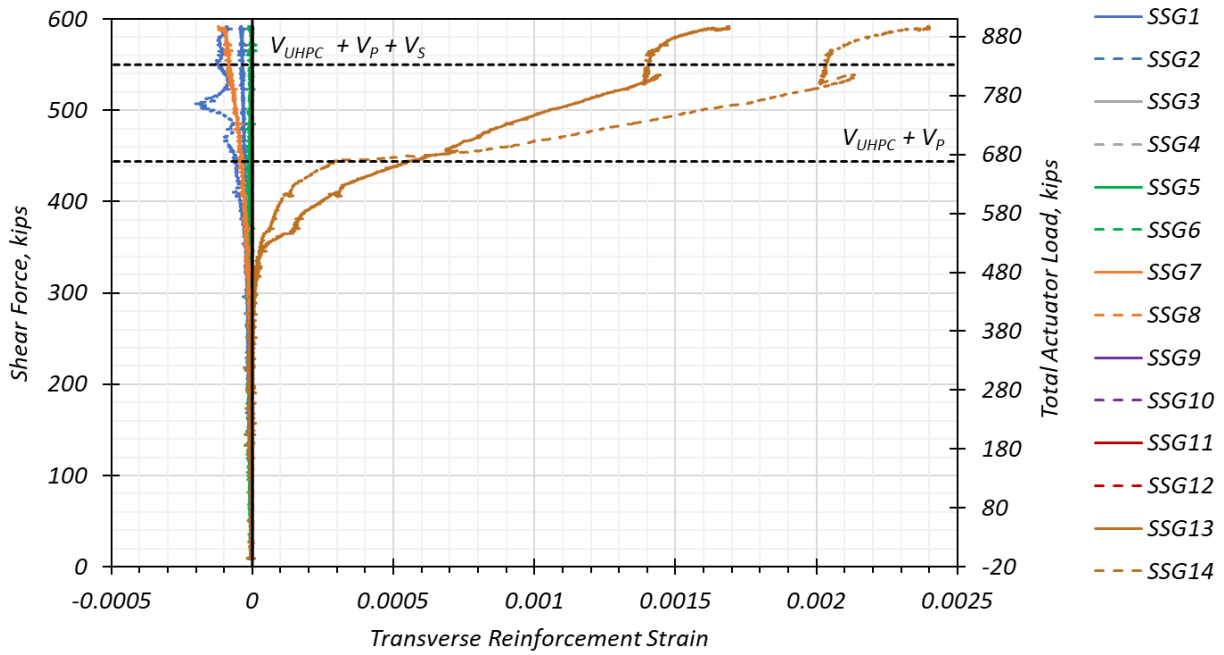

(b) Strains in Transverse Reinforcement Gages

Figure 6.39. Tx34-2 Shear Test 2: Transverse Reinforcement Strain Gages.

6.4.2.2 Additional Strain Measurements and Crack Angle

Figure 6.40(a) shows the arrangement of the LVDT rosette, KSGs, and SGs. Figure 6.40(b) shows the schematic of the LVDT rosette, KSGs, and the SGs on the web. Figure 6.40(c) presents the shear force at the region of major crack development at the reinforced end plotted versus the strains measured by the LVDTs, SGs, and KSGs installed in the directions parallel and perpendicular to existing cracks. The analytically computed crack angle was 27.1 degrees. The crack angle computed from the LVDT rosette was 27 degrees, while the physically measured angle was 26 degrees.

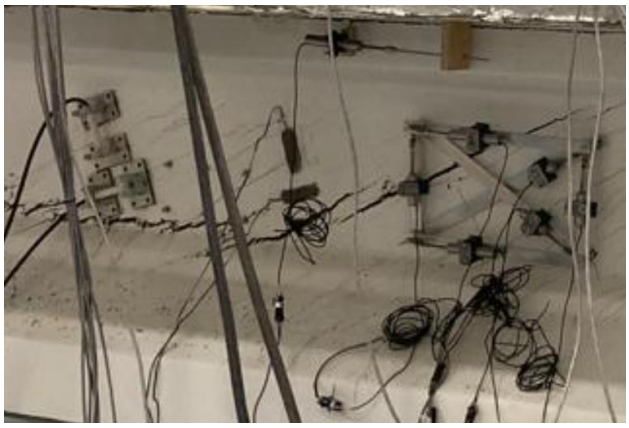

(a) Photograph of Tx34-2 at Peak Load

(b) Instrumentation Schematic of Shear End

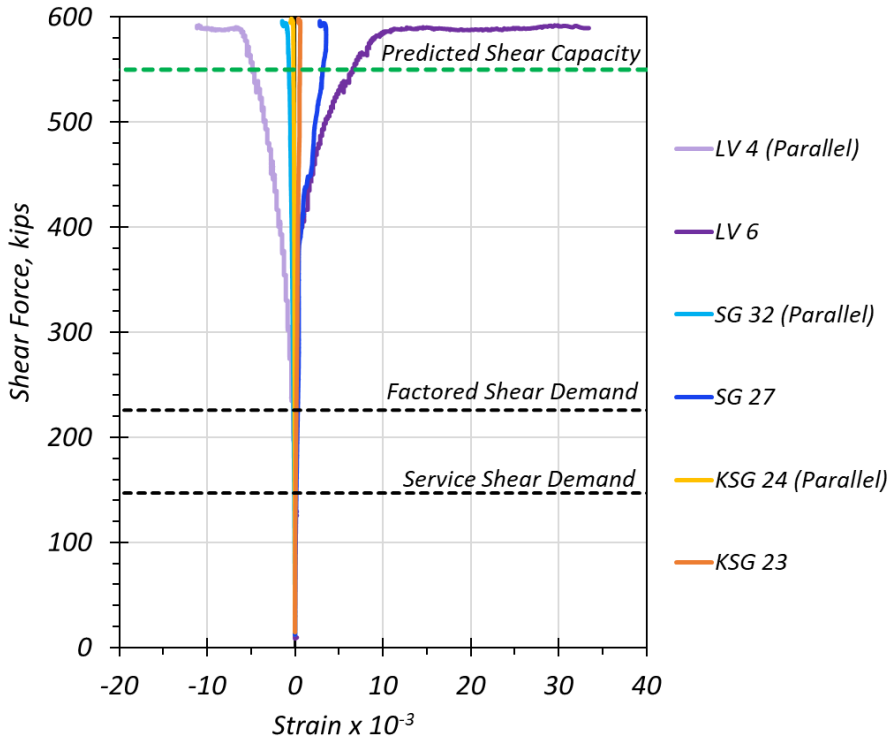

(c) Shear Force Versus Strain

Figure 6.40. Tx34-2 Shear Test 2: Web Strains (Reinforced End).

6.4.2.3 Shear Force versus Deflection

The shear force at the location of the most prominent crack at the reinforced end was plotted versus the maximum deflection observed in the shear span. Figure 6.41 presents the shear force versus the maximum deflection.

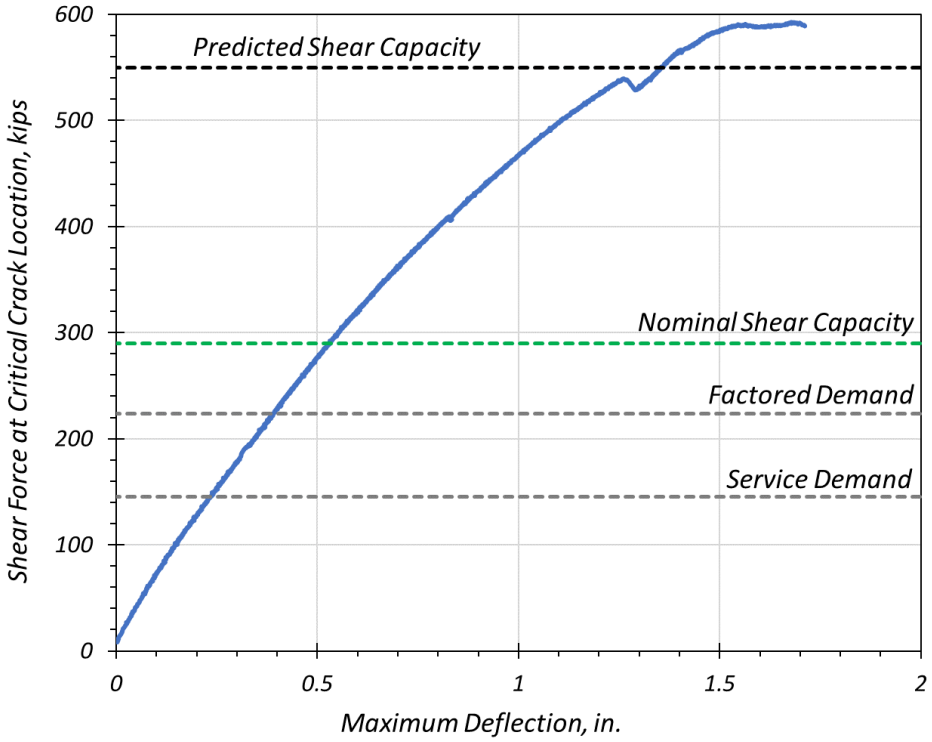

Figure 6.41. Tx34-2 Shear Test 2: Shear Force versus Maximum Deflection (Reinforced End).

6.4.2.4 Flexure Strains between the Actuators

Figure 6.42 presents the layout of the SPs and SGs installed on the top surface of the CC deck and the bottom surface of the UHPC girder. Figure 6.43 shows the strains measured by the strain gages and SPs located at the top and bottom of the composite girder in between the two actuators. These strains were compared to the predicted top and bottom strains computed from the moment-curvature analysis described in Section 5.3.2. The top strains from both SGs and SPs follow the same trend as the prediction. The bottom SP showed almost zero data until the load of test termination, while the SGs showed a greater strain than the prediction. This result was possibly due to not fully capturing the cracking of the girder after the flexure and shear tests in the assumptions used to compute the predicted strains.

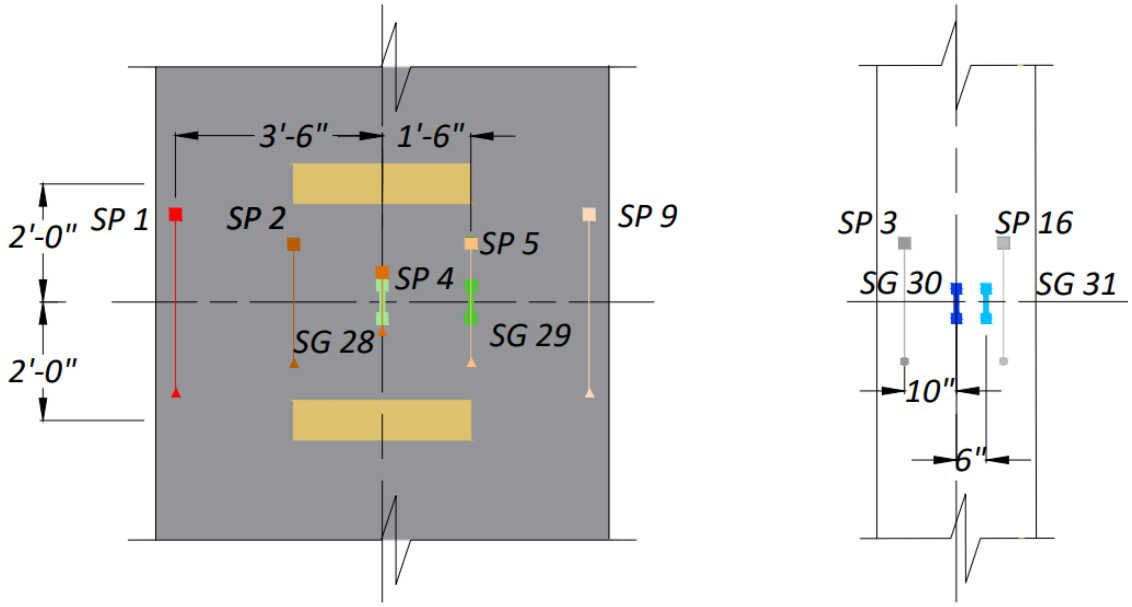

(a) Top of CC Deck Slab *(b) Underside of UHPC Girder Soffit*

Figure 6.42. Tx34-2 Shear Test 2: Layout of SPs (between Actuators).

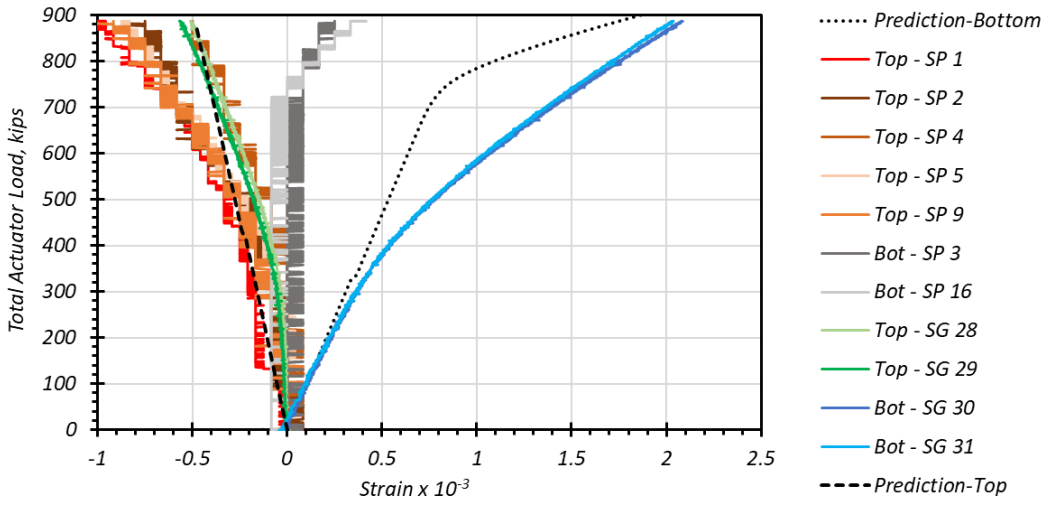

(a) Top and Bottom Strains (SP and SG)

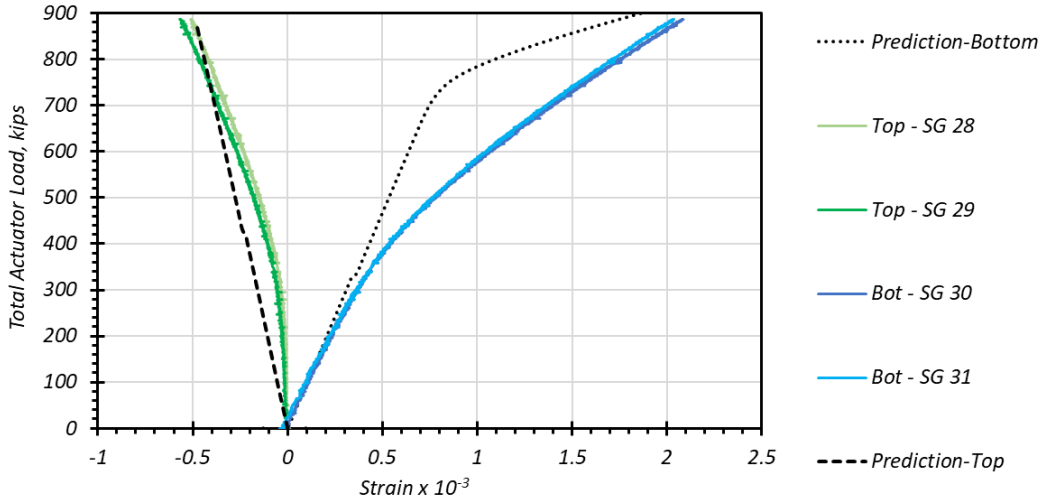

(b) Top and Bottom Strains (SG only)

Figure 6.43. Tx34-2 Shear Test 2: Strains at Top of Deck and Bottom of Girder (between Actuators).

6.4.2.5 Deflection Profile

Figure 6.44(a) presents the schematic of the test setup. Figure 6.44(b) presents the deflection profile measured by SPs installed along the span length. The deflection was less than the previous shear test of the specimen due to the smaller span length of Shear Test 2.

(a) Schematic of Test Setup

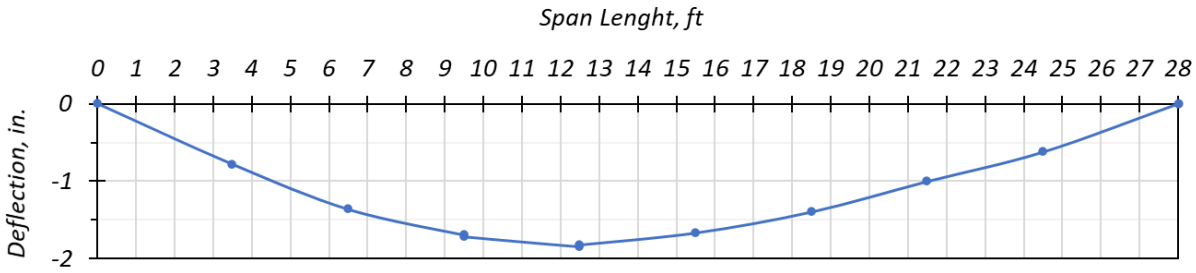

(b) Deflection Profile

Figure 6.44. Tx34-2 Shear Test 2: Deflection Profile.

6.4.2.6 Interface Shear between UHPC Girder and CC Deck

Figure 6.45(a) presents a schematic of the LVDTs installed at the CC deck and UHPC girder interface to measure interface slip. Figure 6.45(b) presents the interface slip measured between the deck and the girder at 5.5 ft from each girder end. The unreinforced end was observed to show less slip when compared to the reinforced end. A maximum interface slip of 0.19 in. was observed at the reinforced end, while a maximum slip of 0.07 in. was observed at the unreinforced end. It can be noted that the unreinforced end had slightly more reinforcement across the interface due to the use of only #5 UC bars, while the reinforced end included #5 UC bars with smaller diameter #4 R-bars. In addition, a higher shear force was applied to the reinforced end.

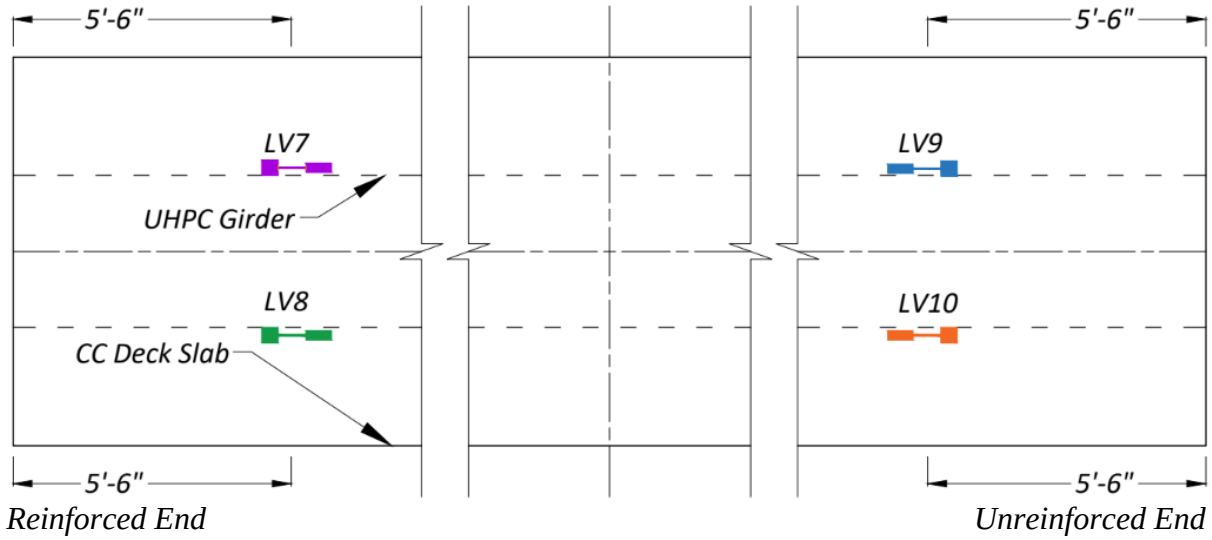

(a) Layout of LVDTs Measuring Interface Slip

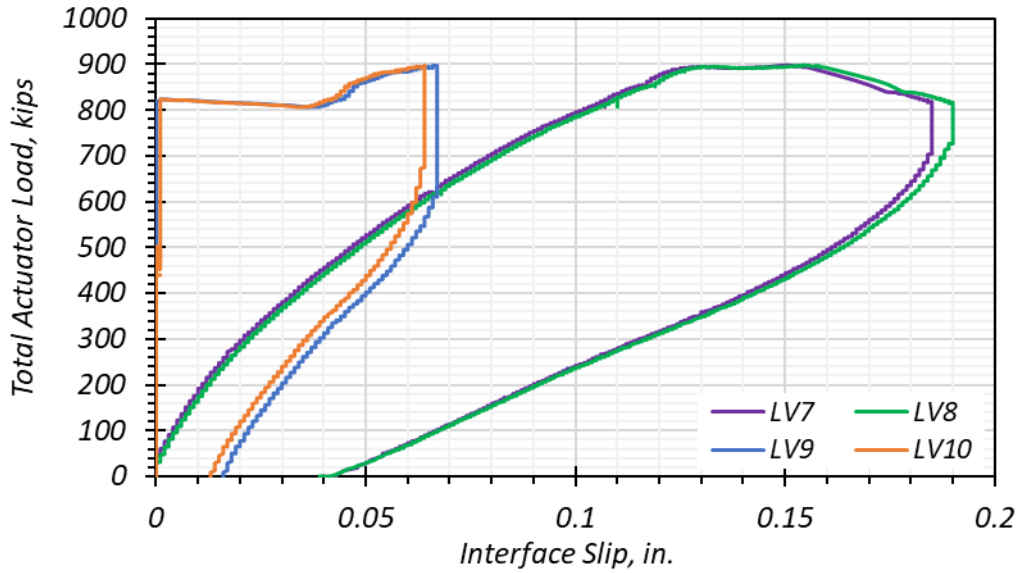

(b) Total Actuator Load versus Interface Slip

Figure 6.45. Tx34-2 Shear Test 2: Interface Slip Measurements.

6.5 TX54 SHEAR TEST RESULTS

The third specimen, Tx54, was expected to have the highest shear capacity due to a deeper web, a greater number of tendons (including more harped tendons), and a greater tensile strength of the companion uniaxial tension specimens than the other girder specimens. Therefore, as in the case of the reinforced end of the Tx34-2, two actuators were used to test the shear strength of the Tx54 specimen until failure. The span-to-depth ratio was maintained at 2.39. The two actuators were 26 in. apart, with the actuator nearer to the bearing located 12.75 ft from the centerline of the bearing. Both the reinforced and unreinforced ends were symmetrical in the test setup and instrumentation. Because the reinforced end was expected to be stronger in shear capacity and the total capacity that could be applied by the two actuators in the lab was limited to 600 kips each, the reinforced end was tested first so that the longer span would aid in testing the full shear capacity of the specimen without running out of the actuator capacity. This step was planned in case there was sudden destructive damage of the unreinforced end of the specimen in shear, rendering the span shorter for the subsequent shear test of the reinforced end. The shorter span would require more load per actuator to test the capacity of the reinforced end. Therefore, unlike the other girder shear tests, the reinforced Tx54 girder end was tested prior to the unreinforced end. The critical points in the two tests are discussed in the following sections and reference the shear force developed at the major crack location. The average first cracking strength obtained from the direct uniaxial tensile strength test for the Tx34-1 girder was 0.95 ksi based on the material-level tests.

6.5.1 Shear Test 1: Reinforced End

Figure 6.7 shows the test setup for Shear Test 1 at the reinforced end of the Tx54 girder specimen. The shear test of the reinforced end was conducted after the flexure test so that the longer span length could be leveraged to test the reinforced end to failure. The LVDTs, SGs, and KSGs were installed at potential critical crack locations. The shear force was computed at the location of the major shear damage, which was at 6.75 ft from the centerline of the bearing pad located at the reinforced end of the girder. The following key observations were noted during the test:

- At a shear force of 483 kips, the first cracking sound was heard.
- At a shear force of approximately 600 kips, there was a cracking sound followed by the appearance of diagonal cracking of 0.004–0.008 in. wide cracks.

- At a shear force of 651 kips, wider cracks began to appear.
- At 722 kips shear force, there were sounds that could be due either to the approaching widening of cracks in the specimen or to interface slip.
- At approximately 777 kips shear force, 0.004–0.2 in. wide cracks were visible. At this stage, the reinforced end with minimum transverse reinforcement showed ductile behavior and continued to hold load with crack widening and cracking sounds. Interface slip leading to engagement of the interface reinforcement for composite action may have also caused the loud dull sound.
- To preserve the beam for shear testing of the unreinforced end, the test was terminated. The top and bottom strains measured midway between the actuators by strain gages and SPs were plotted versus the total load.

Table 6.15 presents the typical, minimum, and maximum crack widths observed at load steps when testing was paused to measure the crack widths.

Table 6.15. Tx54 Shear Test 1: Range of Crack Widths for Reinforced End.

Shear Force, kips	Total Actuator Load, kips	Minimum Width, in.	Maximum Width, in.	Typical Width, in.
600	688	< 0.004	0.008	0.006
722	840	< 0.004	0.02	0.008
777	920	< 0.004	0.2	0.04–0.1

Figure 6.46 presents the schematic of the shear cracks developed at the end of Shear Test 1 of the Tx54 specimen's reinforced end. Figure 6.47 shows the shear span at the reinforced end with the two actuators at ultimate load.

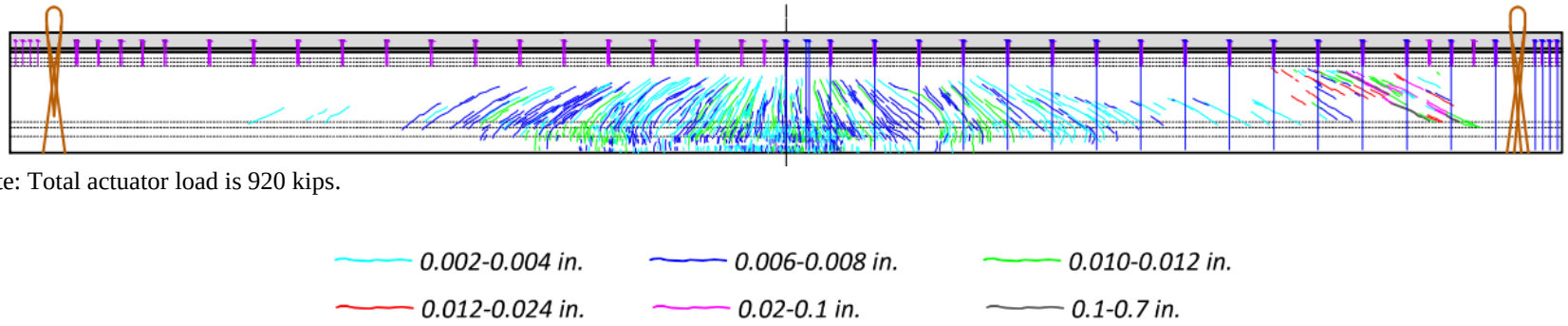

Note: Total actuator load is 920 kips.

Figure 6.46. Tx54 Shear Test 1: Shear Cracks at End of Test.

Figure 6.47. Tx54 Shear Test 1: Shear Span of Reinforced End at Failure.

6.5.1.1 Transverse Reinforcement Strains

Figure 6.48(a) and (b) present the schematic of the SSGs installed on the transverse web reinforcement of the Tx54 girder and the strains in these transverse reinforcement bars. One strain gage was installed on each leg of the selected transverse R-bars. The strain gages in the shear span

indicated the yielding of the bars that are at the location of the shear crack formation at a shear force of more than 500 kips.

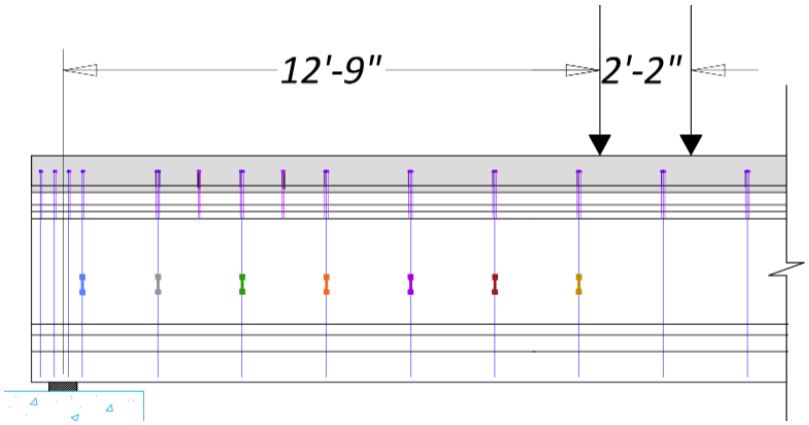

(a) Surface Steel Gages installed on R-bars

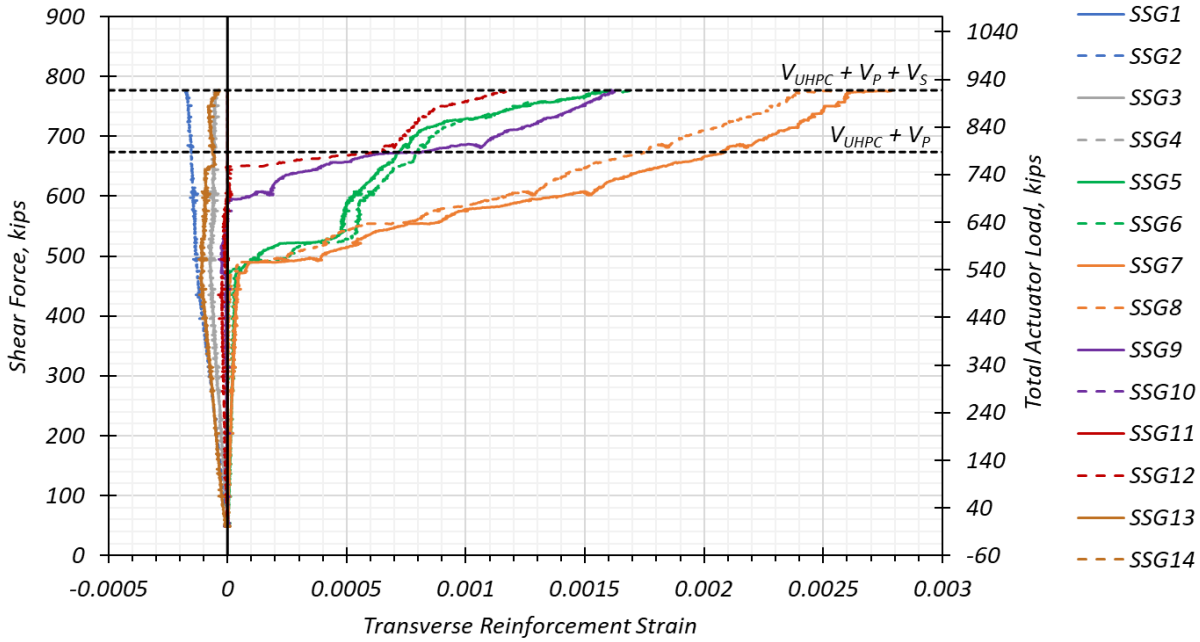

(b) Strains in Transverse Reinforcement Gages

Figure 6.48. Tx54 Shear Test 1: Transverse Reinforcement Strain Gages.

6.5.1.2 Additional Strain Measurements and Crack Angle

Figure 6.49(a) shows the arrangement of the LVDT rosette, KSGs, and SGs. Figure 6.49(b) shows the schematic of the LVDT rosette, KSGs, and the SGs on the web. Figure 6.49(c) presents the shear force at the region of major crack development plotted against the strains measured by the LVDTs, SGs, and KSGs installed in the directions parallel and perpendicular to existing cracks.

The analytically computed crack angle was 31 degrees. The crack angle computed from the LVDT rosette was 27 degrees, while the physically measured angle measured was 29.5 degrees.

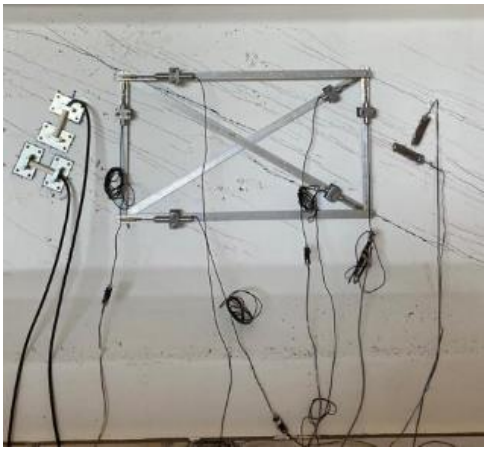

(a) Photograph of Tx54 at Peak Load

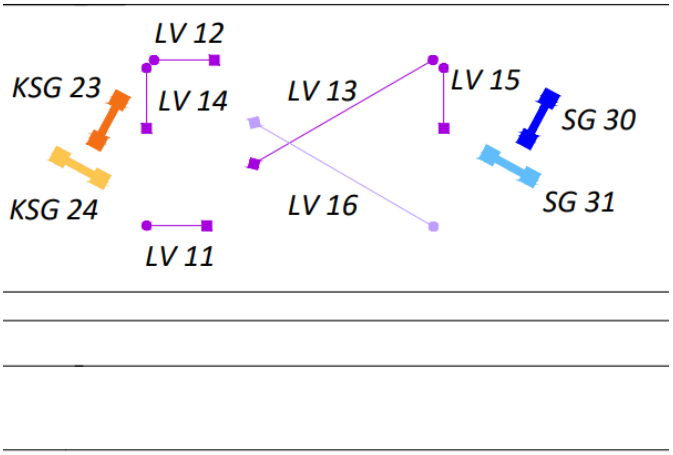

(b) Instrumentation Schematic of Shear End

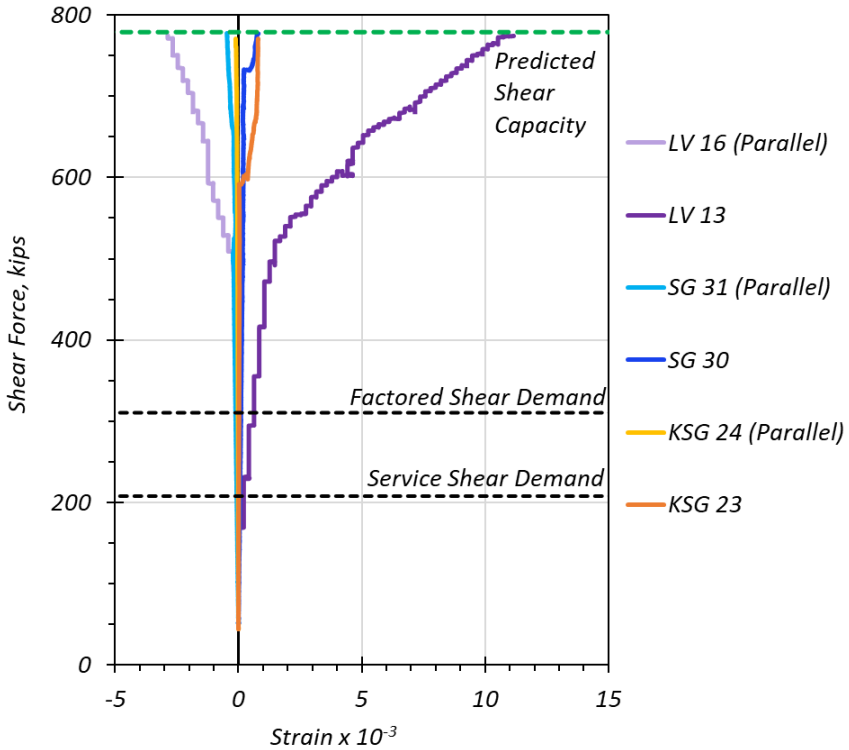

(d) Shear force versus Strain

Figure 6.49. Tx54 Shear Test 1: Web Strains (Reinforced End).

6.5.1.3 Shear Force versus Deflection

The shear force at the location of the most prominent crack is plotted versus the maximum deflection observed in the shear span in Figure 6.50. The prominent crack was located 6.75 ft from

the centerline of the bearing pad located at the reinforced end. The behavior of the girder was linear until at a shear capacity of 500 kips, beyond which the girder showed nonlinear behavior, with a drop in load occurring around the nominal shear capacity.

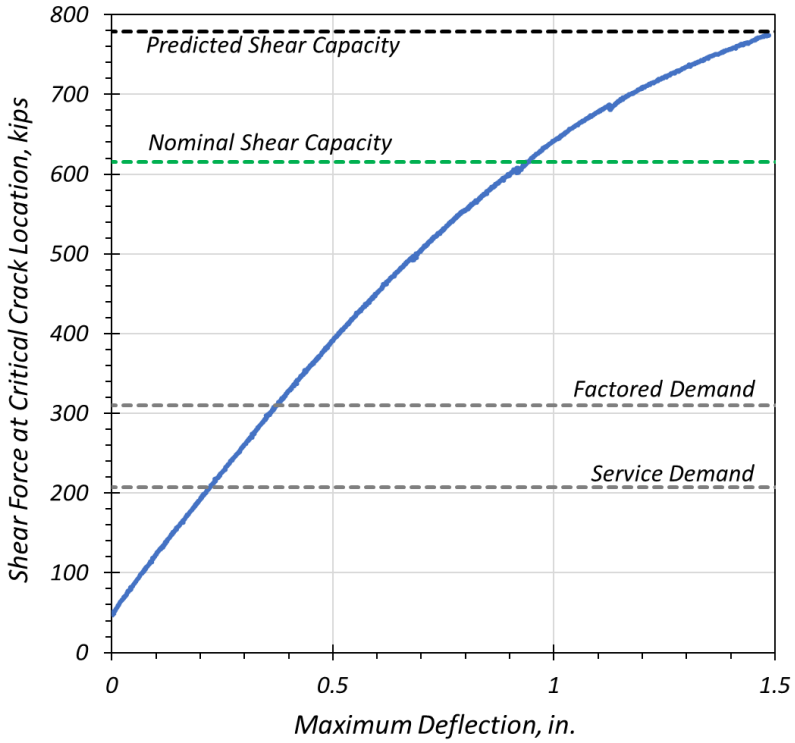

Figure 6.50. Tx54 Shear Test 1: Shear Force versus Maximum Deflection (Reinforced End).

6.5.1.4 Flexure Strains between the Actuators

Figure 6.51 presents the layout of the SPs and SGs installed at the top of the CC deck and the bottom of the UHPC girder. Figure 6.52 shows the strains measured by the strain gages and SPs located at the top and bottom of the composite girder in between the two actuators. These strains were compared with the predicted top and bottom strains computed from the moment-curvature analysis described in Section 5.3.2. Most of the top SPs and SGs and the bottom SGs follow the trend of the prediction curve. One of the top SPs and two bottom SGs seem to not record the data until the termination loads of the test when the strains increase in magnitude.

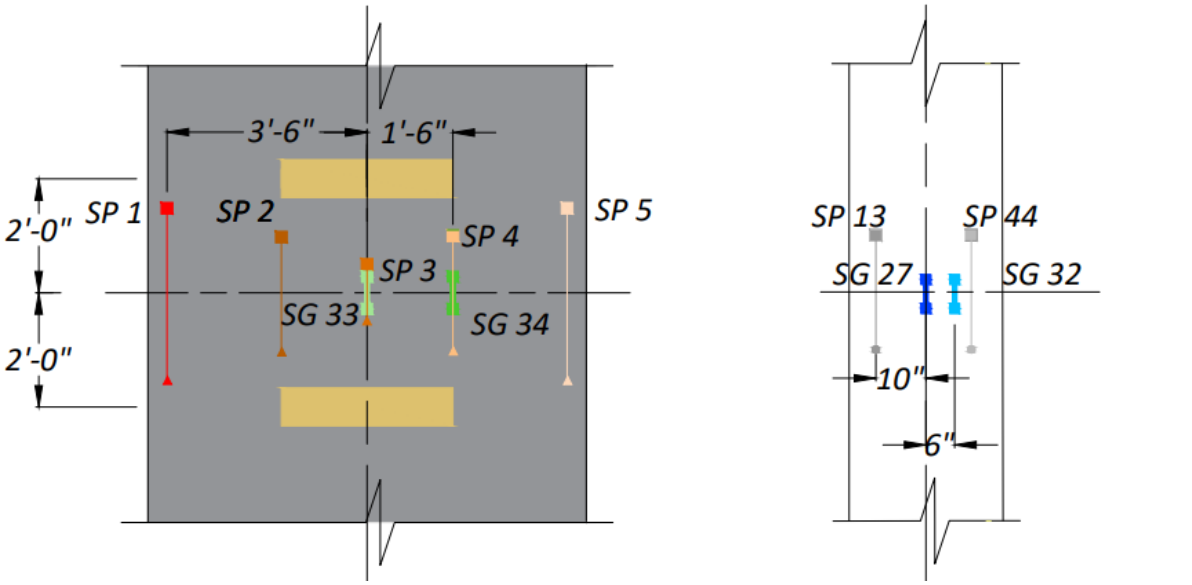

(a) Top of CC deck slab *(b) Underside of UHPC girder soffit*

Figure 6.51. Tx54 Shear Test 1: Layout of SPs (between Actuators).

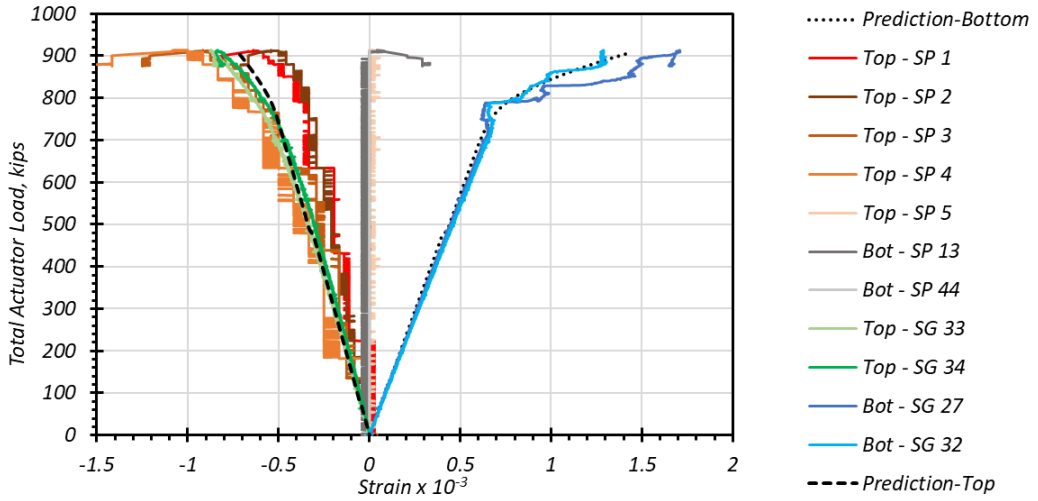

(a) Top and Bottom Strains (SP and SG)

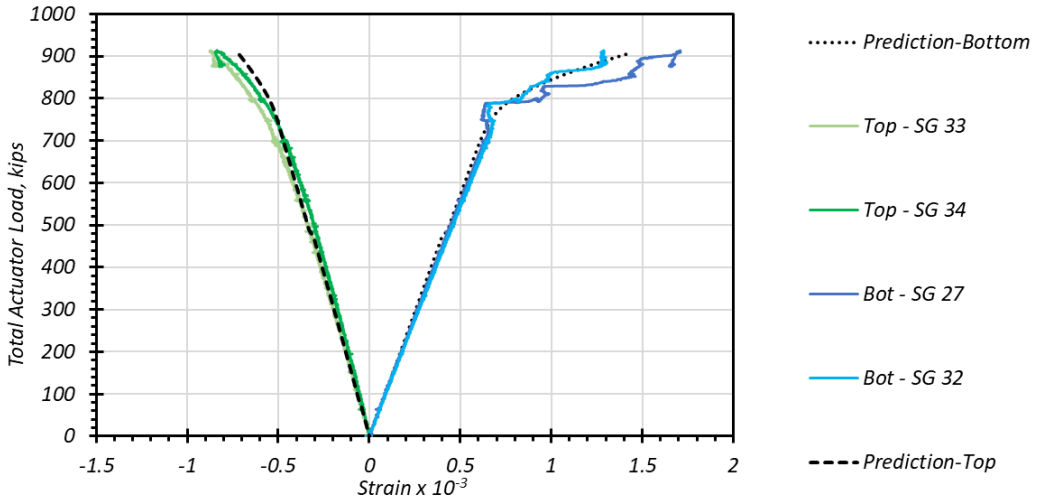

(b) Top and Bottom Strains (SG only)

Figure 6.52. Tx54 Shear Test 1: Strains at Top of Deck and Bottom of Girder (between Actuators).

6.5.1.5 Deflection Profile

Figure 6.53(a) presents the schematic of the test setup. Figure 6.53(b) presents the deflection profile measured by SPs installed along the span length. The maximum deflection of both shear tests is similar and close to 2 in. The deflection observed during this test was slightly over 2 in. because of higher loading on the specimen.

(a) Schematic of Test Setup

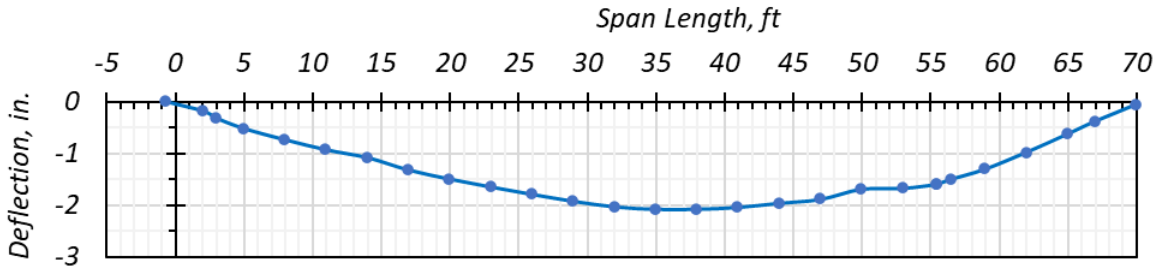

(b) Deflection Profile

Figure 6.53. Tx54 Shear Test 1: Deflection Profile.

6.5.1.6 Interface Shear between UHPC Girder and CC Deck

Figure 6.54(a) presents a schematic of the LVDTs installed at the CC deck and UHPC girder interface. Figure 6.54(b) presents the interface slip measured between the deck and the girder at 5.5 ft from each girder end. A maximum interface slip of 0.056 in. was observed at the reinforced end, while there was no observable slip at the unreinforced end. The lower slip at the unreinforced end may be related to the slightly higher area of interface steel present at the unreinforced end. More significantly, a higher shear force was applied at the reinforced end in this test.

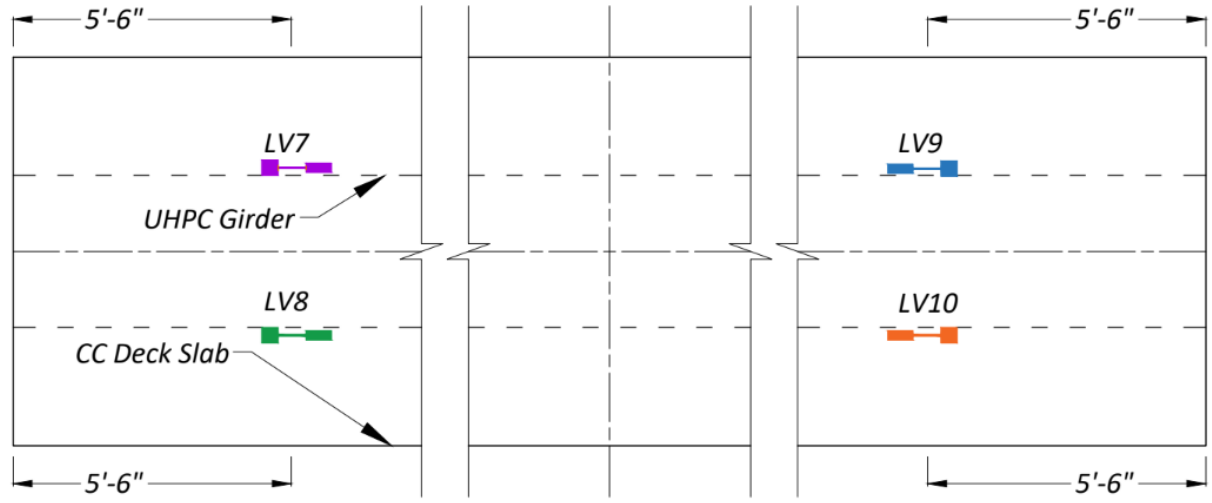

(a) Layout of LVDTs Measuring Interface Slip

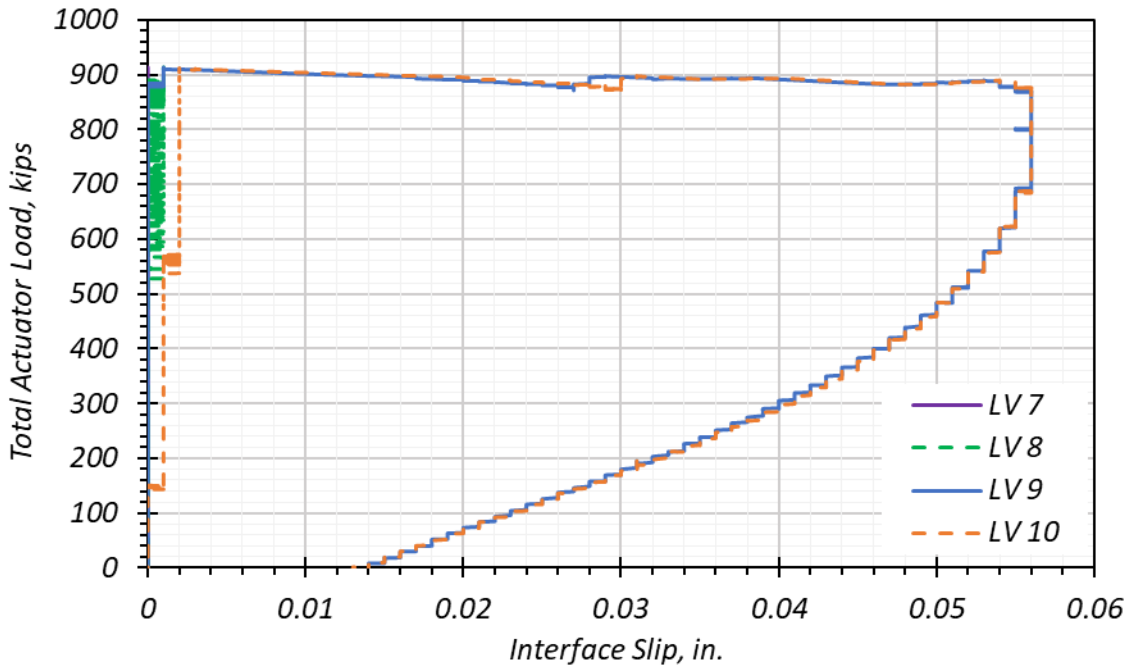

(b) Total Actuator Load versus Interface Slip

Note: LV7 and LV8 read zero data, which is interpreted as zero slip at the unreinforced end.

Figure 6.54. Tx54 Shear Test 1: Interface Slip Measurements.

6.5.2 Shear Test 2: Unreinforced End

Figure 6.9 shows the test setup for Shear Test 2 at the unreinforced end of the Tx54 girder specimen. The total span length of the composite specimen was structurally stable to conduct the shear test on the unreinforced end without altering the span. The test setup was symmetrically opposite to Shear Test 1. The performance of the unreinforced end of the specimen was quite similar to the reinforced end shear test of this specimen. The shear force is reported for the critical shear location, which was taken as 6.75 ft from the bearing pad centerline at the unreinforced end of the girder. Key observations during testing include the following:

- At a shear force of 425 kips, hairline diagonal cracks were observed in the shear span.
- At a shear force of 578 kips, a dull sound was heard, and diagonal cracks widened to 0.005 in.
- As the total load was incremented up to a shear force of 730 kips, 0.004–0.006 in. wide cracks began to appear.
- At approximately 762 kips shear force, the cracks widened and their width ranged from 0.004–0.2 in. with a prominent crack of 0.3 in. width and several hairline cracks.

Figure 6.55 presents the cracks in the web that span from the bottom flange and into the top flange. A vertical crack emerging from the bottom flange into the web is shown at the face of the girder. Figure 6.56 presents the schematic of the shear cracks at the end of Shear Test 2 of the unreinforced end of Tx54. Table 6.16 shows the typical, minimum, and maximum crack widths observed at load steps when testing was paused to measure the crack widths.

Table 6.16. Range of Crack Widths for Tx54 Shear Test 2: Unreinforced End.

Shear Force, kips	Total Actuator Load, kips	Minimum Width, in.	Maximum Width, in.	Typical Width, in.
660	578	< 0.004	0.005	0.004
730	850	< 0.004	0.006	0.005
762	890	< 0.004	0.3	0.004–0.2

Figure 6.55. Tx54 Shear Test 2: Shear Span of Unreinforced End at Failure.

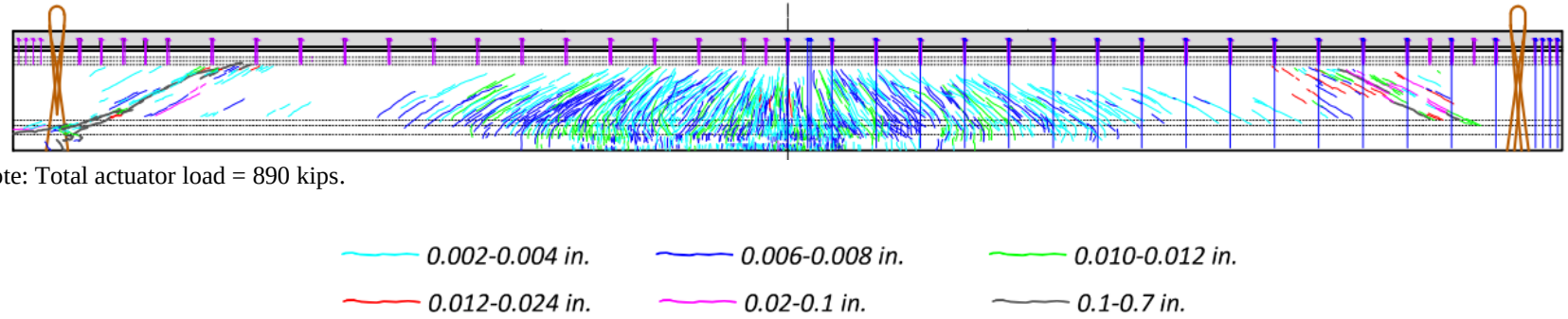

Note: Total actuator load = 890 kips.

Figure 6.56. Tx54 Shear Test 2: Shear Cracks at End of Test.

6.5.2.1 Transverse Reinforcement Strains

Figure 6.57(a) and (b) present the steel surface strain gages mounted on instrumented R-bars and the strains measured during the shear test leading to failure of the unreinforced end. As mentioned in the previous section, one strain gage was installed on each leg of the selected transverse R-bars. Figure 6.57(b) shows the strains measured by these gages plotted versus shear force at the critical crack location, which is 6 ft from the nearest actuator load (6 ft-9 in. from the centerline of the bearing pad). The strains in the transverse reinforcement at the reinforced end were well below the yield strain when the unreinforced end of the girder specimen was loaded.

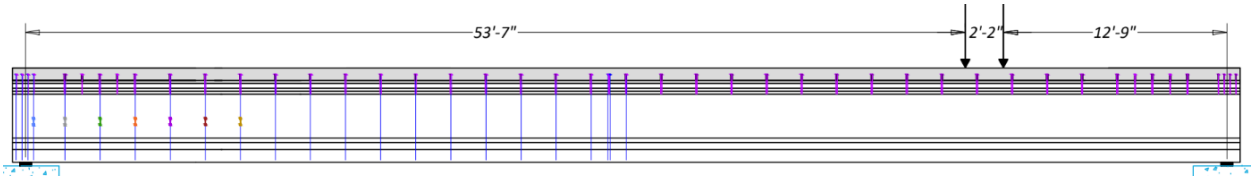

(a) Surface Steel Gages Installed on R-bars

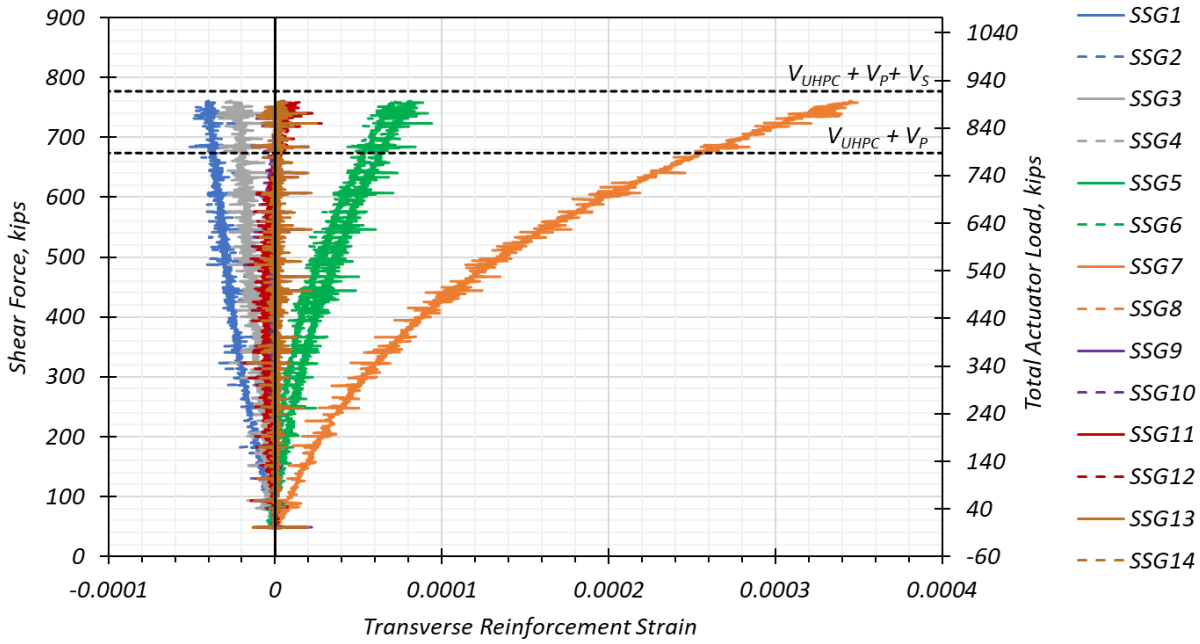

(b) Strains in Transverse Reinforcement Gages

Figure 6.57. Tx54 Shear Test 2: Transverse Reinforcement Strain Gages.

6.5.2.2 Additional Strain Measurements and Crack Angle

Figure 6.58(a) shows the arrangement of the LVDT rosette, KSGs, and SGs. Figure 6.58(b) shows the schematic of the LVDT rosette, KSGs, and the SGs on the web. Figure 6.58(c) presents the shear force at the region of major crack development plotted versus the strains measured by the LVDTs, SGs, and KSGs installed in the directions parallel and perpendicular to existing cracks. The LVDTs transverse to the crack and parallel to the crack show the tension and compression strains being developed in the web when the cracks widen at higher shear forces. The analytically computed crack angle was 29 degrees. The crack angle computed from the LVDT rosette was 26 degrees, while the physically measured angle was 28 degrees.

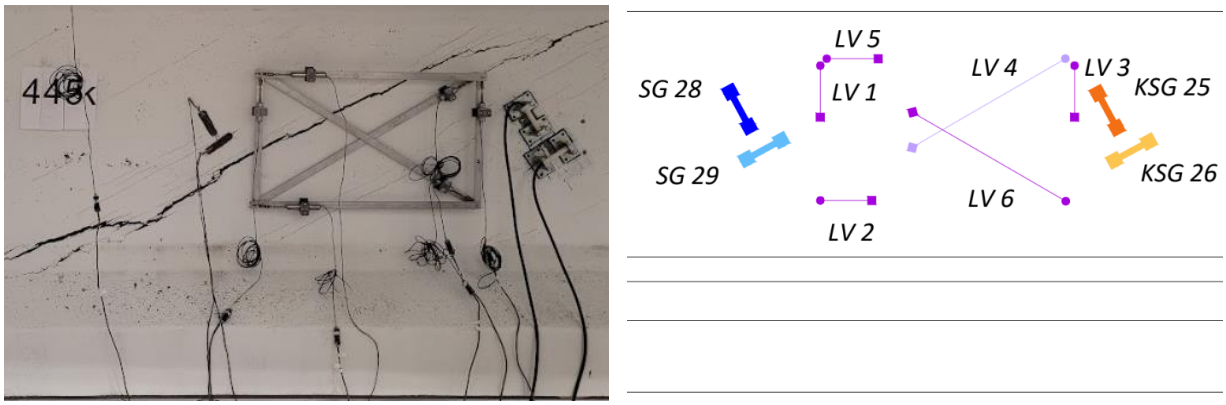

(a) Photograph of Tx54 at Peak Load *(b) Instrumentation Schematic of Shear End*

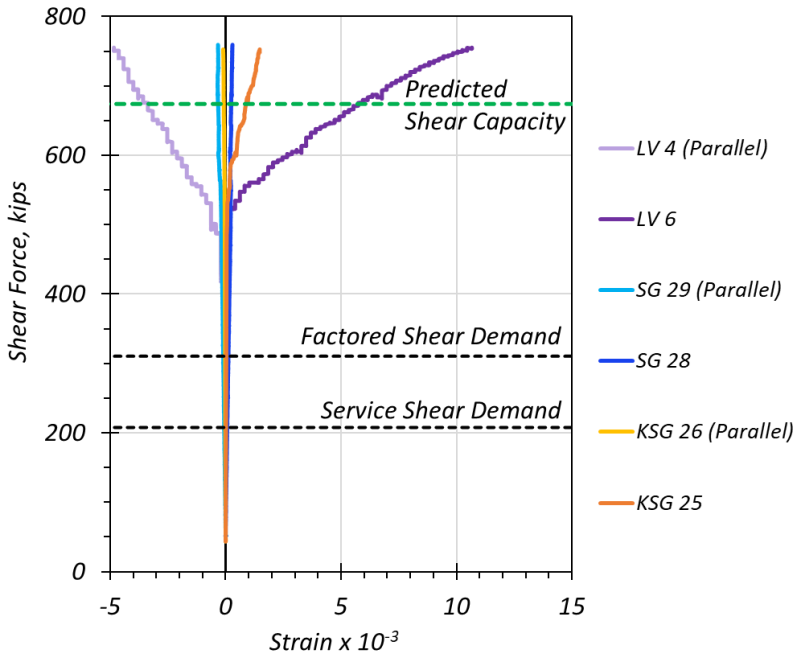

(c) Shear Force versus Strain

Figure 6.58. Tx54 Shear Test 2: Web Strains (Unreinforced End).

6.5.2.3 Shear Force versus Deflection

The shear force at the location of the most prominent crack was plotted versus the maximum deflection observed in the shear span. The shear force was computed at 6.75 ft from the centerline of the bearing pad located at the reinforced end of the girder. Figure 6.59 presents the shear force versus the maximum deflection. The figure illustrates linear behavior until the nominal shear capacity of the girder specimen is reached. Beyond the nominal capacity, the girder specimen exhibits nonlinear behavior.

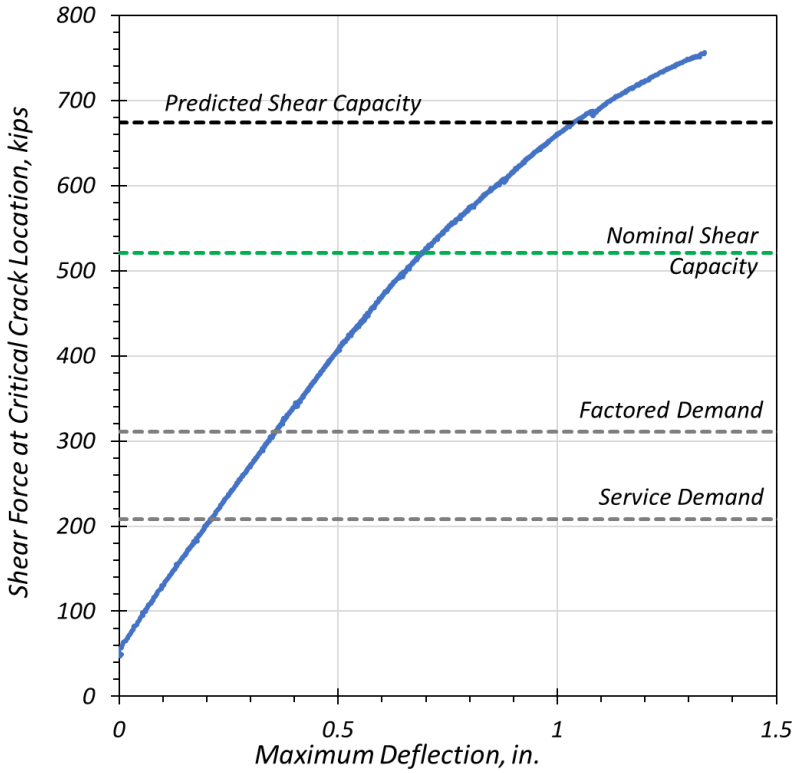

Figure 6.59. Tx54 Shear Test 2: Shear Force versus Maximum Deflection (Unreinforced End).

6.5.2.4 Flexure Strains between the Actuators

Figure 6.60 presents the layout of the SPs and SGs installed at the top of the CC deck and the bottom of the UHPC girder. Figure 6.61 shows the strains measured by the strain gages and SPs located at the top and bottom of the composite girder in between the two actuators. These strains were compared with the predicted top and bottom strains computed from the moment-curvature analysis described in Section 5.3.2. The top and bottom strains from the SGs follow the same trend as the prediction, while the SP values are lower than expected for the majority of the load history. The top and bottom SPs do not seem to show variation in data until large strains are observed at the termination load of the test.

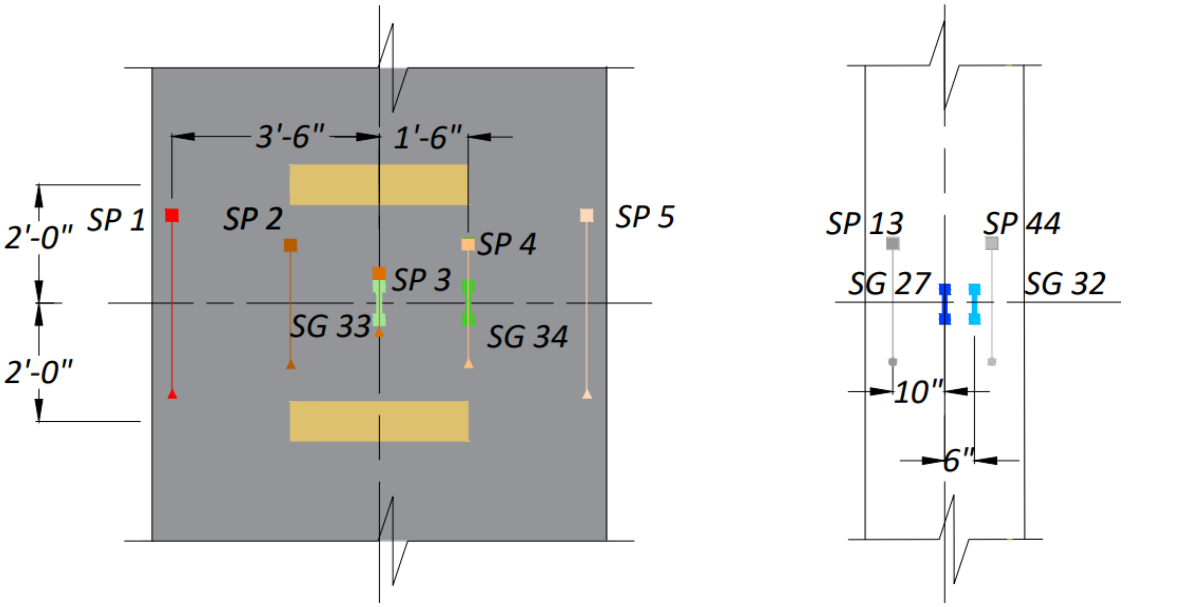

(a) Top of CC Deck Slab *(b) Underside of UHPC Girder Soffit*

Figure 6.60. Tx54 Shear Test 2: Layout of SPs (between Actuators).

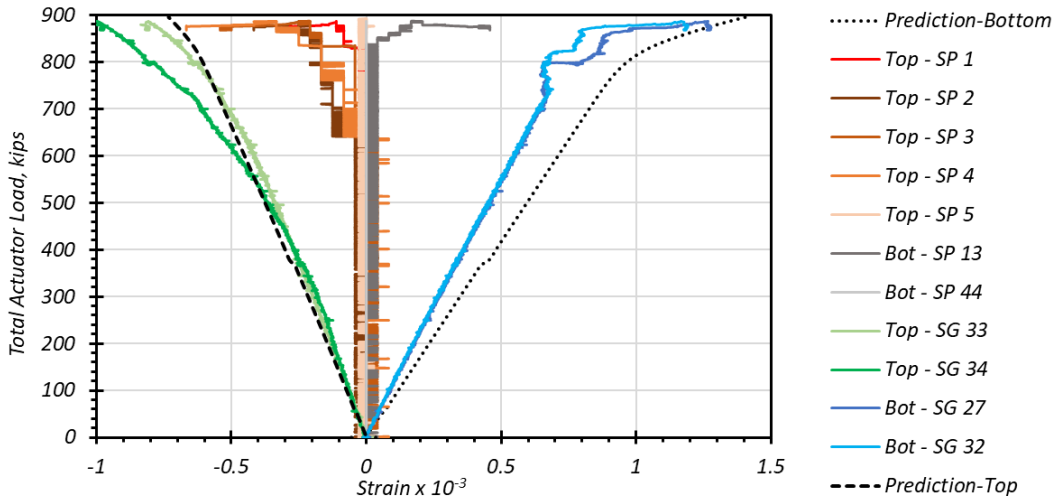

(a) Top and Bottom Strains (SP and SG)

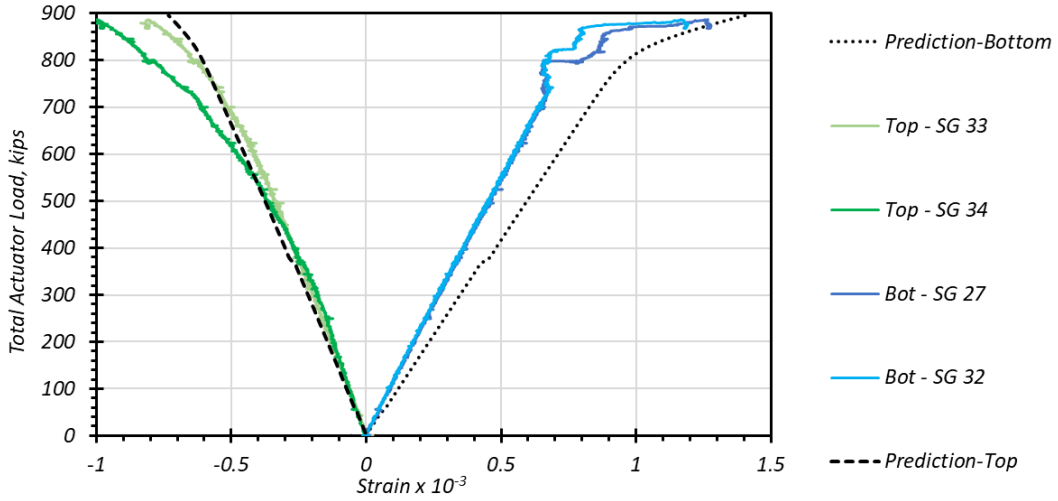

(b) Top and Bottom Strains (SG only)

Figure 6.61. Tx54 Shear Test 2: Strains at Top of Deck and Bottom of Girder (between Actuators).

6.5.2.5 Deflection Profile

Figure 6.62(a) presents a schematic of the test setup. Figure 6.62(b) presents the deflection profile measured by SPs installed along the span length. The maximum deflections of both shear tests are similar and close to 2 in.

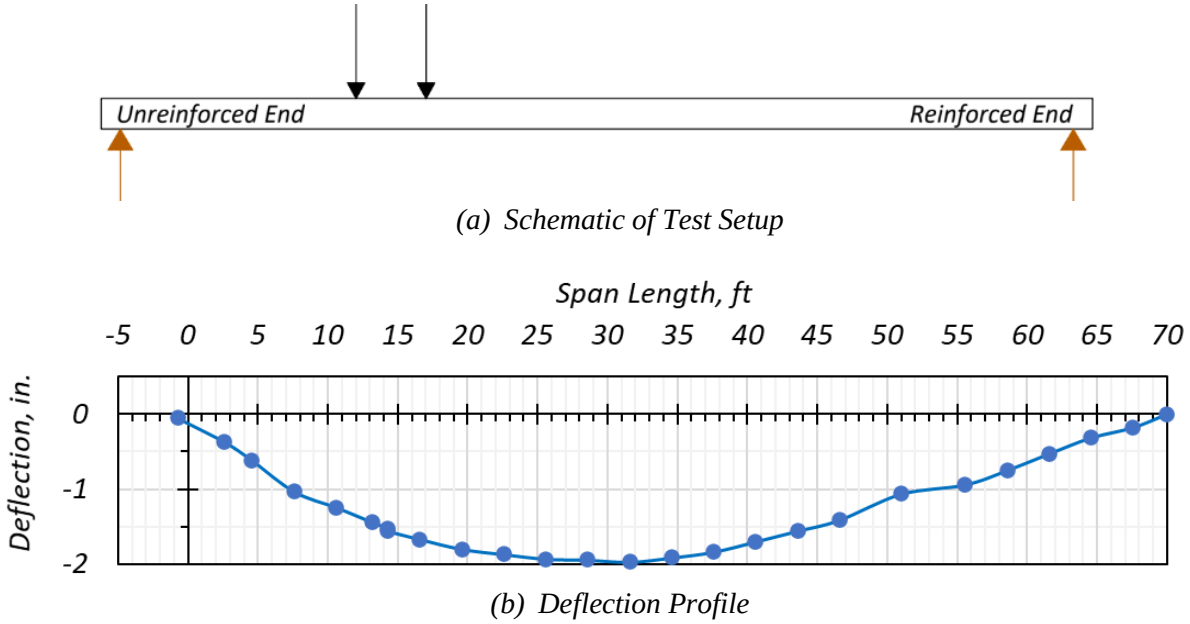

(a) Schematic of Test Setup

(b) Deflection Profile

Figure 6.62. Tx54 Shear Test 2: Deflection Profile.

6.5.2.6 Interface Shear between UHPC Girder and CC Deck

Figure 6.63(a) presents a schematic of the LVDTs installed at the CC deck and UHPC girder interface. Figure 6.63(b) presents the interface slip measured between the deck and the girder at 5.5 ft from each girder end. The unreinforced end was observed to show less slip than the reinforced end during Shear Test 2. A maximum interface slip of 0.008 in. was observed at the reinforced end, while a maximum slip of 0.005 in. was observed at the unreinforced end. The slip was negligible when the unreinforced end was loaded.

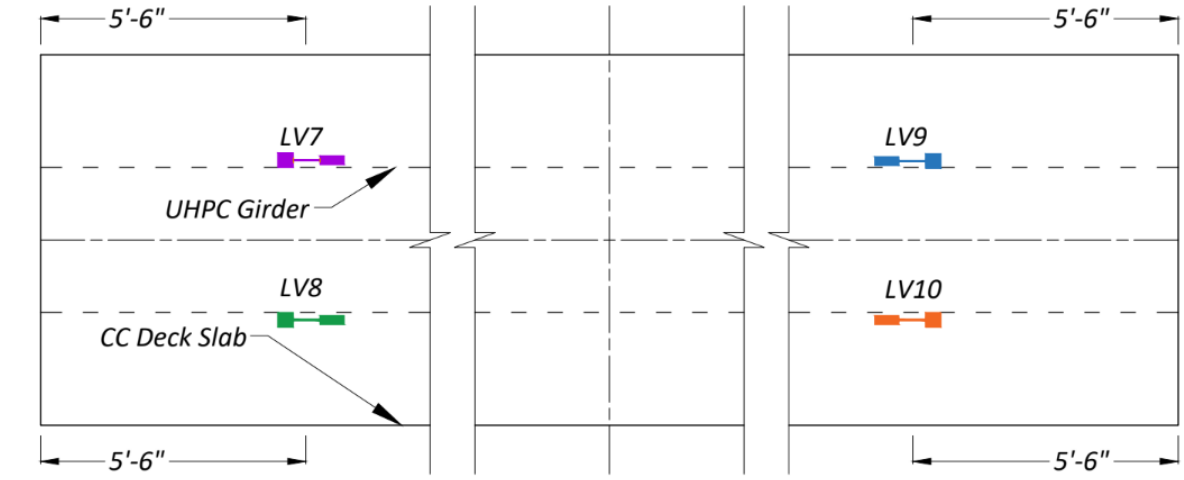

(a) Layout of LVDTs Measuring Interface Slip

[Note: LVDTS are located at interface of UHPC girder and deck.]

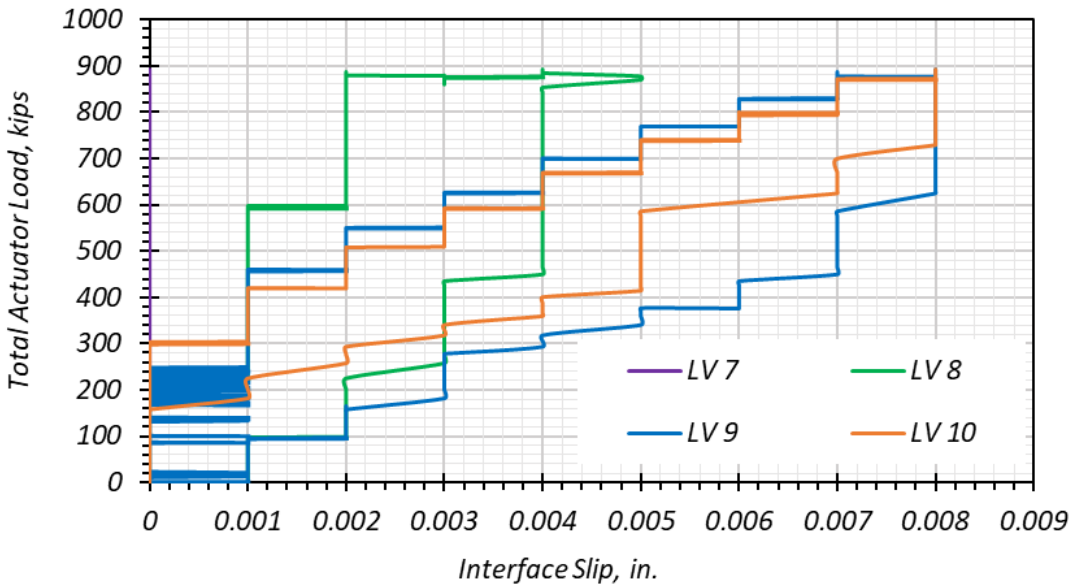

(b) Total Actuator Load versus Interface Slip

Note: LV7 read zero data, which could be due to negligible slip along that edge of the girder.

Figure 6.63. Tx54 Shear Test 2: Interface Slip Measurements.

6.6 COMPARISON OF SHEAR TEST RESULTS

The overall shear performance of all three girders was relatively ductile, and the steel fibers in the UHPC held the matrix together by bridging the cracks and preventing a brittle shear failure. The shear ends continued to carry load even after developing significantly wide cracks. One exception

was the unreinforced end of the Tx34-1 girder, which had a lower tensile strength and a resulting lower shear capacity than the expected shear demand. All the other girder ends showed promising results with respect to the shear performance relative to the service and factored shear demands of the prototype girder designs.

6.6.1 Effect of Tensile Strength on Shear Capacity

Based on the experimental results, the correlation between the tensile strength at first cracking at the material level and the full-scale test was evaluated. The shear performance of the UHPC girders confirmed the importance of the tensile strength measured at a material level with uniaxial tension testing. Key findings include the following:

- The Tx34-1 specimen was designed for the strengths achieved for the laboratory mixture and the precast plant mixture, with a tensile strength at service of 1.0 ksi. Based on the companion specimen tension testing (0.53 ksi first cracking tensile strength), the first specimen was reanalyzed for flexure-shear interaction during the flexure test. The analysis predicted a shear failure in the unreinforced end of the girder prior to flexure failure at midspan. The full-scale testing showed that the tensile strength of the girder was in fact well represented by the companion specimens, and the shear cracks in the unreinforced end occurred around the predicted load of shear failure based on the measured tensile strength.
- For the Tx34-2 specimen, companion small-scale specimens showed slightly improved tensile properties, with a tensile strength of about 0.60 to 0.75 ksi. The Tx34-2 specimen also had harped tendons that improved the shear performance of the girder. There was no premature shear failure for this specimen in the unreinforced end.
- The Tx54 girder specimen had the highest tensile strength measured of all the specimens (0.95 ksi). This finding was evident from the superior shear performance of this specimen. This specimen also had harped tendons that improved the shear performance slightly.

In addition to the tensile strength of the UHPC, shear capacity was provided by the harped prestressing tendons for the Tx34-2 and Tx54 specimens. However, shear resistance due to the aggregate interlock available in CC is not consider in UHPC due to the absence of coarse aggregate. In the reinforced end of each girder specimen, transverse mild steel reinforcement also provided additional shear resistance. The capacity of the shear resistance of the transverse steel

was inversely proportional to the spacing, and the design of the specimens provided for a minimum reinforcement (maximum spacing by design) (AASHTO 2020).

Table 6.17 presents the measured first cracking tensile strength at the time of testing of companion specimens close to the full-scale test day and the predicted and experimental shear capacity. A direct dependence of the shear capacity on the tensile strength at first cracking was confirmed based on the predictions and experiments. The predicted and experimental shear capacities are within 15 percent of each other, with the experimental capacity being higher than the predicted capacity—except for the Tx34-1 unreinforced end, which was not tested to failure. The Tx34-1 reinforced end may have more fiber concentration than the unreinforced end and the companion specimens, which may have led to a higher tensile strength at that end than the value used for predicting the shear capacity based on the companion material-level, direct uniaxial tensile strength test. The details of the fiber distribution of the cores of the girder can be found in Chapter 8 of the Volume 1 report.

Table 6.17. Predicted and Experimental Shear Capacity.

Specimen	Girder End	Measured Tensile Strength at First Cracking, ksi	Predicted Shear Capacity, kips	Experimental Shear Capacity, kips
Tx34-1	Unreinforced	0.53	211	202
Tx34-1	Reinforced	0.53	273	413
Tx34-2	Unreinforced	0.62	444	449
Tx34-2	Reinforced	0.62	550	592
Tx54	Unreinforced	0.95	674	761
Tx54	Reinforced	0.95	779	777

6.6.2 Crack Angle

Based on the computations explained in Section 6.1.3.3, crack angles of the major developed cracks were determined using the strains measured by the LVDT rosette at that location. This value was compared with the physically measured angle of inclination of the crack. The LVDT data from the reinforced end shear test of Tx34-1 and the unreinforced end shear test of Tx34-2 showed that two of the LVDTs forming the rosette were not providing reliable data, thereby leading to zero readings. This outcome may have been due to some of the LVDTs in the rosette not having sufficient mobility to expand or contract during the test. Table 6.18 presents the measured and

computed crack angles. The table also presents the crack angle based on the shear capacity predictions being developed for UHPC by FHWA (2022).

Table 6.18. Angle of Inclination of Developed Shear Cracks.

Specimen	Girder End	Crack Angle Computed from Experimental Strain Data, degrees	Measured Crack Angle, degrees	FHWA Crack Angle, degrees
Tx34-1	Unreinforced	*	32	30.8
Tx34-1	Reinforced	29.5	34	30.8
Tx34-2	Unreinforced	*	20	27.7
Tx34-2	Reinforced	27	26	27.7
Tx54	Unreinforced	26	28	27.2
Tx54	Reinforced	27	29.5	27.2

*Insufficient data available to determine the result.

The computed crack angle using the measured strain data gives a close approximation of the corresponding measured crack angle. The recommendations in Appendix B of the AASHTO draft specifications for UHPC (FHWA 2022) was also found to be effective in predicting the shear crack angle. Note that AFGC (2013) recommends an angle of 30 degrees, while the PCI study (Tadros 2021) recommends the AASHTO (2020) general modified compression field theory.

6.6.3 Interface Shear Slip

Table 6.19 presents the interface shear slip measured at the ends of the girder during the shear tests. The average slip of the two LVDTs at one end is reported in the table. The area of the steel provided at the two ends differed slightly because the unreinforced end contained bundles of three #5 UC-bars, while the reinforced end used two #5 UC-bars bundled with one #4 R-bar. The area of the interface shear reinforcement spanning the slip critical ends of the girder are also listed in the table. Overall, the provided interface shear reinforcement controlled the interface slip up to the factored design loads. Limited slip was observed at higher loads, with a range of average slip for all girders from 0.005–0.19 in.

Table 6.19. Interface Shear Slip Summary.

Shear Test Description	Unreinforced End		Reinforced End	
	Area of Steel, in^2	Interface Slip, in.	Area of Steel, in^2	Interface Slip, in.
Tx34-1 Unreinforced Shear Cracking (Phase I)	8.06	0.011	7.29	0.015
Tx34-1 Unreinforced Shear Cracking (Phase II)	8.06	0.023	7.29	0.086
Tx34-1 Reinforced End	8.06	0	7.29	0.032
Tx34-2 Unreinforced End	8.06	0.075	7.29	0.095
Tx34-2 Reinforced End	8.06	0.065	7.29	0.19
Tx54 Unreinforced End	6.82	0.005	6.16	0.008
Tx54 Reinforced End	6.82	0.001	6.16	0.056

Note: The reinforcement areas are computed over the interface shear critical distance as per AASHTO (2020): Tx34-1 (11.25 ft), Tx34-2 (15.0 ft), Tx54 (10 ft).

6.6.4 Shear Capacity Prediction by Different Methods

Section 6.1.2 elaborates on the different approaches in literature. The present research computed the shear capacity based on the methods and assumptions explained in Section 6.1.3. Figure 6.64 presents shear capacity predictions from the different methods, and Table 6.20 presents the numerical values. With the exception of the unreinforced end of the Tx34-1 girder specimen (due to a lower than expected tensile strength), the FHWA design recommendations provide a conservative estimate of the shear capacity of the girder specimens.

Table 6.20. Comparison of Shear Capacity, kips.

Specimen	Girder End	Experimental	FHWA	PCI	AFGC	Predicted
Tx34-1	Unreinforced	202	337	426	221	211
Tx34-1	Reinforced	413	398	492	284	273
Tx34-2	Unreinforced	449	395	438	263	444
Tx34-2	Reinforced	592	464	504	325	550
Tx54	Unreinforced	761	607	660	542	674
Tx54	Reinforced	777	713	757	636	779

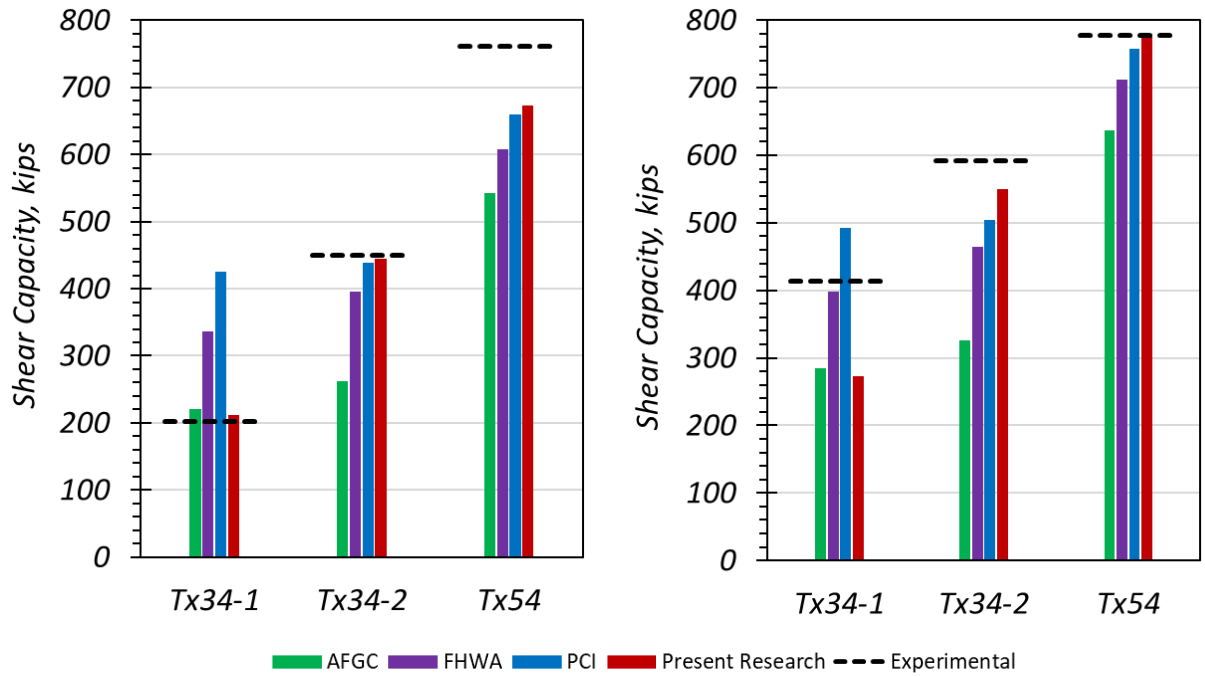

(a) Unreinforced End *(b) Reinforced End*

Figure 6.64. Shear Capacity Comparison.

6.6.5 Shear Demand and Shear Capacity

Table 6.21 and Figure 6.65 summarize the shear demand and shear capacity of the three girder specimens. The design demands for the corresponding prototype bridge girders were computed using AASHTO (2020). The nominal capacity is based on FHWA (2022) recommendations using design target values for UHPC. The predicted capacity is based on the assumptions and methods used in the present research, as explained in Section 6.1.3.

For the Tx34-1 girder, when compared to the assumed design values, the predicted shear capacity was 4 percent higher than the experimental capacity for the end without minimum shear reinforcement (R-bars) because of the low tensile strength at the unreinforced end. The low tensile strength may have occurred due to the settlement of fibers at that end. Conversely, the experimental shear capacity was 34 percent higher than the predicted capacity for the end with minimum transverse reinforcement, which is potentially because of a higher tensile strength at the reinforced end that might occur due to a higher fiber concentration in the web at the reinforced end. This observation was corroborated from the cores of Tx34-1 girder specimens studied for fiber distribution. The details of this study are included in Chapter 8 of the Volume 1 report.

The predicted shear capacity was less than the experimental shear capacity by 15 percent or less for all shear tests conducted for the Tx34-2 and Tx54 girder specimens. The design values assumed for a nonproprietary mix are recommended to be based on experimentally measured strengths of material-level specimens fabricated from UHPC batch volumes required for large-scale girder production to ensure consistency in the design and measured values. The design tensile strength values were slightly higher than the measured tensile strength for the Tx34-1 unreinforced end, which resulted in the nominal strength being less than the experimental capacity for shear strength. The design tensile strength was also higher than the measured tensile strength of Tx34-2. Compared to Tx34-1, the tensile strength was slightly higher for Tx34-2 (19 percent). The assumed design tensile strength values were suitable for the Tx54 girder, for which the measured tensile strength was within 5 percent of the measured tensile strength.

Table 6.21. Shear Demand and Shear Capacity.

Specimen	Girder End	Demand, kips		Capacity, kips		
		Service	Factored	FHWA	Predicted	Experimental
Tx34-1	Unreinforced	138	213	337	211	202
Tx34-1	Reinforced	138	213	398	273	413
Tx34-2	Unreinforced	145	223	395	444	449
Tx34-2	Reinforced	145	223	464	550	592
Tx54	Unreinforced	208	310	607	674	761
Tx54	Reinforced	208	310	713	779	777

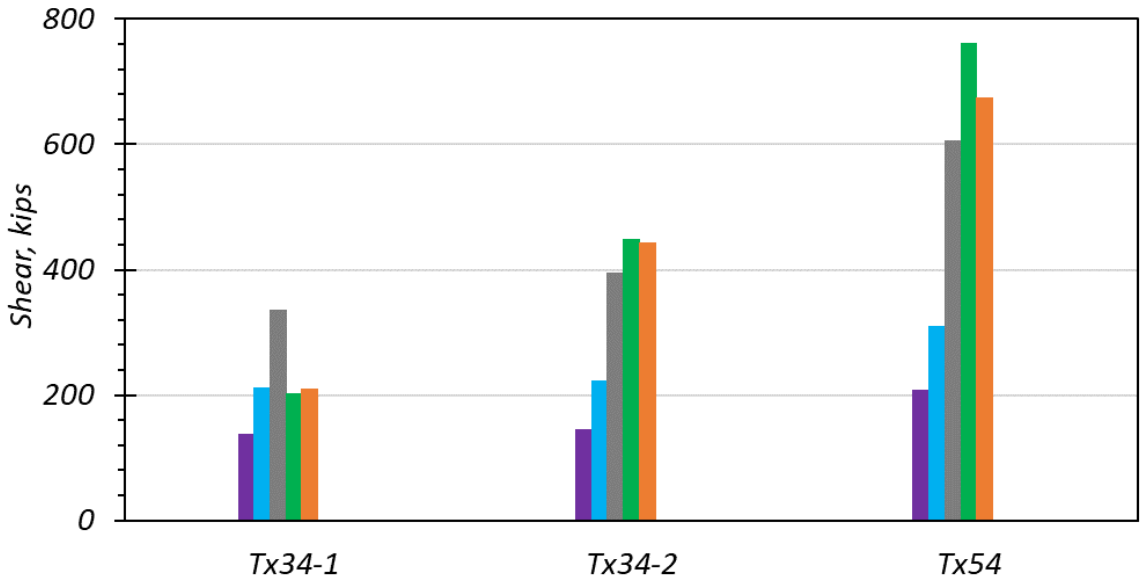

(a) Unreinforced End

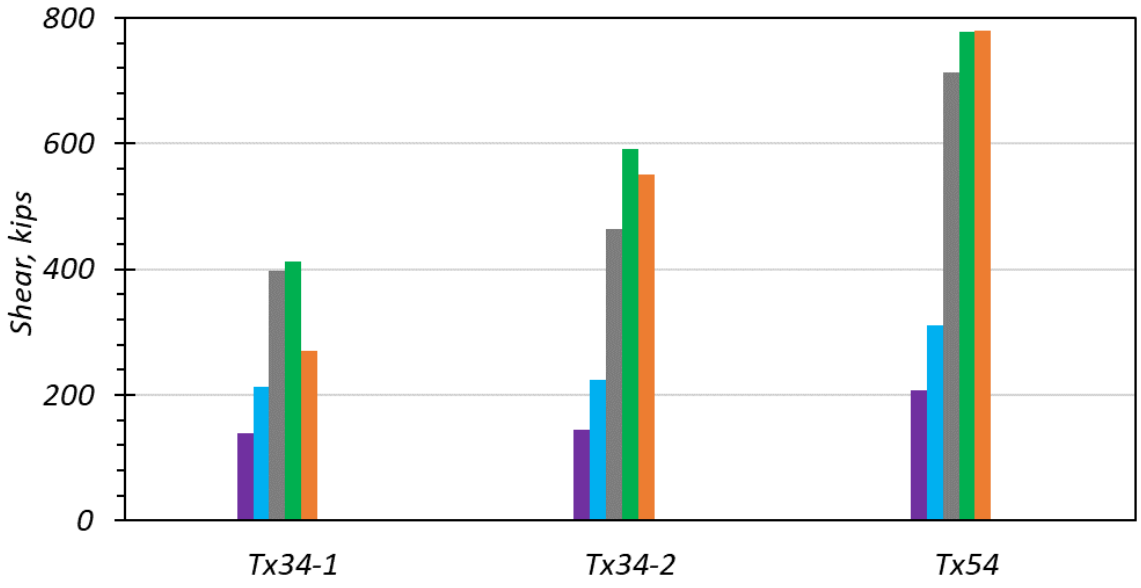

(b) Reinforced End

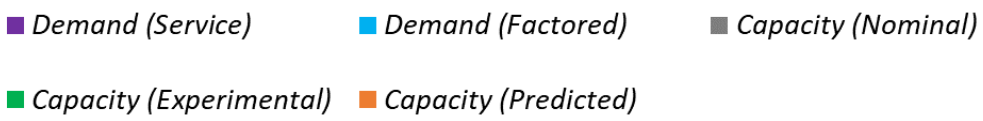

Figure 6.65. Shear Demand and Capacity.

6.7 SUMMARY

The full-scale testing of the shear performance of the girder specimens provided an opportunity to compare the shear capacity and performance with and without minimum transverse reinforcement in the form of R-bars. A span-to-depth ratio greater than 2.0 was used for all shear tests, and the arrangement of the load is described in detail in Chapter 6. One half span of each girder specimen had minimum transverse reinforcement by design in the form of R-bars, while the other half span did not contain web reinforcement. The superior ductility; dependence of the steel fibers on the tensile strength of the mix, particularly in the web; and the comparison between the shear capacity of the ends with and without the minimum transverse web reinforcement were evaluated. Based on the analysis conducted as per the procedures elaborated in Chapter 6.2.5 and the results of the full-scale testing, the following observations and conclusions were drawn:

1. *Analysis and design.* With respect to analysis and design for shear, the following observations were made based on the design and predicted response versus the measured response:
    - The predicted shear strength estimates utilize the expressions recommended for UHPC based on the work done by FHWA and PCI (El-Helou and Graybeal 2022b; Tadros 2021) and on the measured material properties. The FHWA and PCI formulations directly correlate the tensile strength of the UHPC to the shear capacity of the structural element. This result was supported by the current project, wherein the shear capacity of the full-scale specimens was observed to be directly related to the tensile strength measured from the uniaxial tension testing of the companion material-level specimens.
    - The shear test results confirmed that the actual shear capacity of the specimens was closely estimated (showing a difference of less than 13 percent between the prediction and measured maximum shear strength for all the shear tests), with the exception of the Tx34-1 end with minimum web reinforcement, which showed a 53 percent higher experimental capacity.
    - Consideration of the full section depth, including the composite CC deck, also provided more accurate predictions of the shear capacity of the specimens. Note that the deck is not included in the approach recommended by FHWA (El-Helou and Graybeal 2022b).

2. *General shear performance of girder specimens*. The following general observations were made with respect to the shear response and behavior of the girder specimens:
    - The shear performance of UHPC girders is enhanced relative to CC. The UHPC girder specimens did not undergo a sudden brittle shear failure during load testing. The steel fibers impart a crack bridging property to the matrix of UHPC, resulting in the shear components holding load despite the onset of crack openings and strain localization in the shear elements, such as in the webs of the I-shaped girders considered for this project. Despite testing the specimens to the maximum capacity in shear for Tx34-2 and Tx54, the composite girders continued to be stable structurally.
    - The shear capacity is very sensitive to the uniaxial tensile strength of UHPC. The tensile strength of Tx34-1 girder was much lower than anticipated, and fiber segregation was noted in the companion small-scale samples, likely due to higher than expected flow. These two elements could be the prime reasons for the lower shear capacity of the end without reinforcement.
    - The shear capacity of the unreinforced end of the Tx34-1 specimen was lower than the design shear capacity because the measured tensile strength from the companion specimens was lower than the design value. Therefore, the unreinforced end developed shear cracks before flexure crack localization took place at the midspan. The Tx34-2 and Tx54 specimen had greater tensile strength than the Tx34-1 specimen, and no premature shear failure in these sections occurred during flexure testing. The improved performance of the Tx34-2 and Tx54 specimens is also due to higher prestressing forces and harping of some of the tendons, which provided additional shear capacity.
    - In addition to the tensile strength of UHPC, shear capacity is enhanced by other factors, such as harping of some of the prestressing strands, minimum transverse web reinforcement, and deeper girder webs. This result is evident from the lowest shear capacity being observed for the eccentric prestressing strand Tx34-1 specimen, followed by the Tx34-2 with more prestressing strands, some of which were harped. The highest shear capacity was observed for the deeper Tx54 specimen that also contained some harped tendons.
    - The girder ends with minimum transverse web reinforcement were stronger in shear than the ends without transverse reinforcement in the form of R-bars. With the

enhanced shear capacity of UHPC relative to CC, the transverse steel reinforcement can be reduced substantially to the minimum required as per AASHTO (2020) rather than to the standard spacing recommended by TxDOT (2017a). The minimum transverse web reinforcement provides additional ductility to the composite section to delay a sudden failure under overload conditions.

3. *Individual girder shear performance—no web reinforcement*. With respect to the shear response and behavior at the ends of the individual girder specimens with no transverse reinforcement, the following observations were made:
    - *Tx34-1 (Unreinforced End).* The UHPC tensile strength of Tx34-1 was lower than the design tensile strength, which likely led to the shear failure at the unreinforced end of the specimen during the flexure test. Based on the experimental uniaxial tension test data, the *predicted* shear capacity at this end was close to the limiting value in the test (4 percent higher). The experimental capacity of 202 kips was 46 percent higher than the service load of the prototype bridge but was 5 percent lower than the corresponding factored demand load.
    - *Tx34-2 (Unreinforced End).* The shear performance at the unreinforced end of the Tx34-2 girder specimen was enhanced by the improved tensile strength and harped layout of the strands. The shear capacity was 449 kips, which was 1 percent higher than the prediction using the uniaxial tension test data for the companion specimens. The shear capacity of the girder was 210 percent higher than the service load of the corresponding prototype bridge and 101 percent higher than the factored demand load. The harping of the strands and improved tensile strength enhanced the overall shear capacity significantly at the unreinforced end of the Tx34-2 girder in comparison to the unreinforced end of the Tx34-1 girder.
    - *Tx54 (Unreinforced End).* The shear performance of the Tx54 girder was further enhanced over the other two girder specimens due to a higher measured tensile strength, increased prestressing, a harped strand layout, and a deeper web section. The shear capacity was 761 kips (13 percent higher than the prediction). This increase may indicate a higher tensile strength within the girder section than in the companion material-level test specimens. The capacity exceeded the service demand of the

corresponding prototype bridge by 266 percent and the factored demand by 145 percent.

4. *Individual girder shear performance—minimum web reinforcement*. With respect to the shear response and behavior at the ends of the individual girder specimens with minimum transverse reinforcement, the following observations were made:
    - *Tx34-1 (Reinforced End).* The reinforced end of the Tx34-1 specimen was stronger in shear due to the contribution of the steel reinforcement in the web. The maximum applied shear was 413 kips, which was 53 percent higher than the predicted shear capacity. The uniaxial tensile strength data for the companion specimen showed a great deal of variation. It may be possible that the reinforced end of the girder may have had a higher concentration of fibers than the unreinforced end, resulting in higher tensile strength of the girder web and, consequently, higher shear capacity. This activity was later observed in the fiber distribution of the cored specimens of the reinforced end of the Tx34-1 girder. The details of the cored specimen fiber distribution are documented in the Volume 1 report. The capacity was 199 percent higher than the service load of the corresponding prototype bridge and 94 percent higher than the factored demand load.
    - *Tx34-2 (Reinforced End).* The reinforced end of the Tx34-2 girder was unintentionally reinforced with extra transverse bars due to early fabrication at the precast plant, which forced the shortening of the span length of the test specimen for the shear test to avoid testing the portion of the girder with extra transverse R-bars. The shear capacity was 592 kips, which was 8 percent higher than the predicted shear capacity. The capacity exceeded the service demand of the corresponding prototype bridge by 308 percent and the factored demand by 165 percent.
    - *Tx54 (Reinforced End).* The shear capacity of the Tx54 at girder end with minimum transverse reinforcement was 777 kips. The predicted capacity was 779 kips, giving a difference of less than 1 percent. The shear capacity exceeded the service loading of the corresponding prototype bridge by 274 percent and the factored shear demand by 151 percent.
5. *Interface Shear Performance:* There is less friction provided at the UHPC girder interface than at CC girders due to the self-consolidating nature of UHPC and the absence of coarse

aggregate. Bundled interface UC-bars were placed along the unreinforced half span to provide interface shear resistance between the UHPC girder and the CC deck, as described in Chapter 4. The reinforced half span had minimum transverse web shear R-bars (R-bars) that were supplemented with bundled UC-bars to improve the interface shear resistance. These bars were provided for additional interface shear strength due to the low interface shear capacity when surface roughening is not considered for UHPC. The UC-bars (No. 5) were larger in diameter than the R-bars (No. 4) to enhance the interface shear strength:

- The interface shear slip was measured between the CC deck and the UHPC girder. The measurements indicate that the reinforced end slipped more than the unreinforced end, potentially because of a higher area of interface shear steel reinforcement provided by the higher diameter UC-bars combination (UC-bar triplet bundles) in the unreinforced half of the girder than the combination of UC-bars and R-bars (one pair of UC-bars coupled with R-bar) in the reinforced half of the girder. The unplanned use of an SCC topping along the top surface of the unreinforced end of Tx54 girder may be the reason the lowest slip measurement is for this girder. This positive outcome may be useful when considering other approaches to increase the interface shear strength for the UHPC girder. (Note that the use of a small volume of SCC became necessary due to an unexpected shortage of UHPC in the last batch, likely caused by the lower flow spread of the UHPC that led to increased sticking of the material in the mixer and Tuckerbuilt.)
- The provided interface shear reinforcement controlled the interface slip up to the factored design loads. Limited slip was observed at higher loads, with a range of slip for all girders between 0.005–0.19 in.
- The Tx34-1 unreinforced end slipped by 0.027 in. and the reinforced end slipped by 0.086 in. during the shear failure of the unreinforced end. During the testing of the reinforced span, the maximum measured slip was 0.034 in. (The unreinforced end was eliminated during the reinforced end shear test because the major flexure crack at the midspan of the specimen led to shortening the span length for the second shear test.)
- The Tx34-2 unreinforced end slipped by 0.075 in. and the reinforced end slipped by 0.098 in. during the shear failure of the unreinforced end. During the shear testing of the reinforced end, the reinforced end slipped by 0.19 in., while the unreinforced end only slipped by 0.07 in.

- The Tx54 unreinforced end slipped by 0.005 in. and the reinforced end slipped by 0.008 in. during the shear failure of the unreinforced end. During the shear testing of the reinforced end, the reinforced end slipped by 0.056 in., while the unreinforced end only slipped by 0.001 in.

7 TRANSFER LENGTH AND CAMBER

7.1 TRANSFER LENGTH

This section presents the review of transfer length of the prestressing strands in the UHPC girder specimens. Transfer length is affected by bonding mechanisms between prestressing strands and concrete (Bhoem et al. 2010). Due to the different bond characteristics between UHPC and CC, the estimation of transfer length based on the current AASHTO LRFD Bridge Design Specifications may not be applicable for UHPC (AASHTO 2020). Therefore, the prestressing strand transfer length for the developed UHPC mixture was studied in this project. The measured transfer length was compared to both the current AASHTO LRFD Bridge Design Specifications and recommendations for UHPC by other studies. The following sections present the definition of transfer length, the recommended transfer length estimation for CC and UHPC, the experimental plan, and the results.

7.1.1 Definition of Transfer Length

Transfer length is defined as the required length of embedded pretensioned strand to transfer the effective prestress f_{pe} to the concrete by bond (ACI Committee 318 2019). Figure 7.1 shows the transfer length that is the distance from the free end of a strand to the point that the effective prestress can be transferred.

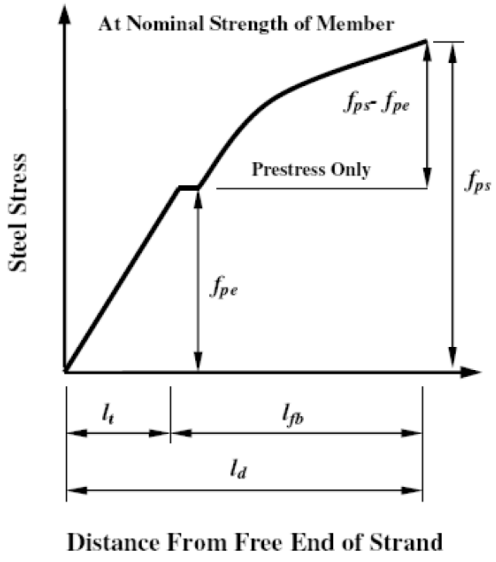

Figure 7.1. Definition of Transfer Length (adapted from Barnes et al. 1999).

7.1.2 Transfer Length Estimation for Conventional Concrete

The current AASHTO LRFD Bridge Design Specifications Section 5.9.4.3.1 provides the transfer length as 60 d_b for design, where d_b is a diameter of a strand (AASHTO 2020). The transfer length expression is limited for use to a compressive strength up to 10 ksi at release and 15 ksi at service, respectively.

National Cooperative Highway Research Program (NCHRP) Report 603 (Ramirez and Russell 2008) suggested the equation for the transfer length of high-strength concrete, which is applicable to concrete with compressive strength up to 9 ksi, is shown in Equation (7.1):

$$l_t = \left(\frac{120}{\sqrt{f'_{ci}}}\right) d_b \tag{7.1}$$

where:

l_t = Transfer length, in.

f'_{ci} = Compressive strength at release, ksi

d_b = Diameter of strand, in.

7.1.3 Recommended Transfer Length Estimation for UHPC

The *Design Guidelines for Reactive Powder Concrete (RPC) Prestressed Concrete Beams* (Gowripalan and Gilbert 2000) used in Australia suggested that transfer length l_t be between $20d_b$ and $40d_b$. Note that the Australian design guidelines were developed for a proprietary UHPC (Ductal) with 2.0 percent fiber volume. A study conducted by the PCI also recommended 20 d_b to 40 d_b for a transfer length of UHPC, with a minimum clear cover and center-to-center spacing of $2d_b$ (eConstruct 2020). The AASHTO Draft Specification for UHPC provides the following estimate equation for transfer length (AASHTO 2020).

$$l_t = \xi 24 d_b \tag{7.2}$$

where:

ξ = Coefficient taken as 0.75 or less for a shorter transfer length used for the service and fatigue limit states, and 1.0 or more for a longer transfer length used for the strength and extreme limit states.

Other researchers measured the transfer length of prestressing strands in UHPC, as shown in Table 7.1. The results range from 17–30 d_b, which shows good agreement with the recommendation for UHPC (20–40 d_b).

Table 7.1. Transfer Length Results of UHPC from Other Studies.

Strand Diameter, in.	Measured Transfer Length, in.	Transfer Length/ Strand Diameter	Volume of Steel Fiber, %	Source
0.6	11–18	18.3–30.0 d_b	2.0	John et al. (2011)
0.5	8.7–11.0	17.4–22.0 d_b	0.9	Bertram and Hegger (2012)
0.7	17–21	24.2–30.0 d_b	-	Maguire et al. (2009)

Note: - : Not available

7.1.4 Experimental Plan

Transfer length of the girder specimens was measured using a DEMEC strain gage, as shown in Figure 7.2. DEMEC points were fabricated using an aluminum sheet for the first two girder specimens and attached on the girders using high-strength glue adhesive immediately after removing the girder forms, as shown in Figure 7.3. For the first girder specimen (Tx34-1), DEMEC points were installed at both ends and both faces, creating a total length of 59 in. from the end with a 2 in. spacing. Note that the diameter of strands was 0.6 in. The time for attaching DEMEC points caused a delay in strand release. Thus, for the second girder specimen (Tx34-2), fewer DEMEC points were installed at the precast plant, with a total length of 13 in. (to ensure 20 d_b) from each end and on both faces with a 2 in. spacing. After transporting the Tx34-2 girder specimen to the laboratory, additional DEMEC points were attached to create a 37 in. distance (to ensure 60 d_b) from the end with a 2 in. spacing at both ends and both faces.

Figure 7.2. DEMEC Device.

The following procedure was used to take the DEMEC point measurements:

1. Zero readings were recorded immediately after demolding the form before strand release.
2. After releasing the strands, initial readings were recorded.
3. After transporting the girder specimens to the laboratory, readings were conducted continuously until the full-scale load testing.

However, the readings for Tx34-1 and Tx34-2 were not reliable. It was hypothesized that this issue was related to the use of aluminum DEMEC points. The aluminum point did not have sufficient hardness for the points of the DEMEC device. Therefore, the center-punched hole on the aluminum plate was widened during the course of taking readings. Consequently, the aluminum DEMEC points were replaced with a stainless steel DEMEC contact seat for the third girder specimen (Tx54), as shown in Figure 7.4. Note that the thread part of the stainless steel DEMEC contact seat was cut to attach it directly to the surface of the girder specimen. The stainless steel DEMEC contact seats provided more stable and reliable readings.

For the Tx54 girder, DEMEC contact seats were installed at both ends of the girder and on one face only to create a 33 in. distance (to ensure more than 40 d_b) from the end with 4 in. spacing. The DEMEC contact seats were installed immediately after removing the forms. Zero and initial readings were recorded before and after the prestressing transfer, respectively. After transporting the girder to the laboratory, readings were recorded once a week up until the full-scale testing.

A prestressed girder cambers upward after prestressing transfer due to the eccentricity of prestressing, thus causing compressive strain at the level of the DEMEC points. In addition, the

self-weight of the girder causes tensile strain below the neutral axis of the girder. The tensile strain from self-weight at the level of the DEMEC points is calculated using Equation (7.3) (Bhoem et al. 2010), and to compensate for this tensile strain, the computed strain was deducted from the surface compressive strain measured from the DEMEC readings:

$$\varepsilon_{weight} = \frac{MY_{DEMEC}}{E_c I_{tr}} \tag{7.3}$$

where:

ε_{weight} = Tensile strain due to self-weight, in/in.

M = Moment due to self-weight, kip-in.

Y_{DEMEC} = Distance between DEMEC seat and centroid of transformed section, in.

E_c = MOE, ksi

I_{tr} = Moment of inertia of transformed section, in^4

Compressive strain readings were smoothed by averaging readings of three adjacent points. Transfer length was determined using the 95 percent average maximum strain method (Russell and Burns 1997).

(a) Attached Aluminum DEMEC Points on Tx34-1

(b) Attached Aluminum DEMEC Points on Tx34-2

Figure 7.3. Installed DEMEC Plates.

(a) Stainless Steel DEMEC Contact Seat

(b) Installed DEMEC Contact Seats

Figure 7.4. DEMEC Contact Seats for Tx54.

7.1.5 Transfer Length Results

The measured compressive strains for Tx34-1 and Tx34-2 using aluminum DEMEC points fluctuated and were deemed unreliable. Thus, the transfer length results for Tx34-1 and Tx34-2 are excluded from this report. Figure 7.5 shows the results of transfer length of Tx54 at the initial readings (immediately after releasing the prestress) and at 33 days (before conducting full-scale testing).

The results were compared to the equations from the AASHTO LRFD Bridge Design Specifications (AASHTO 2020), NCHRP Report 603 (Ramirez and Russell 2008), and Australian (Gowripalan and Gilbert 2000) and PCI recommendation (eConstruct 2020) (between 20 d_b and 40 d_b), as shown in Table 7.2.

Table 7.2. Transfer Length of Tx54.

Age	Live End	Dead End	AASHTO (60 d_b)	NCHRP Report 603	PCI	
					20 d_b	40 d_b
Initial (1 day), in.	18.0	19.5	36.0	18.7	12.0	24.0
33 days, in.	20.5	19.5	36.0	18.7	12.0	24.0

Notes:
1. d_b = 0.6 in.
2. f'_{ci} = 14.8 ksi
3. Fiber volume is 1.5 percent.

The transfer length at the live end (stressed end) was 18.0 in. initially and 20.5 in. at 33 days. The results are between 30 d_b and 34 d_b. The transfer length at the dead end was 19.5 in. both initially and at 33 days, which is 32.5 d_b. The results are in the range of the PCI recommendations and the Australian design guidelines for UHPC, whereas the results are higher than the draft of AASHTO recommendations for UHPC, 24 d_b. Based on these measurements, the current AASHTO transfer length estimation is conservative for UHPC applications. Even though NCHRP Report 603 estimation has a compressive strength limitation (up to 9 ksi), this estimation is comparable to the measured results if the limitation is not considered. For design purposes, a 30 d_b transfer length for the developed UHPC containing 1.5 percent of fiber volume in this project is recommended.

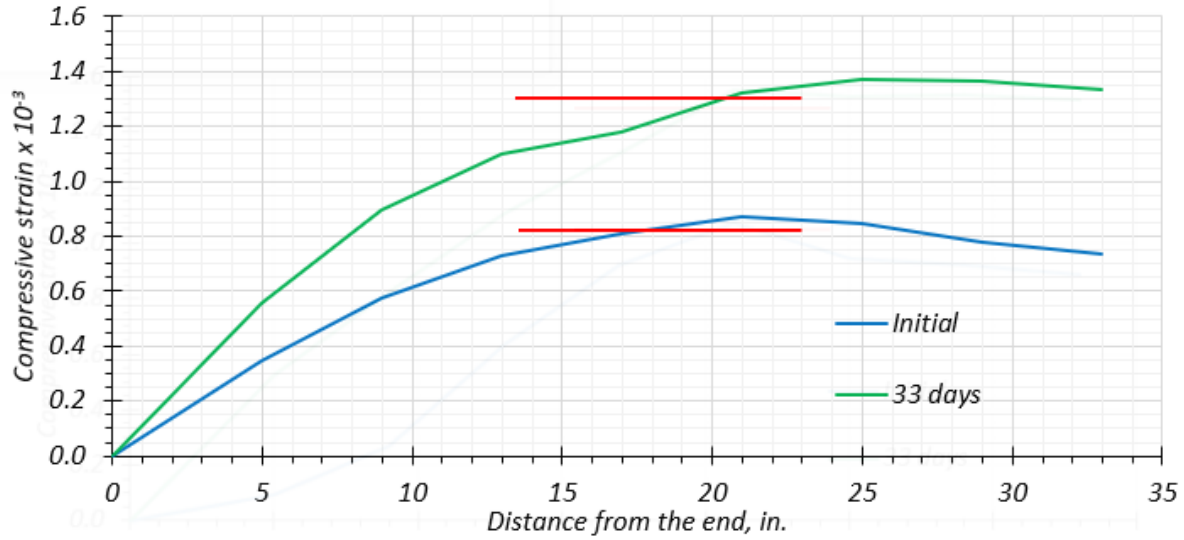

(a) Transfer Length at Live End (Minimum Web Reinforcement)

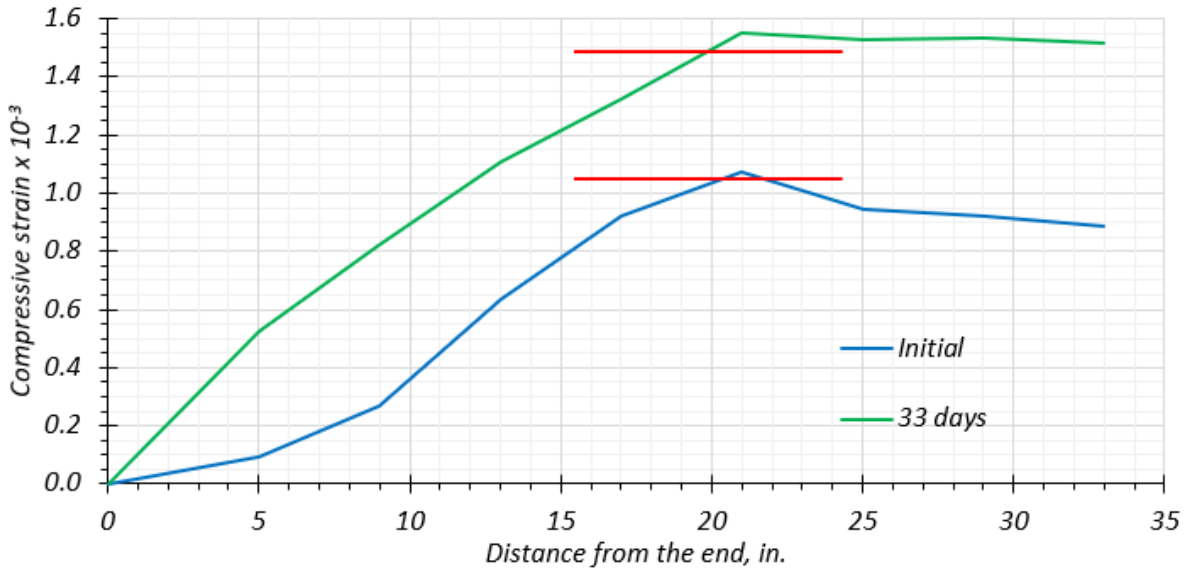

(b) Transfer Length at Dead End (No Web Reinforcement)

Note: Red line = 95% average maximum strain.

Figure 7.5. Transfer Length of Tx54.

7.2 CAMBER AND DEFLECTION

This section presents camber and deflection of the prestressed UHPC girder specimens. Due to the eccentricity of prestressing, camber occurs immediately after prestress release. After initial camber, camber growth is affected by compressive strength, MOE, creep, shrinkage, prestress loss, thermal gradients, deck placement, and live load (Storm et al. 2013). Currently, there is a lack of

knowledge for prestress losses and long-term properties, such as creep and shrinkage, for prestressed UHPC girders. Therefore, guidance for an accurate prediction of camber for prestressed UHPC girders is limited. This section provides measured cambers of the three UHPC girder specimens. In addition, the predicted cambers are provided to consider prestress loss predictions based on the proposed creep and shrinkage prediction models discussed in Sections 6.5.1 and 6.5.2 of the Volume 1 report, respectively.

7.2.1 Experimental Plan

The initial camber of the girder specimens at midspan was measured using a ruler with 1/16 in. accuracy immediately after prestress release at the precast plant. After transporting the girder specimens to the laboratory, readings for camber were conducted using the same ruler over time until conducting full-scale testing. The measured camber values over time are compared with the predicted camber values using an incremental time-step method, as discussed in the following sections.

7.2.2 Measured Camber

Figure 7.6 shows the measured camber of the three girder specimens. Note that the camber value at the transport day (13 days) of Tx34-1 was measured when the girder was placed in the laboratory on four wooden supports (one at each end and one at each quarter point), whereas the camber values of the other two girder specimens on the day of transport were measured when the girder specimens were place on two pedestals (one at each end). Thus, there was an erroneous high value of the camber reading for Tx34-1 at 13 days. For all the three girder specimens, the camber value at the transport day shows a relatively high value temporarily. It may be due to the effects from lifting a girder specimen. Table 7.3 presents camber values of the three girder specimens at specific times, including initially, at deck placement, at removal of deck forms, and at the final day of testing.

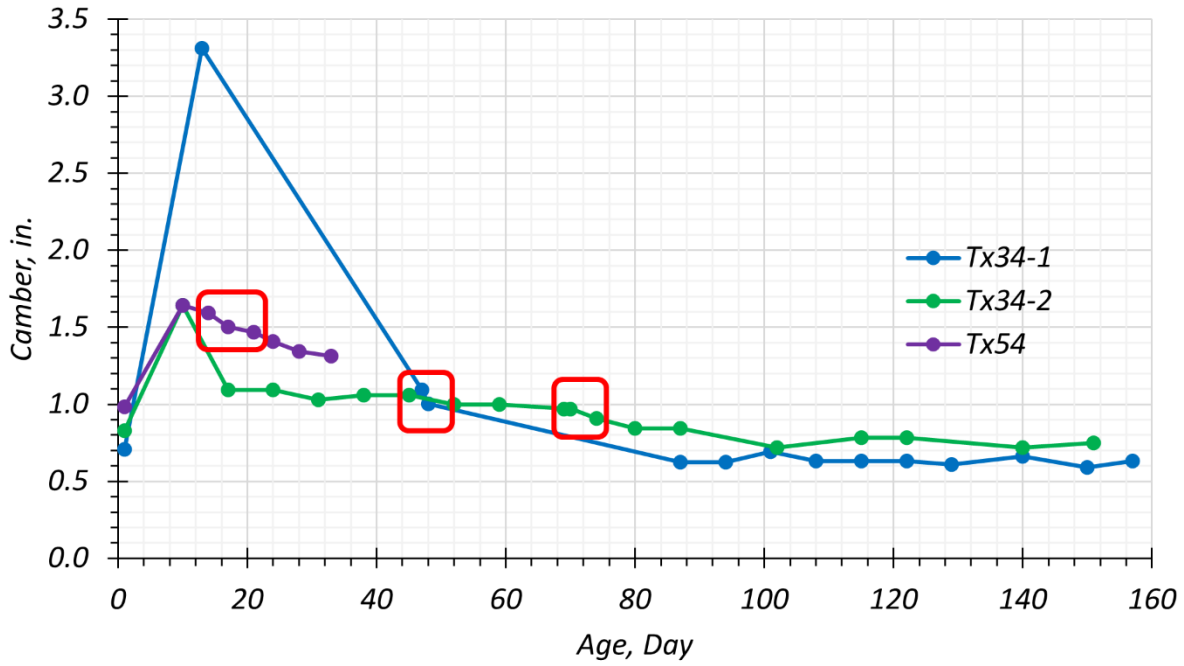

Red Box: Deflection due to deck placement

Figure 7.6. Measured Camber of the Girder Specimens.

Table 7.3. Camber Values of the Girder Specimens.

Girder ID	Initial Camber, in.	Camber before Deck Placement, in.	Camber after Deck Form Removal, in.	Final Camber[1], in.
Tx34-1	0.71	1.09	1.00	0.63
Tx34-2	0.83	0.97	0.91	0.75
Tx54	0.98	1.50	1.41	1.31

Note:

1. The final camber measurement was conducted before full-scale testing. The ages of the final camber readings are 157, 151, and 33 days for Tx34-1, Tx34-2, and Tx54, respectively.

The numbers of strands are 30, 38, and 48 for Tx34-1, Tx34-2, and Tx54, respectively, as shown in Table 4.3. The eccentricity at midspan of Tx34-1, Tx34-2, and Tx54 are 8.61 in., 8.80 in., and 15.10 in., respectively, as shown in Table 4.3. Note that the geometry and the length (50 ft) of Tx34-1 and Tx34-2 are the same, as shown in Figure 4.1 and Figure 4.2. Due to the higher eccentricity and larger number of strands, Tx34-2 has a higher initial camber than Tx34-1. Tx54 is 70 ft long with 48 strands and 15.10 in. eccentricity. As a result, it has the highest initial camber value. The difference in camber before and after deck placement was similar for all three girder specimens (0.09 in., 0.06 in., and 0.09 in. for Tx34-1, Tx34-2, and Tx54, respectively). The difference in camber between the initial and final readings was 0.08 in. for both Tx34-1 and Tx34-

2. Note that camber measurement period for Tx54 was relatively short (33 days) because full-scale testing for Tx54 was conducted at the age of 34 days.

7.2.3 Prediction of Camber

The incremental time-step method was used for the estimation of camber in this project. Camber increases (upward) due to creep and prestressing force, whereas it decreases (downward) due to self-weight of the girder, prestress losses, and deck and haunch weight. Except for the prestress loss due to autogenous shrinkage at transfer and a few selected parameters, the calculation of prestress losses followed the method of refined estimates of time-dependent losses in accordance with the AASHTO LRFD Bridge Design Specifications Section 5.9.3.4 (AASHTO 2020).

7.2.3.1 Initial Camber at Transfer

Initial camber at transfer occurs upward due to the prestressing force, whereas downward deflection occurs immediately after transfer due to a girder self-weight. The initial camber at transfer is calculated using Equation (7.4):

$$\Delta_i = \Delta_{ps,i} - \Delta_{sw,i} \tag{7.4}$$

where:

Δ_i = Net camber at prestress transfer, in.

$\Delta_{ps,i}$ = Camber (upward) at transfer due to prestress, in.

$\Delta_{sw,i}$ = Deflection (downward) at transfer due to girder self-weight, in.

Camber due to prestress at transfer is calculated by Equation (7.5). Transfer length was assumed to be 20 in. based on the measurements discussed in Section 7.1.5. The term of Δp_i in Equation (7.5) includes prestress loss due to elastic shortening and autogenous shrinkage occurring between the final set and transfer.

$$\Delta_{ps,i} = \left(\frac{p_i}{(E_{cg,i})(I_{tran,i})} - \frac{\Delta p_i}{(E_{cg,i})(I_{tran,i})}\right) \times \left(\frac{e_1 L^2}{8} - \frac{(e_1 - e_2)a^2}{6} - \frac{e_1 L_t^2}{6}\right) \tag{7.5}$$

$$p_i = A_{ps} N_s f_{pbt} \tag{7.6}$$

$$\Delta p_i = A_{ps} N_s \Delta f_{pT} \tag{7.7}$$

where:

p_i = Initial prestressing force, kips

$E_{cg,i}$ = MOE of girder at transfer, ksi

$I_{tran,i}$ = Moment of inertia of transformed section of the girder at transfer, in^4

Δp_i = Change in prestressing force due to prestress loss at transfer, kips

e_1 = Eccentricity at midspan, in.

e_2 = Eccentricity at support, in.

L = Girder span, in.

L_t = Transfer length, in.

a = Distance from the end to the harping point, in.

A_{ps} = Area of individual prestressing strand, in^2

N_s = Number of prestressing strands

f_{pbt} = Stress in prestressing steel immediately prior to transfer, $f_{pbt} = 0.75\, f_{pu} = 202.5$ ksi, where $f_{pu} = 270$ ksi

Δf_{pT} = Total prestress loss at transfer, ksi

For CC, elastic shortening of concrete is the only factor for prestress loss at transfer. For UHPC, however, prestress loss due to autogenous shrinkage occurs during the time between final set and transfer and should also be considered. Prestress loss at transfer due to elastic shortening and autogenous shrinkage is calculated by Equation (7.8).

$$\Delta f_{pT} = \Delta f_{pES} + \Delta f_{pshi} \tag{7.8}$$

$$\Delta f_{pES} = \frac{f_{cgp} \times E_p}{E_{cgi}} \tag{7.9}$$

$$\Delta f_{pshi} = \varepsilon_{shi} E_p K_i \tag{7.10}$$

where:

Δf_{pES} = Prestress loss due to elastic shortening at transfer, ksi

f_{cgp} = Concrete stress at the center of gravity of prestressing tendons due to the prestressing force immediately after transfer, ksi

E_p = MOE of prestressing strand, ksi

Δf_{pshi} = Prestress loss due to autogenous shrinkage occurring during the time between final set and transfer, ksi

ε_{shi} = Autogenous shrinkage strain occurring between the time between final set and transfer, in./in.

K_i = Transformed section coefficient that accounts for initial (elastic) interaction between concrete and bonded steel, assumed to be 0.83 according to Section F.1.6.1 of eConstruct (2020).

Establishing an accurate amount of autogenous shrinkage to estimate the prestress loss at transfer is difficult because of the following reasons. First, the autogenous shrinkage that occurs before 24 hours is not captured by the standard test method ASTM C157 (2017) because it recommends measuring shrinkage after 24 hours. As a result, the autogenous shrinkage that occurs before 24 hours is unknown when using the standard test method, as shown in Figure 7.7. Second, even if the autogenous shrinkage that occurs before 24 hours is measured, a portion of the autogenous shrinkage occurs while concrete is in a plastic state. Thus, the time of transition from a plastic to a solid state in concrete should be identified to know the amount of autogenous shrinkage that occurred in the solid state. Third, even though the amount of free autogenous shrinkage is large, restrained shrinkage in a form is much lower than free shrinkage (Yoo et al. 2014a). Yoo et al. (2014a) indicated that the restrained shrinkage value is one-fifth or less than the free shrinkage of the same UHPC mixture design. Therefore, actual shrinkage of a pretensioned girder on a casting bed before demolding may be lower than the autogenous shrinkage. Fourth, the high heat of a UHPC girder due to cement hydration may decrease the prestressing force by thermal expansion of strands. Bruce et al. (1998) reported that the prestressing force can be decreased temporarily up to 11 percent for CC due to thermal expansion resulting from heat of cement hydration. However, some of the prestressing force can be regained by cooling after bonding between concrete and steel. As a result, the prestress loss due to the thermal effect is approximately 6 percent. Storm et al. (2013) also investigated change in prestressing force after initial prestressing due to thermal expansion of strands. The authors reported that prestressing force can be decreased temporarily more than 7 percent for CC due to the thermal effects, including cement hydration and exposure to the sun. The temperature of a UHPC girder is higher than a CC girder due to a large cement content. For example, the maximum measured internal temperatures of the Tx34-1 girder and a

SCC girder fabricated on the same day were 214°F and 142°F, respectively. The temperature of the three girder specimens at 16 hours is in the range of 180–200°F, as discussed in Section 6.3.3 in the Volume 1 report. Thus, the thermal expansion due to the high temperature may affect prestress loss at transfer. Distinguishing the prestress losses due to thermal expansion of strands and due to autogenous shrinkage may be difficult.

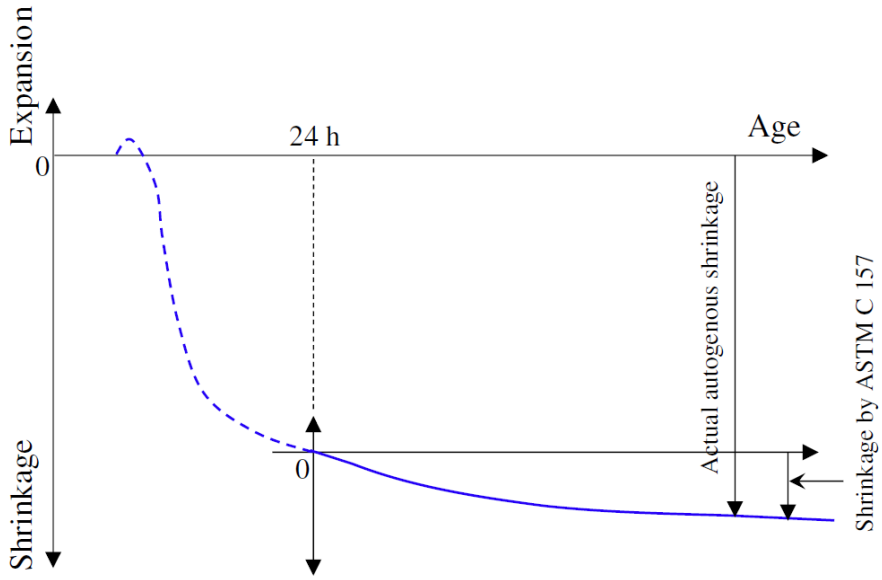

Figure 7.7. Autogenous Shrinkage Occurring between Final Set and Transfer (adapted from (Yoo et al. 2014a).

The recommendation by eConstruct (2020) is 600 με for prestress loss due to autogenous shrinkage during the time between the final set and transfer. However, the amount of autogenous shrinkage may vary depending on the proportions of the UHPC, especially cement content. In addition, this value is conservative; thus, the authors will refine this value through further research. The predicted cambers using 600 με autogenous shrinkage for prestress loss at transfer were underestimated compared to the measured camber at transfer of the three girder specimens. For this project, 200 με of autogenous shrinkage provided a good prediction for the initial cambers of the three girder specimens, as shown in Table 7.4. Thus, 200 με was assumed for the prestress loss at transfer due to autogenous shrinkage. Note that the amount of autogenous shrinkage may depend on temperature development of a girder and the curing time prior to transfer.

Table 7.4. Predicted and Measured Initial Camber.

Girder ID	Measured Initial Camber, in.	Predicted Initial Camber, in.
Tx34-1	0.71	0.71
Tx34-2	0.83	0.86
Tx54	0.98	0.95

Deflection at transfer due to the girder self-weight $\Delta_{sw,i}$ is calculated by Equation (7.11).

$$\Delta_{sw,i} = \frac{5W_g L^4}{384(E_{cg,i})(I_{tran,i})} \tag{7.11}$$

where:

W_g = Girder self-weight, kips/in.

L = Length of girder, in.

7.2.3.2 Camber between Transfer and Deck Placement

Camber between transfer and deck placement is affected by prestress losses and creep over time. Prestress losses occur due to the effects of strand relaxation, creep, and shrinkage, in addition to elastic shortening and autogenous shrinkage at transfer. The associated camber is calculated in time increments using Equation (7.12).

$$\Delta_t = \Delta_{ps,t} + \Delta_{cr,t} - \Delta_{sw} \tag{7.12}$$

where:

Δ_t = Camber at a specific time, in.

$\Delta_{ps,t}$ = Camber due to prestress at a specific time, in.

$\Delta_{cr,t}$ = Camber due to creep at a specific time, in.

Δ_{sw} = Deflection due self-weight at a specific time, kips

7.2.3.2.1 Camber due to Prestress

Camber due to prestress can be computed by Equation (7.13), which includes a term for prestress losses as shown in Equation (7.14).

$$\Delta_{ps,t} = \Delta_{ps,t-1} - \left(\frac{\Delta p_{p,t} - \Delta p_{p,t-1}}{E_{cg,t}\, I_{tran}}\right) \times \left(\frac{e_1 L^2}{8} - \frac{(e_1 - e_2)a^2}{6} - \frac{e_1 L_t^2}{6}\right) \tag{7.13}$$

$$\Delta p_{p,t} = A_{ps} N_s \Delta f_{pT} \quad (7.14)$$

where:

$\Delta_{ps,t-1}$ = Camber due to prestress at the previous time step, in.

$\Delta p_{p,t}$ = Prestressing force due to prestress loss at a specific time, kips

$\Delta p_{p,t-1}$ = Prestressing force due to prestress loss at the previous time step, kips

$E_{cg,t}$ = MOE of girder at a specific time, ksi

I_{tran} = Moment of inertia of transformed section of the girder, in^4

The total prestress loss Δf_{pT} has two components: the first component is the short-term prestress loss occurring at transfer, as described in Equation (7.15), and the second component is the long-term prestress loss occurring due to creep and shrinkage of the UHPC girder and relaxation of prestressing strands, as shown in Equations (7.16) and (7.17).

$$\Delta f_{pT} = (\Delta f_{pES} + \Delta f_{pshi}) + \Delta f_{pLT} \quad (7.16)$$

$$\Delta f_{pLT} = (\Delta f_{pSR} + \Delta f_{pCR} + \Delta f_{pR1}) \quad (7.17)$$

where:

Δf_{pLT} = Long-term prestress loss, ksi

Δf_{pSR} = Prestress loss due to shrinkage of girder occurring between transfer and deck placement, ksi

Δf_{pCR} = Prestress loss due to creep of girder occurring between transfer and deck placement, ksi

Δf_{pR1} = Prestress loss due to relaxation of prestressing strands occurring between transfer and deck placement—1.2 ksi for low-relaxation strands, according to AASHTO LRFD Bridge Design Specifications Section 5.9.3.4.2c (AASHTO 2020).

Prestress losses due to creep and shrinkage can be calculated by Equations (7.18) and (7.19).

$$\Delta f_{pSR} = \varepsilon_t E_p K_{id} \quad (7.18)$$

$$\Delta f_{pCR} = \frac{E_p}{E_{cg}} f_{cgp} \psi_{(t,t_i)} K_{id} \quad (7.19)$$

where:

ε_t = Shrinkage strain of UHPC girder at a specific time

E_p = MOE of prestressing strands, ksi

K_{id} = Transformed section coefficient that accounts for time-dependent interaction between concrete and bonded steel between transfer and deck placement, assumed to be 0.83 according to Section F.1.6.2.1.1 of eConstruct (2020).

$\psi_{(t,t_i)}$ = Creep coefficient of UHPC girder at a specific time due to loading at transfer

The creep coefficient and shrinkage of UHPC can be calculated using the prediction models established for the developed UHPC presented in Sections 6.5.1 and 6.5.2, respectively, in the Volume 1 report.

7.2.3.2.2 Camber due to Creep

Camber increases due to the creep of the UHPC girder under prestressing over time and can be estimated by Equation (7.20).

$$\Delta_{cr,t} = \Delta\psi_{(t,t-1)} \left\{ \frac{\left(\frac{p_t + p_{t-1}}{2}\right)}{(E_{cg,i})(I_{tran,i})} \times \left[\frac{e_1 L^2}{8} - \frac{(e_1 - e_2)a^2}{6} - \frac{e_1 L_t^2}{6} \right] - \Delta_{sw,i} \right\} \quad (7.20)$$

where:

$\Delta\psi_{(t,t-1)}$= Increment in creep coefficient for the time between a specific time step (t) and a previous time step ($t-1$) due to load applied at transfer

p_t = Prestressing force at a specific time (t), kips

p_{t-1} = Prestressing force at the previous time step ($t-1$), kips

7.2.3.2.3 Deflection due to Girder Self-Weight

Deflection during the time between transfer and deck placement due to the girder self-weight is calculated using Equation (7.21).

$$\Delta_{sw} = \frac{5 W_g L^4}{(384 E_{cg,t})(I_{tran})} \quad (7.21)$$

7.2.3.3 Camber after Deck Placement

Deck placement influences the camber by the introduction of the deck self-weight and increase in moment of inertia from composite section. In addition, prestress gain occurs due to shrinkage of the deck concrete. Camber after deck placement is calculated using Equation (7.22).

$$\Delta_t = \Delta_{ps,t} + \Delta_{cr,t} - \Delta_{sw} - \Delta_{deck} \tag{7.22}$$

where:

Δ_{deck} = Deflection of composite section due to self-weight of deck and haunch, in.

7.2.3.3.1 Camber due to Prestress

Camber with the following prestress losses and gain due to prestress after deck placement can be computed by Equation (7.13):

$$\Delta f_{pLT} = (\Delta f_{pSR} + \Delta f_{pCR} + \Delta f_{pR1}) + \Delta f_{pR2} + \Delta f_{pSS} \tag{7.23}$$

where:

Δf_{pR2} = Prestress loss due to relaxation of prestressing strands in composite section between deck placement and final, $\Delta f_{pR2} = \Delta f_{pR1} = 1.2$ ksi for low-relaxation strands according to AASHTO LRFD Bridge Design Specifications Section 5.9.3.4.3c (AASHTO 2020).

Δf_{pSS} = Prestress gain due to shrinkage of deck in composite section, ksi.

$$\Delta f_{pSS} = \frac{E_p}{E_{cg}}(\Delta f_{cdf})(K_{df})[1 + 0.7\psi(t_t, t_d)] \tag{7.24}$$

$$\Delta f_{cdf} = \frac{\varepsilon_{t,d} A_d E_{c\,deck}}{[1+0.7\psi_d(t_t,t_d)]}\left(\frac{1}{A_c} - \frac{e_{pc}e_d}{I_{tran,c}}\right) \tag{7.25}$$

where:

Δf_{cdf} = Change in concrete stress due to shrinkage of deck concrete at centroid of prestressing strands, ksi

K_{df} = Transformed section coefficient that accounts for time-dependent interaction between concrete and bonded steel between deck placement and

final, assumed to be 0.73 according to Section F.1.6.2.1.1 of eConstruct (2020).

$\psi(t_t, t_d)$ = Girder creep coefficient due to loading at deck placement

$\varepsilon_{t,d}$ = Shrinkage strain of deck concrete, in./in.

A_d = Area of deck concrete, in^2

$E_{c\ deck}$ = MOE of deck concrete, ksi

$\psi_d(t_t, t_d)$= Creep coefficient of deck concrete due to loading immediately after deck placement

A_c = Area of composite section, in^2

e_{pc} = Eccentricity of prestressing force with respect to centroid of composite section, in.

e_d = Eccentricity of deck with respect to the gross composite section, in.

$I_{tran,c}$ = Moment of inertia of transformed composite section, in^4

7.2.3.3.2 Camber due to Creep

Camber occurs continuously over time due to creep from the prestressing force. Additional camber after deck placement is calculated using Equation (7.20).

7.2.3.3.3 Deflection due to Self-Weight of Girder, Deck, and Haunch

Deflection due to self-weight of deck and haunch after deck placement is calculated using Equation (7.26). Deflection due to a girder self-weight is calculated by Equation (7.21).

$$\Delta_{deck} = \frac{5(W_d+W_h)L^4}{(384E_{cg,t})(I_{tran,c})} \quad (7.26)$$

where:

W_d = Deck self-weight, kips/in.

W_h = Haunch self-weight, kips/in.

7.2.3.4 Predicted Camber

Table 7.5 provides all the necessary parameters used to predict the camber of the three girder specimens. Table 7.6, Table 7.7, and Table 7.8 shows the prediction results at specific time steps for Tx34-1, Tx34-2, and Tx54, respectively.

Table 7.5. Input Parameters for Camber Prediction.

Parameter	Tx34-1	Tx34-1	Tx54
$E_{cg,i}$, ksi	4891	4891	4891
$I_{tran,i}$, in^4	89,784	90,147	303,347
I_{tran}, in^4	89,461	89,728	322,503
e_1, in.	8.61	8.80	15.04
e_2, in.	8.61	5.64	8.76
W_g, kip/ft	0.697	0.697	0.908
W_d, kip/ft	0.815	0.815	0.815
W_h, kip/ft	0.066	0.066	0.066
L, ft	50	50	70
L_t, in.	20	20	20
a, ft	0	20	30
A_{ps}, in^2	0.217	0.217	0.217
N_s	30	38	48
f_{cgp}, ksi	2.72	2.40	3.44
E_p, ksi	28,500	28,500	28,500
ε_{shi}, in./in.	200	200	200
ε_{ult}, in./in.	700	700	700
Creep Coefficient	0.8	0.8	0.8
A_d, in^2	782	782	782
$E_{c\ deck}$, ksi	3987	3987	3987
A_c, in^2	1207	1213	1411
e_{pc}, in.	19.6	20.0	21.5
e_d, in.	13.7	13.6	10.3
$I_{tran,c}$, in^4	276,011	272,402	396,678
K_{id}	0.83	0.83	0.83
K_{df}	0.73	0.73	0.73
$\Delta_{ps,i}$, in.	0.93	1.07	1.26
$\Delta_{sw,i}$, in.	−0.22	−0.21	−0.31
Δ_i, in.	0.71	0.86	0.95

Table 7.6. Camber Prediction for Tx34-1.

Description and Age, days	Prestress Loss Predictions								Camber and Deflection Predictions				
	Δf_{pES} ksi	Δf_{pshi} ksi	Δf_{pSR} ksi	Δf_{pCR} ksi	Δf_{pR1} ksi	Δf_{pR2} ksi	Δf_{pSS} ksi	Δf_{pT} ksi	$\Delta_{ps,t}$ in.	$\Delta_{cr,t}$ in.	Δ_{sw} in.	Δ_{deck} in.	Δ_t in.
Transfer, 0.9	15.34	4.73	—	—	—	—	—	20.07	0.93	—	−0.22	—	0.71
Before deck placement, 47	15.34	4.73	12.42	5.86	1.20	—	—	39.55	0.84	0.33	−0.18	—	0.99
After deck placement, 59	15.34	4.73	12.88	6.21	1.20	1.20	0.36	41.92	0.83	0.35	−0.18	−0.10	0.90
Final, 157	15.34	4.73	14.29	8.93	1.20	1.20	1.05	46.74	0.83	0.42	−0.18	−0.10	0.97

Note:
1. Positive: prestress loss and upward camber
2. Negative: prestress gain and downward deflection

Table 7.7. Camber Prediction for Tx34-2.

Description and Age, days	Prestress Loss Predictions								Camber and Deflection Predictions				
	Δf_{pES} ksi	Δf_{pshi} ksi	Δf_{pSR} ksi	Δf_{pCR} ksi	Δf_{pR1} ksi	Δf_{pR2} ksi	Δf_{pSS} ksi	Δf_{pT} ksi	$\Delta_{ps,t}$ in.	$\Delta_{cr,t}$ in.	Δ_{sw} in.	Δ_{deck} in.	Δ_t in.
Transfer, 0.9	13.30	4.73	—	—	—	—	—	18.03	1.07	—	−0.21	—	0.86
Before deck placement, 59	13.30	4.73	12.85	5.38	1.2	—	—	37.46	0.96	0.43	−0.18	—	1.21
After deck placement, 74	13.30	4.73	13.24	6.11	1.2	1.2	0.59	40.37	0.94	0.45	−0.18	−0.20	1.01
Final, 151	13.30	4.73	14.27	7.77	1.2	1.2	1.09	43.56	0.94	0.50	−0.18	−0.20	1.06

Note:
1. Positive: prestress loss and upward camber
2. Negative: prestress gain and downward deflection

Table 7.8. Camber Prediction for Tx54.

Description and Age, days	Prestress Loss Predictions								Camber and Deflection Predictions				
	Δf_{pES} ksi	Δf_{pshi} ksi	Δf_{pSR} ksi	Δf_{pCR} ksi	Δf_{pR1} ksi	Δf_{pR2} ksi	Δf_{pSS} ksi	Δf_{pT} ksi	$\Delta_{ps,t}$ in.	$\Delta_{cr,t}$ in.	Δ_{sw} in.	Δ_{deck} in.	Δ_t in.
Transfer, 0.9	19.09	4.73	—	—	—	—	—	23.82	1.26	—	−0.31	—	0.95
Before deck placement, 17	19.09	4.73	10.02	5.58	1.20	—	—	40.62	1.14	0.33	−0.27	—	1.20
After deck placement, 28	19.09	4.73	11.25	6.59	1.20	1.20	−0.05	44.01	1.13	0.38	−0.27	−0.07	1.17
Final, 33	19.09	4.73	11.63	6.93	1.20	1.20	−0.07	44.71	1.12	0.40	−0.27	−0.07	1.18

Note:
1. Positive: prestress loss and upward camber
2. Negative: prestress gain and downward deflection

Figure 7.8 and Table 7.9 show the predicted camber values compared to the measured camber values.

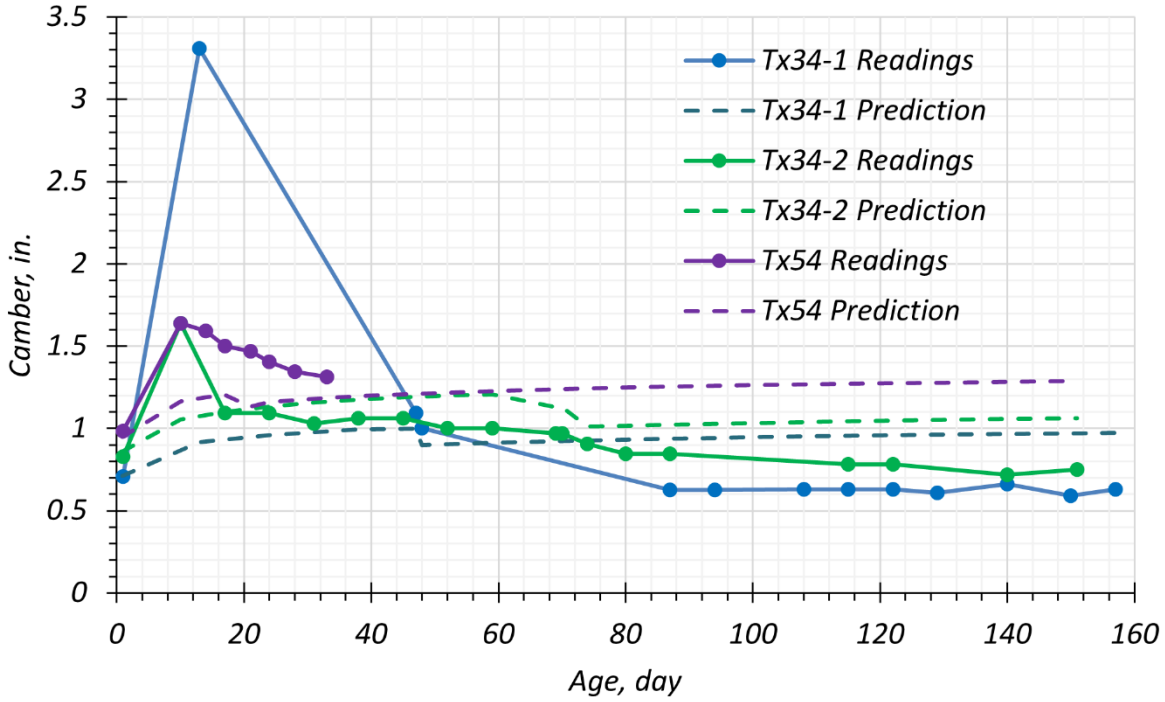

Figure 7.8. Predicted and Measured Camber.

Table 7.9. Measured and Predicted Camber Comparison.

Girder ID	Initial Camber, in.			Final Camber, in.			
	Measured	Predicted	Difference	Age, days	Measured	Predicted	Difference
Tx34-1	0.71	0.71	0.0 (0.0%)	157	0.63	0.97	0.34 (54%)
Tx34-2	0.83	0.86	0.03 (3.6%)	151	0.75	1.06	0.31 (41%)
Tx54	0.98	0.95	−0.03 (−3.1%)	33	1.31	1.18	−0.13 (−9.9%)

The predictions show a good estimation of camber for the precast, pretensioned UHPC girder specimens. The difference between the measured and the predicted camber at the final measurement for Tx34-1 and Tx34-2 is 0.34 and 0.32 in. The trend of the predicted camber after deck placement shows a slight increase, from 0.89 to 0.97 in. for Tx34-1, and from 1.02 to 1.06 in. for Tx34-2, because of the camber due to creep (the increased camber estimation after deck placement is 0.08 in. and 0.04 in. for Tx34-1 and Tx34-2, respectively), whereas the actual camber for Tx34-1 and Tx34-2 decreased to 0.37 in. and 0.15 in. after deck placement, respectively. This

result may be because there is an overestimated camber due to creep. However, it can be refined further in future research. Overall, the difference between the measured and predicted camber is small considering the accuracy of measurements and other effects, such as friction, between the bearing pads and UHPC girder. Therefore, the camber predictions for these precast, pretensioned UHPC girders provides a reasonable estimation.

7.3 SUMMARY

The full-scale girder specimens were also studied to evaluate the transfer length of the prestressing strands and the measured versus predicted camber over time. The following observations and conclusions were made:

1. *Transfer Length*.
    - The transfer lengths for the Tx54 girder specimen were measured over time. The initial transfer length was 18.0 in. and 19.5 in. at the live end and dead end, respectively. The transfer length at 33 days was 20.5 in. at the live end and 19.5 in. at the dead end.
    - The measured results give a transfer length of 30–34 d_b. The results are well-matched with the PCI and Australian recommendations for UHPC, which is 20–40 d_b (eConstruct 2020; Gowripalan and Gilbert 2000). Note that the AASHTO draft specifications for UHPC recommends 24 d_b transfer length for design (FHWA 2022).
2. *Camber*.
    - The camber of the UHPC girder specimens was recorded from the time of prestress transfer at the plant. Tx34-1 and Tx34-2 (50 ft long) had 0.71 and 0.83 in. of initial camber, respectively, and Tx54 (70 ft long) had 0.98 in. of initial camber. The final camber was 0.63 in. for Tx34-1, 0.75 in. for Tx34-2, and 1.31 in. for Tx54. Note that the ages at the time of the final camber measurements were 157, 151, and 33 days for Tx34-1, Tx34-2, and Tx54, respectively.
    - For prediction of camber, the incremental time-step method was used. Unlike CC, prestress loss due to autogenous shrinkage occurring during the time between the final set and transfer was additionally considered for the initial camber of the UHPC girders. In addition, the prediction models for creep and shrinkage presented in the Volume 1 report were used to estimate prestress losses over time. The measured camber was predicted quite accurately using the following parameters for the developed UHPC:

200 με autogenous shrinkage before transfer, 700 με ultimate shrinkage, and 0.8 creep coefficient. The difference between measured and predicted camber values was from −0.03 to 0.03 in. for the initial camber and from −0.12 to 0.34 in. for the final camber.

8 SUMMARY AND CONCLUSIONS

This Volume 2 report primarily discusses the full-scale testing of the UHPC girder specimens fabricated at the precast plant. These girders were cast using a nonproprietary UHPC mixture developed using locally sourced materials in Texas based on detailed feedback from several precasters across the state. This volume presents a literature review of the recommendations and guidelines on the design of UHPC structural elements used for highway bridge structures documented in Chapter 2. The nonproprietary mixture was designed to achieve the target design strengths that were determined based on preliminary designs of precast, pretensioned UHPC bridge girders conceived as part of the analytical feasibility study for several typical TxDOT girder sections. Chapter 3 documents the details of the analytical feasibility study. The Volume 1 report provides information related to the development of the nonproprietary UHPC mixtures and the production of the girder specimens. The designs of the girder specimens with a composite CIP CC deck slab are presented in Chapter 4, with detailed drawings provided in the appendix. Chapter 4 also discusses the full-scale testing setup, loading, and instrumentation of the girders. The performance of the girders under flexure and shear are explained through analytical predictions and experimental data in Chapters 5 and 6, respectively. Chapter -2075909280.□ presents the monitoring of the transfer length and camber for the specimens from the day of release of prestressing strands to the full-scale load testing. The following sections briefly summarize the observations and conclusions drawn from these full-scale testing and related tasks documented in this report volume.

8.1 ANALYTICAL FEASIBILITY STUDY

The analytical feasibility study was the first step toward identifying the potential designs that could be optimized with UHPC. Existing literature on the structural design of UHPC served as the basis of the design considerations for the trial designs. The trial designs—namely (a) 5SB16 PCSB with a side-by-side configuration for short-span bridges, (b) Tx54 prestressed concrete I-girders for medium- to long-span bridges, and (c) Tx62 for prestressed concrete I-girders for long-span bridges—were developed using the strength values of UHPC noted in the literature. The potential benefits of utilizing precast, pretensioned UHPC bridge girders were determined based on the AASHTO design approach, with slight modifications for UHPC. The material target properties, especially for the tension and compression limit states, are based on the design assumptions noted

in Chapter 3. Various parameters, including number of girders, girder spacing, strand diameter, deck thickness, and compressive and tensile strength of concrete were varied to optimize the UHPC girder designs and to study the following research questions:

- What is the maximum possible span length for a given bridge type with specific geometric and material properties?
- What is the possible extension of span length beyond the current standard design when using UHPC girders?
- Is it possible to remove a girder line to optimize a bridge design when using UHPC girders?

The following key findings are noted based on the results of the feasibility study:

1. *Development of potential UHPC design options.* Based on the published range of UHPC properties, such as unit weight, compressive and tensile strengths, and prestress losses, UHPC girder designs were developed for the following slab beam and I-girders:
    - For 5SB15 slab beam girders, in comparison to the standard slab beam girder design using CC, the designs using 0.6 in. diameter strands can provide around a 40 percent longer span length, while the designs using 0.7 in. diameter strands can provide around a 55 percent increase in span length. However, camber is higher for the 0.7 in. diameter strands; harping the strands is beneficial for controlling the camber.
    - For Tx54 girders, longer span lengths were evaluated for (a) varying material strengths of UHPC, (b) different girder spacing, (c) using a 7.0 in. deck with 2.5 in. UHPC PCPs, and (d) varying the strand layout. Increasing span lengths beyond 30–40 percent longer is not practically feasible due to the high compressive and tensile strength requirements for the UHPC mixture. Approximately a 29 percent increase in span length is possible for a Tx54 girder with 0.6 in. strand diameters versus using an 8.5 in. CC deck.
    - For Tx62 girders, longer span lengths were analyzed for (a) different girder spacing, (b) varying strand diameters, (c) different compressive and tensile strengths of UHPC, and (d) varying strand layouts. For 0.6 in. diameter strands, an approximately 30 percent increase in span length can be achieved with a conventional deck thickness and with a thinner deck, while the designs using 0.7 in. diameter strands can provide up to 50 percent longer span length.

2. *Impact of strand diameter*. The full potential of UHPC can be leveraged by using larger diameter (0.7 in.) strands. However, using 0.7 in. diameter strands leads to larger camber values, although they can potentially be mitigated by harping strands. In addition, the optional live load-deflection check might be a concern for these longer span lengths. To maximize the benefits of UHPC, 0.7 in. diameter strands can be considered for future designs.
3. *Recommendations for nonproprietary UHPC mixture.* Based on the findings of the analytical feasibility study, the potential benefits of implementing UHPC for bridge structures compared to CC were highlighted. The target strengths for the nonproprietary UHPC mixture to be developed in this research were set as follows: 14 ksi compressive strength and 0.75 ksi tensile strength at release, and 22 ksi compressive strength and 1.0 ksi tensile strength at service.
4. *Recommendations for full-scale testing program*. Following review of the results and discussions with the TxDOT team, it was decided to test two Tx34 girder shapes for a medium-span-length bridge case and one Tx54 girder shape for a longer-span bridge case with no change to the strand diameter (0.6 in.) or deck thickness.

8.2 FULL-SCALE TESTING PROGRAM

Based on the target values identified from the analytical feasibility study, the nonproprietary UHPC mixtures were developed, and the most promising UHPC mixture was selected for precast, pretensioned UHPC girder fabrication, as documented in the Volume 1 report. In consultation with the TxDOT committee, two Tx34 girder specimens and one Tx54 girder specimen were selected for full-scale testing under shear and flexure. The particulars are described as follows:

1. *Details of UHPC girder specimens.* The material properties of the selected mixture design from various trials conducted in the laboratory and the precast plant were used as design inputs for the prototype designs (compressive strength of 14 ksi at release and 18.9 ksi at service, and a direct uniaxial tensile strength of 0.75 ksi at release and 1.0 ksi at service). The precast plant facility had certain limitations on the capacity and availability of casting beds because of the production schedule. Therefore, limitations on the number of strands were considered in the final design of the prototype girders and girder specimens. For example, the prototype girders were limited in span length because of the restriction on the

number of prestressing strands. Because the flexure and shear behavior of the UHPC girders and their interaction with a CC deck under standard traffic loads were the primary objective of the research project, the three specimens were designed to evaluate the flexure, shear, and transfer length properties of the corresponding prototype bridge girder designs. The specimens were of reduced span length to accommodate limitations in the laboratory. Two Tx34 specimens (50 ft long) and one Tx54 specimen (70 ft long) were produced with UHPC at the precast plant, and a CIP CC deck was constructed for each girder specimen in the laboratory. The main parameters for each girder specimen are as follows: (1) Tx34-1 had 30 eccentric strands with a protype bridge span length of 77 ft, (2) Tx34-2 had 38 strands with 6 harped strands and a protype bridge span length of 85 ft, and (3) Tx54 had 48 strands with 8 harped strands and a protype bridge span length of 121 ft.

2. *Instrumentation, measurements, and inspection at the precast plant.* The girders were instrumented with embedded gages at the midspan to monitor the flexure strain profile along the height of the girder. TCs were also installed along the height of the girder to monitor the temperature development during the first 16 hours at the midspan and the end. The details of the temperature development are documented in Section 6.3.3 of the Volume 1 report. Several instrumented R-bars were installed at the shear end to monitor the strain of the transverse reinforcement under shear loading. Camber and transfer length readings were taken in the field. The surface of the girders was evaluated to document any defects or cracks. Details of the surface evaluation can be found in Section 6.2.2.3, 6.2.3.3, and 6.2.4.3 of the Volume 1 report.
3. *Hardened properties.* Companion material-level test specimens were cast for monitoring the material properties of the UHPC girder specimens and the CIP deck slab of CC. The average values of the material properties that were used for the analysis of the specimens prior to testing are shown in Table 8.1.

Table 8.1. Summary of Short-Term Hardened Properties.

Description	Tx34-1, ksi	Tx34-2, ksi	Tx54, ksi
Compressive Strength (CIP deck slab), 28 days	5.5	6.5	5.1
Compressive Strength (UHPC), 28 days	18.9	18.0	16.5
Compressive Strength (UHPC), test day	19.1 (187 days)	18.9 (165 days)	18.1 (45 days)
Direct Uniaxial Tensile Strength at First Cracking, test day	0.53 (187 days)	0.62 (165 days)	0.95 (45 days)
MOE, 3 days	6662	6446	6742
MOE, 28 days	6330	7163	7446

Note: The test days are noted in parentheses where applicable.

4. *Instrumentation and measurements in the laboratory.* Embedded gages installed in the field were used to monitor internal strains due to flexure at midspan. The SPs and surface strain gages were installed at the midspan to monitor strains due to flexure at the girder surface. These surface strain measuring instruments were also located in between the actuators during the shear tests. SGs, surface mounted concrete gages, and LVDTs were installed at the shear ends to monitor the shear strains. LVDTs were also utilized to monitor the interface slip between the CC deck and the UHPC girder. Finally, SPs were installed along the span length of the specimens to obtain the vertical deflection profile of the specimens under loading conditions. With respect to the instrumentation, the following observations were made:

- The SPs were consistently effective for vertical measurements of larger magnitude for all the tests. However, their effectiveness in capturing strains of low magnitude was not consistent for all the tests, possibly because the sensitivity and the resolution were not effective capturing some smaller horizontal strains occurring during some flexure and shear tests, particularly those resulting in very small deformations at the instrument.
- The transfer length was monitored using a DEMEC strain gage at the girder ends. The use of stainless steel contact seats provided more consistent measurements relative to punched aluminum plates.
- The surface strain gages were very sensitive to small strains and were the most consistent instruments.
- K-gages that were cast in the UHPC girder were less reliable, possibly due to damage during the casting process. The K-gages installed on the surface were more effective in recording data.

- The LVDTs were less sensitive than the strain gages in the range of strains of small magnitude but effective in capturing strains of large magnitude, particularly for wide shear cracks.
- Overall, the use of LVDTs, K-gages, and strain gages provided sufficient redundancy to monitor small and large strains.

8.3 FLEXURE TESTING

A four-point bending full-scale test was conducted on each of the three UHPC girder specimens to simulate the prototype load conditions at the midspan. The responses of the specimens in the constant bending moment region were monitored by a suite of sensors. The responses included the strains and deflections to compute the moment-curvature and load-deflection of the specimen through the progression of load. Based on the analysis conducted as per the procedures elaborated on in Chapter 5 and the results of the full-scale testing, the following observations and conclusions were drawn:

1. *General flexural performance of girder specimens*. The following observations were made with respect to the flexural response and behavior of the girder specimens:
   - Overall, the flexure performance of the three specimens was adequate for the design loads of the corresponding prototype bridge, and the behavior of all the specimens in flexure was ductile even at the peak loads.
   - The maximum flexure capacity of the specimens under flexure prior to destructive damage to the beam was recorded. The girders had to be preserved for subsequent shear tests of both the ends. Therefore, the tests were terminated after crack localization was observed in the constant bending moment region. Tensile strains of approximately 0.009, 0.006, and 0.007 were observed at the peak loads for Tx34-1, Tx34-2, and Tx54, respectively.
   - There was no cracking observed at service and at factored demand conditions.
   - Up to service level demand, all three specimens showed a linear response without cracking. The service load was lower than the experimental capacity by 49 percent, 53 percent, and 53 percent for Tx34-1, Tx34-2, and Tx54, respectively.

- At the factored level demand, some nonlinearity accompanied by incipient cracking was observed. However, the cracks were well within serviceable widths. The factored demand load was lower than the experimental capacity by 23 percent, 31 percent, and 32 percent for Tx34-1, Tx34-2, and Tx54, respectively.
- The flexural performance of the girder was significantly impacted by the material properties of the girder, especially the tensile strength of UHPC. This finding was consistent with the analytical evaluation that showed a direct relationship between the performance of a specimen and the material strength of each of its components. In addition to the material test properties of the components of the specimen, the flexure capacity is also dependent on the span length, type of girder shape, and the type (harped or eccentric) and number of prestressing strands.

2. *Individual girder flexural performance*. With respect to the flexural response and behavior of the individual girder specimens, the following observations were made:
   - *Tx34-1*. This girder specimen had an eccentric strand layout with the lowest prestressing force. The tensile strength (first cracking strength of 0.53 ksi and peak strength of 0.6 ksi) of the companion samples for the girder specimen was lower than the design assumption for the specimen, which led to a shear failure at the girder end without transverse reinforcement before the flexure failure. Therefore, after shear crack widening at the unreinforced end, the actuator at the end near the unreinforced end was disengaged, and the actuator near the reinforced end continued to be loaded until flexure crack localization occurred. The specimen had a maximum measured flexure capacity of 5020 k-ft. Based on the companion prototype bridge design, the service demand was 49 percent lower than the experimental capacity, and the factored demand load was 23 percent lower than the experimental capacity. The crack widths ranged from hairline to 0.008 in., and the localized flexure crack that occurred at the underside of the girder was 0.19 in. wide. Overall, the flexural performance was ductile due to the crack bridging property of the fibers. Due to the slightly higher flow of the Tx34-1 UHPC mixture, fiber settlement was observed in the material-level companion specimens. There may have been similar settlement at the bottom of the Tx34-1 girder, which would tend to enhance the girder flexure performance despite the low tensile strength of the companion material-level specimens.

- *Tx34-2.* This specimen had more prestressing force than Tx34-1, a harped strand layout, and improved tensile strength (first cracking strength of 0.62 ksi and peak strength of 0.7 ksi). The maximum measured flexure strength of this specimen was 6562 k-ft. Based on the companion prototype bridge design, the service demand was 53 percent lower than the experimental capacity, and the factored demand load was 31 percent lower than the experimental capacity. The crack widths at maximum loading ranged from hairline to 0.01 in., with a localized flexure crack at the soffit widening to 0.12 in. at maximum loading. Because the tensile capacity of this specimen was slightly better than the Tx34-1 girder and there was shear resistance due to harping of strands, there was no premature shear failure.
- *Tx54.* This specimen exhibited enhanced performance in flexure relative to the first two girder specimens. The Tx54 specimen had the highest prestressing force, a harped strand layout, and tensile strength comparable to the strengths achieved in the laboratory mixture (first cracking strength of 0.95 ksi and peak strength of 1.16 ksi). There was no damage to the shear ends while conducting the flexure test. The maximum measured flexure strength of this specimen was 12,860 k-ft. Based on the companion prototype bridge design, the service demand was 53 percent lower than the experimental capacity, and the factored demand load was 32 percent lower than the experimental capacity. The cracks in the flexure region ranged from hairline to 0.012 in. at maximum loading. The localized crack at the soffit was 0.06 in. wide at maximum loading. The behavior of the girder was ductile, and the test was terminated at a tensile strain on the bottom soffit of 0.006 to preserve the girder for further testing.

3. *Analysis and design.* With respect to analysis and design for flexure, the following observations were made based on the design and predicted response versus the measured response:
    - The standard first principles of mechanics were found to be effective in predicting the behavior of the UHPC girder specimens with a composite CC deck.
    - Nonlinear stress-strain models were used for the CC deck and UHPC to run an iterative moment-curvature analysis to predict the behavior of the girder specimens under flexure. Load-deflection analysis was conducted to predict the elastic and post-cracking deflection behavior of the specimens.

    - The predictions were largely dependent on the material properties of the girders. The material models used for the analysis had to be modified to account for the assumptions needed to model the behavior of UHPC with higher tensile strength from the steel fibers.
    - The standard analytical methods for the moment-curvature and load-deflection were found to be applicable to the standard TxDOT composite bridge section with UHPC girders. The predictions of the flexural capacity were within 90 percent of the maximum measured flexure strength of the girders.
- The flexural design based on AASHTO LRFD Bridge Design Specifications (AASHTO 2020) is adequate for the standard service and factored demand loads that a prototype bridge would be subjected to in the field. More details regarding the suitability of these assumptions are explained in Section 5.5 and in the recommendations provided in the Volume 3 report.

8.4 SHEAR TESTING

The full-scale testing of the shear performance of the girder specimens provided an opportunity to compare the shear capacity and performance with and without minimum transverse reinforcement in the form of R-bars. Chapter 6 describes in detail the shear testing and load arrangement. A span-to-depth ratio greater than 2.0 was used for all shear tests. One half span of each girder specimen had minimum transverse reinforcement by design in the form of R-bars, while the other half span did not contain web reinforcement. The superior ductility, dependence of the steel fibers on the tensile strength of the mix (particularly in the web), and the comparison between the shear capacity of the ends with and without the minimum transverse web reinforcement were evaluated. Based on the analysis conducted as per the procedures elaborated in Chapter 6 and the results of the full-scale testing, the following observations and conclusions were drawn.

1. *Analysis and design.* With respect to analysis and design for shear, the following observations were made based on the design and predicted response versus the measured response.
    - The predicted shear strength estimates utilize the expressions recommended for UHPC based on the work done by FHWA and PCI (El-Helou and Graybeal 2022b; Tadros 2021) and the measured material properties. The FHWA and PCI formulations directly

correlate the tensile strength of the UHPC to the shear capacity of the structural element. This result was supported by the current project, wherein the shear capacity of the full-scale specimens was observed to be directly related to the tensile strength measured from the uniaxial tension testing of the companion material-level specimens.

- The shear test results confirmed that the actual shear capacity of the specimens was closely estimated (showing a difference of less than 15 percent between the prediction and measured maximum shear strength for all the shear tests), with the exception of the Tx34-1 end with minimum web reinforcement, which showed a 34 percent higher experimental capacity.
- Consideration of the full section depth, including the composite CC deck, also provided more accurate predictions of the shear capacity of the specimens. Note that the deck is not included in the approach recommended by FHWA (El-Helou and Graybeal 2022b).

2. *General shear performance of girder specimens*. The following general observations were made with respect to the shear response and behavior of the girder specimens:
   - The shear performance of the UHPC girders is enhanced relative to CC. The UHPC girder specimens did not undergo a sudden brittle shear failure during load testing. The steel fibers impart a crack bridging property to the matrix of UHPC, resulting in the shear components holding load despite the onset of cracks opening and strain localization in the shear elements, such as the webs of the I-shaped girders considered for this project. Despite testing the specimens to the maximum capacity in shear for Tx34-2 and Tx54, the composite girders continued to be stable structurally.
   - The shear capacity is very sensitive to the uniaxial tensile strength of UHPC. The tensile strength of Tx34-1 girder was much lower than anticipated, and there was fiber segregation noted in the companion small-scale samples, which is likely due to higher than expected flow. These two elements could be the prime reasons for the lower shear capacity of the end without reinforcement.
   - The shear capacity of the unreinforced end of the Tx34-1 specimen was lower than the design shear capacity because the measured tensile strength from the companion specimens was lower than the design value. Therefore, the unreinforced end developed shear cracks before flexure crack localization took place at the midspan. The Tx34-2 and Tx54 specimen had greater tensile strength than the Tx34-1 specimen, and no

premature shear failure in these sections occurred during flexure testing. The improved performance of the Tx34-2 and Tx54 specimens is also due to higher prestressing forces and harping of some of the tendons, which provided additional shear capacity.

- In addition to the tensile strength of the UHPC, the shear capacity is enhanced by other factors, such as harping of some of the prestressing strands, minimum transverse web reinforcement, and deeper girder webs. This enhancement is evident with the lowest shear capacity observed for the eccentric prestressing strand Tx34-1 specimen, followed by the Tx34-2 with more prestressing strands, some of which were harped. The highest shear capacity was observed for the deeper Tx54 specimen with some harped tendons.
- The girder ends with minimum transverse web reinforcement were stronger in shear than the ends without transverse reinforcement in the form of R-bars. With the enhanced shear capacity of UHPC relative to CC, the transverse steel reinforcement can be reduced substantially to the minimum required per AASHTO (2020) rather than the standard spacing recommended by TxDOT (2017a). The minimum transverse web reinforcement provides additional ductility to the composite section to delay a sudden failure under overload conditions.

3. *Individual girder shear performance—no web reinforcement*. With respect to the shear response and behavior at the ends of the individual girder specimens with no transverse reinforcement, the following observations were made:
   - *Tx34-1 (Unreinforced End).* The UHPC tensile strength of Tx34-1 was lower than the design tensile strength, which likely led to the shear failure at the unreinforced end of the specimen during the flexure test. Based on the experimental uniaxial tension test data, the *predicted* shear capacity at this end was close to the limiting value in the test (4 percent higher). The experimental capacity of 202 kips was 46 percent higher than the service load of the prototype bridge but was 5 percent lower than the corresponding factored demand load.
   - *Tx34-2 (Unreinforced End).* The shear performance at the unreinforced end of the Tx34-2 girder specimen was enhanced by the improved tensile strength and harped layout of the strands. The shear capacity was 449 kips, which was 1 percent higher than the prediction using the uniaxial tension test data for the companion specimens. The

shear capacity of the girder was 210 percent higher than the service load of the corresponding prototype bridge and 101 percent higher than the factored demand load. The harping of the strands and improved tensile strength enhanced the overall shear capacity significantly at the unreinforced end of the Tx34-2 girder in comparison to the unreinforced end of the Tx34-1 girder.

- *Tx54 (Unreinforced End).* The shear performance of the Tx54 girder was further enhanced above the other two girder specimens due to a higher measured tensile strength, increased prestressing, a harped strand layout, and a deeper web section. The shear capacity was 761 kips (13 percent higher than the prediction). This increase could indicate a higher tensile strength within the girder section than in the companion material-level test specimens. The capacity exceeded the service demand of the corresponding prototype bridge by 266 percent and exceeded the factored demand by 145 percent.

4. *Individual girder shear performance—minimum web reinforcement*. With respect to the shear response and behavior at the ends of the individual girder specimens with minimum transverse reinforcement, the following observations were made:
    - *Tx34-1 (Reinforced End).* The reinforced end of the Tx34-1 specimen was stronger in shear due to the contribution of the steel reinforcement in the web. The maximum applied shear was 413 kips, which was 53 percent higher than the predicted shear capacity. The uniaxial tensile strength data for the companion specimen of these data showed a great deal of variation. It may be possible that the reinforced end of the girder may have had a higher concentration of fibers than the unreinforced end, resulting in higher tensile strength of the girder web and, consequently, higher shear capacity. This activity was later observed in the fiber distribution of the cored specimens of the reinforced end of the Tx34-1 girder. The details of the cored specimen fiber distribution are documented in the Volume 1 report. The capacity was 199 percent higher than the service load of the corresponding prototype bridge and 94 percent higher than the factored demand load.
    - *Tx34-2 (Reinforced End).* The reinforced end of the Tx34-2 girder was unintentionally reinforced with extra transverse bars due to early fabrication at the precast plant, which forced the shortening of the span length of the test specimen for the shear test to avoid

testing the portion of the girder with extra transverse R-bars. The shear capacity was 592 kips, which was 8 percent higher than the predicted shear capacity. The capacity exceeded the service demand of the corresponding prototype bridge by 308 percent and the factored demand by 165 percent.

- *Tx54 (Reinforced End).* The shear capacity of the Tx54 at girder end with minimum transverse reinforcement was 777 kips. The predicted capacity was 779 kips, giving a difference of less than 1 percent. The shear capacity exceeded the service loading of the corresponding prototype bridge by 274 percent and the factored shear demand by 151 percent.

6. *Interface Shear Performance:* There is less friction provided at the UHPC girder interface than at CC girders due to the self-consolidating nature of UHPC and the absence of coarse aggregate. Bundled interface UC-bars were placed along the unreinforced half span to provide interface shear resistance between the UHPC girder and the CC deck, as described in Chapter 4. The reinforced half span had minimum transverse web shear R-bars (R-bars) that were supplemented with bundled UC-bars to improve the interface shear resistance. These bars were provided for additional interface shear strength due to the low interface shear capacity when surface roughening is not considered for UHPC. The UC-bars (No. 5) were larger in diameter than the R-bars (No. 4) to enhance the interface shear strength:
    - The interface shear slip was measured between the CC deck and the UHPC girder. The measurements indicate that the reinforced end slipped more than the unreinforced end, potentially because of a higher area of interface shear steel reinforcement provided by the higher diameter UC-bars combination (UC-bar triplet bundles) in the unreinforced half of the girder than the combination of UC-bars and R-bars (one pair of UC-bars coupled with R-bar) in the reinforced half of the girder. The unplanned use of an SCC topping along the top surface of the unreinforced end of Tx54 girder may be the reason the lowest slip measurement is for this girder. This positive outcome may be useful when considering other approaches to increase the interface shear strength for the UHPC girder. (Note that the use of a small volume of SCC became necessary due to an unexpected shortage of UHPC in the last batch, likely caused by the lower flow spread of the UHPC that led to increased sticking of the material in the mixer and Tuckerbuilt.)

- The provided interface shear reinforcement controlled the interface slip up to the factored design loads. Limited slip was observed at higher loads, with a range of slip for all girders between 0.005–0.19 in.
- The Tx34-1 unreinforced end slipped by 0.027 in. and the reinforced end slipped by 0.086 in. during the shear failure of the unreinforced end. During the testing of the reinforced span, the maximum measured slip was 0.034 in. (The unreinforced end was eliminated during the reinforced end shear test because the major flexure crack at the midspan of the specimen led to shortening the span length for the second shear test.)
- The Tx34-2 unreinforced end slipped by 0.075 in. and the reinforced end slipped by 0.098 in. during the shear failure of the unreinforced end. During the shear testing of the reinforced end, the reinforced end slipped by 0.19 in., while the unreinforced end only slipped by 0.07 in.
- The Tx54 unreinforced end slipped by 0.005 in. and the reinforced end slipped by 0.008 in. during the shear failure of the unreinforced end. During the shear testing of the reinforced end, the reinforced end slipped by 0.056 in., while the unreinforced end only slipped by 0.001 in.

8.5 TRANSFER LENGTH AND CAMBER

The full-scale girder specimens were also studied to evaluate the transfer length of the prestressing strands and the measured versus predicted camber over time. The following observations and conclusions were made:

1. *Transfer Length*.
    - The transfer lengths for the Tx54 girder specimen were measured over time. The initial transfer length was 18.0 in. and 19.5 in. at the live end and dead end, respectively. The transfer length at 33 days was 20.5 in. and 19.5 in. at the live end and dead end, respectively.
    - The measured results give a transfer length of 30–34 d_b. The results are well-matched with the PCI and Australian recommendations for UHPC, which is 20–40 d_b (eConstruct 2020; Gowripalan and Gilbert 2000). Note that the AASHTO draft specifications for UHPC recommends 24 d_b transfer length for design (FHWA 2022).

2. *Camber*.
    - The camber of the UHPC girder specimens was recorded from the time of prestress transfer at the plant. Tx34-1 and Tx34-2 (50 ft long) had 0.71 and 0.83 in. of initial camber, respectively, and Tx54 (70 ft long) had 0.98 in. of initial camber. The final camber was 0.63, 0.75, and 1.31 in. for Tx34-1, Tx34-2, and Tx54, respectively. Note that the ages at the time of the final camber measurements were 157, 151, and 33 days for Tx34-1, Tx34-2, and Tx54, respectively.
    - For prediction of camber, the incremental time-step method was used. Unlike CC, prestress loss due to autogenous shrinkage occurring during the time between the final set and transfer was additionally considered for the initial camber of the UHPC girders. In addition, the prediction models for creep and shrinkage presented in the Volume 1 report were used to estimate prestress losses over time. The measured camber was predicted quite accurately using the following parameters for the developed UHPC: 200 με autogenous shrinkage before transfer, 700 με ultimate shrinkage, and 0.8 creep coefficient. The difference between measured and predicted camber values was from −0.03 to 0.03 in. for the initial camber and from −0.12 to 0.34 in. for final camber.

8.6 RECOMMENDATIONS FOR UHPC DESIGN

The following are the key recommendations for the design of UHPC girders based on this Volume 2 research project (the Volume 3 report provides more detailed guidelines and design examples):

1. *Material properties.* Experimental material-level testing is important in setting the design assumptions for UHPC bridge girders. The compressive and uniaxial tensile strengths are important because UHPC designs will commonly have higher prestressing forces and design loads for a given girder section. In the absence of experimental data, previously available data or lower bound values may be assumed for preliminary design based on the mixture design and the percentage of fibers.
2. *Flexure design.* SLSs and ULSs were considered for flexural design of the prototype bridges that formed the basis for the girder specimens.

a. Service Limit State:
    i. For the SLS, the stresses in the girder—typically controlled by the stresses at the beam ends at release and at the midspan section at service—should be evaluated and checked.
    ii. It is important to consider appropriate material reduction factors for the compressive and tensile stress limits. The limits used in the AASHTO draft specifications for UHPC (FHWA 2022) are recommended. At release, the compressive stress limit for prestressed members was taken as 65 percent of compressive strength at release; however, the tensile stress limit was taken as 85 percent of tensile strength at release (FHWA 2022). At service, the compressive stress limit was taken as 60 percent of compressive strength at service, while the tensile stress limit was taken as 85 percent of tensile strength at service (FHWA 2022).
b. Ultimate Limit State:
    i. From the research conducted, the theoretical flexure capacity, using a rigorous analysis considering the individual stress-strain models presented in Chapter 5, provides an accurate estimate of flexure capacity.
    ii. The triangular stress block method for UHPC, described by Graybeal (2008), was also a robust method similar to the rigorous nonlinear analysis for determine the nominal flexure capacity.
    iii. It was found that the nominal flexure capacity for the decked I-girder specimens considered in this study can be calculated using the approximate rectangular stress block method defined in the AASHTO LRFD Bridge Design Specifications (AASHTO (2020). This method was found to be effective and gave simple and conservative design estimates for the three girder specimens. The rectangular stress block works effectively for these girders because the primary compression force is resisted by the CC deck concrete.
    iv. For those sections in which the UHPC is primarily resisting both the tension and compression, the triangular stress block recommended by FHWA (2022) gives a more accurate estimate, while the rectangular stress block is

a more approximate estimate. When limited experimental material-level test data for nonproprietary mixtures exists, the more conservative approach is recommended. The use of the AASHTO (2020) rectangular stress block methodology was found to provide a reasonable estimate of moment strength when the primary compression force occurs in the CIP concrete deck, as was the case for the tested girder specimens. This approach ignored the tension strength of the UHPC for the tested girders because the contribution to flexure strength was quite low when compared to contribution of the tension force in the prestressing tendons.

3. *Shear design.*
    a. The nominal shear capacity was considered as a combination of the contributions from the UHPC, transverse steel, and vertical component of prestressing strands (if harped). The contribution of fibers was not considered independently, as recommended by AFGC (2013); instead, it was considered as part of the UHPC shear resistance component. The methodology and formulation to evaluate the shear capacity of UHPC was similar to what Graybeal and El-Helou (2021) and Tadros (2021) used. One difference was the calculation of the initial crack angle was based on the concept of Mohr's circle. The shear capacity of the transverse steel and prestressing strands were based on the AASHTO draft recommendations for UHPC (FHWA 2022).
    b. Shear design should be carried out using the modified compression field theory (MCFT) provided in the AASHTO LRFD Specifications (AASHTO 2020). One of the important parameters to be considered is the first cracking uniaxial tensile strength of UHPC.
    c. Based on the experimental research conducted, the tensile strength of the web section under shear may have been slightly lower than the tensile strength of the bottom flange under flexure due to potential variation in fiber distribution that can occur due to differences in the flow spread values between batches. For example, the flow spread value of the Tx34-1 specimen was slightly higher, leading to fiber settlement in the material samples and, to some degree, in the girder. Therefore, it

is important to ensure that the first cracking tensile strength is adjusted accordingly to account for the uncertainty in the fiber distribution.

   d. Based on the research conducted, the shear capacity of the sections without transverse reinforcement was approximately two times higher than the factored shear demand for the girders with a uniaxial direct tensile strength greater than 0.6 ksi.
   e. Although the sections may be shown to have sufficient shear strength without transverse reinforcement, minimum transverse shear reinforcement is recommended to provide additional ductility and some reserve strength following the onset of shear cracking in an overload condition. This reinforcement can also be used for interface shear transfer.

4. *Interface shear design*. Effective surface roughening of the top surface of the UHPC girder was found to be difficult; therefore, it is highly recommended that bundled UC-bars provide interface shear resistance between the CC deck and UHPC girder. High-strength steel studs can also be considered (Crane 2010). Further research can be conducted on providing a thin layer of SCC topping or similar material to introduce surface roughening for an improved bond between UHPC girders and CC decks.
5. *Splitting resistance reinforcement*. The unreinforced ends of the girders were not damaged after the release of strands or during the service and factored demand load conditions of the girder. Therefore, the improved tensile strength of the UHPC girder due to the presence of steel fibers was determined to be sufficient to withstand the release of the prestressing strands. Consistent with guidelines provided by the PCI study on UHPC (Tadros 2021), it is recommended that the splitting reinforcement be reduced because the current limits are very conservative when applied to UHPC girders.
6. *Transfer Length.* The results of the measured transfer lengths for the Tx54 girder specimen were 30–32.5 d_b at transfer and 32.5–34 d_b at 33 days. A transfer length of 30 d_b is recommended for design using the developed UHPC mixture.
7. *Camber*. The camber values for the UHPC girder specimens were predicted accurately using the AASHTO-refined method to estimate time-dependent loss (AASHTO 2020) with the developed modifications. The recommended modifications for the nonproprietary

UHPC mixture used in this study are (1) 200 με autogenous shrinkage before transfer, (2) 700 με ultimate shrinkage, and (3) 0.8 creep coefficient.

8.7 RECOMMENDATIONS FOR FUTURE WORK

Based on the research conducted, the following future work is recommended for consideration:

1. Optimization of girder cross-sections for UHPC, including consideration of a reduced deck thickness and approaches for accelerated bridge construction, should be explored.
2. The prestressing strands should be increased to 0.7 in. diameter or higher strength strands to leverage the full potential of longer spans with UHPC.
3. The use of UHPC in bridge decks and bridge substructures should be explored to enhance the durability of the overall bridge structure.
4. The interface shear capacity of UHPC girders with CIP concrete deck slabs should be investigated for additional approaches to enhance composite action.
5. Enhancing UHPC girder performance by optimizing the type and volume of fibers and fiber types, including mixing fiber types, should be further investigated.
6. Based on this research, further shear testing of UHPC girders, including the deck, is recommended to develop additional experimental data to support analytical modeling to predict girder performance and to support design recommendations and requirements.

REFERENCES

AASHTO (2002). "Standard Specifications for Highway Bridges, Seventeenth Edition." American Association of State Highway and Transportation Officials, Washington, DC.

AASHTO (2007). "AASHTO LRFD Bridge Design Specifications, Fourth Edition." American Association of State Highway and Transportation Officials, Washington DC.

AASHTO (2010). "AASHTO LRFD Bridge Design Specifications, Fifth Edition." American Association of State Highway and Transportation Officials, Washington DC.

AASHTO (2012). "AASHTO LRFD Bridge Design Specifications, Sixth Edition." American Association of State Highway and Transportation Officials, Washington DC.

AASHTO (2014). "AASHTO LRFD Bridge Design Specifications, Eigth Edition." American Association of State Highway and Transportation Officials, Washington DC.

AASHTO (2020). "AASHTO LRFD Bridge Design Specifications, Ninth Edition." American Association of State Highway and Transportation Officials, Washington DC.

AASHTO T 397 Draft (AASHTO 2022). "Standard Method of Test for Uniaxial Tensile Response of Ultra-High Performance Concrete." American Association of State Highway and Transportation Officials, Washington, DC.

ACI 224R-08 (2001). "Control of Cracking in Concrete Structures." American Concrete Institute, Framington Hills, MI.

ACI 318-08 (2008). "Building Code Requirements for Structural Concrete and Commentary." American Concrete Institute, Farmington Hills, MI.

ACI 318-14 (2014). "Building Code Requirements for Structural Concrete and Commentary." American Concrete Institute, Farmington Hills, MI.

ACI 318-19 (2019). "Building Code Requirements for Structural Concrete and Commentary." American Concrete Institute, Farmington Hills, MI.

ACI 544.4R-18 (2018). "Guide to Design with Fiber-Reinforced Concrete." American Concrete Institute, Farmington Hills, MI.

ACI Committee 318 (2019). "Building Code Requirements for Structural Concrete and Commentary." American Concrete Institute, Farmington Hills, MI.

AFGC (2013). "Ultra High Performance Fibre-Reinforced Concretes (Bétons Fibrés à Ultra-Hautes Performances)." AFGC-SETRA, Bagneux, France.

AFGC/SETRA (2002). "Ultra High Performance Fibre-Reinforced Concretes (Bétons Fibrés À Ultra-Hautes Performances)." *Recommandations provisoires (Interim Recommendations)* Paris, France.

Ahlborn, T. M., Perry, V. H., and Paul, W. (2016). "The First North American Broad Based Structural Design Guide on UHPC – ACI 239C." *First International Interactive Symposium on UHPC – 2016*.

Alahmari, T., Jáuregui, D., and Weldon, B. (2021). "Load Testing of Prestressed Bridge Girders from Locally Developed UHPC and HPC." *Bridge Maintenance, Safety, Management, Life-Cycle Sustainability and Innovations*, CRC Press, 3769-3775.

Astarlioglu, S., and Krauthammer, T. (2014). "Response of Normal-Strength and Ultra-High-Performance Fiber-Reinforced Concrete Columns to Idealized Blast Loads." *Engineering structures*, 61, 1-12.

ASTM C157 (2017). "Standard Test Method for Length Change of Hardened Hydraulic-Cement Mortar and Concrete." ASTM International, West Conshohocken, PA.

ASTM C1609/C1609M (2012). "Standard Test Method for Flexural Performance of Fiber-Reinforced Concrete (Using Beam With Third-Point Loading)." ASTM International, West Conshohocken, PA.

ASTM C1856 (2017). "Standard Practice for Fabricating and Testing Specimens of Ultra-High-Performance Concrete." ASTM International, West Conshohocken, PA.

Baby, F., Marchand, P., and Toutlemonde, F. (2014a). "Shear Behavior of Ultrahigh Performance Fiber-Reinforced Concrete Beams. I: Experimental Investigation." *ASCE Journal of Structural Engineering*, 140(5), 04013111.

Baby, F., Marchand, P., and Toutlemonde, F. (2014b). "Shear behavior of ultrahigh performance fiber-reinforced concrete beams. II: Analysis and design provisions." *ASCE Journal of structural engineering*, 140(5), 04013112.

Barnes, R. W., Burns, N. H., and Kreger, M. E. (1999). "Development Length of 0.6-inch Prestressing Strand in Standard I-Shaped Pretensioned Concrete Beams." University of Texas at Austin. Center for Transportation Research.

Bentz, E. C., Vecchio, F. J., and Collins, M. P. (2006). "Simplified Modified Compression Field Theory for Calculating Shear Strength of Reinforced Concrete Elements." *ACI Structural Journal*, 103(4), 614.

Bertram, G., and Hegger, J. (2012). "Bond Behavior of Strands in UHPC–Tests and Design." *Proceedings of the 3rd International Symposium on UHPC* 525-532.

Bhoem, K. M., Barnes, R. W., and Schindler, A. K. (2010). "Performance of Self-Consolidating Concrete in Prestressed Girders." Auburn University. Highway Research Center.

Bierwagen, D., and Abu-Hawash, A. (2005). "Ultra High Performance Concrete Highway Bridge." *Proc. of the 2005 Mid-Continent Transportation Research Symposium* Ames, Iowa, 1-14.

Bruce, R. N., Russell, H. G., Roller, J. J., and Hassett, B. (1998). "Implementation of High Performance Concrete in Louisiana Bridges."

Cauberg, N., Piérard, J., Parmentier, B., and Remy, O. (2012). "Shear Capacity of UHPC-Beam Tests." *Proc. Hipermat*, 451-458.

Chuang, E. Y., and Ulm, F. J. (2002). "Two-Phase Composite Model for High Performance Cementitious Composites." *Journal of Engineering Mechanics*, 128(12), 1314-1323.

Crane, C. K. (2010). "Shear and Shear Friction of Ultra-High Performance Concrete Bridge Girders." Georgia Institute of Technology.

Crane, C. K., and Kahn, L. F. (2012). "Interface Shear Capacity of Small UHPC/HPC Composite T-Beams." *Ultra-High Performance Concrete and Nanotechnology in Construction. Proceedings of Hipermat 2012. 3rd International Symposium on UHPC and Nanotechnology for High Performance Construction Materials*, 19, 459.

CSA S6:19 (2019). "Canadian Highway Bridge Design Code." Canadian Standards Association (CSA), Toronto, ON: CSA.

DAfStb-Guideline (2017). "Ultra-High Performance Concrete (Draft)." German Committee for Structural Concrete, Berlin.

Devalapura, R. K., and Tadros, M. K. (1992). "Stress-Strain Modeling of 270 ksi Low-Relaxation Prestressing Strands." *PCI Journal*, 37(2), 100-106.

eConstruct (2020). "Implementation of Ultra-High-Performance Concrete in Long-Span Precast Pretensioned Elements for Concrete Buildings and Bridges." Wiss, Janney, Elstner Associates, University of Nebraska-Lincoln, The NCSU Constructed Facilities Laboratory, Precast/Prestressed Concrete Institute, Chicago, IL.

El-Helou, R. G., and Graybeal, B. A. (2022a). "Flexural Behavior and Design of Ultrahigh-Performance Concrete Beams." *ASCE Journal of Structural Engineering*, 148(4), 04022013.

El-Helou, R. G., and Graybeal, B. A. (2022b). "Shear Behavior of Ultrahigh-Performance Concrete Pretensioned Bridge Girders." *ASCE Journal of Structural Engineering*, 148(4), 04022017.

El-Helou, R. G., and Graybeal, B. A. (2023). "Shear Design of Strain–Hardening Fiber-Reinforced Concrete Beams." *ASCE Journal of Structural Engineering*.

El-Helou, R. G., Haber, Z. B., and Graybeal, B. A. (2022). "Mechanical Behavior and Design Properties of Ultra-High-Performance Concrete." *ACI Materials Journal*, 119(1).

Empelmann, M., and Oettel, V. (2012). "UHPFRC Box Girders under Torsion." *Proceedings of the 3rd International Symposium on UHPC and Nanotechnology for High Performance Construction Materials*, 517-524.

EN 1992 Eurocode 2 (2004). "Design of Concrete Structures." European Committee for Standardization, Rue de Stassart, 36 B-1050 Brussels, Belgium.

EN 14651 (2005). "Test Method for Metallic Fibre Concrete – Measuring the Flexural Tensile Strength (Limit of Proportionality (LOP), Residual)." European Committee for Standardization, Brussels, Belgium.

Fehling, E., Leutbecher, T., Röder, F., and Stürwald, S. (2008). "Structural Behavior of UHPC under Biaxial Loading." *Ultra High Performance Concrete*, 2, 05-07.

FHWA (2022). "Proposed AASHTO LRFD Guide Specifications for Structural Design with UHPC." *Draft Under Review*, American Association of State Highway and Transportation Officials, Washington, DC.

fib (2013). "Model Code for Concrete Structures 2010." Fédération Internationale du Béton (*fib*), Berlin: Wilhelm Ernst & Sohn.

fib Task Group 8.6 (2013). "Ultra High Performance Fiber Reinforced Concrete." Fe´deration Internationale du Be´ton (*fib*), Lausanne, Switzerland.

German Research Program (2005-2013). "Sustainable Building With Ultra-High-Performance Concrete, SSP 1182." German Research Foundation (DFG), Bonn, Germany.

Giesler, A. J., McGinnis, M. J., and Weldon, B. D. (2018). "Flexural Behavior and Analysis of Prestressed Ultra-High-Performance Concrete Beams Made from Locally Available Materials." *PCI Journal*, 63(6).

Gowripalan, N., and Gilbert, R. (2000). "Design Guidelines for RPC Prestressed Concrete Beams." *Sydney, Australia: School of Civil and Environmental Engineering*.

Graybeal, B. (2019). "UHPC Presentation at Concrete Bridges Committee (AFF30) Meeting." *The Transportation Research Board (TRB) 98th Annual Meeting* Washington, DC.

Graybeal, B., and El-Helou, R. (2021). "Design Example of a UHPC Girder Bridge with Convention Concrete Deck." AASHTO CBS T-10 Committee Meeting, FHWA, Technical Committee for Concrete Design T-10, Web Meeting.

Graybeal, B. A. (2006a). "Material Property Characterization of Ultra-High Performance Concrete." Federal Highway Administration, McLean, VA.

Graybeal, B. A. (2006b). "Structural Behavior of Ultra High Performance Concrete Prestressed I-Girders." Federal Highway Administration, McLean, VA.

Graybeal, B. A. (2008). "Flexural Behavior of an Ultrahigh-Performance Concrete I-Girder." *Journal of Bridge Engineering*, 13(6), 602-610.

Graybeal, B. A. (2009). "Structural Behavior of a Prototype Ultra-High Performance Concrete Pi-Girder." *FHWA, U.S. Department of Transportation, Report No. FHWA-HRT-10-027.*

Graybeal, B. A. (2014). "Design and Construction of Field-Cast UHPC Connections." Federal Highway Administration, McLean, VA.

Grünewald, S., Ferrara, L., and Dehn, F. (2010). "Structural Design with Flowable Concrete-A fib-Recommendation for Tailor-Made Concrete." *Design, Production and Placement of Self-Consolidating Concrete*, Springer, 13-23.

Gunasekaran, D. (2020). "Mechanics and Design of Prestressed Girder Bridges using Ultra High Performance Concrete." (Texas A&M University).

Gunes, O., Yesilmen, S., Gunes, B., and Ulm, F. J. (2012). "Use of UHPC in Bridge Structures: Material Modeling and Design." *Advances in Materials Science and Engineering*, 2012.

Haber, Z. B., De la Varga, I., Graybeal, B. A., Nakashoji, B., and El-Helou, R. (2018). "Properties and Behavior of UHPC-class Materials." Federal Highway Administration, McLean, VA.

John, E. E., Ruiz, E. D., Floyd, R. W., and Hale, W. M. (2011). "Transfer and Development Lengths and Prestress Losses in Ultra-High-Performance Concrete Beams." *Transportation Research Record*, 2251(1), 76-81.

JSCE (2004). "Recommendations for Design and Construction of Ultra High-Strength Fiber-Reinforced Concrete Structures." Japan Society of Civil Engineers, Tokyo, Japan.

Karthik, M. M., and Mander, J. B. (2011). "Stress-Block Parameters for Unconfined and Confined Concrete Based on a Unified Stress-Strain Model." *ASCE Journal of Structural Engineering*, 137(2), 270-273.

Lin, T. Y., and Burns, N. H. (2010). "Design of Prestressed Concrete Structures."

Maguire, M., Morcous, G., Hanna, K., and Tadros, M. (2009). "Ultra-High-Performance Concrete in Standard Precast/Prestressed Concrete Products." *Proceedings of the PCI National Bridge Conference*.

Mander, J. B. (1983). "Seismic Design of Bridge Piers." Christchurch.

Manning, M. P., Weldon, B. D., McGinnis, M. J., Jáuregui, D. V., and Newtson, C. M. (2016). "Behavior Comparison of Prestressed Channel Girders from High-Performance and Ultrahigh-Performance Concrete." *Transportation Research Record*, 2577(1), 60-68.

Matthews, S., Bigaj-van Vliet, A., Walraven, J., Mancini, G., and Dieteren, G. (2018). "*fib* Model Code 2020: Towards A General Code for Both New and Existing Concrete Structures." *Structural Concrete*, 19(4), 969-979.

Mobasher, B., Bakhshi, M., and Barsby, C. (2014). "Backcalculation of Residual Tensile Strength of Regular and High Performance Fiber Reinforced Concrete from Flexural Tests." *Construction and Building Materials*, 70, 243-253.

Model Code (1993). "Model Code 1990, CEB FIP, fib." *Comite Euro-International Du Beton, Paris*.

Mohebbi, A., and Graybeal, B. (2022). "Prestress Loss Model for Ultra-High Performance Concrete." *Engineering Structures*, 252, 113645.

Mohebbi, A., Graybeal, B., and Haber, Z. (2022). "Time-Dependent Properties of Ultra High-Performance Concrete: Compressive Creep and Shrinkage." *Journal of Materials in Civil Engineering*, 34(6), 04022096.

Muzenski, S., Haber, Z. B., and Graybeal, B. (2022). "Interface Shear of Ultra-High-Performance Concrete." *ACI Structural Journal*, 119(1).

NF-P-18-451 (2018). "French Standard Execution of Concrete Structures - Specific Rules for UHPFRC." AFNOR, La Plaine Saint-Denis, France.

NF-P-18-470 (2016). "French Standard Concrete – Ultra-High Performance Fibre-Reinforced Concretes – Specifications, Performance, Production and Conformity." AFNOR, La Plaine Saint-Denis, France.

NF-P-18-710 (2016). "French Standard National Addition to Eurocode 2 – Design of Concrete Structures: Specific Rules for Ultra-High Performance Fibre-Reinforced Concretes (UHPFRC)." AFNOR, La Plaine Saint-Denis, France.

NF EN 13670/CN (2013). "Execution of Concrete Structures – National Addition to NF EN 13670:2013." AFNOR, La Plaine Saint-Denis, France.

Patnaik, A., Baah, P., Ricciardi, P., and Khalifa, W. (2017). "Reduction of Crack Widths in Steel Reinforced Concrete Bridge Decks with Fiber Addition." *American Concrete Institute Special Publication*, 319, 1.1-1.20.

Patnaik, A. K. (1994). "Horizontal Shear Strength of Composite Concrete Beams with a Rough Interface."

PCI (2017). "PCI Design Handbook." Precast/Prestressed Concrete Institute.

Pirayeh Gar, S., Mander, J. B., and Hurlebaus, S. (2018). "Deflection of FRP Prestressed Concrete Beams." *Journal of Composites for Construction*, 22(2), 04017049.

Ramirez, J. A., and Russell, B. W. (2008). "Transfer, Development, and Splice length for Strand/Reinforcement in High-Strength Concrete." 603.

Resplendino, J. (2014). "French Recommendations and Feedback on Experience With Ultra-High-Performance Fibre-Reinforced Concrete (UHPFRC)." *American Concrete Institute, ACI Special Publication*, 61-74.

Rilem (1994). "RILEM Recommendations for the Testing and Use of Constructions Materials." 6, 218220.

RILEM TC 162-TDF (2002). "Test and Design Methods for Steel Fibre Reinforced Concrete, Recommendations." Materials and Structures, 579–582.

Rouse, J. M., Wipf, T. J., Phares, B., Fanous, F., and Berg, O. (2011). "Design, Construction, and Field Testing of An Ultra-High Performance Concrete Pi-Girder Bridge."Ames, IA.

Russell, B. W., and Burns, N. H. (1997). "Measurement of Transfer Lengths on Pretensioned Concrete Elements." *ASCE Journal of Structural Engineering*, 123(5), 541-549.

Schmidt, M., and Fröhlich, S. (2015). "UHPC From Research to Standardization: European Approaches." *Advances in Civil Engineering Materials*, 4(2), 144-170.

Schmidt, M., Leutbecher, T., Piotrowski, S., and Wiens, U. (2017). "The German Guideline for Ultra-High Performance Concrete." *AFGC-ACI-fib-RILEM Int. Symposium on Ultra-High Performance Fibre-Reinforced Concrete*, UHPFRC 2017, Montpellier, France.

Schmidt, M., and Teichmann, T. (2007). "Ultra-High-Performance Concrete: Basis for Sustainable Structures." *Proceedings of the CESB Conference* Prague, 83-88.

Shao, Y., and Billington, S. (2019). "Utilizing Full UHPC Compressive Strength in Steel Reinforced UHPC Beams." *International Interactive Symposium on Ultra-High Performance Concrete*, Iowa State University Digital Press.

Sritharan, S. (2015a). "Design of UHPC Structural Members: Lessons Learned and ASTM Test Requirements." *Advances in Civil Engineering Materials*, 4(2), 113-131.

Sritharan, S. (2015b). "Design of UHPC Structural Members: Lessons Mearned and ASTM Test Requirements." *Advances in Civil Engineering Materials*, 4(2), 113-131.

Steinberg, E., and Lubbers, A. (2003). "Bond of Prestressing Strands in UHPC." *Proceedings, 2003 International Symposium on High Performance Concrete*.

Storm, T. K., Rizkalla, S. H., and Zia, P. Z. (2013). "Effects of Production Practices on Camber of Prestressed Concrete Bridge Girders." *PCI journal*, 58(1).

Swiss Society of Engineers and Architects (2013). "Bétons fibrés Ultra-Performant: Matériaux, Dimensionnement et Exécution (UHPC: Materials, Design and Construction)." Swiss Society of Engineers and Architects, Zurich.

Tadros, M. (2021). "Application of PCI Ultra-High-Performance Concrete to Bridge Super Structures." AASHTO CBS T-10 Committee Meeting, Presenter-Maher Tadros, Technical Committee for Concrete Design T-10, Web Meeting.

Toutlemonde, F., Bernadi, S., Brugeaud, Y., and Simon, A. (2018). "Twenty Years-Long French Experience in UHPFRC Application and Paths Opened from The Completion of The Standards for UHPFRC." *The 2nd International Conference on UHPC Materials and Structures (UHPC2018-China)*, International Union of Laboratories and Experts in Construction Materials.

Toutlemonde, F., Généreux, G., Delort, M., and Resplendino, J. (2016). "Product and Design Standards for UHPFRC in France." *First International Interactive Symposium on UHPC 2016*, 1-8.

TxDOT (2017a). "Prestressed Concrete I-Girder Details." TxDOT Bridge Division Standard, Austin, TX.

TxDOT (2017b). "State FY 2017 Low Bid Average for New and Replaced Bridges with DCIS Estimate." Texas Department of Bridge Transportation, Austin, Texas.

TxDOT (2019). "TxDOT Bridge Standards." Texas Department of Transportation, Austin, TX.

TxDOT (2021). "TxDOT Bridge Design Manual - LRFD." Texas Department of Transportation, Austin, TX.

TxDOT (2023). "Bridge Design Manual - LRFD." Texas Department of Transportation, Austin, TX.

Urmson, C. R., and Mander, J. B. (2012). "Local Buckling Analysis of Longitudinal Reinforcing Bars." *ASCE Journal of Structural Engineering*, 138(1), 62-71.

Vecchio, F. J., and Collins, M. P. (1986). "The Modified Compression-Field Theory for Reinforced Concrete Elements Subjected to Shear." *ACI J.*, 83(2), 219-231.

Visage, E. T., Perera, K., Weldon, B. D., Jauregui, D. V., Newtson, C., and Guaderrama, L. (2012). "Experimental and Analytical Analysis of the Flexural Behavior of UHPC Beams." *Proceedings of Hipermat 3rd International Symposium on UHPC and Nanotechnology for High Performance Construction Materials*, 403-410.

Visage, E. T., Weldon, B. D., Jauregui, D. V., and Newtson, C. M. (2019). "Flexural Performance of Ultrahigh-Performance Concrete Developed Using Local Materials." *Journal of Materials in Civil Engineering*, 31(5), 04019050.

Voo, Y. L., Poon, W. K., and Foster, S. J. (2010). "Shear Strength of Steel Fiber-Reinforced Ultrahigh-Performance Concrete Beams without Stirrups." *ASCE Journal of Structural Engineering*, 136(11), 1393-1400.

Weldon, B. D., Jauregui, D. V., Newtson, C. M., Taylor, C. W., Montoya, K. F., and Allena, S. (2010). "Feasibility Analysis of Ultra High Performance Concrete for Prestressed Concrete Bridge Applications."Las Cruces, NM.

Wille, K., El-Tawil, S., and Naaman, A. (2014a). "Properties of Strain Hardening Ultra High Performance Fiber Reinforced Concrete (UHP-FRC) under Direct Tensile Loading." *Cement and Concrete Composites*, 48, 53-66.

Wille, K., Tue, N. V., and Parra-Montesinos, G. J. (2014b). "Fiber Distribution and Orientation in UHP-FRC Beams and Their Effect on Backward Analysis." *Materials and Structures*, 47(11), 1825-1838.

Yang, I.-H., Joh, C., Lee, J. W., and Kim, B.-S. (2013). "Torsional Behavior of Ultra-High Performance Concrete Squared Beams." *Engineering Structures*, 56, 372-383.

Yoo, D.-Y., Min, K.-H., Lee, J.-H., and Yoon, Y.-S. (2014a). "Shrinkage and Cracking of Restrained Ultra-High-Performance Fiber-Reinforced Concrete Slabs at Early Age." *Construction and Building Materials*, 73, 357-365.

Yoo, D.-Y., Shin, H.-O., Yang, J.-M., and Yoon, Y.-S. (2014). "Material and bond properties of ultra high performance fiber reinforced concrete with micro steel fibers." *Composites Part B: Engineering*, 58, 122-133.

Yoo, D.-Y., and Yoon, Y.-S. (2015). "Structural Performance of Ultra-High-Performance Concrete Beams with Different Steel Fibers." *Engineering Structures*, 102, 409-423.

Yoo, D. Y., and Yoon, Y. S. (2016). "A Review on Structural Behavior, Design, and Application of Ultra-High-Performance Fiber-Reinforced Concrete." *International Journal of Concrete Structures and Materials*, 10(2), 125-142.

Yuan, J., and Graybeal, B. (2016). "Full-Scale Testing of Shear Key Details for Precast Concrete Box-Beam Bridges." *Journal of Bridge Engineering*, 21(9), 04016043.

Zhang, G., and Graybeal, B. A. (2014). "Development of UHPC Pi-Girder Sections for Span Length up to 41 m." *Journal of Bridge Engineering*, 20(3), 04014068.

APPENDIX: DRAWING SHEETS

The drawing sheets that were delivered to the precaster prior to the fabrication of the girder specimens are enclosed in this section. The drawings present the structural details and other fabrication notes that the research team communicated to the personnel at the precast plant.

ULTRA HIGH PERFORMANCE CONCRETE PRECAST PRESTRESSED BRIDGE GIRDER SPECIMENS

TXDOT PROJECT NO. 0-6982

TEXAS A&M TRANSPORTATION INSTITUTE
TEXAS A&M UNIVERSITY
COLLEGE STATION

Texas A&M Transportation Institute *Texas A&M University*		
Utilization of UHPC Bridge Superstructures in Texas		
Tx34-1 *Cover Sheet*		
TxDOT Project No.	*Drawing No.*	*Date*
0-6982	*S6982 – 0*	*06/07/2021*

GIRDER DIMENSIONS AND SECTION PROPERTIES

Girder Type	"D" (in.)	"B" (in.)	"Yt" (in.)	"Yb" (in.)	Area ($in.^2$)	"Ix" ($in.^4$)	"Iy" ($in.^4$)	Weight ⑥ (plf)
Tx34	34	12	18.49	15.51	627	88,355	40,731	697

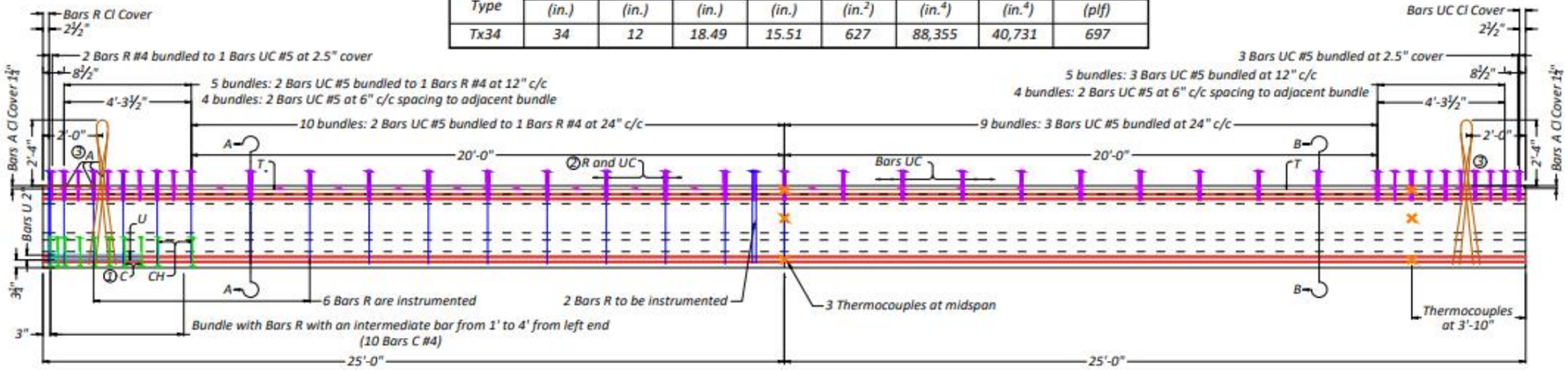

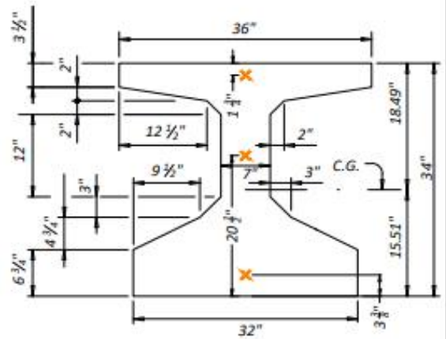

Cross-section Geometry

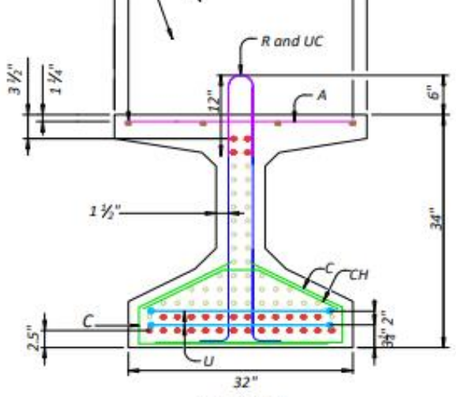

SECTION A-A

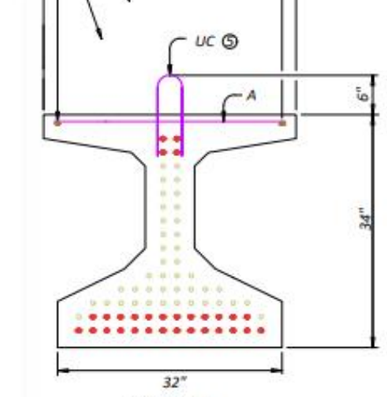

SECTION B-B

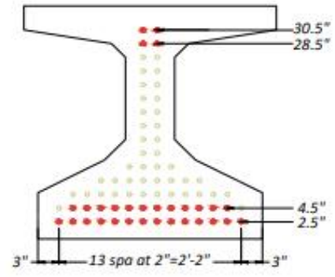

①Bundled with Bars R with intermediates in between bars R from 1' to 4' on left end only.

②The average of the top and bottom spacing of Bars R cannot exceed the required spacing. Bars R are bundled with UC bars. For bundle detail please see drawing S6982 – 2

③Bars A at 6" c/c tied to hoop bundles up to 5'-0" from left end, at 12" c/c tied to Bars R beyond 5'-0" from left end – intermediates in between the Bars R tied to Bars T
Bars A tied to hoop bundles in right half – at 6" c/c up to 5'-0" from right end and at 24" c/c beyond 5'-0" right end

④2 Bars T 49'-9" long at 2" side cover at both sides of top flange and 2 Bars T 25'-0" long at equal spacing in between the 49'-9" Bars T only on left end.

⑤Projection of Bars UC above the top flange of girder is between 5"-6".

⑥Based on 160 pcf total weight of UHPC and reinforcing steel.

General Notes:

1. Half span with minimum transverse (web) reinforcement, the other half without shear reinforcement in the web.
2. U-composite bars (Bars UC) are provided for interface shear between the girder and the deck slab.
3. For bar bending details, see drawing S6982 – 3.
4. 1½" clear cover unless noted otherwise.
5. Cover dimensions are clear dimensions, unless noted otherwise.
6. Reinforcing bar dimensions shown are out-to-out of bar.
7. 0.6 in. diameter, low relaxation prestressing strands: 26 at bottom and 4 at top. Bars UC to be tied to top strands.
8. Total girder length of this sheet is 50'-0".

Texas A&M Transportation Institute Texas A&M University		
Utilization of UHPC Bridge Superstructures in Texas		
Tx34-1 Elevation and Cross-sections		
TxDOT Project No.	Drawing No.	Date
0-6982	S6982 – 1	06/07/2021

GIRDER DIMENSIONS AND SECTION PROPERTIES								
Girder Type	"D" (in.)	"B" (in.)	"Yt" (in.)	"Yb" (in.)	Area ($in.^2$)	"Ix" ($in.^4$)	"Iy" ($in.^4$)	Weight (plf)
Tx34	34	12	18.49	15.51	627	88,355	40,731	697

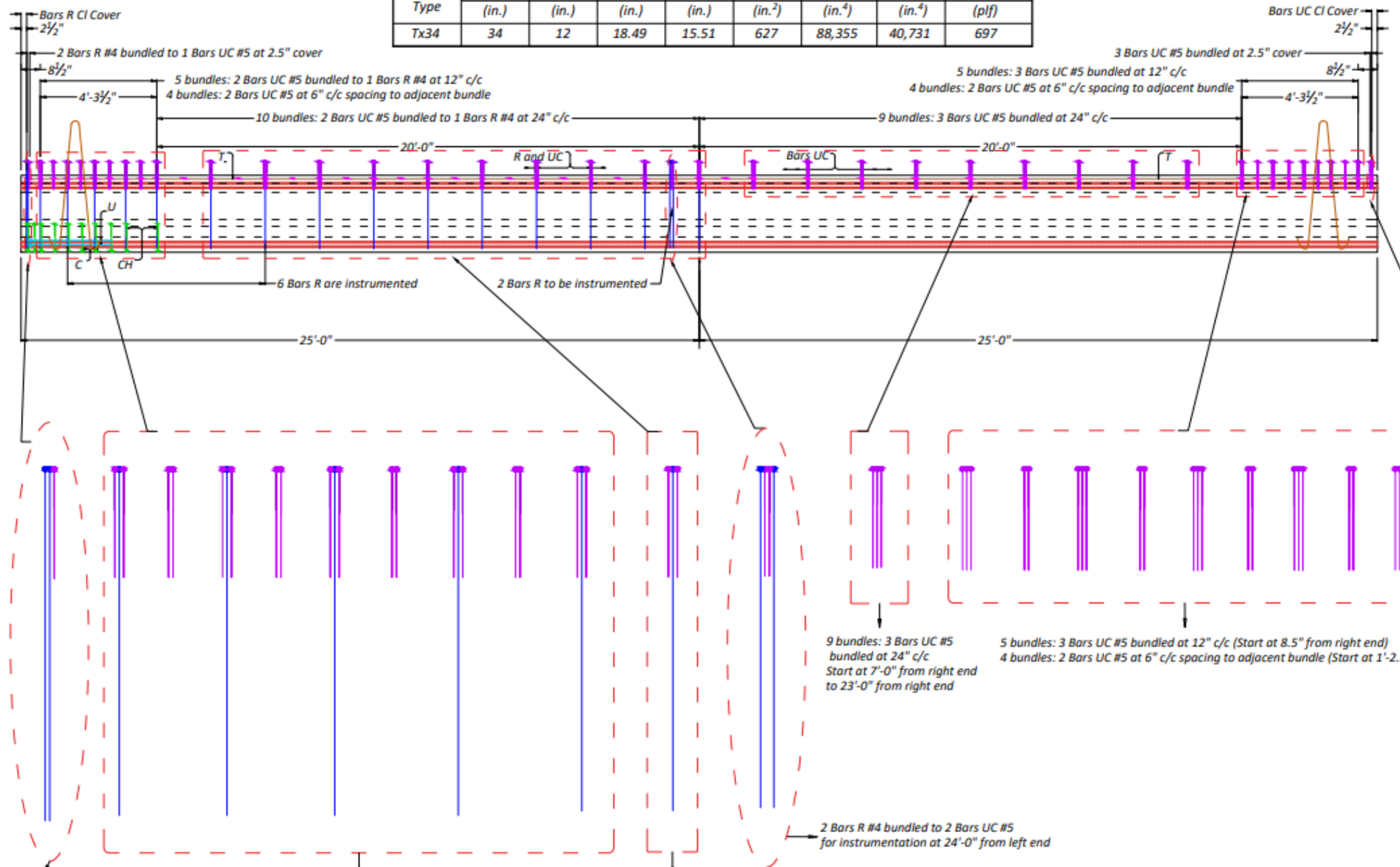

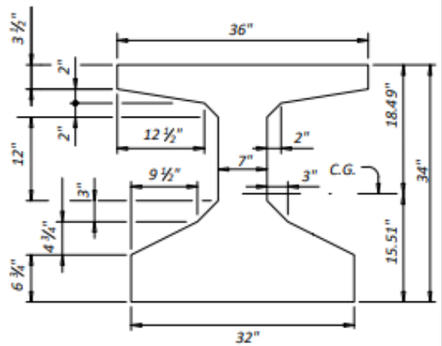

Cross-section Geometry

Texas A&M Transportation Institute Texas A&M University		
Utilization of UHPC Bridge Superstructures in Texas		
Tx34-1 Details of Bars R and Bars UC		
TxDOT Project No.	Drawing No.	Date
0-6982	S6982 – 2	06/07/2021

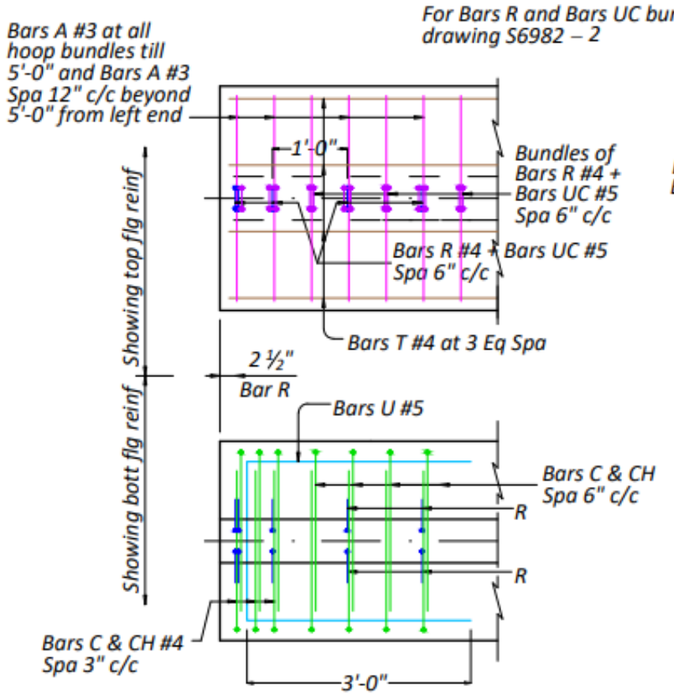

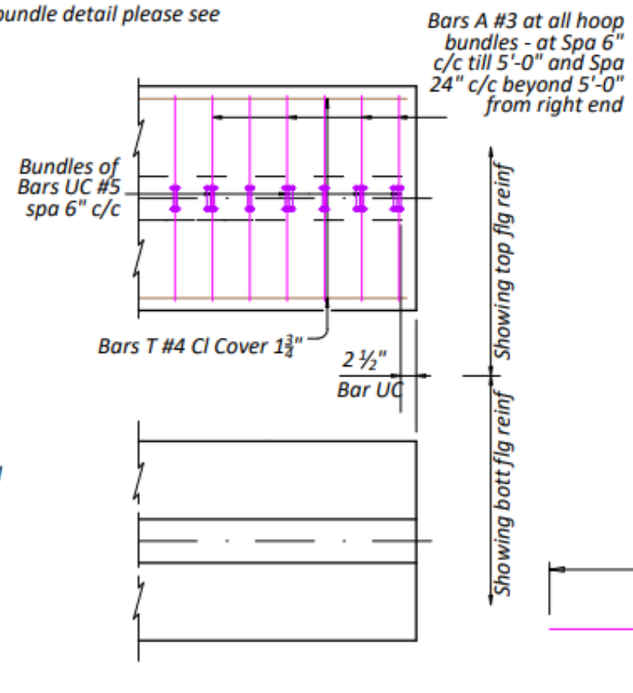

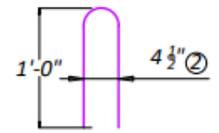

BARS UC34 (#5)

① No portion of bar less than 10 ft.

② Out-to-out dimension

Bill of Reinforcing Steel				
Specimen 1 – Eccentric				
Bar	Size	No. of Bars	Length	Weight, lb
A34	#3	41	2'-9"*	43
C34	#4	20	4'-0"*	26
CH34	#4	10	2'-6"*	17
R34	#4	19	7'-6"*	95
T34	#4	2	49'-9"	67
T34	#4	2	25'-0"	34
U34	#5	2	8'-3"*	18
UC34	#5	94	2'-4"	226

* Standard length for Tx34 girder reinforcement

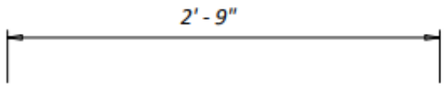

BARS A34 (#3)

To control top flange cracking that may occur during form removal, additional top flange reinforcing may be placed as shown in girder ends at the Fabricator's option.

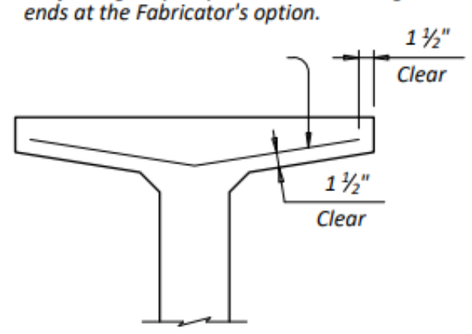

OPTIONAL TOP FLANGE REINFORCING DETAIL

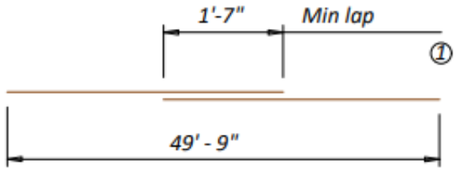

BARS T34 (#4)

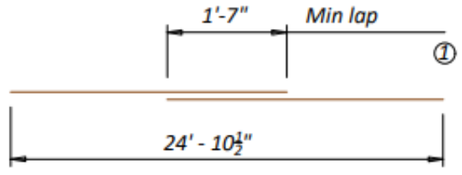

BARS T34 (#4)

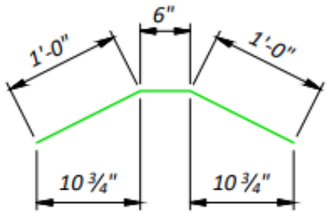

BARS CH34 (#4)

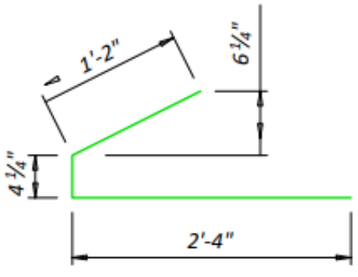

BARS C34 (#4)

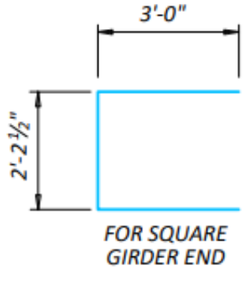

BARS U34 (#5)

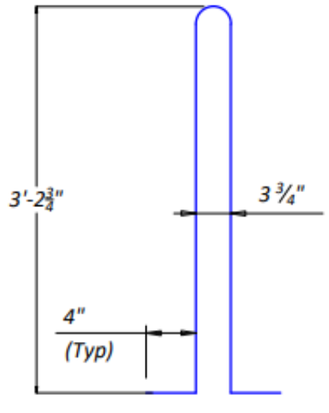

BARS R34 (#4)

Texas A&M Transportation Institute Texas A&M University		
Utilization of UHPC Bridge Superstructures in Texas		
Tx34-1 Bar Bending and Flange Details		
TxDOT Project No.	Drawing No.	Date
0-6982	S6982 – 3	06/07/2021

ULTRA HIGH PERFORMANCE CONCRETE PRECAST PRESTRESSED BRIDGE GIRDER SPECIMENS

TXDOT PROJECT NO. 0-6982

TEXAS A&M TRANSPORTATION INSTITUTE
TEXAS A&M UNIVERSITY
COLLEGE STATION

Texas A&M Transportation Institute *Texas A&M University*		
Utilization of UHPC Bridge Superstructures in Texas		
Tx34-2 *Cover Sheet*		
TxDOT Project No.	*Drawing No.*	*Date*
0-6982	*S6982 – 0*	*08/02/2021*

GIRDER DIMENSIONS AND SECTION PROPERTIES

Girder Type	"D" (in.)	"B" (in.)	"Yt" (in.)	"Yb" (in.)	Area ($in.^2$)	"Ix" ($in.^4$)	"Iy" ($in.^4$)	Weight ⑥ (plf)
Tx34	34	12	18.49	15.51	627	88,355	40,731	697

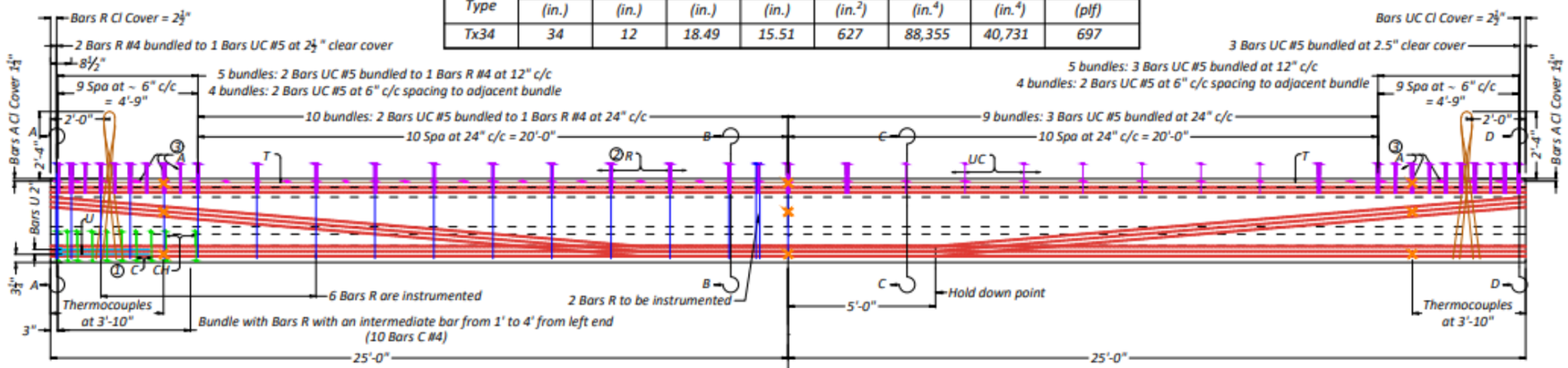

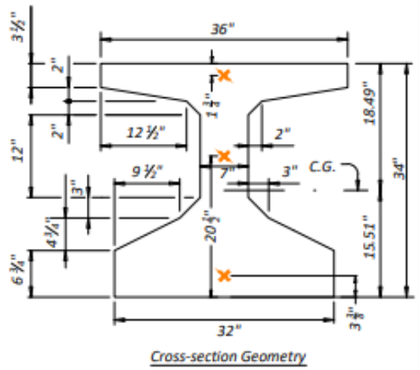

Cross-section Geometry

SECTION A-A

SECTION B-B

SECTION C-C

SECTION D-D

① Bundled with Bars R with intermediates in between bars R from 1' to 4' on left end only.

② The average of the top and bottom spacing of Bars R cannot exceed the required spacing. Bars R are bundled with UC bars. For bundle detail please see drawing S6982 – 2

③ Bars A at 6" c/c tied to hoop bundles up to 5'-0" from left end, at 12" c/c tied to Bars R beyond 5'-0" from left end – intermediates in between the Bars R tied to Bars T
Bars A tied to hoop bundles in right half – at 6" c/c up to 5'-0" from right end and at 24" c/c beyond 5'-0" right end

④ 2 Bars T 49'-9" long at 2" side cover at both sides of top flange and 2 Bars T 25'-0" long at equal spacing in between the 49'-9" Bars T only on left end.

⑤ Projection of Bars UC above the top flange of girder is between 5"-6".

⑥ Based on 160 pcf total weight of UHPC and reinforcing steel.

General Notes:

1. Half span with minimum transverse (web) reinforcement, the other half without shear reinforcement in the web.
2. U-composite bars (Bars UC) are provided for interface shear between the girder and the deck slab.
3. For bar bending details, see drawing S6982 – 3
4. 1½" clear cover unless noted otherwise.
5. Cover dimensions are clear dimensions, unless noted otherwise.
6. Reinforcing bar dimensions shown are out-to-out of bar.
7. 0.6 in. diameter, low relaxation prestressing strands, 6 strands are draped: 28 at bottom and 10 at top at ends; 34 at bottom and 4 at top at midspan. For strand and force details, see drawing S6982 – 2. Bars UC to be tied to top strands.
8. Total girder length of this sheet is 50'-0".
9. When cutting the strands, maintain 18" of strand projecting from each girder end. (Final dimension can be coordinated with the research team.)
10. Prior to delivery, cut the strands such that 2" of strand projects from each girder end.

Texas A&M Transportation Institute
Texas A&M University

Utilization of UHPC Bridge Superstructures in Texas

Tx34-2

Elevation and Cross-sections

TxDOT Project No.	Drawing No.	Date
0-6982	S6982 – 1	08/02/2021

GIRDER DIMENSIONS AND SECTION PROPERTIES

Girder Type	"D" (in.)	"B" (in.)	"Yt" (in.)	"Yb" (in.)	Area ($in.^2$)	"Ix" ($in.^4$)	"Iy" ($in.^4$)	Weight (plf)
Tx34	34	12	18.49	15.51	627	88,355	40,731	697

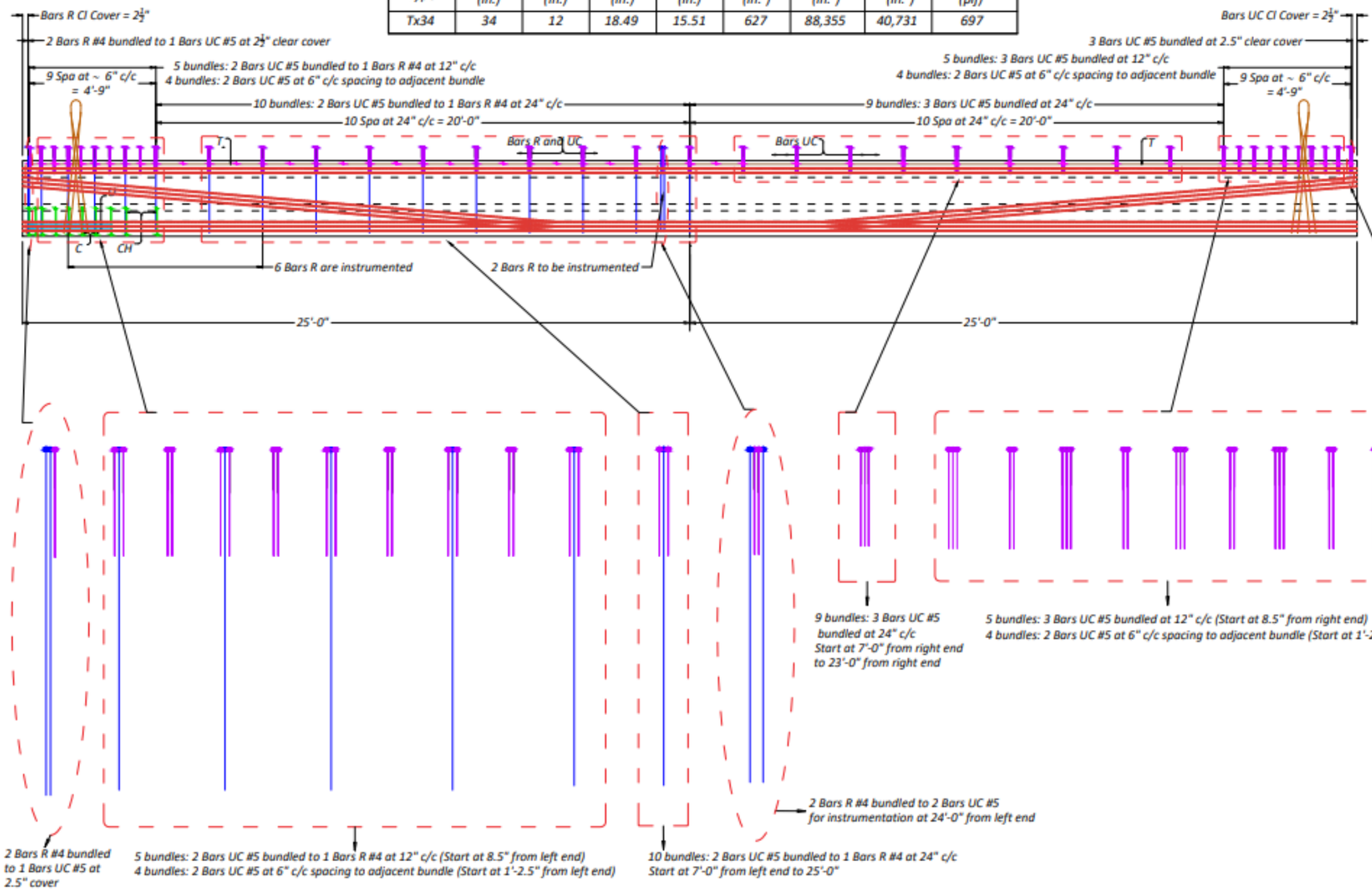

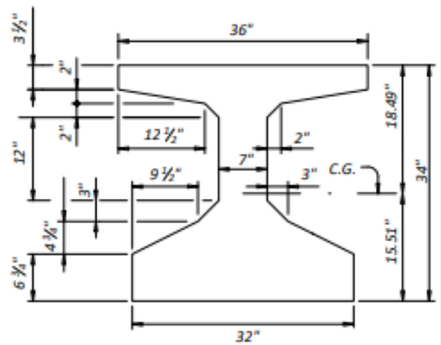

Cross-section Geometry

Low Relaxation (270 ksi) Strand Pattern
Number of strands: 38 ~ 0.6"∅ @ 44 k per strand
Number of straight strands: 32 (28 Bot & 4 Top)
Number of deflected strands: 6 @ 26.50"
Concrete release strength: 11.7 ksi
Concrete design strength: 18.0 ksi
Eccentricity @ ℄: 8.80" and @ end: 5.64"

Texas A&M Transportation Institute Texas A&M University		
Utilization of UHPC Bridge Superstructures in Texas		
Tx34-2 Details of Bars R, Bars UC, and Strands		
TxDOT Project No.	Drawing No.	Date
0-6982	S6982 – 2	08/02/2021

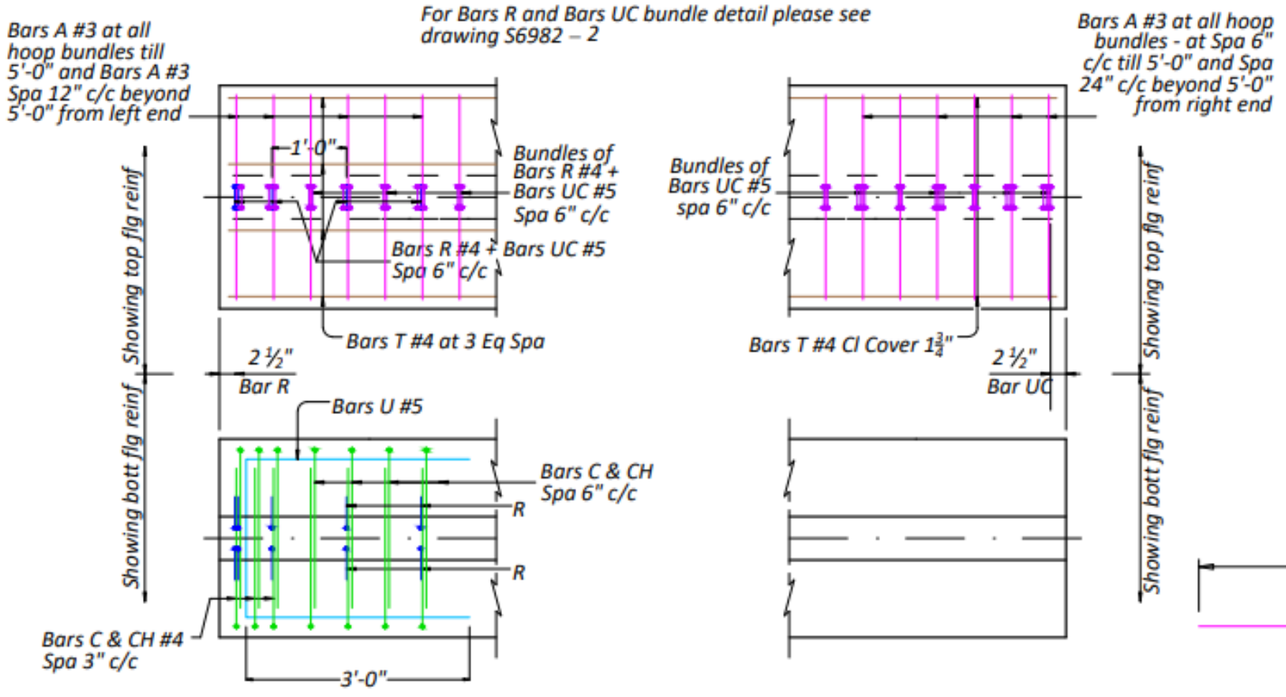

① No portion of bar less than 10 ft.

② Out-to-out dimension

Bill of Reinforcing Steel

Specimen 1 – Eccentric

Bar	Size	No. of Bars	Length	Weight, lb
A34	#3	41	2'-9"*	43
C34	#4	20	4'-0"*	26
CH34	#4	10	2'-6"*	17
R34	#4	19	7'-6"*	95
T34	#4	2	49'-9"	67
T34	#4	2	25'-0"	34
U34	#5	2	8'-3"*	18
UC34	#5	94	2'-4"	226

* Standard length for Tx34 girder reinforcement

To control top flange cracking that may occur during form removal, additional top flange reinforcing may be placed as shown in girder ends at the Fabricator's option.

Texas A&M Transportation Institute
Texas A&M University

Utilization of UHPC Bridge Superstructures in Texas

Tx34-2

Bar Bending and Flange Details

TxDOT Project No.	Drawing No.	Date
0-6982	S6982 – 3	08/02/2021

ULTRA HIGH PERFORMANCE CONCRETE PRECAST PRESTRESSED BRIDGE GIRDER SPECIMENS

TXDOT PROJECT NO. 0-6982

TEXAS A&M TRANSPORTATION INSTITUTE
TEXAS A&M UNIVERSITY
COLLEGE STATION

Texas A&M Transportation Institute *Texas A&M University*		
Utilization of UHPC Bridge Superstructures in Texas		
Tx54 *Cover Sheet*		
TxDOT Project No.	*Drawing No.*	*Date*
0-6982	*S6982 – 0*	*02/15/2022*

GIRDER DIMENSIONS AND SECTION PROPERTIES

Girder Type	"D" (in.)	"B" (in.)	"Yt" (in.)	"Yb" (in.)	Area ($in.^2$)	"Ix" ($in.^4$)	"Iy" ($in.^4$)	Weight ⑦ (plf)
Tx54	54	30	30.49	23.51	817	299,740	46,707	908

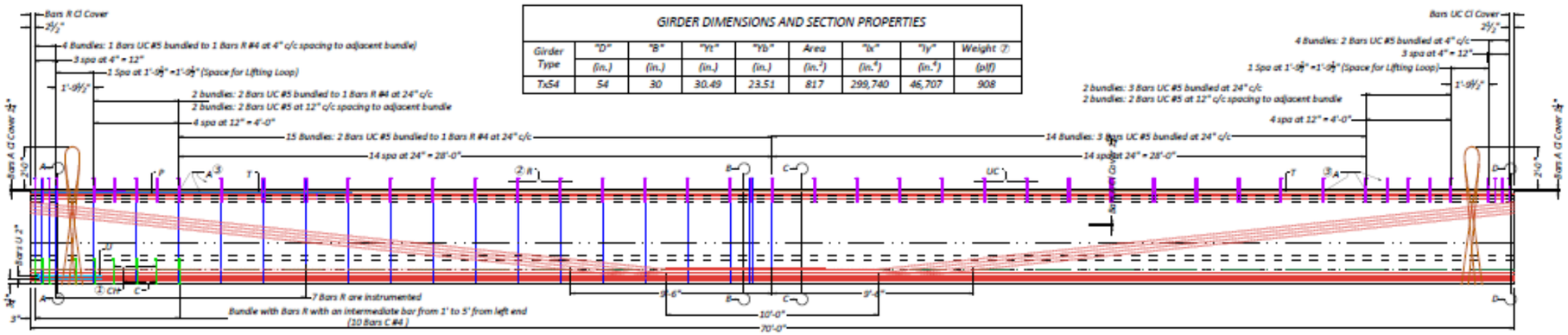

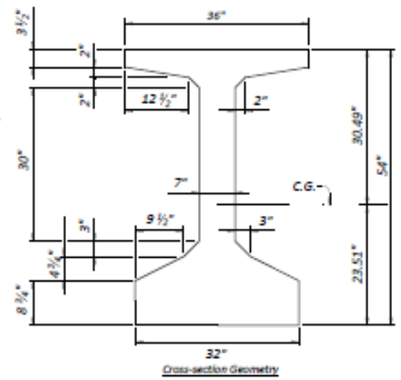

Cross-section Geometry

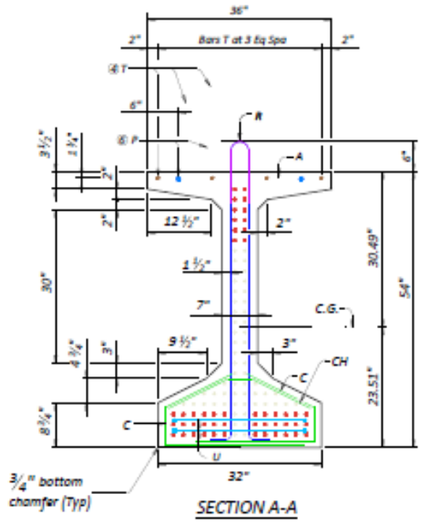

SECTION A-A

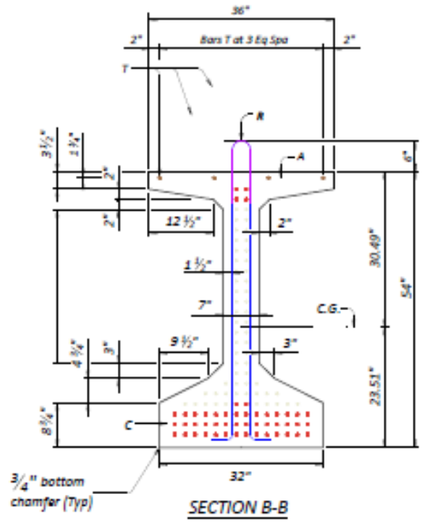

SECTION B-B

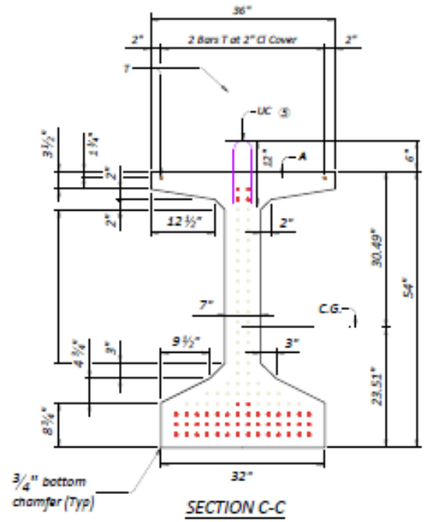

SECTION C-C

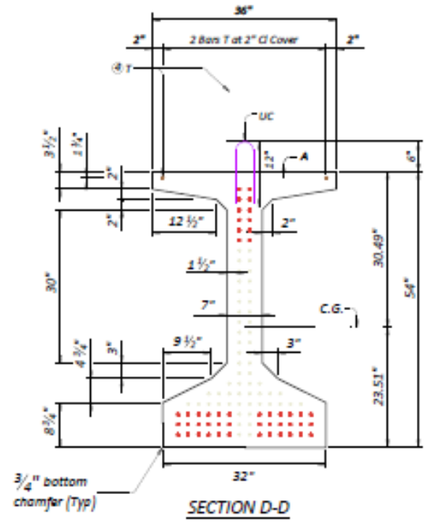

SECTION D-D

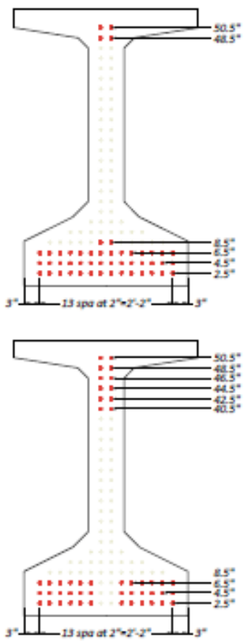

① Bundled with Bars R with intermediates in between bars R from 1' to 5' on left end only.

② The average of the top and bottom spacing of Bars R cannot exceed the required spacing.

③ Bars A at 12" c/c on left half only and tied to Bars R (except 2nd Bar R from left end) where possible
– Intermediates in between the the bars tied to Bars T
Bars A at 24" c/c on right half at 5' from the right. Tied to Bars UC bars (except 2nd Bar UC from right end)

④ 2 Bars T 49'-9" long at 2" side cover (effective) at both sides of top flange and 2 Bars T 25'-0" long at equal space in between the 49'-9" Bars T only on left end.

⑤ Projection of U composite bars above the top flange of girder is between 5-6".

⑥ 2 Bars P #6 15' long on left end only at 6" spacing from end at both sides of top flange.

⑦ Based on 160 pcf total weight of UHPC and reinforcing steel.

General Notes:

1. Half span with minimum transverse (web) reinforcement, the other half without shear reinforcement in the web.
2. U-composite bars in the half without web reinforcement is provided for interface shear between the girder and the deck slab.
3. For bar bending details, see drawing S6982 – 6
4. 1" clear cover unless noted otherwise.
5. Cover dimensions are clear dimensions, unless noted otherwise.
6. Reinforcing bar dimensions shown are out-to-out of bar.
7. Research team needs to be present for the installation of R bars to ensure the correct location of the gaged bars.
8. 0.6 in. diameter, low relaxation prestressing strands, 8 strands are draped: 36 at bottom and 12 at top at ends; 44 at bottom and 4 at top at midspan. For strand and force details, see drawing S6982 – 2. Bars UC to be tied to top strands.
9. Total girder length of this sheet is 70'-0".
10. When cutting the strands, maintain 18" of strand projecting from each girder end. (Final dimension can be coordinated with the research team.)
11. Prior to delivery, cut the strands such that 2" of strand projects from each girder end.

Texas A&M Transportation Institute Texas A&M University Utilization of UHPC Bridge Superstructures in Texas		
Tx54 Elevation and Cross-sections		
TxDOT Project No.	Drawing No.	Date
0-6982	S6982 – 1	02/15/2022

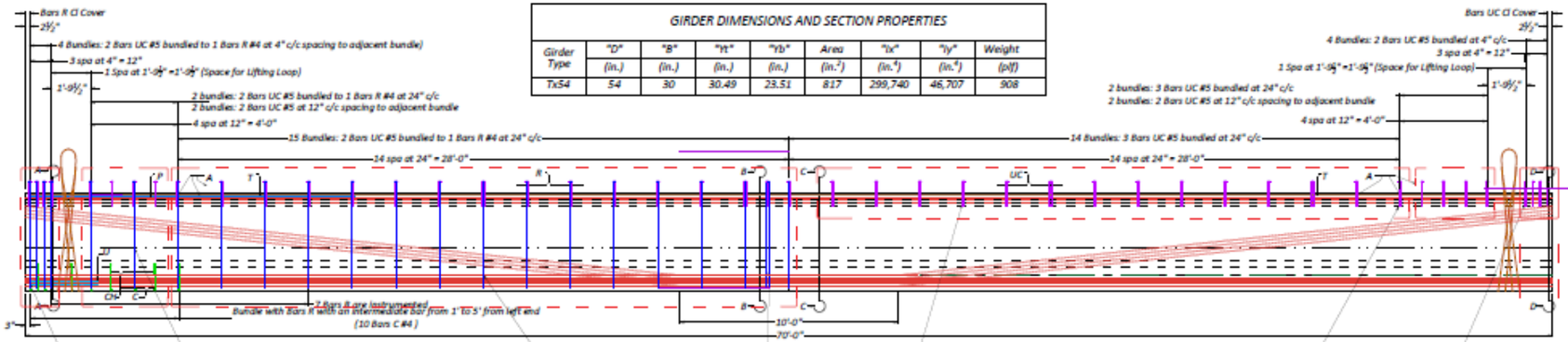

GIRDER DIMENSIONS AND SECTION PROPERTIES								
Girder Type	"D" (in.)	"B" (in.)	"Yt" (in.)	"Yb" (in.)	Area ($in.^2$)	"Ix" ($in.^4$)	"Iy" ($in.^4$)	Weight (plf)
Tx54	54	30	30.49	23.51	817	299,740	46,707	908

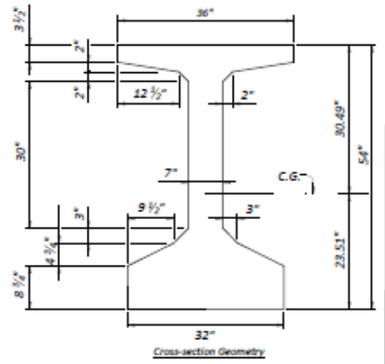

Cross-section Geometry

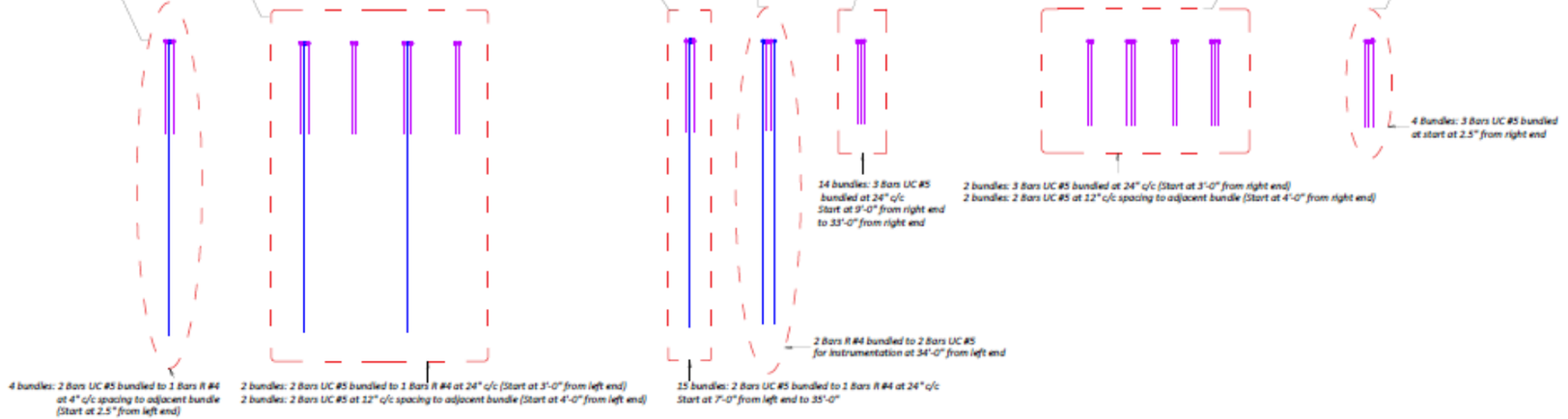

Low Relaxation (270 ksi) Strand Pattern
Number of strands: 48 – 0.6"∅ @ 44 k per strand
Number of straight strands: 40 (36 Bot & 4 Top)
Number of deflected strands: 8 @ 46.50"
Concrete release strength: 11.7 ksi
Concrete design strength: 18.0 ksi
Eccentricity @ C: 15.09" and @ end: 8.76"

Texas A&M Transportation Institute Texas A&M University		
Utilization of UHPC Bridge Superstructures in Texas		
Tx54 Details of Bars R, Bars UC, and Strands		
TxDOT Project No.	Drawing No.	Date
0-6982	S6982 – 2	02/15/2022

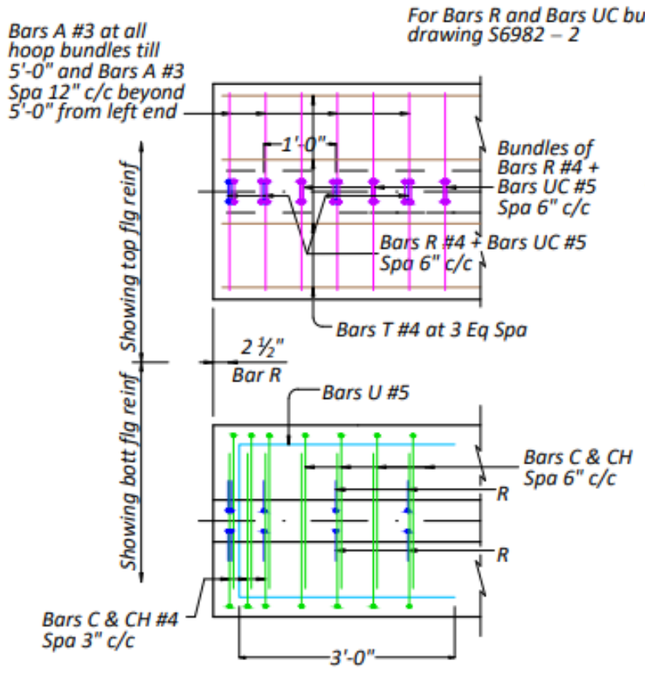

For Bars R and Bars UC bundle detail please see drawing S6982 – 2

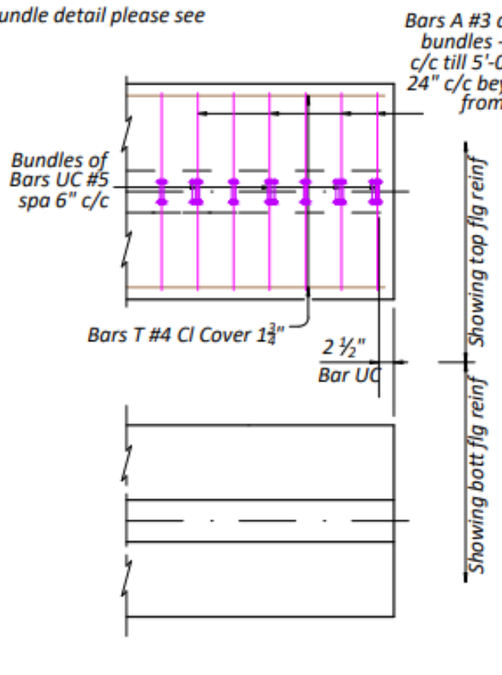

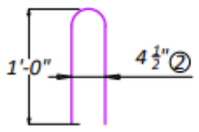

BARS UC34 (#5)

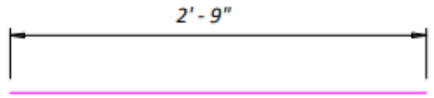

BARS A34 (#3)

① No portion of bar less than 10 ft.

② Out-to-out dimension

Bill of Reinforcing Steel				
Specimen 1 – Eccentric				
Bar	Size	No. of Bars	Length	Weight, lb
A34	#3	41	2'-9"*	43
C34	#4	20	4'-0"*	26
CH34	#4	10	2'-6"*	17
R34	#4	19	7'-6"*	95
T34	#4	2	49'-9"	67
T34	#4	2	25'-0"	34
U34	#5	2	8'-3"*	18
UC34	#5	94	2'-4"	226

* Standard length for Tx34 girder reinforcement

To control top flange cracking that may occur during form removal, additional top flange reinforcing may be placed as shown in girder ends at the Fabricator's option.

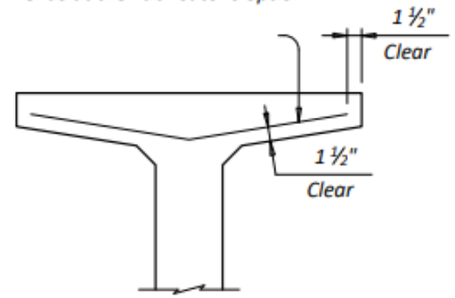

OPTIONAL TOP FLANGE REINFORCING DETAIL

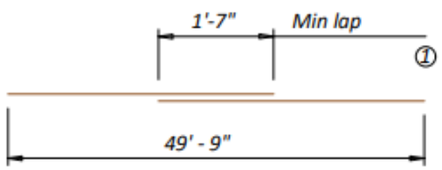

BARS T34 (#4)

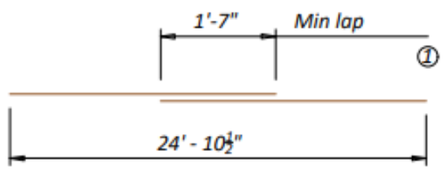

BARS T34 (#4)

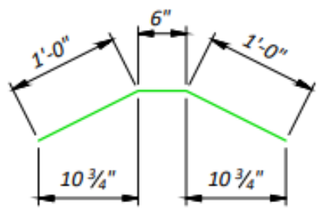

BARS CH34 (#4)

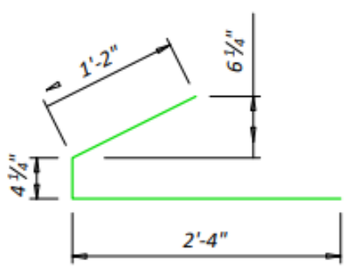

BARS C34 (#4)

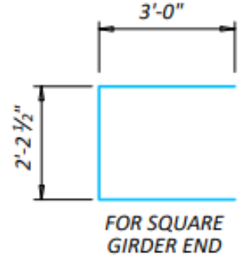

BARS U34 (#5)

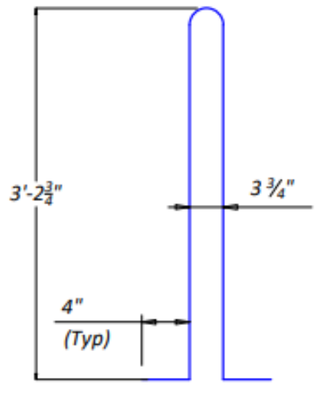

BARS R34 (#4)

Texas A&M Transportation Institute Texas A&M University		
Utilization of UHPC Bridge Superstructures in Texas		
Tx54 Bar Bending and Flange Details		
TxDOT Project No.	Drawing No.	Date
0-6982	S6982 – 3	08/02/2021